



HAL
open science

Chronology of the diversification of anurans

Alfred Lemierre

► **To cite this version:**

Alfred Lemierre. Chronology of the diversification of anurans. Paleontology. Museum national d'histoire naturelle - MNHN PARIS, 2022. English. NNT : 2022MNHN0010 . tel-04959419

HAL Id: tel-04959419

<https://theses.hal.science/tel-04959419v1>

Submitted on 20 Feb 2025

HAL is a multi-disciplinary open access archive for the deposit and dissemination of scientific research documents, whether they are published or not. The documents may come from teaching and research institutions in France or abroad, or from public or private research centers.

L'archive ouverte pluridisciplinaire **HAL**, est destinée au dépôt et à la diffusion de documents scientifiques de niveau recherche, publiés ou non, émanant des établissements d'enseignement et de recherche français ou étrangers, des laboratoires publics ou privés.



MUSEUM NATIONAL D'HISTOIRE NATURELLE
Ecole Doctorale Sciences de la Nature et de l'Homme – ED 227

Année 2022

N° attribué par la
bibliothèque

□□□□□□□□□□□□□□□□

THESE

Pour obtenir le grade de

DOCTEUR DU MUSEUM NATIONAL D'HISTOIRE NATURELLE

Spécialité : Paléontologie

Présentée et soutenue publiquement par

Alfred Lemierre

Le 18 novembre 2022

Chronologie de la diversification des anoures

Sous la direction de :

Michel Laurin, Directeur de recherche, CNRS

Salvador Bailon, Ingénieur de recherche, MNHN

Annelise Folie, Chargée de collection, IRSNB

JURY :

James Gardner	Curator, Royal Tyrrell Museum, Canada	Rapporteur
Massimo Delfino	Profesor, Università di Torino, Turin, Italie	Rapporteur
Gilles Didier	Chargé de recherche, Institut montpellierain Alexander Grothendieck, Montpellier, France	Examinateur
Nadia Fröbisch	Profesor, Museum für Naturkunde, Berlin, Allemagne	Examinatrice
Annemarie Ohler	Professeure, Muséum national d'histoire naturelle, Paris, France	Examinatrice
Michel Laurin	Directeur de recherche, Centre national de la recherche scientifique, Paris, France	Directeur de thèse
Annelise Folie	Chargé de collection, Institut royal des sciences naturelles de Belgique, Bruxelles, Belgique	Encadrant de thèse

*« S'il fallait tenir compte des services rendus à la science,
la grenouille occuperait la première place »*

Claude Bernard, *Etude de la médecine expérimentale*, 1865

« Faites l'anouere, pas la guerre ! »

Julien Sly Barbier, 2022

REMERCIEMENTS

Je tiens tout d'abord à remercier mes trois encadrants, Michel Laurin, Annelise Folie et Salvador Bailon, qui ont été présents tout au long de ces trois années et sans qui ce manuscrit n'existerait pas. Merci à Michel de m'avoir fait confiance pour réaliser ce projet, et de continuer mon rêve d'enfant, être paléontologue. Merci encore de m'avoir guidé au travers des méandres des publications. Merci à Salvador et Annelise de m'avoir accompagné dans mes premiers pas au sein de la paléoherpétologie et de la description de ces petites grenouilles, et s'être échinés à vérifier chacune de mes identifications sur tous mes petits bouts d'os. Merci enfin à tous les trois pour m'avoir relu, corrigé et commenté mes manuscrits, et de m'avoir aidé à les transformer en véritables objets scientifiques.

Je tiens à adresser mes remerciements les plus sincères aux membres du jury de cette thèse : Annemarie Ohler, Nadia Fröbisch, Gilles Didier, Massimo Delfino et James Gardner. I wish to express my most sincere thanks to the members of the jury. It is an honor for me to have you all reviewing and assessing my work. Merci à Annemarie Ohler de représenter le muséum, et de m'avoir aidé lors de mes errements sur la nomenclature de *Thaumastosaurus* et des momies du Quercy. Gilles, merci de m'avoir apporté ton aide et ton expertise lors des analyses des temps de divergence pour les pipidés. Nadia Fröbisch, thanks for accepting to be a part of this jury. Massimo Delfino, thanks for accepting to be a reviewer of this manuscript. Jim, thanks a lot for accepting to review this large manuscript, and for our discussion on amphibians from the Cretaceous of In Becetén and Sudan.

Je tiens particulièrement à remercier Damien Germain, pour m'avoir fait découvrir un peu plus la recherche au travers d'un stage pendant mon Master 2, et de m'avoir aidé pour la rédaction et la publication de mon premier article scientifique. Merci encore

pour m'avoir soutenu pendant mon année de bénévolat, et de m'avoir laissé un quasi-« libre » accès aux collections de grenouilles au Muséum, et surtout d'avoir supporté mes longues discussions, encore plus autour d'un verre. Je remercie aussi Thomas Arbez et Gael Clément, pour m'avoir fait découvrir la recherche, et de m'avoir initié à la tomographie et à la modélisation 3D.

Je tiens à remercier Cromie, Petit-père, Grand-papa, Isa, Guillaume et Paul, et la Fondation pour la Recherche sur la Biodiversité, sans qui cette thèse n'aurait jamais pu voir le jour, et qui m'ont permis, grâce à leur soutien financier, de poursuivre dans cette voie.

Je tiens à remercier Florent Goussard et Nathalie Poulet pour leur aide à la réalisation de jolis modèle 3D et à manipuler les images obtenues par tomographie. Je remercie aussi Martha Bellato et Patricia Wils pour leur aide à la réalisation des scans sur mes petits morceaux de grenouilles du Crétacé.

Je tiens à remercier Sylvie Crasquin, Sylvain Charbonnier, Angelina Bastos, Suzy Colas et Nadia Guerguad pour m'avoir accueilli au sein du CR2P pendant ces trois années. Je tiens à remercier Nour-Eddine Jalhil pour son aide sur les différentes occurrences de grenouilles au sein du registre fossile africain. Merci à Didier Dutheil et Paolo de Brito pour leur discussions sur les anoures mésozoïques du Gondwana, et sur l'évolution des faunes Sud-Américaines et Africaines pendant le Crétacé.

Merci à Thierry Pélissié, Maëva Orliac, Renaud Lebrun, Gilles Escarguel, Monique Vianey-Liaud et toute l'équipe du Quercy pour m'avoir accueilli à la phosphatière du Cloup d'Aural depuis deux ans, et de m'inclure au sein de ce vaste projet d'étude des fossiles des Phosphatières du Quercy. Merci pour ces semaines à trier du sédiment à la recherche de mes grenouilles et de petits lézards, ainsi qu'à nos discussions sur ces faunes et leurs origines. Merci à Damien Gendry et Romain Vullo pour m'avoir accueilli pendant quelques jours au sein du laboratoire de Rennes, et d'avoir travaillé sur un superbe spécimen historique de la région. Merci à Yves Laurent pour m'avoir accueilli deux fois au sein du Muséum de Toulouse, pendant que je parlais à la recherche de petits bouts de *Thaumastosaurus*.

I wish to extend my thanks to David Blackburn and Jaimie Grey. Dave, thanks a lot for giving me the opportunity to work on most of anuran from the Kem Kem Formation and discussing on African anurans evolution and fossil record. Jaimie, thanks for the discussion on pipid brains and endocast.

Je tiens à remercier mes deux collègues de bureau, Valentin Buffa et Jordan Gônet. Merci à vous deux pour m'avoir tenu compagnie pendant ces trois ans et pour toutes nos discussions, plus ou moins sérieuses. Valentin, merci pour m'avoir encouragé et guidé dans mes premiers dessins scientifiques, bien que je reste bien en deçà de tes résultats. Merci aussi pour toutes ces pauses café, qui nous ont sûrement permis de tenir pendant ces trois dernières années. Merci à Elvis, Guillaume, Marjorie, Béatrice, Marine, Vincent, Mathieu, Nicolas, Ségolène, Vincente, Marine, Rémi et Christophe pour ces moments d'escapade de la thèse entre doctorants, que ce soit à Paris ou pendant des congrès.

Merci à tout le crew du master et des Verredredi, Léo, Julien, Jocerand, Morgane, Téophane, Cécile, Vincent, Rodrigue, Camille et Hugues, pour m'avoir soutenu et accompagné tout au long de ces trois années, quand nous n'étions pas confinés chez nous. Ces soirées passées à discuter et à boire ont été de vrais moments d'escapades entre potes.

Je tiens à remercier Tracy, pour m'avoir supporté et pour avoir été présente à mes côtés depuis plus de sept ans. Ta présence m'a permis de tenir pendant les moments plus difficiles, que ce soit avant ou pendant cette thèse. Merci également à Karacrouqs et Marie, ces deux petites boules de poils qui partagent ma vie depuis quatre mois maintenant.

Enfin, et pour conclure, merci à toute ma famille, Adé, Arthur, Daddy, Maman, Cromie, Petit Père, Grand-papa et Isa pour m'avoir soutenu et accompagné et écouté parler de fossiles et maintenant de grenouilles, depuis que je suis tout petit. Merci à vous de m'avoir accompagné visiter ces musées d'histoire naturelle au travers de nos voyages, y compris les plus lointains, et de m'avoir encouragé à poursuivre mon rêve d'enfants.

TABLE OF CONTENTS

Extended abstract	14
General Introduction	21
Section I–Early evolution and chronology of pipid diversification throughout Mesozoic and Paleogene Africa.....	36
Chapter I–The Pipimorph fossil record	38
Chapter II–Pipimorphs of In Becetén and their implication for pipid diversification in Mesozoic Africa.....	48
II.1 Introduction.....	50
II.2 Materials and Methods	51
II.3 Systematic Paleontology	51
II.4 Osteological Description.....	53
II.5 Phylogenetic Analysis.....	63
II.6 Discussion	64
II.7 Conclusion	67
II.8 Appendix.....	68
Chapter III–A new pipid from the Cretaceous of Africa (In Becetén, Niger) and early evolution of Pipidae.....	68
II.1 Introduction.....	70
III.2 Geological Context.....	72
III.3 Materials and Methods	74
III.4 Systematic Palaeontology.....	76

III.5 Results.....	80
III.6 Nomenclatural Note	92
III.7 Phylogenetic Analyses.....	103
III.8 Discussion	109
III.9 Conclusion.....	117
III.10 Appendix.....	118
Chapter IV–Big brain in strange body: Description of new Pachycentrata remains and the first fossil amphibian ‘brain’	139
IV.1 Introduction.....	141
IV.2 Materials and Methods.....	142
IV.3 Systematic Palaeontology	143
IV.4 Osteological Description	144
IV.5 Internal Anatomy	148
IV.6 Discussion	159
IV.7 Conclusion	163
IV.8 Appendix.....	163
Chapter V–Bridging the gap ? Dating early pipid evolutionary radiation	166
V.1 Introduction.....	168
V.2 Materials and Methods	169
V.3 Systematic Palaeontology	173
V.4 Results	176
V.5 Discussion.....	179
V.6 Conclusion.....	188
Chapter VI–Conclusions on early pipid diversification.....	190

Section II–Diversification of the neobatrachians in Mesozoic African and Paleogene Europe	196
Chapter VII–The early neobatrachian fossil record.....	198
Chapter VIII–A new genus and species from the Kem Kem (Morocco), the oldest neobatrachian from Cretaceous Africa.....	208
VIII.1 Introduction.....	210
VIII.2 Geological Context.....	212
VIII.3 Materials and Methods.....	213
VIII.4 Systematic Paleontology.....	216
VIII.5 Description.....	220
VIII.6 Phylogenetic Analyses	241
VIII.7 Discussion.....	247
VIII.8 Conclusion	250
VIII.9 Appendix.....	251
Chapter IX– The neobatrachians of In Beceté: The earliest coexistence of an hyloid and a ranoid ?.....	254
IX.1 Introduction.....	256
IX.2 Geological Context.....	257
IX.3 Materials and Methods	257
IX.4 Systematic Paleontology.....	258
IX.5 Phylogenetic Analyses.....	278
IX.6 Discussion	279
IX.7 Conclusion.....	281

IX. 8 Appendix.....	281
Chapter X–The return of the mummy: <i>Thaumastosaurus</i> , an Eocene pyxicephalid from Western Europe	284
I. From Toad to Frog, a CT-based reconsideration of <i>Bufo servatus</i> , an Eocene anuran mummy from Quercy (France)	287
X.1 Introduction.....	287
X.2 Geological Context.....	289
X. 3 Materials and Methods	292
X.4 Systematic Paleontology.....	296
X.5 Description.....	300
X.6 Taxonomy	327
X.7 Ontogenetic assessment	330
X.8 Phylogeny.....	331
X. 9 Paleobiogeographic implications	353
X.10 Conclusion.....	356
X.11 Appendix.....	357
2. Conversion of the names Pyxicephaloidea, Pyxicephalidae and Pyxicephalinae (Anura, Ranoidea) into phylogenetic nomenclature	375
X.12 Introduction.....	375
X.13 Typographic conventions.....	375
X.14 Phylogenetic nomenclature	376
X.15 Concluding remarks	384
Chapter XI– Conclusions on the early diversification of African neobatrachians	387
 Conclusions and perspectives	392
 References	400
 Appendix – Articles.....	444

DISCLAIMER OF INTENT TO PUBLISH

Following article 8.2 of the International code of Zoological nomenclature, 4th edition (International commission on zoological nomenclature, 2000), the author declare that this work is not edited with a nomenclatural goal, and hence is not published, in regard to the Code. Thus, nomenclatural acts presented in this work are not available in regard to the Code.

EXTENDED ABSTRACT

EXTENDED ABSTRACT

Among Lissamphibia, Anura represents the most diverse clade, with more than 7500 species currently recognized, present on almost every continent and environment. This diversity is a result of a long and rich evolutionary history, with molecular clock analyses tracing its origin more than 250 Ma ago. In the fossil record, anurans are present on almost all continents since the Jurassic. However, numerous disparities exist between continents, clades and eras. As such, most African neobatrachian clades still lack a fossil record and their early diversification and evolution are poorly known. Even the early diversification of Pipidae, an endemic African and South American clade, is poorly documented on both continents. Thus, the evolutionary history of Anura is not known in detail, with numerous gaps in it. In particular, most of the early diversification of African extant clades, like Pipidae and Neobatrachia, remains cryptic. Hence, this hinders efforts to reconstruct the paleobiogeographical evolution of this clade, and assess the impact of the extinction crises on them. The objectives of this dissertation are to improve our understanding of anuran diversification through the study of the early diversification of African neobatrachians and Pipidae during the Mesozoic and Paleogene.

This study focuses on two African sites, the Kem Kem Formation from the Late Cretaceous of Morocco, and In Becetén, from the Late Cretaceous of Niger, where both pipids and neobatrachians have been mentioned, but never described in detail. In addition, the exceptional preserved ranoid *Thaumastosaurus*, from the Eocene of Western Europe, is also studied, as previous reports suggested that it could be related to endemic African ranoids. The study of the anurans from In Becetén reveals the most diverse site of Mesozoic Africa, with at least 7 anuran taxa identified, including 4 pipimorphs and likely two neobatrachians, showing that both clades were already diverse by the middle Late Cretaceous. The presence of a neobatrachian in both the Kem Kem and In Becetén pushes back the oldest occurrence of the clade in Africa by more than 20 My. The study of *Thaumastosaurus* confirmed its African ranoid affinities, as a Pyxicephalidae, and endemic African clade. *Thaumastosaurus* expands both the

EXTENDED ABSTRACT

stratigraphic and geographical range of the clade and highlights that several endemic ranoid clades might have inhabited other continents in the past. Pipimorphs of In Becetén include two pipids, one of them preserving the endocast of its “brain”, which suggests that its hearing, olfactive and optic capacities were similar to those of extant *Pipa*.

The phylogenetic analyses of pipimorphs highlight that the conflict between morphological and molecular topologies for extant pipids impacts greatly the position of numerous extinct pipids. Estimates of the divergence time between Pipidae and its sister-clade, Shelaniinae, depends on the affinities of putative pipids in the Early Cretaceous of Africa. If pipids are indeed present in Western Africa (Koum basin), the divergence between Pipidae and Shelaniinae is estimated around 125 Ma, whereas it would be around 105 Ma if they are absent. The emergence of pipid was followed by a rapid evolutionary radiation in the next 10 My. This radiation may be linked to the opening of the Southern Atlantic Ocean, more precisely on the opening of the Central or Equatorial segment. All divergence time analyses point against transatlantic dispersal events within the pipid diversification, contrary to previous paleobiogeographic hypotheses. In addition, the divergence between South American and African lineages is estimated around the Early/Late Cretaceous boundaries, thus implying that long ghost lineages for the main extant pipid clades are present. This dissertation highlights that Africa played a key role in the early diversification of both Neobatrachia and Pipidae.

GENERAL INTRODUCTION

GENERAL INTRODUCTION

Among the three lissamphibians clades (Caudata, Gymnophiona and Anura), Anura represents the majority of the recognized known extant species, with recognized 7492 species (out of 8455 species of Lissamphibia; Frost, 2021). This makes this clade the third most diverse among tetrapods, below Squamata (11820 species; Uetz et al., 2022) and Aves (10824 species; Billerman et al., 2022) and far more than Mammalia (5495 species; Mammal Diversity Database, 2022). Anurans are today present almost in every continental ecosystem (Duellman and Trueb, 1994). They are present on every continent, except for Antarctica (Duellman and Trueb, 1994). They are present in almost all habitat, from the Kalahari Desert (Channing and Rödel, 2019) to high mountains within the Andes (Frost, 2021), with various lifestyles, from “gliding” (Olivier, 1951; Reilley and Jorgensen, 2011) to swimming (Reilley and Jorgensen, 2011). This ecological diversity reflects their high adaptation potential (Duellman and Trueb, 1994). Indeed, anurans are known to develop numerous myological, osteological, muscular traits to survive and thrive in their environments (Duellman and Trueb, 1994). However, as all amphibians (Urodela and Gymnophiona), they are highly sensitive to perturbation and modification of their environment (Duellman and Trueb, 1994). Hence, anurans are particularly vulnerable to the artificialization and anthropization of their habitats (Navas et al., 2012). Furthermore, anurans are widely threatened by the fungus *Batrachochytrium dendrobatidis* (Longcore et al., 1999), a worldwide parasite (Fisher and Garner, 2007; Fisher et al., 2009) that has already driven several anuran species to extinction (Fisher et al., 2009). Its dispersal has been linked to the amphibian trade and poor handling of wild specimens (Fisher and Garner, 2007). Thus, more than 50% of extant anuran species are now threatened, and protection measures are beginning to be implemented to preserve their diversity (Drinkrow and Cherry, 1995; Griffiths and Pavajeau, 2008; Pellens and Grandcolas, 2016; Rezende Oliveira, 2019; Vasconcelos and Prado, 2019).

The large diversity within anurans is also the result of a long and rich evolutionary history. Molecular clock analyses have proposed that Lissamphibia emerged within the Paleozoic, around 267 Ma (Zhang et al., 2005; Marjanović and

GENERAL INTRODUCTION

Laurin, 2007: table 2, 2014; Cannatella et al., 2009; Pyron, 2011), while the divergence between Salientia (Anura and its closest taxa) and Caudata (Urodela and its closest taxa) has been estimated during the Middle Permian (Guadalupian) around 264 Ma. However, no lissamphibian has currently been identified within Paleozoic outcrops. Two clades of “Amphibia” that arose during the Paleozoic have been proposed as the stem-clade of Lissamphibia: *Lepospondyli* Zittel, 1888 and *Temnospondyli* Zittel, 1888. In the last two decades, several analyses have been performed, to support each of the two hypotheses (Bolt, 1977; Laurin et al., 2022; Marjanović and Laurin, 2014, 2019; Pardo et al., 2017; Atkins et al., 2017; Schoch, 2019; Queiroz et al., 2020). A recent analysis proposed that the three lissamphibians groups might not form a clade within *Temnospondyli*, with extant amphibians being di- or triphyletic (Pardo et al., 2017; but see Marjanović and Laurin, 2019; Santos et al., 2020). The earliest true known lissamphibian is a salientian, *Triadobatrachus massinoti* Piveteau, 1936. Recovered from an unknown locality within the Early Triassic outcrops of Madagascar (250 My; Piveteau, 1937), this salientian has been widely studied to understand and assess the osteological evolution of lissamphibians near the origin of anurans, e.g. with the reduction of vertebrae and fusion of several bones (Rage and Roček, 1989; Sigurdson et al., 2011; Ascarrunz et al., 2016). Within the Triassic, three other occurrences of Salientia are known (*Czatkobatrachus* in Poland, Evans and Borsuk-Bialynicka, 1998; Borsuk-Bialynicka and Evans, 2002; indeterminate Salientia from Arizona, Stocker et al., 2019; indeterminate Salientia from Greenland, Jésus et al., 2022) and points to an already worldwide repartition of the clade. Other Salientia are also known in the Early Jurassic, like *Prosalirus bitis* Shubin and Jenkins, 1995 from North America (Roček, 2013). During the same epoch, the earliest anuran, *Vieraella herbstii* Reig, 1961 from the latest Early Jurassic of Patagonia has been recovered. Several anurans are known in both Laurasia (*Eodiscoglossus oxoniensis* Evans et al., 1990 from England and indeterminate anurans from North America; Roček, 2013) and Gondwana (*Notobatrachus* Reig, 1956; indeterminate anurans in Africa, South America and India according to Roček, 2013; Gardner and Rage, 2016; Barcelos et al., 2022) during the

GENERAL INTRODUCTION

Middle-Late Jurassic. Although their phylogenetic position within Anura is still unresolved, their attribution to this clade is well-supported (Báez and Gómez, 2016; Gao and Chen, 2017). An anuran assigned with strong support to extant anuran clades are known in the Late Jurassic, with *Rhadinostenus parvus* Henrici, 1998 from the Morisson Formation of Utah (USA; 156-147 Ma) assigned to Pipoidea (Rhinophrynidae + Pipidae). Within the Early Cretaceous, several pipimorphs (Pipidae and all taxa closer to Pipidae than to Rhinophrynidae) are known in Europe, South America, and Africa (Gardner and Rage, 2016; Barcelos and dos Santos, 2022; see the present thesis). At the end of the Early Cretaceous, the first neobatrachians are documented in the Crato Formation in Brazil (113-109 Ma, Martill et al., 2007). During the Early and Late Cretaceous, anurans are known in all continents (except Antarctica; Roček, 2013; Gardner and Rage, 2016; Xing et al., 2018; Barcelos and dos Santos, 2022). Although most specimens are fragmentary, isolated bones (Roček, 2013), the anuran diversity seems widely different in Laurasia and Gondwana (and continents that emerged from their breakup). In Laurasia, the anuran diversity seems dominated by Discoglossoidea and anurans of indeterminate affinities (Gardner and DeMar, 2013; Roček, 2013), while Gondwanan continents seem dominated by pipimorphs and neobatrachians (Gardner and Rage, 2016; Barcelos and dos Santos, 2022). Few anurans are known from the Paleocene, but neobatrachians have been reported from almost all continents. Furthermore, the only (currently) known anuran specimens from Antarctica have been assigned to a neobatrachian (Mörs et al., 2020), implying that the clade had already dispersed across all continents at least in the early Paleogene. Neobatrachians represent a majority of anuran specimens recovered in the fossil record only during the Eocene, in peculiar within Europe and North America (Holman, 2003; Rage, 2006, 2016). Within the Oligocene, several extant genera, like *Pelophylax*, *Rana* and *Ptychadena*, have been identified (Sanchíz, 1998; Roček, 2013). During the Pliocene, extant species, like *Pelophylax kl. esculentus*, are known (Roček, 2013).

Thus, the anuran fossil record is rich, spanning the entire Mesozoic and Cenozoic, on all continents. Furthermore, molecular clock analyses consider that most

GENERAL INTRODUCTION

large anuran clades emerged during the late Mesozoic (Cretaceous) and early Cenozoic (Pyron, 2011; Frazão et al., 2015; Feng et al., 2017). However, this apparent richness masks great disparities within this record, between continents, periods, and clades. Within Anura, numerous clades are still lacking a fossil record (Gardner and Rage, 2016). Furthermore, the fossil record of most clades does not extend past the Neogene (Roček, 2013; Marjanović and Laurin, 2014; Gardner and Rage, 2016; Barcelos and dos Santos, 2022). For example, the fossil record of the Leiopelmatidae, considered the sister-clade to all other extant anuran clades (Frost et al., 2006; Wiens et al., 2011), starts in the Miocene (Worthy et al., 2013). As most anuran specimens are found as disarticulated and isolated bones, precise assessment of taxonomic affinities is sometimes difficult. This is especially true during the Mesozoic and early Paleogene. As an example, although the Late Cretaceous of North America has yielded a vast diversity of anuran taxa, most of them cannot be assigned to any anuran clade because of their preservation state (Gardner, 2008; Roček, 2013). To the contrary, Pipidae and its total-clade, Pipimorpha, do possess an extensive fossil record, likely linked to their aquatic lifestyle and peculiar osteological synapomorphies (e.g., fusion of the sacral vertebra and urostyle, loss of the posterolateral expansions of the parasphenoid). Disparities within the fossil record among continents are also great. In North America and Europe, numerous sites, with sometimes hundreds of anuran bones, are recorded from the Jurassic to the end of the Neogene (Roček, 2013; Rage, 2016). On the contrary, less than fifteen occurrences of Anura have been reported from the entire Mesozoic of Africa (Gardner and Rage, 2016), with less than half of them published and described. Finally, hundreds of sites have been reported from the Neogene, while far less have been reported from the Paleogene and Mesozoic, leading to some gaps within the Paleogene (Gardner and Rage, 2016).

Thus, while the evolutionary history of Anura is known in detail through molecular phylogenies, it remains poorly documented in the fossil record, with numerous temporal gaps in it. Most of the early diversification of extant clades, like Pipidae or Neobatrachia, is poorly known. This led to a lack of node constraints for

GENERAL INTRODUCTION

molecular clock analyses, and estimation of time of divergence between anurans clades can yield large uncertainties and is poorly reflected in the fossil record (Marjanović and Laurin, 2007; Frazão et al., 2015; Feng et al., 2017). This also hinders our efforts to reconstruct the paleobiogeographical evolution of several clades, and to understand the impact of the various biological crises on Anura.

The objectives of this dissertation are to improve our understanding of anuran diversification and its chronology, with a focus on pipids and African neobatrachians during the Mesozoic and Early Paleogene. The focus on African anurans is linked to the presence of several undescribed sites in Mesozoic Africa, where anurans have been reported for decades, but never fully studied (Broin et al., 1974; Báez and Rage, 1998, 2004; Rage and Dutheil, 2008; Gardner and Rage, 2016). Furthermore, Africa, with South America, has been considered as the region where Neobatrachia and Pipidae emerged and first diversified, during the Cretaceous (Frazão et al., 2015; Feng et al., 2017).

GENERAL INTRODUCTION

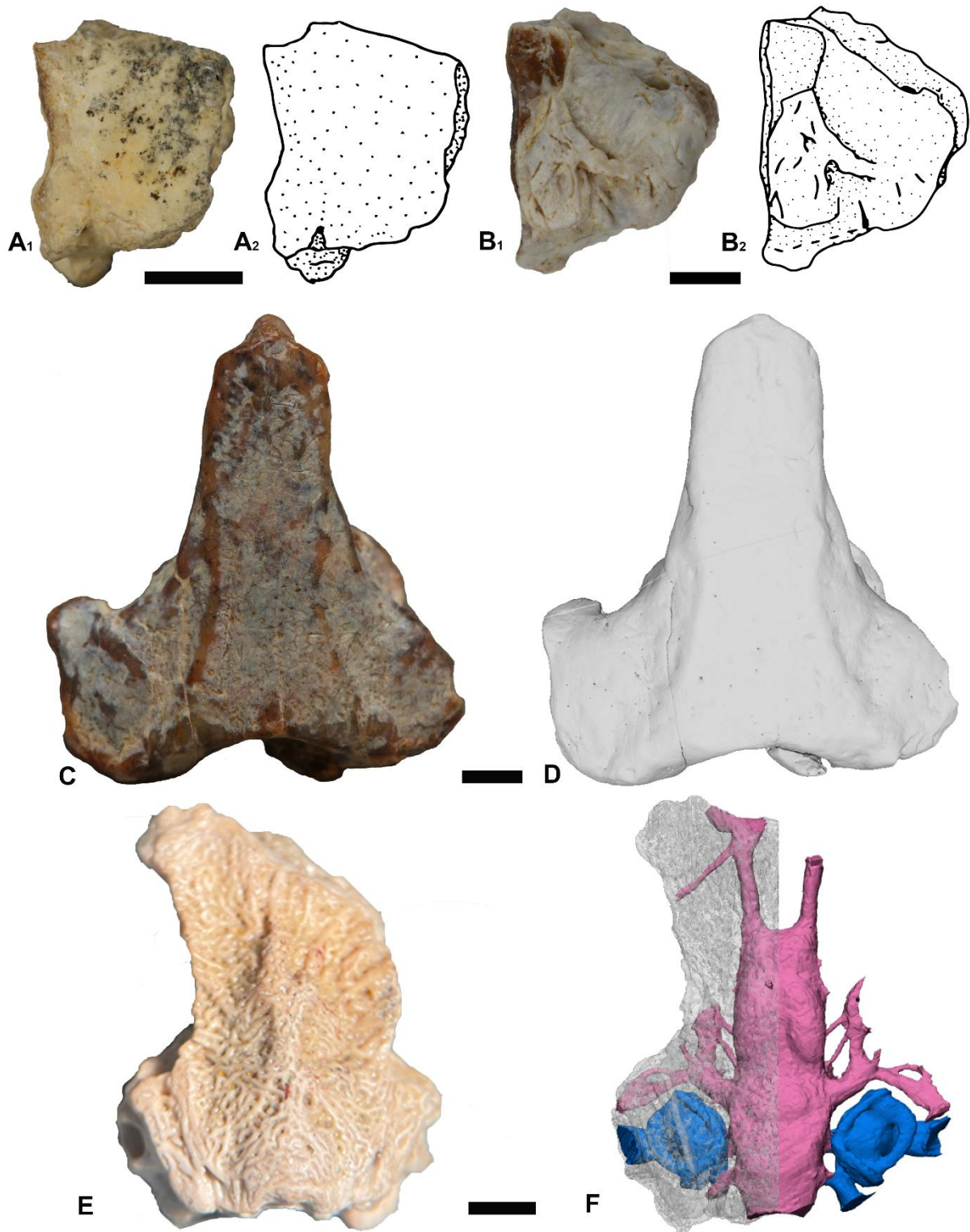


FIGURE I-1. Selected anuran specimens from the Cretaceous of In Becetén assigned to **Pipimorpha**. **A**, MNHN.F.IBC1626, incomplete right prooticoccipital of an undescribed pipimorph in **A₁**, dorsal view and **A₂**, interpretative drawing of the specimen in dorsal view; **B**, newly identified specimen (no collection number), incomplete right prooticoccipital of an undescribed pipimorph in **B₁**, dorsal view and **B₂**, interpretative drawing of the specimen in dorsal view; **C–D**, MNHN.F.IBC1602, incomplete braincase of an unnamed ‘Xenopodinomorpha’ in **C**, dorsal view and **D**, 3D model of the same braincase in dorsal view;

GENERAL INTRODUCTION

E–F, MNHN.F.IBC1604, holotype and braincase of *Pachycentrata taqueti* in E, dorsal view, F, 3D model of the same specimen, with bony elements transparent to show the colored endocast.

The first section of this dissertation focuses on the analyses of the pipimorphs from the Cretaceous of In Becetén (Niger), and their use into novel time divergence analyses for Pipidae. In In Becetén, two pipids, *Pachycentrata taqueti* (Báez and Rage, 1998) and an unnamed presumed Xenopodinomorpha, were described almost twenty-five years ago. However, numerous other pipimorph bones were neither described nor studied. Among them, several cranial elements indicate that more than two pipids are present in the site. In addition, several bones are newly referred to *Pachycentrata* and the unnamed xenopodinomorph. I will first present my results on the analyses of the numerous unassigned pipimorphs bones in In Becetén and conclude on the pipimorph diversity of the site (Chapter II; Fig. I-1A, B). I will then present my work on the redescription of the unnamed xenopodinomorph (Chapter III), with newly characters obtained from the CT-scan of the braincase of this taxon (Fig. I-1C, D). I also include this new taxon within phylogenetic analyses that include several newly described pipimorphs. I also take this opportunity to include the putative pipimorph *Aygroa anoualensis* Jones et al., 2003 to test its affinities. If *Aygroa* is indeed a pipimorph, it could be the stratigraphically oldest of the clade. I then study new *Pachycentrata* specimens through CT-scans of the braincase (holotype; Fig. I-1E), first vertebra (atlantal vertebra), presacral vertebra and sacrococcyx, which reveal their internal anatomy and their endocast. The analysis of the cranial endocast of *Pachycentrata* reveals numerous brain structures preserved as imprint, in addition to numerous cranial nerves (Fig. I-1F). These structures are used to infer several sensory capabilities and ecological parameters for *Pachycentrata* (Chapter IV). Finally, I perform several time divergence analyses using the novel method developed by Didier and Laurin (2020). It is based on the ‘Fossilized Birth Death’ process, which models diversification and allows estimating three parameters: cladogenesis, sometimes called speciation

GENERAL INTRODUCTION

(when a lineage splits into two), extinction, which are modelled by the older Birth-Death model, and fossilization (Chapter V). This novel method requires only on a topology (or a set thereof) and the geological age of each horizon that has yielded fossil of the studied taxa. Thus, using various geological datasets and topologies, I am able to propose sets of age estimates, and I discuss the paleobiogeographic implications of each scenario.

The second section of this dissertation focuses on several neobatrachians remains from Mesozoic Africa and Paleogene Europe. Neobatrachia represents today the most diverse anuran clade (~96% of extant species; Frost et al., 2021). They are considered to have emerged during the Early Cretaceous and are considered to have undergone a diversification event during the Cretaceous (Feng et al., 2017). One of the main neobatrachian clades, Ranoidea, is thought to have emerged in the Mesozoic of Africa (Frazão et al., 2015; Feng et al., 2017). Similarly, the Hyloides, another main anuran clade, is considered to have emerged in the Mesozoic of South America (Frazão et al., 2015; Feng et al., 2017). Unfortunately, Ranoidea currently does not have a fossil record in the Mesozoic (excluding undescribed fossils from the Cenomanian of Sudan; Báez and Rage, 1998). In Africa, a single neobatrachian, *Beelzebufo ampinga* Evans et al., 2014, has been reported from the latest Late Cretaceous of Madagascar (Maastrichtian, Evans et al., 2008, 2014). *B. ampinga* has been considered an hyloid in recent analyses (Báez and Gómez, 2018; Lemierre et al., 2021; Lemierre and Blackburn, 2022). However, anurans have been reported from several other sites in Africa during the Early/Late Cretaceous and could potentially yield new neobatrachian taxa. The first section of this dissertation will be focus on the study of anurans from two African Cretaceous sites, Kem Kem in Morocco (Chapter VIII) and In Becetén in Niger (Chapter IX) and one extinct European taxon from the Paleogene of the Quercy, France with putative African affinities (Chapter X).

GENERAL INTRODUCTION

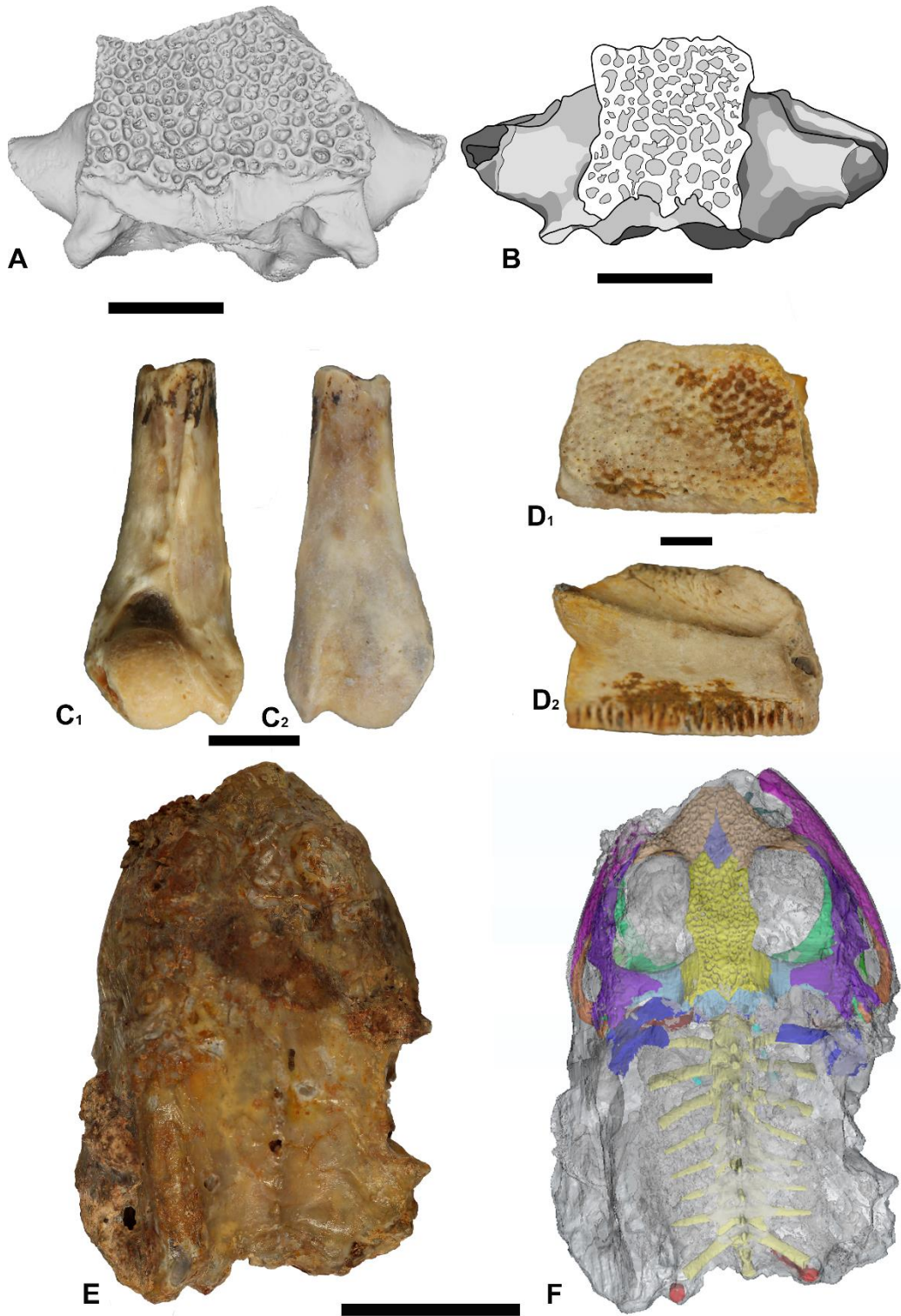


FIGURE I-2. Selected neobatrachians specimens studied in this dissertation. A, UCRC-PV94, posterior braincase of an indeterminate anuran from the Cretaceous Kem Kem Formation (Morocco) in dorsal view; B, MHNT.PAL.2020.0.36.1, neotype of *Thaumastosaurus botti* De Stefano, 1903, from the Late Eocene of Quercy (France), posterior braincase in dorsal view; C, MNHN.F.IBC1603, humerus from In Becetén (Cretaceous, Niger) previously assigned to Ranidae in C₁, ventral and C₂, dorsal views; D, incomplete left maxilla from In Becetén of an undescribed ornamented anuran in D₁, labial and D₂, lingual views; E-F, MNHN.F.QU17381,

GENERAL INTRODUCTION

mummy of *Bufo servatus* from the Eocene of Quercy (France), E, in dorsal view and F, 3D model of the same mummy, with the soft tissues in transparent to show the underlying colored skeleton.

I first studied two Cretaceous sites from Africa : (1) the Kem Kem Formation from Morocco and (2) the site of In Becetén in Niger. The anurans of the Kem Kem (Cenomanian) were previously described in a preliminary study in 2008 (Rage and Dutheil, 2008). Within this study, a pipid, *Oumtkoutia anae*, was described, in addition to several indeterminate anurans. Among those indeterminate anurans, several elements (cranial and postcranial) belong to a hyperossified and ornamented anuran (Fig. I-2A). The ornamentation and general aspects of the posterior braincase of this hyperossified taxon is reminiscent of *Thaumastosaurus* (Fig. I-2B). This hyperossified taxon from the Kem Kem has been considered recently (Gardner and Rage, 2016) as a putative neobatrachian, and could represent the oldest occurrence of the clade in Africa. I took the opportunity to CT-scan of the anurans from the Kem Kem site to describe this new hyperossified taxon and include it within a phylogenetical analysis to test its putative neobatrachian affinities.

In Becetén is a rich site from the middle Late Cretaceous of southeastern Niger. The faunal list from the original publication (de Broin et al., 1974) mentioned several anurans, including pipids, and bones assigned to Ranidae (equivalent to Ranoidea; Fig. I-2C₁₋₂). A few pipids were described almost twenty-five years later, with the recognition of two distinct taxa : *Pachycentrata taqueti* and an unnamed Xenopodinomorph (Báez and Rage, 1998). Most of the other anuran specimens were left unstudied and undescribed. However, a hyperossified anuran was mentioned in a recent review of lissamphibian fossil from Africa (Gardner and Rage, 2016: 180). More anurans taxa could therefore be present within this site, involving that it could be the richest from the Mesozoic of Africa, and one of the richest from the Cretaceous of Gondwana. Thus, I studied all anuran specimens that were collected by the MNHN during the 70s from this locality (de Broin et al., 1974). As specimens belonging to pipimorphs will be studied in the previous section (Chapters II-IV), I will present my

GENERAL INTRODUCTION

results on the remaining anuran specimens. Among these specimen, one hyperossified ornamented taxon was identified (Fig. I-2D₁₋₂); it shares osteological characteristics with several hyloids. I include this taxon in a phylogenetic analysis to test its neobatrachian affinities. I also describe and review the different specimens previously assigned to Ranoidea, to assess if this assignment could still be valid. If valid, In Becetén could be the first Mesozoic occurrence where a hyloid and a ranoid coexisted.

Finally, in the tenth chapter, I will present my work on the Eocene *Thaumastosaurus*. This latter European taxon is the ranoid *Thaumastosaurus* De Stefano, 1903 from the Eocene (Paleogene, 40-33.5 Ma) of Western Europe. This taxon is known not only by isolated bones, but also by almost complete mummies, that preserved an articulated skeleton, skin and organs (Laloy et al., 2013; Tissier et al., 2016, 2017). Recent phylogenetical analyses have assigned *Thaumastosaurus* to the Natatanura, a large clade within Ranoidea, and proposed that it was close to African natatanurans, like *Pyxicephalus* (Báez and Gomez, 2018). This attribution to Natatanura makes *Thaumastosaurus* the stratigraphically (currently) oldest taxon of the clade, even though it emerged in the Cretaceous (Feng et al., 2017). I studied one anuran mummy from the Quercy Phosphorites, which had been assigned to the Bufonidae (Neobatrachia, Hyloides), as *Bufo servatus* (Fig. I-2E). As the CT-scan quickly revealed that this mummy could be reassigned to *Thaumastosaurus* (Fig. I-2B, F), I decided to focus on this peculiar taxon, to reassess its phylogenetic position, and to investigate its African affinities. A well-corroborated systematic position for *Thaumastosaurus* would allow to better use it as a calibration constrain in molecular clock analyses.

Section I

*EARLY EVOLUTION AND CHRONOLOGY OF
PIPIMORPH DIVERSIFICATION THROUGHOUT
MESOZOIC AND PALEOGENE AFRICA*

Chapter I

THE PIPIMORPH FOSSIL RECORD

The pipimorph fossil record

The Pipidae is an anuran clade composed of bizarre anuran taxa. All pipids live the majority (and some the totality) of their life in the aquatic environment (Duellman and Trueb, 1994; Trueb et al., 2000; Measey, 2016) and possess several unique morphological traits. One of the best known is their loss of tongue (thus, pipids are dubbed “tongueless frogs”; Duellman and Trueb, 1994) or in the case of *Pipa*, the modification of the jaw apparatus to allow suction feeding (Trueb et al., 2000). Several osteological adaptations to an aquatic lifestyle are also uniquely present within pipids, such as the loss of an ossified posterolateral extension of the parasphenoid (i. e. Eustachian canals visible in ventral view on the braincase) or the fusion of the sacral vertebra and urostyle into a single bone, the sacrococcyx (Ford and Cannatella, 1993). Pipids are also widely known through the pipid *Xenopus* Wagler, 1827, more precisely its type species, *Xenopus laevis* Wagler, 1827. This taxon has been used since the 30s (Gurdon and Hopwood, 2000; De Robertis and Gurdon, 2021) as a model organism in biology (Van Sittert and Measey, 2016), and was used in studying brain evolution in tetrapods (Lee-Liu et al., 2017; Streidter and Northcutt, 2020), blood circulation system (Warkman and Krieg, 2007), molecular biology (Slater et al., 2009) and even as a model in disease mechanisms studies (Fainsod and Moody, 2022). Furthermore, *Xenopus* was also used to detect human pregnancies (*Xenopus* in contact with pregnant women urine would produce oocyte; Shapiro and Zwarenstein, 1934), and was introduced in the Northern Hemisphere, where it managed to establish itself into the wild (Fouquet, 2001; Measey et al., 2012). Thus, *Xenopus laevis* is today considered an invasive species in North America, Europe and even some regions of Africa, its home continent (Ilhlow et al., 2016; Measey et al., 2012; 2016; Vogt et al., 2017).

Pipids are currently native only to two continent, South America and Africa (Duellman and Trueb, 1994). More than 30 species are currently recognized, with numerous cryptic species (Evans et al., 2015). They are unequally incorporated within five genera: *Pipa* (seven species), *Xenopus* (28 species), *Silurana* (one species, considered

The pipimorph fossil record

as a subgenus of *Xenopus* in numerous recent studies; Channing and Rödel, 2019), *Hymenochirus* (four species), and *Pseudhymenochirus* (one species). Of those five genera, only *Pipa* inhabits South America, whereas the remaining four are present in Africa. Among the African genera, *Xenopus* possess the widest geographical range. This wide range is linked to a large number of cryptic species, due to the relative isolation of its environment (murky lakes, temporary ponds; Channing and Rödel, 2019). A similar pattern has recently been identified in *Pipa*, on which molecular analyses have identified the presence of more species than currently recognized (at least eight new lineages; Fouquet et al., 2022). Morphological and molecular phylogenetical analyses all agree that the sister-clade of Pipidae is the endemic North American Rhinophrynidae (and its single taxon, *Rhinophrynus dorsalis* Duméril and Bibron, 1841). Within the fossil record, several extinct taxa have been identified as phylogenetically closer to Pipidae than Rhinophrynidae. Thus, the clade Pipimorpha (Ford and Cannatella, 1993) has been coined as the total clade of Pipidae. Pipimorpha are known since the Late Jurassic/Early Cretaceous of Africa (Jones et al., 2003; Lasseron et al., 2019). The paleogeographical range of pipimorph is wider than the current geographic range of pipids, with several occurrences in Europe and in the Middle East (Fig. I-1A). All early pipimorphs are located near the Tethys, with several occurrence in Spain during the Early Cretaceous (Buffetaut et al., 1996; Báez and Sanchíz, 2007; Báez, 2013; Fig. I-1A) and in Israel during the latest Early Cretaceous (Nevo, 1968; Estes et al., 1978; Trueb and Báez, 2006). Two pipimorphs have been recovered from the latest Early Cretaceous, within the Crato Formation, in Brazil (Fig. I-1B; Báez et al., 2021). In the Late Cretaceous, two or three pipids are known from the earliest Late Cretaceous of Africa : (1) *Oumtkoutia anae* Rage and Dutheil, 2008, from the Cenomanian of Morocco, the oldest known pipid (Fig. I-1B), (2) *Pachycentrata taqueti* (Báez and Rage, 1998) from the Coniacian-Santonian of Niger (Báez and Rage, 1998) and (3) an unidentified pipid from the same site.

Several pipids are known in the latest Late Cretaceous of Africa (Gardner and Rage, 2016), and an endemic south American clade of pipimorph, the Shelaniinae,

The pipimorph fossil record

appears in the fossil record of the continent during the latest Late Cretaceous (Barcelos and dos Santos, 2022). Within the Paleogene, a single pipid is known in the Paleocene, '*Xenopus*' *romeri* Estes, 1975 from Brazil, while several pipids are known in the Eocene of Africa (Gardner and Rage, 2016) and South America (Barcelos and dos Santos, 2022). Shelaniinae are also present until the Late Eocene of Argentina (Barcelos and dos Santos, 2022). Fossils attributed to extant genera have been recovered since the Late Eocene (*Xenopus arabiensis* Henrici and Báez, 2001) and Miocene (*Pipa* sp.; Delfino and Sánchez-Villagra, 2018). Thus, the fossil record of pipimorph, while almost continuous since the Early Cretaceous, is unevenly present across three continents, with several large gaps in Africa and South America. Hence, although most molecular clock analyses estimate the emergence of Pipidae around the Early/Late Cretaceous boundary (Cannatella, 2015; Frazão et al., 2015; Feng et al., 2017; Hime et al., 2021), no pipids are known in the Early Cretaceous of Africa and from the entire Cretaceous of South America (only pipimorphs or shelaniins) Barcelos and dos Santos, 2022). Molecular clock analyses also proposed that the lineages that led to extant genera emerged during the Late Cretaceous/Paleogene, implying the existence of long ghost lineages (Cannatella, 2015; Feng et al., 2017).

The pipimorph fossil record



Figure I-1. Maps showing pipimorphs occurrence throughout the Mesozoic and Paleogene. A, Map of the Mediterranean region showing pipimorphs occurrence during the Cretaceous; B, Map of South America and Africa showing pipimorphs occurrence during the Cretaceous and Paleogene. Red stars represent studied sites (1) Kem Kem Formation, (2) In Becetén and (3) Koum Basin; light blue stars represent Early Cretaceous pipimorphs, gray circles represent Late Cretaceous pipimorphs; gray outlined circle represents undescribed early cretaceous pipimorphs; black circles represent Paleogene pipimorphs and black outlined circles represent undescribed Paleogene pipimorphs.

The pipimorph fossil record

This disparity within the fossil record hinders our capacity to assess and understand the early diversification of Pipidae, and their paleogeographical range. Several studies have proposed the existence of numerous transatlantic dispersal events across the Southern Atlantic Ocean during the Late Cretaceous and Early Paleogene (Aranciaga-Rolando et al., 2019) as a driver of pipid diversification. However, pipids are not known to be long-distance land-walkers (Measey, 2016) and tolerate only moderate saline waters (around half the salinity of the ocean; Munsey, 1972; Albert and McCoy, 2017). Hence, the hypothesis of multiple dispersal across the Atlantic Ocean seems unlikely. Thus, more divergence time analyses are required to assess the timing of pipid diversification.

My objective in this section is to propose (1) new phylogenetic relationships among Gondwanian pipimorphs and pipids and (2) new hypotheses for the chronology of early pipid diversification during the Cretaceous and Paleogene.

The first three chapters of this section focus on the study and description of new pipimorphs from one of the stratigraphically oldest African sites, In Becetén. This site is located in Southeast Niger (Fig. I-1B), east of the town of Tahoua. All specimens were collected from sediments brought back from the MNHN expedition in the 70s (de Broin et al., 1974). Stratigraphic and sedimentary analyses have dated the In Becetén Formation to Coniacian-Santonian age (Moody and Stutcliffe, 1991). The site possesses a rich vertebrate fauna, although most of it has neither been described nor illustrated. Among anurans, two pipids have nevertheless been mentioned and illustrated (Báez and Rage, 1998): *Pachycentrata taqueti* and an unnamed presumed xenopodinomorph that was only briefly described (Báez and Rage, 1998).

In the first chapter, I will present my results on the identification and description of numerous pipimorph remains that could not be attributed to the two pipid taxa of In Becetén. Among them, I was able to identify two new anuran taxa. Although fragmentary, both taxa can be referred to the Pipimorpha. I included them in my morphological dataset for Pipimorpha to test their phylogenetic relationships.

The pipimorph fossil record

Furthermore, In Becetén is important for studies on pipid diversification, as it is the first known site where more than one pipid taxon is known. I had the opportunity to CT-scan the holotype of *P. taqueti* (a braincase) and several vertebral elements, and the braincase of the second pipid.

In the second chapter, I will present my result on the study of the unnamed pipid from In Becetén. The tomography of this second pipid allowed for a complete description of the braincase, including part of its internal anatomy, alongside vertebral elements (putatively) associated with the braincase. This newly described taxon was included into phylogenetic analyses of Pipimorpha. I chose to perform one of these analyses using a topologic constraint to follow the molecular topology retrieved for extant pipid taxa. I also took this opportunity to include the putative pipimorph *Aygroa anoualensis* Jones et al., 2003, from the Late Jurassic/Early Cretaceous of Morocco, to assess its position within pipimorphs, as it could be the stratigraphically oldest pipimorph. I also had access to the 3D model and CT-scan of the oldest pipid, *Oumtkoutia anae* from the Cenomanian of Morocco. I was able to rescore several morphological characters within my phylogenetical dataset.

In the third chapter, I studied the 3D model and internal anatomy of *P. taqueti*, to retrieve and reconstruct one of the most complete fossil brain endocast found in an amphibian, and discuss its palaeoecological and palaeobiological inferences.

Finally, in the fourth chapter, I performed several analyses of divergence time estimation, using a novel method developed by Didier and Laurin (2020) using the 'Fossilized Birth Death' model. This analysis was performed using the topologies obtained from my previous phylogenetic analyses and a dataset of all stratigraphic occurrences of gondwanian pipimorphs that I compiled from the literature and from my personal observations on original material. These analyses allowed me to propose several timelines for early pipid diversification and the palaeogeographical scenarios that can explain them. When I constructed the occurrence dataset, I had the opportunity to study the undescribed anurans of the Koum Basin (Fig. I-1B). The site is located in Northern Cameroon and the material was collected during the late 1980s

The pipimorph fossil record

by an Americano-Franco-Cameroonese scientific team (Brunet et al., 1988; Flynn et al., 1988; Jacobs et al., 1988). This site is considered of Barremian-Albian age and anurans were mentioned, but never published (Gardner and Rage, 2016). I recently rediscovered most of the materials within the MNHN collection (with SMU collection numbers). Most of the materials, including a partial pipimorph braincase, is still under study, several vertebrae were worthy of being incorporated within this thesis. They resemble *Pachycentrata* vertebrae and could represent the earliest occurrence of pipid in the fossil record. Thus, their incorporation into my occurrence dataset, albeit with caution, was essential.

Chapter II

*PIPIMORPHS OF IN BECETÉN AND THEIR
IMPLICATION FOR PIPID DIVERSIFICATION IN
MESOZOIC AFRICA*

Pipimorphs of In Becetén and their implication for pipid diversification in Mesozoic Africa

II.1 Introduction

Pipidae is a clade composed of exclusively aquatic anurans. This particularity and the osteological characteristics of such a lifestyle have made fossils of this clade more easily identifiable than other anurans in Africa (Gardner and Rage, 2016). As such, pipimorphs possess one of the most extensive fossil records of all anurans in Gondwana. Their oldest member, *Aygroa anoualensis* Jones et al., 2003, is known in the Late Jurassic-Early Cretaceous of Northern Africa (Lasseron et al., 2019). Pipimorphs are also known during the Cretaceous throughout Europe, South America and Africa (Chapter III). The earliest taxa attributed to its crown-clade Pipidae were found in the earliest Late Cretaceous of Africa. These taxa are *Oumtkoutia anae* (Rage and Dutheil, 2008), *Pachycentrata taqueti* (Báez and Rage, 1998) and *Inbecetenanura ragei* (Chapter II). Among them, two taxa, *P. taqueti* and *I. ragei*, were described from the site of In Becetén (Niger), one of the most diverse and richest Mesozoic sites for anurans in Africa (Gardner and Rage, 2016; Chapters I, III). The former taxon was identified as a strange pipid in a preliminary study (de Broin et al., 1974), then described as *Pachycentrata taqueti* (*Pachybatrachus taqueti* in Báez and Rage, 1998) from the Coniacian-Santonian beds. This taxon is now known by several braincases and vertebral elements. The second taxon, *Inbecetenanura ragei* was recently described (Chapter III) based on a braincase and vertebral elements. Phylogenetic analyses placed both taxa within Pipidae, making In Becetén the first co-occurrence of at least two pipids in a given locality.

As part of an ongoing study on the anurans of In Becetén, we take the opportunity to here describe two new, unnamed, pipimorph taxa, based on cranial and vertebral elements. These new taxa are also included in phylogenetical analyses of pipimorphs taxa to test its affinities with Pipidae. We also include the brief description of several postcranial elements assigned to a Pipimorpha indet. Finally, we discuss the

Pipimorphs of In Becetén and their implication for pipid diversification in Mesozoic Africa

implication of the identifications of three pipimorphs from the anuran diversity and paleoenvironment of In Becetén.

II.2 Materials and Methods

Institutional abbreviations—MNHN: Muséum national d’Histoire naturelle, Paris, France. All specimens are stored within the Paleontological collection of the MNHN of Paris (France) in the Amphibians and Reptiles section, under the collection number MNHN.F.IBC.

The anatomical terminology used herein is based on Roček (1980) and Biton et al. (2016) for cranial features, Sanchíz (1998) for postcranial and Gómez and Turazzini (2016) for ilial ones.

Phylogenetic analysis—Our data matrix (Appendix S1) includes 44 taxa and 176 osteological characters and is derived from that of Chapter III. We added the new pipimorphs from this publication to the dataset. The analysis was performed using TNT v.1.5 (Goloboff and Catalano, 2016) under equal weights. All analyses were conducted with cline characters ordered (characters 18, 32, 33, 36, 38, 39, 59, 74, 82, 97, 98, 120, 141, 149) (Rineau et al., 2015; 2018). The analysis consisted of heuristic searches with 1000 random addition sequences of taxa, followed by tree bisection reconnection (TBR) branch swapping, holding 10 trees per repetitions. The final trees were rooted on *Ascaphus truei* (Ascaphidae), and when more than one most parsimonious tree was found, a strict consensus was obtained.

II.3 Systematic Paleontology

ANURA Duméril, 1805

XENOANURA Starrett, 1973

PIPIMORPHA Ford and Cannatella, 1993

Pipimorphs of In Becetén and their implication for pipid diversification in Mesozoic Africa

PIPIMORPHA INDET. 1

Referred material—One right prooticoccipital (MNHN.F.IBCMNHN.F.IBC 1626) and one atlantal complex (MNHN.F.IBCMNHN.F.IBC 1968).

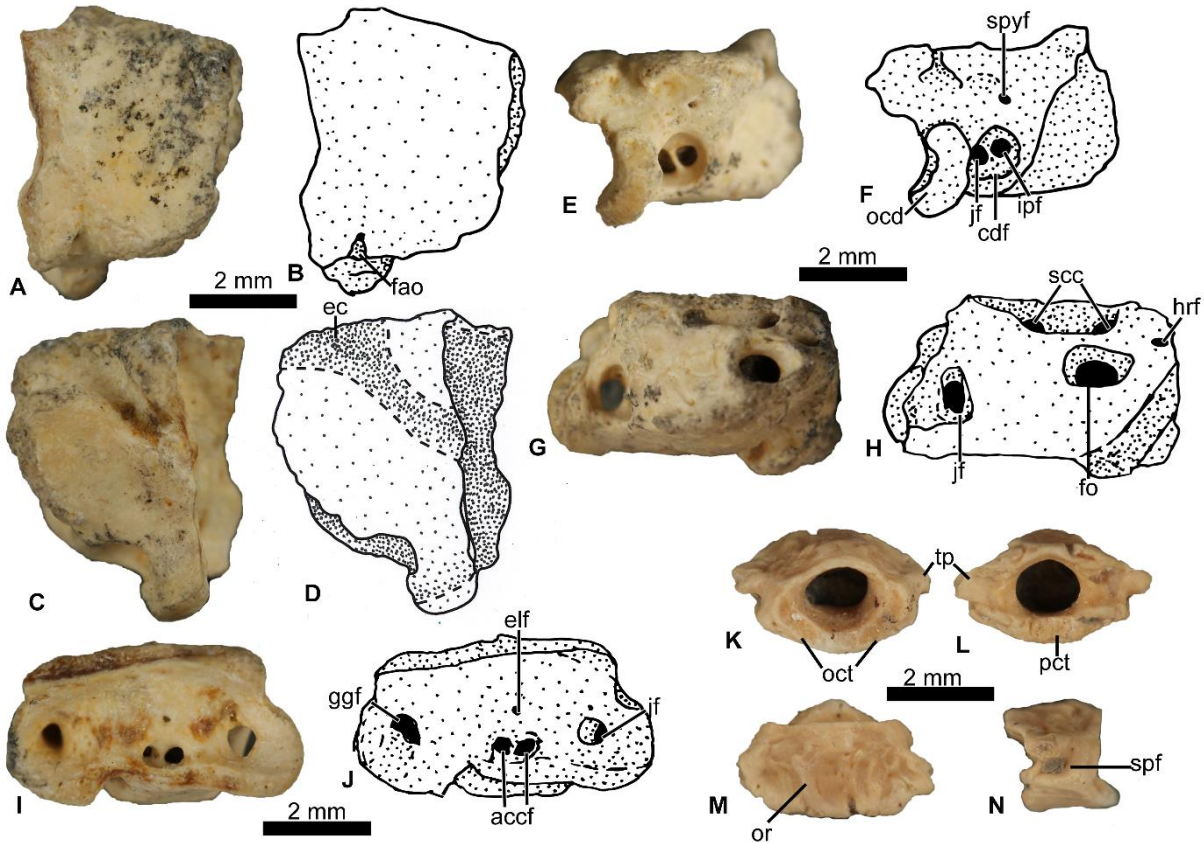


Figure II-1. Cranial and postcranial elements of a Pipimorpha indet. 1 of In Becetén. A right prooticoccipital (MNHN.F.IBC 1626) in dorsal view, B interpretative drawing of A, C, MNHN.F.IBC1626 in ventral view, D interpretative drawing of C, E MNHN.F.IBC1626 in posterior view, F, interpretative drawing of E, G, MNHN.F.IBC1626 in lateral view, H interpretative drawing of G, I, MNHN.F.IBC1626 in medial view, J, interpretative drawing of I; K–N, atlantal (MNHN.F.IBC 1968) in K, anterior, L, posterior, M, dorsal, and N, right lateral views. **Abbreviations:** accf, acoustic foramen; fao, foramen for the arteria occipitalis; cdf, condyloid fossa; ec, Eustachian canal; elf, endolymphatic foramen; ggf, Gasserian ganglion fossa; hrf, hyomandibular nerve foramen; ipf, inferior perilymphatic foramen; jf, jugular foramen; ocd, occipital condyle; oct, occipital cotyle; or, ornamentation; fo, fenestra ovalis; pct, posterior cotyle; scc, semicircular canals; spf, spinal foramen; spyf, superior perilymphatic foramen; tp, transverse process.

II.4 Osteological Description

Prooticooccipital

Only half of the prooticooccipital is preserved (Fig. II-1A-J). There is no ventral nor dorsal ornamentation (Fig. II-1A, C). There is no lateral extension of the crista parotica. In dorsal view, the surface is smooth (Fig. II-1A). On the posterior margin of the dorsal surface, a small shallow groove opens into the foramen for the arteria occipitalis (Fig. IV-1A, B). In ventral view, the Eustachian canal is narrow posteromedially and widens anterolaterally (Fig. II-1C, D).

In posterior view, the occipital condyle is crescentic and ventrolateral to the foramen magnum. Lateral to the occipital condyle, the condyloid fossa is circular and is half the dorso-ventral size of the occipital condyle (Fig. II-1E-F). The jugular foramen (medial foramen within the fossa) is bigger than the inferior perilymphatic foramen (lateral foramen within the condyloid fossa). The jugular foramen opens posteromedially within the condyloid fossa (Fig. II-1E, F). Dorsal to the condyloid fossa, a small superior perilymphatic foramen is visible (Fig. II-1E). In lateral view, the fenestra ovalis is located very anteriorly on the otic capsule, at the level of the Eustachian canal (Fig. II-1G, H). The fenestra is small and circular. Two small foramina are visible dorsal to the fenestra ovalis (Fig. II-1G, H). They all represent part of the semi-circular canals visible due to breakage. Another small opening, located anterior to fenestra ovalis, is visible (Fig. II-1G, H). Although partially filled, it connects to a large and deep fossa within the braincase (see below). It is here interpreted, due to its position, as the foramen for hyomandibular ramus of the cranial nerve VII.

Atlantal complex

MNHN.F.IBC 1968 is a complete atlantal complex (vertebrae I + II) compressed dorsoventrally (Fig. II-1K-N). It bears a posterior cotyle, indicating an opisthocoelous condition for the vertebrae. Its centrum is wider than long (Fig. II-1M). In anterior

Pipimorphs of In Becetén and their implication for pipid diversification in Mesozoic Africa

view, the vertebral canal is large and circular. The two occipital cotyles are thin, crescentic and ventrolateral to the vertebral canal (Fig. II-1K). A thin lip of bone separates the two articular surfaces so that it corresponds to the Type II of Lynch (1971). In posterior view, the posterior cotyle is small and compressed dorsoventrally. There is no neural spine. The posterior half of the dorsal surface of the neural arch bears irregular ridges slightly projected posteriorly (Fig. II-1M). In lateral view, a large spinal foramen (filled with sediment) is visible under the remnant of a slightly cylindrical transverse process (Fig. II-1N).

Discussion—MNHN.F.IBC 1626 can be differentiated from the braincase of *Pachycentrata* in (i) lacking pachyosteosclerosis, (ii) lacking a dorsal and ventral ornamentation, (iii) lacking a lateral expansion of the crista parotica and (iv) having a fenestra ovalis opening more anteriorly. It cannot be attributed to a juvenile of *Pachycentrata*, as all braincase of the latter taxon, even those smaller than MNHN.F.IBC 1626, all display dorsal ornamentation (ref). It can also be differentiated from *Inbecetenanura ragei* in (i) lacking a lateral expansion of the crista parotica, (ii) having crescentic occipital condyles (ovoid in *Inbecetenanura*) and (iii) having occipital condyles ventrolateral to the foramen magnum (ventral in *Inbecetenanura*).

MNHN.F.IBC 1968 can be distinguished from all atlantals of *Pachycentrata* in (i) lacking a neural spine, (ii) lacking pachyosteosclerosis, (iii) lacking a dorsal vermicular ornamentation and (iiii) having less separated cotyles. It can also be differentiated from *Inbecetenanura* in having (i) crescentic cotyle (likely ovoid in *Inbecetenanura*). However, it shares with MNHN.F.IBC 1626, (i) crescentic occipital condyle/cotyles and (ii) occipital condyle/cotyles ventrolaterally placed to the foramen magnum. Both the braincase MNHN.F.IBC 1968 and the atlantal complex MNHN.F.IBC 1626 are therefore here attributed to the same taxon, a Pipimorpha by (i) the absence of posterolateral expansion of the parasphenoid (i.e., Eustachian canals visible in ventral view) and (ii) the presence of opisthocoelous vertebrae. Unfortunately, the present

Pipimorphs of In Becetén and their implication for pipid diversification in Mesozoic Africa

known material is too fragmentary to propose a name, hence it will be referred as “Pipimorpha indet. 1”. Nevertheless, it represents a third pipoid taxon in In Becetén.

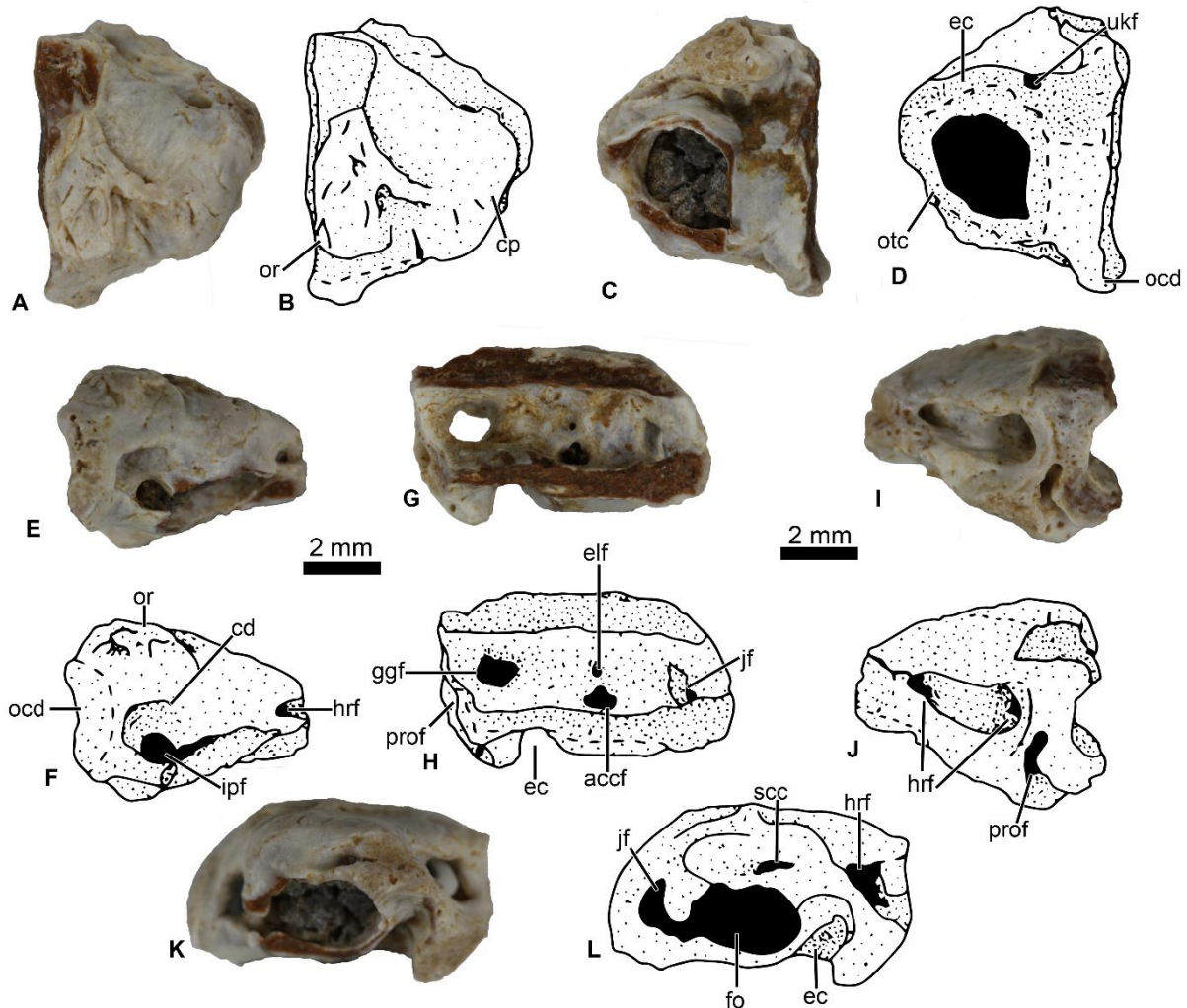


Figure II-2. Partial right prooticoccipital (Unnumbered specimen) of *Pipimorpha indet. 2* from In Becetén. A, in dorsal view, B, interpretative drawing of A, C, in ventral view, D, interpretative drawing of C, E, in posterior view, F, interpretative drawing of E, G, in medial view, H interpretative drawing of G, I, in anterior view, J, interpretative drawing of I, K, in lateral view and L, interpretative drawing of K. **Abbreviations: *accf*, fused acoustic foramina; *cd*, condyloid fossa; *cp*, crista parotica; *ec*, eustachian canal; *elf*, endolymphatic foramen; *ggf*, Gasserian ganglion fossa; *hrf*, hyomandibular nerves foramina and groove; *jf*, jugulare foramen; *ocd*, occipital condyle; *or*, ornamentation; *otc*, otic capsule; *fo*, fenestra ovalis; *pct*, posterior cotyle; *pf*, perilymphatic foramen; *prof*, prootic foramen; *ukf*, unknown foramen.**

Pipimorphs of In Becetén and their implication for pipid diversification in Mesozoic Africa

Pipimorpha indet. 2

Referred material—One left prooticoccipital (Unnumbered specimen)

Description—The prooticoccipital is almost fully preserved (Fig. II-2). The dorsal surface of the prooticoccipital bears a shallow dorsal ornamentation on its medial region composed by narrow and dispersed grooves (Fig. II-2A-B). There is no lateral expansion of the crista parotica. In ventral view, the Eustachian canal forms a narrow groove along the anterior margin of the otic capsule, before widening posteromedially to otic capsule (Fig. II-2C-D). Two foramina of unknown homology pierce the Eustachian canal at midlength. The otic capsule is broken, but all fragments have been collected and glued back together. It is large and forms an expanded ventral bulge. In posterior view, the occipital condyle is broken off, but it was likely crescentic (Fig. II-2E-F). There is no superior perilymphatic foramen. In medial view, the jugular foramen opens as the posteriormost foramen (Fig. II-2G-H). Midlength of the medial wall of the cavum cranii, the fused acoustic foramina open as the largest opening. Dorsal to this opening, the endolymphatic foramen is small and circular. On the anterior region of the medial wall of the cavum cranii, a large fossa is preserved. It opens extracranially on the lateral surface of the prooticoccipital (Fig. II-2I, J). This fossa is interpreted as the Gasserian ganglion (= trigeminofacial ganglion).

A small foramen opens within the cavum cranii anteriorly. The foramen is compressed anteroposteriorly (Fig. II-2I-J). Due to its position, it is interpreted as a prootic foramen. On the lateral surface of the prooticoccipital, a small hyomandibular ramus of the nerve VII is preserved (Fig. II-2K). Although broken, remnants of the foramen ovale shows it is located forward on the crista parotica.

Discussion—This specimen can be differentiated from *Pachycentrata* in in (i) lacking pachyosteosclerosis; (ii) lacking ventral ornamentation and (iii) lacking a superior perilymphatic foramen. It can also be differentiated from *Inbecetenanura* in (i) lacking a lateral expansion of the crista parotica, (ii) having crescentic occipital condyles (ovoid

Pipimorphs of In Becetén and their implication for pipid diversification in Mesozoic Africa

in Inbecetenanura); (iii) having shallow ornamentation on the dorsal surface of the prooticoccipital and (iv) having one unknown foramina piercing the Eustachian canal. Finally, this unnumbered specimen is similar to the Unnamed genus and species (*Pipimorpha* indet.) in (i) having crescent-shaped occipital condyles; (ii) having an inferior perilymphatic foramen lateral to the jugular foramen

However, it can be differentiated from the latter taxon in (i) lacking a superior perilymphatic foramen; (ii) having shallow ornamentation on the dorsal surface of the prooticoccipital; (iii) having lateral occipital condyles (ventrolateral in *Pipimorpha* indet.) and (iv) having one foramen of unknown homology piercing the Eustachian canals.

Therefore, this unnumbered specimen can be differentiated from all three known pipimorph taxa from In Becetén. However, it can also be referred to *Pipimorpha* by lacking a posteromedial expansion of the parasphenoid (i.e. visible Eustachian canal in ventral view). Unfortunately, as for *Pipimorpha* indet. 1, the present known material is too fragmentary to propose a new name, hence it is here referred as “*Pipimorpha* indet. 2”.

Other specimens attributed to indeterminate *Pipimorpha*

Numerous fragmentary bones from pipimorphs were identified in In Becetén. It was not possible to attribute them to any of the four known taxa, or to a distinct taxon. They are nevertheless here shortly described.

Referred material—Two incomplete angulars (MNHN.F.IBC 1631, 1964), 14 centra (MNHN.F.IBC 1997; all centra have been assigned the same collection number); three incomplete scapulae (MNHN.F.IBC 1632, 1633 and 1974), 21 incomplete humeri (MNHN.F. IBC1651-1655, 1977-1981; several humeri have been assigned to the same collection number); 51 ilia (MNHN.F.IBC 1635-1649, 1975; several ilia have been assigned the same collection number); four femora (MNHN.F.IBC 2000a-d) and six tibiofibulae (MNHN.F.IBC 2001a-f).

Pipimorphs of In Bacetén and their implication for pipid diversification in Mesozoic Africa

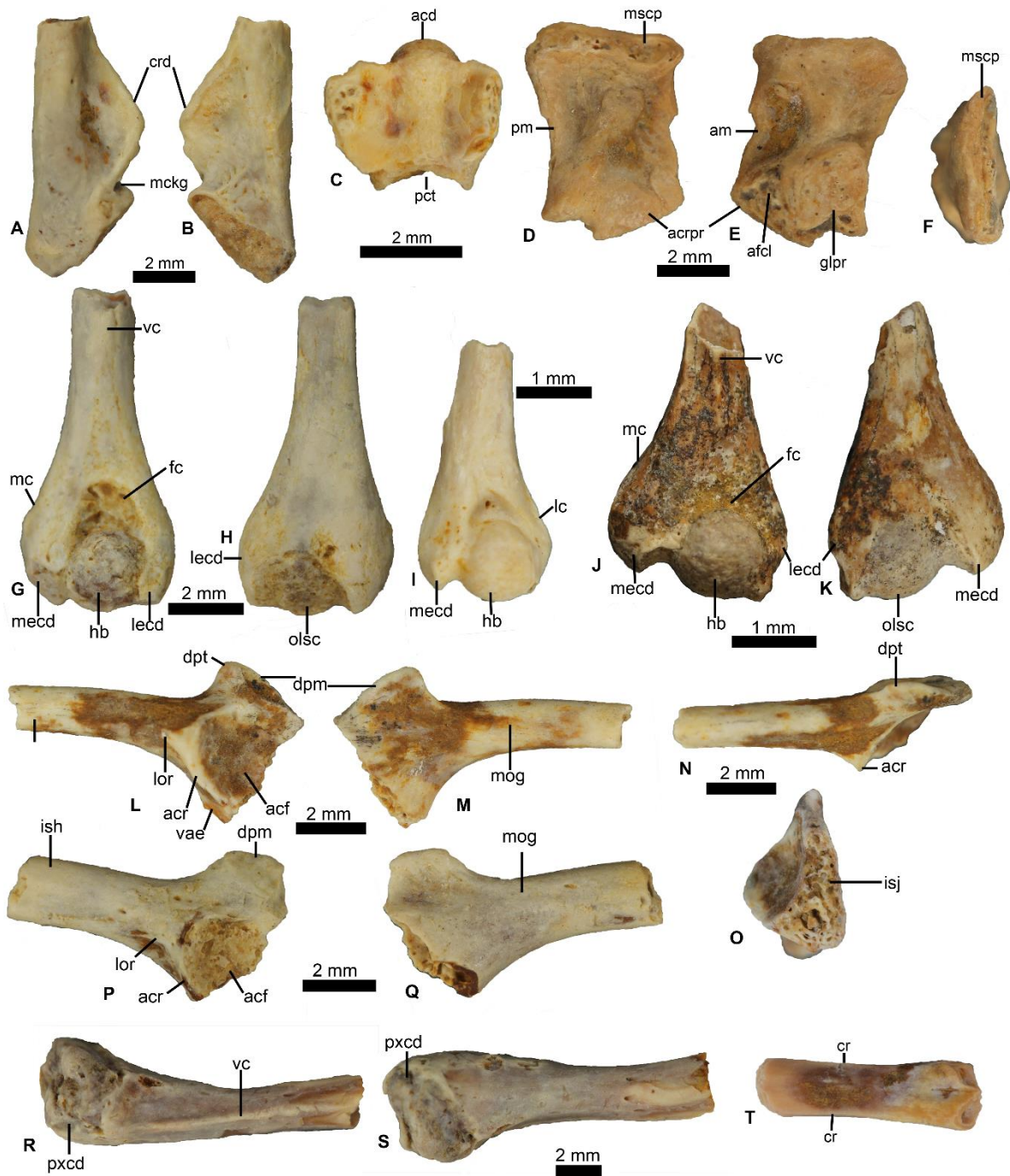


Figure II-3. Diverse elements attributed to indeterminate Pipimorpha. A–B, left angular (MNHN.F.IBC 1964) in A, medial and B, lateral; C, vertebra centrum (MNHN.F.IBC 1997e) in dorsal view; D – F, incomplete right scapula (MNHN.F.IBC1974) in D, dorsal, E, ventral and F, medial views; G–H, humerus (MNHN.F.IBC 1977a) assigned to morphotype A in G, ventral and H, dorsal views; I, humerus (MNHN.F.IBC 1980) in ventral view; J–K, humerus (MNHN.F.IBC 1655) assigned to morphotype B in J, ventral and K, dorsal views; L – O, left ilium (MNHN.F.IBC1635) assigned to morphotype A (?*Pachycentrata taqueti*) in L, lateral, M, medial, N, dorsal and O, posterior views; P–Q, left ilium (MNHN.F.IBC 1649) assigned

Pipimorphs of In Becetén and their implication for pipid diversification in Mesozoic Africa

to morphotype B in **P**, lateral and **Q**, medial views; **R** – **S**, left or right? Femur (MNHN.F.IBC 2000a) in **R**, ventral and **S**, lateral views; **T**, left or right ? tibiofibula (MNHN.F.IBC 2001a) in **T**, lateral view. **Abbreviations:** **acd**, anterior condyle; **acf**, acetabular fossa; **acr**, acetabular rim; **acrpr**, acromial process; **afcl**, articular facet for the clavicle; **am**, anterior margin; **cr**, crest; **crd**, coronoid process; **dpm**, dorsal prominence; **dpt**, dorsal protuberance; **fc**, ventral fossa (= fossa cubitalis); **glpr**, glenoid process; **hb**, humeral ball; **ish**, ilial shaft; **isj**, ilioischiatic juncture; ; **lc**, lateral crest; **lecd**, lateral epicondyle; **lor**, lateral oblique ridge; **ma**, anterior margin; **mc**, medial crest; **mckg**, Meckelian groove; **mecd**, medial epicondyle; **mp**, posterior margin; **mog**, medial oblique groove; **mscp**, suprascapular margin; **olsc**, olecranon scar; **pct**, posterior cotyle; **pxcd**, proximal condyle impression; **vae**, ventral acetabular expansion; **vc**, ventral crest.

Angulars

MNHN.F.IBC 1631 and 1964 both represent the posterior region of the bone. The coronoid process is large and extends into a flange (Fig. II-3A). The Meckelian groove is close posteriorly (Fig. II-3A-B).

Centra

All centra are opisthocelous. They are elongate anteroposteriorly (Fig. II-3C). No bony accretion is present, so they cannot be attributed to *Pachycentrata*. They are too incomplete to be compared to *Inbecetenanura*, and no presacral centra (excluding atlantal) are known for the third and fourth pipimorph taxa.

Scapulae

All three scapulae (MNHN.F.IBC 1632, 1633 and 1974) possess a similar gross morphology and likely belong to the same taxon. MNHN.F.IBC 1632 is the most complete and has been already described (Báez and Rage, 1998). Scapulae are short and compressed lateromedially (Fig. II-3D). The greatest width (at the articulation with the suprascapular) is almost two-third of the length of the bone (Fig. II-3D–F). The anterior margin is slightly concave in MNHN.F.IBC 1974 (straight in the others) and bears a large anterior crest (Fig. II-3E). The glenoid fossa represents around half

Pipimorphs of In Becetén and their implication for pipid diversification in Mesozoic Africa

of the shaft length. The posterior margin is concave. A small articular facet is present on the anterior margin, implying that the clavicle was not fused to the scapula (Báez and Rage, 1998). The pars glenoidalis seems to be distinct from the pars acromialis (Fig. II-3E). An interglenoidalis sinus likely separated both processus.

Humeri

21 humeri have been recovered (MNHN.F. IBC1651-1655, 1977-1981). All can be attributed to Pipimorpha based on (i) well-developed epicondyles, (ii) small humeral ball (compared to maximum width of the humerus), (iii) short medial crest, (iv) straight diaphysis and (v) a deep ventral fossa (= fossa cubitalis). Two morphotypes, A and B, can be distinguished at In Becetén. Morphotype A is represented by eleven humeri (MNHN.F. IBC1651-1654, 1977, 1981 1980?). Morphotype B is represented by eight humeri (MNHN.F. IBC1655, 1979). Two humeri (MNHN.F. IBC1978a-b) are poorly preserved and no referred to a morphotype.

Morphotype A—The ventral fossa is ovoid, elongate anteroposteriorly and deep (Fig. II-3G). In the best-preserved specimens, the distal end of the ventral crest (= deltoid crest) is present as a thin sharp ridge (Fig. II-3G). The medial epicondyle (= ulnar epicondyle) protrudes (medially) more from the humeri than the lateral epicondyle (= radial epicondyle). However, both epicondyles are well developed, giving a symmetrical aspect to some humeri (Fig. II-3G). A small, short medial crest is present (Fig. II-3G-I). A lateral crest is also present in some specimens, such as MNHN.F. IBC1980, which resembles humeri of morphotype A (Fig. II-3I). However, the humeral ball seems shifted laterally, and its radial epicondyle seems smaller than in Morphotype A. Unfortunately, this specimen belongs to an immature individual, so the attribution to morphotype A is putative.

Morphotype B—Humeri of this morphotype present a ventral fossa, which is reduced to a shallow groove pressed against the humeral ball (Fig. II-3J). As in morphotype A, both epicondyles are well-developed. However, the medial epicondyle appears larger

Pipimorphs of In Becetén and their implication for pipid diversification in Mesozoic Africa

and more developed than the lateral epicondyle (Fig. II- 3J-K). It is also larger than the one found in morphotype A. As in morphotype A, the medial crest is short. No lateral crest has been recovered.

Remarks—Both morphotypes represent common variation of humeri within pipimorphs (Gómez, 2016). Unfortunately, there is no clear synapomorphies that could allow an attribution of these morphotype to any of the four pipimorph taxa of In Becetén.

Ilia

Fifty-one ilia have been identified as belonging to pipimorph. This is based on (i) reduction of absence or a ventral acetabular expansion, (ii) the presence of a anterolateral oblique ridge on the shaft, (iii) the anteroventral portion of the acetabular rim protruding laterally and (iv) a large ilioischiatric junction. Twenty-two ilia can be attributed to two morphotypes. Morphotype A is represented by twenty ilia (MNHN.F. IBC1635-1647, 1975) and Morphotype B by two ilia (MNHN.F. IBC1648, 1649).

Morphotype A— The dorsal prominence is small, triangular and slightly projected laterally. Its anterior margin is more steeply inclined than its posterior margin (Fig. II- 3L-M). Several specimens preserve an ovoid dorsal protuberance instead of triangular. The medial oblique groove starts from the anterior border of the dorsal prominence on the medial surface of the ilium. Ilia assigned to Morphotype A seem to lack a dorsal crest. A lateral oblique ridge is present and extends anteriorly from the acetabular rim (Fig. II-3N). The ventral acetabular expansion is strongly oriented medially, with a minimal lateral exposure. The dorsal acetabular expansion (~pars ascendens) is indistinct from the dorsal surface (Fig. II-3L-N). When preserved (such as on the specimen MNHN.F.IBC 1935), the ilioischiatric junction is large. The interiliac tubercle is poorly preserved, but seems ample at least ventrally.

Pipimorphs of In Becetén and their implication for pipid diversification in Mesozoic Africa

Morphotype B— This morphotype is distinct of morphotype A in (i) lacking a dorsal protuberance (Fig. II-3P-Q). The dorsal prominence is bell-shaped, almost rectangular. An oblique ridge is present laterally (Fig. II-3Q).

The remaining ilia are too fragmentary to be assigned to any morphotypes.

Remarks—Morphotype A is similar to *Singidella latecostata* (recovered as a sister-taxon to *Pachycentrata*) and *Pseudohymenochirus* (extant taxa close to *Pachycentrata*) in having a low triangular dorsal prominence and an inconspicuous dorsal acetabular expansion (Báez and Harrison, 2005). Among In Becetén taxa, *Pachycentrata* is considered to be closely related to *Singidella*, and both are placed as stem-Hymenochirini in most phylogenetic analyses (Gómez, 2016; Section II, Chapter II). In addition, the frequency of ilia of morphotype A (90% of recovered pipid ilia) suggests that it might belong to the dominant pipid taxon. Thus, we could refer this morphotype to *Pachycentrata*. However, this attribution is very putative, and we refrain from using these specimens for future phylogenetic analyses. Morphotype B slightly resembles the ilia of *Kuruleufenia*, in having a rather tall bell-shaped dorsal prominence.

Femora

Four incomplete femora (MNHN.F. IBC 2000) are attributed to Pipidae due to the presence of a ventral crest on their ventral surface (Fig. II-3R-S). The ventral crest is low, thin and sharp.

Tibiofibulae

Six incomplete tibiofibulae (MNHN.F. IBC 2001) are attributed to Pipidae on the presence of a medial and lateral crest on their diaphysis. The crests are shallow but well visible (Fig. II-3T).

Pipimorphs of In Becetén and their implication for pipid diversification in Mesozoic Africa

II.5 Phylogenetic Analysis

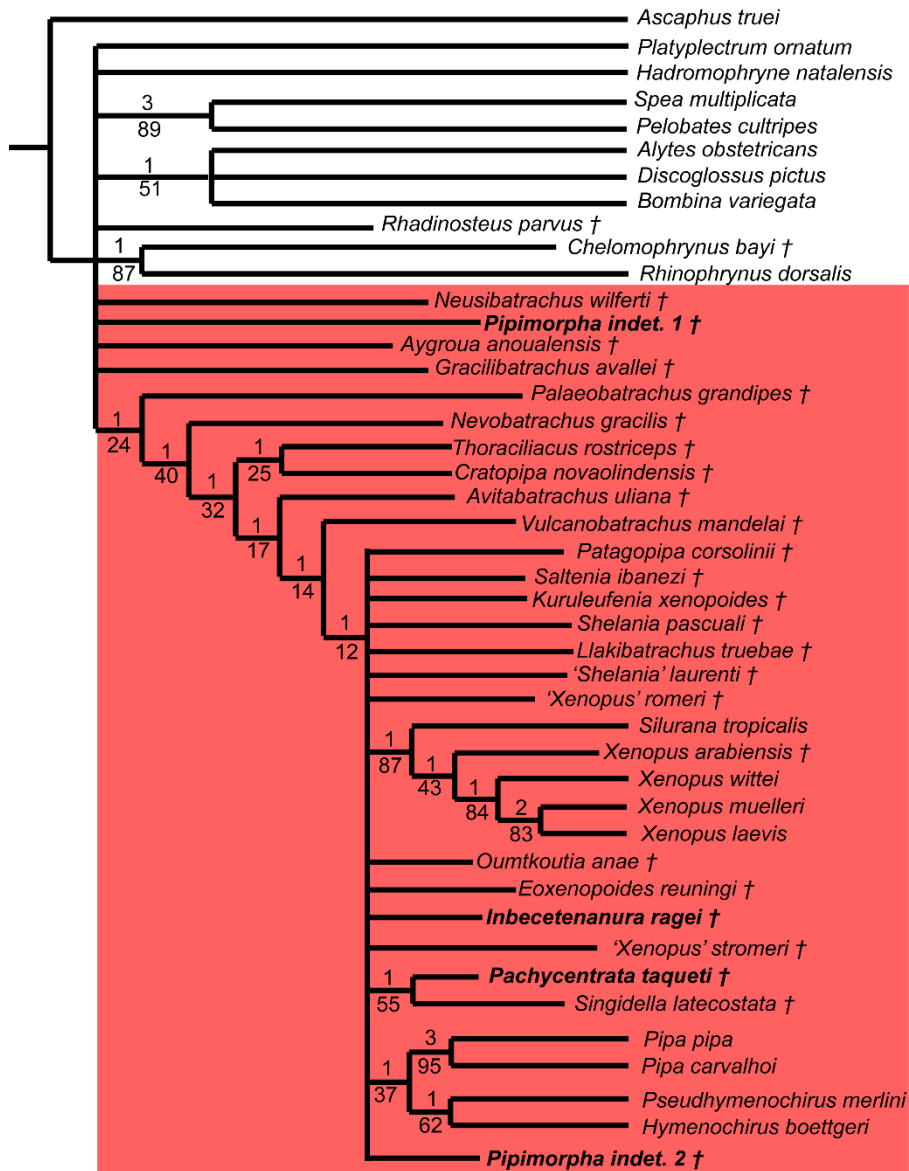


Figure II-4. Strict consensus of 144 MPTs of 647 steps from the analysis performed under equal weight, multistate characters ordered (CI = 0.287; RI = 0.557). † represents extinct taxa; In Becetén taxa are represent in bold italic; the red rectangle highlights pipimorph taxa; numbers above branches designate Bremer support; those below are bootstrap frequencies.

Results

A phylogenetic analysis performed under equal weight and cline characters ordered yielded 144 MPTs with a score of 647 steps. The strict consensus (CI = 0.287 RI = 0.557; Fig. II-4) includes a large basal polytomy that neither rejects nor confirms the

Pipimorphs of In Becetén and their implication for pipid diversification in Mesozoic Africa

pipimorph affinities of some taxa that are normally considered to belong to this clade (*Aygroua*, *Gracilibatrachus*, and *Neusibatrachus*) and of *Pipimorpha* indet. 1 (Fig. II-4). Several pipimorphs, like *Aygroua* and *Pipimorpha* indet. 1 from In Becetén, are indeed recovered in an unresolved polytomy with Pelobatidae, Alytidae, Neobatrachia, Rhinophrynidae and a clade composed of several pipimorphs and all gondwanopipids. *Pipimorpha* indet. 2 is recovered within the latter clade, placed in an unresolved polytomy with all gondwanopipids. This latter clade is supported by four synapomorphies, (1) an inconspicuous zygomatic ramus (32: 1→0); (2) the loss of maxillary teeth (34:0→1); (3) posteromedial processes of the hyoid ossified on more than one half of the anteroposterior length of the lower jaw (79: 0→1) and (4) posteromedial processes of the hyoid symmetrical or with a narrower anterior end than its posterior end (80: 0→1). Furthermore, *Pipimorpha* indet. 1 is recovered as a pipimorph in 71% of all MPTs, while *Pipimorpha* indet. 2 is recovered as a pipid in 57% of all MPTs (Fig. II-5).

II.6 Discussion

Phylogenetic analyses

The phylogenetic position of *Pachycentrata taqueti* and *Inbecetenanura ragei* within Pipids is consistent with previous analyses (Gómez, 2016; Aranciaga Rolando et al., 2019; Chapter III). *Pipimorpha* indet. 2 is also recovered as a pipimorph at minimum, while *Pipimorpha* indet. 1 is not always recovered as a pipimorph. This uncertainty is linked to the absence of several key skeletal elements and the very fragmentary materials. Most pipimorph synapomorphies are present on the sphenethmoid, ilium and sacrococcyx (Gómez, 2016; Chapter III), all elements lacking for both *Pipimorpha* indet. 1 and 2. However, examination of all MPTs obtained suggests that both taxa possess a very strong affinity with the pipimorphs. Furthermore, several pipimorph synapomorphies are present in these taxa. Thus, we attribute both *Pipimorpha* indet. 1 and 2 to *Pipimorpha*. Furthermore, *Pipimorpha* indet. 2 has been recovered in a

Pipimorphs of In Becetén and their implication for pipid diversification in Mesozoic Africa

majority of MPTs as a pipidae (Fig. II-5), crownward of *Oumtkoutia anae* in 54% of MPTs. Thus, we also consider that *Pipimorpha* indet. 2 has putative pipid affinities.

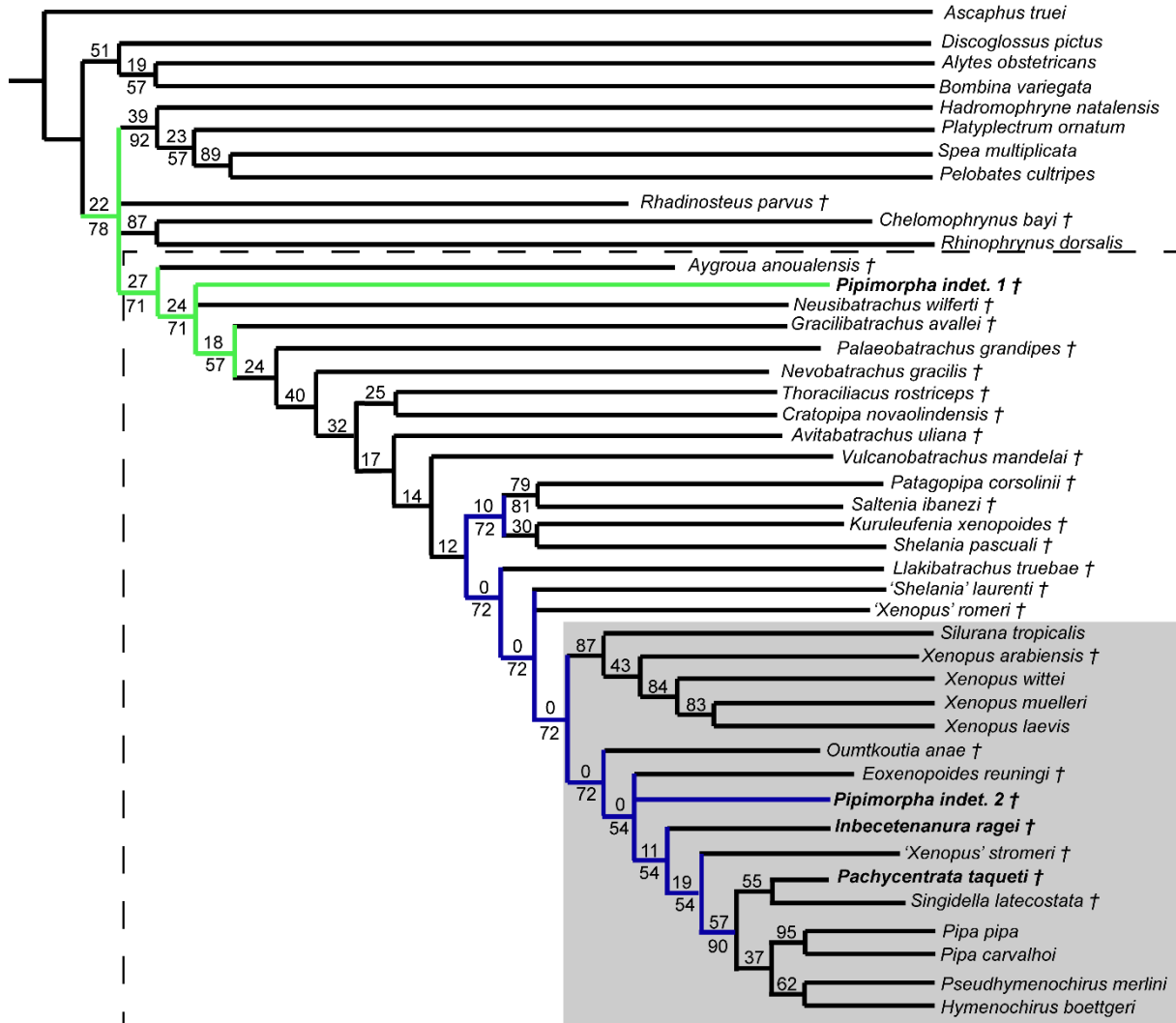


Figure II-5. Majority consensus of 144 MPTs of 647 steps from the analysis performed under equal weight, multistate characters ordered, showing the various positions of the two new In Becetén taxa inferred. † represents extinct taxa; bold italic taxa are from In Becetén; green branches represent phylogenetic position for *Pipimorpha* indet. 1 on the MPTs; blue branches represent phylogenetical position for *Pipimorpha* indet. 2 on the MPTs; dotted rectangle represents *Pipimorpha*; light gray rectangle represents Pipidae; number above branches represent bootstrap frequencies, those below are the % of MPTs where the branch was recovered.

Pipimorphs of In Becetén and their implication for pipid diversification in Mesozoic Africa

Anuran diversity of In Becetén

In Becetén is one of the oldest sites yielding pipids taxa (Chapter III). The presence of four pipimorph taxa makes it the richest Cretaceous site for the clade, surpassing the lagerstätte of the Crato Formation where currently two pipimorphs are known (Báez et al., 2021). In addition, several non-pipimorph anurans are present within In Becetén (de Broin et al., 1974; Gardner and Rage, 2016; Chapter IX). With at least five anuran taxa, and several urodeles (Gardner and Rage, 2016), In Becetén is the richest amphibian site of Mesozoic and Paleogene (Early Cenozoic) from Africa. However, few sites have been studied in Africa (Gardner and Rage, 2016), and unstudied sites might harbor a similar diversity.

Interestingly, *Pachycentrata* is by far the dominant anuran within In Becetén. *Pachycentrata* represents around 16% of the total pipimorph specimens identified, and 67% of total specimens attributed to a named taxon. This dominance within the site is likely due to the pachyosteosclerosis of its braincase and vertebrae. This feature explains the better preservation than other taxa. In addition, the peculiar ornamentation and aspect associated with this feature allows for easy attribution of incomplete elements.

In extant ecosystem, it is common for at least two pipid taxa to coexist (Tinsley, 1975, 1979; Kobel et al., 1981; Fouquet et al., 2022). A diversity of four pipid taxa or more (similar to In Becetén case) has been recovered in the Amazonian Basin (Fouquet et al., 2022) and within the Great lakes in Africa (Tinsley, 1975, 1979). Both regions have been commonly considered biodiversity hotspots (Salzburger et al., 2014; Vasconcellos et al., 2020), and a similar claim for In Becetén could be made. However, it is possible that all four taxa are not synchronous. In addition, co-existing *Xenopus* taxa are known to hybridize between themselves (Tinsley, 1975, 1979; Kobel et al., 1981), and possess few (if any) osteological differences. Thus, it is likely that the pipimorph skeletal disparity in In Becetén is much greater than in most extant ecosystems.

Pipimorphs of In Becetén and their implication for pipid diversification in Mesozoic Africa

Interestingly, pipids are known to be voracious anurophages (Vogt et al., 2017). Hence, predation among pipid taxa is high. It is likely that a similar interaction occurred in In Becetén.

Paleoenvironmental implications

Current analyses of the paleoenvironment of In Becetén have proposed a fluvio-lacustrine environment (Moody and Sutcliffe, 1991; Mateer et al., 1992). This is similar to other (and older sites) Cretaceous sites, like Gadoufaoua (Taquet, 1976) or the Kem Kem (Ibrahim et al., 2020a). However, the presence of at least four pipimorph taxa in In Becetén argues for a different paleoenvironment. Indeed, as extant pipids are known to dwell within calm lakes and ponds (Channing and Rödel, 2019), their diversity suggests that In Becetén was a more lacustrine environment than previously thought.

II.7 Conclusion

In conclusion, analysis of new anuran materials from In Becetén led to the identification of new specimens of *Pachycentrata taqueti*. Two potential new, unnamed, pipimorph taxa are identified within the site. Our phylogenetic analyses do not allow to propose a more precise phylogenetical position for these new taxa. This mainly linked to the very few (only two) known elements attributed to these taxa. However, several osteological characters show likely close relationships with pipids. One of the two unnamed pipimorph taxa may represent a third pipid taxon from In Becetén, and the fifth from Mesozoic Africa. Numerous pipimorph bones are present, but many are not attributable to any taxa of In Becetén anurans. This makes In Becetén, the most diverse pipimorph site within Mesozoic and Paleogene Gondwana.

Pipimorphs of In Becetén and their implication for pipid diversification in Mesozoic Africa

Finally, the presence of four pipimorph taxa implies that the paleoenvironment was more lacustrine than previously thought, in peculiar in contrast to other Mesozoic western African sites, like Gadoufaoua or the Kem Kem.

II.8 Appendix

Appendix S1. Morphological dataset used for phylogenetical analyses

The dataset used is the one from Chapter III, with the addition of Pipimorpha indet.

1 and 2.

	1	2	3	4	5	6	7	8	9	10	11	12	13	14	15	16	17	18	19	20
Pipimorpha indet. 1	?	?	?	?	?	?	?	?	?	0	?	?	?	?	?	?	0	?	?	?
Pipimorpha indet. 2	?	?	?	?	?	?	?	?	?	0	?	?	?	?	?	?	1	?	?	?
	21	22	23	24	25	26	27	28	29	30	31	32	33	34	35	36	37	38	39	40
Pipimorpha indet. 1	?	?	?	?	?	?	?	?	?	?	?	?	?	?	?	?	?	?	?	?
Pipimorpha indet. 2	?	?	?	?	?	?	?	?	?	?	?	?	?	?	?	?	?	?	?	?
	41	42	43	44	45	46	47	48	49	50	51	52	53	54	55	56	57	58	59	60
Pipimorpha indet. 1	?	?	?	?	?	?	?	?	?	2	?	?	?	?	?	?	1	1	?	?
Pipimorpha indet. 2	?	?	?	?	?	?	?	?	?	?	?	?	?	?	?	?	1	1	0	1
	61	62	63	64	65	66	67	68	69	70	71	72	73	74	75	76	77	78	79	80
Pipimorpha indet. 1	0	0	0	1	0	1	0	0	0	0	?	?	?	?	?	?	?	?	?	?
Pipimorpha indet. 2	0	1	1	?	0	?	0	0	0	1	?	?	?	?	?	?	?	?	?	?
	81	82	83	84	85	86	87	88	89	90	91	92	93	94	95	96	97	98	99	100
Pipimorpha indet. 1	?	?	?	?	1	1	1	3&4	?	?	?	?	?	?	?	?	?	?	?	?

Pipimorphs of In Becetén and their implication for pipid diversification in Mesozoic Africa

Pipimorpha indet. 2	?	?	?	?	?	?	?	?	?	?	?	?	?	?	?	?	?	?	?	?
	101	102	103	104	105	106	107	108	109	110	111	112	113	114	115	116	117	118	119	120
Pipimorpha indet. 1	?	?	?	?	?	?	?	?	?	?	?	?	?	?	?	?	?	?	?	?
Pipimorpha indet. 2	?	?	?	?	?	?	?	?	?	?	?	?	?	?	?	?	?	?	?	?
	121	122	123	124	125	126	127	128	129	130	131	132	133	134	135	136	137	138	139	140
Pipimorpha indet. 1	?	?	?	?	?	?	?	?	?	?	?	?	?	?	?	?	?	?	?	?
Pipimorpha indet. 2	?	?	?	?	?	?	?	?	?	?	?	?	?	?	?	?	?	?	?	?
	141	142	143	144	145	146	147	148	149	150	151	152	153	154	155	156	157	158	159	160
Pipimorpha indet. 1	?	?	?	?	?	?	?	?	?	?	?	?	?	?	?	?	?	?	?	?
Pipimorpha indet. 2																				
	161	162	163	164	165	166	167	168	169	170	171	172	173	174	175	176				
Pipimorpha indet. 1	?	?	?	?	?	?	?	?	?	?	?	?	?	?	?	?				
Pipimorpha indet. 2	?	?	?	?	?	?	?	?	?	?	?	?	?	?	?	?				

Appendix S2. Taxa list for the phylogenetical analyses

The list is the same as in Chapter III, with the addition of Pipimorpha 1 and 2.

Appendix S3. Character list

The list is the same as in Chapter III.

Chapter III

*A NEW PIPID FROM THE CRETACEOUS OF AFRICA
(IN BECETÉN, NIGER) AND EARLY EVOLUTION OF
PIPIDAE*

A new pipid from the Cretaceous of Africa (In Becetén, Niger) and early evolution of Pipidae

II.1 Introduction

The aquatic pipids and other pipimorphs in their stem-group possess one of the most extensive fossil record of any anuran clade, with numerous remains attributed to the clade since the Early Cretaceous (Marjanović and Laurin, 2014; Báez et al., 2021). In peculiar, they possess an extensive Cretaceous fossil record from both Gondwana and Laurasia continents (Gardner and Rage, 2016; Báez et al., 2021). This period is key for the evolutionary history of pipimorphs as the clade diversified rapidly (Frazão et al., 2015; Feng et al., 2017), possibly driven by the breakup of the West Gondwanian subcontinent, made of South America and Africa (Powell et al., 1980; Gaina et al., 2013; Will and Frimmel, 2018). During the last decade, several well-preserved pipimorphs have been described from South America (Leal and Brito, 2006; Báez et al., 2009, 2021; Carvalho et al., 2019), documenting the early diversification and evolution of this clade in peculiar during the Early/Late Cretaceous, around the time when Africa and South America (Báez et al., 2021) became separated.

Few pipimorphs are known in the Cretaceous of Africa, and these are mostly restricted to Sub-Saharan Africa or Arabia (Báez and Harrison, 2005; Trueb et al., 2005; Gardner and Rage, 2016). In addition, they are restricted either to Early Cretaceous outcrops (Arabian Peninsula; Gardner and Rage, 2016) or to latest Late Cretaceous outcrops (Trueb et al., 2005). In the Early Cretaceous of the Arabian Peninsula, three pipimorph taxa are known, *Nevobatrachus* (replacement name for *Cordicephalus*; Mahony, 2019) *gracilis* Nevo, 1968, *Thoraciliacus rostriceps* Nevo, 1968 and *Shomronella* Estes et al., 1978. Two pipimorph taxa are known in the latest Late Cretaceous, *Vulcanobatrachus* Trueb et al., 2005 and *Eoxenopoides* Haughton, 1931. Regarding pipids, only two Cretaceous taxa are known, *Oumtkoutia anae* Rage and Dutheil, 2008 from Morocco and *Pachycentrata* (replacement name for *Pachybatrachus* Báez and Rage, 2004)

A new pipid from the Cretaceous of Africa (In Becetén, Niger) and early evolution of Pipidae

taqueti Báez and Rage, 1998 from Niger. Both are from earliest Late Cretaceous outcrops.

During the late 1990s, a strange pipid, *Pachycentrata taqueti* (*Pachybatrachus taqueti* in Báez and Rage, 1998), was described from the Coniacian-Santonian beds of Ibeceten (Niger; Báez and Rage, 1998, 2004). In addition to this taxon, a braincase, attributed to an indeterminate xenopodinomorph, a clade composed of Xenopodines (*Xenopus* + *Silurana*) and all taxa closer to the latter than to all other extant pipids, was described (Báez and Rage, 1998: fig. 3H-K). Only *P. taqueti* has been included in phylogenetical analyses (Trueb et al., 2005; Báez et al., 2007; Gómez, 2016; Carvalho et al., 2019; Aranciaga Rolando et al., 2019). As part of an ongoing study of the anuran diversity of In Becetén, we here take the opportunity to redescribed this braincase, along with several vertebral elements, all assigned to the same taxon. We also include this taxon into a phylogenetic analysis of the pipimorphs to test the xenopodinomorph attribution proposed in the original description. In addition, the phylogenetic analysis also suggests several scenarii about pipid dispersals between South America and Africa. This constrains the separation timing of these two continents by the South Atlantic Ocean, as we show below.

A new pipid from the Cretaceous of Africa (In Becetén, Niger) and early evolution of Pipidae

III.2 Geological Context

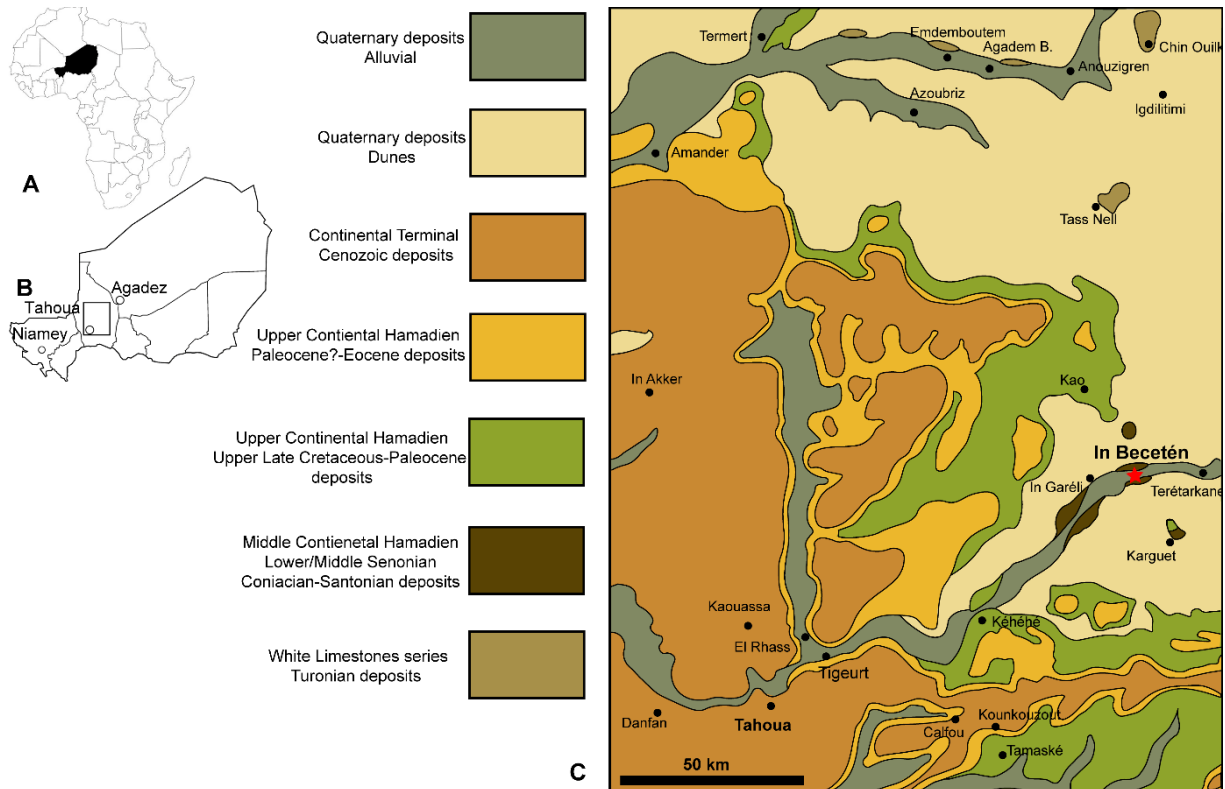


Figure III-1. Map of the In Becetén locality. A, map of Africa, with Niger highlighted in black; B, map of Niger with the Tahoua region highlighted in black square outline; C, simplified geological map of the Tahoua and In Becetén region, modified from Greigert and Pougnet (1965). Red star (grey in print version) indicates the In Becetén site.

All specimens came from the site of In Becetén (also known as In Becetem, In Beceten, In'Betetén, In Béceten, Ibesseten and erroneously Ibeceten; pers. Com. D. Dutheil, Dec. 2021). They were collected during three expeditions in 1970, 1972 and 1973, organised by the Muséum national d'Histoire naturelle de Paris (France), led by P. Taquet and D. Russell (Broin et al., 1974). The site of In Becetén is located 80 km east north-east of the town of Tahoua, in the South-western region of the Republic of Niger (Fig. III-1; Báez and Rage, 1998: fig. 1). This site has been known since the 1970s, for its diverse vertebrate fauna (de Broin et al., 1974), as apart from mammals, all large continental vertebrate clades have been identified (Broin et al., 1974; Patterson, 1993; Gayet and

A new pipid from the Cretaceous of Africa (In Becetén, Niger) and early evolution of Pipidae

Meunier, 1996; Báez and Rage, 1998; Lapparent, 2000; Gardner and Rage, 2016; Lapparent de Broin et al., 2020).

The site of In Becetén is located within the Iullemmeden (or Iullmeden) Basin. It represents a vast sedimentary basin from Northern Africa, characterised by an alternation of marine and continental deposits during the Cretaceous and the Paleogene (Greigert, 1966; Greigert and Pougnet, 1967; Broin et al., 1974; Moody and Sutcliffe, 1991). Within this basin, fossiliferous layers, including those of In Becetén, are part of the Ibeceten Formation (Moody and Sutcliffe, 1991). This Formation is composed of an alternation of shales and sandstones (Moody and Sutcliffe, 1991). Anurans specimens were recovered from thin black/grey shale beds (de Broin et al., 1974; Moody and Sutcliffe, 1991; Meunier and Larsson, 2018) either during screen-washing operations or were exposed on the ground surface (de Broin et al., 1974).

A precise age for the Ibeceten Formation is currently difficult to propose, as it is the case for most continental Formations from the Late Cretaceous of Africa, with most of them referred to the Senonian (part of the Late Cretaceous, from the Coniacian to Maastrichtian; Moody and Sutcliff, 1991). The Ibeceten Formation has been incorporated into the Damergou Series, which spans from Late Cretaceous to Eocene (Moody and Sutcliffe, 1991).

The base of the Damergou series, the Talrass Formation, rests uncomfortably on Cenomanian deposits. This formation is overlaid by the 'White Limestone' Formation composed of marine limestone, dated and correlated to the Late Turonian transgression (Moody and Sutcliffe, 1991). The Ibeceten Formation overlays this 'White Limestone' Formation and represents nonmarine and marine deposits. The base of the Formation is composed of nonmarine beds, where anurans specimens were collected (Broin et al., 1974; Moody and Sutcliffe, 1991), and upper marine beds dated from the Santonian/Campanian marine transgression (Moody and Sutcliffe, 1991). The unit overlaying the Ibeceten Formation is composed of marine beds dated to the Campanian-Maastrichtian (Greigart and Pougnet, 1967; Moody and Sutcliffe, 1991).

A new pipid from the Cretaceous of Africa (In Becetén, Niger) and early evolution of Pipidae

The Ibeceten Formation is thus dated to the Coniacian or Santonian (Early Senonian; Broin et al., 1974). However, correlations of the Iullemeden Basin with other African cretaceous basins suggest that the Ibeceten Formation dates from the Santonian (Mateer et al., 1992). Nevertheless, in the absence of recent stratigraphical work on the In Becetén site, we follow previous paleontological studies and considered the site to be Coniacian or Santonian.

The nonmarine Ibeceten beds are considered to represent fluvial-lacustrine deposits, based on fossil evidence (Greigart, 1966; Moody and Sutcliffe, 1991). However, paleogeographical studies of the region during the Late Cretaceous have shown that several transgression/regression events took place in the Iullemeden Basin (Moody and Sutcliffe, 1991). Stratigraphical evidence from neighbouring sites (based on fossil evidence; Moody and Sutcliffe, 1991) indicates that paleoshoreline was near the site (Moody and Sutcliffe, 1991). Marine influence within the fossiliferous beds thus cannot be excluded.

III.3 Materials and Methods

Institutional abbreviations

MNHN: Muséum national d'Histoire naturelle, Paris, France. All specimens are stored within the Paleontological collection of the MNHN of Paris (France) in the Amphibians and Reptiles section, under the collection number MNHN.F.IBC XXXX.

Micro-CT scan tomography

MNHN.F.IBC 1602 was micro-CT scanned at the AST-RX (Accès Scientifique à la Tomographie à Rayons X) at the UMS 2700, MNHN (Paris France). A nanofocus beam of 180 kV of the CT scanner was used with the following parameters: voltage, 125 kV; current, 245 μ A; voxel size, 7.847 μ m; slice resolution, 1666 x 1676 pixels. A total of 2312 virtual slices were reconstructed. These slices were imported into the 3D

A new pipid from the Cretaceous of Africa (In Becetén, Niger) and early evolution of Pipidae

reconstruction software Mimics 21.0 (Materialise, Leuven, Belgium). Before importation, slices were cropped to maximally remove the empty spaces. To decrease data size, slices were converted from 16 to 8 bits. The dataset thus includes 1868 slices, with an image resolution of 1300 × 1222 pixels and a voxel size of 15.69 μm for the volume file (see Appendix S1). The 3D model was produced by segmentation of each bone using the ‘thresholding’ function (using the contrast on grayscale images). We used the same voxel resolution of 15.69 μm, with a smoothing factor of 3 for one iteration, to homogenize the model resulting from manual segmentation. Data produced by segmentation were exported in the software 3matic 9.0 as a separate file (see Appendix S2, S3).

The anatomical terminology used herein is based on Roček (1980) and Biton et al. (2016) for cranial features, and Sanchíz (1998) for postcranial ones. Anatomical terminology for cranial nerves follows Gaupp (1896).

Phylogenetic analyses

Our data matrix (Appendix S4) includes 43 taxa and 176 osteological characters and is derived from that of Aranciaga Rolando et al. (2019; see Appendix S5 for the list of characters). We added 5 new extinct pipimorph taxa; (1) *Aygroua anoualensis* Jones et al., 2003, (2) *Cratopipa novaolindensis* Carvalho et al., 2019; (3) *Xenopus arabiensis* Henrici and Báez, 2001; (4) ‘*Xenopus*’ *stromeri* Ahl, 1926 and (5) *Inbecetanura ragei* gen. nov. et sp. nov. (see Appendix S6). Except for *Inbecetanura* gen. nov., newly added taxa were scored from both personal observation and literature (Henrici and Báez, 2001; Jones et al., 2003; Carvalho et al., 2019; Lasseron et al., 2019; Báez et al., 2021). Several other taxa were rescored (see Appendix S7) from both personal observations on specimens and on a 3D model (holotype of *Oumtkoutia anae*), and literature (Estes, 1975; Trueb, 1999; Rage, 2008).

All analyses were performed using TNT v.1.5 (Goloboff and Catalano, 2016) under equal weights. All analyses were conducted with cline characters ordered

A new pipid from the Cretaceous of Africa (In Becetén, Niger) and early evolution of Pipidae

(characters 18, 32, 33, 36, 38, 39, 59, 74, 82, 97, 98, 120, 141, 149) in the analyses with or without topological constraint (Rineau et al., 2015; 2018). All analyses consisted of heuristic searches with 1000 random addition sequences of taxa, followed by tree bisection reconnection (TBR) branch swapping, holding 10 trees per repetitions. The final trees were rooted on *Ascaphus truei* (Ascaphidae), and when more than one most parsimonious tree was found, a strict consensus was obtained. Constrained analysis was performed using the topology of Jetz and Pyron (2018) for extant taxa (Fig. S1). Node supports were expressed using Bremer support and standard bootstrap, with traditional searches of 1000 replicates, collapsing groups below 5% frequency.

Nomenclatural typographic conventions

Throughout this paper, we use the following conventions for the writing of different kinds of nomina (scientific names):

[A] Nomina managed under the current International Code of Zoological Nomenclature are presented according to the following standard formats: italic lower-case letters for nomina of species and genera (e.g. *Inbecetenanura*, *Inbecetenanura ragei*)

[B] Nomina managed under the PhyloCode (following Recommendations 6.1A) are presented in bold italic lower-case letters (e.g., ***Pipidae***).

~ : but not.

∇ : clade.

RegNum registration number: registration number of the name definition on the RegNum website <https://www.phyloregnum.org>

III.4 Systematic Palaeontology

ANURA Duméril, 1805

XENOANURA Starrett, 1973 (= DORSIPARES Blainville, 1816)

PIPIMORPHA Ford and Cannatella, 1993

A new pipid from the Cretaceous of Africa (In Becetén, Niger) and early evolution of Pipidae

GONDWANOPIPIDAE Lemierre et al., nomen novum

PIPIDAE Gray, 1825

?PIPINOMORPHA Báez and Púgener, 2003

Genus *INBECETENANURA* gen. nov.

Type species—*Inbeceteanura ragei* nov. sp.

Diagnosis—As for the sole species.

Derivation of the name—The name *Inbeceteanura* is a combination of In Becetén, the type locality and “anura”, latin word for the clade regrouping frogs and toads.

INBECETENANURA RAGEI gen. nov. and sp. nov.

Unidentified genus and species: Báez and Rage, 1998 p. 680-684, text-figs 3H-K, pl. 1 : figs 8-11.

Holotype—One braincase with otic capsules (MNHN.F.IBC 1602).

Derivation of the name—Named after the late Dr. Jean-Claude Rage, palaeontologist from the MNHN, to honour his work on amphibian from Africa, including from In Becetén.

Stratigraphic range—Coniacian or Santonian (91,1 to 83,4 Ma).

Referred material—One presacral vertebra (MNHN.F.IBC 1650), four presacral centra (MNHN.F.IBC 1997a-d) and three sacrococcyges (MNHN.F.IBC 1972, 1973a, b).

Diagnosis—Pipid frog that differs from all other Pipidae in having the following combination of characters: (1) braincase heavily ossified, with frontoparietal and parasphenoid fused respectively ventrally and dorsally to sphenethmoid and prootics; (2) septum nasi fully ossified and projected anteriorly; (3) large optic foramen; (4) large lateromedially elongate prootic foramen; (5) foramen magnum dorsal and ventral

A new pipid from the Cretaceous of Africa (In Becetén, Niger) and early evolution of Pipidae

margins ossified; (6) lanceolate parasphenoid; (7) cultriform process of the parasphenoid extending anterior to the planum anteorbitale.

Differs from all Xenopodinomorpha by its heavily ossified skull, especially in the ethmoidal region; differs furthermore by having a shorter posterior extension of the parasphenoid, which ends at the mid-level of the otic capsules.

Differs from all other Pipinomorpha in having a rounded braincase in lateral view and large lateral expansions of the parasphenoid; differs also by lacking a superior perilymphatic foramen opening extracranially on the posterior surface of the prooticoccipital and lacking an anterolateral process of the sphenethmoid; differs furthermore in lacking crest on the dorsal surface of the otic capsules (exception for the epiotic eminence) for the insertion of the adductor mandibulae muscle.

Differs from *Pachycentrata taqueti* in lacking a vermicular ornamentation on the cranial dermal bones and lacking the posterior bony expansion of the prooticoccipital, located posterolaterally to the occipital condyles and in having ovoid occipital condyles.

A new pipid from the Cretaceous of Africa (In Becetén, Niger) and early evolution of Pipidae

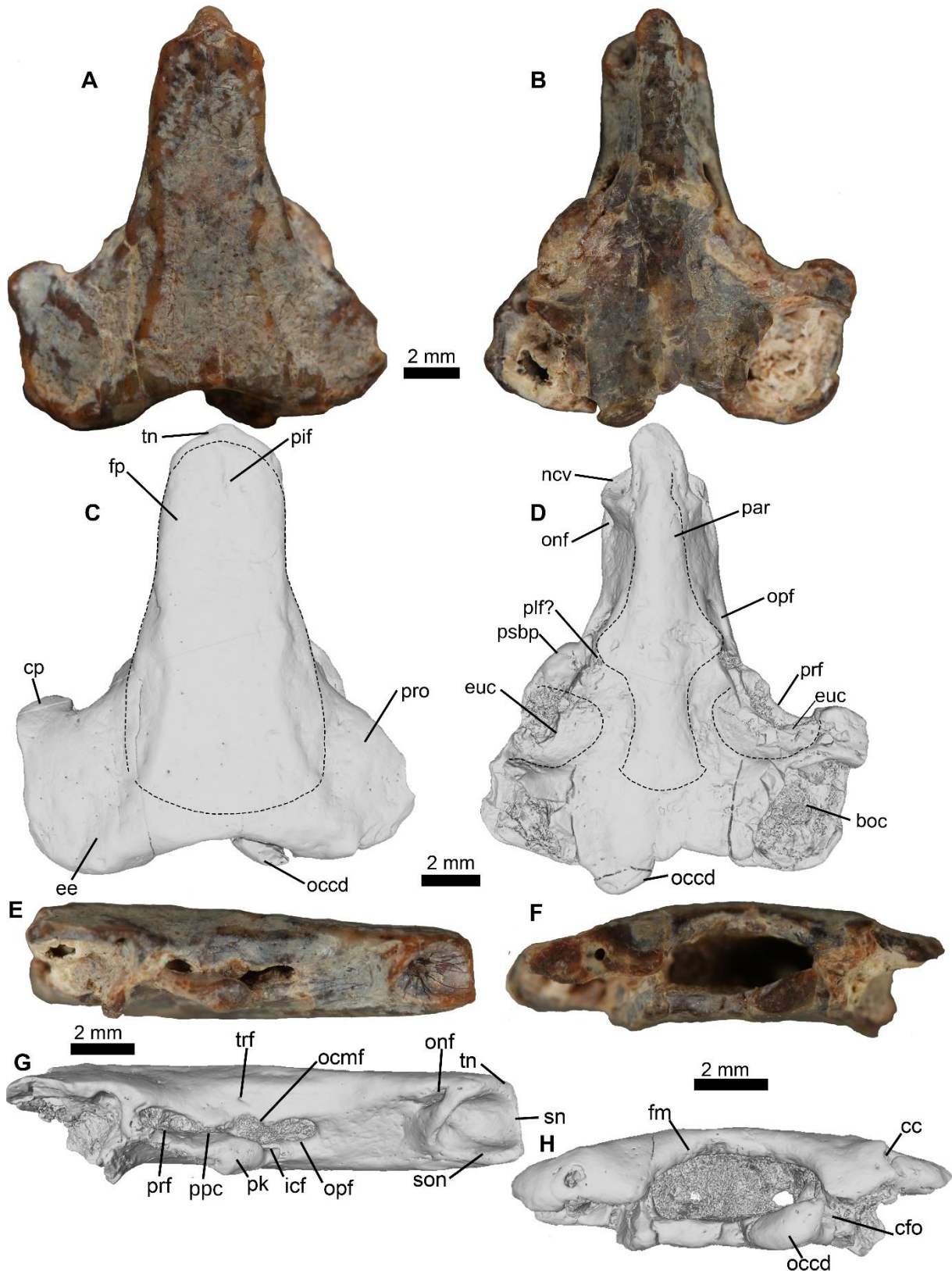


Figure III-2. Braincase of *Inbecetenanura ragei* sp. nov. (MNHN.F.IBC 1602, holotype). A–B, MNHN.F.IBC 1602 in A, dorsal and B, ventral views; C–D, 3D model of MNHN.F.IBC 1602 in C, dorsal and D, ventral views; E–F, MNHN.F.IBC 1602 in E, right lateral and F, posterior views; G–H, 3D model of MNHN.F.IBC 1602 in G, left lateral and H, posterior views.

A new pipid from the Cretaceous of Africa (In Becetén, Niger) and early evolution of Pipidae

Abbreviations: boc, broken remnants of otic capsule; cc, carotid canal; cfo, condyloid fossa; cp, crista parotica; ee, epiotic eminence; euc, eustachian canal; fm, foramen magnum; fp, frontoparietal; icf, internal carotid foramen; ncv, nasal cavity; occd, occipital condyle; ocmf, oculomotor foramen; onf, orbitonasal foramen; opf, optic foramen; par, parasphenoid; pif, pineal foramen; plf?, putative palatine foramen; ppc, prepalatine connection; prf, prootic foramen; pro, prootic; psbp, pseudobasal process; son, solum nasi; sn, septum nasi; tn, tectum nasi; trf, trochlear foramen. Dotted lines represent limits of frontoparietal, parasphenoid and Eustachian canals.

III.5 Results

Description of *Inbecetenanura ragei* sp. nov

The holotype is an incomplete braincase, with the following bones preserved: frontoparietals, sphenethmoid, parasphenoid, prootic and exoccipitals. The last two bones are fully fused together, forming a prooticooccipital complex. This braincase exhibits an intense hyperossification, with a fusion of all bones, leaving the sutures barely visible (Fig. III-2). In addition, several bones are strongly ossified, allowing the braincase to be fully enclosed in bone, with the lateral walls fully ossified except for several foramina (Fig. III-2). In lateral view, the braincase is rounded.

Frontoparietals—The frontoparietals are fully fused, without any trace of medial suture and forming an azygous bone. Hence, they will be referred to as a single bone in the description. The fusion to the neighbouring bones made its segmentation difficult. However, its margins are still distinguishable (Fig. III-2C). The anterior region of the frontoparietal is smaller than the posterior region, indicating a slight orbital constriction.

A new pipid from the Cretaceous of Africa (In Becetén, Niger) and early evolution of Pipidae

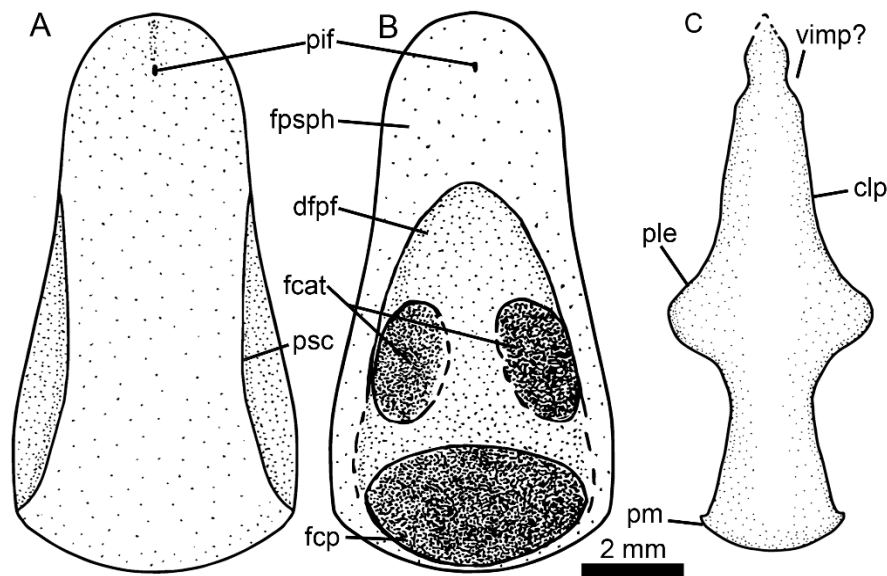


Figure III-3. Interpretative drawing and reconstruction of the frontoparietal and parasphenoid of *Inbecetenanura ragei* sp. nov. (based on MNHN.F.IBC 1602). Frontoparietal in A, dorsal and B, ventral views; C, parasphenoid in ventral view. Abbreviations: clp, cultriform process; dfpf, dorsal imprint of the fenestra frontoparietalis; fcat, facies cerebralis anterior; fcp, facies cerebralis posterior; fpsph, frontoparietal-sphenethmoid articulation area; pif, pineal foramen; pm, posterior margin; ple, posterolateral expansion; psc, parasagittal crest; vimp?, putative vomer imprint.

The frontoparietal is lacking anterodorsal, rostral and posterolateral processes (Figs. III-2A, 3A). In dorsal view, faint parasagittal crests are present on each side, delimiting a flat and smooth frontoparietal table (Figs. III-2C, 3A). On the frontoparietal table, several shallow pits are visible. They likely represent damage caused by taphonomy or diagenesis. Other artefacts, such as striations extending anteroposteriorly, are visible on the frontoparietal table (Fig. III-2E).

The anterior margin of the frontoparietal is convex. The bone covers most of the sphenethmoid, leaving only a small region visible in dorsal view (= tectum nasi in Fig. III-2A). This exposed region would have been covered by the nasals. On the anterior region of the frontoparietal, the pineal foramen is present in medial position (Fig. III-2A, E). On the dorsal surface of the frontoparietal, a shallow groove extends from the latter foramen up to the anterior margin of the bone. Posteriorly, the frontoparietal is

A new pipid from the Cretaceous of Africa (In Becetén, Niger) and early evolution of Pipidae

extended and covers most of the medial region of the prooticoccipital. The posterior margin of the bone is convex posteriorly.

In ventral view, the anterior region of the bone is smooth. It is delimited posteriorly by the fenestra frontoparietalis that occupies most of the ventral surface of the frontoparietal (Fig. III-3B). The anterior margin of the fenestra is convex. Midlength of the fenestra frontoparietalis, the facies cerebralis anterior (Jarošová and Roček, 1982) is a paired anteroposteriorly elongate ovoid imprints. Posteriorly, the facies cerebralis posterior is large and transversely elongate (Fig. III-3B). This configuration of incrustation frontoparietalis occurs in several extant and extinct pipids, like *Xenopus laevis* (Špinar, 1976) and *Shelania pascuali* (Báez and Púgener, 1998). This indicates that a taenia tecti transversalis was present as a cartilaginous element (Špinar, 1976; Jarošová and Roček, 1982).

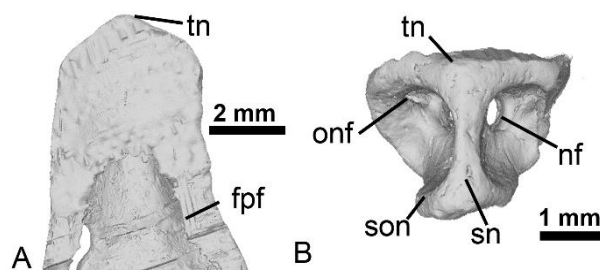


Figure III-4. 3D reconstruction of the anterior region of the sphenethmoid and parasphenoid of *Inbecetenanura ragei* sp. nov. (MNHN.F.IBC 1602). Model in A, dorsal and B, anterior views. Abbreviations: fpf, fenestra frontoparietalis; nf, nasal foramen; onf; orbitonasal foramen; sn, septum nasi; son, solum nasi; tn, tectum nasi.

Sphenethmoid—The sphenethmoid is a rhomboid bone. It is fused ventrally to the parasphenoid and posterolaterally to the prooticoccipital. Thus, the sphenethmoid forms the anterior and lateral walls and floor of the braincase.

In dorsal view, the anterior region of the bone is covered by the frontoparietal except for the tectum nasi. The latter is thick and strongly ossified (Fig. III-2A, C). The anterior margin of the frontoparietal fenestra is deeply concave anteriorly (Fig. III-4A). The solum nasi is thick (Fig. III-4).

A new pipid from the Cretaceous of Africa (In Becetén, Niger) and early evolution of Pipidae

The septum nasi is ossified and elongate anteroposteriorly (Fig. III-4B). Its anterior margin is broken but it likely projected anteriorly outside the braincase. This septum separates the two nasal cavities medially. Each nasal cavity is large and opens anterolaterally (Fig. III-4B). In each nasal cavity, two foramina (the orbitonasal foramina) are preserved. It opens externally into an anteroposteriorly elongated foramen on the lateral side of the sphenethmoid (Figs. III-2G, 4B). At the bottom of each nasal cavity, the nasal foramen is small and circular (Fig. III-4B). On the surface of the intern walls of the nasal cavities, shallow anteroposteriorly oriented striations are visible (Fig. III-2E). They likely resulted from diagenetic damages. No sella amplificans is present.

The sphenethmoid is ossified on all its length, fusing posteriorly with the prooticooccipital around the level of posterior margin of the optic foramen (Fig. III-2B, D). Posterior to the orbitonasal foramen, several anteroposteriorly oriented shallow striations are present on each lateral wall of the sphenethmoid. They likely represent diagenetic damages. Posteriorly, a large opening, the fused optic and oculomotor foramina, is present. This opening is elongate anteroposteriorly and constricted at midlength. This constriction is likely a remnant of the prepalatine connection, that separated optic and oculomotor foramina (Fig. III-2G). At the level of the oculomotor foramen, a small canal and internal carotid foramen are located media to the pseudobasal articulation. This foramen opens anteriorly (Fig. III-2G). Ventral to this foramen, a small circular foramen (putative palatine foramen) is present (Fig. III-2D). Dorsal to the oculomotor foramen, a small circular trochlear foramen is also present. In ventral view, the cultriform process of the parasphenoid covers most of the ventral surface of the bone (Figs. III-2D, 3C).

Prooticooccipital complex—The prooticooccipital is strongly ossified, without a trace of sutures between the different bones, forming one complex fused dorsally to the frontoparietal, and ventrally to the parasphenoid (Fig. III-2A- D). In dorsal view, the crista parotica is fully ossified, with an anterolateral expansion (Fig. III-2A, C). Except

A new pipid from the Cretaceous of Africa (In Becetén, Niger) and early evolution of Pipidae

for the epiotic eminence present medially on each side, there are no crests. Medially, both exoccipital are fused dorsally, forming a thin bridge that roofs the posteriormost portion of the braincase, posterior to the frontoparietal. Lateral to the prepalatine connection, the right pseudobasal process is anteroposteriorly elongated (Fig. III-2E, G).

In ventral view, a shallow depression is visible between the posterior margin of the pterygoid knob and the anterior margin of the otic capsules (Fig. III-2D). This depression seems to extend laterally into a small canal. This can be interpreted as the remnants of the Eustachian canals (Fig. III-2D). The otic capsules are crushed and broken, so almost no information can be recovered. However, the broken base of the anterior walls of the otic capsules shows that the capsules were elevated (Fig. III-2H). In posterior view, the foramen magnum is lateromedially wide (Fig. III-2F, H). The preserved right occipital condyle is dorsolaterally-ventromedially elongated. Judging by the putative position of the occipital condyles, they were not connected posteromedially. The occipital articulation should have been a Type II of Lynch, 1971. Laterally, and partially hidden in posterior view, a large condyloid fossa is preserved. Unfortunately, it is not possible to distinguish the jugular and inferior perilymphatic foramina. The carotid foramen is small and located on each side of the posterior margin of epiotic eminence (Fig. III-2H). It opens into a canal, extending anteromedially and exiting intracranially into the braincase.

Parasphenoid—This unpaired bone is fused to the surrounding elements and has been slightly crushed; its limits are hard to differentiate (Fig. III-2B, D). The parasphenoid is a lanceolate bone that lacks subotic alae.

The cultriform process extends anteriorly to the level of the nasal cavities, but it does not seem complete (Figs. III-2D, 3C). It narrows anteriorly, and likely ended into a pointed end. Posterior to the level of the orbitonasal foramen, the margin of the parasphenoid is difficult to discern, but the cultriform process seems to widen gradually up to the level of the optic foramen. The bone widens abruptly at the anterior

A new pipid from the Cretaceous of Africa (In Becetén, Niger) and early evolution of Pipidae

margin of the optic foramen, forming a large lateral expansion, occupying most of the ventral width of the braincase (Figs. III-2B, D; 3C). The cultriform process then narrows posterior to the anterior margin of the prootic foramen. The posterior margin of the parasphenoid is convex and slightly tapered (Figs. III-2D; 3C). This margin is located well anterior to the foramen magnum, at the mid-level of the otic capsules.

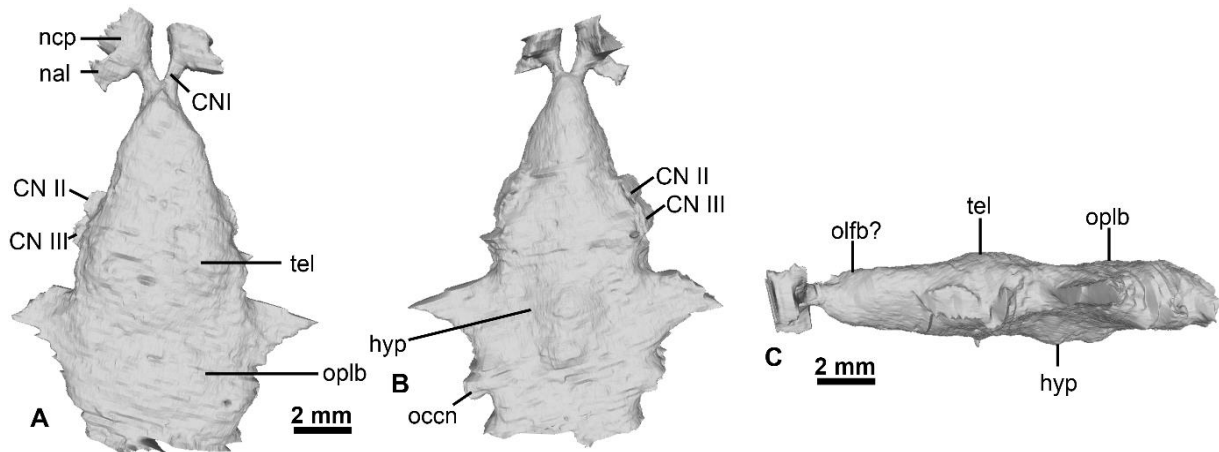


Figure III-5. 3D model of the endocast of the braincase of *Inbecetenanura ragei* sp. nov. (MNHN.F.IBC 1602). Model in A, dorsal, B, ventral and C, left lateral views. Abbreviations: CN I, olfactory nerves pathways; CN II, optic nerves pathways; CN III, oculomotor nerves pathways; hyp, hypothalamus; nal, orbitonasal duct; ncp, base of nasal capsule; occn, pathway for occipital nerves; olfb?, olfactory bulb ?; oplb, optic lobe; tel, telencephalon.

Endocast of the braincase—The preservation of the braincase allowed for the segmentation of most of its endocast, except the otic capsules region. In addition, most of details from the cranium region were not discernible, likely due to poor preservation of the bone. The pathway for the olfactory nerve (CN I) is very short anteroposteriorly (Fig. III-5A), and a barely discernible bulge ventral to the base of the CN I might be olfactory bulbs. The orbitonasal duct is short anteroposteriorly and flattened dorsoventrally. Both hemispheres of the telencephalon diverge (from each other) and protrude posteriorly (Fig. III-5A, C). They are elongate anterolaterally, and their impressions on both endocast and frontoparietal are small (Figs. III-3B, 5A). Lateral to the telencephalon, both optic and oculomotor nerves pathways (respectively CN II and CN III) are present (Fig. III-5A, C). Posterior to the telencephalon no cranial nerves are discernible at the level of the prootic foramen (Fig. III-5A, B). The optic lobe is an ovoid

A new pipid from the Cretaceous of Africa (In Becetén, Niger) and early evolution of Pipidae

bulge elongate transversally. Anterior to the optic lobe, the hypothalamus is protruding as two small ovoid bulges on the ventral surface of the endocast (Fig. III-5B, C). A partial pathway for the occipital nerves is preserved on the right side (Fig. II-5B). These nerves exit the skull via the condyloid fossa.

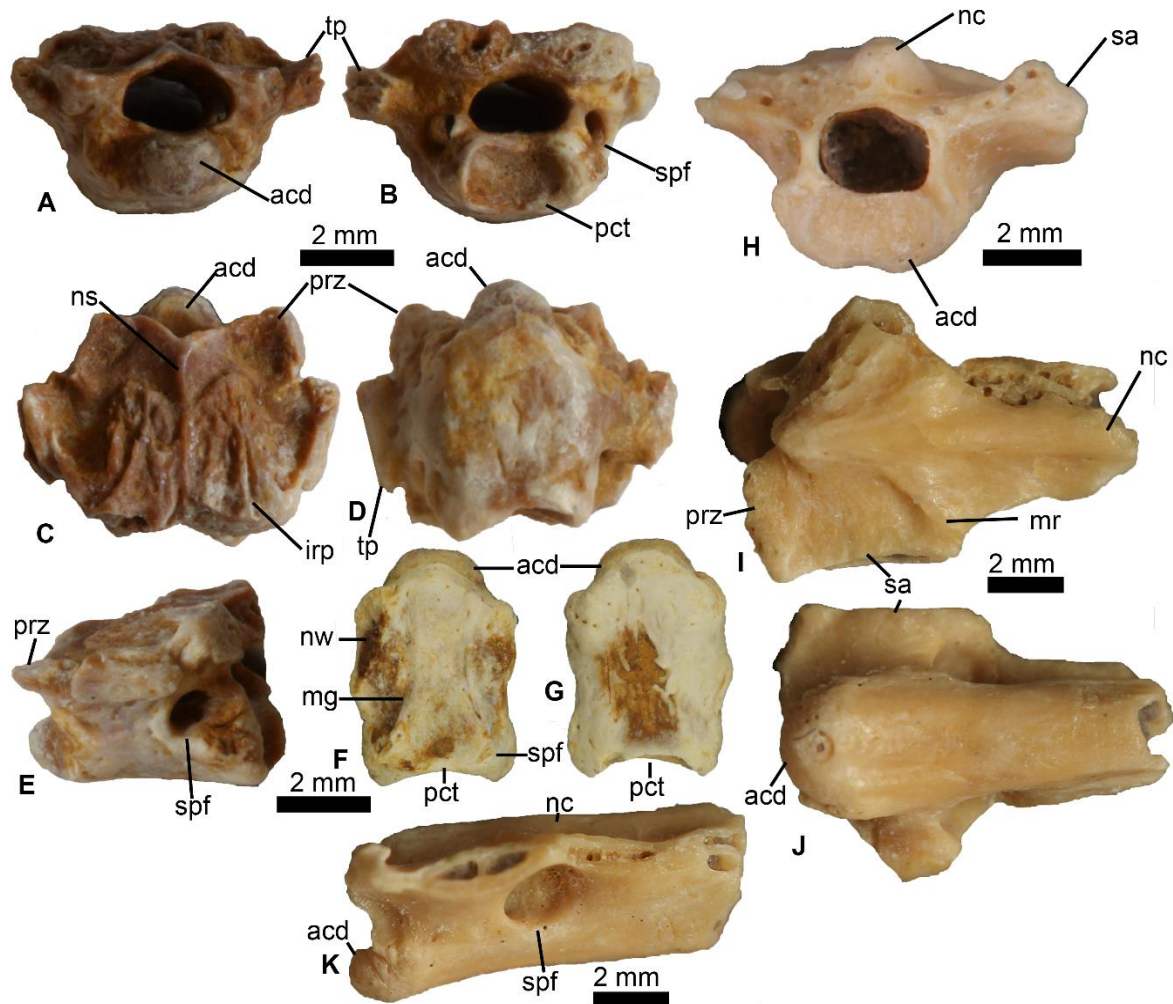


Figure III-6. Vertebral elements of *Inbecetenanura ragei* sp. nov. A–E, presacral vertebra (MNHN.F.IBC 1650) in A, anterior, B, posterior, C, dorsal, D, ventral and E, right lateral views; F–G, presacral centrum (MNHN.F.IBC 1997a) in F dorsal and G ventral views; H–K, sacrococcyges (MNHN.F.IBC 1972) in H, anterior, I, dorsal, J, ventral and K, left lateral views. Abbreviations: acd, anterior condyle; irp, irregular projection; mg, medial groove; mr, medial ridge; nc, neural crest; ns, neural spine; nw, neural wall; pct, posterior cotyle; prz, prezygapophyse; sa, sacral apophyse; spf, spinal foramen; tp, transverse process.

Vertebral column

A new pipid from the Cretaceous of Africa (In Becetén, Niger) and early evolution of Pipidae

Presacral vertebrae—MNHN.F.IBC 1650 is opisthocoelous and bears a well individualized but low neural spine (Fig. III-6A-E). The anterior condyle is dorsoventrally compressed and protrudes anteriorly. A small shallow depression is present on each side of this anterior projection. The vertebral canal is large and oval. Such as the cotyle, the condyle is also dorsoventrally compressed (Fig. III-6B). Lateral to the vertebral canal, a large spinal foramen opens posterolaterally on each side of the neural walls (Fig. III-6B, E).

In dorsal view, the prezygapophysis is rectangular and bear a flat dorsally oriented articular surface (Fig. III-6C). The anterior region of MNHN.F.IBC 1650 is smooth, except for a thin neural ridge. The anterior margin of the dorsal surface bears a medial notch. The postzygapophyses are not preserved, but they were located close to the medial region of the vertebral canal.

Posteriorly, the dorsal surface of the neural arch is covered by irregular ridges on both sides of the neural spine. The neural spine is very low and reduced to a thin ridge that projects posteriorly. Its posterior end is not preserved (Fig. III-6C). With the presence of the notch on the anterior margin, this indicate that neural spines overlapped each other, and vertebrae were imbricated. There is no anteroposterior grooves nor bone deposits on the ventral surface (Fig. III-6D). The transverse processes are broken at their base (Fig. III-6A-E). The base of the processes is dorsoventrally flattened.

Four centra bearing an anterior condyle compressed dorsoventrally and a wide posterior cotyle are also attributed to *Inbecetenanura* (Fig. III-6F). Shallow depressions are present on each side of the anterior condyle (Fig. III-6F). In dorsal view, the neural walls do not extend on the whole length of the centrum, leaving a posterior opening. Medially, the opening extends into a shallow medial groove that extends anteriorly towards the anterior condyle. The groove can be interpreted as the canal for the spinal nerve. Broken bases of bony walls within the centra indicates that a spinal foramen was present. The centra thus share sufficient similarities with MNHN.F.IBC 1650 to be referred to the same taxon.

A new pipid from the Cretaceous of Africa (In Becetén, Niger) and early evolution of Pipidae

Sacrococcyges—Three incomplete sacrococcyges (fused sacral vertebra and urostyle), MNHN.IBC 1972, 1973a, b are attributed to *Inbecetenanura*.

The anterior condyle is compressed dorsoventrally and protrudes anteriorly. The vertebral canal is subrectangular and wide (Fig. III-6G). There is no sign of bone accretion on the anterior surface of the bone. On the best-preserved specimen, the posterior region of the left prezygapophysis (MNHN.F.IBC 1972; Fig. III-6H) is preserved and shows that the articular surface is flat and subrectangular. The neural crest (fusion of the neural spine of the sacral vertebra and the dorsal crest of the urostyle) is low. It is present on the whole length of the sacrococcyges fragments (Fig. III-6H). Anteriorly, a deep sagittal notch opens on the neural arch. This indicates that the sacrococcyx was imbricated with the preceding presacral vertebra. The sacral apophyses are broken at their bases. Nevertheless, the apophyses were obviously large and anteroposteriorly expanded. A thin oblique medial ridge is present on each side of the neural crest. It extends posterolaterally following the posterior margin of the sacral apophyses (Fig. III-6H). Shallow longitudinal grooves are present on the ventral surface in MNHN.F.IBC1973 and may correspond to more mature individual (as in *Pachycentrata*, Báez and Rage, 1998).

In lateral view, a single large spinal foramen is present (Fig. III-6J, K). This indicates that only the sacral vertebra and urostyle are incorporated into the sacrococcyges. The two remaining sacrococcyges (MNHN.F.IBC 1973a, b) are very incomplete, preserving the anteriormost portion of the element. However, they are similar to MNHN.F.IBC 1972 in bearing (1) a low neural crest; (2) a thin oblique medial ridge on each side of the neural crest. They are all attributed to the same taxon.

Discussion

The braincase of *Inbecetenanura* (MNHN.F. IBC1602) can be referred to pipids in (1) having orbitonasal foramina fully enclosed in bone; (2) having a lanceolate parasphenoid lacking subotic alae; (3) having optic foramina fully enclosed in bone;

A new pipid from the Cretaceous of Africa (In Becetén, Niger) and early evolution of Pipidae

(4) having an azygous frontoparietal (also present in numerous anuran clades) and (5) having fused parasphenoid and braincase. This braincase can be differentiated from *Pachycentrata* in (1) lacking pachyosteosclerosis, (2) lacking vermicular ornamentation on its dorsal surface; (3) lacking anterolateral process on the frontoparietal; (4) having ovoid occipital condyles (crescent shaped in *Pachycentrata*); (5) having a rounded braincase in lateral view (wedge-shaped in *Pachycentrata*). It can also be differentiated from *Eoxenopoides* in (1) having a heavily ossified skull with large fusion of frontoparietal, braincase and parasphenoid (all bones are sutured together and not fused in *Eoxenopoides*); (2) having a rounded posterior margin of the frontoparietal (pointed in *Eoxenopoides*); (3) having parasagittal crests; (4) having an ossified anterior region of the prooticooccipitals and (5) having a posterior end of the parasphenoid well anterior to the ventral margin of the foramen magnum. *Inbecetenanura* also differs from *Oumtkoutia* in (1) having parasagittal crest on its frontoparietal; (2) having a large pseudobasal process; (3) having ovoid occipital condyles and (4) not having the frontoparietal narrowing anteriorly.

As mentioned in its original description ('Unidentified genus and species' in Báez and Rage, 1998: [680-684]), *Inbecetenanura* resembles '*Xenopus*' *romeri* in having (1) highly ossified ethmoidal region; (2) anteriorly extended ossified septum nasi; (3) large pseudobasal process anterior to the Eustachian canal; (4) cultriform process of the parasphenoid extending anterior to the nasal cavities level; (5) pineal foramen anterior on the frontoparietal and (6) crista parotica lacking dorsal crest. However, *Inbecetenanura* differs from '*Xenopus*' *romeri* in (1) lacking anterolateral process on the frontoparietal and in having (2) ovoid occipital condyles; (3) a posterior margin of the parasphenoid well anterior to the ventral margin of the foramen magnum; (4) a broader anterior region of the cultriform process and (5) a wider foramen magnum. The posterior cotyle of MNHN.F.IBC 1650 (a presacral vertebra; Fig. III-6B) match relatively well in shape and size to the anterior condyle of MNHN.F.IBC 1972 and 1973 (sacrococcyges, Fig. III-6H). In addition, the prezygapophyses of the presacral vertebra

A new pipid from the Cretaceous of Africa (In Becetén, Niger) and early evolution of Pipidae

(Fig. III-6C) and the ones preserved on the sacrococcyx (Fig. 6I) all have flat and subrectangular articular facets. The inferred position of the postzygapophyses in MNHN.F.IBC 1650 (Fig. III-6C) correspond to the position of the prezygapophyses in MNHN.F.IBC 1972 (Fig. III-6I). For these reasons, we here interpret and decide to attribute the presacral vertebra and the two sacrococcyx to the same taxon, *Inbecetenanura ragei* sp. nov. The presence of opisthocoelous vertebrae and sacrococcyx is characteristic of pipids (Gómez, 2016). The presence of large spinal foramen on presacral vertebrae is uncommon in mature anurans. Its presence is usually a marker of immaturity (Duelleman and Trueb, 1994) except in several extinct pelobatids retaining large spinal foramina in the adult stage (Sanchiz and Mlynarski, 1979; Augé et al., 1997; Rage and Augé, 2015). In pipids, this is known in Xenopodines, but only on the atlantal complex (Cannatella and Trueb, 1998). The presence of irregular ridges on the dorsal surface of the presacral vertebrae is also known in '*Xenopus*' *stromeri* (Rage, 2008). This combination of vertebral characters appears to be unique within Anura (at least within Xenoanura). Presacral vertebra MNHN.F.IBC 1650 and sacrococcyges MNHN.F.IBC 1972, 1973a, b are lacking the vermicular ornamentation and pachyostosis present in *Pachycentrata taqueti*. The sacrococcyges also bear a single pair of spinal foramina (two pairs of spinal foramina in *P. taqueti*). The vertebrae and sacrococcyges described here cannot therefore be attributed to *P. taqueti*. Association between the postcranial bones and the braincase of *Inbecetenanura* is not directly possible because they have not been found in connexion. However, it would be unlikely that two distinct pipid taxa, one known by cranial elements, the second by postcranial elements, are present in In Becetén (in addition to *Pachycentrata*). Therefore, we here tentatively attribute the vertebrae, sacrococcyges and cranial elements to *Inbecetenanura ragei* based on circumstantial evidence. Nevertheless, due to this uncertainty of the attribution of the vertebral elements to *Inbecetenanura ragei*, we based the diagnosis of *Inbecetenanura ragei* only on its braincase.

A new pipid from the Cretaceous of Africa (In Becetén, Niger) and early evolution of Pipidae

To sum up, we attribute the presacral vertebra MNHN.F.IBC 1650, the four presacral centra MNHN.F.IBC 1997a–to 1997d and three sacrococcyges MNHN.F.IBC 1972, and 1973a and 1973b as well as the braincase MNHN.F.IBC 1602 to *Inbecetenanura ragei* sp. nov.

?*INBECETENANURA*

Cranial bones—Three incomplete sphenethmoids are tentatively referred to *Inbecetenanura*: MNHN.F.IBC 1969a, b, 2061.

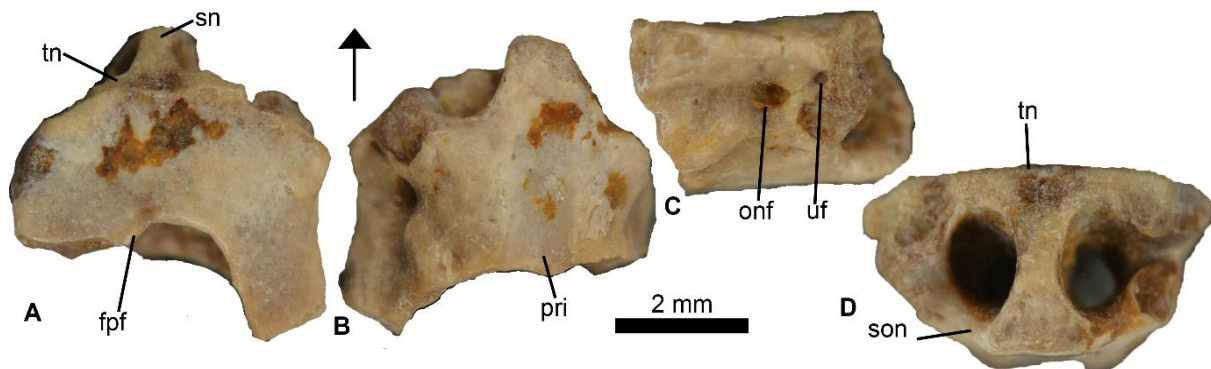


Figure III-7 Sphenethmoid of *Inbecetenanura*? Sphenethmoid (MNHN.F.IBC 1969a) tentatively assigned to *Inbecetenanura* gen. nov. in **A**, dorsal, **B**, ventral and **C**, right lateral views. **Abbreviations:** **fpf**, fenestra frontoparietalis; **onf**, orbitonasal foramen; **pri**, parasphenoid imprint; **sn**, septum nasi; **tn**, tectum nasi.

They bear a bony septum nasi that seems to project anteriorly (Fig. III-7A, C). Their orbitonasal foramina are fully enclosed in bone (Fig. III-7). They are small and anteroposteriorly elongated. On the dorsal surface of the sphenethmoids, the anterior margin of the fenestra frontoparietalis is deeply concave anteriorly (Fig. III-7A). In ventral view, the parasphenoid imprint shows that the cultriform process of the parasphenoid narrows anteriorly and is extended anteriorly, past the orbitonasal foramina (Fig. III-7B). The nasal cavities are large and elongate laterally (Fig. III-7D). A small circular foramen is present anterior to the orbitonasal foramen (Fig. III-7C). It opens within the nasal cavity, but its function is unknown.

A new pipid from the Cretaceous of Africa (In Becetén, Niger) and early evolution of Pipidae

Discussion and attribution—Enclosure of the orbitonasal foramen in bone is characteristic of pipids. The shape and size of this foramen is consistent with the one of *Inbecetenanura* (holotype specimen, MNHN.F.IBC 1650). In addition, the parasphenoid imprint matches the shape of the parasphenoid recovered in *Inbecetenanura* (Fig. III-2D). The sphenethmoids are distinct from the sphenethmoid of *P. taqueti* in lacking ventral ornamentation. These elements could be referred to *Inbecetenanura*, but their poorly preserved stage and the fact that they are disarticulated (see below) render the attribution questionable.

The presence of isolated sphenethmoids are puzzling. In *Inbecetenanura* and *P. taqueti* the sphenethmoid is fused to the rest of the braincase. Disarticulated sphenethmoids could pertain to immature specimens, but they are at least as large as that of *Inbecetenanura*. This could indicate either that the holotype of *Inbecetenanura*, MNHN.F.IBC 1602, belongs to a small individual, or that these sphenethmoids belong to a third taxon from Ibeceten.

III.6 Nomenclatural Note

Báez and Púgener (2003: 454) erected the taxa Pipinomorpha and Xenopodinomorpha and provided the following phylogenetic definition for the former: “Pipinomorpha includes Pipinae and fossil taxa, as *Eoxenopoides* according to this analysis, more closely related to this crown group than to Xenopodinae.”. Báez and Púgener (2003) did not define explicitly Xenopodinomorpha or Pipinae, but they provided this additional information that allows to infer their intent (Báez and Púgener, 2003: 454): “Pipidae comprises two clades for which we propose the stem-based names Pipinomorpha and Xenopodinomorpha”. Thus, it is clear that Pipidae was conceptualized as a crown-group, while Pipinomorpha and Xenopodinomorpha must be total groups to preserve the arrangement Pipidae = Pipinomorpha + Xenopodinomorpha. Their topology was based on a morphological analysis that incorporated many extinct taxa; it is thus

A new pipid from the Cretaceous of Africa (In Becetén, Niger) and early evolution of Pipidae

comparable to our unconstrained analysis, notably in placing Hymenochirini closer to *Pipa* than to *Xenopus*. Thus, Báez and Púgener (2003: fig. 13) included Hymenochirini in Pipinae. Under our constrained analysis, as in molecular phylogenies of pipids (Frost et al., 2006; Cannatella, 2015), the taxon Hymenochirini is closer to *Xenopus* than to *Pipa*.

In order to apply the names Xenopodinomorpha and Pipinomorpha in the context of our constrained analysis (and of recent molecular phylogenies), it is necessary to reformulate slightly the phylogenetic definitions. In conformity with the recommendations of Taylor (2007), we attempt to capture as best as we can the intent of Báez and Púgener (2003: 454) while keeping in mind the requirements of the PhyloCode (Cantino and de Queiroz, 2020). We also consider the updated phylogenetic context provided by many molecular phylogenies published since 2003, which show that the position of Hymenochirini differs between trees based on morphological data, which place Hymenochirini close to *Pipa*, and trees based on molecular data, which place Hymenochirini close to *Xenopus*. Given that the names Xenopodinomorpha and Pipinomorpha derive from *Xenopus* and *Pipa* respectively, their phylogenetic definition should be based on the type-species of these two nominal genera, in conformity with Article 11.10 of the PhyloCode (Cantino and de Queiroz, 2020). We therefore suggest the following phylogenetic definition of Pipidae, Xenopodinomorpha and Pipinomorpha:

Pipidae Gray, 1825, converted clade name

RegNum registration number : 809

Definition—Pipidae is the smallest clade that includes *Xenopus laevis* Daudin 1802 and *Pipa pipa* Linnaeus 1758. Abbreviated definition: min crown ∇ (*Xenopus laevis* Wagler, 1827 and *Pipa pipa* Linnaeus, 1758).

Etymology—Named after the eponym genus *Pipa*.

A new pipid from the Cretaceous of Africa (In Becetén, Niger) and early evolution of Pipidae

Reference phylogeny—The primary reference phylogeny is the equal weight unconstrained analysis from this study (Fig. III-8). Other reference phylogenies include the equal weight constrained analysis from this study (Fig. III-9), Báez et al (2007: fig. 6), Gómez (2016: fig. 5), Aranciaga Rolando et al (2019: fig. 4) and Cannatella (2015: fig. 3).

Composition—Under unconstrained morphological analyses (Fig. III-8), which were published in most paleontological studies of Pipidae, it includes the extant *Xenopus* Wagler, 1827, *Silurana* Gray, 1864, *Pipa* Linnaeus, 1758, *Hymenochirus* Boulanger, 1896, *Pseudhymenochirus* Chabanaud, 1960 and the extinct '*Xenopus*' *stromeri* Ahl, 1926, *Eoxenopoides* Haughton, 1931, *Singidella* Báez and Harrison, 2005, *Oumtkoutia* Rage and Dutheil, 2008, *Pachycentrata* Báez and Rage, 2004 and *Inbecetenanura* nov. gen. Under molecular-based or constrained analyses (Fig. III-9), this clade could encompass all above taxa and the extinct *Saltenia* Reig, 1959, *Shelania* Casamiquela, 1960, '*Xenopus*' *romeri* Estes, 1975, '*Shelania*' *laurenti* Báez and Púgener, 1998, *Llankibatrachus* Báez and Púgener, 2003, *Kuruleufenia* Gómez, 2016 and *Patagopipa* Aranciaga Rolando et al., 2019.

Diagnostic apomorphies—Under unconstrained morphological analyses, *Pipidae* is supported by a combination of five non-unique synapomorphies: (1) parasphenoid fused to the braincase; (2) antorbital process of the maxilla absent or weakly developed; (3) posteromedial margin of neural arches of posterior presacral vertebrae slightly concave to straight; (4) transverse process of the sixth vertebra markedly forward and (5) fused ilium and ischium. Under constrained morphological analyses, *Pipidae* is supported by a combination of nine non-unique synapomorphies: (1) anterior process of the pterygoid dorsal to the maxilla; (2) antorbital process of the maxilla absent or weakly developed; (3) sphenethmoid fused to the frontoparietal; (4) posterior margin of the frontoparietal rounded; (5) presacral vertebrae squared (as wide as long) in dorsal view; (6) distal margin of the sacral apophyses straight; (7)

A new pipid from the Cretaceous of Africa (In Becetén, Niger) and early evolution of Pipidae

neural arch of the sacrum longer than wide; (8) anterior and posterior processes of the sacral apophyses tapered and (9) an interiliac scar ample both ventrally and dorsally.

Xenopodinomorpha Báez and Púgener, 2003, converted clade name

RegNum registration number :810

Definition—*Xenopodinomorpha* is the largest clade that includes *Xenopus laevis* Daudin 1802 but not *Pipa pipa* Linnaeus 1758. Abbreviated definition : max total ∇ (*Xenopus laevis* Daudin, 1802 and ~ *Pipa pipa* Linnaeus, 1758).

Etymology—Named after the eponym genus *Xenopus*.

Reference phylogeny—The primary reference phylogeny is the equal weight unconstrained analysis from this study (Fig. III-8). Other reference phylogenies include the equal weight constrained analysis from this study (Fig. III-9), Báez et al (2007: fig. 6), Gómez (2016: fig. 5), Aranciaga Rolando et al (2019: fig. 4) and Cannatella (2015: fig. 3).

Compositions—Under unconstrained morphological analyses, which were published in most paleontological studies of this taxon, the clade includes *Xenopus* Wagler, 1827 and *Silurana* Gray, 1864. Under molecular-based or constrained analyses (Fig. 9), this clade could encompass the extant *Xenopus* Wagler, 1827, *Silurana* Gray, 1864, *Hymenochirus* Boulanger, 1896, *Pseudhymenochirus* Chabanaud, 1960 and the extinct *Patagopipa* Aranciaga Rolando et al., 2019, '*Xenopus*' *stromeri* Ahl, 1926, *Shelania* Casamiquela, 1960, '*Shelania*' *laurenti* Báez and Púgener, 1998, *Eoxenopoides* Haughton, 1931, *Inbecetenanura* nov. gen., *Pachycentrata* Báez and Rage, 2004, *Singidella* Báez and Harrison, 2005, '*Xenopus*' *romeri* Estes, 1975, *Saltenia* Reig, 1959, *Kuruleufenia* Gómez, 2016, *Oumtkoutia* Rage and Dutheil, 2008 and *Llankibatrachus* Báez and Púgener, 2003.

Diagnostic apomorphies—Under unconstrained morphological analyses, *Xenopodinomorpha* (redundant with Xenopodines) is supported by a combination of fifteen non-unique synapomorphies, (1) an anterior process of the pterygoid reaching the level of the antorbital plane; (2) zygomatic process of the squamosal well

A new pipid from the Cretaceous of Africa (In Becetén, Niger) and early evolution of Pipidae

developed and articulating with the maxilla; (3) absence of teeth on maxillary arcade; (4) anterior margin of the frontoparietal window of the sphenethmoid not delimited in bone; (5) margin of olfactive foramina incompletely bound in bone; (6) margin of orbitonasal foramina incompletely bound in bone; (7) inferior perilymphatic foramen of the otic capsules opening extracranially posterior to the jugular foramen; (8) presence of a posteroventral process ventrolateral to the condyloid fossa; (9) articular facets of the postzygapophyses of the presacral vertebrae with grooves and ridges; (10) neural arch of the sacrum longer than wide; (11) medial end of clavicles expanded medially; (12) short scapula (glenoid fossa wider than maximum width of the shaft); (13) dorsal prominence of the ilium very high; (14) dorsal prominence asymmetrical, with posterior margin convex and anterior margin steep and highly concave and (15) dorsal prominence around the level of the anterior margin of the acetabular fossa. Under constrained morphological analyses, *Xenopodinomorpha* is supported by a combination of four non-unique synapomorphies: (1) presence of parasagittal crests on the frontoparietal table; (2) anterior margin of the frontoparietal window of the sphenethmoid not delimited in bone; (3) inferior perilymphatic foramen of the otic capsules opening extracranially ventral to the jugular foramen and (4) absence of superior perilymphatic foramen.

Pipinomorpha Báez and Púgener, 2003, converted clade name

RegNum registration number :811

Definition—Pipinomorpha is the largest clade that includes *Pipa pipa* Linnaeus 1758 but not *Xenopus laevis* Daudin 1802. Abbreviated definition: max total ∇ (*Pipa pipa* Linnaeus, 1758 and \sim *Xenopus laevis* Daudin, 1802).

Etymology—Named after the eponym genus *Pipa*.

Reference phylogeny—The primary reference phylogeny is the equal weight unconstrained analysis from this study (Fig. III-8). Other reference phylogenies

A new pipid from the Cretaceous of Africa (In Becetén, Niger) and early evolution of Pipidae

include the equal weight constrained analysis from this study (Fig. III-9), Báez et al (2007: fig. 6), Gómez (2016: fig. 5), Aranciaga Rolando et al (2019: fig. 4).

Compositions—Following morphological based unconstrained analyses (Fig. 8), this clade could include the extant *Pipa* Linnaeus, 1758, *Hymenochirus* Boulanger, 1896 and *Pseudhymenochirus* Chabanaud, 1960 and the extinct *Eoxenopoides* Haughton, 1931, *Inbecetenanura* nov. sp., *Pachycentrata* Báez and Rage, 2004, *Singidella* Báez and Harrison, 2005, *Oumtkoutia* Rage and Dutheil, 2008 and '*Xenopus*' *stromeri* Ahl, 1926. According to phylogenies based on molecular data or phylogenies based on morphological data but constrained by the molecular topology, this clade includes only *Pipa* Linnaeus, 1758.

Diagnostic apomorphies—Under unconstrained morphological analyses, *Pipinomorpha* is supported by a non-unique synapomorphy, the loss of a distinct pterygoid knob on the basal process of the otic capsule. Under constrained morphological analyses, *Pipinomorpha* (redundant with Pipinae) is supported by a combination of fourteen non-unique synapomorphies: (1) a well-developed premaxilla; (2) absence of inferior perilymphatic foramen on the otic capsule; (3) occipital condyles with flat and circular articular facet; (4) occipital condyles with posterolaterally oriented articular facet; (5) cranio-quadrate passage, exit foramen completely bound by the prootic; (6) posteromedial margin of neural arches of posterior presacral vertebrae deeply notched; (7) a dorsal ridge of the urostyle present and moderately to well-developed; (8) absence of medial notch of the scapula; (9) posterolateral expansion of the epicoracoids cartilages surpassing the lateral margin of the sternum; (10) absence of a parietal crest (= crista paraventralis) on the humerus; (11) distal region of the ilial shaft flattened, and compressed dorsoventrally; (12) dorsal crest of the ilium directed laterally; (13) presence of longitudinal crests on tibiale and fibulare and (14) absence of prehallux.

This set of three definitions forms a node-stem triplet (as defined by Sereno, 1998) that preserves the intended nomenclature of Báez and Púgener (2003: 454),

A new pipid from the Cretaceous of Africa (In Becetén, Niger) and early evolution of Pipidae

namely that Pipidae includes (only) two clades, Xenopodinomorpha and Pipinomorpha.

A recent study by Aranciaga Rolando et al. (2019) retrieved several pipimorphs as a clade, placed as the sister-group of Pipidae. To accommodate these relationships, they erected the names Shelaniinae (for the new clade) and Panpipidae (as Shelaniinae + Pipidae and others taxa). They provided the following definitions : Panpipidae as “the stem-based clade consisting of *Patagopipa* and all species that share a more common ancestor with *Shelania laurenti*, *Pipa*, and *Xenopus laevis* than with *Vulcanobatrachus mandelai*, *Avitabatrachus uliana*, *Cordicephalus gracilis*, or *Palaeobatrachus grandipes*” and Shelaniinae as “The stem-based clade consisting of *Patagopipa* and all species that share a more common ancestor with *Shelania laurenti* than with *Pipa*, *Silurana*, *Xenopus*, or *Eoxenopoides*”. Their topology (Aranciaga-Rolando et al., 2019: fig. 4) was based on a morphological analysis that incorporated many extinct taxa; it is thus comparable to our unconstrained analysis, notably in placing Hymenochirini closer to *Pipa* than to *Xenopus*, and recovering several extinct pipids as pipinomorphs. However, both definitions include the taxon ‘*Shelania laurenti*’ as an internal specifier. This taxon is not the type-species of *Shelania* Casamiquela, 1960; rather, the type-species is *Shelania pascuali* Casamiquela, 1960. Thus, neither definition follows Article 11.10 of the PhyloCode (Cantino and de Queiroz, 2020).

In addition, the use of the prefix ‘Pan’, according to Articles 10.3 and 10.5 of the PhyloCode, should be reserved for total clades, which are delimited by extant clades. Thus, the name Pan-pipidae should be used to defined the total-group of Pipidae rather than the crown-group Pipidae and part of its stem-group (as proposed by Aranciaga Rolando et al., 2019). This means that Pan-pipidae would correspond to the definition proposed by Ford and Cannatella (1993: 104) for Pipimorpha : “We define the new stem-based name Pipimorpha to be those taxa that are more closely related to living Pipidae than to living *Rhinophrynus*”. Articles 10.1 and 10.2 of the PhyloCode indicate that clades names can either be converted (from a pre-existing name) or

A new pipid from the Cretaceous of Africa (In Becetén, Niger) and early evolution of Pipidae

established. Regarding total clades, if a name needs to be established, the prefix “Pan-” needs to be used (Article 10.3), as within Pan-Pipidae. However, Article 10.6 states that “If there is a pre-existing name that has been applied to a particular total clade, that name may be converted or a panclade name may be established instead” (the choice is left to the discretion of the authors; following Recommendation 10.1). As Pipimorpha was clearly established as a total (stem-based) clade by its authors, we chose to convert Pipimorpha as the total clade of Pipidae. Similarly, we prefer to define the names *Xenopodinomorpha* and *Pipinomorpha* (which were clearly conceptualized as total clades by their authors) in conformity with the PhyloCode than to erect panclade names for these total clades. We note that these names have been used several times since these taxa were erected (*Pipimorpha*, *Xenopodinomorpha* and *Pipinomorpha* respectively yield 77, 15, and 11 references in Google Scholar, as of March 29, 2022), which is one of the justifications for our choice.

Thus, we propose an emended definition of Shelaniinae and Pipimorpha. In addition, we also propose a replacement name for Pan-Pipidae, Gondwanopipidae, and propose the following definitions:

Pipimorpha Ford and Cannatella, 1993, converted clade name

RegNum registration number : 812

Definition—The total clade composed of the crown clade *Pipidae*, and all extinct organisms or species that share a more common ancestor with *Pipidae* than with any extant taxa that are not members of *Pipidae*. Abbreviated definition: total ∇ of *Pipidae*.

Etymology—Combination of the clade name “Pipidae” and “morpha”, derived from the Greek “morphé” meaning shape, appearance.

Reference phylogeny—The primary reference phylogeny is the equal weight unconstrained analysis from this study (Fig. III-8). Other reference phylogenies include the equal weight constrained analysis from this study (Fig. III-9), Báez et al

A new pipid from the Cretaceous of Africa (In Becetén, Niger) and early evolution of Pipidae

(2007: fig. 6), Gómez (2016: fig. 5), Aranciaga Rolando et al (2019: fig. 4) and Cannatella (2015: fig. 3).

Composition. Pipimorpha includes the extant *Xenopus* Wagler, 1827, *Pipa* Linnaeus, 1758, *Hymenochirus* Boulenger, 1896, *Pseudhymenochirus* Chabanaud, 1920 and *Silurana* Gray, 1864. It also (currently) includes the extinct *Aygroua* Jones et al., 2003, *Neobatrachus* Mahony, 2019, *Thoraciliacus* Nevo, 1968, *Cratopipa* Carvalho et al., 2019, *Avitabatrachus* Báez et al., 2000, *Vulcanobatrachus* Trueb et al., 2005, *Neusibatrachus* Seiffert, 1972, *Gracilibatrachus* Báez, 2013, *Pachycentrata* Báez and Rage, 2004, *Inbecetenanura* Lemierre et al., gen. nov., *Singidella* Báez and Harrison, 2005, '*Xenopus*' *romeri* Estes, 1975, '*Xenopus*' *stromeri*, Ahl, 1926, *Shelania* Casamiquela, 1960, '*Shelania*' *laurenti* Báez and Púgener, 1998, '*Xenopus*' *hasaunus* Špinar, 1978, *Shomronella jordanica* Estes et al., 1978, *Oumtkoutia* Rage and Dutheil, 2008, *Eoxenopoides* Haughton, 1931, *Llankibatrachus* Báez and Púgener, 2003, *Kuruleufenia* Gómez, 2016, *Patagopipa* Aranciaga Rolando et al., 2019, *Saltenia* Reig, 1959, and Palaeobatrachidae Cope, 1865.

Diagnostic apomorphies—Numerous synapomorphies have been proposed for this clade (see Gómez, 2016), mostly based on *Neusibatrachus* and *Gracilibatrachus* well-preserved skeletons. However, the inclusion of *Aygroua* (still poorly known) as a sister-taxon to all other pipimorphs in phylogenetical analyses (Figs. 9, 10) supported *Pipimorpha* by a combination of three non-unique synapomorphies : (1) the distal region of the ilial shaft circular and not compressed mediolaterally in cross-section; (2) the presence of a low ridge on the dorsal surface of the ilium and (3) an interiliac scar ample but restricted to the ventral part of the ilia.

Gondwanopipidae nomen novum

RegNum registration number :813

Definition—The smallest clade that includes *Shelania pascuali*, *Pipa pipa*, *Hymenochirus boettgeri*, *Xenopus laevis* and *Silurana tropicalis*. Abbreviated definition: min total ∇

A new pipid from the Cretaceous of Africa (In Becetén, Niger) and early evolution of Pipidae

(*Shelania pascuali* Casamiquela, 1960, *Xenopus laevis* Daudin, 1802, *Hymenochirus boettgeri* Tornier, 1896, *Pipa pipa* Linnaeus, 1758 and *Silurana tropicalis* Gray, 1864).

Etymology—Combination of the name ‘Gondwana’ and the clade name Pipidae.

Reference phylogeny—The primary reference phylogeny is the equal weight unconstrained analysis from this study (Fig. III-8). Other reference phylogenies include Báez et al (2007: fig. 6), Gómez (2016: fig. 5) and Aranciaga Rolando et al (2019: fig. 4).

Composition. Following morphology-based unconstrained analyses (Fig. 8), this clade includes Shelaniinae, ‘*Shelania*’ *laurenti*, *Llankibatrachus trubei*, ‘*Xenopus*’ *romeri* and Pipidae. Following phylogenies based on molecular data or phylogenies based on morphological data but constrained by the molecular topology, this clade includes *Pipidae* (see the definition for *Pipidae* above). Gondwanopipidae as here defined can be identified in both analyses (Figs. III-8-11; Aranciaga-Rolando et al., 2019; Carvalho et al., 2020). However, according to phylogenies based on molecular data or phylogenies based on morphological data but constrained by the molecular topology, this clade is redundant (and even synonymous) with *Pipidae* (Fig. III-9, 11), and the latter should be preferred.

Diagnostic apomorphies—Following morphology-based unconstrained analyses (Fig. 8; Aranciaga Rolando et al., 2019), *Gondwanopipidae* is supported by a combination of seven non-unique synapomorphies: (1) anterior process of the pterygoid dorsal to the maxilla; (2) lateral flange of the pterygoid transversally wide and restricted posteriorly; (3) no prefacial commissure (septum between prootic and palatine foramina); (4) cleithrum covering the posterior edge of the suprascapular cartilage; (5) a distal margin of the sacral apophyses straight; (6) apophyses anterior and posterior of the sacrum tapered and (7) an interiliac scar ample both ventrally and dorsally.

Shelaniinae Aranciaga Rolando et al., 2019, converted clade name

A new pipid from the Cretaceous of Africa (In Becetén, Niger) and early evolution of Pipidae

RegNum registration number : 814

Definition—The largest clade that includes *Shelania pascuali* but not *Pipa pipa*, *Hymenochirus boettgeri*, *Silurana tropicalis*, and *Xenopus laevis*. Abbreviated definition: max total ∇ (*Shelania pascuali* Casamiquela, 1960 and ~ *Xenopus laevis* Daudin, 1802, *Hymenochirus boettgeri* Tornier, 1896, *Pipa pipa* Linnaeus, 1758 and *Silurana tropicalis* Gray, 1864).

Etymology—Named after the eponym genus *Shelania*.

Reference phylogeny—The primary reference phylogeny is the equal weight unconstrained analysis from this study (Fig. III-8). Other reference phylogenies include Báez et al (2007: fig. 6), Gómez (2016: fig. 5) and Aranciaga Rolando et al (2019: fig. 4).

Composition—Under the unconstrained analysis (figs. 8, 10), this taxon includes the extinct *Shelania pascuali* Casamiquela, 1960, *Saltenia* Reig, 1959, *Kuruleufenia* Gómez, 2016 and *Patagopipa* Aranciaga Rolando et al., 2019. Shelaniinae has been recovered in morphological unconstrained analyses (Fig. III-8; Aranciaga-Rolando et al., 2019; Carvalho et al., 2020). However, according to phylogenies based on molecular data or phylogenies based on morphological data but constrained by the molecular topology, this clade is redundant with *Shelania pascuali*, or it includes the latter and possibly *Kuruleufenia xenopoides* and a clade that includes *Saltenia ibanezi* and *Patagopipa corsolinii*, depending on how a polytomy is resolved (Figs. III-9, 11).

Diagnostic apomorphies—Following morphology-based unconstrained analyses (Fig. III-8; Aranciaga Rolando et al., 2019) *Shelaniinae* is supported by a combination of six non-unique synapomorphies: (1) an anterior process of the pterygoid reaching the level of the antorbital plane; (2) eight distinct presacral vertebrae; (3) presacral vertebrae I and II not fused but rather broadly imbricated medially; (4) transverse process of the sixth vertebra markedly forward; (5) pair of ribs of the second vertebra oriented anterolaterally and (6) the distal region of the ilial shaft flattened, and compressed dorsoventrally.

A new pipid from the Cretaceous of Africa (In Becetén, Niger) and early evolution of Pipidae

III.7 Phylogenetic Analyses

Phylogenetic relationships of extant and extinct xenoanurans have been controversial for the past decade, with several recently described extinct taxa (Báez et al., 2007; Rage and Dutheil, 2008; Gómez, 2016; Carvalho et al., 2019; Aranciaga Rolando et al., 2019; Báez et al., 2021) variably placed either close to Xenopodinae (*Xenopus* + *Silurana*) or Pipinae (*Pipa* + Hymenochirini). To accommodate these extinct taxa, several clade names have been proposed, following the work of Báez and Púgener (2003). *Xenopodinomorpha* and *Pipinomorpha* were erected to accommodate extinct taxa closer to Xenopodinae or Pipinae respectively (Báez and Púgener, 2003; also see the nomenclatural note above).

A new pipid from the Cretaceous of Africa (In Becetén, Niger) and early evolution of Pipidae

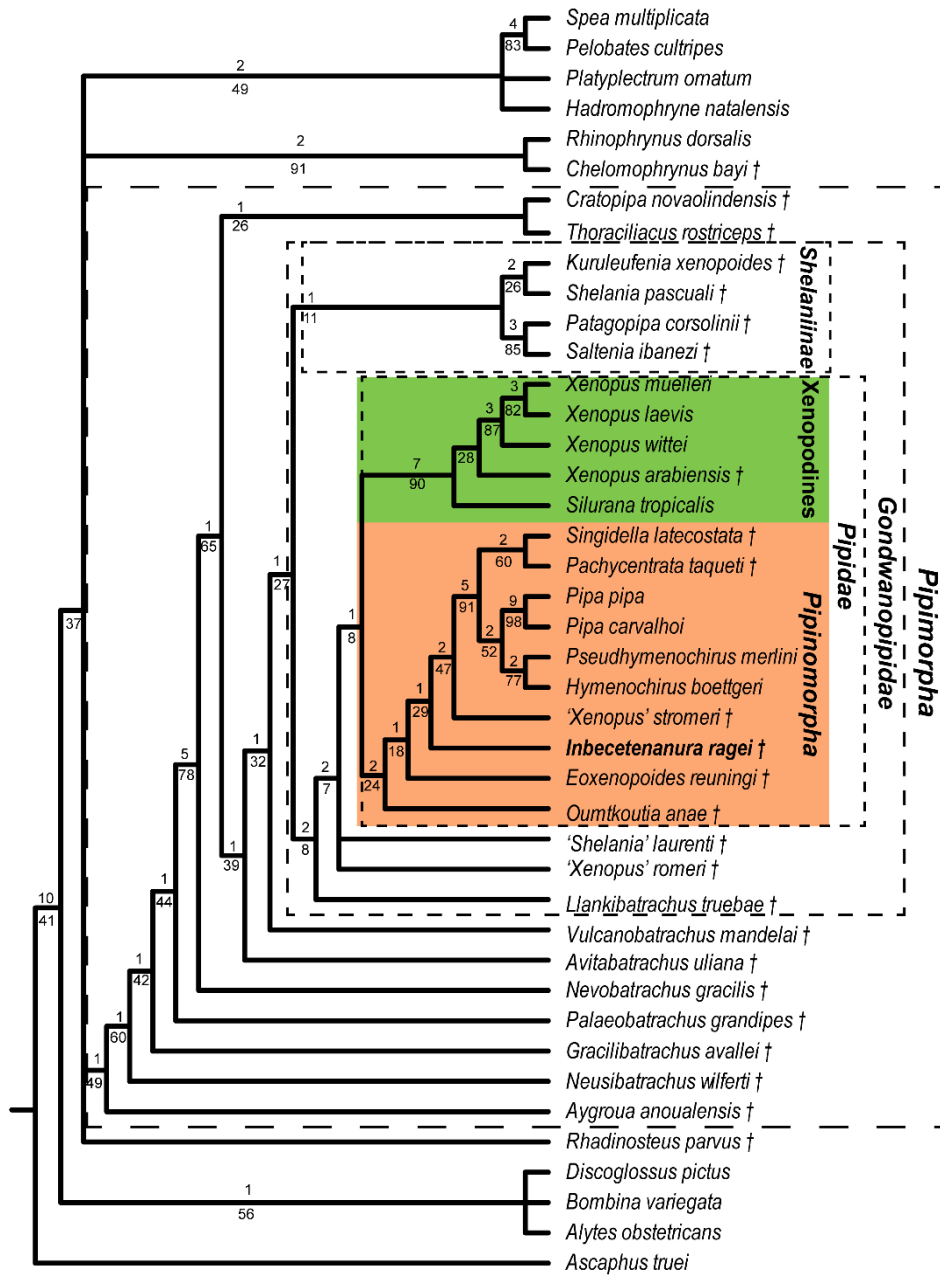


Figure III-8. Strict consensus of 4 MPTs of 649 steps from the unconstrained analysis under equal weights, with multistate characters ordered (CI = 0,352; RI = 0, 682). The † symbol identifies extinct taxa; clade names in bold italic represent names converted in PhyloCode (except *Inbecetenanura ragei*); orange clade represents Pipimorpha; green clade represents Xenopodines; numbers above branches designate Bremer support; those below are bootstrap frequencies.

Equal weight analysis—A phylogenetic analysis under equal weight and ordered yielded 4 MPTs with a score of 649 steps. The strict consensus (CI = 0, 364; RI = 0, 698; Fig. III-8) recovered a *Pipimorpha* clade placed within a tetrachotomy with the extinct

A new pipid from the Cretaceous of Africa (In Becetén, Niger) and early evolution of Pipidae

Rhinophrynus parvus, a clade composed of *Rhinophrynus dorsalis* + *Chelomorphrynus bayi*, and a clade made of Pelobatidae (*Spea*; *Pelobates*) + *Hadromophryne*. *Pipimorpha* is poorly supported by three synapomorphies: (1) the distal region of the ilial shaft circular and not compressed mediolaterally in cross-section (character 137, 0→1); (2) the presence of a low ridge on the dorsal surface of the ilium (character 145: 0→1); and (3) an interiliac scar ample but restricted to the ventral part of the ilia (character 149, 0→1).

Interestingly, the extinct African *Aygroa anoualensis* Jones et al., 2003 is recovered as the sister-taxon to all pipimorph, supported by three synapomorphies, all on the ilium. The pipimorph *Cratopipa novaolindensis* Carvalho et al., 2019 appears to form a clade with the Cretaceous *Thoraciliacus rostriceps*, but this is poorly supported by two synapomorphies: (1), the presence of transverse process on the urostyle (character 105, 1→0) and (2), fusion of the ilium and ischium (character 152, 0→1). This clade is a sister-clade to all other gondwanian pipimorphs.

Gondwanopipidae is recovered, poorly supported by seven synapomorphies (see Appendix S7). *Shelaniinae* is poorly supported by six synapomorphies (see Appendix S8; identical to the ones recovered in Aranciaga Rolando et al., 2019). Within *Gondwanopipidae*, we also find *Shelania pascuali* Casamiquela, 1961 and '*Xenopus*' *romeri* Estes, 1975 within a trichotomy with *Pipidae*. *Pipidae* is supported by five synapomorphies (see Appendix S8). Within *Pipidae*, Xenopodines is redundant with *Xenopodinomorpha*. Xenopodines is recovered as the sister-clade of *Pipinomorpha*, containing the extant *Pipa*, *Hymenochirus* and *Pseudohymenochirus* and several extinct taxa.

Xenopodines is here composed of *Silurana* and a clade that includes the extant *Xenopus* species and the extinct *Xenopus arabiensis*. Xenopodines is strongly supported by eighteen synapomorphies, many of them recovered within other phylogenetic analyses (Báez and Púgener, 2003; Gómez, 2016) and used as diagnostic apomorphies for this clade (Frost et al., 2006). *Pipinomorpha* is poorly supported by one

A new pipid from the Cretaceous of Africa (In Becetén, Niger) and early evolution of Pipidae

synapomorphy, the loss of a distinct pterygoid knob on the basal process of the otic capsule (character 59: 2→0).

Inbecetenanura is placed within *Pipinomorpha* (Fig. III-8) as the sister-group of a clade composed of “*Xenopus*” *stromeri* + ((*Singidella latecostata* + *Pachycentrata taqueti*)+(Pipinae)), which is poorly supported by three synapomorphies: (1) the reduction of the posteromedial region of the parasphenoid, ending well anterior to the ventral margin of the foramen magnum (20: 0→1); (2) the presence of a posteroventral process of the otic capsule ventral to condyloid fossa (67: 0→1); (3) a neural arch lamina of the sacral vertebra longitudinally rectangular (longer than wide; 101: 0→2).

P. taqueti is recovered as a sister-taxon to the Eocene *S. latecostata*, moderately supported by two synapomorphies: (1) the presence of an occipital artery housed in a closed canal (10, 0→1) and (2) the anterior extension of the cultriform process of the parasphenoid ending at antorbital level (18, 3→1). Extant pipines are recovered as a clade strongly supported by seven synapomorphies (see Appendix S8).

A new pipid from the Cretaceous of Africa (In Becetén, Niger) and early evolution of Pipidae

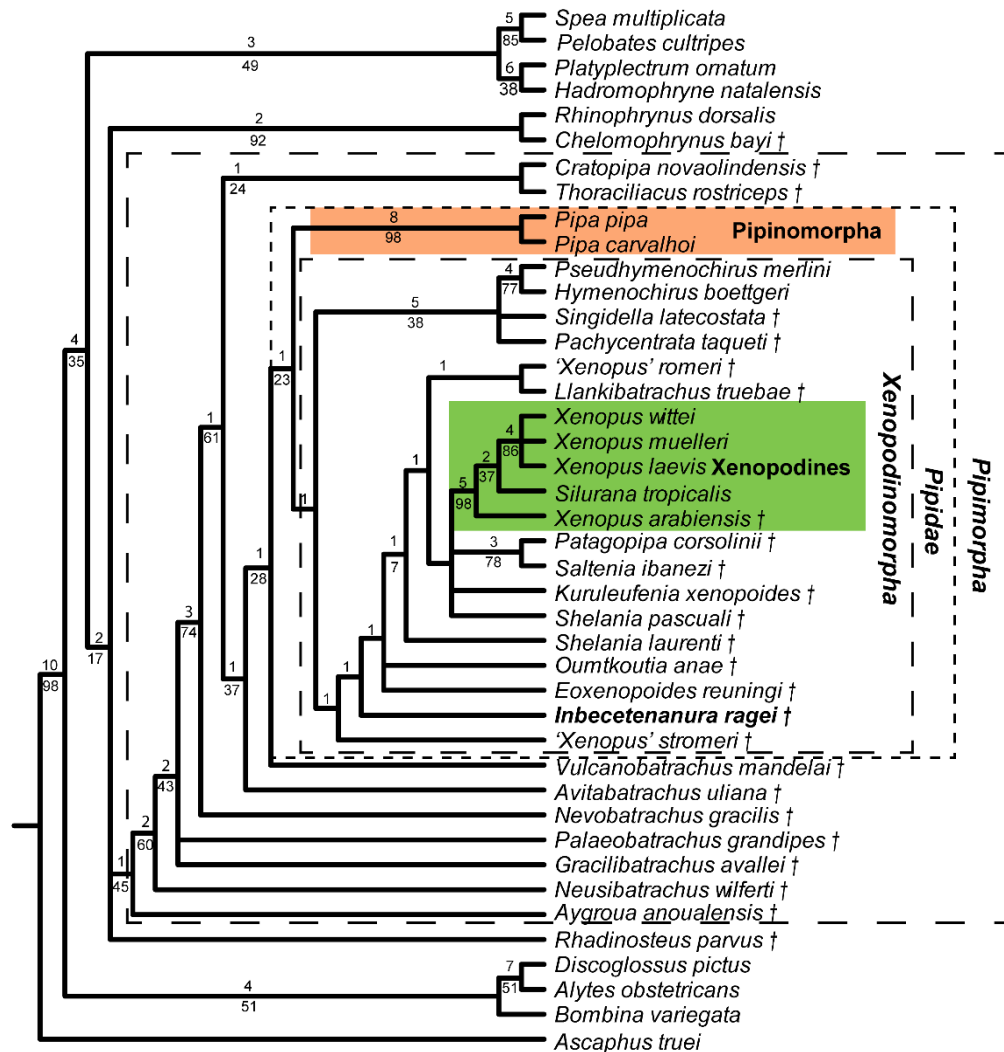


Figure III-9. Strict consensus of 47 MPTs of 675 steps from the constrained analysis using a molecular scaffold tree from Jetz and Pyron (2018), performed under EW with multistate characters ordered (CI = 0.352; RI = 0.682). The † symbol identifies extinct taxa; clade names in bold italic represent names converted in PhyloCode (except *Inbecetenanura ragei*); orange clade represents Pipinomorpha; green clade represents Xenopodines; numbers above branches designate Bremer support; those below are bootstrap frequencies.

Constrained analysis

Three main extant pipids clade are recognized in literature (Frost et al., 2006; Jetz and Pyron, 2018), Xenopodinae (*Xenopus* + *Silurana*), Hymenochirini (*Hymenochirus* + *Pseudohymenochirus*) and Pipinae (*Pipa*). The first major phylogenetic analyses (based on osteological characters; Cannatella and Trueb, 1988; Ford and Cannatella, 1993)

A new pipid from the Cretaceous of Africa (In Becetén, Niger) and early evolution of Pipidae

recovered the Xenopodines as a sister-clade to all other *Pipidae*, and placed Hymenochirini as a clade of Pipinae. Addition of several extinct pipimorphs and pipids did not raise doubts about these relationships (Báez and Trueb, 1997; Báez and Púgener, 1998; Trueb, 1999; Báez and Púgener, 2003; Trueb et al., 2005; Gómez, 2016). However, the rise of molecular phylogenetical analyses proposed a completely different relationships for extant Pipidae (Frost et al., 2006; Pyron and Wiens, 2011; Jetz and Pyron, 2018; Dubois et al., 2021), with Pipinae composed of only *Pipa*, as a sister-clade to Dactylethrinae (Xenopodines + Hymenochirini). This conflict between morphological and molecular phylogenetic analyses is still unresolved (Bewick et al., 2012) and the relationships and position of the various extinct *Pipidae* might differ between both topologies.

To address this conflict, we performed phylogenetic analyses constrained on a topology taken from Jetz and Pyron (2018), to see if the placement of In Becetén taxa is impacted.

Constrained equal weight analysis—We recovered 47 MPTs with a score of 675 steps. The strict consensus (CI = 0,352; RI = 0, 682; Fig. III-9) recovered Xenoanura, *Pipimorpha* and *Pipidae*. Xenoanura is supported by four synapomorphies: (1), frontoparietals completely fused (character 4, 0→1); (2), absence of subotic alae of the parasphenoid (character 17, 0→1); (3) cultriform process of the parasphenoid extending up to the vomers anteriorly (character 19, 0→2); (4) sphenethmoid not exposed dorsally (between the roofing dermal bones; character 48, 1→0). *Pipimorpha* is supported by four synapomorphies, three of them recovered in previous analyses for the clade. *A. anoualensis* is a sister-taxa to all pipimorphs.

C. novaolindensis and *T. rostriceps* form a clade, supported by the same two synapomorphies as in previous analyses (see Appendix S8). *Shelaniinae* was not recovered as clade. Taxa attributed to this clade were instead recovered within *Xenopodinomorpha* (Fig. III-9). This makes *Gondwanopipidae* redundant with *Pipidae*. This clade is poorly supported by nine synapomorphies (see Appendix S8).

A new pipid from the Cretaceous of Africa (In Becetén, Niger) and early evolution of Pipidae

Xenopodinomorpha is here redundant with Dactylethrinae (Xenopdines+ Hymenochirini, a name used only so far with extant taxa; Dubois et al., 2021). *Xenopodinomorpha* is supported by three synapomorphies: (1), the presence of posteroventral process ventrolateral to the condyloid fossa on the otic capsules (synapomorphies of *Xenopodinomorpha* according to Gómez, 2016; character 67, 0->1); (2), clavicle fused to scapula (character 108, 1->2; lost in *Shelania pascuali* and *Saltenia ibanezi*); (3), presence of ribs expansions along their shafts (lost in several extinct taxa and *Pseudohymenochirus*; character 175, 1->0). *S. latecostata* and *P. taqueti* appear to be stem-Hymenochirini. Hymenochirini is strongly supported by nine synapomorphies (Appendix S8). Crown-Hymenochirini are strongly supported by eight synapomorphies (see Appendix S8).

Stem-Xenopodines includes numerous extinct taxa (Fig. III-9) and is supported by four cranial synapomorphies: (1) presence of parasagittal crests on the frontoparietal (lost in *Patagopipa corsolinii*; character 8, 0->1); (2), anterior margin of the frontoparietal fenestra delimited in bone (reversed in Xenopodines; character 45, 2->0); (3), inferior perilymphatic foramen of the otic capsules opening extracranially ventral to jugular foramen (lost in *Xenopus*; character 62, 1->2); (4), absence of superior perilymphatic foramen (character 63, 0->1). *Inbecetenanura* appears to be a stem-Xenopodines.

III.8 Discussion

Ontogenetic stage

In the original description of MNHN.F.IBC 1602, the authors suggested that the braincase belonged to an immature individual (Báez and Rage, 1998). This hypothesis was based on (1) a long anterior extension of the otic capsules; (2) a separation of prootic and optic foramina by a bony wall and (3) the presence of weak parasagittal crests on the frontoparietal. However, a similar extension of the otic capsules in

A new pipid from the Cretaceous of Africa (In Becetén, Niger) and early evolution of Pipidae

Inbecetenanura ragei occurs in several mature individuals of pipid taxa (Trueb et al., 2000). A bony wall between prootic and optic foramina also occurs in mature individuals of several extant and extinct pipids (Estes, 1975; Trueb and Hanken, 1992). Furthermore, parasagittal crests are highly variable in pipids, from absent, as in *Patagopipa* (Aranciaga Rolando et al., 2019) to well-defined, as in *Pipa* (Trueb et al., 2000). As an example, mature specimens of *Shelania pascuali* still bear weak parasagittal crests (Báez and Trueb, 1997). Presence of weak parasagittal crests cannot be taken as a sign of immaturity. In conclusion there is no indication that MNHN.F.IBC 1602 represents an immature individual. Moreover, comparison with immature and mature individuals of *Pachycentrata taqueti* can be made. The extreme fusion of dermal, palate and endocranial bones of the braincase displayed by *Inbecetenanura* does not occur in braincases of immature *P. taqueti*, but it resembles braincases of mature individuals.

Status and attribution of In Becetén taxa

Pachycentrata taqueti and *Inbecetenanura* both appear to be pipids. *Inbecetenanura* and *Pachycentrata* are found among pipinomorphs in non-constrained analyses. However, in constrained analyses, they are recovered as a xenopodinomorphs. Previous mention of the holotype of *Inbecetenanura* considered it a xenopodinomorph (Báez and Rage, 1998; Gardner and Rage, 2016), but they were not based on phylogenetic analyses. *Pachycentrata* has only been recovered as a pipinomorph within previous analyses (Báez and Rage, 1998; Gómez, 2016). Other extinct taxa, like *Oumtkoutia anae*, were also suggested to be xenopodinomorph. This conflict seems linked to the position of the Hymenochirini and to the polarization of several characters. As mentioned above, morphological and molecular analyses support conflicting positions of Hymenochirini (Bewick et al., 2012). In addition, molecular – morphological compound analyses yielded results similar to molecular analyses (Bewick et al., 2012). Homologies on key characters for Hymenochirini and *Pipa* have to be reconsidered and investigated, in peculiar in the Hymenochirini (Bewick et al., 2012). The only secure attribution for

A new pipid from the Cretaceous of Africa (In Becetén, Niger) and early evolution of Pipidae

Inbecetenanura is to *Pipidae*. We putatively refer *Inbecetenanura* to *Pipinomorpha*, as it is the position recovered in unconstrained analysis.

In conclusion, the two pipimorph taxa from In Becetén are attributed to *Pipidae*. This is the second-oldest occurrence of pipid taxa, fifteen million years after *Oumtkoutia anae* from the Cenomanian beds of Morocco (Rage and Dutheil, 2008). More importantly, In Becetén is the oldest co-occurrence of at least two pipid taxa in a given locality, and the oldest occurrence of a pipine taxon.

Pipimorph phylogeny

In its original description, Jones et al. (2003) considered *A. anoualensis* was close to Xenoanura (~Pipoidea) based on ilium osteological characters. We recovered *A. anoualensis* as a pipimorph, sister-taxon to all other pipimorphs in every analysis, and thus confirmed its attribution to *Pipimorpha*. *A. anoualensis* has been identified in the Ksar Metlili site (Eastern Morocco; Jones et al., 2003; Lasseron et al., 2019) from the Ksar Metlili Formation. This Formation was previously considered to be Early Cretaceous (Berriasian) age (Haddoumi et al., 2016) but recent faunistic analyses revealed numerous similarities with Middle-Late Jurassic fauna (Lasseron et al., 2019). Although a lower Berriasian age cannot be excluded (Lasseron pers. Com), *A. anoualensis* is slightly older than two pipimorph occurrences, *Neusibatrachus wilferti* (Báez and Sanchiz, 2007) and *Shomronella jordanica* Estes et al., 1978 from the Middle-Upper Berriasian. This makes *A. anoualensis* the oldest pipimorph known and the second oldest xenoanuran (Fig. III-9).

The recently described *Cratopipa novaolindensis* (Carvalho et al., 2019; Báez et al., 2021) appears to be a pipimorph and to form a clade with *Thoraciliacus rostriceps*. Both taxa are Aptian age (*T. rostriceps* is slightly older; Gardner and Rage, 2016; Carvalho et al., 2019) but they are geographically far away. This result is different from the position of *C. novaolindensis* (in *Shelaniinae*) originally proposed by Carvalho et al. (2019). This

A new pipid from the Cretaceous of Africa (In Becetén, Niger) and early evolution of Pipidae

difference is likely linked to the rescoring of several key characters (such as the sacro-urostyler articulation) following the redescription of Báez et al (2021).

Gondwanopipid and pipid phylogeny

Gondwanopipidae (~Panpipidae in Aranciaga Rolando et al., 2019), recently proposed by Aranciaga Rolando et al (2019) is here recovered only when performing the unconstrained analysis (Fig. III-8). This clade includes *Shelaniinae* as the sister-clade to a clade made of *Llankibatrachus* + trichotomy of *Pipidae* and two gondwanopipids, '*Shelania*' *laurenti* and '*Xenopus*' *romeri*. This condition is similar to the one recovered in Aranciaga Rolando et al (2019: fig. 3). However, when performing under constrained analysis, neither *Gondwanopipidae* nor *Shelaniinae* were recovered (Fig. III-9). All gondwanopipids were instead recovered as pipids. This result is more similar to previous analyses (Báez and Púgener, 2003; Gómez, 2016) where all gondwanopipids were found nested within either *Xenopodinomorpha* or *Pipinomorpha*. This difference is linked to the position of Hymenochirini, either close to *Pipa* or Xenopodines.

A new pipid from the Cretaceous of Africa (In Becetén, Niger) and early evolution of Pipidae

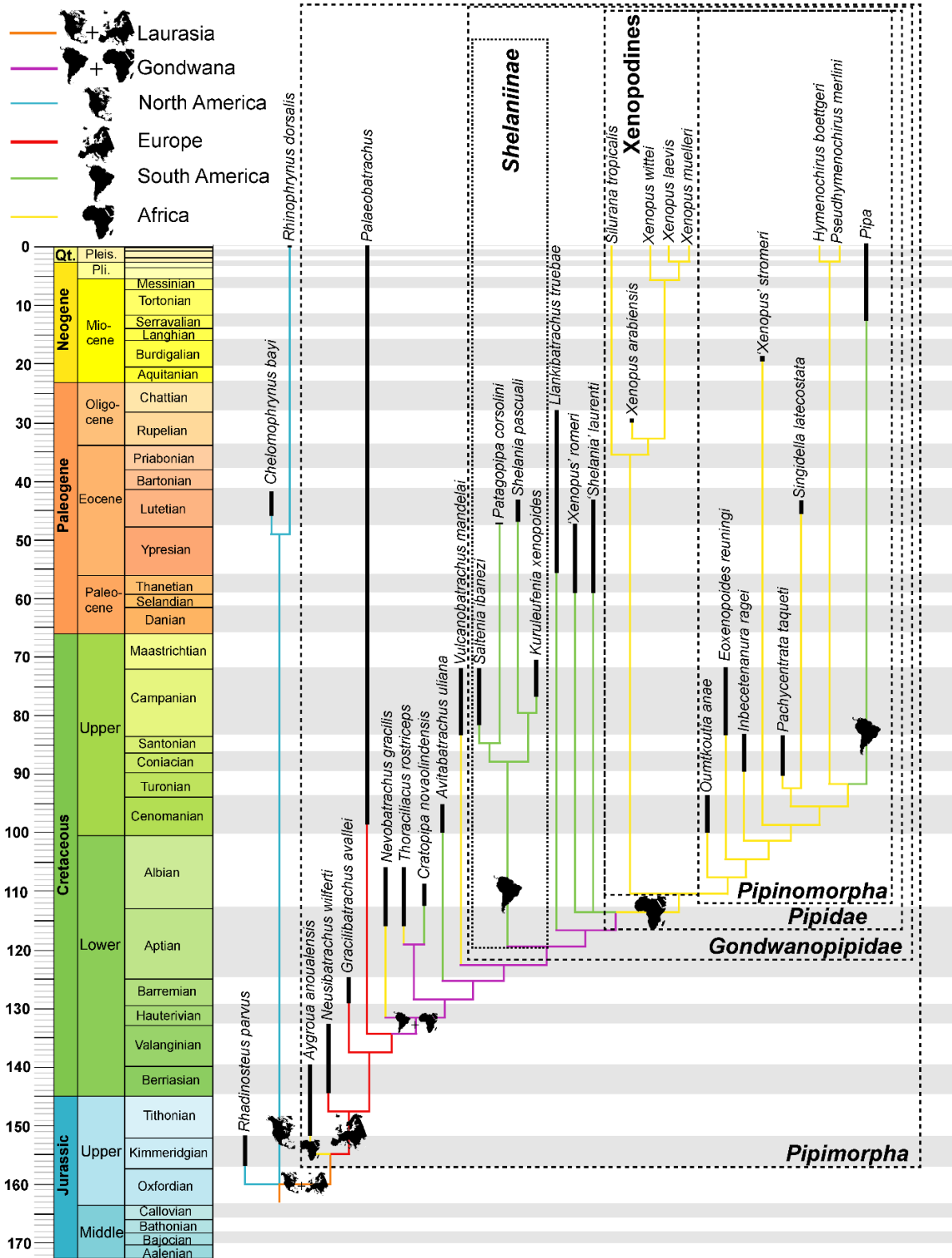


Figure III-10. Strict consensus of the unconstrained analysis under equal weights mapped onto the stratigraphical chart, with their geographical occurrences. Black bar over branches indicates known fossil record and clade names in bold italic represent names converted in PhyloCode. Position of nodes does not reflect time-calibrated ages. The phylogenetical position of *Palaeobatrachus* is inferred on the position of *Palaeobatrachus grandipes*.

A new pipid from the Cretaceous of Africa (In Becetén, Niger) and early evolution of Pipidae

Paleobiogeographical implications

Xenoanuran diversification and dispersal through the globe is still unclear. The oldest xenoanuran, *Rhadinostenus parvus* was recovered from the Late Jurassic of North America (Kimmeridgian, 157-152 ma). The oldest pipimorph seems to be *Aygroa anoualensis* from the Late Jurassic-Early Cretaceous of North Africa (Tithonian-Berriasian, 152-140 ma; Lasseron et al., 2020). These two taxa document the early divergence of two large extant clades (Rhinophrynidae and *Pipimorpha*). Molecular analyses have dated the divergence between these two main xenoanuran clades to the Middle Jurassic, around 165 Ma (Feng et al., 2017), and this is compatible with the fossil record (Marjanović and Laurin, 2014). However, it should be noted that the taxa used for calibration of the *Pipimorpha* by Feng et al. (2017) were not the oldest representatives of the clade and early pipimorphs were included within a basal polytomy by Marjanović and Laurin (2014). Inclusion of these pipimorphs as node calibration could push further back the divergence of Xenoanura. All early occurrences of *Pipimorpha* are centered around the Tethys, in Morocco (Jones et al., 2003), Spain (Báez and Sanchiz, 2007) and Israel (Estes et al., 1978; Gardner and Rage, 2016), which suggests that early diversification of pipimorphs occurred in that area (Figs. III-10, 11).

A new pipid from the Cretaceous of Africa (In Becetén, Niger) and early evolution of Pipidae

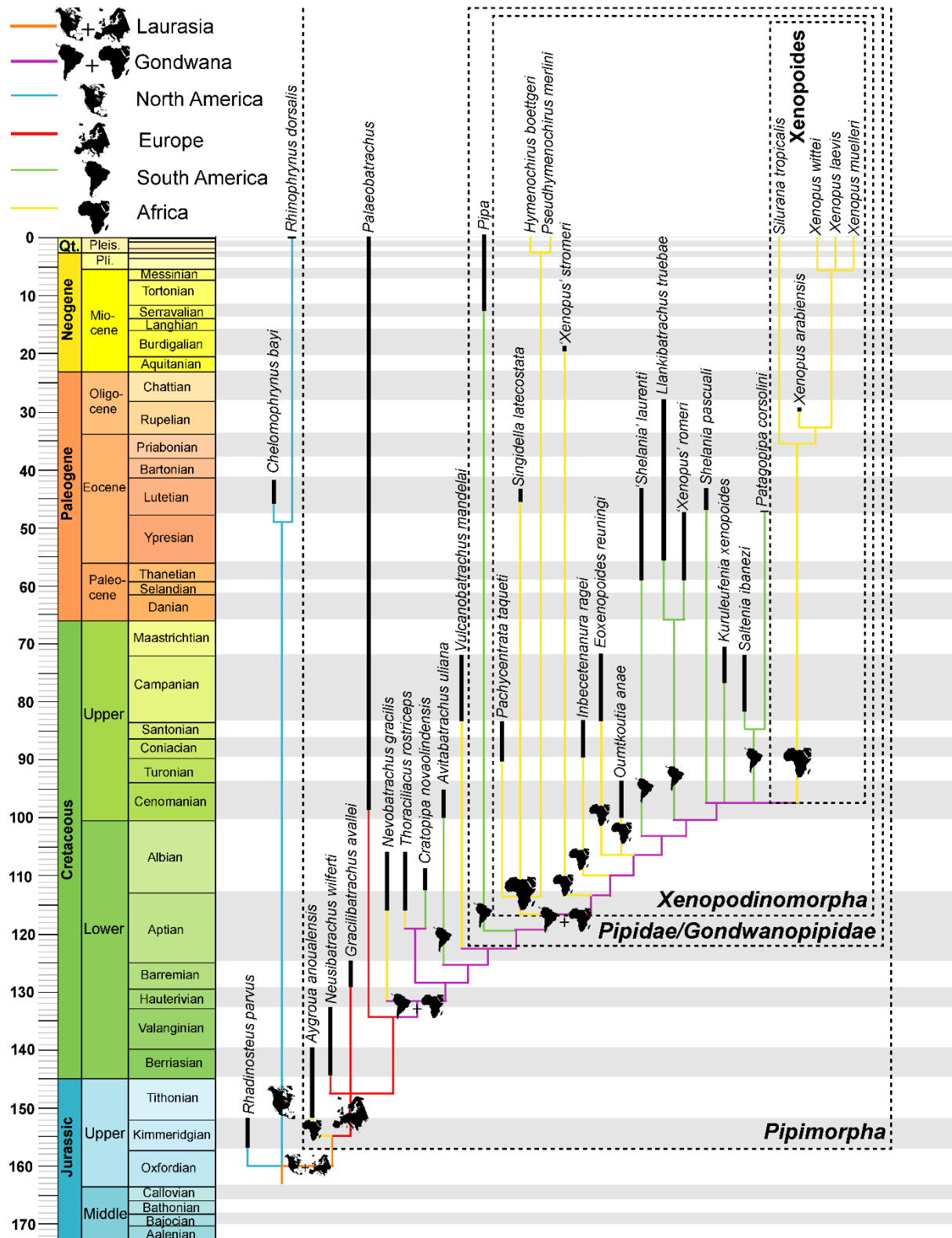


Figure III-11. Strict consensus of the constrained analysis under equal weights mapped onto the stratigraphical chart, with their geographical occurrences. Black bar over branches indicates known fossil record and clade names in bold italic represent names converted in PhyloCode. Position of nodes does not reflect time-calibrated ages. The phylogenetical position of *Palaeobatrachus* is inferred on the position of *Palaeobatrachus grandipes*.

A new pipid from the Cretaceous of Africa (In Becetén, Niger) and early evolution of Pipidae

During the latest part of the Early Cretaceous (Aptian-Albian) and beginning of the Late Cretaceous (Cenomanian), there are numerous occurrences of pipimorphs across Gondwana (Fig. III-10; Gardner and Rage, 2016; Báez et al., 2021), indicating that the clade was already widespread. Later in the late Cretaceous, pipimorphs are represented by pipids in Africa (Cenomanian; Gardner and Rage, 2016) and *Shelaniinae* in South America (Fig. III-10), although the South American taxa may be interpreted as pipids under the constrained topology (Fig. III-11).

The rich fossil record of pipinomorphs (unconstrained analysis; Fig. III-10) or xenopodinomorphs (constrained analysis: Fig. III-11) spans across Africa and South America. Phylogenetic results show close relationships between South American and African taxa under both topologies (Figs III-10, 11), implying that pipids were able to easily move from one continent to another. Despite the strong aquatic adaptations of extant pipids, this dispersal may not have been as difficult as it might first seem, for two reasons. First, at least some pipids, such as the African pipid *Xenopus laevis*, are known to tolerate moderately salinity (around 20-40% of sea water salinity; Munsey, 1972; Hopkins and Brodie Jr, 2015); second, at least six *Xenopus* species (including *X. laevis*) can move overland (Measey, 2016). The taxonomic distribution of these abilities among other pipids (outside *Xenopus*) is unknown, but the taxon is obviously adaptable in ways that can facilitate overland dispersal and across brackish water. However, it would seem very unlikely to see these anurans crossed the sea (in transatlantic dispersal) contrary to more terrestrial vertebrates with a more water-proof skin (mammals, squamates...). Thus, the successive divergences between African and South American gondwanopipids that occurred until the mid-Cretaceous (according to a literal interpretation of the fossil record) suggest a permanent connection between Africa and South America at that time. This is congruent with current analyses that place the loss of this connection in the mid-Cretaceous, around the Early/Late Cretaceous transition (Fairhead, 1988; Nürnberg and Müller, 1991; Binks and Fairhead, 1992; McLoughlin, 2001; Will and Frimmel, 2018). After this

A new pipid from the Cretaceous of Africa (In Becetén, Niger) and early evolution of Pipidae

separation, gondwanopipids were presumably unable to disperse between both continents, as we see appears to be the case from the mid-Cretaceous onwards.

This scenario does not require over-water dispersal, contrary to other scenarios proposed recently (Gómez, 2016; Aranciaga Rolando et al., 2019). In addition, it implies that lineages leading to all major extant pipid clades (Pipinae, Hymenochirini and Xenopodines) likely emerged during the Cretaceous, which implies long ghost lineages for these clades, which are poorly documented in the fossil record.

III.9 Conclusion

In conclusion, the redescription of an indeterminate pipid from Ibeceten leads to the establishment of a new pipid taxon, *Inbecetenanura ragei* nov. sp. Several postcranial elements from the site are also attributed to the same taxon. Phylogenetic analyses confirm its placement within *Pipidae*, although some uncertainties remain on its attribution within the clade. We also took the opportunity to convert *Pipimorpha*, *Gondwanopipidae*, *Shelaniinae*, *Pipidae*, *Xenopodinomorpha* and *Pipinomorpha* into the phylogenetical nomenclature as implemented in the *PhyloCode*. In Becetén is the oldest site where more than one pipid taxon is known, and the oldest site where a pipine is recovered. Inclusion of the gondwanian *Aygroua anoualensis* suggests that this taxon is a pipimorph and the sister-taxon to all other pipimorphs. We recover *Shelaniinae*, a recently proposed pipimorph clade, as the closest clade to the *Pipidae* in the unconstrained analysis. However, the analysis constrained to reflect the topology of extant taxa recovered by the numerous molecular analyses finds the various shelaniines among xenopodinomorphs, where they do not necessarily form a clade. The position of several extinct pipid taxa, recovered either as pipinomorph or xenopodinomorph, thus strongly depends on the topology of the extant taxa. Phylogenetic results indicate that repeated dispersals of gondwanopipids between Africa and South America until the mid-Cretaceous at the latest suggests that these

A new pipid from the Cretaceous of Africa (In Becetén, Niger) and early evolution of Pipidae

continents were still connected, at least through a limited land bridge, until then. Main pipid clades likely originated during the Cretaceous, when the final opening of Southern and Central Atlantic Ocean. This geological context may have driven a pipid evolutionary radiation around the Early/Late Cretaceous transition. This confirms that the Cretaceous is a key period of the evolutionary history of the *Pipimorpha*.

III.10 Appendix

Appendix S1. CT-scan of MNHN.F.IBC1602

The appendix can be found on Zenodo at : <https://doi.org/10.5281/zenodo.6624939>

Appendix S2. 3D model of MNHN.F.IBC1602

The appendix can be found on Zenodo at : <https://doi.org/10.5281/zenodo.6624939>

Appendix S3. 3D model of the endocast of MNHN.F.IBC1602

The appendix can be found on Zenodo at : <https://doi.org/10.5281/zenodo.6624939>

Appendix S4. Matrix used in phylogenetical analyses.

The appendix can be found on Zenodo at : <https://doi.org/10.5281/zenodo.6624939>

Appendix S5. List of characters used.

Description of characters used in phylogenetic analysis follows Aranciaga-Rolando et al. (2019). This character list is founded on those published by Báez et al. (2009, 2012), Báez (2013), Cannatella and Trueb (1988) and Gómez (2016). All character statements refer to the adult stage, unless stated otherwise. Abbreviations: B13: (Báez, 2013); BGT12: (Báez et al., 2012); BMG09: (Báez et al., 2009); BP03: (Báez & Pugener, 2003); BT97: (Báez & Trueb, 1997); CT88: (Cannatella & Trueb, 1988); F06: (Fabrezi, 2006); G16: (Gómez, 2016); H03: (Haas, 2003); PMT03: (Pugener et al., 2003).

A new pipid from the Cretaceous of Africa (In Becetén, Niger) and early evolution of Pipidae

Cranium

1. Skull, preorbital region, relative length with respect to the skull length: (0) one-third, or more; (1) one quarter, or less. (BGT12:1)
2. Nasals, fusion to one another: (0) absent; (1) present. (BGT12:2)
3. Frontoparietals, relation with nasals: (0) not overlapping; (1) overlapping. (BGT12:3)
4. Frontoparietals, fusion to one another: (0) not fused or partially fused; (1) completely fused. (BGT12:4)
5. Frontoparietals, anterolateral processes: (0) absent; (1) present. (CT88:10)
6. Frontoparietals, posterolateral extensions: (0) absent; (1) present. (BGT12:5)
7. Frontoparietals, supraorbital flange: (0) absent; (1) present. (B13:5)
8. Frontoparietals, parasagittal crests: (0) absent; (1) present. (G16)
9. Frontoparietals, pineal foramen (as an opening on the dorsal surface): (0) absent; (1) present. (B13:6)
10. Occipital artery, location: (0) dorsal to skull roof; (1) housed in a closed canal. (B13:25)
11. Vomer: (0) present; (1) absent. (BGT12:21)
12. Vomeres, fusion : (0) paired; (1) fused to one another. (BGT12:22)
13. Vomer, relative position with respect to the choana: (0) medial; (1) posterior. (BP03:16, part)
14. Vomer, plate-like anterior portion: (0) poorly developed; (1) well developed. (B13:17)
15. Vomer, postchoanal process: (0) absent; (1) present. (B13:18)
16. Palatine: (0) absent; (1) present. (B13:19)
17. Parasphenoid, subotic alae: (0) present; (1) absent. (BGT12:24)

A new pipid from the Cretaceous of Africa (In Becetén, Niger) and early evolution of Pipidae

18. Parasphenoid, cultriform process, anterior extent with respect to antorbital level: (0) posterior; (1) about the same level (2) anterior, between vomers; (3) well beyond, reaching (or nearly so) maxillary arcade. (BGT12:25)
19. Parasphenoid, cultriform process, shape of anterior third: (0) moderately wide, round or finely serrated; (1) broad, markedly serrated; (2) very narrow, pointed or strongly tapering. (BMG09:23)
20. Parasphenoid, posteromedial extent: (0) extending near the ventral margin of the foramen magnum; (1) ending well anterior to the ventral margin of the foramen magnum. (BGT12:26)
21. Parasphenoid, relation to braincase: (0) not fused; (1) partially or completely fused. (BGT12:23)
22. Pterygoid, anterior ramus: (0) present; (1) absent. (BGT12:30)
23. Pterygoid, anterior ramus, relative position with respect to the maxilla:(0) medial; (1) dorsal. (BGT12:31)
24. Pterygoid, anterior ramus, anterior extent relative to the antorbital plane: (0) well posterior to it; (1) reaching it or nearly so. (B13:27)
25. Pterygoid, anterior ramus, ventral flange: (0) absent, (1) present. (CT88:14)
26. Pterygoid, medial ramus: (0) present, well developed; (1) reduced. (BGT12:32)
27. Pterygoid, medial ramus, indentation on distal margin: (0) absent; (1) present. (BGT12:33)
28. Pterygoid, medial ramus, contact with parasphenoid: (0) absent; (1) present. (BGT12:35)
29. Pterygoid, medial ramus, relation to otic capsule: (0) not fused; (1) fused. (BGT12:36)
30. Pterygoid, medial and posterior rami, configuration in otic region: (0) not expanded; (1) expanded to form an otic plate. (BGT12:34)
31. Squamosal, relation to annulus tympanicus: (0) separated; (1) fused in a conch-shaped bone. (BGT12:27)

A new pipid from the Cretaceous of Africa (In Becetén, Niger) and early evolution of Pipidae

32. Squamosal, zygomatic ramus: (0) inconspicuous; (1) moderately to well developed, free-ending; (2) well developed, articulating with maxilla; (3) well developed, articulating with pterygoid. (BTG12:28, part; B13:22)
33. Squamosal, otic ramus: (0) poorly to moderately developed, medial process poorly differentiated; (1) present, with distinct medial process that rests on the crista parotica; (2) present, with extensive medial process that rests on the otoccipital. (B13:23)
34. Maxillary arcade, teeth: (0) present; (1) absent. (BGT12:40)
35. Maxillary arcade, teeth, crown morphology: (0) bicuspid, labial cuspid may be present as low blade (1) monocuspid. (CT88:31, part)
36. Premaxilla, palatine process, shape: (0) weakly or moderately developed; (1) well-developed, long; (2) very long, daggerlike. (BGT12:15)
37. Premaxilla, alary process, distinctiveness from the rest of the pars facialis: (0) distinct; (1) indistinct. (CT88:25)
38. Maxilla, relation with premaxilla: (0) not or slightly overlapping premaxilla; (1) overlapping premaxilla with pointed process of the pars facialis that reaches alary process; (2) nearly or completely overlapping premaxilla anteriorly. (BGT12:16)
39. Maxilla, antorbital/preorbital process: (0) absent or weakly developed; (1) present, well-developed but thin; (2) present, well-developed and wide.
40. Maxilla, partes (i.e., facialis, palatina, dentalis) in the orbital region, distinctiveness from one another: (0) distinct; (1) not distinct. (BGT12:18)
41. Maxilla, pars facialis, palatine process: (0) absent; (1) present. (B13:14)
42. Quadratojugal: (0) present; (1) absent. (BGT12:19)
43. Septomaxilla, shape: (0) convolute; (1) flat. (BGT12:20)
44. Braincase, floor in the orbital region, shape: (0) rounded; (1) distinctly angled. (BGT12:10)
45. Sphenethmoid, frontoparietal fenestra, anterior margin condition: (0) delimited in bone; (1) not delimited in bone. (BGT12:6)

A new pipid from the Cretaceous of Africa (In Becetén, Niger) and early evolution of Pipidae

46. Sphenethmoid, frontoparietal fenestra, bony anterior margin shape: (0) round arch; (1) with tapering embayment or notch. (G)
47. Sphenethmoid, lateral wall of braincase in the orbital region, origin: (0) chondral; (1) membranous. (BT97:2, part)
48. Sphenethmoid, dorsal exposure between dermal roofing bones: (0) absent; (1) present. (B13:8)
49. Sphenethmoid, relation with frontoparietal: (0) not fused; (1) fused. (G)
50. Cavum cranii, cartilaginous roofing configuration: (0) completely open; (1) taenia transversalis present only; (2) taenia transversalis et medialis; (3) tectum parietale; (4) almost completely chondrified; (5) taeniae tecti medialis only. (H03:96)
51. Planum antorbitale, ossification: (0) completely cartilaginous or ossified/mineralized less than one half; (1) ossified/mineralized more than one half. (BGT12:8)
52. Septum nasi, ossification: (0) completely cartilaginous; (1) incompletely ossified; (2) completely ossified. (CT88:8)
53. Olfactory foramina, margin: (0) bound completely or partially in bone; (1) bound completely in cartilage. (BGT12:7)
54. Orbitonasal foramina, margin: (0) bound completely in bone; (1) bound incompletely in bone or in cartilage. (CT88:9)
55. Optic foramina, margins: (0) bound in cartilage or cartilage and bone; (1) bound completely in bone. (BGT12:9)
56. Prefacial commissure (septum between prootic and palatine foramina): (0) present; (1) absent. (PMT03:8)
57. Otic capsules, Eustachian canal: (0) absent; (1) present. (BGT12:11)
58. Otic capsules, Eustachian canal, configuration: (0) shallow anteroventral depression; (1) ventral deep furrow. (BP03:7, part)

A new pipid from the Cretaceous of Africa (In Becetén, Niger) and early evolution of Pipidae

59. Otic capsules, basal process, shape: (0) poorly differentiated from the rest of prootic, shallow excavation; (1) distinct, short anteroventral process; (2) conspicuous, medially located pterygoid knob. (BGT12:29)
60. Otic capsules, contact area for palatoquadrate, orientation: (0) anterior or anterolateral; (1) completely ventral; (2) completely lateral. (G16)
61. Otic capsules, inferior perilymphatic foramina: (0) present; (1) absent. (BGT12:12)
62. Otic capsules, inferior perilymphatic foramina, position: (0) open intracranially anterior to jugular foramen; (1) open extracranially posterior to jugular foramen; (2) open extracranially ventral to jugular foramen. (BGT12:13)
63. Otic capsules, superior perilymphatic foramina: (0) present; (1) absent. (BGT12:14)
64. Otic capsules, superior perilymphatic foramina, position: (0) open intracranially anterior to jugular foramen; (1) open extracranially posterior to jugular foramen. (B13:11, part)
65. Otic capsules, occipital condyles, shape of articular surface: (0) convex, ovoid or reniform; (1) flat, circular. (CT88:37, BR98:9)
66. Otic capsules, occipital condyles, orientation of articular surface in ventral view: (0) posteromedial; (1) posterolateral. (CT88:36, BR98:10)
67. Otic capsules, posteroventral process ventrolateral to condyloid fossa: (0) absent; (1) present. (G16)
68. Otic capsules, crista parotica, transverse dorsal crest: (0) absent; (1) present. (CT88:34)
69. Otic capsules, bony cranio-quadrate passage (sensu Goodrich, 1930; Paterson, 1946) on anterior wall of prootic: (0) as a more or less distinct groove; (1) as a close canal formed by anteroventral extension of crista parotica. (G16)

A new pipid from the Cretaceous of Africa (In Becetén, Niger) and early evolution of Pipidae

70. Otic capsules, cranio-quadrant passage, exit foramen (opening into the tympanum), margin: (0) bound only medially by prootic or in cartilage; (1) bound completely by prootic. (G16)
71. Columella: (0) absent; (1) present. (CT88:21)
72. Tympanic annulus: (0) absent, (1) present. (G16)
73. Mentomeckelian bone: (0) present; (1) absent. (BGT12:38)
74. Angulosplenial, coronoid process: (0) poorly developed; (1) well-developed but short; (2) long, blade-like. (BGT12:37)
75. Jaw articulation, position relative to otic capsule: (0) lateral; (1) at the anterolateral corner; (2) posterior. (BGT12:39)

Hyoid Apparatus

76. Hyoid apparatus, hyale, general configuration: (0) complete, arising laterally; (1) narrowly discontinuous, arising laterally; (2) complete or narrowly discontinuous, arising from a medial bridge; (3) broadly discontinuous, arising from a medial bridge; (4) mostly incomplete, only medial bridge. (BMG09:26)
77. Hyoid apparatus, hyale, ossification: (0) not ossified; (1) ossified. (BGT12:44)
78. Hyoid apparatus, anterolateral processes of hyoid plate: (0) absent; (1) present. (BMG09:28)
79. Hyoid apparatus, posteromedial process, length of ossified portion: (0) less than one half of the anteroposterior length of the lower jaw; (1) more than one half of the anteroposterior length of the lower jaw. (BGT12:41)
80. Hyoid apparatus, posteromedial process, shape (as anterior end width relative to that of posterior end): (0) wider anterior than posterior; (1) symmetrical or narrower anterior than posterior. (BGT12:42)
81. Hyoid apparatus, parahyoid bone: (0) present; (1) absent. (BGT12:43)

A new pipid from the Cretaceous of Africa (In Becetén, Niger) and early evolution of Pipidae

Vertebral Column

82. Presacral vertebrae, number of discrete elements: (0) nine; (1) eight; (2) seven; (3) six. (B13:34)
83. Presacral vertebrae, centra, formation: (0) perichordal; (1) epichordal. (BGT12:45)
84. Presacral vertebrae, postzygapophyses, configuration of articulation facets: (0) flat; (1) with grooves and ridges; (2) curved ventrally. (BGT12:47)
85. Presacral vertebrae, cotyle, relative width with respect to vertebral canal maximum width: (0) nearly as wide as; (1) clearly narrower. (G16)
86. Presacral vertebra I, anterior cotyles, interrelation: (0) closely juxtaposed (including a single articulation facet; type III of Lynch, 1971); (1) moderately separated (type II of Lynch, 1971); (2) well separated (type I of Lynch, 1971). (B13:35)
87. Presacral vertebra I, anterior cotyles, position relative to neural canal: (0) completely ventral, (1) ventrolateral. (G16)
88. Presacral vertebrae I and II, relation: (0) not fused, weak or no imbrication; (1) not fused, broad imbrication medially only; (2) not fused, broad imbrication involving all the neural laminae; (3) synostotically fused; (4) synchondrotically fused. (BGT12:49)
89. Presacral vertebra III, transverse processes, uncinat process: (0) present; (1) absent. (BMG09:41)
90. Presacral vertebrae, posterior presacrals (except last presacral), posteromedial margin of neural arch: (0) slightly concave to straight or with a minute neural spine; (1) projecting in a well-developed neural spine; (2) deeply notched; (3) with irregular projections. (BGT12:48)
91. Presacral vertebra IV, transverse process, shape in dorsal/ventral aspect: (0) straight or nearly so; (1) markedly curved posteriorly. (CT88:46)
92. Presacral vertebra IV, transverse processes (plus ribs if present), proximal-distal length in comparison to sacral diapophyses length: (0) nearly equal or slightly longer, (1) much longer (25% or more). (G16)

A new pipid from the Cretaceous of Africa (In Becetén, Niger) and early evolution of Pipidae

93. Presacral vertebra V, transverse process, orientation in dorsal/ventral aspect with respect to sagittal plane: (0) nearly perpendicular; (1) moderately forward; (2) markedly forward; (3) posterior. (G16)
94. Presacral vertebra VI, transverse processes, orientation in dorsal/ventral aspect with respect to sagittal plane: (0) nearly perpendicular; (1) moderately forward; (2) markedly forward; (3) posterior. (B13:41)
95. Presacral vertebra VI, transverse processes, proximal-distal length in comparison to sacral diapophyses length: (0) clearly shorter; (1) nearly equal or longer. (B13:39)
96. Presacral vertebrae, last presacral, articulation facets of centrum: (0) notochordal; (1) opisthocoelous; (2) procoelous; (3) amphicoelus. (BGT12:46; B13:37)
97. Ribs, as discrete elements: (0) present in larvae and adults; (1) present in larvae and ankylosed to transverse processes in adults; (2) absent in larvae and adults. (BGT12:50)
98. Sacrum, diapophyses, distal expansion in dorsal/ventral view (as ratio of distal length and mediolateral width): (0) weakly expanded or unexpanded (ratio < 0.75); (1) moderately expanded (0.75 < ratio < 1.5); (2) widely expanded (ratio > 1.5). (B13:45)
99. Sacrum, diapophyses, distal margin in dorsal view: (0) laterally convex; (1) straight; (2) laterally concave. (B13:46)
100. Sacrum, diapophyses, anterior margin, orientation with respect to sagittal plane in dorsal view: (0) posterolateral; (1) nearly perpendicular; (2) anterolateral. (B13:47)
101. Sacrum, neural arch lamina, proportions (minimum length at base of diapophysis relative to external interzygapophyseal width): (0) transversely rectangular, wider than long (ratio ≤ 0.6); (1) nearly square, nearly as long as it is wide ($1 \geq \text{ratio} > 0.6$); (2) longitudinally rectangular, longer than wide (ratio > 1). (G16)
102. Sacrum, neural arch lamina, medial ridge or crest: (0) absent; (1) present. (CT88:48)
103. Sacrum, number of vertebrae: (0) one; (1) two or more. (G16)

A new pipid from the Cretaceous of Africa (In Becetén, Niger) and early evolution of Pipidae

104. Sacrum, articulation with urostyle: (0) non-synovial, notochordal; (1) monocondylar; (2) bicondylar; (3) fused. (BGT12:51; B13:43)
105. Urostyle, transverse processes: (0) present; (1) absent. (B13:48)
106. Urostyle, dorsal ridge: (0) inconspicuous or low; (1) present, moderately to well developed. (B13:49)

Pectoral Girdle

107. Clavicle, medial end, shape: (0) not expanded; (1) expanded. (BGT12:53)
108. Clavicle, relationship to scapula: (0) lateral end contacts medial edge of pars acromialis; (1) lateral end overlaps anterior edge of pars acromialis; (2) lateral end is fused to scapula. (BGT12:52)
109. Scapula, proportions (as ratio between maximum width of glenoid fossa and maximum width of shaft): (0) ratio > 1; (1) 1 > ratio > 0.5; (2) ratio < 0.5. (BMG09: 57; BGT12:54)
110. Scapula, relative length with respect to the clavicle: (0) shorter; (1) longer; (2) nearly as long as. (B13:52)
111. Scapula, medial notch: (0) present; (1) absent. (BGT12:55)
112. Scapula, anterior lamina: (0) present; (1) absent. (B13:53)
113. Cleithrum, general shape: (0) not forked; (1) forked. (B13:54)
114. Cleithrum, relation to posterior edge of suprascapular cartilage: (0) not covering; (1) covering. (BGT12:56)
115. Coracoid, sternal end, expansion (as ratio between its width and coracoid length): (0) ratio < 0.5; (1) ratio nearly 0.5; (2) ratio nearly 1. (BGT12:57)
116. Omosternum: (0) present; (1) absent. (B13:56)
117. Sternum: (0) present; (1) absent. (B13:58)
118. Sternum, condition: (0) cartilaginous; (1) ossified. (B13:59)

A new pipid from the Cretaceous of Africa (In Becetén, Niger) and early evolution of Pipidae

119. Sternum, shape: (0) wide and relatively short, semicircular or romboid; (1) proximally bifurcated into two slender prongs; (2) anchor or arrow shape, peduncle slender or broad; (3) broad, oval to subrectangular, typically notched posteriorly. (G16)
120. Epicoracoid cartilages, interrelation in the coracoideal region: (0) broadly overlapping; (1) narrowly overlapping or abutted; (2) completely fused. (BMG09:56)
121. Epicoracoid cartilages, posterolateral expansion: (0) absent; (1) present. (CT88:50)
122. Epicoracoid cartilages, posterolateral expansion, lateral extent relative to the lateral margin of the sternum: (0) not surpassing; (1) surpassing. (CT88:51)

Forelimb

123. Humerus, shaft, general shape: (0) columnar; (1) ventrally curved. (B13:60)
124. Humerus, humeral ball (= eminentia capitata), relative size (as transverse diameter relative to maximum distal width at epicondyle level): (0) small (ratio < 0.58); (1) large (ratio > 0.58). (G16)
125. Humerus, medial and lateral epicondyles, relative development: (0) medial well developed, lateral much reduced, pressed against the humeral ball; (1) medial well developed, lateral reduced but projected laterally; (2) equally well developed, distal humerus almost symmetrical; (3) medial greatly expanded, lateral moderately developed. (G16)
126. Humerus, deltoid crest (= crista ventralis), relative length (with respect to the humeral length): (0) short (ratio nearly 1/3); (1) long (ratio nearly 1/2). (G16)
127. Humerus, parietal crest (= crista paraventralis): (0) absent; (1) present. (G16)
128. Humerus, medial epicondylar crest (= radial crest): (0) absent; (1) present, moderately to well developed. (G16)
129. Humerus, mid-length cross section, medullary space relative to cortical bone: (0) broad; (1) narrow. (G16)
130. Carpus, carpal torsion: (0) absent; (1) present. (B13:62)

A new pipid from the Cretaceous of Africa (In Becetén, Niger) and early evolution of Pipidae

131. Carpus, preaxial carpals (element Y and distal 2): (0) separate, (1) fused. (F06:65)
132. Carpus, post axial carpals (ulnare, distal carpals 3, 4, and 5): (0) all discrete; (1) distal carpals 4 and 5 fused; (2) distal carpals 3, 4, and 5 fused; (3) ulnare and distal carpal 5 fused, distal carpal 4 discrete. (B13:61)
133. Prepollex: (0) present; (1) absent. (G16)
134. Prepollex, number and shape of prepollical elements: (0) one, spherical or elongate, (1) two, distal may be elongate, (2) three or more, spherical or elongate, (3) two, distal hypermorphic axe-head-shaped. (BMG09:62)
135. Metacarpals, maximum length relative to radio-ulna length: (0) relatively short (ratio < 0.65); (1) long, (ratio > 0.7). (B13:63)

Pelvic Girdle

136. Ilium, ilial shaft, shape of the proximal cross-section: (0) circular or nearly so, iliac shaft not compressed mediolaterally; (1) vertically oval, iliac shaft compressed mediolaterally. (BGT12:58)
137. Ilium, ilial shaft, shape of the distal cross-section: (0) circular or nearly so, iliac shaft uncompressed dorsoventrally; (1) horizontally oval, iliac shaft fairly compressed dorsoventrally; (2) flattened, iliac shaft much compressed dorsoventrally. (BGT12:59)
138. Ilium, dorsal prominence, relative height with respect to that of the acetabular fossa: (0) very low; (1) low to moderately high; (2) very high. (BGT12:60)
139. Ilium, dorsal prominence, shape in lateral profile: (0) bell-shaped, symmetrical or nearly so with both anterior and posterior margins gently sloping; (1) rectangular-shaped, symmetrical or nearly so with both anterior and posterior margins steep; (2) clearly asymmetrical with a posterior convex slope and an anterior margin steep and slightly concave. (BGT12:61)
140. Ilium, dorsal prominence, orientation in dorsal aspect: (0) not inclined, vertically directed; (1) inclined medially; (2) inclined laterally. (BGT12:62)

A new pipid from the Cretaceous of Africa (In Becetén, Niger) and early evolution of Pipidae

141. Ilium, dorsal prominence, relative position of its apex with respect to the anterior margin of acetabular fossa: (0) clearly posterior; (1) approximately same level; (2) clearly anterior. (BGT12:63)
142. Ilium, dorsal protuberance: (0) inconspicuous; (1) conspicuous. (BGT12:64)
143. Ilium, dorsal protuberance, shape: (0) elongate, projecting laterally; (1) nearly rounded, projecting laterally; (2) globose, projecting dorsolaterally. (BGT12:65)
144. Ilium, spiral groove on shaft: (0) absent; (1) present. (B13:64)
145. Ilium, dorsal crest: (0) inconspicuous; (1) present as a low ridge; (2) well developed as a flange (wider than one half of the shaft width). (BGT12:66)
146. Ilium, dorsal crest, longitudinal extension relative to iliac shaft length: (0) restricted to distal half of the iliac shaft; (1) extends along the anterior three fourths of the iliac shaft; (2) extends lengthwise or nearly so; (3) restricted to the proximal part of the iliac shaft. (BGT12:67)
147. Ilium, dorsal crest, orientation: (0) directed dorsally; (1) directed dorsolaterally; (2) directed laterally. (BGT12:68)
148. Ilium, lateral oblique ridge: (0) absent; (1) present. (BGT12:69)
149. Ilium, interiliac scar: (0) inconspicuous; (1) ample, but restricted to ventral part of ilia; (2) ample both ventrally and dorsally. (BGT12:70)
150. Ilium, angle between the margin of the ventral acetabular expansion and the ventral margin of the iliac shaft in acetabular view: (0) acute; (1) nearly straight; (2) obtuse. (BGT12:71)
151. Ilium, dorsal acetabular expansion, lateral exposure in acetabular view: (0) broad; (1) narrow but distinct; (2) minimal, inconspicuous. (BGT12:72)
152. Ilium, relation with ischium: (0) not fused; (1) fused to each other. (BGT12:73)
153. Ischium, shape of the posterior wall of the acetabulum in dorsal view: (0) slightly concave; (1) deeply concave. (BGT12:74)
154. Ischium, shape in lateral view: (0) long, with a nearly rectangular outline; (1) short, with semicircular outline. (B13:68)

A new pipid from the Cretaceous of Africa (In Becetén, Niger) and early evolution of Pipidae

155. Pubis, condition: (0) cartilaginous; (1) partially or completely ossified. (BGT12:75)

156. Epipubis: (0) absent, (1) present. (CT88:72; BMG09:67)

Hindlimb

157. Femur, femoral crest: (0) absent; (1) present. (BMG09:68)

158. Femur, length relative to tibiofibula length: (0) shorter (ratio < 0.9); (1) nearly equal (ratio around 1); (2) longer (ratio > 1.1). (B13:70)

159. Tarsus, tibiale-fibulare, relative length (as % of the limb [femur + tibiofibula + tibial-fibular] length): (0) less than 20%; (1) more than 20%. (G16)

160. Tarsus, tibiale-fibulare, longitudinal crests: (0) absent; (1) present. (CT88:73)

161. Tarsus, distal tarsal 1, as a discrete element: (0) absent, (1) present. (BMG09:71)

162. Tarsus, distal tarsals 2 and 3, configuration: (0) not fused; (1) fused. (B13:72)

163. Prehallux: (0) present; (1) absent. (G16)

164. Prehallux, number and shape of prehallical elements: (0) one, spherical or elongate (1) two, spherical or elongate, (2) three or more, spherical or elongate, (3) two, distal hypermorphic axe-head-shaped, (4) three or more, axe-head-shaped. (BMG09:72)

165. Distal of sesamoides tarsale: (0) absent; (1) present. (BGT12:76)

Characters added by Aranciago et al., 2019

166. Posterior end of the frontoparietal bone: 0, rounded; 1, convergent margins resulting in an acute posterior end of the bone.

167. Lateral flange on pterygoid: 0, absent; 1, present but transversally wide and restricted posteriorly; 2, present but anteroposteriorly long and thin.

168. Posterior margin of otic capsules: 0, at same level of the occipital condyles; 1, posteriorly expanded, surpassing the posterior margin of the occipital condyles.

A new pipid from the Cretaceous of Africa (In Becetén, Niger) and early evolution of Pipidae

169. Frontoparietal, shape of the anterior margin: acuminate (0); or rounded (1).
170. Frontoparietal, interorbital constriction: (0) present; (1) absent.
171. Prootic, with epiotic prominences on its medial margin: (0) absent; (1) present.
172. Vertebrae, shape of centrum in dorsal view: (0) squared (almost as anteroposteriorly long as transversely wide) minimal space between vertebrae; (1) rectangular (wider than long) with gap between vertebrae greater than half their length.
173. Sacrum, shape of diapophyseal processes: (0) anterior and posterior process rounded; (1) anterior process tapering and posterior process rounded; (2) anterior and posterior processes tapering.
174. II pair of ribs: (0) laterally or posterolaterally projected; (1) anterolaterally oriented.
175. Ribs, expansions along its shaft: (0) present; (1) absent.
176. Illium, shape in dorsal view: (0) anterior half of iliac shaft subparallel each other; (1) anterior half of iliac shaft divergent each other, resulting in a V-shape contour.

Ordered Characters: 18, 32, 33, 36, 38, 39, 59, 74, 82, 97, 98, 120, 141, 149,

Appendix S6. Taxa list. † symbol represents extinct taxon and bold name represent new taxa from those of Aranciago Rolando et al (2019)

Alytes obstetricans

Ascaphus truei

Avitabatrachus uliana †

***Aygroua anoualensis* †**

Bombina variegata

Chelomophrynus bayi †

***Cratopipa novaolindensis* †**

Discoglossus pictus

A new pipid from the Cretaceous of Africa (In Becetén, Niger) and early evolution of Pipidae

Eoxenopoides reuningi †

Hadromophryne natalensis

Hymenochirus boettgeri

Inbecetenanura ragei †

Kuruleufenia xenopoides †

Llankibatrachus truebae †

Neusibatrachus wilferti †

Nevoatrachus gracilis (*Cordicephalus gracilis*) †

Oumtkoutia anae †

Pachycentrata taqueti †

Patagopipa corsolini †

Pelobates cultripes

Pipa carvalhoi

Pipa pipa

Platyplectrum ornatum

Pseudhymenochirus merlini

Rhadinosteus parvus †

Rhinophrynus dorsalis

Saltenia ibanezi †

'*Shelania*' *pascuali* †

Silurana tropicalis

Singidella latecostata †

Spea multiplicata

Thoraciliacus rostriceps †

Vulcanobatrachus mandelai †

Xenopus arabiensis †

Xenopus laevis

Xenopus muelleri

A new pipid from the Cretaceous of Africa (In Becetén, Niger) and early evolution of Pipidae

'Xenopus' romeri †

'Xenopus' stromeri †

Xenopus wittei

Appendix S7. Change on character codification from Aranciago Rolando et al., 2019

Changes on *Pachycentrata taqueti* are based on observation made on specimens (A. Lemierre). Changes on *'Xenopus' stromeri* are based on the description of materials given by Rage et al. (2008). Changes on *'Xenopus' romeri* are based on the description given by Estes (1975). Changes on *Thoraciliacus rostripes* are based on Trueb (1999). Changes on *Cratopipia novaolindensis* are based on the redescriptions given by Báez et al. (2021). Changes on *Avitabatrachus uliana* are based on the recent revision of the genus by Báez et al. (2022).

Pachycentrata taqueti: Character 5, 0 to 1; Character 9, 0 to 1; Character 11, 1 to ?; Character 18, ? to 0&1; Character 19, ? to 1; Character 52, 1 to 1&2; Character 82, ? to 3; Character 166, ? to 0; Character 168, ? to 1; Character 169, ? to 0; Character 170, ? to 0; Character 172, ? to 1.

'Xenopus' stromeri : Character 1, ? to 1; Character 2, ? to 0; Character 3, ? to 1; Character 7, 0 to 1; [Character 18, ? to 1]; Character 20, ? to 1; Character 61, 1 to 0; Character 62, 0 to 2; Character 63, 0 to 1; Character 82, ? to 2; Character 103, ? to 0; Character 104, ? to 3; [Character 109, ? to 2]; Character 112, ? to 1; Character 123, 1 to 0; [Character, 125, 3 to 2]; Character 126, 0 to 1; [Character 128, 0 to 1]; Character 151, 1&2 to 2; Character 168, ? to 0; Character 170, 1 to 0; [Character 171, ? to 0].

Thoraciliacus rostripes : character 57, 0 to 1; character 58, ? to 0; character 104, 2 to 1.

Cratopipia novaolindensis: Character 5, 0 to 1; Character 23, 1 to ?; Character 25, 1 to ?; Character 31, 1 to 0; Character 32, ? to 1; Character 34, 1 to 0; Character 42, ? to 1; Character 43, ? to 0; Character 48, ? to 0; Character 49, ? to 1; Character 65, 0 to ?; Character 71, ? to 1; Character 82, 2 to 1; Character 88, 3 to 2; Character 104, 3 to ?; Character 105, 1 to 0; Character 126, 0 to 1; Character 138, ? to 0&1; Character 139, ? to

A new pipid from the Cretaceous of Africa (In Becetén, Niger) and early evolution of Pipidae

0; Character 140, ? to 2, Character 141, ? to 0; Character 145, 0 to 0&1; Character 152, 0 to 1; Character 155, 1 to 0; Character 168, 1 to 0.

Avitabatrachus uliana: Character 104, 3 to 1&3.

Appendix S8. List of synapomorphies for selected clades.

Equal weight, ordered analysis

Pipimorpha : 137, 0→1; 145, 0→1; 149, 0→1

Pipimorpha, excluding *Aygroa anoualensis*: 136, 1→0; 142, 0→1, 2; 152, 0→1.

Pipimorpha, node excluding *Nevobatrachus* and *Cratopipia* + *Thoraciliacus*: 31, 0→1; 58, 0→1; 60, 0→1; 74, 0→1.

Vulcanobatrachus + Gondwanopipidae: 27, 0→1; 34, 0→1; 79, 0→1; 80, 0→1.

Cratopipa novaolindensis + *Thoraciliacus rostriceps*: 105, 1→0; 152, 0→1.

Gondwanopipidae: 23, 0→1; 56, 1→0; 99, 0→1; 114, 0→1; 149, 1→2; 167, 0→1; 173, 0→2.

Shelaniinae: 24, 0→1; 82, 2→1; 88, 3→1; 94, 1→2; 137, 1→2; 174, 0→1.

Pipidae: 21, 0→1; 39, 1→0; 90, 3→0; 94, 1→2; 152, 0→1.

Xenopodinae: 24, 0→1; 32, 1→2, 3; 34, 1→0; 45, 0→1; 53, 0→1; 54, 0→1; 62, 2→1; 67, 0→1; 84, 0→1; 101, 0→1; 107, 0→1; 109, 1→0; 138, 1→2; 139, 0→2; 141, 0→1.

Pipinomorpha: 59, 2→0.

Pipinomorpha (node excluding *Inbecetenanura*): 7, 0→1; 171, 1→0.

Singidella + *Pachycentrata* clade: 9, 0→1; 18, 3→1.

Pipinae: 36, 0→1; 68, 0→1; 75, 0→1; 92, 0→2; 106, 0→1; 127, 1→0; 160, 0→1.

Equal Weight analysis, constrained on the topology of Jetz and Pyron (2018)

Xenoanura : 4, 0→1; 17, 0→1; 19, 0→2; 48, 1→0.

Pipimorpha: 137, 0→1; 145, 0→1; 149, 0→1

Rhinophrynididae: 56, 0→1; 97, 0→1,2; 109, 0→1; 130, 0→1; 159, 1→0.

Pipimorpha, node excluding *A. anoualensis* : 88, 1→4; 141, 0→1,2; 151, 0→1.

A new pipid from the Cretaceous of Africa (In Becetén, Niger) and early evolution of Pipidae

C. novaolindensis + *T. rostriceps*: 105, 1→0; 152, 0→1.

Pipidae: 23, 0→1; 39, 1→0; 49, 0→1; 99, 0→1; 101, 0→2; 149, 1→2; 166, 1→0; 172, 1→0; 173, 0→2.

Xenopodinomorpha: 67, 0→1; 108, 1→2; 175, 1→0.

Stem-Xenopodines: 8, 0→1; 45, 2→0; 62, 1→2; 63, 0→1.

Stem-Xenopodines, node including *Inbecetenanura*: 7, 1→0; 170, 0→1; 171, 0→1.

Stem-Xenopodines, node excluding *Inbecetenanura*: 20, 1→0; 49, 1→0; 66, 1→0; 101, 2→0.

Xenopodines: 32, 1→2; 34, 1→0; 39, 1→0; 45, 0→1; 84, 0→1; 93, 0→; 107, 0→1; 138, 1→2; 139, 1→2; 145, 0→1.

Stem-Hymenocherini: 6, 0→1; 18, 3→1; 22, 0→1; 38, 1→2; 51, 0→1; 52, 1→2; 82, 2→3; 84, 0→2; 92, 1→0.

Crown-Hymenocherini: 36, 0→2; 68, 0→1; 77, 0→1; 85, 0→1; 90, 0→2; 93, 0→1

A new pipid from the Cretaceous of Africa (In Becetén, Niger) and early evolution of Pipidae

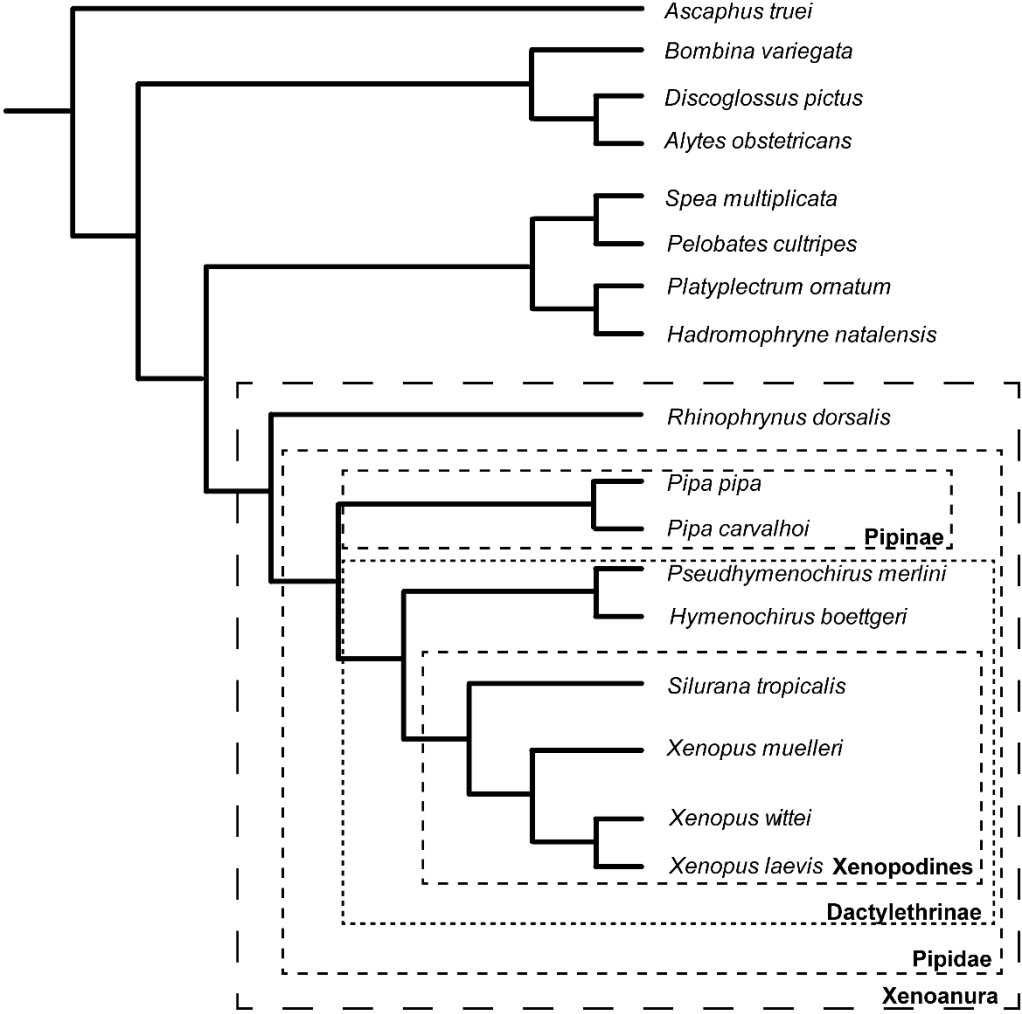


FIGURE S1. Tree used for the constrained analyses under a phylogeny inferred from Jetz and Pyron (2018).

Chapter IV

***BIG BRAIN IN STRANGE BODY:
DESCRIPTION OF NEW PACHYCENTRATA REMAINS
AND THE FIRST FOSSIL AMPHIBIAN 'BRAIN'***

Big brain in strange body: Description of new *Pachycentrata* remains and the first fossil amphibian ‘brain’

IV.1 Introduction

When the pipid *Pachycentrata taqueti* was first described in the original study of the In Becetén fauna, its extreme ornamentation was already considered a unique feature among pipids (“La seconde forme es tunc forme nouvelle [...] l’ornementation osseuse (pachyostose) extrêmement développée” in Broin et al., 1974). The detailed description and illustration of this peculiar pipid also noted this aspect, even considering that *Pachycentrata* exhibited pachyosteosclerosis (Báez and Rage, 1998). The authors interpreted the unique aspect of the braincase and vertebral elements as probable specializations to underwater burrowing (Báez and Rage, 1998) as in living *Pipa* (Emerson, 1976). However, the presence of pachyosteosclerosis, if attested, is puzzling. This condition has never been recovered in any amphibians, even in putative stem-Lissamphibia, like the temnospondyls or Lemospondyls (Romer and Edinger, 1942). It is known in several amniotes, from sirenians (Houssaye, 2009) to extinct aquatic snakes (Houssaye et al., 2013; Rage et al., 2016; Houssaye et al., 2019). In amniotes, pachyosteosclerosis has been identified as a ballast for buoyancy control and hydrostatic regulation of body trim, as amniotes have to dive with their lungs filled with air (Ricqlès and Buffrénil, 2001). As pipids (and anurans) are known to be able to dive with empty lungs, and breath via cutaneous exchanges (Duellman and Trueb, 1994), pachyosteosclerosis could have a different impact on the lifestyle of *Pachycentrata*. This extreme ossification could also have great impacts on the preservation of internal anatomy features.

I will here present my preliminary results on the analyses of the internal anatomy of the braincase and vertebral elements of *Pachycentrata taqueti* with CT-scanned specimens, and the osteological description of several new *Pachycentrata* remains from In Becetén.

Big brain in strange body: Description of new *Pachycentrata* remains and the first fossil amphibian ‘brain’

IV.2 Materials and Methods

Institutional abbreviations

MNHN: Muséum national d’Histoire naturelle, Paris, France. All specimens are stored within the Paleontological collection of the MNHN of Paris (France) in the Amphibians and Reptiles section, under the collection number MNHN.F.IBC XXXX.

Micro-CT scan tomography

MNHN.F.IBC 1604, 1611, 1616 and 1623 were micro-CT scanned at the AST-RX (Accès Scientifique à la Tomographie à Rayons X) at the UMS 2700, MNHN (Paris France). A nanofocus beam of 180 kV of the CT scanner was used with the following parameters: voltage, 125 kV; current, 245 μ A; voxel size, 7.847 μ m; slice resolution, 1666 x 1676 pixels. A total of 2312 virtual slices were reconstructed. These slices were imported into the 3D reconstruction software Mimics 21.0 (Materialise, Leuven, Belgium). Before importation, slices were cropped to maximally remove the empty spaces. To decrease data size, slices were converted from 16 to 8 bits. The dataset thus includes 1868 slices, with an image resolution of 1300 x 1222 pixels and a voxel size of 15.69 μ m for the volume file (see Appendix S1). The 3D model was produced by segmentation of each bone using the ‘thresholding’ function (using the contrast on grayscale images). We used the same voxel resolution of 15.69 μ m, with a smoothing factor of 3 for one iteration, to homogenize the model resulting from manual segmentation. Data

Big brain in strange body: Description of new *Pachycentrata* remains and the first fossil amphibian ‘brain’

produced by segmentation were exported in the software 3matic 9.0 as a separate file (see Appendix S2, S3).

The anatomical terminology used herein is based on Roček (1980) and Biton et al. (2016) for cranial features, and Sanchíz (1998) for postcranial ones. Anatomical terminology for cranial nerves and brain structures follows Ecker (1889) and Púgener (2002) for spinal nerves.

IV.3 Systematic Palaeontology

ANURA Duméril, 1805

XENOANURA Starrett, 1973

PIPIMORPHA Ford and Cannatella, 1993

PIPIDAE Gray, 1825

PACHYCENTRATA Báez and Rage, 2004

Pachycentrata taqueti (Báez and Rage, 1998)

1998 *Pachybatrachus taqueti* Báez and Rage, p. 671-680, text-figs 2, 3, pl. 1 : figs 1-6.

Holotype—one braincase and otic capsules (MNHN.F.IBC 1604; erroneously reported as IBC 1404 in Báez & Rage 1998: 671).

Stratigraphic range—Coniacian to Santonian (89-86 Ma).

Newly referred materials—four prooticooccipitals (MNHN.F.IBC 1607, 1608, unnumbered specimens), one atlantal complex (MNHN.F.IBC 1965), four presacral vertebrae (MNHN.F.IBC 1615-1618) and four sacrococcyges (= sacral vertebrae + urostyle) (MNHN.F.IBC 1621-1623, 1967).

Big brain in strange body: Description of new *Pachycentrata* remains and the first fossil amphibian ‘brain’

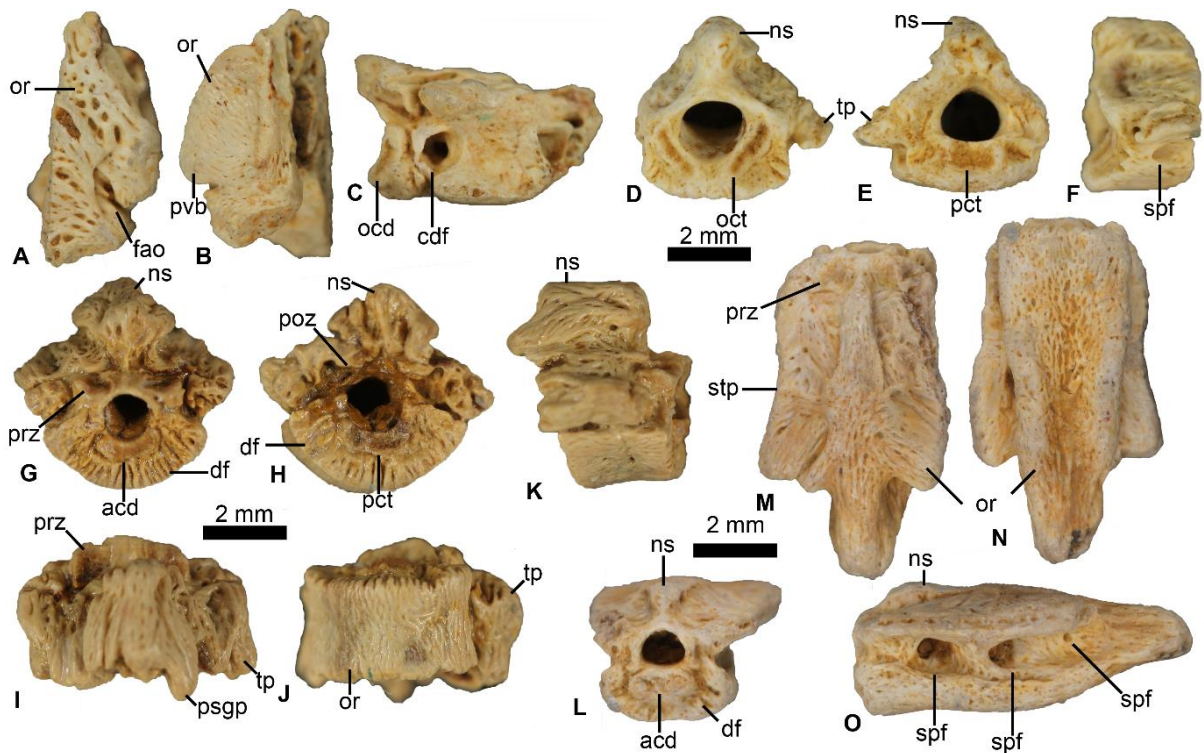


Figure IV-1. Cranial and postcranial elements of *Pachycentrata taqueti*. A – C, right prooticoccipital (MNHN.F.IBC 1607) in A, dorsal, B, ventral and C, right lateral views; D–F, atlantal (MNHN.F.IBC 1965) in D, anterior, E, posterior and F, right lateral views; G–K, presacral vertebra (MNHN.F.IBC 1616) in G, anterior, H, posterior, I, dorsal, J, ventral and K, right lateral views; L–O, sacrococcyx (MNHN.F.IBC 1623) in L, anterior, M, dorsal, N, ventral and O, left lateral views. **Abbreviations:** *acd*, anterior condyle; *cdf*, condyloid fossa; *df*, deep furrows; *fao*, foramen for the arteria occipitalis; *ns*, neural spine; *ocd*, occipital condyle; *oct*, occipital cotyle; *or*, ornamentation; *pct*, posterior cotyle; *poz*, postzygapophysis; *prz*, prezygapophysis; *psgp*, parasagittal process; *pvb*, posteroventral bulge; *spf*, spinal foramen; *stp*, sacral transverse process; *tp*, transverse process.

IV.4 Osteological Description

Prooticoccipitals—All four elements represent respectively left (MNHN.F.IBC 1608, unnumbered specimen) and right (MNHN.F.IBC 1607, unnumbered specimen) halves of the posterior region of the braincase (i.e. prooticoccipital; Fig. IV-1A–C). All bear (1) a vermicular dorsal ornamentation, (2) grooves on their ventral surface and (3) possess a thickened aspect (Fig. IV-1A–B). The foramen for the arteria occipitalis is visible within a shallow groove (Fig. IV-1A). The occipital condyle is thin and crescentic, with a large bulge posteroventrolateral to the condyle fossa (Fig. IV-1C).

Big brain in strange body: Description of new *Pachycentrata* remains and the first fossil amphibian ‘brain’

Atlantal complex—This element is represented by complete atlantal vertebrae (fused atlas + presacral vertebra II, Fig. IV-1D–F). The atlantal complex is thick and bloated, due to pachyosteosclerosis. Its dorsal and ventral surfaces are ornamented (respectively with vermicular and shallow grooves). This fusion commonly occurs in Pipimorpha, Bufonidae and Pelobatidae (Duellman and Trueb, 1994). The presence of a small spinal foramen midlength of the atlantal indicates the limit between the fused vertebrae. The centrum is wider than long. The occipital cotyles are small, crescentic (Fig. IV-1D). They are flanked laterally by two large depressions (articulation with the paired occipital bulges). Occipital cotyles are separated by a protruding limb of bone, similar (but not necessarily homologous) to the odontoid process of Caudata (Duellman and Trueb, 1994). The posterior cotyle is rectangular (i.e. length > height). The neural spine is high and widens posteriorly (Fig. IV-1D – F). One small and dorsoventrally flattened transverse process is preserved.

Presacral vertebrae—All four presacrals are opisthocoelous, with a dorsoventrally thickened and bloated centrum (Fig. IV-1G–K). Their dorsal surface is covered by a vermicular ornamentation, while their ventral surface is also ornamented with deep grooves (Fig. IV-1I–J). The neural arches show that they were imbricated, and bear short parasagittal processes posteriorly (Fig. IV-1I, K). Anterior and posterior surfaces of the centra bear deep furrows (Fig. IV-1G – H), reinforcing connection between vertebrae. The zygapophyses bear short smooth circular articular facets (Fig. IV-1I, J). The prezygapophysis are oriented dorsally, with their lateral margin raised vertically (Fig. IV-1G). the postzygapophysis are oriented ventrally, and their lateral margins bears a deep groove, forming a tongue-and-groove articulation with the prezygapophyses.

Sacrococcyges—Only the sacral region and anterior portion of the urostyle are preserved on the four identified sacrococcyges (Fig. IV-1L–O). As in previous elements, the dorsal surface is covered by a vermicular ornamentation (Fig. IV-1M), while the ventral surface is covered by an ornamentation made of anteroposteriorly elongated deep grooves (Fig. IV-1N). The centrum is dorsoventrally thickened. The neural spine

Big brain in strange body: Description of new *Pachycentrata* remains and the first fossil amphibian ‘brain’

is low but extends posteriorly (Fig. IV-1M). The prezygapophyses bears short and smooth circular articular facets (Fig. IV-1M). These facets are dorsally oriented. In lateral view, the presence of two large spinal foramina indicates that two vertebrae are included (in addition to the urostyle) within the sacrococcyx (Fig. IV-1O). The first vertebra that fuses with the urostyle is the sacral vertebra, forming the sacrococcyx. The second vertebra that can fuse is the last presacral vertebra. As all known anurans, except Ascaphidae (only known by *Ascaphus truei*), possess eight presacral vertebrae (Duelleman and Trueb, 1994). Hence, the VIIIth presacral vertebra is incorporated within the sacrococcyx. Thus, the anteriormost spinal foramen marks the posterior limit of the VIIIth presacral vertebra region, while the sacral vertebra region is delimited anteriorly by this spinal foramen (Fig. IV-1O) and posteriorly by the second large spinal foramen. A third small foramen is located posterior to the large foramina (Fig. IV-1O). It is interpreted as the spinal foramen of the urostyle.

Discussion—All vertebral elements can be referred to a single taxon, on the basis of (1) a vermicular dorsal ornamentation; (2) ventral ornamentation made of deep grooves; (3) deep furrows on anterior and posterior surface of the centra; (4) rectangular (wider than height) and (5) thickened and bloated aspect due to pachyosteosis. The braincases can be referred to the same taxon as the vertebrae based on (1) vermicular dorsal ornamentation; (2) occipital articular facet reduced and crescentic; (3) large secondary occipital articulation posteroventral to the occipital condyles; (4) pachyosteosis. All elements can be referred to Pipidae on the basis of (1) absence of posterolateral expansion of the parasphenoid (i.e. Eustachian canals visible on ventral view); (2) margins of the optic foramina fully ossified; (3) azygous frontoparietal; (4) parasphenoid fused to the braincase; (5) opisthocoelous presacral vertebrae and (6) fused sacral vertebra and urostyle into a sacrococcyx. All elements are referred to *Pachycentrata*, based on (1) their dorsal and ventral ornamentation; and (2) bone dorsoventrally thickened due to pachyosteosclerosis. They also belong to the only known species of this genus, *Pachycentrata taqueti*. This taxon is the most recognizable anuran from In Becetén, and the most represented. Indeed, no other

Big brain in strange body: Description of new *Pachycentrata* remains and the first fossil amphibian ‘brain’

amphibians exhibit pachyosteosclerosis and this feature is unique to *Pachycentrata*. Recent analyses (Chapter II) confirmed the position of *Pachycentrata* as the oldest pipine, close to extant Hymenocherini and the extinct Eocene *Singidella* Báez and Harrison, 2005. All these taxa share a reduction of the number of presacral vertebrae, down to six free presacral vertebrae.

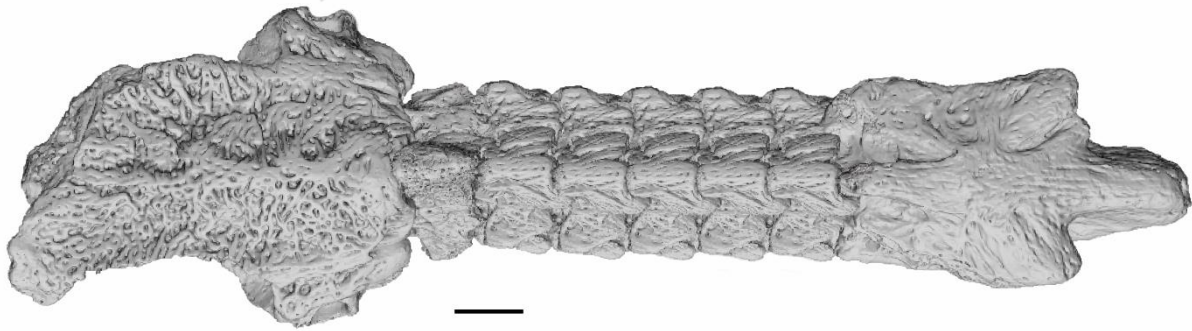


Figure IV-2. Proposed reconstruction of the vertebral column and skull of *Pachycentrata taqueti*. Scale bar represents 2 mm.

We were able to CT-scan the most complete braincase, MNHN.F.IBC 1604 (holotype of *P. taqueti*), one atlantal vertebra (MNHN.F.IBC 1611), a complete presacral vertebra (MNHN.F.IBC 1616) and the most complete sacrocoelium (MNHN.F.IBC 1623). Thus, it was possible to propose a schematic reconstruction of the *Pachycentrata* known skeleton (Fig. IV-2). Hence, the individual represented by the braincase MNHN.F.IBC 1604 was likely around 35-40 mm long from snout to the end of the sacrocoelium. This size is similar to the small extant pipids, like *Hymenochirus* and *Pseudhymenochirus* (Channing and Rödel, 2019).

Within the braincase and vertebrae, we were able to reconstruct the endocast of the both endocranial cavity (Fig. IV-3) and the vertebral canal. Within these endocasts, several structures were identified, and will be described here.

Big brain in strange body: Description of new *Pachycentrata* remains and the first fossil amphibian ‘brain’

IV.5 Internal Anatomy

Cranial endocast : a brain ?

When studying extinct vertebrates, the shape, size, and evolution of the brain has always been widely studied, especially in regard of the brain evolution during terrestrialization (Jerison, 1973; Streidter and Northcutt, 2020). The analyses of the endocranial cavity, and its endocast has been well developed in mammals (Mackintosh et al., 1985; Macrini et al., 2007; Lefebvre et al., 2011; Rowe et al., 2011; Jerison, 2012; Orliac et al., 2014) and has been recently developed on dinosaurs (Brochu, 2000; Evans, 2005; Witmer and Ridgely, 2008; Miyashita et al., 2011; Buchlotz, 2012; Paulina-Carabajol et al., 2016; Riamon et al., 2021). These analyses allowed to infer numerous biological capacities of extinct taxa, such as their visual, auditive and olfactive capacities (Edinger, 1921; Taylor et al., 1995; Witmer and Ridgely, 2008). Although extant anuran taxa, like *Rana* or *Xenopus*, have been used as model for “basic” tetrapod brain anatomy (Lee-Liu et al., 2017; Streidter and Northcutt, 2020), few studies have focused on their endocast and its application to extinct taxa. This is mainly due to the poor preservation of the brain structures within the endocast. Within amphibians (Dempster, 1935; Romer and Edinger, 1942; Herrick, 1948; Pardo and Anderson, 2016; Dutel et al., 2019; Clement et al., 2016, 2021), the brain does not fill the entire endocranial cavity. Hence the endocast only preserves a few main structures, such as the telencephalon or the optic tecta (Romer and Edinger, 1942; Clement et al., 2021). Some anurans preserve more structures, like *Breviceps* (Clement et al., 2021). Interestingly, the endocast of *Pachycentrata* (Fig. IV-3) widely differs from the one retrieved in *Inbecetenanura ragei* (Fig. III-5) with numerous structures present and discernable. Furthermore, even when comparing the endocast of *Pachycentrata* with the endocast of well ossified taxa, *Pipa* and *Breviceps*, *Pachycentrata* preserves even more brain structures. Thus, we can interpret most of the brain structures and sizes. Hence, we consider that the preserved endocast is an anuran “brain”. This is the first

Big brain in strange body: Description of new *Pachycentrata* remains and the first fossil amphibian ‘brain’

time that the imprint of a brain has been identified not only in anuran, but in all lissamphibians and extinct amphibians (Romer and Edinger, 1942).

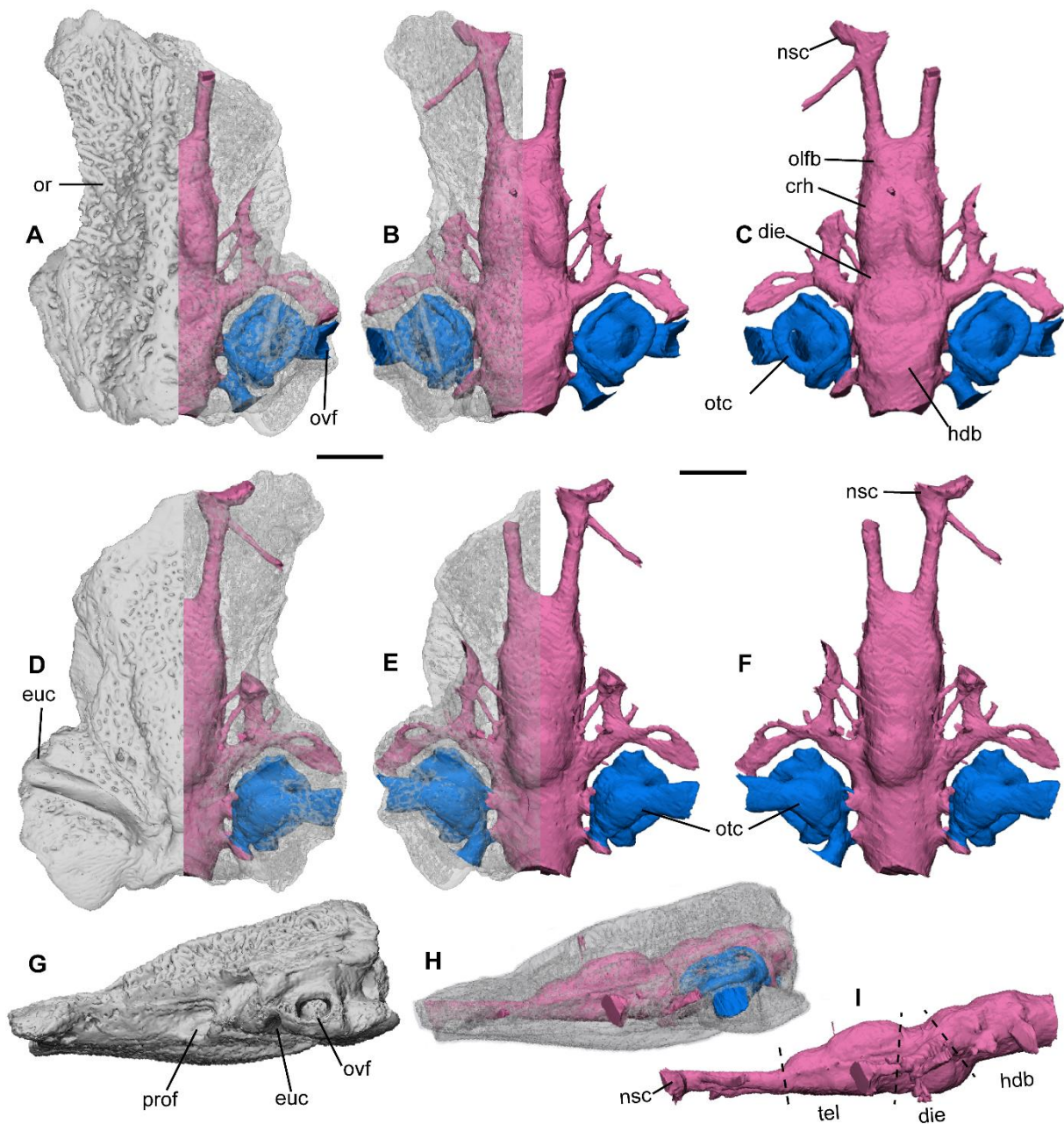


Figure IV-3. 3D models of the braincase (MNHN.F.IBC 1604) of *Pachycentrata taqueti* and its endocast. A-C, 3D model of MNHN.F.IBC 1604 in dorsal view, A, dorsal view showing the ornamentation (left side) and the underlying endocast (right side), B, dorsal view showing the underlying endocast and C, dorsal view of the endocast; D-F, MNHN.F.IBC 1604 in ventral view, D, ventral view showing the ornamentation (left side) and the underlying endocast (right side), E, ventral view showing the underlying endocast and F, ventral view of the endocast; G-I, MNHN.F.IBC 1604 in left lateral view, G, 3D model of the braincase, H, same model transparent to show the underlying endocast and I, 3D model of the endocast.

Big brain in strange body: Description of new *Pachycentrata* remains and the first fossil amphibian ‘brain’

Abbreviations: **crh**, cerebral hemisphere; **die**, diencephalon; **euc**, Eustachian canal; **hdb**, hindbrain; **nsc**, nasal capsule; **olfb**, olfactory bulbs; **or**; ornamentation; **otc**, otic capsule; **ovf**, oval fenestra; **prof**, prootic foramen; **tel**, telencephalon. Scale bars represent 2 mm.

The endocast is 10.5 mm long (from exoccipital to sphenethmoid) and 9.2 mm wide (widest point; Fig. IV-4A-C). On the anteriormost portion, the olfactory bulbs are distinct from the cerebral hemispheres but a lateral constriction (Fig. IV-4A). The paired olfactory bulbs are short(1 mm length) but thick (1.5 mm height). The telencephalon is not prominent, as in *Pipa*, but resembles the one of *Xenopus* (Fig. IV-4D-H). On its dorsal surface, a wide shallow sulcus divides the telencephalon into two cerebral hemispheres (Fig. IV-4A). Contrary to *Pipa*, the hemispheres are parallel to one another (Fig. IV-4A) and do not protrude posteriorly. A small elongate bulge is present on each side of the anterolateral region of the cerebral hemispheres. This small, paired structures is interpreted as the accessory olfactory bulbs (Fig. IV-4B, C). Thus, the identified olfactory bulbs are in fact the main olfactory bulbs. A shallow groove seems to delimit the ventral margin of the pallium (Fig. IV-4B). It is not possible to distinct the dorsal, lateral, medial and ventral sections of the pallium. Posterior to the telencephalon, the dorsal surface of the diencephalon is a shallow depression, with no habenal discernable (Fig. IV-4A).

On the ventral surface of the diencephalon, two protuberances, located midwidth of the brain, are visible (Fig. IV-4B). The anteriormost protuberance is small (Fig. IV-4C), barely visible in ventral view (Fig. IV-4B). This protuberance, located midlength of the brain, is tentatively interpreted as remnants of the optic chiasma (Fig. IV-4B). The second protuberance is tall (i.e., it strongly protrudes ventrally; Fig. IV-4B, C) and large. It is interpreted as the hypothalamus. On the anterior region of the dorsal surface of the midbrain, posterior to the diencephalon, the optic tectum forms a rather ovoid structure. A faint constriction midlength of the structure might indicates the limit between the two lobes. The optic tectum is poorly developed, short, and do not protrude laterally (Fig. IV-4A, C). Posterior to the optic tectum, the cerebellum is a faint flattened structure present on the dorsal brain surface (Fig. IV-4A). A wide but

Big brain in strange body: Description of new *Pachycentrata* remains and the first fossil amphibian ‘brain’

anteroposteriorly short structure, posterior to the cerebellum, is interpreted as the fourth ventricle (Fig. IV-4A, C). Posterior to the fourth ventricle, the medulla oblongata narrows laterally until the exoccipital (Fig. IV-4A).

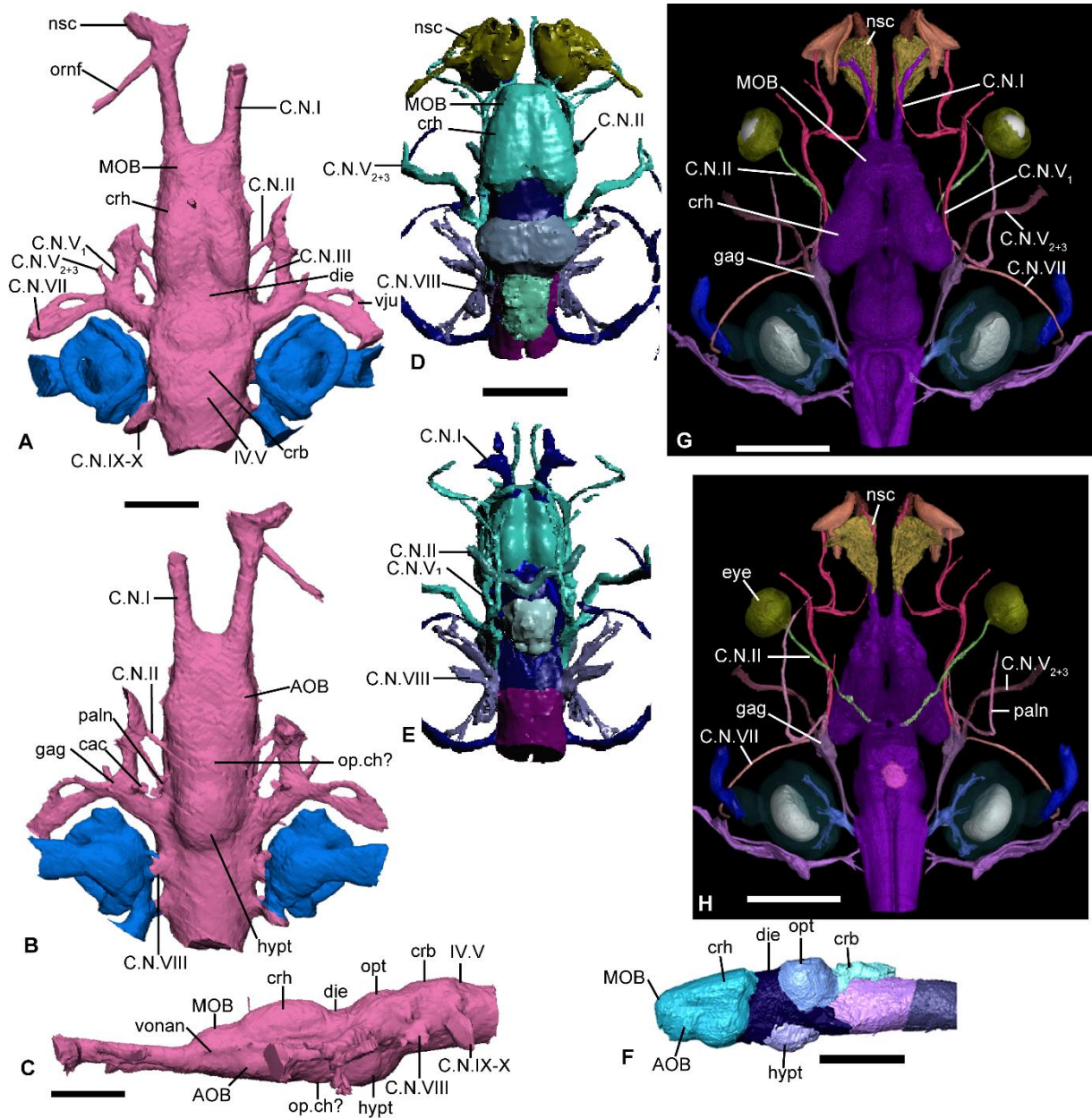


Figure IV-4. Endocast of *Pachycentrata taqueti* and brain of extant pipids. A-C, endocast and “brain of *Pachycentrata* in A, dorsal, B, ventral and C, lateral views; D-F, 3D model of the brain of *Xenopus laevis* (taken from Porro and Richards, 2017) in D, dorsal, E, ventral and F, left lateral views; G-H, 3D model of the brain of *Pipa* (realized by Jaimi Gray) in G, dorsal and H ventral views. **Abbreviations:** AOB, accessory olfactory bulb; cac, canal for carotid artery; C.N I-X, cranial nerves I-X; crb, cerebellum; crh, cerebral hemisphere; die, diencephalon; gag, Gasserian ganglion; hypt, hypothalamus; MOB, main olfactory bulb; nsc, nasal capsule; op.ch?, putative optic chiasma; opt, optic tectum; ornf, orbitonasal duct; plan, palatine nerve; vju, jugular vein; vonan, vomeronasal duct.

Big brain in strange body: Description of new *Pachycentrata* remains and the first fossil amphibian ‘brain’

Cranial nerves and vascular system

Several paired canals were identified. Most of them exit the braincase via cranial foramina (Fig. IV-3A-B, D-E). Thus, we were able to identify most anuran cranial nerves. Within anurans, ten pairs of cranial nerves (C.N.) are known in skeletally mature individuals (Ecker, 1889; Púgener, 2002; Porro and Richards, 2017).

The first pair of canals are long and extend anteriorly from the anterior region of the olfactory bulbs and accessory olfactory bulbs to the base of the nasal capsule (see below). This pair is interpreted as the olfactory nerves (C.N. I). Just posterior to the anterior end of both C.N. I, a small canal diverges posterolaterally (Fig. IV-4A, B). This canal exists the sphenethmoid posterolaterally via the orbitonasal foramen. Thus, these paired canals are interpreted as the nasolacrimal duct. A small pair of canals arise from the accessory olfactory bulbs and extend anteriorly at midheight of the Main olfactory bulbs (MOB). They fuse to the C.N.I. Thus, they are interpreted as the vomeronasal nerves (Jungblut et al., 2013). Midlength of the brain, three pairs of canals diverge from the brain, and seems to exit the braincase via a single large foramen (Figs. IV-3G, H, 4A, B; Báez and Rage, 1998). However, tomography revealed that all three pairs exit the braincase via distinct foramina. These foramina all open within a large lateral fossa, present on each side of the braincase (Fig. IV-3G).

The anteriormost paired canals are thin and small (Fig. IV-4A). They diverge from the braincase anterolaterally at the level of the optic chiasma (Fig. IV-4B). Thus, they are interpreted as the optic nerves (C.N. II). Hence, the exit foramina of C.N II is interpreted as the optic foramina. The second paired canals are also small and thin (Fig. IV-4A). They exit the braincase via a pair of small and circular foramina, located posterior to the optic foramina (Fig. IV-4A). Due to this position, the foramina are interpreted as the oculomotor foramina. Hence, the second paired canals are interpreted as the motor oculi nerves (C.N. III). At the base of the C.N.III, a pair of thin and short canals diverge from the C.N. III and extend ventrally. They exit the braincase via two small and circular foramina that pierced the floor of the braincase near the

Big brain in strange body: Description of new *Pachycentrata* remains and the first fossil amphibian ‘brain’

parasphenoid (Fig. IV-3D). In the original description of MNHN.F.IBC1602, these foramina were interpreted as putative exit foramina for the carotid artery (Báez and Rage, 1998: 675), while the second pair of ventral foramina, located laterally to the first pair (Fig. IV-4B) had been interpreted as the palatine foramina (Báez and Rage, 1998: 675: fig. 2B). As the second paired canals do not connect with the C.N. V (see below), we interpret them as part of the carotid arteries. Thus, we confirm the proposition of Báez and Rage (1998) that the medial ventral foramina are exit foramina for the carotid artery. The third paired canals arise from the anterior region of the medulla oblongata (Fig. IV-4A). These canals are large (Fig. IV-4A, C) and exit the braincase anteriorly into large, paired foramina (Fig. IV-3B). Interestingly, the foramina open into a large groove that extends anteriorly on the lateral surface of the braincase, where the optic and oculomotor foramina open (Fig. IV-3G). These canals are the largest identified within the braincase. Thus, we interpret them as the trigeminal nerves (C.N. V). Hence, the exit foramina are interpreted as the prootic foramina (Fig. IV-3G).

Furthermore, the lateral groove extending anteriorly alongside the lateral wall of the braincase is interpreted as the groove for the ophthalmic ramus of C.N. V (C.N. V₁ in Porro and Richards, 2017). Just before the prootic foramen, a thickening is present on the C.N.V. Its position allows us to interpret it as the Gasserian ganglion (Ecker, 1889; Porro and Richards, 2017). A short pair of canals arise ventrally from the Gasserian ganglions (Fig. IV-4A, B). They exit the braincase via the palatine foramina, piercing the floor of the braincase (Fig. IV-4B). Thus, they are interpreted as the palatine nerves (“palatine ramus” of Ecker, 1889). A second, small, paired canal emerge from the Gasserian ganglions dorsal to the C.N.V₁. These canals exit the braincase via a pair of small foramina posterolateral to the large prootic foramina. The origin and orientation of these canals allow to interpret them as the maxillo-mandibular ramus of the C.N.V (C.N.V₂₊₃). A third pair of canals arise laterally from the Gasserian ganglions (Fig. IV-4A). They are large and extend laterally alongside the anterior margin of the otic capsules (Figs. IV-3A; 4A). They exit the skull posterolaterally, via a pair of foramina opening slightly dorsoposteriorly within the

Big brain in strange body: Description of new *Pachycentrata* remains and the first fossil amphibian ‘brain’

fenestra ovalis (Fig. IV-3G). Thus, they are interpreted as the hyomandibular branch of the facial nerves (C.N.VII). Midlength of the hyomandibular branch of C.N.VII, a small canal diverges anteriorly briefly, before fusing laterally with the large C.N.VII. It is interpreted as part of the internal jugular vein, while the remaining is likely indistinct from the hyomandibular branch of C.N.VII. A pair of short but wide canals arise from the brain around the level of the cerebellum (Fig. IV-4A, B). They connect laterally to the inner ear via two small acoustic foramina (Fig. IV-4A). They are interpreted as the auditory nerves (C.N.VIII). Finally, a pair of large canals arise from the posterior region of the medulla oblongata (Fig. IV-4A). They are short and exit the braincase via the condyloid fossa (Fig. IV-3B, E). These large canals are interpreted as the indistinct imprint of the glossopharyngeal and vagus nerves (C.N.IX and C.N.X), the internal jugular vein and part of the lymphatic system.

Two pairs cranial nerves could not be identified within *Pachycentrata* braincase, the trochlear (C.N.IV) and abducens (C.N.VI) nerves. It is unsurprising, as the trochlear nerves pathway is parallel and close to the ophthalmic ramus of C.N.V, even sharing the same protection sheath (Ecker, 1889), and is difficult to discern in several extant taxon (Porro and Richards, 2017). Regarding the abducens nerves, they arise within the brain, before extending into the Gasserian ganglions and following the same pathway as the ophthalmic ramus of C.N.V (Ecker, 1889; Porro and Richards, 2017). Thus, its ‘absence’ within the preserved endocast is unsurprising.

Big brain in strange body: Description of new *Pachycentrata* remains and the first fossil amphibian ‘brain’

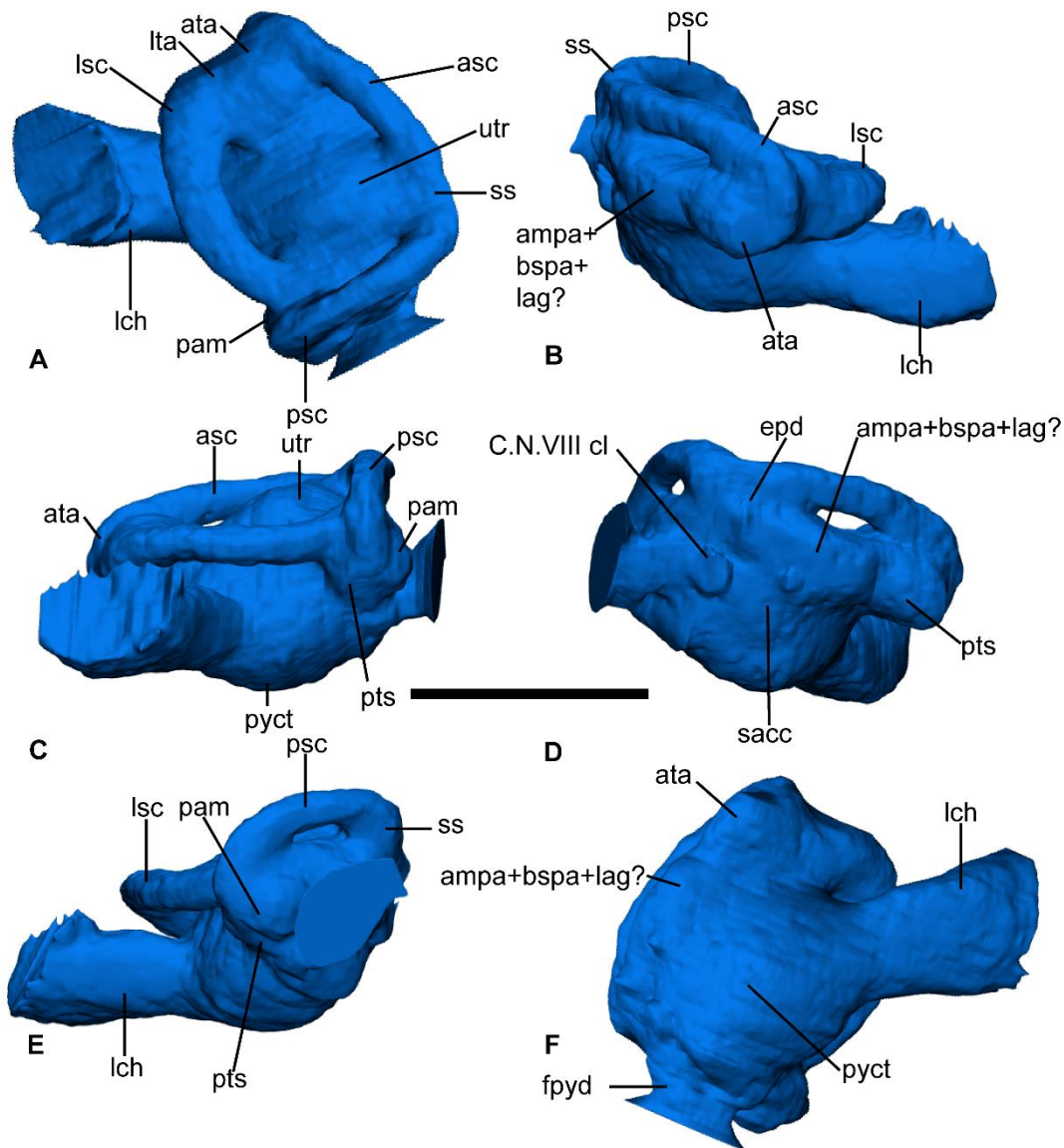


Figure IV-5. Endocast of the left inner ear of *Pachycentrata taqueti*, based on MNHN.F.IBC 1604. Endocast in A, dorsal, B, anterior, C, lateral, D, medial, E, posterior and F, ventral. Abbreviations: ampa+bspa+lag?, fused imprint of amphibian and basilar papillae and lagena; asc, anterior semicircular canal; ata, anterior ampulla; C.N.VIII cl, canal for the C.N.VIII; epd, endolymphatic duct; fpyd, fused perilymphatic ducts; lch, lateral chamber; lsc, lateral semicircular canal; ita, lateral ampulla; pam, posterior ampulla; psc, posterior semicircular canal; pts, posterior sinus; psc, posterior semicircular canal; pyct, perilymphatic cistern; sacc, saccule; ss, superior sinus; utr, utricle. Scale bar represents 2 mm.

Inner ear

Both otic capsules are complete, and their endocast preserve part of the vestibular apparatus and otic chamber.

The inner ear is well-developed laterally, with an enlarged perilymphatic space (Fig. IV-5). This space opens laterally into the fenestra ovalis (Fig. IV-3A). The

Big brain in strange body: Description of new *Pachycentrata* remains and the first fossil amphibian 'brain'

vestibular apparatus is fully preserved. The anterior, lateral and posterior semi-circular canals are distinct and thick. The lateral semi-circular canal is smaller than the other two and flattened dorsoventrally (Fig. IV-5A-C). The anterior ampulla is thick and protrudes anterolaterally at the base of the anterior semi-circular canal (Fig. IV-5B). The lateral ampullae is also thick and protrudes anterolaterally near the anterior ampulla. Thus, both ampullae are indistinct in anterior view (Fig. IV-5A, B). The posterior ampulla protrudes posterolaterally at the base of the posterior semi-circular canal (Fig. IV-5C, E). The superior sinus (common crus) is wide and low (Fig. IV-5A, E). The posterior sinus protrudes posterolaterally from the posterior ampulla (Fig. IV-5E). The utricle and utricular recess form a single indistinct thick structure (Fig. IV-5A). Medial to the utricle, an anteroposteriorly elongated structure protrudes medially (Fig. IV-5D). It is tentatively interpreted as the amphibian and basilar papillae, and lagena. In total the vestibular apparatus represents more than half the total height of the inner ear.

A small canal arises from the utricle and opens into the braincase via a small circular foramen. It is interpreted as the endolymphatic duct, and the foramen, as the endolymphatic foramen (Fig. IV-5D, F). The otic chamber is bulbous but does not extend ventrally (Fig. IV-5B). The sacculus is discernible as a faint protuberance on the anterior surface of the otic chamber. The perilymphatic cistern represents the rest of the chamber (Fig. IV-5B). The cistern is bulbous ventrally and is separated from the laterally elongated perilymphatic space by a slight constriction. On the medial surface of the perilymphatic cistern, part of the C.N.VIII are preserved. On the posterior surface of the cistern, a short but wide canal opens within the condyloid fossa (Fig. IV-3A). It is interpreted as fused perilymphatic ducts.

Big brain in strange body: Description of new *Pachycentrata* remains and the first fossil amphibian ‘brain’

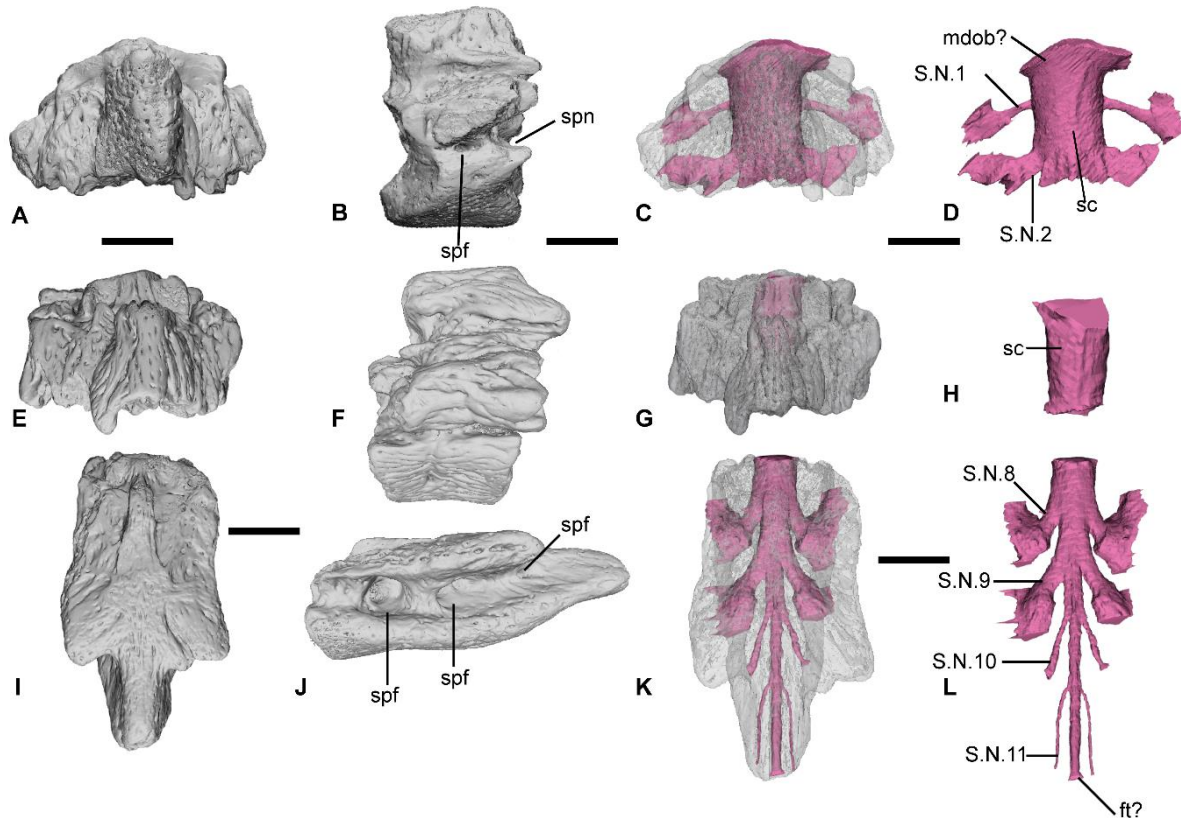


Figure IV-6 Endocast of the central nervous system of *Pachycentrata taqueti*. A-D, atlantal complex of *P. taqueti* (MNHN.F.IBC 1611), A, dorsal and B, left lateral views, C, same specimen transparent with the underlying endocast in dorsal view and D, endocast of the anterior region of the central nervous system in dorsal view; E-H, presacral vertebra of *P. taqueti* (MNHN.F.IBC 1616) in E, dorsal and F, left lateral views, G, same specimen transparent with the underlying endocast and H, endocast of the central region of the central nervous system in dorsal view; I-L, sacrococcyx of *P. taqueti* (MNHN.F.IBC 1623) in I, dorsal and J, left lateral views, K, same specimen transparent with the underlying endocast in dorsal view and L, endocast of the posterior region of the central nervous system in dorsal view. **Abbreviations:** ft?, putative filium terminale; mdob?, putative medulla oblongata; sc, spinal cord; spf, spinal foramen; spn, spinal foramen; S.N.1-11, spinal nerve 1-11.

Central Nervous System (CNS)

Within anurans, the Central Nervous System and its vertebral nerves (Púgener, 2002) exit the vertebral column intravertebrally (i.e., spinal foramina are not present on a single vertebra). As such, it is almost impossible to infer and reconstruct most of the CNS when studying isolated vertebrae. However, in *Pachycentrata*, the first spinal foramen is preserved on the atlantal (fusion of 1st and 2nd vertebrae; Fig. IV-6A-C). Furthermore, at least three spinal foramina seem preserved on its sacrococcyx (Fig.

Big brain in strange body: Description of new *Pachycentrata* remains and the first fossil amphibian ‘brain’

IV-6J, K). As *Pachycentrata* possesses 6 discrete presacral vertebrae, we can infer the minimal number of pairs of spinal foramina present, at least ten. This estimation is similar to the number of spinal foramina present in *Hymenochirus* (Pügener, 2002). The spinal cord is preserved mostly as a rather smooth cylindrical-shaped structure (Fig. IV-6D, H, L). Within the atlantal, the anterior region of the spinal cord thickens dorsally (Fig. IV-6D). It is tentatively interpreted as the posterior end of the medulla oblongata. Within the sacrococcyx, the posterior end of the spinal cord thickens into a small bulge (Fig. IV-6K, L). It is tentatively interpreted as part of the filum terminale. Within the endocast of the atlantal, a pair of small canals diverged from the spinal cord (Fig. IV-4D). These canals exit the atlantal via a small circular pair of spinal foramina midlength of the complex (Fig. IV-4B, C). These canals are interpreted as the first spinal nerve (fused S.N 1 and 2 of Ecker, 1889)

In the posterior region of the atlantal, the spinal cord seems to diverge into two large canals, whose full extension cannot be assessed (i.e. no third vertebra connected). They exit the atlantal via a deep notch on the posterior end of the lateral surface of the atlantal. These canals are interpreted as half of the second spinal nerve. Although we do not have a completed articulated vertebral column, the notches present both anteriorly and posteriorly on the lateral surface of the presacral vertebra (Fig. IV-6F) confirms that all presacral nerves are located intervertebrally. Thus, we cannot reconstruct spinal nerves 3 to 7. Within the sacrococcyx, a first pair of large canals diverge from the spinal cord (Fig. IV-6K, L). They exit the bone via the anteriormost spinal foramina, and thus are interpreted as the eighth spinal nerves. A second large pair of canals diverge posterior to the eighth spinal nerves (Fig. IV-6K, L), also exiting the sacrococcyx via a pair of large spinal foramina. These canals are interpreted as the ninth spinal nerve. A third pair of canals, smaller, also exit the sacrococcyx, via the posteriormost spinal foramina. They are interpreted as the tenth spinal nerves. Finally, a fourth pair of very small canals diverge on the posterior portion of the spinal cord. They do not exit the bone on its preserved portion. They are interpreted as the eleventh spinal nerves. The posteriormost region of the spinal cord

Big brain in strange body: Description of new *Pachycentrata* remains and the first fossil amphibian ‘brain’

IV.6 Discussion

Olfactive capacities—Within the brain of *Pachycentrata*, the telencephalon is the most developed region of the brain (xx mm), consisting of almost 50% of the total endocast volume. When comparing the MOB and AOB of *Pachycentrata* to those of *Xenopus* and *Pipa*, they are more prominent and more developed (Fig. IV-4A, D, G). Three distinct pairs of olfactive organs have identified within the nasal capsules of pipids (*Xenopus*; Weiss et al., 2021). One of them, the vomeronasal organ (VNO, also known as Jacobs organ) arise from the AOB (via the vomeronasal nerve), while the remaining two, the principal and middle cavities (PC and MC respectively) arise from the MOB. (Weiss et al., 2021). The use of the middle cavity within the nasal capsule as an olfactive organ is unique to pipids (Helling, 1939; Eisthen, 1992). Several analyses have linked the increase in volume (i.e. prominence) of the MOB to an increase in size of the linked olfactive organs (Noble, 1931; Jungblut et al., 2021; Weiss et al., 2021). Thus, we can interpret that *Pachycentrata* possessed bigger (relatively) olfactive organs than *Xenopus* or *Pipa*, at least regarding the principal and middle cavities. Within pipids, the principal cavity serves as the olfactory organ for the ‘air’ nose (as in all anurans; Weiss et al., 2021), while the middle cavity is the olfactory organ for the water nose (Eisthen, 1992). Thus, we interpret that *Pachycentrata* likely had better olfactive capacities than other pipids.

Visual capacities—The optic nerves of *Pachycentrata* are very thin, smaller than in *Xenopus* (Porro and Richards, 2017), but similar to the ones recovered in *Pipa*. Thus, we can interpret that *Pachycentrata* had small eyes, like *Pipa* (Thomas et al., 2020; other references). Furthermore, the reduced optic tectum seems smaller than in *Pipa* (although it could due to the brain not fully filling the endocranial space). The volume of the optic tectum has been related to the capacity in anurans to detect moving object

Big brain in strange body: Description of new *Pachycentrata* remains and the first fossil amphibian ‘brain’

(Ingle, 1973a, b). Thus, *Pachycentrata* likely had poor visual capacities, like *Pipa* (Thomas et al., 2020).

Auditory capacities—Within extant pipids, the ear system has undergone major evolution compared to other anurans, to accommodate for their aquatic lifestyle (Wever, 1985). They have lost their external ear, and the tympanic annulus is ossified and fused to the squamosal into a conch-shaped bone (Wever, 1985; Trueb et al., 2000). Using the extant phylogenetic bracket approach (Witmer, 1995), we infer that *Pachycentrata* also lacked an external ear, and possessed an ossified tympanic annulus. Although not fully preserved, the middle ear cavity, represented by the Eustachian canal, extended medially on the floor of the otic capsule from the level of the fenestra ovalis to the posterior margin of the parasphenoid. Both middle ear cavities would have been connected medially via the pharyngeal cavity (not preserved here; Wever, 1985). The laterally elongated perilymphatic space connecting the perilymphatic cistern to the fenestra ovalis is reminiscent, albeit shorter, of the lateral passage recovered in *Pipa pipa* (Wever, 1985) and *Xenopus* (Mason et al., 2015). The homology, or function of this lateral passage is still unknown (Mason et al., 2015), but as it is only present in pipids, it is likely linked to their aquatic lifestyle.

To recap, *Pachycentrata* was an aquatic pipids with small poorly functional eyes, a great sense of smell and an auditory apparatus adapted for its lifestyle.

Central nervous system and spinal nerves

The first pair of spinal nerves are very small, largely reduced than in other anurans, such as in *Bombina*, but similar to the size of the first spinal nerves of *Xenopus* and *Hymenochirus* (Púgener, 2002: fig. II.24C). Within extant pipids, the reduction of the hypoglossal nerves has been linked to the loss of the tongue, as tongue nerves originate from the hypoglossal nerves (Scholsser and Roth, 1995; Púgener, 2002). Using the extant phylogenetical bracket approach, and a similar reduction of the hypoglossal nerves in *Pachycentrata*, this extinct taxon likely lacked a tongue. Although the absence

Big brain in strange body: Description of new *Pachycentrata* remains and the first fossil amphibian ‘brain’

of a tongue could be considered a synapomorphy for Pipidae (Frost et al., 2006), this character has never been identified in any extinct pipid, until known.

The CNS of *Pachycentrata* seems to follow a rather standard pattern for anurans, with the modification known in *Pipa* and *Xenopus* (Púgener, 2002). Interestingly, whereas the reduction of the number of presacral vertebrae, via the incorporation of the eighth vertebra into the sacrococcyx, has been proposed as an argument for a close relationship between *Pachycentrata* and the Hymenocherini (Báez and Rage, 1998; Báez and Harrison, 2005), the CNS pattern of *Pachycentrata* differs from the one of *Hymenochirus*. In *Hymenochirus*, there is a reduction of the number of distinct sciatic plexus nerves from four (S.N. 9-12) to three, with the fusion of S.N. 10 and 11. Thus, in *Hymenochirus*, the sciatic plexus nerves are the following : seventh spinal nerve (S.N. 9), eighth spinal nerve (S.N. 10+11) and ninth spinal nerve (S.N.12). This is linked to larger eighth spinal nerve canals. However, in *Pachycentrata*, both eighth and ninth spinal canal are large. Hence, there is no fusion of the S.N.10 and 11 in *Pachycentrata*. The tenth and eleventh spinal nerves correspond to the S.N 12 and 13. Thus, *Pachycentrata* possessed thirteen pair of spinal nerves, albeit only eleven discrete pair. Hence, the incorporation of the eighth presacral vertebra into the sacrococcyx of *Pachycentrata* did not follow the same ontogenetical pattern as in *Hymenochirus* or *Pseudhymenochirus* (following Púgener, 2002).

Ecological inferences—The absence of an external ear, the presence of an ossified tympanic annulus and a sacrococcyx indicates that *Pachycentrata* was a fully aquatic anuran, like all pipids (Duelleman and Trueb, 1994). With its small eyes and poor visual capacity, *Pachycentrata* could be considered a poor hunter. However, pipids are known to sometimes use a mix of olfactive, tactile and auditory inputs during prey hunting or to detect predators (Kramer, 1933; Altmer, 1962). Hence, it is likely that *Pachycentrata* relied more on its smell than its vision. In addition, pipids are able to detect predators solely via olfactive inputs (Wells, 2007).

Big brain in strange body: Description of new *Pachycentrata* remains and the first fossil amphibian ‘brain’

The extreme ossification of the braincase, with pachyosteosclerosis, is unique among amphibians, and extremely rare even in amniotes (Houssaye, 2009, 2013). The development of pachyosteosclerosis in *Pachycentrata* remains puzzling. Although it reinforced the skull and vertebrae, the bony deposits likely hinder most movements of the vertebral column, while the lateral movements of the head were also limited. It could also have help *Pachycentrata* to quickly sink to the bottom of the lake or pond it lived. The lack of amphibian taxa to compare makes the interpretation of the development of pachyosteosclerosis in *Pachycentrata* very difficult. In the original description of *Pachycentrata*, the pachyosteosclerosis was interpreted as an indicator of burrowing capacities (Báez and Rage, 1998). Although we consider that pachyosteosclerosis cannot be the result of burrowing behavior, the strong ossification of the anterior portion of the braincase, in peculiar the sphenethmoid, is interesting. This ossification, combined with an anteroposteriorly elongate C.N.I indicates that *Pachycentrata* was likely a burrower (Whiting, 1961; Emerson, 1976). The shape of the skull, wedge-shaped, with its anterior end narrower than its posterior region (Fig. IV-2) has also been considered as an adaptation for using the skull as a locomotor organ (Wake, 1993). It is not possible to assess if burrowing was frequent or not in *Pachycentrata*. However, this pipid likely burrowed with its head into muddy bottom of lakes, as the extant *Pipa* (Emerson, 1976).

Pachycentrata resembles *Pipa*, in having poor vision, better sense of smell and burrowing headfirst. Thus, it is likely that *Pachycentrata* inhabited similar environment, such as the bottom of turbid, muddy, and dark lakes or ponds. In this kind of environment, the poor vision of *Pachycentrata* would not have been a disadvantage, and its good sense of smell would have allowed it to easily detect preys. Its capacity to burrow could have been used to forage the ground for food, or to survive within moist soils if the lakes dried up, as extant *Pipa* does (Emerson, 1976). We have no information on its jaw apparatus; thus, we cannot assess if *Pachycentrata* had teeth, nor if it possesses a *Pipa*-like jaw apparatus, allowing for suction-feeding (Trueb et al., 2000). However, it should be noted that the maxilla-mandibular ramus of

Big brain in strange body: Description of new *Pachycentrata* remains and the first fossil amphibian ‘brain’

the C.N. V, that innerves the jaws elements is thin, as in *Pipa*, unlike in *Xenopus* or *Hymenochirus* (Trueb et al., 2000; Porro and Richards, 2017). A link between this nerve ramus and *Pipa* jaw modification has never been explored but could yield interesting results.

IV.7 Conclusion

In conclusion, new cranial and vertebral elements of *Pachycentrata* have been identified in In Becetén. All bear the vermicular dorsal ornamentation and pachyosteosclerosis. The tomography of the braincase and vertebral elements allowed to reconstruct its cranial and spinal cord endocasts. The cranial endocast of *Pachycentrata* is in fact the imprint of at least 80% of its brain, a unique feat among amphibians. Thus, the endocast can be interpreted as the brain. Six pairs of cranial nerves are identified, alongside most of the inner ear structures. Five pairs of spinal nerves have also been identified. Comparison to extant pipids allowed us to infer that *Pachycentrata* had small poorly functioning eyes, a great sense of smell, lacked an external ear, had an inner ear modified for an aquatic lifestyle and also lacked a tongue. Thus, *Pachycentrata* likely lived at the bottom of turbid, muddy dark lakes or ponds, and was able to burrow within its bottom to feed, escape predators, or even to survive a drought that would dry its watery environment.

IV.8 Appendix

Table S1. List of CT-scan and associated 3D model of *Pachycentrata taqueti*.

Specimen number	Element	Taxon	CT-Scan files	3D Models
MNHN.F.IBC 1604	Braincase	<i>Pachycentrata taqueti</i>	ark:/87602/m4/472084	ark:/87602/m4/472087

Big brain in strange body: Description of new *Pachycentrata* remains and the first fossil amphibian ‘brain’

MNHN.F.IBC1604_endocast	‘Brain’	<i>Pachycentrata taqueti</i>	ark:/87602/m4/472084	ark:/87602/m4/397536
MNHN.F.IBC1604_left inner ear	Endocast of left inner ear	<i>Pachycentrata taqueti</i>	ark:/87602/m4/472084	ark:/87602/m4/397547
MNHN.F.IBC1604_right inner ear	Endocast of right inner ear	<i>Pachycentrata taqueti</i>	ark:/87602/m4/472084	ark:/87602/m4/397552
MNHN.F.IBC1611	Atlantal	<i>Pachycentrata taqueti</i>	ark:/87602/m4/472091	ark:/87602/m4/472102
MNHN.F.IBC1611_endocast	Endocast	<i>Pachycentrata taqueti</i>	ark:/87602/m4/472091	ark:/87602/m4/472105
MNHN.F.IBC1616	Presacral	<i>Pachycentrata taqueti</i>	ark:/87602/m4/472095	ark:/87602/m4/472108
MNHN.F.IBC1616_endocast	Endocast	<i>Pachycentrata taqueti</i>	ark:/87602/m4/472095	ark:/87602/m4/472114
MNHN.F.IBC1623	Sacrococcyx	<i>Pachycentrata taqueti</i>	ark:/87602/m4/472099	ark:/87602/m4/472117
MNHN.F.IBC1623_endocast	Endocast	<i>Pachycentrata taqueti</i>	ark:/87602/m4/472099	ark:/87602/m4/472120
Proposed reconstruction of <i>Pachycentrata</i> skeletal elements	Braincase and vertebral column	<i>Pachycentrata taqueti</i>		ark:/87602/m4/472111

Chapter V

*BRIDGING THE GAP ? DATING EARLY PIPID
EVOLUTIONARY RADIATION*

V.1 Introduction

Pipidae and its total group, Pipimorpha, are peculiar and enigmatic anuran clades. All known taxa, both extant and extinct, are exclusively aquatic (Duelleman and Trueb, 1994; although *Xenopus* is able to walk on the land; see references). Pipimorphs are today restricted to Africa and South America (Frost et al., 2006). However, their past geographical range is wider, with known occurrences in the fossil record during the Mesozoic in Europe, South America and Africa (Lemierre et al., 2022). Furthermore, the oldest pipimorphs (excluding *Aygroua anoualensis* Jones et al., 2003) are located in Europe, indicating a rich evolutionary history and multiple dispersal events across at least three continents. The oldest pipids are known in the earliest Late Cretaceous of Northwest Africa, with the occurrence of *Oumtkoutia anae* Rage and Dutheil, 2008 from the Cenomanian of Morocco (Rage and Dutheil, 2008) and *Pachycentrata taqueti* Baez and Rage, 1998 and *Inbecetenanura ragei* from the Coniacian-Santonian of Niger (Chapter III). Within South America, an endemic clade of pipimorphs, the Shelaniinae, thrived during the Late Cretaceous and Early Paleogene (Barcelos and dos Santos, 2022), with no pipid known in the South American fossil record until the Eocene (Barcelos and dos Santos, 2022). Among this rich fossil record (in peculiar for anuran in Africa and South America), several uncertainties remain on the chronology and timeline of pipid emergence and diversification. Molecular clock analyses have proposed an emergence of Pipidae during the Early Cretaceous (Cannatella, 2015; Feng et al., 2017), but no pipids are known until the early Late Cretaceous.

Furthermore, their absence from the Mesozoic fossil record of South America is puzzling. The emergence of Pipidae has been considered for a decade to be correlated with the opening of the South Atlantic Ocean (SAO) during the latest Early Cretaceous (Báez and Pugener, 2003; Gómez, 2016; Aranciaga-Rolando et al., 2019; Carvalho et al., 2019). The opening led to the breakup of West Gondwana into South America and

Bridging the gap ? Chronology of the early pipid diversification

Africa (Fairhead, 1988). The absence of pipids in the fossil record of the Late Cretaceous in South America has been interpreted as an absence of pipid taxa on the continent (Aranciaga-Rolando et al., 2019), placing the emergence and diversification of the clade solely on the African continent. Several transatlantic dispersal events, allowing for the establishment of south American and African lineages during the Paleogene, have been proposed to explain their extant presence (Aranciaga-Rolando et al., 2019). However, the scarce pipid remains in Late Cretaceous of Africa (representing only four known taxa), hardly reflect the proposed diversification of the previous studies. Hence, the timing of pipid diversification during the Cretaceous remains poorly understood. In addition, molecular clock analyses have estimated that several extant taxa (*Pipa*, Xenopodines, Hymenocherini) emerged during the Cretaceous, implying long ghost lineages (Cannatella, 2015).

To resolve these uncertainties on early pipid diversification, we decided to perform several divergence times analyses, using an FBD model, on two pipimorph phylogenies and two alternative interpretations of the fossil record. We then discuss the different proposed scenarios and their paleobiogeographical implications.

V.2 Materials and Methods

Fossilized Birth Death model (FBD model)—The Fossilized Birth-Death model (FBD) was first developed and introduced by Stadler (2010), Didier et al. (2012), and Heath et al., (2014). The FBD models diversification and allows estimating three parameters: cladogenesis (λ), sometimes called speciation (when a lineage splits into two), extinction (μ ; 'death' of the lineage), which are modelled by the older Birth-Death model, and fossilization (ψ ; a fossil of a given lineage is left and dated at the time of the event). In addition, the FBD model considers that a single lineage is present at the origin time of the diversification process and that extant lineages are samples with probability q . The method used below to estimate the divergence time is the one developed by Didier et al. (2017) and Didier and Laurin (2020), which requires only a

Bridging the gap ? Chronology of the early pipid diversification

topology (or a set thereof) and the geological age of each horizon that has yielded fossils of the relevant taxa. To obtain the probability density of the extinction times of taxa, we used the method developed by Didier and Laurin (2021).

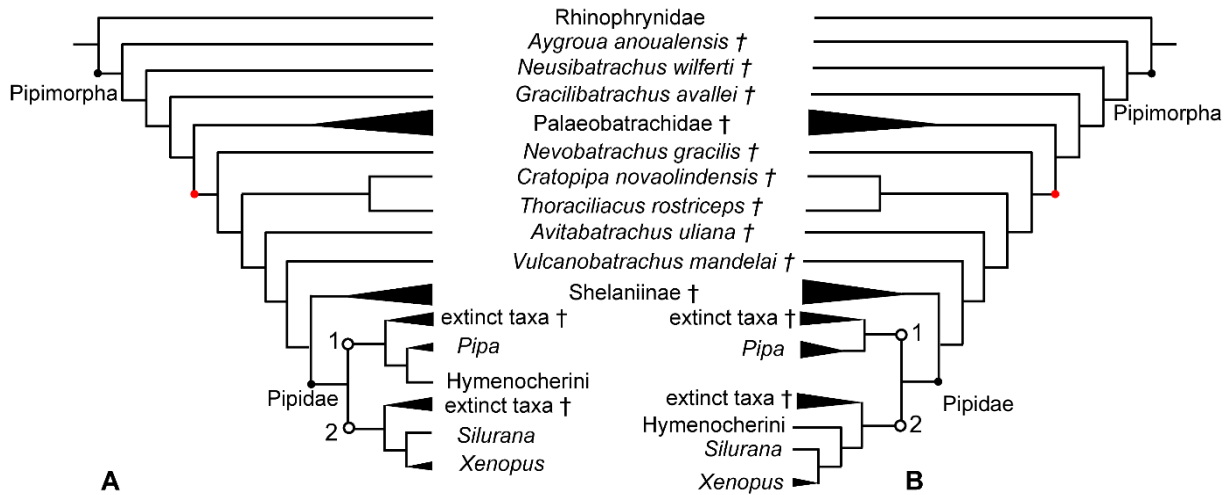


Figure V-1. Proposed topologies for pipimorph phylogeny. **A**, topology following the [Xenopodinae [*Pipa* + Hymenocherini]] hypothesis (supported by morphological data); **B**, topology following the [*Pipa* [Xenopodinae + Hymenocherini]] hypothesis (supported by molecular data and used to build the topological constraint). Clades present past the red circle are used in our analyses and white circles indicate (1) Pipimorpha node and (2) Xenopodinomorpha node; † indicates extinct taxon.

Pipimorph phylogeny—Pipimorpha includes Pipidae and all taxa phylogenetically closer to the latter than to Rhinophrynidae. All non-pipid pipimorphs are extinct taxa, the oldest of which date from the earliest Early Cretaceous (Jones et al., 2003; Lemierre et al., 2022). Within Pipimorpha, an endemic clade of South American taxa, Shelaniinae, has recently been recovered in several analyses (Aranciaga-Rolando et al., 2019; Lemierre et al., 2022). Furthermore, Shelaniinae may be the sister-clade to Pipidae (Lemierre et al., 2022). Within Pipidae, three extant clades are known, Pipinae (includes at least *Pipa* and its stem), Xenopodines (*Xenopus* + *Silurana*) and Hymenocherini (*Hymenochirus* + *Pseudhymenochirus*). Both Pipinae and Xenopodines possess total clades, Pipimorpha and Xenopodinomorpha respectively (Fig. V-1).

Phylogenetic analyses—The morphological dataset for phylogenetic analyses includes 45 taxa and 176 characters. It is derived from the dataset of Chapter III. We added two extinct pipimorphs, “*Xenopus*” *hasaunus* from the Oligocene of Libya

Bridging the gap ? Chronology of the early pipid diversification

(Špinar, 1980) and *Xenopus* sp. from the Oligocene of Ethiopia (Blackburn et al., 2019). All analyses were performed using TNT v.1.5 (Goloboff and Catalano, 2016) under equal weights. All analyses were conducted with cline characters ordered (characters 18, 32, 33, 36, 38, 39, 59, 74, 82, 97, 98, 120, 141, 149) in the analyses with or without topological constraint (Rineau et al., 2015; 2018). All analyses consisted of heuristic searches with 1000 random addition sequences of taxa, followed by tree bisection reconnection (TBR) branch swapping, holding 10 trees per repetitions. The final trees were rooted on *Ascaphus truei* (Ascaphidae), and when more than one most parsimonious tree was found, a strict consensus was obtained. To resolve the polytomies among the studied taxa (see below), we inferred their position based on majority-rule consensus trees. Constrained analysis was performed using the topology of Jetz and Pyron (2018) for extant taxa.

Topologies—Phylogenetical analyses based on morphological dataset have always recovered the following topology for extant pipids genera: [Xenopodines [Hymenocherini + *Pipa*]] (Fig. V-1A; Estes, 1975; Cannatella and Trueb, 1988; Ford and Cannatella, 1993). The inclusion of extinct pipimorphs (Nevo, 1968; Báez and Harrison, 2005) or pipids (Báez and Rage, 1998; Báez and Pugener, 2003) within phylogenetical analyses recovered a similar topology, with extinct taxa assigned to Xenopodinomorpha, Pipinomorpha or stem-Hymenocherini. However, the development and implementation of molecular analyses yield a radically different topology: [*Pipa* [Xenopodines + Hymenochirini]] (Fig. V-1B). This topology, with *Pipa* as the sister-taxon to all extant Pipids, has been recovered in all phylogenetical analyses when molecular data is included (Frost et al., 2006; Pyron and Wiens, 2011; Cannatella, 2015; Jetz and Pyron, 2018). This second topology is important, as extant taxa are not always recovered in the same phylogenetical position (Lemierre et al., 2022). Thus, we ran two phylogenetical analyses, with one with topological constrains (based on Jetz and Pyron, 2018). The unconstrained analyses yielded 199 trees of 674 score, while the constrained one yielded 160 trees of 698 score.

Bridging the gap ? Chronology of the early pipid diversification

Our analyses are focused on gondwanian pipimorphs and pipids. This focus allowed to discuss early diversification of pipids within Gondwanan. Furthermore, the sister-taxon to *Nevobatrachus* (sister-taxon to all gondwanian pipimorphs) in our analyses is *Palaeobatrachus*. This taxon represents the Palaeobatrachidae, an endemic extinct clade of Europe. However, no complete phylogenetical analysis of this clade is currently known to us. Hence, we cannot include this clade within our analyses. We also decided to not include the enigmatic pipid '*Xenopus*' *stromeri* Ahl, 1926, as it is younger (Early Miocene, see below; Rage, 2008) than our stratigraphical range. Thus, the time divergence analyses were made on 25 taxa.

Stratigraphical range and dataset—As in previous studies using this method (Didier et al., 2017; Didier and Laurin, 2020; Didier and Laurin, 2021), we used a flat distribution between upper and lower bounds on the estimate of the age of each taxon. This age was estimated using the stratigraphic occurrences of the fossiliferous localities yielding the studied taxa. Thus, we constructed a database of known occurrences of all 25 taxa. We restricted younger occurrences to the Oligocene-Miocene transition, at 23.03 Ma. Neogene occurrences were not considered, as most specimens are assigned only to the genus level to extant genera (*Pipa*, *Xenopus*, *Silurana*; see Gardner and Rage, 2016; Báez et al., 2021). We also only included occurrences known to us in the early 2022 (excluding new occurrences from Barcelos and dos Santos, 2022). Within the African Mesozoic pipids, one problem arose with the occurrences of *Pachycentrata* Báez and Rage, 2004. This taxon is known by several isolated cranial and vertebral elements in the Coniacian-Santonian of In Becetén (Niger, Báez and Rage, 1998).

However, among the anurans of the Koum Basin (also known as Mayo-Key Basin, Northern Cameroon) currently studied by one of us (A. Lemierre), several vertebrae have been identified as *Pachycentrata*-like elements (Rage et al., 2013; see below). The attribution is still putative but needs to be considered. Thus, we ran two sets of analyses, one with this older occurrence, the second without. In total, we

Bridging the gap ? Chronology of the early pipid diversification

performed four different analyses, using two topologies and two stratigraphical dataset.

A pipid in the Early Cretaceous ?—The Koum Basin (also known as Mayo-Rey Basin) is located in Northern Cameroon, 150 km Southeast of the town of Garoua (Fig. V-2A). It is a large Cretaceous-Cenozoic sedimentary Basin (Brunet et al., 1988). The anuran remains came from the KB-6 locality. They were collected during the 1980s, as part of the Programme International de Recherches dans le Crétacé-Cénozoïque d’Afrique de l’Ouest au Cameroun (P.I.R.C.A.O.C; Brunet et al., 1988; Flynn et al., 1988). The anuran specimens are currently housed in the Southern Methodist University (SMU, Dallas, USA) fossil vertebrate collection. Around 2312 anuran specimens have been identified. We had access to 80 of them. Among these specimens, we here described five presacral centra that resemble *Pachycentrata* vertebral elements.

V.3 Systematic Palaeontology

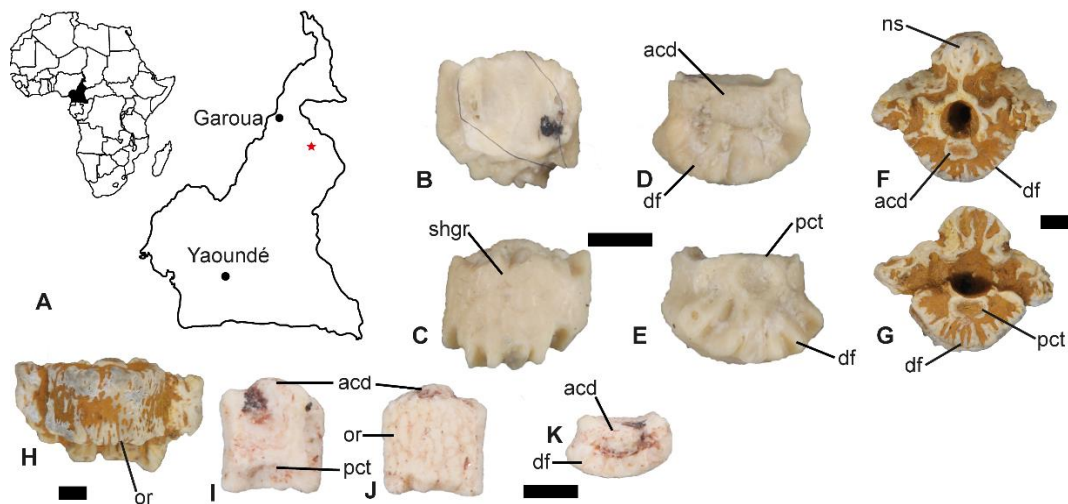


Figure V-2. Putative *Pachycentrata* vertebral remains from Cameroon. A, Map of Africa and Cameroon, showing the location (red star) of the Koum Basin; B—E, SMU74716, centrum of *Pachycentrata* sp. in B, dorsal, C, ventral, D, anterior and E, posterior views; F—H, MNHN.F.IBC 1613, presacral vertebra of *Pachycentrata taqueti* from In Becetén in F, anterior, G, posterior and H, ventral views; I—K, SMU74715a, centrum of ?*Pachycentrata* in I, dorsal, J, ventral and K, anterior views. **Abbreviations:** *acd*, anterior condyle; *df*, furrows; *ns*, neural spine; *or*, ornamentation; *pct*, posterior cotyle.

Bridging the gap ? Chronology of the early pipid diversification

ANURA Duméril, 1804

XENOANURA Starrett, 1973

PIPIMORPHA Ford and Cannatella, 1993

PIPIDAE Gary, 1825

Pachycentrata Báez and Rage, 2004

Referred material—an incomplete presacral vertebra (SMU74716)

SMU74716 is a presacral vertebra missing most of its neural arch and neural walls. The centrum is wider than long (Fig. V-2B, C). It is thickened and bloated lateroventrally (Fig. V-2D). The centrum bears an anterior condyle (Fig. V-2D) and a posterior cotyle (Fig. V-2E), indicating an opisthocoelous condition for the vertebra. The condyle and cotyle are slightly compressed dorsoventrally, with a diameter slightly smaller than the width of the vertebral canal (Fig. V-2D, E). The ventral surface of its centrum is ornamented, with longitudinally extended shallow grooves on its surface (Fig. V-2C). Its anterior and posterior surface also bear deep furrows, reinforcing the connection between vertebrae (Fig. V-2D, E).

Discussion and attribution—The bloated aspect of the centrum and the presence of deep furrows is interpreted as pachyosteosis. In amphibians, pachyosteosis occurs only (to our knowledge) in the pipid *Pachycentrata* (it co-occurs with osteosclerosis). SMU74716 resembles centra of *Pachycentrata taqueti* in (1) having a bloated and thickened aspect (Fig. V-2F, G), (2) a ventral ornamentation made of longitudinally extended shallow grooves (Fig. V-2H), (3) reduced articular facets. It seems to differ in having smaller articular facet diameter than the width of the vertebral canal. However, several vertebrae assigned to *Pachycentrata taqueti* also bear articular facets smaller than the width of the vertebral canal (Fig. V-2F, G; MNHN.F.IBC 1613). As SMU74716 is smaller than most *Pachycentrata* vertebrae, it could represent an immature individual. Hence, we attribute SMU74716 to *Pachycentrata* sp.

Bridging the gap ? Chronology of the early pipid diversification

?*Pachycentrata* Báez and Rage, 2004

Referred materials—four presacral centra (SMU74714a, b, 74715a,b)

All four centra are opisthocoelous, with an anterior condyle and a posterior cotyle (Fig. V-2I—K). Their articular facets are dorsoventrally compressed. Their diameter is the same as the vertebral canal width (Fig. V-2K). The centra are slightly thickened lateroventrally by bony deposit (Fig. V-2K). The ventral surface of the centra is slightly ornamented with faint longitudinal grooves (Fig. V-2J). Their anterior and posterior surface bear shallow furrows (Fig. V-2K).

Discussion and attribution—As for SMU74716, the thickened aspect of SMU74714-74715 can be interpreted as pachyosteosis. SMU74714, 74715 resemble *Pachycentrata* in (1) having ventral ornamentation, (2) dorsoventrally compressed articular facets; (3) diameter of the articular facets similar to the width of the vertebral canal. However, the four centra differ from *Pachycentrata* in (1) having faint grooves as a ventral ornamentation and (2) shallow furrows on their anterior and posterior surfaces. The presence of pachyosteosis in SMU74714-74715 makes it tempting to attribute the four centra to *Pachycentrata*. However, pachyosteosis markers (thickening of the bone, ventral ornamentation, furrows) are less distinct on these centra than in SMU74716. These centra are small and could belong to immature individual(s). Hence, we assign SMU74714, 74715 to ?*Pachycentrata* to reflect these differences.

Bridging the gap ? Chronology of the early pipid diversification

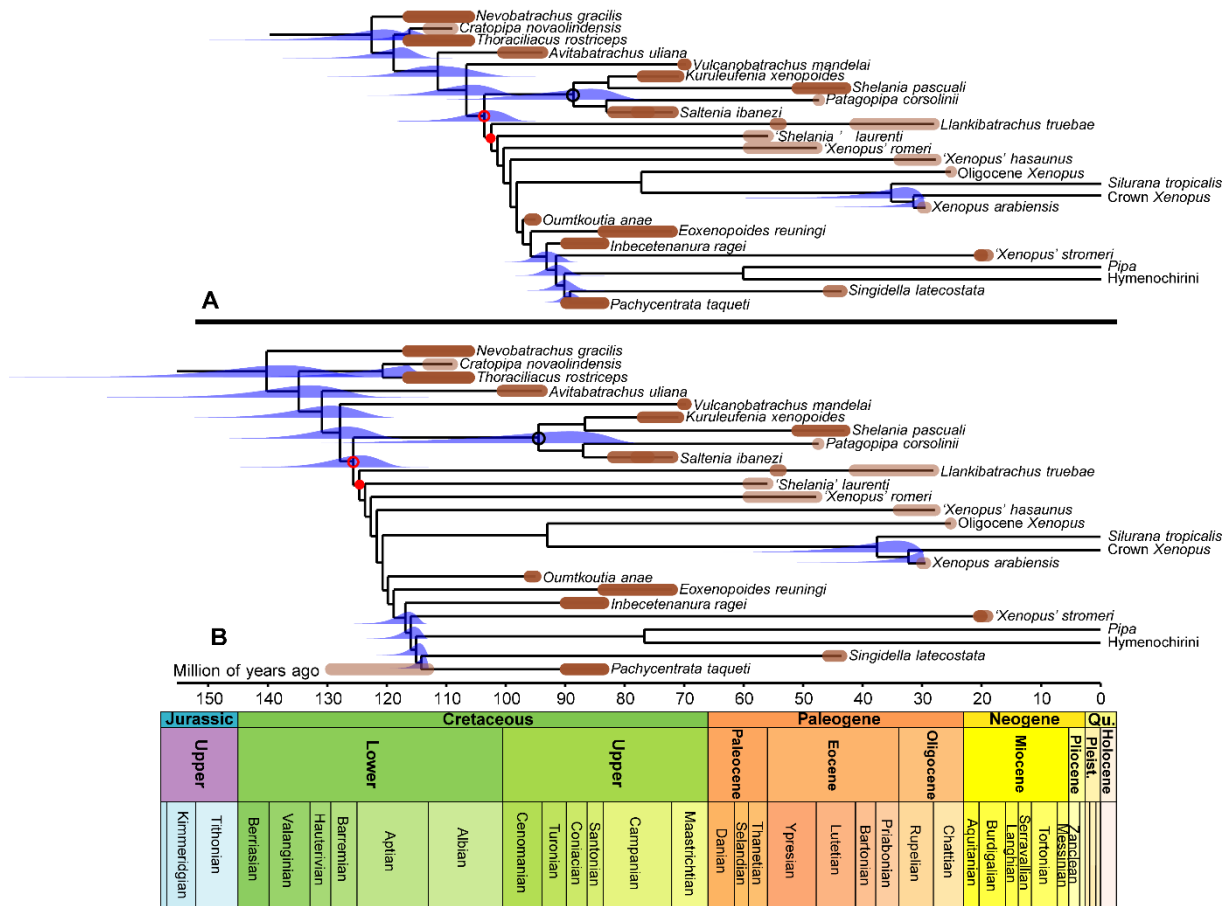


Figure V-3. Divergence time analyses results from the dataset using the topology yielded by the unconstrained analysis. A, analysis using the ‘young *Pachycentrata* occurrence’ stratigraphical dataset and **B,** analysis using the ‘old *Pachycentrata* occurrence’ stratigraphical dataset. The divergence time probability distributions are represented in blue. The brown highlighting of the branches represents the bounds of the range of plausible ages of fossil occurrences; darker brown indicates more than one record in the same time interval; red outlined circle represents the node Shelaniinae + Pipidae, dark outlined circle represents the node Shelaniinae, red circle represents the node Pipidae.

V.4 Results

Divergence times

Topology [Xenopodines [Hymenochirini + *Pipa*]], stratigraphic dataset without old *Pachycentrata*—The probability density of divergence time for the pipid node put their emergence between the Aptian (120 Ma) and early Cenomanian (98 Ma). The peak density places this emergence within the Albian, around 103 Ma, just before the

Bridging the gap ? Chronology of the early pipid diversification

Early/ Late Cretaceous transition. The probability density of divergence time for several pipid clades shows that both pipinomorphs and xenopodinomorphs diverged during the early Late Cretaceous (Fig. V-3A). Within pipinomorphs, the probability densities show a rapid diversification, with all clades emerging in 6 Ma, between 96 and 90 Ma. Thus, all pipid clades emerged within 13 Ma, between 103 (emergence of Pipidae) and 90 Ma (last diversification event within the Mesozoic). The sister-clade of Pipidae, Shelaniinae, underwent a diversification within the Late Cretaceous, and peak density places the diversification around 85 Ma. Probability density places the divergence between *Xenopus* and *Silurana* between 55 and 30 Ma, with peak density placing it around 35 Ma.

Unconstrained topology [Xenopodines [Hymenochirini + *Pipa*]], stratigraphic dataset with old *Pachycentrata*—The inclusion of the old *Pachycentrata* occurrence pushes the emergence of Pipidae within the Early Cretaceous. Probability density of divergence between Shelaniinae and Pipidae places the divergence between 140 and 115 Ma. The peak density places this divergence around 125 Ma (Fig. V-3B). Probability density of divergence between pipinomorphs and xenopodinomorphs places the divergence between 120 and 115 Ma. Pipinomorpha underwent a diversification event between 130 and 113 Ma. Thus, Pipidae underwent a diversification event between 125 and 113 Ma, with all major clades diverging then. Within Shelaniinae, probability density places the basal divergence within the clade between 125 and 78 Ma, with peak density around 89 Ma.

Bridging the gap ? Chronology of the early pipid diversification

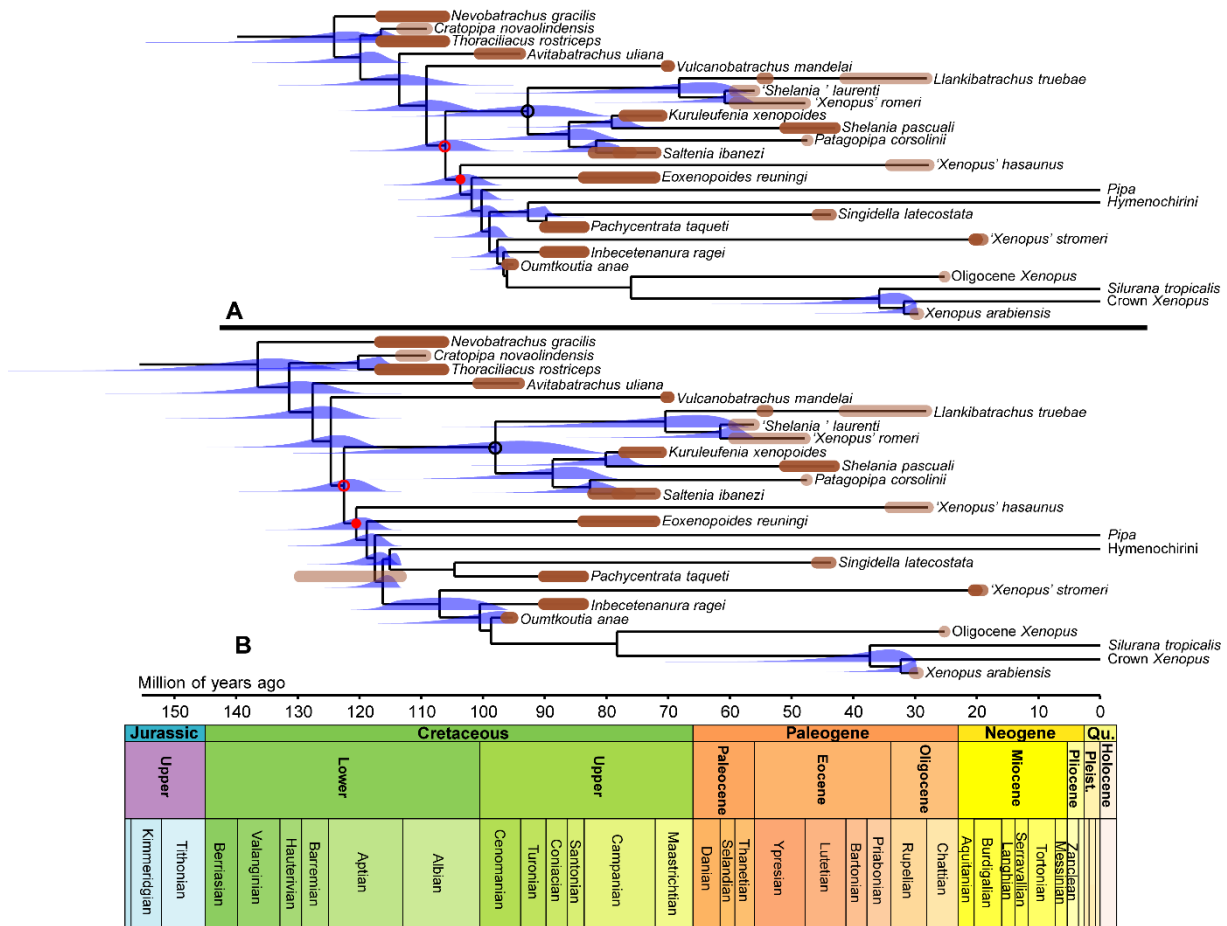


Figure V-4. Divergence time analyses results from the dataset yielded by the constrained analysis. A, analysis using the 'young *Pachycentrata* occurrence' stratigraphical dataset and B, analysis using the 'old *Pachycentrata* occurrence' stratigraphical dataset. The divergence time probability distributions are represented in blue. The brown highlighting of the branches represents the bounds of the range of plausible ages of fossil occurrences; darker brown indicates more than one record in the same time interval; red outlined circle represents the node Shelaniinae + Pipidae, dark outlined circle represents the node Shelaniinae, red circle represents the node Pipidae.

Constrained topology [*Pipa* [Hymenocherini + Xenopodines]], stratigraphic dataset without old *Pachycentrata*—The use of topological constraints change numerous relationships within Pipids and Shelaniines. Several extinct taxa recovered previously as pipids are here not recovered within the clade (Fig. V-4A). Probability density places the divergence between Shelaniinae and pipids between 120 and 100 Ma, with peak density around 105 Ma. The *Pipa* lineage diverged from the remaining pipids between 110 and 95 Ma, with peak density around 101 Ma. A large diversification within xenopodinomorphs takes place between 98 and 90 Ma. Thus, pipids underwent a

Bridging the gap ? Chronology of the early pipid diversification

diversification event between 105 and 90 Ma. The Hymenocherini lineage diverged from the *Pachycentrata-Singidella* clade between 102 and 88 Ma, with a peak density around 90.5 Ma. *Xenopus* and *Silurana* lineages diverged between 55 and 30 Ma, with a peak density around 35 Ma.

Constrained topology [*Pipa* [Hymenocherini + Xenopodines]], stratigraphic dataset with old *Pachycentrata*—As in the analysis with the topology with constrain, the inclusion of the older occurrence of *Pachycentrata* pushes pipid diversification well within the Early Cretaceous. The divergence between Pipidae and Shelaniinae is placed between 130 and 115 Ma, with the peak density of probability around 121 Ma. The *Pipa* lineage diverged from the remaining pipids between 128 and 115 Ma, with peak density around 118 Ma (Fig. V-4B). A large diversification within xenopodinomorphs occurred between 118 and 115 Ma. Thus, the pipid quickly diversified between 121 and 115 Ma. A second, small diversification event occurred within Xenopodinomorpha between 105 and 98 Ma. *Xenopus* and *Silurana* lineages diverged between 60 and 30 Ma, with peak density around 35 Ma. Hymenocherini diverged from the *Pachycentrata-Singidella* clade around 115 Ma. Within Shelaniinae, a diversification event occurred during the Late Cretaceous, between 86 and 78 Ma.

V.5 Discussion

Age of the Koum Basin—When including the old occurrence of *Pachycentrata* from the Koum Basin in our dataset, the divergence between *Pachycentrata* and *Singidella* is estimated around 113-115 Ma (Figs. V-3B, 4B). Interestingly, the Koum Basin age is estimated between 129 and 113 Ma (Brunet et al., 1988). Hence, our analyses propose that the Koum Basin is likely no older than 121-125 Ma (divergence Pipidae/Shelaniinae), and should be considered Aptian age, if *Pachycentrata* (or another pipid) is indeed present.

Bridging the gap ? Chronology of the early pipid diversification

Results from all analyses point to two different scenarios for diversification of gondwanian pipimorphs and pipids during the Mesozoic and Paleogene. These two scenarios are not based on topological differences, but rather on the presence (or absence) of the “older” occurrence of *Pachycentrata*. Hence, the first scenario is dubbed “old pipid emergence” and the second, “young pipid emergence”.

Old pipid emergence scenario—Pipidae and Shelaniinae diverged in this scenario during the early Aptian (latest Early Cretaceous), around 123 Ma (Figs. V-3B, 4B). Shelaniinae underwent a single diversification event during the Cenomanian (earliest Late Cretaceous), around 95-85 Ma. Analyses on both topologies also highlight and identify an evolutionary radiation within Pipidae following its divergence from Shelaniinae. This radiation probably lasted from 123 to 114 Ma (Aptian) and our study is the first to identify this event within Pipidae. This evolutionary radiation is currently not known within the fossil record, as a single pipid occurrence is known (*Pachycentrata*, Koum Basin, Cameroon). During this event, the lineages that lead to the three main extant pipid clades, Pipinae, Xenopodinae and Hymenocherini, are considered to have emerged (Figs. V-3B, 4B), even though their fossil record starts only in the late Paleogene (Xenopodines) or Neogene (Pipinae and Hymenocherini). This implies that long ghost lineages at the base of these three clades in Africa and South America. Among Pipinae, the oldest *Pipa* is from the Miocene of Venezuela, around 12.7 Ma (Delfino and Sánchez-Villagra, 2018), indicating a ghost lineage of 105.3 My. For Hymenocherini, no fossil is currently known (Gardner and Rage, 2016). Hence the ghost lineage of Hymenocherini spans 115 My. Xenopodines possess an older fossil record, with *Xenopus* taxa known within the Oligocene (Figs. V-3B, 4B), which implies a ghost lineage of 61 My.

Young pipid emergence scenario—Analyses on both topologies yield a similar age estimation for the divergence between Shelaniinae and Pipidae, around 103 Ma (Albian, Early Cretaceous). This age estimation is similar to several molecular clock analyses (Cannatella, 2015) that used extinct taxa as node constrains. For Shelaniinae,

Bridging the gap ? Chronology of the early pipid diversification

a diversification event occurred (as in the “old” scenario) during the Coniacian (89-85 Ma). As in the previous scenario, pipids underwent an evolutionary radiation from 103 to 94 ma (Early/Late Cretaceous transition). This radiation has previously been considered to have taken place within the Late Cretaceous only, in peculiar for xenopodinomorphs (Lemierre et al., 2022). Furthermore, as for the previous scenario, only a single pipid, *Oumtkoutia anae* (Rage and Dutheil, 2008) is known for the period. Hence the fossil record does not (currently) record this radiation. During this event, the lineages that lead to the three main extant pipid clades, Pipinae, Xenopodinae and Hymenocherini, are considered to have emerged (Figs. V-3A, 4A) as in the previous scenario.

Early diversification of Pipidae—All four analyses point to a rapid diversification event following the emergence of pipids. This study is the first to identify this event within Pipidae. When considering the “older” dataset, this event took place within the latest Early Cretaceous (125-115 Ma), and is currently not directly documented within the fossil record, as a single pipid occurrence is known (*Pachycentrata*, Cameroon). During this event, the lineages at the base of the three main extant pipid clades, Pipinae, Xenopodinae and Hymenocherini, are inferred to have emerged (Figs. V-3, 4) in all scenarios.

Bridging the gap ? Chronology of the early pipid diversification

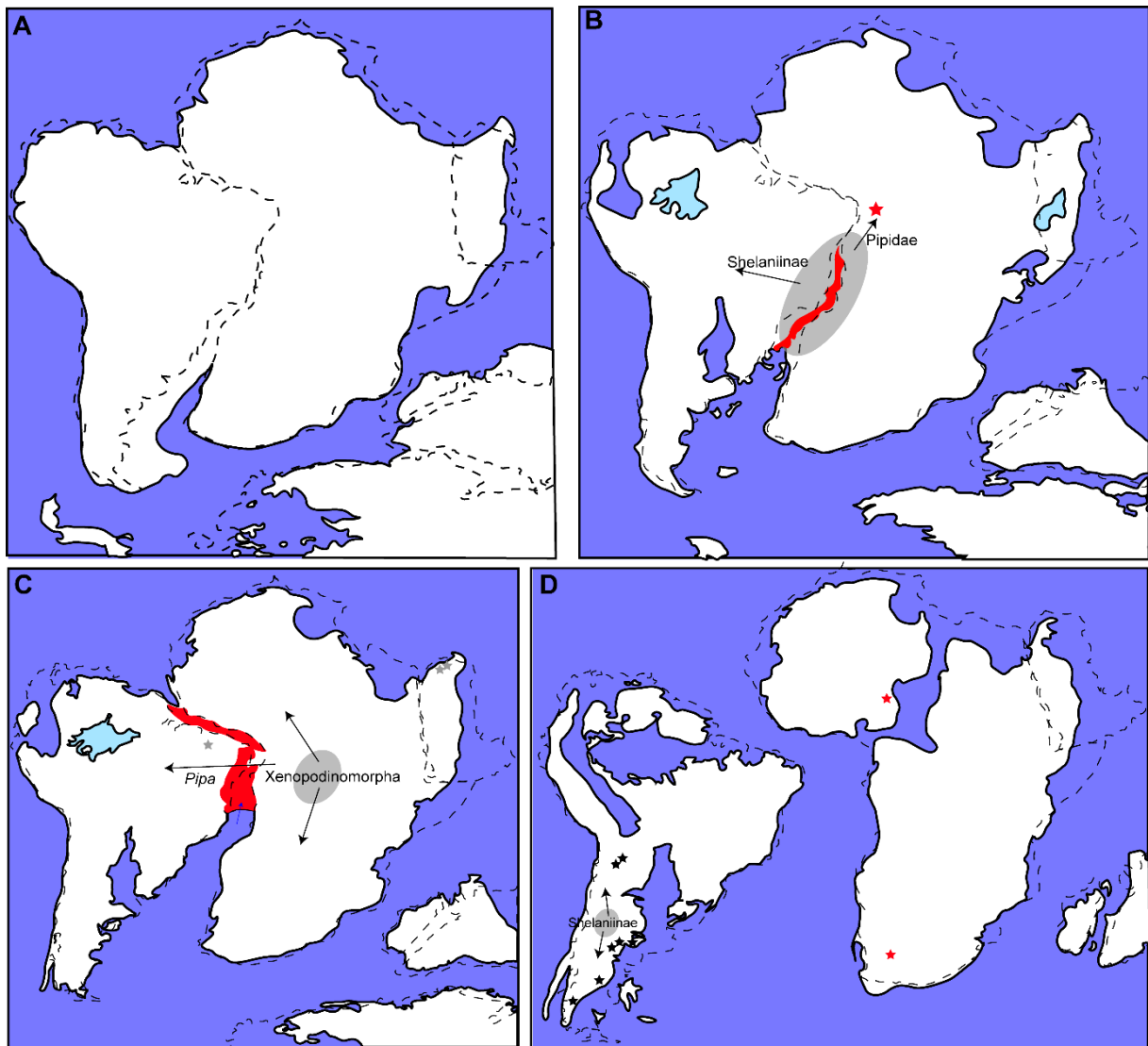


Figure V-5. Evolution of the paleobiogeography of West Gondwana and pipid diversification using the ‘old pipid emergence’ scenario from 135 to 85 Ma. **A**, West Gondwana during the Barremian (135 Ma); **B**, West Gondwana during the lower Aptian (125 Ma); **C**, West Gondwana during the Aptian/Albian boundary (115 Ma) and **D**, West Gondwana during the lower-middle Late Cretaceous (95-80 Ma). Red areas represent active rifting regions; light gray areas represent likely regions of evolutionary radiations; dotted outlines represent extant landmasses; white filled area represents landmasses at the time chosen; arrows represent pipid or shelaniine dispersal; red stars represent pipid fossil occurrences; black stars represent shelaniine occurrences and grey stars represent gondwanian pipimorphs that are not Shelaniinae nor Pipidae. Paleobiogeography of extinct landmasses is taken from Scotese (2016), geodynamics movement (rifting) are taken from Moulin et al. (2010) and Chaboureau et al. (2013).

Bridging the gap ? Chronology of the early pipid diversification

Both scenarios (differing by the age of the oldest occurrence of *Pachycentrata*) are nearly identical, the only differences being the age estimates for the divergence between Shelaniinae and Pipidae and the timing of the pipid evolutionary radiation. Interestingly, they both point to a previously unrecognized radiation just after the emergence of the clade. Although several studies highlighted the likely existence of a pipid evolutionary radiation during the Late Cretaceous (Gómez, 2016; Aranciaga-Rolando et al., 2019; Carvalho et al., 2019; Lemierre et al., 2022), most of them placed it during the middle Late Cretaceous and extended during most the Late Cretaceous period (Gómez, 2016; Aranciaga-Rolando et al., 2019). Both scenarios also point to an absence of other diversification events within pipids in South America after this radiation, and a single event in Africa during the Eocene. Within South America, the endemic shelaniines underwent a diversification event, within the middle Late Cretaceous in both scenarios.

Paleobiogeography implications

Old pipid occurrence scenario—The age estimated for the divergence between Shelaniinae and Pipidae is 123 Ma, during the early Aptian. This can be correlated with the active rifting phase of the central segment of the Southern Atlantic Ocean (SAO), which started during the Valanginian (~135 Ma, Fig. V-5A; Chaboureau et al., 2013) and led to the dispersal of Pipidae to Africa with the presence of *Pachycentrata* northeast of the rifting area (Fig. V-5B). The Shelaniinae likely spread within South America at the same period. During the next 10 my, a large evolutionary radiation occurred within the pipids, leading to the establishment of the *Pipa* lineage in South America, while other pipids diversified in Africa (Fig. V-5C). The end of the radiation coincides with the establishment of a permanent seaway passage within the Central segment of the SAO, around the Aptian/Albian boundary (Fairhead and Binks, 1991; Moulin et al., 2010; Aslanian and Moulin, 2013; Chaboureau et al., 2013). During this radiation, several temporary marine incursions have been recorded within the Central segment (Chaboureau et al., 2013). Although their geographical and temporal

Bridging the gap ? Chronology of the early pipid diversification

extensions are unknown (Chaboureau et al., 2013), it is possible that these incursions might have driven the radiation, by isolating regions within the large central segment (~2000 km length; Chaboureau et al., 2013). Interestingly, no diversification within the Pipidae is known during the opening of the Equatorial segment (115-105/100 ma), when a terrestrial connection was still present (Moulin et al., 2010). This absence of diversification could be due to (1) a reduced geographical range of pipids, restricted to more southern basins; (2) geographical barrier, like the West and Central African rifting system (Fairhead, 1988); (3) a bias in the fossil record, as no pipid is currently known in the Albian of West Gondwana and (4) the diversification was not driven by a large-scale geographic isolation. Within South America, the diversification of Shelaniinae is estimated around 89-85 Ma, with known fossils (~ 84 Ma for the earliest) placing it around the southern region of the continent (Fig. V-5D). This event could be linked to the progressive isolation of several Mesozoic sedimentary basins during the middle-upper Late Cretaceous (Donato et al., 2003; Franzese et al., 2003) due to the first Atlantic transgressions.

Bridging the gap ? Chronology of the early pipid diversification

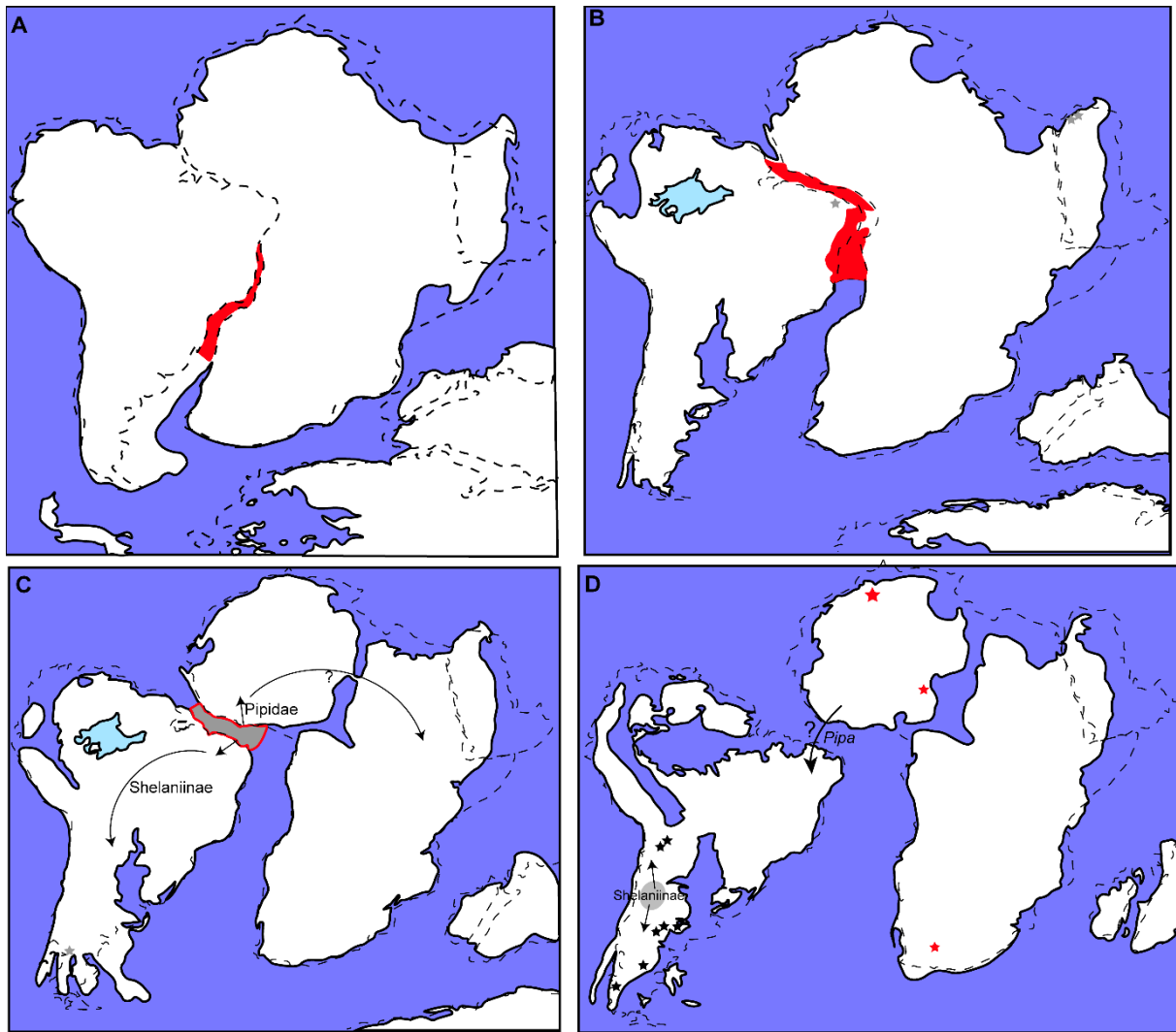


Figure V-6. Evolution of the paleobiogeography of West Gondwana and pipid diversification using the ‘young pipid emergence’ scenario from 125 to 85 Ma. A, West Gondwana during the lower Aptian (125 Ma); B, West Gondwana during the Aptian/Albian boundary (115 Ma); C, West Gondwana during the upper Albian boundary (105 Ma) and D, West Gondwana during the lower-middle Late Cretaceous (95-80 Ma). Red areas represent active rifting region; light gray areas represent likely region of diversification events; dotted outlines represent extant landmasses; white filled area represents landmasses at the time; red outlined area in C represents a rifting area where an emerged landmass has recently been identified (Moulin et al., 2010); arrows represent pipid or shelaniine dispersal; ? represent putative dispersal of pipids across Africa in C and transatlantic dispersal of *Pipa* lineage in D; red stars represent pipid fossil occurrences; black stars represent shelaniines occurrences and grey stars represent non-gondwanopipid pipimorph occurrences. Paleobiogeography of extinct landmasses is taken from Scotese (2016), geodynamics movement (rifting) are taken from Moulin et al. (2010) and Chaboureaux et al. (2013).

‘Young pipid occurrence’ scenario—The age estimated for the divergence between Shelaniinae and Pipidae is 103 Ma, during the upper Albian. This divergence coincides with the final phase of the opening of the Equatorial segment of the SAO (115 to 100

Bridging the gap ? Chronology of the early pipid diversification

Ma according to Fairhead and Blinks, 1991; Fig. V-6A, B). Since 105 Ma, known marines incursions have been recorded within the rifting arc of the Equatorial segment (Moulin et al., 2010) that possibly caused this diversification. During the next 10 My, pipids underwent a large radiation, with two possible scenarios, based on the two topologies. The results from the analysis performed using the topology [*Pipa* [Xenopodines + Hymenocherini]] suggests a divergence between South American (*Pipa*) and the African lineage (which led to Xenopodines and Hymenocherini) around 101 Ma, just 2 My after the emergence of Pipidae. This early divergence between South American and African pipids suggests that terrestrial connection between the two continents may have already been interrupted at this time (Fig. V-6C). The radiation continued within African pipids for at least 8 My, possibly driven by the progressive isolation of Africa and the opening of the Trans-Saharan seaway during the Late Cretaceous.

The result from the analysis performed using the topology [Xenopodines [*Pipa* + Hymenocherini]] proposes that the divergence between *Pipa* and Hymenocherini is no older than 90 Ma (Fig. V-3A), within the earliest Late Cretaceous, at the end of the radiation. As only African lineages diverged from the node [*Pipa* + Hymenocherini], most of the radiation appears to be located within the African continent (Fig. V-6C). The divergence between *Pipa* and Hymenocherini is inferred to have taken place after the terrestrial connection between Africa and South America was lost. Thus, this scenario implies that at least one transatlantic dispersal took place within pipids during the Late Cretaceous to explain the geographic distribution of extant lineages. However, extant pipids, such as *Pipa*, are known to inhabit still and murky ponds and lakes (Duellman and Trueb, 1994; Trueb et al., 2000), and tolerate only slightly saline waters (this was tested only on *Xenopus laevis*; Munsey, 1972; Hopkins and Brodie, 2015). Hence, a transatlantic dispersal using rafting, as proposed for several mammals (Seiffert et al., 2020) and squamates (Vidal et al., 2008), appears unlikely. Similarly, the island-hopping dispersal, also proposed for mammal dispersal during the Cenozoic (Bandoni de Oliveira et al., 2003), also appears unlikely. Another possibility might be the presence of temporary land bridges between South America and Africa during the

Bridging the gap ? Chronology of the early pipid diversification

Late Cretaceous and Paleogene. This type of land bridges has recently been identified between Africa and Madagascar during the Cenozoic (Masters et al., 2021). Thus, such land bridges may have existed between Africa and South America, but we currently have no evidence for this. Hence, our results using the ‘young pipid occurrence’ dataset indirectly support the constrained topology that has been supported by molecular analyses. The diversification of Shelaniinae during the Late Cretaceous (Fig. V-6D) in South America may be linked, as in the ‘old pipid occurrence’ scenario, to the progressive isolation of southern south America sedimentary basins during the first Atlantic transgressions (Franzese et al., 2003).

All scenarios are compatible with (but do not prove) the opening of the Southern Atlantic Ocean as the main driver for the emergence and radiation of the Pipidae throughout the Early/Late Cretaceous, with different segments driving various phases of the evolutionary radiation. Interestingly, all scenarios also point to an absence of diversification events within pipids during the Paleogene (except for the divergence between *Silurana* and *Xenopus*). This common signal might be linked to the unevenness of the pipid fossil record across both continents during the Mesozoic and Paleogene. No pipids are known in South America during the Mesozoic, a single taxon, ‘*Xenopus*’ *romeri*, is known during the Paleocene (Estes, 1975) and pipids are represented in the South American fossil record by few fossils during the Eocene (Barcelos and dos Santos, 2022). Hence, the fossil record is virtually silent on pipid diversity in South America for more than 60-70 My. Within Africa, no pipid is known within the Paleocene, with several occurrences during the early Eocene (Rage et al., 2021). However, most of the Eocene African occurrences are isolated remains, and only indicate that pipids were present across the whole African continent (Gardner and Rage, 2016). Thus, the apparent lack of diversification of pipids during the Paleogene may reflect a taphonomic artefact.

V.6 Conclusion

In conclusion, our analyses point to two possible ages for the divergence between Pipidae and its sister-clade Shelaniinae, 125 or 105 Ma, both within the latest Early Cretaceous. All analyses identify a rapid evolutionary radiation in South America and Africa. This study improves our estimate of the duration (~10 My) of this radiation, placing it within the Early Cretaceous or Early/Late Cretaceous transition. The Shelaniinae also underwent a diversification event, probably during the middle Late Cretaceous. The pipid radiation may have been driven by the opening of the Central or Equatorial segment of the South Atlantic Ocean, depending on the age of the oldest pipids in Africa during the Early Cretaceous. Three of the four analyses also point to an absence of any transatlantic dispersal, indicating that South American and African lineages had already diverged at the Early/Late Cretaceous boundary. All also point to the existence of long ghost lineages for the three main extant pipid clades.

Chapter VI

CONCLUSIONS ON EARLY PIPID DIVERSIFICATION

Conclusions on early pipid diversification

To conclude the first Section of this thesis, we can establish from the second and third Chapters that the study of the anuran fauna from the site of In Becetén, Niger in peculiar the pipimorph remains, reveals two new pipimorphs taxa from Africa (Pipimorph indet. 1 and 2) additionally to *Pachycentrata taqueti* from the Conacian-Santonian of In Becetén (Báez and Rage, 1998), and confirms the presence of a second pipid, *Inbecetenanura ragei*. Thus, with at least four pipimorphs, including two pipids, In Becetén yields the most diverse pipimorph assemblage in the Mesozoic and Paleogene, surpassing the Cretaceous Lagerstätte of the Crato Formation in Brazil. The presence of two pipids, a unique feature of the site during the Mesozoic of Africa, indicates that the clade likely diversified in the region within the latest Early/earliest Late Cretaceous.

The fourth Chapter allowed the identification and description of the first anuran fossil brain endocast inside the holotype of *Pachycentrata taqueti* and gives a preliminary assessment of its olfactive and optical capacities. It shows that *P. taqueti* likely relied mostly on olfaction, rather than vision, for feeding and likely had a lifestyle similar to several extant pipids. Furthermore, we have evidence that *Pachycentrata* likely lacked a tongue, as in extant pipids. Although it is not possible to determine if *P. taqueti* possessed a modified jaw apparatus like *Pipa*, the study of its extreme ossification (pachyosteosclerosis) could bring new information on its lifestyle, and some insight on its feeding capacities.

The new phylogenies obtained in the third Chapter of this Section confirms the pipimorph affinity of *Aygroua anoualensis* from the late Jurassic/Early Cretaceous of Anoual (Morocco), almost twenty years after its original description (Jones et al., 2003). *A. anoualensis* is here recovered as the sister-taxon to all other pipimorphs, in addition to being the oldest (stratigraphically) known pipimorph. Previous analyses (Gómez, 2016; Aranciaga-Rolando et al., 2019) considered that early diversification of pipimorphs was in Laurasia (Europe + North America + mainland Asia), as the two earliest pipimorphs (excluding *A. anoualensis*) were from Europe, and the sister-clade to Pipimorpha, the Rhinophrynidae, is endemic from North America (known since the Jurassic; Henrici, 1991). However, the phylogenetic and stratigraphic position of *A. anoualensis* could argue against this hypothesis. Nevertheless, recent studies have shown that the vertebrate fauna of Anoual (Morocco) shares numerous affinities with Laurasian fauna from the same period

Conclusions on early pipid diversification

(Lasseron et al., 2019) rather than Gondwanian fauna. Hence, the presence of the earliest pipimorph in Anoual could result from dispersion from Laurasia.

In the same Chapter, we also recovered, in topologically unconstrained analyses, the Shelaniinae (an endemic South American clade of pipimorphs) as the sister-group of Pipidae. This south American clade thrived from the Early Cretaceous to the Eocene/Oligocene transition on the continent and seems (from the fossil record) to be concentrated within its southern region. However, phylogenetic analyses performed using molecular topological constrains recovered several putative pipinomorphs in a different position, instead recovered as xenopodinomorphs, leaving *Pipa* “alone” (i.e., no pipinomorph is known, see Chapter III). The position of these extinct pipid taxa seems linked to the polarization of several characters within pipids, and to the position of the Hymenocherini.

Finally, from the fifth Chapter, we established that the divergence time analyses yielded interesting and novel hypotheses for the early diversification of pipids. Although four analyses were performed, two main scenarios can be proposed, based on analyses that exclude the possible early occurrence of *Pachycentrata taqueti*. Both scenarios place the divergence between Pipidae and Shelaniinae during the latest Early Cretaceous (120 or 103 Ma) and highlight the presence of a large pipid radiation in the 10 My following their emergence. This radiation led to the emergence of all extinct and extant pipid lineages in Africa and South America. This rapid radiation has never been identified in previous analyses, and previous authors suggested that the pipid diversification took place during the Late Cretaceous instead, according with a literal reading of the fossil record (Gómez, 2016; Aranciaga-Rolando et al., 2019; Chapter III). Both scenarios point to the final opening of the South Atlantic Ocean (SAO) as a driver for the pipid emergence and evolutionary radiation, albeit differing on the timing. If we considered that *Pachycentrata taqueti* is present in the fossil record of Early Cretaceous Africa (see Chapter V), pipid emergence was driven by the rifting across the Central segment of the SAO, and the subsequent radiation by the progressive opening of the segment and the arrival of permanent seawater within the latter. By the end of the Albian, all South American and African lineages had diverged, and no contact between Africa and South America nor transatlantic dispersal is identified. In the

Conclusions on early pipid diversification

second scenario ('young pipid occurrence' scenario in Chapter V), the emergence and radiation of pipid is driven by the final opening of the Equatorial segment of the SAO. In this scenario, South American and African pipid lineages diverged before 100 Ma, and African pipids continued their radiation in the earliest Late Cretaceous. This scenario also does not imply any transatlantic dispersals.

Hence, Pipidae emergence and early diversification is fully driven by the opening of the last two segment of the South Atlantic Ocean, during the latest ages of the Early Cretaceous. The absence of almost any diversification (except the *Xenopus/Silurana* divergence) in Pipidae within the Paleogene is puzzling. However, it is likely linked to the poor fossil record of the clade during the Paleocene, with a single taxon known (Estes, 1975) and the presence of numerous isolated pipid elements within several Eocene sites, that have yet to be included (if possible) into phylogenetical analyses to assess the pipid diversity during the Paleogene. These scenarios of an early radiation of Pipidae also implies the existence of long ghost lineages for extant genera, from 90 My (*Pipa* lineage) to 60 My (*Xenopodines* lineage).

As a perspective and to continue the study of the pipid diversification, it would be essential to study pipimorph fossils from two periods : the Early Cretaceous and the Paleogene. As mentioned earlier (Chapters I, V), several undescribed pipimorphs have been documented in the Early Cretaceous of Africa, and it would be crucial to assess their phylogenetic position, to confirm (or infirm) the presence of Pipidae within the Early Cretaceous. Within the Eocene, several pipids have been reported from both South America and Africa. It would be interesting to include these taxa within phylogenetic analyses to assess their affinities to extant lineages. This would likely reduce the ghost lineage of several taxa (in peculiar *Pipa*) but could also help to identify new diversification events during the Paleogene.

SECTION II

*DIVERSIFICATION OF THE NEOBATRACHIANS IN
MESOZOIC AFRICA AND PALEOGENE EUROPE*

Chapter VII

THE EARLY NEOBATRACHIAN FOSSIL RECORD

The early neobatrachian fossil record

Neobatrachians represent today more than 6100 recognized species (~96% of extant anurans) and are present in all continents (except for Antarctica; Duellman and Trueb, 1994; Frost et al., 2021). They also display a wide range of ecologies, from aquatic to arboreal (Duellman and Trueb, 1994), within a variety of environments. Within Neobatrachia, two especially speciose clades, Hyloidea and Ranoidea, have been established for several decades (Scott, 2005; Frost et al., 2006; Pyron and Wiens, 2011; Feng et al., 2017; Jetz and Pyron, 2018; Hime et al., 2021). These two clades are known mostly from extant taxa (Duellman and Trueb, 1994) and only a few fossils are known (Gardner and Rage, 2016; Barcelos and dos Santos, 2022). Although their interrelationships are still not fully resolved or stable (Hime et al., 2021), both fossil and extant specimens indicate that hyloids and ranoids were diversified and had a vast and rich evolutionary history. As such, molecular analyses have proposed that neobatrachians emerged within the Early Cretaceous, likely in Gondwana, an ancient landmass constituted of South America, Africa, India, Antarctica, and Australia (Blakey, 2008). Hyloidea and Ranoidea would have diverged around 125 Ma (late Early Cretaceous), during the fragmentation of the western Gondwana, with the hyloids emerging in South America, while the ranoids emerged in Africa (Feng et al., 2017). Both clades rapidly spread and diversified throughout their respective continents and reached Europe and India by the end of the Cretaceous.

Although the fossil record of anurans is mostly composed of neobatrachians during the Neogene (Roček, 2013), a scarce in the Mesozoic documents their early evolutionary history. As for other fossil anurans, most known specimens are recovered as isolated bones, more or less attributed to distinct taxa. This type of fossil preservation makes it often difficult to include the specimens within a morphological dataset for phylogenetical analyses. Therefore, several specimens were assigned to the neobatrachians based on characters located on isolated bones, like the ilium (Roček, 2013; Rage et al., 2020), without any phylogenetic analyses. However, these characters have been shown to display homoplasy by molecular/morphological analyses on neobatrachians (Frost et al., 2006). Therefore, the evolutionary history of Neobatrachia

The early neobatrachian fossil record

is not so clear and poorly understood during the Mesozoic for which they are known in Africa, South America, Europe, and (putatively) India (Fig. VII-1A). Apart from South America, all known occurrences are only from the latest period of the Cretaceous (Evans et al., 2014, Rage et al., 2020; Venczel et al., 2021).

In South America, several anuran taxa have been described (Moura et al., 2021). Most of them have been recovered from the Crato Formation in Brazil. This Formation is dated to the Aptian-Albian (Early Cretaceous) and yielded several exceptionally preserved specimens (Báez et al., 2021). Five Crato anurans, *Arariphrynus placidoi*, Leal and Brito, 2006; *Cratia gracilis*, Báez et al., 2009; *Eurycephalella alcinae* Báez et al., 2009; *Kururubatrachus gondwanicus* Agnolin et al., 2020 and *Primaevorana cratensis* Moura et al., 2021 have been attributed to the Neobatrachia, and represent the earliest occurrences of the clade. The two other taxa are assigned to Pipimorpha (see Chapters I-III). In addition, three other neobatrachians are known within the Late Cretaceous of South America. *Baurubatrachus pricei* Báez and Perí, 1989 and *Uberabatrachus carvalhoi* Báez et al., 2012, from the Maastrichtian of the Marilia Formation (Minas Gerais, Brazil), *Baurubatrachus santosdoroii* Muzzopappa et al., 2022 from the Maastrichtian of the Adamantina Formation (Sao Paulo, Brazil) and *Calyptocephalella satan* Agnolin, 2012, from the Maastrichtian of Patagonia (Argentina). A fourth neobatrachian taxon represented by several articulated specimens (Carvalho, 2006) has been reported from the Late Cretaceous of Brazil (Campanian-Maastrichtian; Carvalho et al., 2003). Unfortunately, this taxon remains unnamed and undescribed for the moment (Barcelos and dos Santos, 2022). Finally, two occurrences of Calyptocephalellidae indet. are known in the Campanian of Argentina (Barcelos and dos Santos, 2022).

The early neobatrachian fossil record

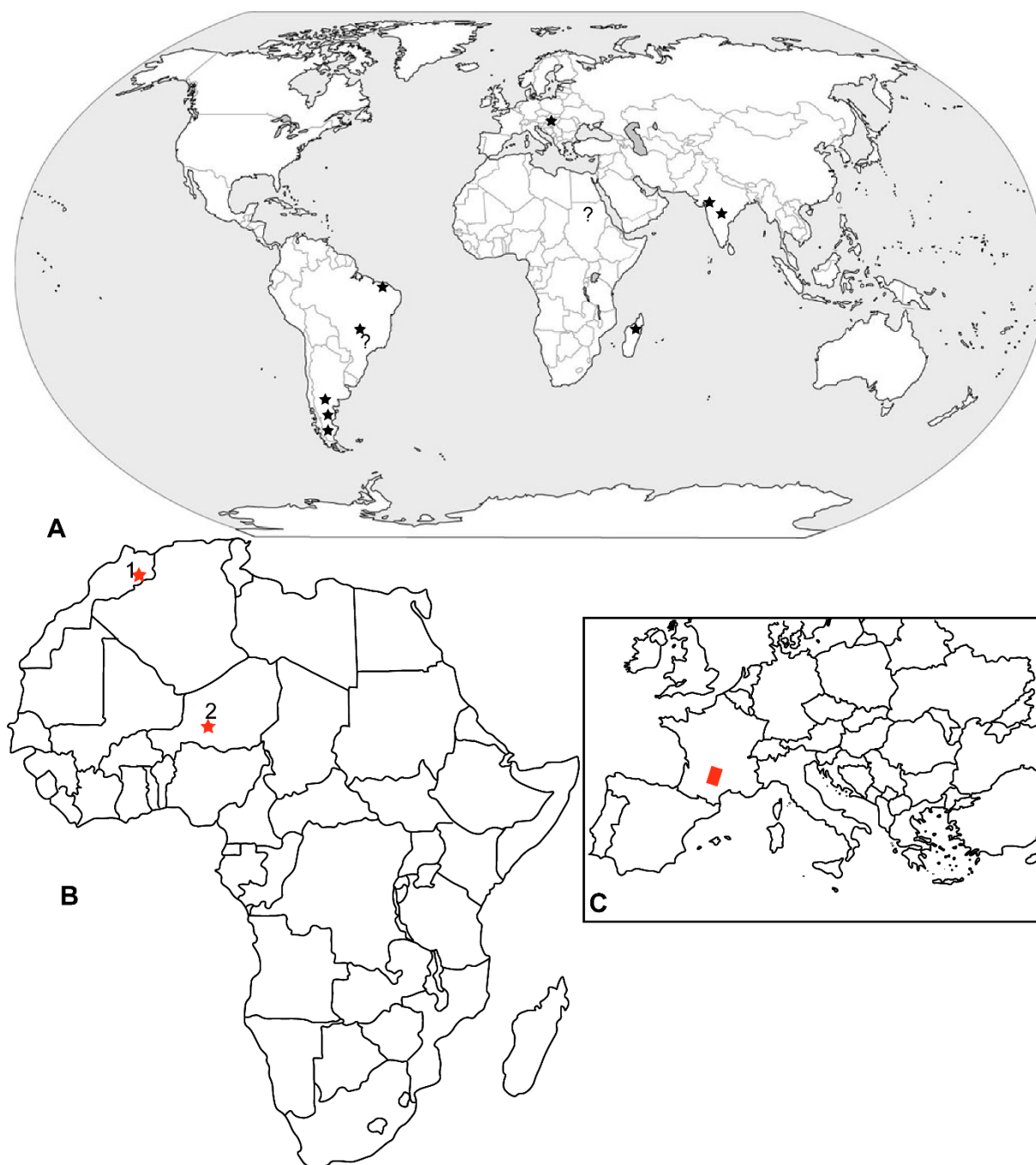


Figure VII-1. Maps showing Neobatrachian fossiliferous localities. **A**, world map showing published neobatrachian occurrences during the Mesozoic (black stars); **B**, map of Africa showing the studied Mesozoic sites (red stars) with (1): Kem Kem Formation and (2): In Becetén and **C**, map of Europe showing the location of the Quercy Phosphorites (red rectangle). ? in **A** represents mentioned but unpublished neobatrachian occurrences.

In Africa, although several isolated bones from the Cenomanian of Sudan of Wadi Abu Hasim are referred to Ranoidea, none have been illustrated or described (Báez and Werner, 1996; Gardner and Rage, 2016). Only, a single neobatrachian taxon,

The early neobatrachian fossil record

Beelzebufo ampinga Evans et al., 2008, is described from the Maastrichtian (Late Cretaceous) of Madagascar (Evans et al., 2014).

In Europe, *Hungarobatrachus* Szentesi and Venczel, 2010 from the Late Cretaceous (Campanian) of Hungary has recently been assigned as a neobatrachian, based on a phylogenetic analysis (Venczel et al., 2021).

Finally, several isolated bones have been described and attributed to neobatrachians from the Maastrichtian of India (Rage and Prasad, 2004; Rage et al., 2020). However, these attributions are not based on phylogenetic analyses or known synapomorphies of neobatrachians, ranoids or hyloids (Rage et al., 2020).

Therefore, a large stratigraphical and geographical gap currently exists between the Aptian-Albian and the Campano-Maastrichtian neobatrachians during the Mesozoic. The earliest neobatrachians are all concentrated in South America (Moura et al., 2021) whereas about 50 My later, they are reported in four continents already separated by oceans. Interestingly, all known Mesozoic neobatrachians have been referred to as hyloids when included in phylogenetic analyses (Báez and Gómez, 2018; Venczel et al., 2021). Apart from undescribed fossils from Africa (Broin et al., 1974; Báez and Werner, 1996), no ranoid is currently known from the Mesozoic. Therefore, a large part of the neobatrachian diversification during this period is unknown. Furthermore, the fossil record of ranoid is also scarce during the Paleogene, with few specimens attributed to the clade, and a single named taxon, *Thaumastosaurus* De Stefano, 1903. This taxon was recently attributed to the natatanuran (a clade of Ranoidea) and is now used as a dating constrain for molecular analyses (Feng et al., 2017). However, some uncertainties remain on its precise position within the natatanurans.

This second section of this thesis is centered on the identification of new neobatrachians and the revision of some already published taxa and their inclusion within phylogenetic dataset to assess or reassess their position. This allows to use them as constrain in molecular clock analyses and should also lead to a better understanding of the neobatrachians diversification and dispersal during the Mesozoic and

The early neobatrachian fossil record

Paleogene. To fulfill this objective, I first focused my work on two Mesozoic African sites (Fig. VII-1B) where neobatrachians were mentioned, the Kem Kem Formation (Morocco; Lemierre et al., 2022; see Chapter VIII) and In Becetén (Niger; see Chapter IX).

The eighth chapter is centered on the study of putative neobatrachians from the Cenomanian of the Kem Kem (Morocco). The Kem Kem beds are located in Southern Morocco (Fig. VII-1B). These beds are dated from the Cenomanian (early Late Cretaceous) and are among the best known and studied sites from Africa, because of their rich continental vertebrate fauna (Sereno et al., 1996; Ibrahim et al., 2020a). The Kem Kem are mostly known by their dinosaur fauna, which includes the iconic *Spinosaurus* (Ibrahim et al., 2020b), and by numerous actinopterygian and chondrichthyan fishes (Dutheil, 1999; Ibrahim et al., 2020b). Squamates are solely known by several snakes (Vullo, 2019) and an undescribed “lizard” (the specimen is unfortunately lost; Martill et al., 2011). Amphibians within the Kem Kem are scarce, with several specimens of *Kababisha*, an enigmatic amphibian, one pipid, *Oumtkoutia anae* Rage and Dutheil, 2008, and several unidentified anurans (Rage and Dutheil, 2008). Among the unidentified anuran remains, several belong to a hyperossified and ornamented taxon similar to recently described neobatrachians, like *Beelzebufo* and *Baurubatrachus* (Agnolín et al., 2012; Gardner and Rage, 2016). I had the opportunity to have access to the CT-scan of the unidentified anuran material. I was able to describe this new ornamented taxon, known by cranial and vertebral elements (Lemierre et al., 2022; see Chapter VIII). I also included this new taxon within a phylogenetic dataset, and ran two phylogenetic analyses to assess its neobatrachian affinities. This taxon may be the oldest African neobatrachian and the first occurrence on mainland Africa. It sheds new light on the dispersal of neobatrachian during the Late Cretaceous.

The ninth chapter will be focused on the study of a second Late Cretaceous site, In Becetén (Niger, Africa). In Becetén is located in southwestern Niger (Fig. VII-1B) and is dated from the Coniacian-Santonian (89.8-83.6 Ma). The site was discovered and specimens collected almost fifty years ago, as part of expeditions in the Cretaceous

The early neobatrachian fossil record

outcrops of Niger (Broin et al., 1974; Taquet, 1976). A list of several anuran taxa, including putative neobatrachian (“ranidé” in Broin et al., 1974) and pipid remains was published, but no specimen was illustrated at the time. An isolated humerus was illustrated and briefly described twenty years later, but without a clear attribution (Rage, 1984). Furthermore, the presence of an ornamented anuran, similar to neobatrachians, was recently mentioned but again not illustrated (Gardner and Rage, 2016). This ornamented taxon and the “ranidé” remains might represent a third occurrence of neobatrachians in Africa and might also be the oldest occurrence of ranoids in the fossil record. My work was centered on the study of all the anuran material from In Becetén, some of which were attributed to pipids (Chapters II-IV). I will here present my result on the identification of the other anurans. Although most of this material cannot be assigned to small clades (see Chapter IX), the new ornamented anuran has clear morphological affinities with Neobatrachia. I chose to include this new taxon within the morphological dataset used in the analyses of the Kem Kem taxon, to assess its neobatrachian affinities. I also discuss the importance of the site of In Becetén for anuran diversity and neobatrachian diversification during the earliest Late Cretaceous.

Finally, in the tenth chapter, I will present my study on the exceptionally well-preserved *Thaumastosaurus* mummies from the Quercy Phosphorites (France; Fig. VII-1C).

The Quercy Phosphorites represent hundreds of karstic sites (around 200 currently known; Pélissié et al., 2021) located in Southern France. Those sites document the evolution of the fauna, especially mammals, and flora of the region during the Early Eocene to the Miocene (around 30 My of deposits). Most of the sites are centered around the Eocene/Oligocene transition, where a large turnover has been identified within the mammal fauna (Pélissié et al., 2021). Within the known anuran specimens of the Quercy, three are exceptionally well-preserved mummies, with traces of soft-tissues. Two taxa have been erected, *Rana plicata* (*Rana cadurcorum* in Martín et al., 2012) and *Bufo servatus*. Subsequent tomography and analyses allowed to reattribute

The early neobatrachian fossil record

the mummies of *Rana plicata* to *Thaumastosaurus*, an Eocene genus of ranoid frog (Laloy et al., 2013). My objective with the specimen of *Bufo servatus* was to describe the specimen with new information brought by the CT-scan tomography of the mummy. *Bufo servatus* was considered to be one of the oldest occurrences of Bufonidae in Europe (Rage, 2016) and the oldest valid taxon assigned to the clade (Sanchíz, 1998). However, the identification and osteological description of the preserved skeleton within the *Bufo servatus* mummy revealed that it belongs to *Thaumastosaurus*, a ranoid (Lemierre et al., 2021). Therefore, I took this opportunity to also include *Thaumastosaurus* within phylogenetic analyses to propose a more precise phylogenetic position of this taxon.

Chapter VIII

*A NEW GENUS AND SPECIES FROM THE KEM KEM
(MOROCCO), THE SECOND NEOBATRACHIAN
FROM CRETACEOUS AFRICA*

A new genus and species from the Kem Kem (Morocco), the second neobatrachian from Cretaceous Africa

VIII.1 Introduction

The Cretaceous is a key period in anuran evolution and diversification including the emergence of major extant clades such as the Neobatrachia and Pipidae (Frazão et al., 2015; Feng et al., 2017). The breakup of the Western Gondwana paleocontinent during the Late Jurassic and Early Cretaceous (McLoughlin, 2001; Blakey et al., 2008)—leading to the creation of the Central and Southern Atlantic Oceans—may have contributed to the early diversification of the Neobatrachia, just as it likely did for the Pipidae (Frazão et al., 2015; Feng et al., 2017). Several neobatrachian taxa have been described in the last decade from the Cretaceous beds of South America (Báez et al., 2009; 2012; Báez and Gómez, 2018; Agnolin et al., 2020), contributing to a better understanding of early diversification of the Neobatrachia. Unfortunately, the fossil record of Neobatrachia is scarce for the Cretaceous of Africa and includes only a single described taxon: *Beelzebufo ampinga* Evans et al., 2008 from the Cretaceous of Madagascar (Evans et al., 2014). However, the lack of both study and sampling is not limited to either African Cretaceous outgroups or extinct Neobatrachia. In general, there are few well-preserved and identifiable anuran fossils in Africa, with numerous sites yielding only few and fragmentary remains (e.g., de Broin et al., 1974; Báez and Werner, 1996; Rage, 2008; Gardner and Rage, 2016) that are not easily incorporated into phylogenetic analyses. This contrasts with South American neobatrachians, several of which are known from well-preserved and mostly articulated specimens preserving much or all of the skeleton (Báez et al., 2012). In Africa, only a handful of sites contain enough fragmentary fossils referred to the same taxon to allow for comparisons to other frogs and inclusion in phylogenetic analyses (Evans et al., 2008, 2014). These few sites are critical to filling the gap in the fossil record of Neobatrachia and central to understanding their early diversification in Africa.

The Kem Kem beds of Morocco (Cretaceous, 100–95 Ma; Ibrahim et al., 2020a) are known for their rich terrestrial vertebrate fauna with numerous dinosaurs, fishes,

A new genus and species from the Kem Kem (Morocco), the second neobatrachian from Cretaceous Africa

sharks, turtles, and crocodiles (Zouhri, 2017). This fauna has been studied extensively in recent decades (Ibrahim et al., 2020a, b) but there is only a single study of its amphibians. Rage and Dutheil (2008) provided evidence for three different anurans, including one pipid that they described as *Oumtkoutia anae* based on a neurocranium, as well as two indeterminate non-pipid anurans based on postcranial remains (Rage and Dutheil, 2008). They attributed several cranial fragments to an undescribed species (mainly based on relative size of the cranial and postcranial elements) with an ornamented and hyperossified skull, one of the earliest known from the Cretaceous of Africa. A decade ago, Agnolin (2012) described a neobatrachian taxon (Calyptocephalellidae) from the Late Cretaceous of Argentina and reviewed several Gondwanan anurans with hyperossified skulls. In that study, Agnolin (2012: 156) included Kem Kem fossils which he referred to Calyptocephalellidae based on cranial and postcranial characters. Because several subsequent studies (Báez and Gómez, 2018; Muzzopappa et al., 2020) highlighted anatomical and analytical errors in Agnolin (2012), attribution of the Kem Kem fossils to the Calyptocephalellidae is questionable. Because Agnolin (2012) considered all of the “indeterminate” anuran remains from the Kem Kem Formation to be a single taxon in his study, several characters supporting the affiliation of these fossils with the Neobatrachia are based on postcranial elements that are not clearly referable to the hyperossified cranial elements. Further, because Agnolin (2012) did not include the Kem Kem fossils in his phylogenetic analysis, their relationships were never formally tested. Reevaluation of the anatomy and phylogenetic affinities of this hyperossified Kem Kem frog may be important for deciphering the early diversification of neobatrachians during the earliest Late Cretaceous of Gondwana and filling a notable gap in the fossil record of African anurans.

Here, we use microcomputed tomographic scans (MicroCT scans) to provide new information about the anatomy of the hyperossified Kem Kem frog. These new data allow for a more complete anatomical study of this taxon, comparisons to other

A new genus and species from the Kem Kem (Morocco), the second neobatrachian from Cretaceous Africa

Cretaceous anurans, and a phylogenetic analysis to estimate its relationships. We describe this material as a new genus and discuss its importance for understanding neobatrachian diversification in Gondwana during the Cretaceous.

VIII.2 Geological Context

The specimens were collected in 1995 during an expedition organized by the University of Chicago and the Service géologique du Maroc at four different localities near Taouz and Oum Tkout (OT1c, TD1, TZ8a1 and TZ8a2 from Dutheil, 1999) from the Kem Kem beds (Ettachfini and Andreu, 2004; Cavin et al., 2010). The term “Kem Kem beds” (Serenio et al., 1996) refers to a large escarpment extending across southeastern Morocco, near the Morocco-Algerian border (Ibrahim et al., 2020a: fig. 1A, C), with numerous exposures along its length. More recently, these beds have been referred to as the Kem Kem group (Ibrahim et al., 2020a), containing two formations: the Gara Sbaa and the Douira Formations. The anuran specimens discussed here were recovered from layers that can be correlated to the Douira Formation of the Kem Kem group (upper part of the Kem Kem; Ibrahim et al., 2020a). The Douira Formation (as well as the Gara Sbaa Formation) has been correlated to the Bahariya Formation in Egypt (Serenio et al., 1996; Cavin et al., 2010), which is dated to the Early Cenomanian (Cavin et al., 2010). The Kem Kem group is topped by marine sediments correlated to the Cenomanian-Turonian transition (Cavin et al., 2010). Other analyses have confirmed the Cenomanian age (Ibrahim et al., 2020a) and considered the Kem Kem group a single continuous deposit sequence from 100 to 95 Ma. The boundary between the Gara Sbaa and the Douira Formations is dated to 96 Ma and linked to the Mid-Cenomanian Event (Ibrahim et al., 2020a). The Douira Formation—and the anuran specimens discussed here—are thus dated to the middle Cenomanian, approximately 96 to 95 Ma (Ibrahim et al., 2020a).

A new genus and species from the Kem Kem (Morocco), the second neobatrachian from Cretaceous Africa

The Douira Formation contains strata that show a marine influence that increases over time. The deposits in the lower part of the formation, composed of sandstones and mudstones, are consistent with a river delta, whereas the deposits in the upper part, composed of interbedded mudstone with claystone, are characteristic of coastal and sabkha environments (see Ibrahim et al., 2020a for a complete description). There is no indication of whether the materials came from either lower or upper part of the Douira Formation.

VIII.3 Materials and Methods

Institutional Abbreviations

MNHN: Muséum National d'Histoire Naturelle, Paris (France); **UCRC-PV**: University of Chicago research collection, Chicago (USA). The anuran fossils are curated in the vertebrate palaeontology research collection of the University of Chicago.

CT-scan parameters

We generated MicroCT scans at the University of Florida's Nanoscale Research Facility using a Phoenix v|tome|x M (GE Measurement & Control Solutions, Boston, MA, USA). Voltage and current were customized for each specimen to balance resolution and intensity contrast; scanning parameters are included in the metadata associated with the scans on MorphoSource. The x-ray images were converted into tomogram slices using GE's reconstruction software datos|x (see Table S1 in Supplemental Data 1). Each stack of slices produced was imported in the 3D reconstruction software Mimics 21.0 (Materialise, Leuven, Belgium); before importation, slices were cropped to remove empty spaces. To further decrease the data size, the slices were converted from 16 bits to 8 bits. The resulting slices have an image resolution of 1580 × 2144 pixels and a voxel size of 5.7 µm for the volume size. 3D models were produced by segmenting each element using the 'thresholding' function (using the contrast on

A new genus and species from the Kem Kem (Morocco), the second neobatrachian from Cretaceous Africa

greyscale images). A 3D model of the endocast was produced by segmenting each element using the “add” function. We used the same voxel resolution of 5.7 µm, with a smoothing factor of 3 for one iteration, to homogenize the model resulting from the segmentation. Data produced by segmentation were exported in the software 3matic 9.0 as separate files (see Table S1 in Supplemental Data 1).

The electronic version of this article in Portable Document Format (PDF) will represent a published work according to the International Commission on Zoological Nomenclature (ICZN), and hence the new names contained in the electronic version are effectively published under that Code from the electronic edition alone. This published work and the nomenclatural acts it contains have been registered in ZooBank, the online registration system for the ICZN. The ZooBank LSIDs (Life Science Identifiers) can be resolved and the associated information viewed through any standard web browser by appending the LSID to the prefix <http://zoobank.org/>. The LSID for this publication is: urn:lsid:zoobank.org:pub:DCACD333-53AA-4A6D-A0F0-9F9C180F0DD. The online version of this work is archived and available from the following digital repositories: PeerJ, PubMed Central SCIE, and CLOCKSS.

Phylogenetic analyses

Our data matrix includes 88 taxa and 150 morphological characters (62 cranial and 75 postcranial characters, 12 from the hyobranchial apparatus, and one from soft-tissues) and is derived from that of Lemierre et al. (2021; see Appendix S1–3). We added two extinct hyperossified neobatrachian taxa (the new taxon described below from the Kem Kem, and *Hungarobatrachus szukacsi*) to test their affinities. *Hungarobatrachus szukacsi* Szentesi and Venczel, 2010 has recently been included in a reduced phylogenetic analysis (Venczel et al., 2021) and is considered a neobatrachian. It is the oldest neobatrachian outside of Gondwana and essential to understand the diversification of the clade during the Cretaceous. These new taxa were scored from observation on 3D mesh files created for this study based on segmenting newly

A new genus and species from the Kem Kem (Morocco), the second neobatrachian from Cretaceous Africa

generated MicroCT scans (see above) and from literature (Szentesi and Venczel, 2010; Venczel et al., 2021).

All analyses were performed using TNT v.1.5 (Goloboff and Catalano, 2016). All analyses were conducted with cline (also called multi-state) characters ordered (characters 3, 9, 10, 14, 26, 34, 51, 52, 68, 93, 112, 121, 124, 125 and 126). Cline characters were ordered as several studies (Rineau et al., 2015, 2018) showed that analyses using ordered morphocline characters outperformed analyses using unordered characters, even when the ordering scheme is wrong (Rineau et al., 2018). Analyses consisted of heuristic searches with 1000 random addition sequences of taxa, followed by tree bisection reconnection (TBR) branch swapping, withholding 10 trees per repetition. The final trees were rooted using *Ascaphus* Stejneger, 1899 (Ascaphidae, Anura) and a strict consensus was created. Node supports were evaluated using Bremer support and standard nonparametric bootstrapping, with searches of 1000 replicates and collapsing groups below 5% frequency.

Because the phylogeny resulting from the above analysis is strongly at odds with relationships inferred from those inferred with molecular genetic data, we performed an additional analysis using a constraint tree reflecting a consensus of recent molecular phylogenetic analyses. This included constraining the backbone of the tree to reflect early divergences in anuran evolution, as well as large-scale patterns of relationships within the two major clades of Neobatrachia (Hyoidea, Ranoidea). Within Hyoidea, we constrained four clades: Calyptocephalellidae, Neoaustrarana (Feng et al., 2017; Streicher et al., 2018), the genus *Telmatobius* Wiegmann, 1834 as monophyletic, and a clade representing all other hyloids. Within Ranoidea, we constrained three clades: Afrobatrachia, Microhylidae, and Natatanura. We did not constrain the placement of any extinct taxa and we also left relationships within constraint clades (e.g., Pelobatoidea, Myobatrachoidea, Natatanura) as polytomies so that relationships within them could be inferred by our morphological data. This constraint tree (available in the Supplemental Materials) was generated by hand and

A new genus and species from the Kem Kem (Morocco), the second neobatrachian from Cretaceous Africa

represents a broad-scale consensus of phylogenetic relationships presented in recent phylogenomic analyses for most frog families (Feng et al., 2017: fig. 1; Hime et al., 2021: fig. 1) and those specific to hylids (Streicher et al., 2018: fig. 6) and ranoids (Yuan et al., 2018: fig 2).

The anatomical terminology used herein is based on Roček (1980), Sanchíz (1998), and Biton et al. (2016) for cranial features, Sanchíz (1998) for postcranial ones, Gómez and Turazzini (2021) for humerus anatomy, and Gómez and Turazzini (2016) for ilium anatomy. Anatomical terminology for cranial nerves follows Gaupp (1896).

VIII.4 Systematic Paleontology

ANURA Duméril, 1804

NEOBATRACHIA Reig, 1958

CRETADHEFDAA gen. nov.

Type (and only known) species *Cretadhefdaa taouzensis* sp. nov.

CRETADHEFDAA TAOUZENSIS sp. nov.

Holotype

UCRC-PV94, posterior portion of the skull preserving co-ossified and incomplete frontoparietals, parasphenoid, and the prooticooccipital (the co-ossified prootics and exoccipitals sensu Roček, 1980)

Type locality

TD1, near the city of Taouz in southeastern Morocco (see Dutheil, 1999 for more information on Kem Kem localities).

Stratigraphic range

A new genus and species from the Kem Kem (Morocco), the second neobatrachian from Cretaceous Africa

Middle Cenomanian (96–95 Ma).

Referred materials

One incomplete squamosal from TD1 (UCRC-PV95); one incomplete maxilla from Tz8a1 (UCRC-PV96); three incomplete presacral vertebrae, two from TD1 (UCRC-PV97–98) and one from Tz8a1 (UCRC-PV101); one incomplete sacral vertebra from OT1c (UCRC-PV103).

Etymology

The genus nomen *Cretadhefdaa* is a combination of the word Cretaceous and a transliteration of the pronunciation of the Arabic word ضفدع or *dhefdaa* (also sometimes written as *dheftha* or *thedfaa*), meaning “frog.” The specific epithet *taouzensis* recognizes the type locality, Taouz.

Diagnosis

A neobatrachian anuran with a hyperossified skull differing from all other anurans by the following unique combination of characters: (1) frontoparietals coossified, lacking a midline suture, and covered in ornamentation of pits and ridges; (2) frontoparietals bearing a smooth occipital flange; (3) no incrassation frontoparietalis on the ventral surface of the frontoparietals; (4) presence of a deep, groove-like central recess on the posterodorsal surface of the braincase to each side of the foramen magnum, and housing the foramen for the arteria occipitalis.

Cretadhefdaa can be differentiated from *Beelzebufo* in (1) having a smooth occipital flange on the posterior margin of the frontoparietals; (2) having a ventral extension of maxillary ornamentation on the pars dentalis and (3) lacking an ornamented table sitting atop neural spine of anterior presacral vertebrae. *Cretadhefdaa* can be differentiated from *Baurubatrachus* in (1) having a fully ossified dorsal margin of the foramen magnum; (2) lacking a distinct palatine shelf of the maxilla; (3) having

**A new genus and species from the Kem Kem (Morocco), the second
neobatrachian from Cretaceous Africa**

a smooth occipital flange on the posterior margin of the frontoparietals; and (4) having a slender and shorter neural spine on presacral vertebrae. *Cretadhefdaa* can be differentiated from *Calyptocephalella satan* Agnolin, 2012 in (1) lacking a distinct shelf on the maxilla; (2) having a smooth occipital flange on the posterior margin of the frontoparietals; (3) lacking median suture between frontoparietals; and (4) having weakly expanded sacral transverse processes. *Cretadhefdaa* can be differentiated from *Hungarobatrachus* in (1) lacking an incrasation frontoparietalis on the ventral surface of the frontoparietals; (2) having the arteria occipitalis foramen within a deep recess; and (3) lacking a distinct palatine shelf of the maxilla. Diagnosis for the species is same as for the genus.

A new genus and species from the Kem Kem (Morocco), the second neobatrachian from Cretaceous Africa

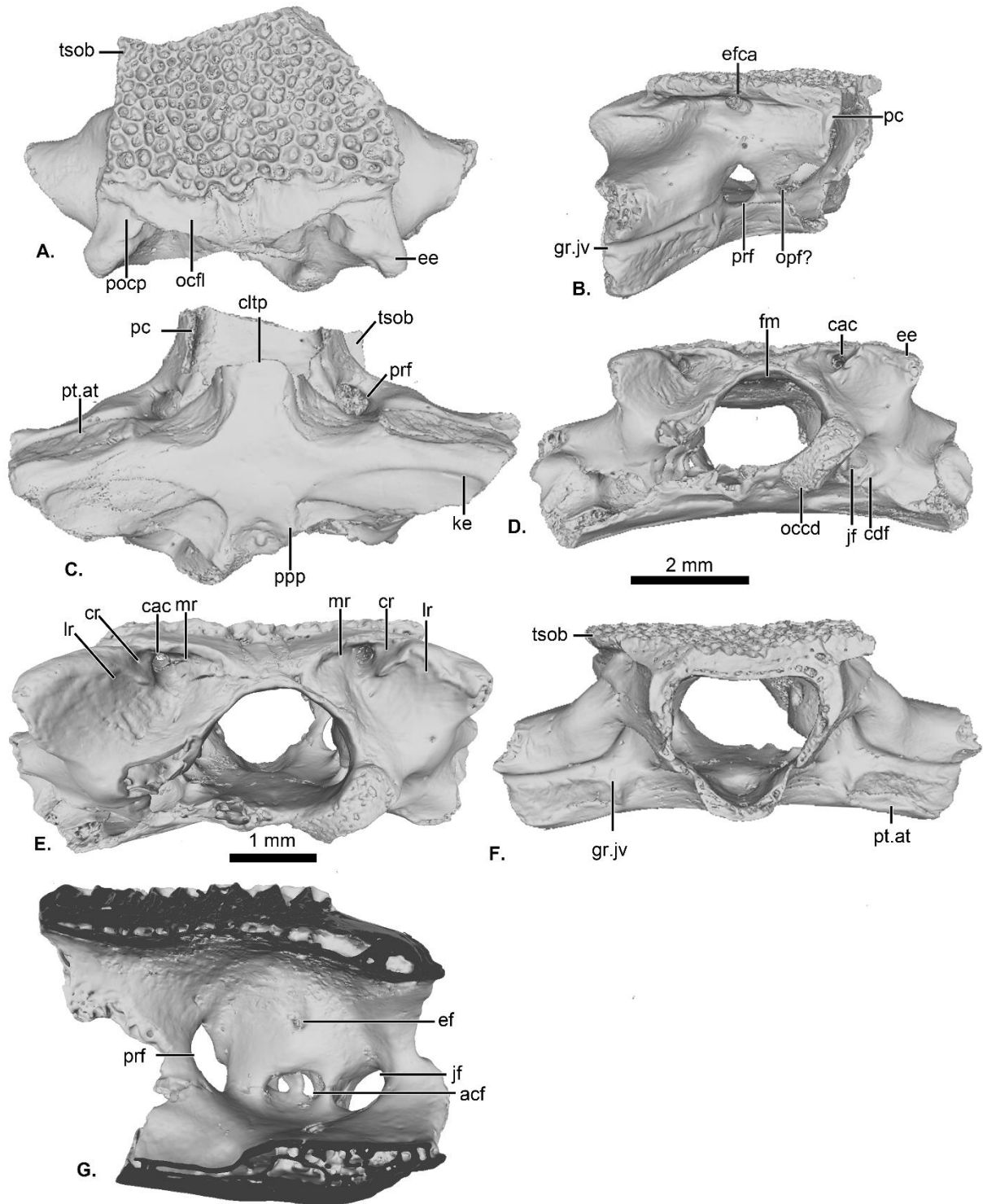


FIGURE VIII-1. UCRC-PV64, holotype of *Cretadhefdaa*. Incomplete braincase in **A** dorsal; **B** right lateral; **C** ventral; **D** posterior; **E** posterodorsal view with a close up on the recesses system; **F** anterior and **G** medial views. **Abbreviations:** *acf?*, fused acoustic foramina; *cac*, canal for arteria occipitalis; *cdf*, condyloid fossa; *cltp*, cultriform process; *cr?*, central recess; *ee*, epiotic eminence; *efca*, exit foramen for arteria orbitonasalis; *fm*, foramen magnum; *gr.jv*, groove for the jugular vein; *jf*, foramen jugulare; *ke*, median keel; *lr*, lateral

A new genus and species from the Kem Kem (Morocco), the second neobatrachian from Cretaceous Africa

recess; **mr**, medial recess; **occd**, occipital condyle; **opt?**, optic foramen; **pc**, pars contacta; **pf**, endolymphatic foramen; **poep**, paraoccipital process; **ppp**, posterior process of the parasphenoid; **prf**, prootic foramen; **pt.at**, pterygoid attachment area; **tsob**, tectum supraorbitale.

VIII.5 Description

Description of the holotype (UCRC-PV94)

Osteological description—UCRC-PV94 is the preserved posterior region of the skull of *Cretadhefdaa*. All bones are co-ossified and the sutures between prooticooccipitals and the frontoparietals are difficult to discern (Fig. VIII-1A–G).

The posterior portion of the frontoparietals is preserved. The two frontoparietals are coossified to one another, and no suture is visible on the frontoparietal table (Fig. VIII-1A). The frontoparietal table is large and covered in an ornamentation of pits and ridges. The posterior margin of the frontoparietals is flanked by a large occipital flange that lacks ornamentation (Fig. VIII-1A). The paraoccipital processes are reduced and fused to the underlying epiotic eminence (prominentia circularis ducti posterior of Roček and Lamaud, 1995), and the posterior process of the frontoparietals is not distinct (Fig. VIII-1A). There is no pineal foramen visible. In lateral view, the preserved portion of the pars contacta is a straight vertical lamina (Fig. VIII-1B). In ventral view, the frontoparietal table extends lateral to the pars contacta into a tectum supraorbitale, but its full extent is unknown because it is broken (Fig. VIII-1A, B). There is no visible frontoparietal incassation on the ventral surface of the frontoparietals (i.e., there is no imprint of the dorsal surface of the endocranium). The absence of frontoparietal incassation could be linked to the coossification of the tecta and thickening of this region of the frontoparietals (Z. Roček, pers. com.). In posterior view, the boundary between the frontoparietals and prooticooccipitals bears a series of deep recesses (Fig. VIII-1D, E). The recesses are located between the tall epiotic eminence and the posterior margin of the frontoparietal table and appear to form a single large, deep groove on each side of the braincase. However, three different

A new genus and species from the Kem Kem (Morocco), the second neobatrachian from Cretaceous Africa

recesses can be distinguished within each groove (medial, central, and lateral recesses in Fig. VIII-1E) that are each separated by well-defined ridges. Both the lateral and medial recesses are shallow, whereas the central recess is deep and houses a large, circular foramen for the arteria occipitalis. The foramen for the arteria orbitonasalis is visible on each lateral surface of the frontoparietal, ventral to the lateral extension of the table (Fig. VIII-1B).

The posterior region of the parasphenoid is preserved. The cultriform process is broken, preserving only its base. The alae are large and cover the ventral surface of the otic capsules. In ventral view, the alae bear a median keel on its surface, extending from its lateral margin to and slightly curving towards the posterior process of the bone (Fig. VIII-1C). The posterior process is divided into two well-separated small extensions, oriented posterolaterally. These expansions are fused to the base of the occipital condyles (Fig. VIII-1C).

The prootic and exoccipital are coossified into a single prooticooccipital complex without a visible suture. Each prooticooccipital is co-ossified to the other along their medial margins, as well as to the frontoparietals (dorsally) and parasphenoid (ventrally). In dorsal view, the epiotic eminence is large, forming a broad lamina (Fig. VIII-1A, D). The dorsal surface of the prootic is smooth. The crista parotica is not fully persevered, but likely had an ossified lateral expansion. There is no trace of an articulation facet for the squamosal on the preserved portion of the prooticooccipital (Fig. VIII-1A). In anterolateral view, a large prootic foramen is present on the anterior surface of the prooticooccipital (Fig. VIII-1B, G), and is fully enclosed in bone. In lateral view, anterior to the prootic foramen, a notch is visible on the anteriormost bony margin of the braincase (Fig. VIII-1B) and might represent the posterior portion of the optic foramen. In anterior view, a well-delimited, narrow groove, likely for the jugular vein, extends from a large depression at the border of the prootic foramen to the lateral margin of the prootic (Fig. VIII-1F). Beneath this groove, a large depression is present from the lateral margin of the prootic to the midpoint of

A new genus and species from the Kem Kem (Morocco), the second neobatrachian from Cretaceous Africa

its anterior surface. This is likely an articular facet for the medial ramus of the pterygoid. In posterior view, the left occipital condyle is missing (Fig. VIII-1D), but the right occipital condyle is slightly ventrolateral to the large foramen magnum (Fig. VIII-1D). The occipital condyle obscures the foramen jugulare that remains partially visible laterally (Fig. VIII-1D). In medial view, several foramina are visible in the wall of the braincase. The posteriormost opening is the foramen jugulare (Fig. 1G). Separated from the latter foramen by a thin bony pillar, a large opening is present on the lateral braincase wall (Fig. VIII-1G). This opening likely represents the fused acoustics foramina, a fusion that is common in many anurans (Z. Roček, pers. comm.). A similar preservation is also present in the exceptionally preserved *Thaumastosaurus servatus* Filhol, 1877 (Lemierre et al., 2021; Chapter X).

Inner Ear—The preservation of the endocast of the otic capsule allowed us to segment the otic chamber and semi-circular canals (vestibular apparatus) of *Cretadhefdaa*. The anterior, posterior, and lateral canals are all preserved and clearly identifiable (Fig. VIII-2A, B). In anterior view, the base of the anterior canal bears a bulge, containing the anterior ampulla (Fig. VIII-2A). In dorsal view, at the base of both anterior and lateral canals, the bulges contain the anterior and lateral ampullae (Fig. VIII-2C). At the base of the posterior sinus (connecting the lateral and posterior canals), a similar bulge contains the posterior ampulla (Fig. VIII-2B, D). In anterior and posterior views, the common crus (superior sinus), connecting the anterior and posterior canals, is well preserved (Fig. VIII-2A–C). The base of the superior sinus is thick and is part of the utricle. The utricle forms the ventral portion of the vestibular apparatus. The vestibular apparatus occupies approximately half of total height of the endocast. The auditory region is large and bulbous (Fig. VIII-2), and the posterior region (perilymphatic cistern + sacculus + lagena) occupies most of the endocast.

**A new genus and species from the Kem Kem (Morocco), the second
neobatrachian from Cretaceous Africa**

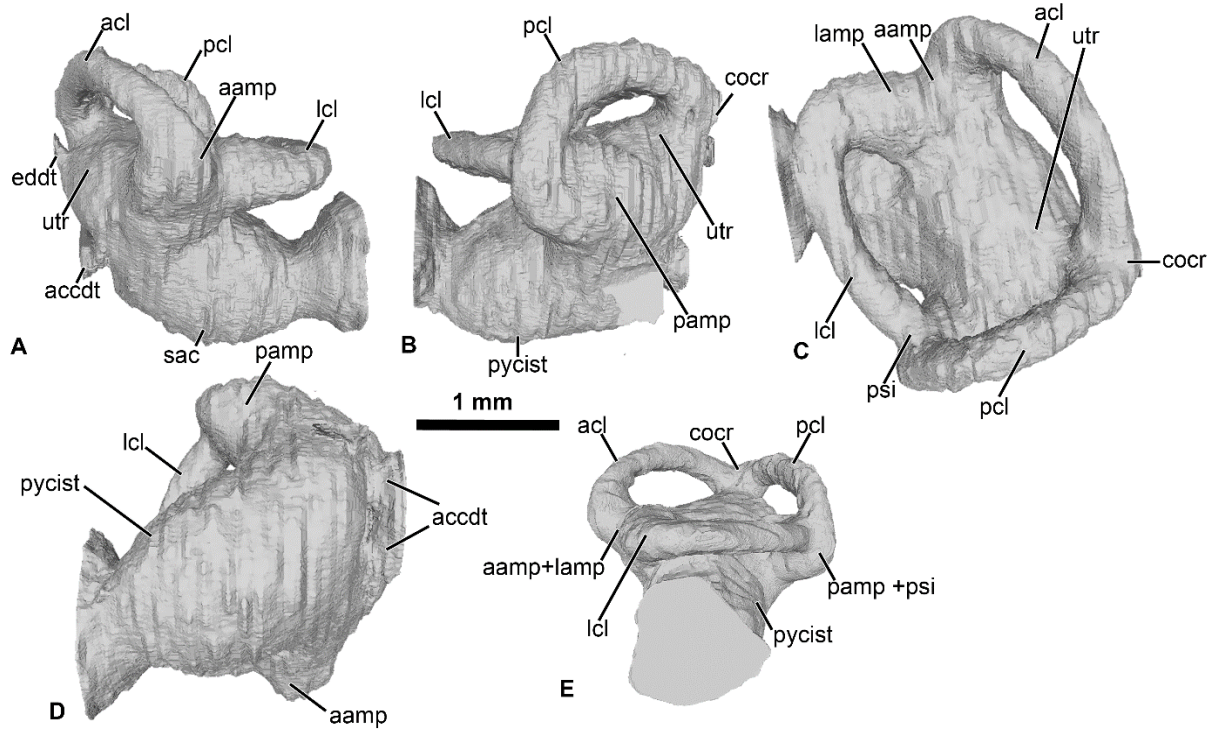


FIGURE VIII-2. Internal morphology of the otic capsule of *Cretadhefdaa*. Endocast of the left otic capsule in **A** anterior; **B** posterior; **C** dorsal; **D** ventral and **E** lateral views. **Abbreviations:** **aamp**, anterior ampulla; **accdt**, transverse section through perilymphatic space containing stat-acoustic nerve; **acl**, anterior semicircular canal; **cocr**, common crus; **eddt**, endolymphatic duct; **lamp**, lateral ampulla; **lch**, lateral chamber; **lcl**, lateral semicircular canal; **otch**, otic chamber; **ovw**, oval window; **pamp**, posterior ampulla; **pcl**, posterior semicircular canal; **psi**, posterior sinus; **pycist**, perilymphatic cistern; **sac**, sacculus; **utr**, utricle.

Within this posterior region, the perilymphatic cistern occupies the posteromedial region (Fig. VIII-2B), while the sacculus occupies the anteriormost portion of this region (Fig. VIII-2A). Lateral to the posterior region, a small region is delimited from the rest of the ventral volume by a slight constriction (Fig. VIII-2A, B). This region can be identified as the transverse section through the perilymphatic space close to the fenestra ovalis. Near the perilymphatic cistern, a short and large canal, representing the perilymphatic ducts, opens posteriorly (Fig. VIII-2B, D) into the braincase and the condyloid fossa (fused perilymphatic foramina). Another large duct is visible in the medial region of the otic chamber, entering the braincase through the

A new genus and species from the Kem Kem (Morocco), the second neobatrachian from Cretaceous Africa

fused acoustic foramina. However, this canal comprises two smaller ducts that are fused medially (Fig. VIII-2) and housed the pathway of the cranial nerve VIII (Gaupp, 1896), representing the auditory nerve (Duellman and Trueb, 1994). A second medial, smaller duct is visible in the medial region of the vestibular apparatus, leading to the dorsalmost foramen of the lateral wall of the braincase (Fig. VIII-1G). This duct is identified as the endolymphatic duct, leading to the endolymphatic sac that was present in the braincase (Frishkof and Goldstein, 1963; Duellman and Trueb, 1994).

Referred Cranial Material to *Cretadhefdaa taouzensis*

UCRC-PV95—The specimen is a fragment of a right squamosal preserving part of the lamella alaris (otic plate of Evans et al., 2014) and the base of the processus posterolateralis (Fig. VIII-3). The dorsal and lateral surface of the bone is covered with an ornamentation made of deep longitudinal pits and ridges in the orbital and lateral region, and deep, nearly circular pits and ridges in the posterior and otic region (Fig. VIII-3A). This ornamentation is slightly different from that observed in UCRC-PV94, though it is not uncommon for anuran cranial bones to display variation in ornamentation within an individual (Buffrénil et al., 2015, 2016). Thus, we interpret UCRC-PV95 as belonging to the same taxon as UCRC-PV94. The size of the squamosal is consistent with the size of the braincase (UCRC-PV94), but there is no indication that the two bones belong to the same individual. The lamella alaris is well developed (~3 mm length preserved, anterior to posterior) with an anterior extension ventrolaterally oriented (Fig. VIII-3B). Posteriorly, the lamella alaris bears a vertical lamina, likely the base of the processus posterolateralis (Fig. VIII-3C). Near this lamina, on the ventral surface of the lamella alaris, a small broken ridge is present. It might be the base of the ramus paroticus.

A new genus and species from the Kem Kem (Morocco), the second neobatrachian from Cretaceous Africa

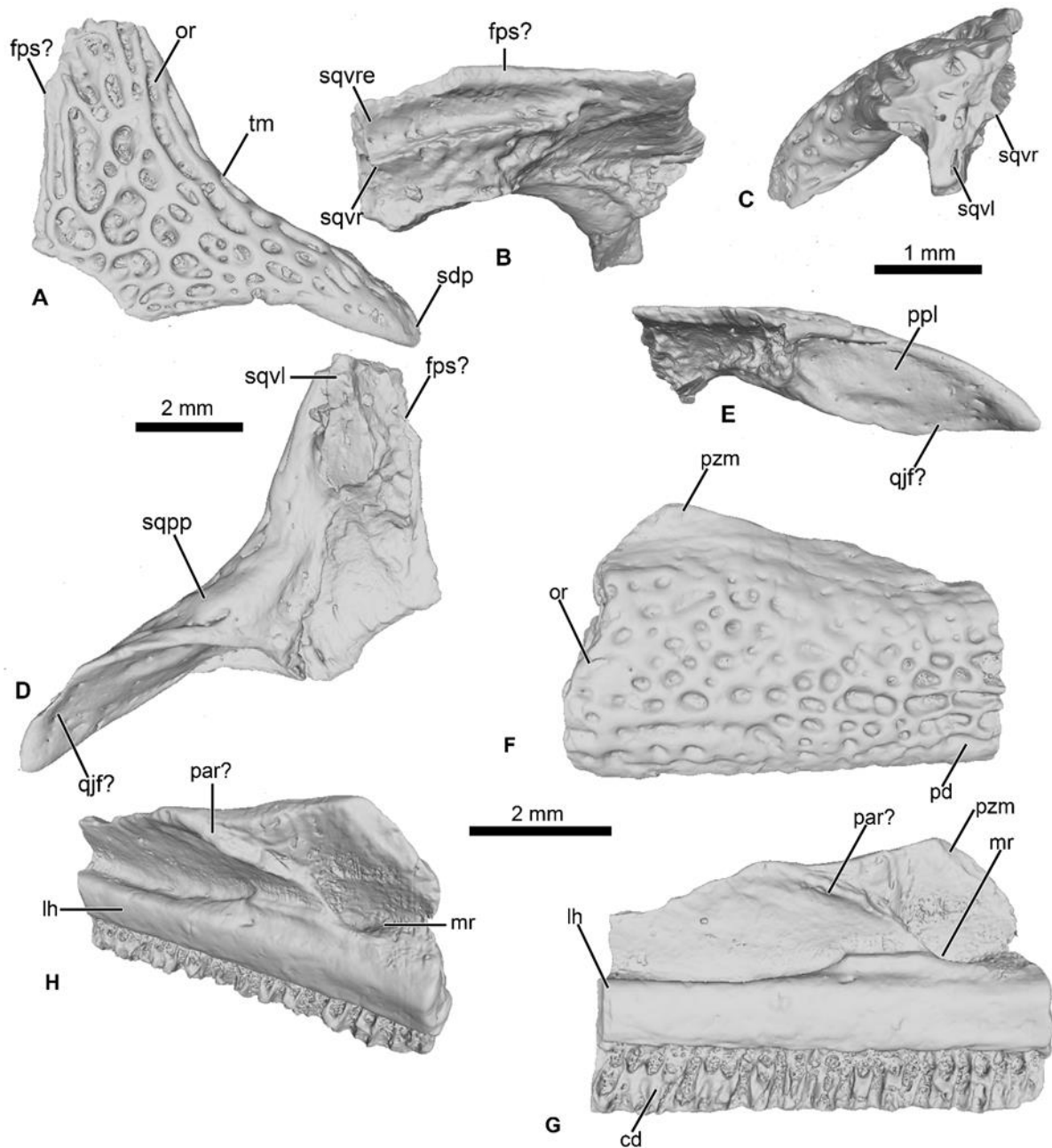


Figure VIII-3. Cranial elements of *Cretadhefdaa*. A – E UCRC-PV95, incomplete squamosal in A, dorsal; B medial; C anterior; D posterior and E ventral views; F–G UCRC-PV94, incomplete maxilla in F lateral, G medial and H dorsomedial views. **Abbreviations:** *cd*, crista dentalis; *fps?*, frontoparietal suture ?; *lh*, lamina horizontalis; *mr*, maxillary recess; *or*, ornamentation; *par?*, palatine articulation; *ppl*, processus posterolateralis of the squamosal; *pzm*, processus zygomatico-maxillaris; *qjf?*, quadratojugal facet ?; *sqvl*, squamosal ventral lamina; *sqvr*, squamosal ventral ridge; *sqvre*, squamosal ventral recess; *tm*, temporal margin

**A new genus and species from the Kem Kem (Morocco), the second
neobatrachian from Cretaceous Africa**

UCRC-PV96—This represents a partial anterior portion of a right maxilla. The maxilla is toothed and its lateral surface is covered in a pits and ridges ornamentation. The ornamentation covers almost all of the lateral surface, save for a thin strip of bone ventrally and its dorsalmost portion. Dorsally, the base of the large processus frontoparietalis is preserved (Fig. VIII-3E, F). In medial view, the pars dentalis is straight, with a small sulcus dentalis (Fig. VIII-F, G; also visible in ventral view). The lamina horizontalis is faint, almost non-distinct from the medial surface of the maxilla (Fig. VIII-3F). It forms a small ridge, with a shallow dorsal groove for the palatoquadrate (Fig. VIII-3G). A deep maxillary recess is present medially (Fig. VIII-3F). A groove for maxillary nerves extends dorsally from the maxillary recess to the dorsal part of the maxilla. Because only the bases of several teeth are preserved, nothing can be said of the tooth morphology of *Cretadhefdaa*.

A new genus and species from the Kem Kem (Morocco), the second
neobatrachian from Cretaceous Africa

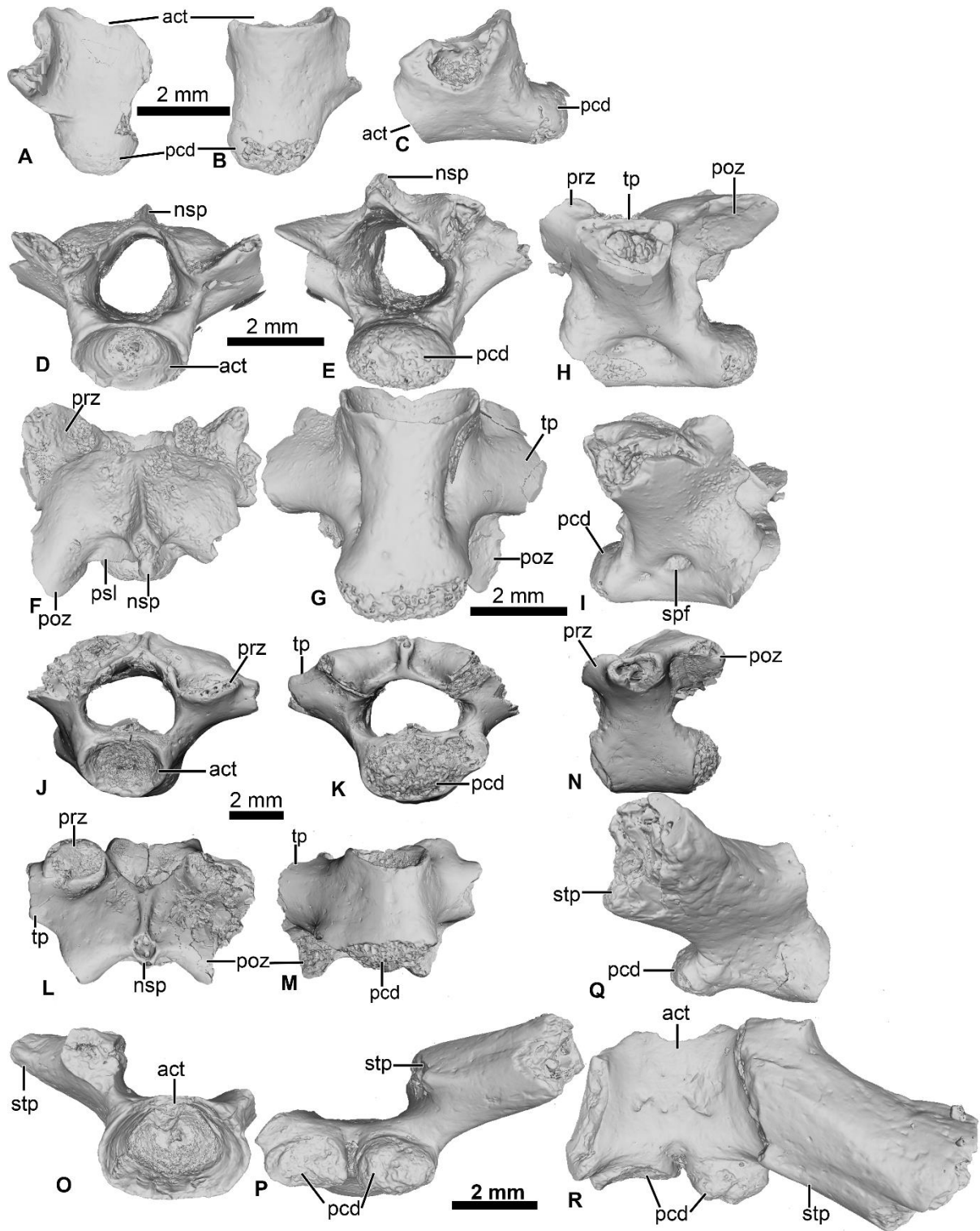


Figure VIII-4. Vertebral element of *Cretadhefdaa*. A–C UCRC-PV97, presacral centrum in A dorsal; B ventral and C right lateral views; D–I UCRC-PV98 incomplete possible presacral vertebra IV in D anterior; E posterior; F dorsal; G ventral; H left lateral and I right lateral views; J–N UCRC-PV101, incomplete possible presacral VIII in J anterior; K posterior; L dorsal; M ventral and N left lateral views; O–R UCRC-PV103, incomplete sacral vertebra in O anterior; P posterior; Q right lateral and R ventral

A new genus and species from the Kem Kem (Morocco), the second neobatrachian from Cretaceous Africa

views. **Abbreviations:** **act**, anterior cotyle; **nsp**, neural spine; **pcd**, posterior condyle; **poz**, postzygapophysis; **prz**, prezygapophysis; **psl**, posterior lamina; **spf**, spinal foramen; **stp**, sacral transverse process; **tp**, transverse process.

Referred Vertebrae

The four vertebrae attributed to *Cretadhefdaa* all have an anterior cotyle and a posterior condyle, indicating a procoelous condition of the vertebral column. Although the length of the centrum varies among these specimens (UCRC-PV97, UCRC-PV101 and UCRC-PV103 are shorter than UCRC-PV98), their similar size and the shape of articular facets and zygapophyses suggests that they all represent the same taxon. In addition, the two best preserved vertebrae, UCRC-PV101 and UCRC-PV98, each has a similarly shaped low and short neural spine that is oriented posteriorly. In other anurans, there is documented variation in the length of the centra of presacral vertebrae throughout the vertebral column (Trueb, 1973; Duellman and Trueb, 1994; Pugener, 2002; Evans et al., 2014; Lemierre et al., 2021: fig. 9). We attribute the above cranial elements and these vertebrae to *Cretadhefdaa* because they all represent non-pipid individuals of similar body size (following Rage and Dutheil, 2008).

UCRC-PV97—This specimen is a centrum of a procoelous vertebra, with the neural walls not preserved (Fig. VIII-4A–C). The centrum is longer than wide (Fig. VIII-4A, B). The posterior condyle is large and wide.

UCRC-PV98—This presacral vertebra is better preserved than UCRC-PV97, with most of the transverse process, one postzygapophysis, and the distal end of the neural spine missing (Fig. VIII-4D–I). The width of the posterior condyle is the same as that of the vertebral canal. The neural walls are thick, with the base of the transverse processes protruding laterally. In dorsal view, the remnants of the transverse processes are subcylindrical and oriented posteriorly. Each prezygapophysis bears a large flat and ovoid-shaped articular facet that is oriented dorsomedially (Fig. VIII-4F). The medial margin of this articular facet is a sharp, straight lamina constituting the medial end of

A new genus and species from the Kem Kem (Morocco), the second neobatrachian from Cretaceous Africa

the dorsal wall of the vertebral canal. The neural spine is low and was likely short, though it is broken distally. The postzygapophysis is long, with an ovoid and flattened articular surface that is oriented ventrally (Fig. VIII-4F). A small posterior lamina connects the neural spine and the medial margin of the postzygapophysis. The centrum is more elongate than UCRC-PV97 (Fig. VIII-4G). In ventral view, the centrum is compressed lateromedially at midlength, giving the ventral surface an hourglass shape (Fig. VIII-4G). In lateral view, a shallow fossa is visible at the midpoint of the vertebra and might be a remnant of a spinal foramen (Fig. VIII-4H, I). The elongate centrum indicates that this vertebra is from the mid-column of *Cretadhefdaa*, possibly representing presacral vertebra IV.

UCRC-PV101—This element is an incomplete presacral vertebra preserving the centrum and neural arch (Fig. VIII-4J–N). The centrum is short, almost as wide as long. The vertebra is procoelous, with an anterior cotyle and a posterior condyle (Fig. VIII-4J, K). The condyle is poorly preserved but seems elongated lateromedially. The prezygapophyses bear a flat articular facet that is oriented dorsomedially (Fig. VIII-4L). In dorsal view, the anterior margin of the neural arch is concave, and a sharp ridge is visible on the dorsal surface of the neural arch, marking the beginning of the neural spine. The neural spine is very short (shorter than the one recovered in UCRC-PV98) and oriented posteriorly. Each postzygapophysis bears a flat articular surface that is oriented ventrolaterally. The transverse processes are broken at their bases. The base of these processes is cylindrical in shape and elongate anteroposteriorly, oriented perpendicular to the anteroposterior axis of the centrum (Fig. VIII-4L, N). The anteroposteriorly short centrum and the low and posteriorly oriented neural spine indicate that UCRC-PV101 is one of the posterior presacral vertebrae (VI to VIII). The posterior condyle of UCRC-PV101 is similar in size to the anterior cotyle of the identified sacral vertebra (UCRC-PV103) and the inferred position of the prezygapophyses of UCRC-PV103 seems to match the position of the

A new genus and species from the Kem Kem (Morocco), the second neobatrachian from Cretaceous Africa

postzygapophyses of UCRC-PV101. UCRC-PV101 might represent the last presacral vertebra (VIII).

UCRC-PV103—This incomplete sacral vertebra bears an anterior cotyle and two posterior condyles (Fig. VIII-4O–R). The centrum of UCRC-PV103 is shorter than the other three vertebrae, but the anterior cotyle is similar to those of UCRC-PV97–98 and 101. The two posterior condyles are well separated and are wider than tall, and thus elliptical. The preserved transverse process is posterolaterally oriented and the preserved portion does not expand distally. In lateral view, the sacral transverse process is extended anteroposteriorly, and is not cylindrical or rod-like. The dorsal expansion of the transverse process is visible in dorsal view (Fig. VIII-4R).

Osteological comparison to hyperossified anurans

Hyperossified (*sensu* Trueb, 1973) ornamented cranial bones occur in both extinct and extant anurans, from pipoids (Báez and Rage, 1998; Trueb et al., 2000) to diverse lineages of neobatrachians, and has evolved more than 20 times independently across extant frogs (Paluh et al., 2020). Hyperossified cranial elements are known in numerous Cretaceous anurans from both Laurasian and Gondwanan sites (Jacobs et al., 1990; Rage and Roček, 2003; Roček, 2013; Gardner and Rage, 2016). In the Gondwanan fossil record, Cretaceous hyperossified anurans are known that belong to both the Pipimorpha and Neobatrachia (Gardner and Rage, 2016; Gómez and Báez, 2018).

Comparison to non-neobatrachian taxa—Ornamented and co-ossified cranial bones are relatively uncommon in the first four diverging lineages of extant frogs: Leiopelmatoidea, Alytoidea, Pipoidea, and Pelobatoidea. Neither of the two extant leiopelmatoids, *Ascaphus* and *Leiopelma* Fitzinger, 1861, exhibit any characteristics unique to hyperossified anuran skulls. Among the extant alytoids, ornamented dermal bones are found only in the genus *Latonia* Meyer, 1843 which is known from the

A new genus and species from the Kem Kem (Morocco), the second neobatrachian from Cretaceous Africa

Paleogene and Neogene of Laurasia and Africa (Roček, 1994; 2013; Biton et al., 2016). However, *Cretadhefdaa* differs from *Latonia* in having a foramen for the occipital artery (lacking in *Latonia*) and frontoparietals that fuse with the prooticooccipitals (see Roček, 1994: fig. 7). The extinct Gobiidae from the Cretaceous of Asia (Roček, 2008; 2013) also exhibits ornamented dermal bones. However, *Cretadhefdaa* can be differentiated from all Gobiidae in having fused frontoparietals without a visible suture (frontoparietals not fused or in contact with each other in Gobiidae), complete fusion of the prootic and exoccipital (suture visible between the two bones in Gobiidae; Roček, 2008), and presacral vertebrae that are procoelous (amphicoelous in Gobiidae).

Cretadhefdaa can be differentiated from all pipoid anurans in having alae of the parasphenoid that cover the ventral surface of the otic capsules (Fig. VIII-1C). Some members of the Pelobatoidea also have ornamented skull bones, but as an integral part of the bone and not as a secondary exostosis (Rage and Roček, 2007; Roček, 2013; Roček et al., 2014). *Cretadhefdaa* can be differentiated from *Eopelobates* Parker, 1929 in (1) having ornamentation as a secondary exostosis (ornamentation is an integral part of the bones in *Eopelobates*); and (2) lacking anteroposterior expansion of the distal part of the sacral apophyses (Roček et al., 2014).

In addition, several fragmentary remains of ornamented maxillae and procoelous vertebrae were recovered in the Cretaceous outcrops of Texas and might represent one of the early diverging frog lineages, but the phylogenetic affinities of these fossils remain unclear (Roček, 2013).

Two hyperossified taxa of uncertain affinities are known from the Late Cretaceous of North America: *Scotiophryne* Estes, 1969 and *Theatoni* Fox, 1976. *Cretadhefdaa* can be differentiated from *Scotiophryne* in (1) having ornamentation made of pits and ridges (fine beadlike tubercles in *Scotiophryne*; Gardner, 2008); (2) having fused frontoparietals without a median suture (frontoparietals not fused in *Scotiophryne*); (3) having a well-delimited lamina horizontalis on the maxilla; and (4) having a well-

A new genus and species from the Kem Kem (Morocco), the second neobatrachian from Cretaceous Africa

developed ramus paroticus of the squamosal that articulates with the frontoparietal. *Cretadhefdaa* can be differentiated from *Theatoniuss* in (1) having teeth on the maxillae (maxillae are edentate in *Theatoniuss*; Gardner, 2008); and (2) having fused frontoparietals without a median suture (frontoparietal fused with a median suture in *Theatoniuss*; Gardner, 2008).

Based on the above comparisons, we exclude *Cretadhefdaa* from the Leiopelmatoidea, Alytoidea, Pipoidea, and Pelobatoidea. The vast majority of extant frog species belong to the Neobatrachia. *Cretadhefdaa* shares with Neobatrachia the presence of well-separated occipital condyles and a bicondylar articulation between the sacrum and urostyle. However, others synapomorphies used to diagnose Neobatrachia (in combination with the two mentioned above), such as the presence of palatines (also called neopalatines in neobatrachians; Báez et al., 2009) cannot be assessed based on the preserved elements of *Cretadhefdaa*.

Comparison to Cretaceous hyperossified taxa—The best known non-pipimorph ornamented taxon described from the Mesozoic fossil record of Africa is *Beelzebubo ampinga*, from the Maastrichtian of Madagascar (Evans et al., 2008, 2014). *Beelzebubo* is known from numerous cranial and some postcranial elements. The ornamentation of *Cretadhefdaa*, comprised of pits and ridges, is similar to that of *Beelzebubo*. Both taxa also have a series of three recesses on the posterodorsal surface of the skull, with the foramen for the arteria occipitalis located within the central recess, which is the deepest recess in both taxa (Fig. VIII-5). *Cretadhefdaa* also differs from *Beelzebubo* in having a smooth occipital flange on the posterior region of the frontoparietals. The poor preservation of the tectum supraorbitale of the frontoparietals of *Cretadhefdaa* (UCRC-PV94) means that we cannot evaluate whether it is similar to the expansion in *Beelzebubo*, in which the tectum supraorbitale is elongate laterally along on its entire length, covering the lateral region of the braincase (Evans et al., 2014). The parasphenoid of *Cretadhefdaa* is similar to that of *Beelzebubo* in having narrow alae (alary process of Evans et al., 2014) with a median keel. *Cretadhefdaa* is similar to *Beelzebubo* in

A new genus and species from the Kem Kem (Morocco), the second neobatrachian from Cretaceous Africa

lacking a distinct palatine shelf on the medial surface of the maxilla, but differs in having ornamentation of the pars facialis on the lateral surface of the maxilla that extends ventrally to the pars dentalis (the ornamentation ends before the pars dentalis in *Beelzebufo*).

The presacral vertebrae of *Cretadhefdaa* differ from most of those referred to *Beelzebufo* by lacking a well-developed neural spine, and lacking an expanded and ornamented “table” sitting atop the spine (Evans et al., 2014: fig. 34–36). In addition, even the shortest neural spine of the posteriormost presacral of *Beelzebufo* is taller than that of any vertebrae that we refer to *Cretadhefdaa* (Fig. VIII-4F, L). The sacral vertebra of *Cretadhefdaa* is similar to that of *Beelzebufo* in having two elliptical posterior condyles for the sacro-urostyler articulation and a centrum that is wider than longer (Fig. VIII-4P). However, the sacral transverse processes of *Beelzebufo* are slightly more expanded distally than that preserved for *Cretadhefdaa* (Fig. VIII-4R).

Another neobatrachian from Gondwana with an ornamented skull is *Baurubatrachus pricei* Báez and Perí, 1989 from the Crato Formation of Brazil (latest Early Cretaceous). The poor preservation of the frontoparietals of the holotype (and only known specimen), which is still embedded in matrix, prevents comparisons of the braincase of *Cretadhefdaa* to *Baurubatrachus*. However, its frontoparietals seem to be similar in having ornamentation comprised of pits and ridges that extend posteriorly to the margin of the foramen magnum. *Cretadhefdaa* also differs from *B. pricei* in having a fully ossified dorsal margin of the foramen magnum, and a foramen for the arteria orbitonasalis dorsal to the prootic foramen. The maxilla of *Cretadhefdaa* is similar to *B. pricei* in having ornamentation on the lateral surface of the pars facialis that extends ventrally to the pars dentalis, but differs in lacking a distinct palatine shelf. *Cretadhefdaa* differs from *B. pricei* in having an occipital flange and a system of recesses on the posterodorsal region of the braincase. *Cretadhefdaa* also differs from *B. pricei* in having more slender and shorter neural spines on presacral vertebrae and slightly expanded sacral transverse processes.

A new genus and species from the Kem Kem (Morocco), the second neobatrachian from Cretaceous Africa

In his 2012 review, Agnolin described several specimens as *Calyptocephalella satan*, the oldest calyptocephalellid described (Agnolin, 2012). Although these specimens need to be reassessed (Báez and Gómez, 2018) and likely represent more than one taxon (Muzzopappa et al., 2020), their attribution to Neobatrachia is certain. *Cretadhefdaa* resembles *C. satan* in having dermal skull bones covered with an ornamentation of pits and ridges, but differs in lacking a distinct palatine shelf (all calyptocephalellids exhibit a distinct palatine shelf; Muzzopappa and Báez, 2009; Agnolin, 2012), in having fused frontoparietals without a median suture, and in having an occipital flange on the frontoparietals (Fig. VIII-1A). The postcranial elements of *Cretadhefdaa* resemble *C. satan* in having procoelous vertebrae with anteroposteriorly elongate centra for the anterior presacral vertebrae, and shorter centra for posterior presacral and sacral vertebrae (Agnolin, 2012). The sacral vertebra bears a bicondylar articulation in both taxa, but *Cretadhefdaa* differs in having sacral transverse processes that are weakly expanded distally, whereas *C. satan* exhibits greatly expanded sacral transverse processes (Agnolin, 2012: fig. 10A, B).

One last ornamented Cretaceous neobatrachian taxon is *Hungarobatrachus szukacsi* from the Late Cretaceous of Hungary. Its vertebral elements are not known, but several skull fragments were recently described (Venczel et al., 2021). Both taxa have fused frontoparietals without a trace of suture along their medial margin. However, *Cretadhefdaa* differs from *H. szukacsi* in having a system of recesses on each side of the posterior surface of its frontoparietals (divided by the foramen magnum) with the foramen for the occipital artery opening in a deep recess and an occipital flange on the frontoparietals. In *H. szukacsi*, the posterior surface of the frontoparietals is smooth with a slight depression and the foramen for the occipital artery opens on each side of the foramen magnum (Venczel et al., 2021: fig.3). The frontoparietals of *H. szukacsi* also bear an *incrassatio frontoparietalis* on the ventral surface whereas *Cretadhefdaa* does not. The maxilla of *Cretadhefdaa* differs from that of *H. szukacsi* in lacking a distinct palatine shelf (Venczel et al., 2021: fig. 5).

A new genus and species from the Kem Kem (Morocco), the second neobatrachian from Cretaceous Africa

Comparison to hyperossified extinct ranoids—Two other hyperossified taxa are relevant for comparisons to *Cretadhefdaa*: *Rocekophryne ornata* Rage et al., 2021 from the Early Eocene of Algeria (Rage et al., 2021) and *Thaumastosaurus servatus* from the Middle to Late Eocene of southwestern France (Lemierre et al., 2021). These are the oldest occurrences of ornamented ranoids in the fossil record (Lemierre et al., 2021; Rage et al., 2021).

Rocekophryne ornata is known from fragmentary cranial and postcranial remains. *Cretadhefdaa* resembles *Rocekophryne* in having fused frontoparietals without a median suture and bearing an ornamentation of pits and ridges, an occipital flange, and in lacking an *incrassatio frontoparietalis* on the ventral surface of the frontoparietals. In addition, *Cretadhefdaa* and *Rocekophryne* both bear ornamentation on the lateral surface of the *pars facialis* of the maxilla that extends ventrally to the *pars dentalis* (Fig. VIII-3F). However, *Cretadhefdaa* differs in lacking a lateral flange on the posterior surface of the frontoparietal, lacking a distinct palatine shelf, and in having very short paraoccipital processes (well-developed in *Rocekophryne*; Rage et al., 2021: fig. 3A—F) and a series of recesses on the posterodorsal surface of the braincase. In addition, the sacral vertebra of *Rocekophryne* bears an anterior condyle (instead of an anterior cotyle in *Cretadhefdaa*) that indicates that the vertebral column is diplasiocoelous (Rage et al., 2021: fig. 4A, B) and possesses transverse processes that are circular in lateral view (not circular in *Cretadhefdaa*).

Thaumastosaurus servatus is known from fragmentary remains and three partially complete and articulated skeletons (Rage and Roček, 2007; Lemierre et al., 2021). As with *R. ornata*, *Cretadhefdaa* and *T. servatus* have fused and ornamented frontoparietals without a medial suture. The anterior surface of the prooticooccipitals of both taxa exhibit a well-delimited but shallow and narrow groove for the jugular vein (Rage and Roček, 2007: fig. 7; Lemierre et al., 2021: fig. 8F). However, *Cretadhefdaa* differs from *T. servatus* in having an occipital flange and reduced paraoccipital processes, lateromedially compressed occipital condyles (instead of crescent shaped),

**A new genus and species from the Kem Kem (Morocco), the second
neobatrachian from Cretaceous Africa**

and a series of recesses in the posterodorsal surface of the braincase (Fig. VIII-1). *Cretadhefdaa* also differs from *T. servatus* in lacking a single, tapered posterior process of the parasphenoid and an incrassatio frontoparietalis on the ventral surface of the frontoparietals (Fig. VIII-1C). In addition, the vertebral column of *T. servatus* is diplasiocoelous instead of procoelous as in *Cretadhefdaa*.

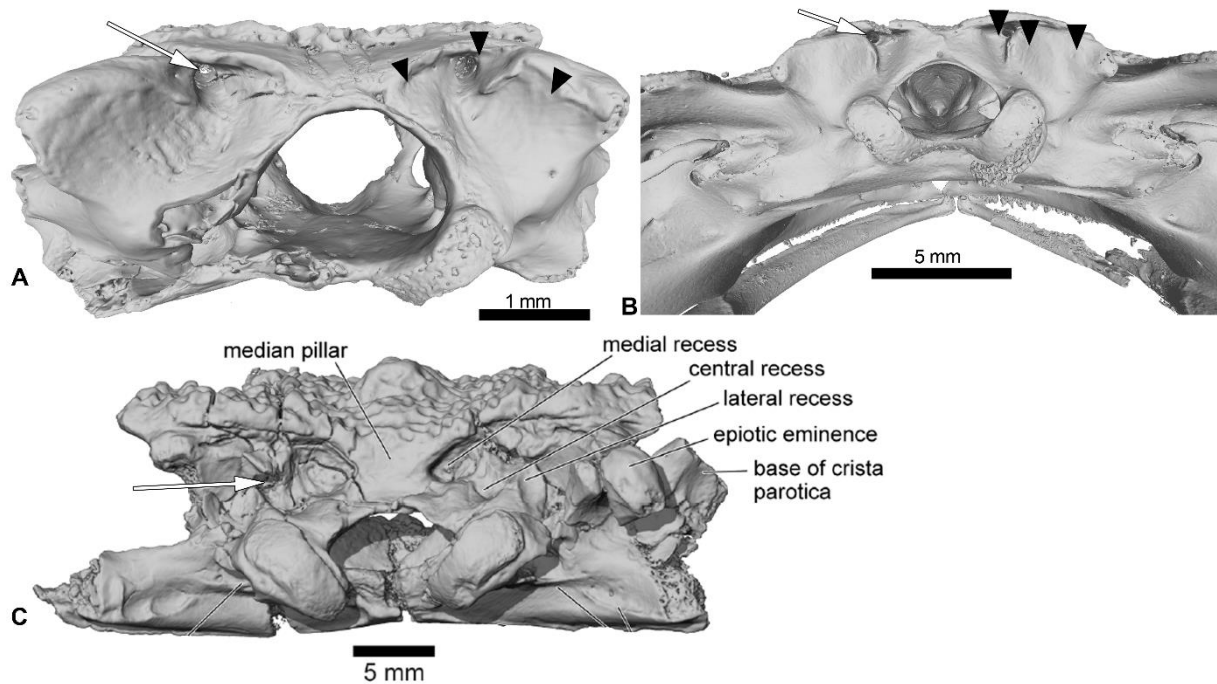


Figure VIII-5. Comparison between the braincases of *Cretadhefdaa*, *Beelzebufo* and *Ceratophryidae*. A *Cretadhefdaa* in posterior view (UCRC-PV64); B *Beelzebufo* braincase in posterior view (taken from Evans et al., 2014: fig. 22C) and C braincase of *Ceratophrys aurita* in posterior view (CAS:Herp:84998; MorphoSource ARK: ark:/87602/m4/M16099). Black arrows point to the recesses discussed in the text.

Comparisons to extant hyperossified hylids—*Cretadhefdaa* shares numerous characters with ornamented extant Neobatrachia. Most of these similarities are associated with hyperossification, but two characters deserve further attention. The first is the presence of contact between the squamosal and frontoparietals, which occurs frequently (but not uniquely) in Hyloidea (e.g., Calyptocephalellidae, Ceratophryidae, or the hylid *Triprion* Cope, 1866). The second is the series of recesses on the posterodorsal surface of the braincase in *Cretadhefdaa*. This is known only in *Beelzebufo* and in *Ceratophrys* Wied-Neuwied, 1824 (Evans et al., 2014; Fig. VIII-5B, C).

A new genus and species from the Kem Kem (Morocco), the second neobatrachian from Cretaceous Africa

However, both *Cretadhefdaa* and *Beelzebufo* differ from *Ceratophrys* in having the foramen for the occipital artery located in the central recess, whereas it is found in the medial recess in extant taxa (Fig. VIII-5). The braincase of *Ceratophrys* is similar to *Cretadhefdaa* in having fused frontoparietals, no distinct posterior process, and barely distinct paraoccipital processes. *Cretadhefdaa* differs from *Ceratophrys* in having an occipital flange, a well-delimited groove for the jugular vein, and in lacking the expanded “table” atop the neural spine of presacral vertebrae. The extant *Tripriion* differs from *Cretadhefdaa* in having a frontoparietal extending posteriorly up to the end of the epiotic eminence, covering it dorsally. *Tripriion petasatus* Cope, 1865 also lacks the system of recesses on the posterodorsal surface of the braincase. *Tripriion spatulatus* Günther, 1882 bears recesses on its posterodorsal region of the braincase, but differs from *Cretadhefdaa* in having the foramen for the arteria occipitalis not located within a recess.

NEOBATRACHIA? Reig, 1958

RANOIDEA? Rafinesque, 1814

Forelimb (UCRC-PV104)

This specimen is an incomplete humerus missing its proximal end and part of the diaphysis (Fig. VIII-6). The diaphysis is straight, and a thin ventral ridge on the proximal end of the bone extends distally to the midlength of the diaphysis (Fig. VIII-6A, C). The fossa cubitalis is very reduced, being shallow and not well-delimited, and visible in ventral view only as a thin crescent around the humeral ball (Fig. VIII-6A). The humeral ball is large and in-line with the main axis of the diaphysis. The epicondyles are not symmetrical, with the ulnar epicondyle well-developed and the radial epicondyle reduced and barely visible in ventral view (Fig. VIII-6A). In dorsal view, the olecranon scar is short, with a tapered and pointed end (Fig. VIII-6B).

A new genus and species from the Kem Kem (Morocco), the second neobatrachian from Cretaceous Africa

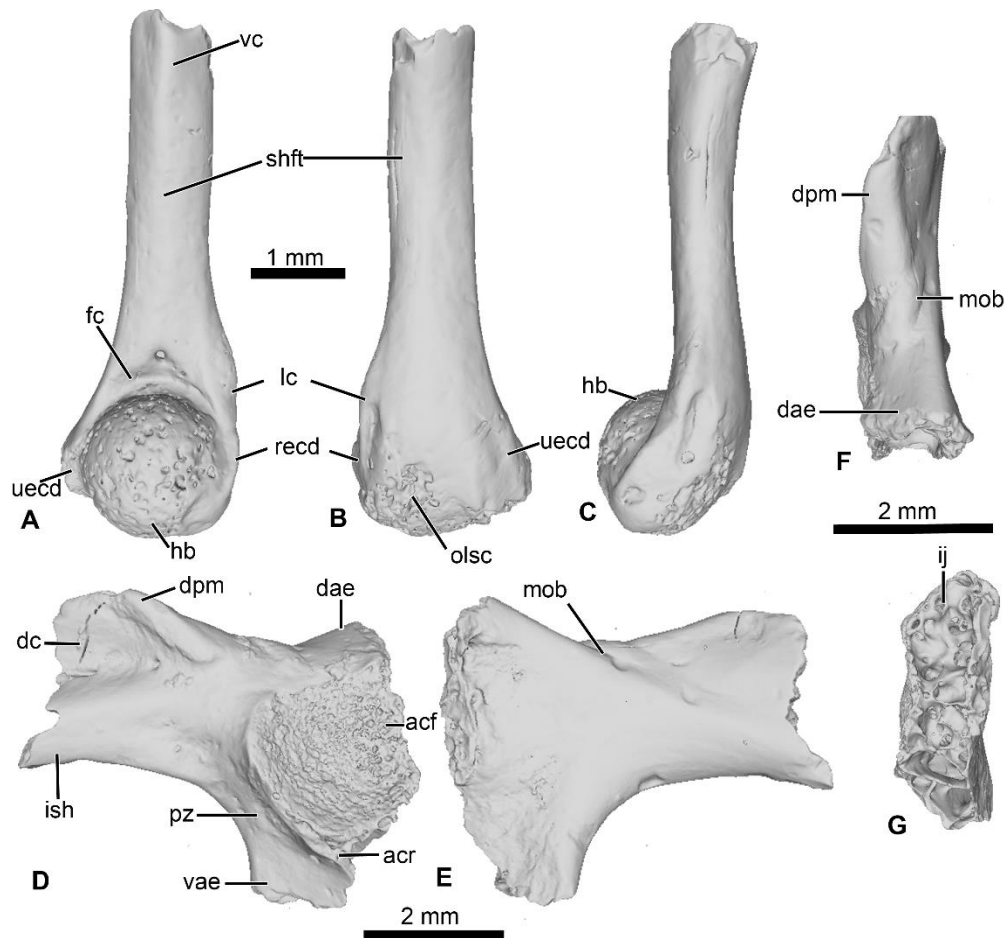


Figure VIII-6. ?*Neobatrachia* humerus and indeterminate ilium from Kem Kem beds. A–C, UCRC-PV104, incomplete humerus in A ventral; B dorsal and C lateral views; D–G, UCRC-PV105, left ilium in D lateral; E medial; F posterior and G dorsal views. **Abbreviations:** acf, acetabular fossa; acr, acetabular rim; dae, dorsal acetabular expansion; dc, dorsal crest; dpm, dorsal prominence; fc, fossa cubitalis; hb, humeral ball; ij, ilioischiatric junction; ish, iliac shaft; lc, lateral crest; mob, medial oblique ridge; olsc, olecranon scar; pz, preacetabular zone; recd, radial (lateral) epicondyle; shft, shaft; uecd, ulnare (medial) epicondyle; vae, ventral acetabular expansion; vc, ventral crest.

Comparisons—The combination of a large humeral ball and asymmetrically developed epicondyles is diagnostic for most Neobatrachia (Prasad and Rage, 2004; Rage et al., 2013), although this combination of characters has not been evaluated in phylogenetic analyses. The presence of a straight diaphysis, a humeral ball in line with the axis of the diaphysis, and a shallow, poorly delimited fossa cubitalis are found in

A new genus and species from the Kem Kem (Morocco), the second neobatrachian from Cretaceous Africa

most ranoids (Rage et al., 2013; de Lapparent de Broin et al., 2020). It differs from the humerus of *Thaumastosaurus servatus*, one of the earliest known ranoids, in having a crescent-shaped fossa cubitalis (triangular in *T. servatus*) and a less developed ulnar epicondyle. Among the Cretaceous neobatrachian taxa, only *Eurycephalella alcinae* Báez et al., 2009 and *Arariphrynus placidoi* Leal and Brito, 2006 have preserved humeri with their ventral surface exposed. The humerus of *A. placidoi* differs from UCRC-PV104 in having two well-developed epicondyles (instead of a reduced radial epicondyle) and a deep fossa cubitalis (instead of a shallow fossa in UCRC-PV104).

These comparisons suggest that UCRC-PV104 should be referred to the Neobatrachia. UCRC-PV104 shares several characters with extant and extinct Ranoidea, as well as with the oldest (putative) member of the Ranoidea (*Thaumastosaurus servatus*). However, because no phylogenetic analyses have yet shown synapomorphies for Ranoidea related to the humerus, we refer this fossil to the Neobatrachia and recognize the assignment to Ranoidea as tentative.

INCERTAE SEDIS

Pelvic girdle (UCRC-PV105)

This element is an incomplete left ilium, preserving most of its acetabular region. UCRC-PV105 bears a high and well-developed dorsal crest, although its extension on the iliac shaft is unknown (Fig. VIII-7I–J). The dorsal crest appears to be lacking its dorsalmost portion, indicating that it was more extensive (Fig. VIII-7I, K). The dorsal prominence is low and elongate anteroposteriorly, and the dorsal protuberance is strongly oriented laterally (Fig. VIII-7K). The acetabular rim is well developed on its ventral region. Although not complete, both the dorsal and ventral acetabular expansions are developed. The dorsal acetabular expansion is inclined posteromedially (Fig. VIII-7I). The ventral acetabular expansion is poorly preserved. However, the preserved portion shows it was well-developed (Fig. VIII-4I). The

A new genus and species from the Kem Kem (Morocco), the second neobatrachian from Cretaceous Africa

preacetabular angle is obtuse and the preacetabular zone is narrow (Fig. VIII-7I). In medial view, a shallow but well delimited medial ridge is present, starting from the base or the dorsal acetabular expansion to the anteriormost preserved portion (Fig. VIII-7J). In posterior view, the ilioischadic juncture is moderately wide and an interiliac tubercle is absent (Fig. VIII-7L).

Comparisons—Ilia are one of the most common anuran elements recovered in the fossil record (Roček, 2000; Rage and Roček, 2003; Roček, 2013; Roček et al., 2013; Gardner and Rage, 2016) and several authors have proposed characters to identify the ilia of the different clades (Gardner et al., 2010; Gómez and Turazzini, 2016; Matthews et al., 2019). However, these are largely based on extant anurans and can be difficult to apply to Mesozoic anurans (Roček et al., 2010; Roček, 2013). The presence of a well-developed dorsal crest is found in several clades (Alytoidea, Pipoidea, and Neobatrachia, especially Ranoidea), but likely reflects similarity in locomotion rather than close phylogenetic relationships (Roček, 2013). The absence of an interiliac tubercle is diagnostic for many neobatrachians, with notable exceptions such as *H. szukacsi* and the aquatic hylid *Pseudis* Wagler, 1830 (Gómez and Turazzini, 2016; Venczel et al., 2021). However, the utility of this character has not been tested thoroughly in a taxon-rich phylogenetic analysis (Gómez and Turazzini, 2016). Agnolin (2012) argued that the presence of a broad preacetabular zone and large acetabular fossa was diagnostic for the Calyptocephalellidae but this was not evaluated in a phylogenetic analysis and may represent an example of convergent evolution. There are no characters that allow for a precise attribution of this ilium (UCRC-PV105) to the other anurans from the Kem Kem or other specific anuran lineages.

VIII.6 Phylogenetic Analyses

Recent phylogenetic analyses (Báez and Gómez, 2018; Lemierre et al., 2021) are based on a similar dataset. This dataset was first elaborated by Báez et al. (2009), based on the dataset of Fabrezi (2006) that was developed for a phylogenetic analysis of ceratophryids. The dataset from Báez et al. (2009) includes 42 taxa—three of which are extinct taxa—and 75 characters. In a separate analysis, Báez and Gómez (2018) modified the dataset from Fabrezi (2006) further by adding 29 neobatrachian taxa and redefining some characters to test the impact of characters related to hyperossification. They expanded the taxon sampling to 71 taxa and added 68 characters (for a total of 143 characters), as well as redefined several characters. Finally, Lemierre et al. (2021) further enlarged the dataset from Báez and Gomez (2018), by adding 15 extant natatanuran ranoid taxa (for a total of 20 natatanuran taxa). The vast majority of extant anurans belong to the Neobatrachia (Feng et al., 2017), which includes two large clades, Hyloidea and the Ranoidea. To date, phylogenetic analyses based solely on morphological characters (e.g., Scott, 2005) do not recover many of the clades found in recent molecular phylogenetic analyses (e.g., Roelants et al. 2007; Feng et al., 2017; Jetz and Pyron, 2018; Hime et al., 2021). To evaluate the phylogenetic placement of *Cretadhefdaa*, we analyzed our character matrix using different sets of assumptions as well as one analysis using a constraint tree reflecting recent results from molecular phylogenetic analyses.

A new genus and species from the Kem Kem (Morocco), the second neobatrachian from Cretaceous Africa

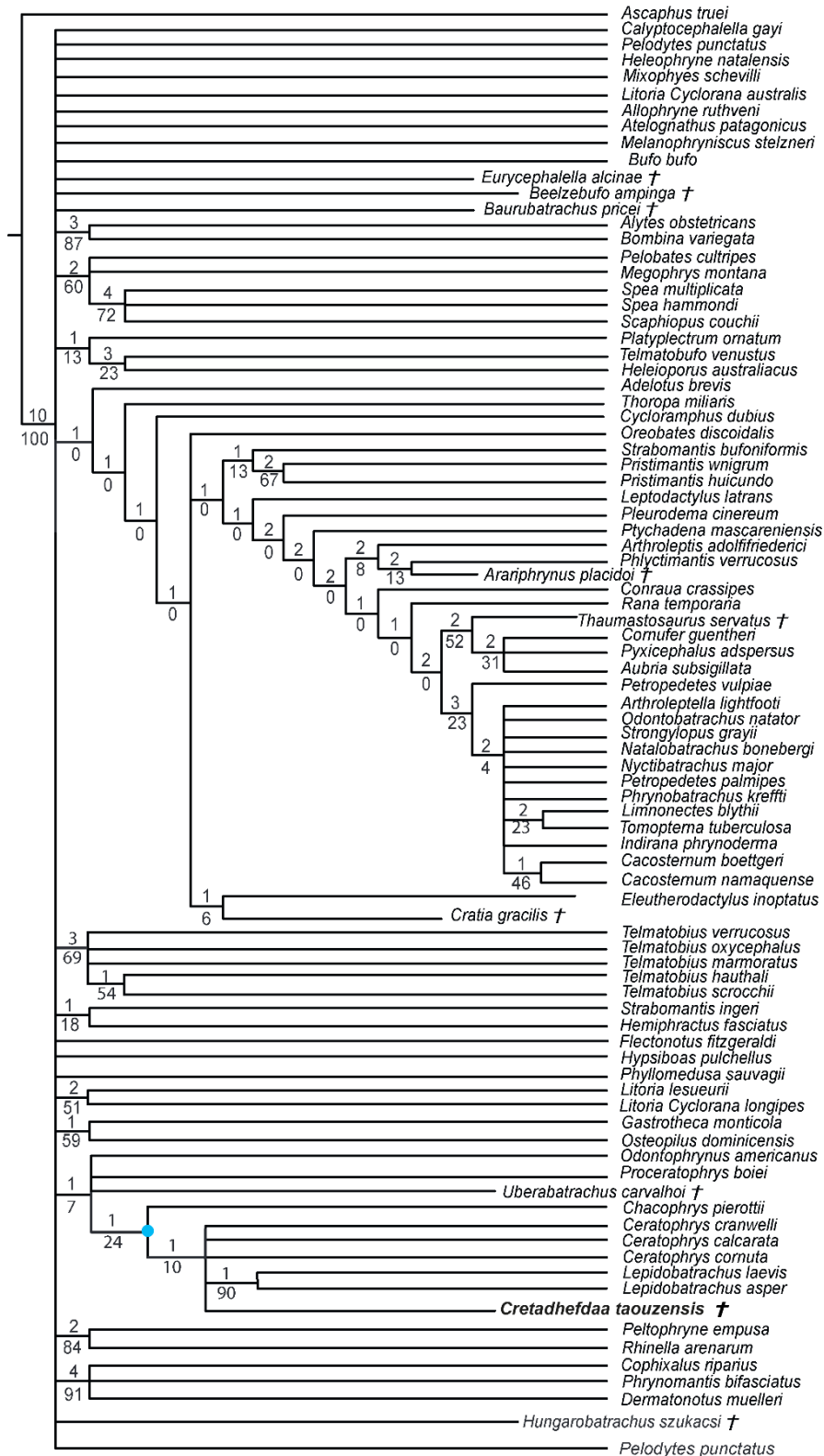


Figure VIII-7. Strict consensus of 60 MPTs of 1362 steps (CI = 0.139; RI = 0.418) from the analysis under EW. † represents extinct taxon, light blue circle represents Ceratophryidae node; numbers above branches designate Bremer support; those below are bootstrap frequencies.

A new genus and species from the Kem Kem (Morocco), the second neobatrachian from Cretaceous Africa

We obtained 60 MPTs (most parsimonious trees) of 1362 steps (CI = 0.139; RI = 0.418) with the analysis performed under equal weight with cline characters ordered. The strict consensus (Fig. VIII-7) shows large polytomies, and the monophyly of the Neobatrachia is not recovered. This seems related to the uncertainties regarding the position of *Arariphrynus placidoi*, and the lack of characters scored for *Cretadhefdaa* and *Hungarobatrachus szukacsi* (13 and 11% of characters scored, respectively). *Cretadhefdaa* is recovered within a clade containing *Uberabatrachus carvalhoi* Báez et al., 2012 and the Ceratophryidae. This clade is supported by three synapomorphies, all of which are character states found in other groups of frogs: (1) a position of articulation of lower jaw and skull at the level of occiput (character 61: 0→1); (2) cotyle of the atlas widely separated (76: 1→2) and (3) angle between iliac shaft and ventral acetabular expansion obtuse (125: 1→2). *Cretadhefdaa* is placed within this clade in a polytomy with the Ceratophryidae. This clade is supported by five synapomorphies mainly related to hyperossified cranial characters (see Appendix S4).

When excluding *Arariphrynus*, we obtained 10 trees of 1355 steps. The strict consensus (CI = 0.174; RI = 0.556; Fig. VIII-8) shows a trichotomy with Pelobatoidae, *Heleophryne* Sclater, 1898, and the remaining Neobatrachia. The 'Neobatrachia' (the clade exclusive of *Heleophryne*) is supported by a five synapomorphies: (1) otic ramus of the squamosal short, overlapping only the most lateral portion of the crista parotica (9: 0→1); (2) absence of process or crest on the anterior margin of the scapula (114: 3→0); (3) configuration of the postaxial carpals as ulnare free, 3+4+5 (119: 0→2); (4) well developed posterodorsal expansion of the ischium (131: 0→1) and (5) horizontal pupil shape (143: 0→2). Among the Neobatrachia, we recovered a large hyperossified clade, supported by six synapomorphies (see Appendix S4). *Hungarobatrachus* is within a poorly supported trichotomy with *Eurycephalella* and *Calyptocephalella* Strand, 1928, for which there are three synapomorphies: (1) contact between lamella alaris of the squamosal and frontoparietals on the dorsal surface of the otic capsule (8: 0→2); (2)

**A new genus and species from the Kem Kem (Morocco), the second
neobatrachian from Cretaceous Africa**

anterior ramus of the pterygoid not reaching planum antorbitale (12: 0→1) and (3) postaxial carpal with ulnare and 3 free (119: 2→1). *Cretadhefdaa* is recovered within a large polytomy with extant Ceratophryidae, poorly supported by four synapomorphies (see Appendix S4).

A new genus and species from the Kem Kem (Morocco), the second neobatrachian from Cretaceous Africa



Figure VIII-8. Strict consensus of 10 MPTs of 1355 steps (CI = 0.174; RI = 0.556) from the analysis under EW excluding *Arariphrynus placidoi*. † represents extinct taxon, red circle represents Neobatrachia node (excluding *Heleophryne*), light blue circle represents Ceratophryidae node; numbers above branches designate Bremer support; those below are bootstrap frequencies.

A new genus and species from the Kem Kem (Morocco), the second neobatrachian from Cretaceous Africa

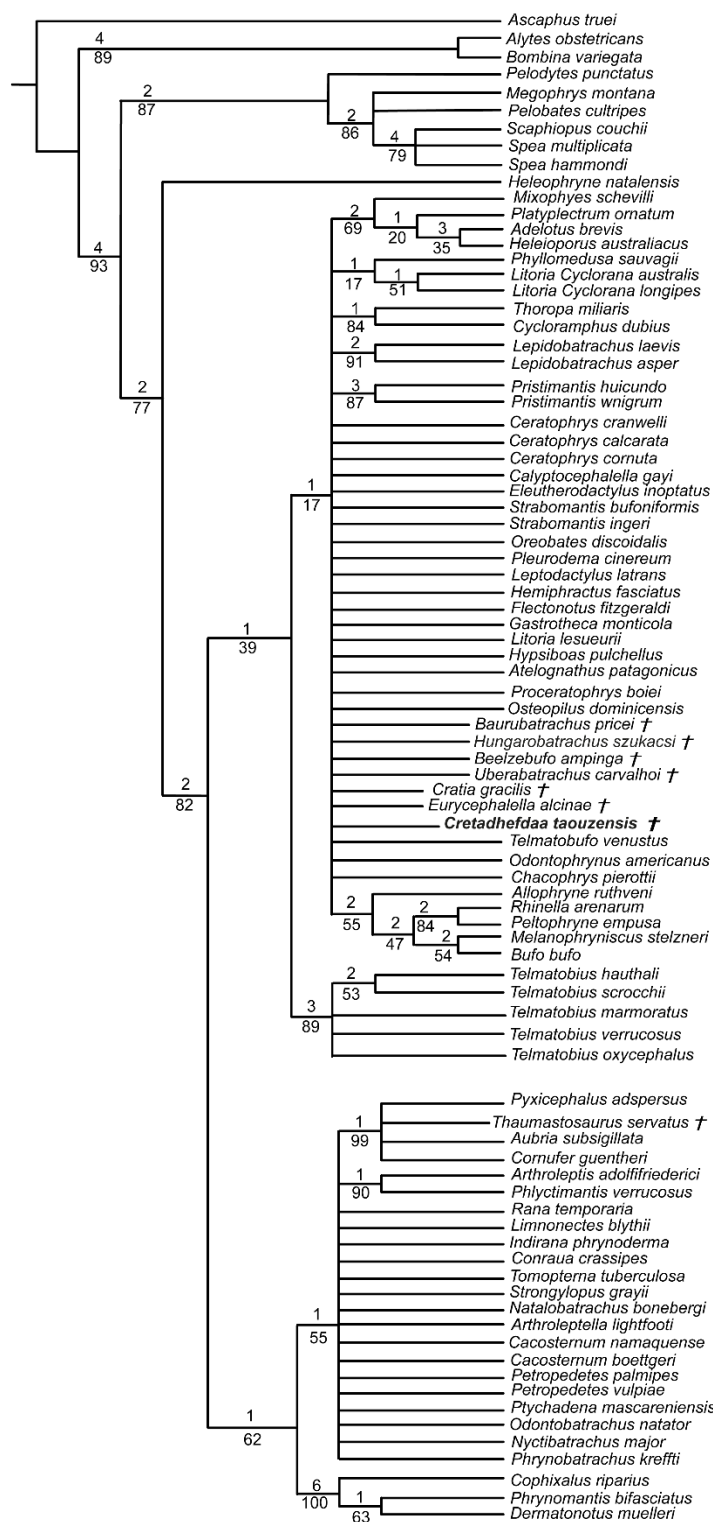


Figure VIII-9. Strict consensus of 190 MPTs of 1395 steps (CI =0.126 ; RI = 0.247) from the analysis under EW, excluding *Arariphrynus placidoi* and using a constraint topology based on molecular phylogenetic analyses. † represents extinct taxon and numbers above branches designate Bremer support; those below are bootstrap frequencies.

A new genus and species from the Kem Kem (Morocco), the second neobatrachian from Cretaceous Africa

In analyses using a topological constraint (and excluding *Arariphrynus placidoi*), we obtained 190 trees, with a score of 1395 steps. The strict consensus (CI = 0.126, RI = 0.247; Fig. VIII-9) shows a monophyletic Neobatrachia, Ranoidea, and Hyloidea, but all of the monophyly of each was enforced in the constraint tree. Within Hyloidea, most taxa are placed within a large unresolved clade (Fig. VIII-9). *Cretadhefdaa* is recovered in a large polytomy within Hyloidea as are *Baurubatrachus*, *Beelzebufo*, *Cratia* Báez et al., 2009, *Eurycephalella*, *Hungarobatrachus*, and *Uberabatrachus*. The only extinct taxon to be recovered elsewhere in the phylogeny is *Thaumastosaurus*, which is recovered in a clade of Ranoidea with *Aubria* Boulenger, 1917, *Cornufer* Tschudi, 1838, and *Pyxicephalus* Tschudi, 1838.

VIII.7 Discussion

Phylogenetic analyses

The poor resolution of the topology obtained when performing phylogenetic analysis under equal weights is not surprising. *Hungarobatrachus szukacsi* has only 16 scored characters within the dataset, none of which are clear neobatrachian synapomorphies, and the skeleton of *Arariphrynus* is very incomplete leading to few scored characters, especially those for the pectoral girdle and vertebrae (51 scored characters in total; see Báez et al., 2009). In addition, most of the scored cranial characters for *Hungarobatrachus* and *Cretadhefdaa* are linked to hyperossification, a recurrent feature in anuran evolution (see above) that likely obscures the phylogenetic relationships of *Cretadhefdaa*.

The phylogenetic positions of *Cretadhefdaa* and *Hungarobatrachus* are similar to several hyperossified extinct Cretaceous taxa by being close to either the Ceratophryidae or Calyptocephalellidae. Recent analyses (Báez and Gómez, 2018) have highlighted that convergence due to hyperossification likely plays a role in the position recovered for other hyperossified extinct neobatrachian taxa. This could

A new genus and species from the Kem Kem (Morocco), the second neobatrachian from Cretaceous Africa

influence the position of *Cretadhefdaa* as well. Nevertheless, the combination of characters of *Cretadhefdaa* confirms its assignment to Neobatrachia. In addition, one character mentioned in the description of the braincase, the presence of a series of recesses in posterodorsal region of the braincase, deserves attention. In addition to *Cretadhefdaa*, a similar (but not clearly homologous) morphology has only been identified in *Beelzebufo* and in the Ceratophryidae (except in *Chacophrys*). To our knowledge, this character has not been used in phylogenetic analyses (e.g., Gómez and Turazzini, 2021). However, the two extant taxa possessing these recesses are closely related (*Ceratophrys* and *Lepidobatrachus* Budgett, 1899), and the extinct *Beelzebufo* has been proposed as a stem member of the Ceratophryidae (Báez and Gómez, 2018; Lemierre et al., 2021). Interestingly, *Cretadhefdaa* is recovered in a more crownward position within Ceratophryidae than *Beelzebufo*, even in other analyses (Báez and Gómez, 2018; Lemierre et al., 2021). It is necessary to test the phylogenetic significance of this character to confirm this hypothesis, which is beyond the scope of this paper. When using a topological constraint based on recent phylogenomic analyses, most extinct taxa—including *Cretadhefdaa*—included in the analysis were recovered as part of Hyloidea, though as part of a large polytomy. In conclusion, our phylogenetic analyses point to *Cretadhefdaa* being within the Neobatrachia, even if most of the synapomorphies diagnostic of this clade are not scored, and several analyses support a hyloid affinity.

Paleobiogeographical implications

Neobatrachians are known in the fossil record during the Late Cretaceous from three main locations: Madagascar (Maastrichtian; Evans et al., 2014), Europe (Santonian; Venczel et al., 2021), and South America (Maastrichtian; Báez and Gómez, 2018). The South American fossil record is of particular importance with numerous taxa known from articulated specimens (Báez et al., 2009; Báez and Gómez, 2018; Agnolin et al., 2020; Moura et al., 2021). In contrast, only fragmentary remains of two taxa have been

A new genus and species from the Kem Kem (Morocco), the second neobatrachian from Cretaceous Africa

recovered from Madagascar and Europe (Evans et al., 2008; 2014; Venczel et al., 2021). There are other reports of neobatrachians from the Cretaceous (Báez and Werner, 1996; Prasad and Rage, 2004; Rage, 1984; Rage et al., 2020) but the attribution of these to the Neobatrachia remains uncertain because diagnostic elements are often not preserved and these other fossils have not been included in phylogenetic analyses. Because *Cretadhefdaa* is from the Mid-Cenomanian, it is the oldest neobatrachian of Africa.

The oldest occurrence of the Neobatrachia is from the Brazilian Crato Formation (Leal and Brito, 2006; Báez et al., 2009; Agnolin et al., 2020; Moura et al., 2021), which preserves extinct anurans from the Aptian (Early Cretaceous). However, *Cretadhefdaa* is still the oldest occurrence of Neobatrachia outside of South America. The Neobatrachia began to diversify during the earliest Cretaceous, including an early split into two major lineages, Hyloidea and Ranoidea, each of which was largely restricted to a portion of western Gondwana, respectively, South America and Africa (Frazão et al., 2015; Feng et al., 2017). Time-calibrated molecular phylogenetic analyses (e.g., Feng et al., 2017) suggest that by 96–95 Ma (i.e., the period from which *Cretadhefdaa* was recovered), the Neobatrachia was already separated into a number of lineages that are restricted today to specific biogeographic regions. These include the Myobatrachidae of Australia, the hyloids of South America, the Microhylidae (widespread today across the tropics), the Afrobatrachia of sub-Saharan Africa, the natatanuran ranoids, and the lineage leading to the Sooglossidae and Nasikabatrachidae that are today restricted, respectively, to the Seychelles Islands and the Western Ghats of India. There remains ample opportunity for both additional sampling and study of neobatrachian fossils from Gondwanan landmasses that could add new insights into the early evolution and biogeography of these major extant frog lineages that diversified in the Early Cretaceous.

The current absence of Ranoidea from the Cretaceous fossil record is puzzling. Except for undescribed and unillustrated material that was attributed to Ranoidea two decades ago (Báez and Werner, 1996), there are surprisingly few ranoid fossils

A new genus and species from the Kem Kem (Morocco), the second neobatrachian from Cretaceous Africa

especially in comparison to the hyloid fossils discovered in South America, Europe, and Africa. Their absence could be due to several factors. The first and most obvious is the lack of anuran specimens from the fossil record of Africa, due both to a lack of targeted collecting and little academic research on existing material. One example that highlights this problem is the Pyxicephalidae, a clade of ranoids endemic to Africa (Channing and Rödel, 2019) and for which time-calibrated molecular phylogenetic analyses suggest a divergence from other natatanurans around 60 Ma (Early Paleocene). Yet, the oldest occurrence of this family is *Thaumastosaurus* from the Middle-Late Eocene of Europe, whereas the earliest African fossil is from only 5 Ma (Matthews et al., 2015; Lemierre et al., 2021). The large gap in the fossil record of this family is found in many other families of Ranoidea, and many clades with an African origin completely lack a fossil record. Another bias could be that the vast majority of Ranoidea are not hyperossified anurans, including many small-sized species, and thus less likely to be preserved as intact and diagnosable fossils. In addition, numerous synapomorphies of Ranoidea are for postcranial elements, such as the vertebrae and the pectoral girdle, that are less likely to be identified and/or preserved (Scott, 2005; Frost et al., 2006). A final bias is simply that there has been sustained interest from South American paleontologists in the fossil record of anurans from countries such as Bolivia, Brazil, and Argentina, whereas there have been exceedingly few African paleontologists dedicated to studying anurans.

VIII.8 Conclusion

Our study confirms the report of Rage and Dutheil (2008) that at least three anuran taxa are present in the Kem Kem beds of Morocco. The newly described *Cretadhefdaa taouzensis* can be attributed to the Neobatrachia, making it both the oldest occurrence of the clade outside of South America and only the second occurrence in the Cretaceous of Africa. Several postcranial bones also point to an affinity with the

**A new genus and species from the Kem Kem (Morocco), the second
neobatrachian from Cretaceous Africa**

Neobatrachia but cannot be associated definitively with either *Cretadhefdaa* or another taxon. The presence of a neobatrachian in the Kem Kem in the Cenomanian demonstrates that neobatrachians were already widespread on Gondwana during the earliest Late Cretaceous.

VIII.9 Appendix

Table S1. List of CT-scan and 3D models of UCRC-PV94– 98, 101, 103– 105

Specimen number	Element	Taxon	CT-Scan files	DOI	3D Models	DOI
UCRC-PV94	Incomplete posterior braincase	<i>Cretadhefda a taouzensis</i>	ark:/87602/m4/42696	https://doi.org/10.17602/M2/M168041	ark:/87602/m4/42696	https://doi.org/10.17602/M2/M427199
UCRC-PV94_Inner ear	Endocast of Inner Ear	<i>Cretadhefda a taouzensis</i>	ark:/87602/m4/42719	https://doi.org/10.17602/M2/M168041	ark:/87602/m4/42719	https://doi.org/10.17602/M2/M427199
UCRC-PV95	Incomplete squamosal	<i>Cretadhefda a taouzensis</i>	ark:/87602/m4/42721	https://doi.org/10.17602/M2/M351726	ark:/87602/m4/42721	https://doi.org/10.17602/M2/M427218
UCRC-PV96	Incomplete maxilla	<i>Cretadhefda a taouzensis</i>	ark:/87602/m4/4271	https://doi.org/10.17602/M2/M389771	ark:/87602/m4/4271	https://doi.org/10.17602/M2/M427196
UCRC-PV97	presacral vertebra	<i>Cretadhefda a taouzensis</i>	ark:/87602/m4/42721	https://doi.org/10.17602/M2/M351731	ark:/87602/m4/42721	https://doi.org/10.17602/M2/M427215
UCRC-PV98	presacral vertebra	<i>Cretadhefda a taouzensis</i>	ark:/87602/m4/42721	https://doi.org/10.17602/M2/M351736	ark:/87602/m4/42721	https://doi.org/10.17602/M2/M427212

**A new genus and species from the Kem Kem (Morocco), the second
neobatrachian from Cretaceous Africa**

UCRC- PV101	presacral vertebra	<i>Cretadhefda a taouzensis</i>	ark:/87602/m4/351753	https://doi.org/10.17602/M2/M351753	ark:/87602/m4/427227	https://doi.org/10.17602/M2/M427227
UCRC- PV103	Sacral vertebra	<i>Cretadhefda a taouzensis</i>	ark:/87602/m4/351822	https://doi.org/10.17602/M2/M351822	ark:/87602/m4/4272202	https://doi.org/10.17602/M2/M427202
UCRC- PV104	Humerus	Neobatrachia ?	ark:/87602/m4/351812	https://doi.org/10.17602/M2/M351812	ark:/87602/m4/4272209	https://doi.org/10.17602/M2/M427209
UCRC- PV105	Ilium	Anura Indet.	ark:/87602/m4/351817	https://doi.org/10.17602/M2/M351817	ark:/87602/m4/4272206	https://doi.org/10.17602/M2/M427206

Appendix S1. Characters list for analyses: The character list is similar to the one from Chapter X

Appendix S2. Taxa list : The taxa list contains the same taxa as in Chapter X, Appendix S4, with the addition of the extinct *Cretadhefda taouzensis* sp. nov. and *Hungarobatrachus szukacsi* Szentesi and Venczel, 2010.

Appendix S3. Nexus file containing the matrix used for all analyses: The nexus file is available at : <https://peerj.com/articles/13699/#supplemental-information>

Appendix S4. List of synapomorphies for selected clades for all analyses.

Analysis under EW, ordered: Ceratophryoidea + *Uberabatrachus* + *Cretadhefda*: 61: 0->1; 76: 1->2; 125: 1->2.

Ceratophryoidea + *Cretadhefda*: 6: 0->1; 8: 0->2; 12: 0->1; 25: 1->0; 49: 0->2.

Analysis under EW, excluding *Arariphrynus placidoi*, ordered: 'Neobatrachia' (excluding *Heleophryne*): 9: 0->1; 114: 3->0; 119: 0->2; 130: 0->1.

Hyperossified clade : 6: 0->1; 10: 1->2; 25: 1->0; 61: 0->2; 68: 1->2; 121: 1->2.

Hungarobatrachus + *Eurycephalella*+ *Calyptocephalella*: 8: 0->2; 12: 0->1; 119: 2->1.

Cretadhefda + Ceratophryidae: 8: 0->1; 29: 1->0; 37: 0->1; 61: 1->2.

Chapter IX

*THE NEOBATRACHIANS OF IN BECETÉN: THE
EARLIEST COEXISTENCE OF AN HYLOID AND A
RANOID ?*

IX.1 Introduction

In Becetén is a rich vertebrate locality from the Late Cretaceous of Niger (Broin et al., 1974). In the original description of the fauna, actinopterygians, dipnoans, crocodiles, dinosaurs, chelonians, squamates and lissamphibians were identified (Broin et al., 1974; Buffetaut, 1974a, b; Buffetaut, 1976; Gayet and Meunier 1996; Gayet et al., 1997; Báez and Rage, 1998, 2004). However, no material was illustrated at the time. Several studies followed (Rage, 1991; Gayet and Meunier, 1996; Gayet et al., 1997; Báez and Rage, 1998, 2004; Meunier and Larsson, 2018), but the fauna remains incompletely studied. The herpetofauna has not been well studied, with only some pipids and a snake vertebra identified and described (Rage, 1991; Báez and Rage, 1998) and one anuran humerus illustrated (Rage, 1984: fig. 1A).

Recent studies on the anurans of In Becetén have revealed that pipimorphs (total-clade of Pipidae) were actually numerous and well diversified (Chapters II, III). This diversity of pipimorphs is unique among other African sites (at least until the Neogene; Gardner and Rage, 2016). However, little information exists on non-pipids anuran from In Becetén. The original study mentioned several bones attributed to an undetermined “Ranidae” (Broin et al., 1974). One humerus was illustrated (Rage, 1984: fig.1A) and the mention of another ornamented anuran was made in a review of the African fossil record of lissamphibians (Gardner and Rage, 2016). Unfortunately, most of the specimens have neither been studied.

As part of an ongoing study on the anurans of In Becetén, we here describe numerous unidentified anuran remains that are not attributed to pipids. We also describe and illustrate the hyperossified anuran mentioned in 2016 (Gardner and Rage, 2016). We also include this latter identified taxon within phylogenetic analyses of neobatrachians to assess its affinities with Neobatrachia. Finally, we compare the anuran diversity of In Becetén to other African sites.

IX.2 Geological Context

All specimens come from the site of In Bécetén (also known as In Becetem, In Beceten, In'Betetén, In Béceten and erroneously Ibeceten). They were collected during three expeditions in 1970, 1972 and 1973, organised by the Muséum national d'Histoire naturelle (Paris, France), and led by P. Taquet and D. Russell (de Broin et al., 1974). The site of In Bécetén is located 80 km east of the town of Tahoua, in the South-eastern region of the Republic of Niger (Chapter III for detailed information). The site is considered Coniacian or Santonian (Late Cretaceous, 91.1 to 83.4 Ma my, see Chapter III for details).

IX.3 Materials and Methods

Institutional Abbreviations MNHN: Muséum national d'Histoire naturelle, Paris, France. All specimens are stored within the Paleontological collection in the Amphibians and Reptiles section, under the collection number MNHN.F.IBC XXXX. The anatomical terminology used herein is based on Roček (1980) and Biton et al. (2016) for cranial features, Sanchíz (1998) for postcranial and Gómez and Turazzini (2016) for ilial terminology.

Phylogenetic analysis Our data matrix includes 88 taxa and 143 morphological characters and is derived from that of Lemierre and Blackburn (2022; see Appendix S1–4). We added the hyperossified anuran mentioned in Gardner and Rage (2016) to test its neobatrachian affinities. This new taxon was scored using personal observations based on direct examination of the specimens. The analysis was performed using TNT v.1.5 (Goloboff and Catalano, 2016) under equal weights. All analyses were conducted

The neobatrachians of In Becetén: The earliest coexistence of hyloid and ranoid ?

with cline characters ordered (characters 18, 32, 33, 36, 38, 39, 59, 74, 82, 97, 98, 120, 141, 149) in the analysis (Rineau et al., 2015, 2018). The analysis consisted of heuristic searches with 1000 random addition sequences of taxa, followed by tree bisection reconnection (TBR) branch swapping, holding 10 trees per repetitions. The final trees were rooted on *Ascaphus truei* (Ascaphidae), and when more than one most parsimonious tree was found, a strict consensus was obtained. Node supports were evaluated using Bremer support and standard nonparametric bootstrapping, with searches of 1000 replicates and collapsing groups below 5% frequency.

IX.4 Systematic Paleontology

NEOBATRACHIA Reig, 1958

RANOIDEA Rafinesque, 1814

Indeterminate ranoid

Referred material

One incomplete humerus (MNHN.F.IBC 1603).

Description—The diaphysis is straight (Fig. IX-1A, B). The diaphysis is thick, with almost the same width as the distal head. The ventral crest (= crista ventralis) is well developed (Fig. IX-1D, F). Midlength to the preserved region of the diaphysis to the fossa cubitalis, the ventral crest is divided into two ridges, with an elongate groove in between (Fig. IX-1A, D). The ulnare crest (= crista paraventralis; Fig. IX-1D, F) is a thin ridge. The fossa cubitalis is triangular and large (width greater than height). The fossa is shallow but well delimited (Fig. IX-1A, D). The humeral ball is not shifted laterally from the diaphysis axis and is well developed (Fig. IX-1A, C, D, F). The ulnare epicondyle is short but distinct, well developed, and it protrudes medially (Fig. IX-1A, B, D, E). The radial epicondyle is not fully preserved but it does not seem to be distinct from the main distal head (Fig. IX-1A, B, D, E). The olecranon scar is extended proximally, with a pointed and tapered proximal margin (Fig. IX-1B, E).

The neobatrachians of In Becetén: The earliest coexistence of hyloid and ranoid ?

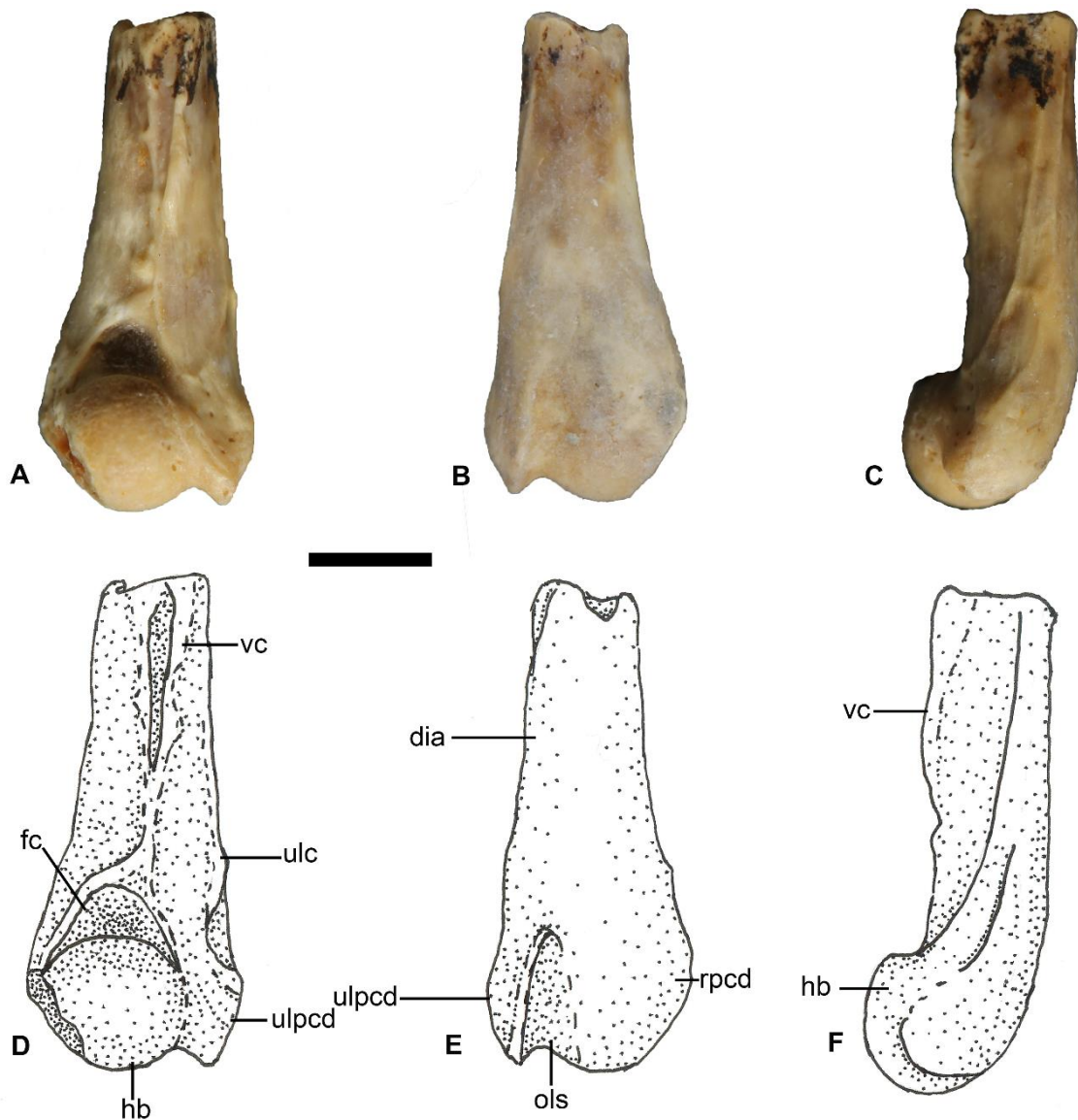


Figure IX-1. Indeterminate Ranoidea of In Becetén. A—C, MNHN.F.IBC1602 in A, ventral, B, dorsal and C medial views; D—F, interpretative drawing of the same specimen in D ventral, E dorsal and F medial views. **Abbreviations:** **dia**, diaphysis; **fc**, fossa cubitalis; **hb**, humeral ball; **ols**, olecranon scar; **rpcd**, radial epicondyle; **vc**, ventral crest; **ulc**, ulnare crest; **ulpcd**, ulnare epicondyle. Scale bar represents 2 mm

Discussion— This humerus was regarded as possible Ranidae in the first publication of the In Becetén fauna (de Broin et al., 1974). The specimen MNHN.F.IBC 1603 was illustrated and shortly described in 1984 (Rage, 1984: fig. 1A) and was considered as a “Ranoid”. This humerus is indeed similar with the Neobatrachian morphotype in

The neobatrachians of In Becetén: The earliest coexistence of hyloid and ranoid ?

having (1) a well-developed humeral ball and (2) likely non-symmetrical epicondyles (Prasad and Rage, 2004; Rage et al., 2021). Furthermore, the presence of a ventral crest divided into two ridges has been recovered in some neobatrachians (as muscular insertion; Otero et al., 2014; Keeffe and Blackburn, 2020). Moreover, the presence of (1) a straight diaphysis; (2) a shallow fossa cubitalis; (3) a humeral ball not shifted laterally and (4) a medial epicondyle more developed than the lateral epicondyle, is consistent with the ranoid morphology (Rage, 2013; de Broin et al., 2020). In addition, the presence of a well-delimited fossa cubitalis, although rare (Rage, 1984), is recovered in several ranoid taxa from the Eocene of the Quercy Phosphorites (Rage, 2016) and among extant ranoids (Worthy, 2001). MNHN.F.IBC 1603 is consistent with a ranoid morphology and can be attributed to the Ranoidea. However, this attribution should be considered provisional. Indeed, the presence of a medial crest is often linked to sexual and/or ontogenetic dimorphism (Duellman and Trueb, 1994). This suggests that this humerus might belong to a male ranoid. A humerus from the Cenomanian of the Kem Kem with ranoid affinities has also been recently described (UCRC-PV 104; see Lemierre and Blackburn, 2022: fig. 6A-C; Chapter VIII). Both humeri share (1) a straight diaphysis, (2) a well-developed humeral ball, (3) asymmetrically developed epicondyles, (4) a humeral ball not shifted from the diaphysis axis and (5) a shallow fossa cubitalis. However, MNHN.F.IBC 1603 differs from UCRC-PV 104 in (1) having a more developed ventral crest divided into two ridges, (2) a well-delimited fossa cubitalis, (3) a more protruding ulnare epicondyle, (4) an olecranon scar more extended anteriorly and (5) an absence of developed lateral crest. Therefore, both humeri are here considered as belonging to two distinct taxa. Furthermore, MNHN.F.IBC 1603 possesses more Ranoidea characters than UCRC-PV 104. In summary, MNHN.IBC 1603 is here attributed to an unidentified ranoid, and thus represents the oldest occurrence of the clade.

The neobatrachians of In Becetén: The earliest coexistence of hyloid and ranoid ?

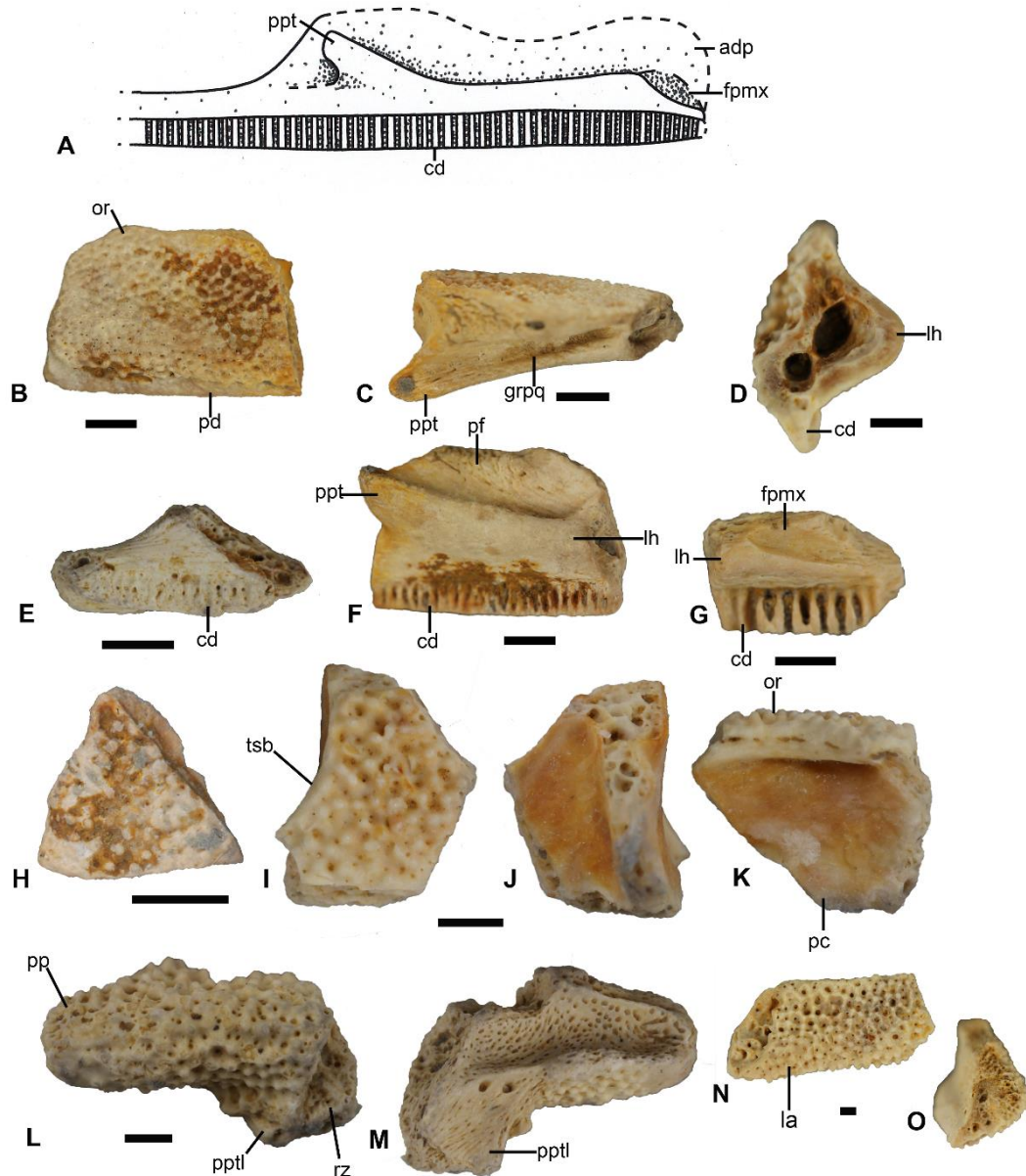


FIGURE IX-2. Cranial elements of *Taxon N*. A, proposed reconstruction of the left maxilla of *Taxon N* in lingual view; B-C, MNHN.F.IBC 1985a, incomplete left maxilla in B, labial and C, dorsal views; D, MNHN.F.IBC 1985b, incomplete left maxilla in cross section (posterior view); E, MNHN.F.IBC 1985c, incomplete posterior left maxilla in lingual view; F, MNHN.F.IBC 1985a in lingual view; G, MNHN.F.IBC 1985e, incomplete anterior left maxilla in lingual view; H, MNHN.F.IBC 1986a, putative incomplete nasal in dorsal view; I-K, MNHN.F.IBC 1986b incomplete frontoparietal in I, dorsal, J, ventral and K, lateral views; L-M, MNHN.F.IBC 1986c, posterior region of a right squamosal in L, lateral and M, medial views; N-O, likely anterior incomplete region of a squamosal (MNHN.F.IBC 1986d) in N, labial and O, lingual views. **Abbreviations:** cd, crista dentalis; fpmx, fossa for the insertion of the premaxilla; grpq, groove for the palatoquadrate bar; la, lamella alaris; lh, lamina horizontalis; or, ornamentation; pc, pars contacta; pd, pars dentalis; pf, pars facialis; pp, processus posterior; pptl, processus posterolateralis; ppt, pterygoid process; rz, ramus zygomaticus; tsb, tectum supraorbitale. Scale bars represent 2 mm (B-H) and 1 mm (I-M).

The neobatrachians of In Becetén: The earliest coexistence of hyloid and ranoid ?

NEOBATRACHIA Reig, 1958

Incertias sedis

“*Taxon N*”

Referred material

22 fragmentary maxillae (MNHN.F. IBC 1983, 1984a-d, 1985a-p) and 8 fragments of exocranium (MNHN.F.IBC 1986a-h) that include incomplete frontoparietal, nasal and squamosal.

Description

Maxilla—the maxilla is thick and strongly ossified (Fig. IX-2). All fragments bear an ornamentation made of small closely spaced tubercles arranged in lines (in most of the fragments; Fig. IX-2B, C). The ornamentation covers most of the preserved labial surface of maxillae, except for a narrow strip along the ventral margin. The pars facialis is incomplete, but seem high on most of its length (Fig. IX-2B). The pars palatina is thick. The lamina horizontalis is deep and rounded (in cross-section) but does not project lingually (Fig. IX-2D, F). Although no teeth are preserved, the pars dentalis shows that the maxilla was toothed (Fig. IX-2E-G). The pars dentalis is dorsoventrally shallow, and extends posteriorly past the pterygoid process (Fig. IX-2E). The pterygoid process is well developed and project lingually (Fig. IX-2F). Posterior to this process, the maxilla narrows dorsally (Fig. IX-2E). Unfortunately, none of the specimen preserved the posterior end of the maxilla so that we do not know what it looks like. Anterior to the pterygoid process, the lamina horizontalis bears a shallow groove for the palatoquadrate (Fig. IX-2C). No palatine process is preserved on any maxilla fragments. The pars facialis is moderately high near the anterior margin of the maxilla, and our interpretation indicates the presence of an anterodorsal process (Fig. IX-2A, G) such as in *Calyptocephalella* or *Ceratophrys*. The anterior tip of the maxilla shows a lingual deep slot facet for the dorsal process of the premaxilla (Fig. IX-2G).

The neobatrachians of In Becetén: The earliest coexistence of hyloid and ranoid ?

Nasal—Two fragments (MNHN.F.IBC 1986a, e) are slender flat pieces of bone. The dorsal surface is covered with the same ornamentation as in maxillae (Fig. IX-2H).

Frontoparietal— The dorsal surface bears an ornamentation similar to the one recovered in maxillae and nasal fragments (Fig. IX-2I). A vertical lamina is interpreted as remnants of the pars contacta. The pars contacta is curved externally (Fig. IX-2J, K). This lamina delimits a dorsal flange which is interpreted as the tectum supraorbitale (Fig. IX-2I, J). Although broken laterally, the lateral margin of the frontoparietal is clearly concave medially (Fig. IX-2J, K).

Squamosal—Five fragments of ornamented bones are interpreted here as fragments of the squamosal. The best preserved specimen (MNHN.F.IBC 1986c, f; Fig. IX-2L-M) represents the posterior process which bears a rounded posterior margin (Fig. IX-2L). It is missing its medial margin, which implies that it might have been more extended and that a ramus paroticus was present (Fig. IX-2M). The anteroventral part of the specimen shows the base of two other processes, one posteroventral and the second anteriorly oriented (Fig. IX-2L, M). The first process is likely the process posterolateralis and the second the ramus zygomaticus. Three other specimens preserve part of the lamella alaris (MNHN.F.IBC 1986d, g, h; Fig. IX-2N, O). The labial surface is ornamented and thickened lingually, forming a triangular-shaped surface (Fig. IX-2O). This fragment likely represents the lamella alaris of the processus zygomaticus. Unfortunately, there is no indication if and how the squamosal articulates with the maxilla.

Discussion—Ornamentation on dermal bones in anurans is recovered solely in when hyperossification is also present (Duellman and Trueb, 1994), and this occurs in various anuran clades (Paluh et al., 2020). However, combination of osteological characters can be used to exclude certain major clades. *Latonia* (Alytidae) is the only known alytid exhibiting dermal ornamentation (Roček, 1994). However, its current stratigraphic range is limited only to Oligocene and Neogene of Europe and Northern Africa (Gardner and Rage, 2016; Syromyatnikova et al., 2019). Moreover, *Taxon N* can

The neobatrachians of In Becetén: The earliest coexistence of hyloid and ranoid ?

be differentiated from *Latonia* in (1) having a rounded medial margin of this lamina (pointed in *Latonia*). Pelobatids are known to exhibit dermal ornamentation (Roček, 2013) that resembles the one of *Taxon N*. However, *Taxon N* differs from all pelobatids in lacking an elongate palatine process of the maxilla (Roček, 2013). *Taxon N* can also be differentiated from Pipimorpha in (1) having a well-developed squamosal and (2) a rather dorso-ventrally thick maxilla (slender maxillae in Pipimorpha). Two anurans of indeterminate phylogenetic position from North America possess a similar ornamentation: *Scotiophryne* and *Theatoniuss*. *Scotiophryne* is known from the Late Cretaceous, and might also occur in Early Cretaceous and Paleocene (Gardner and DeMar, 2013; Roček, 2013). This taxon differs from *Taxon N* in having (1) tubercles from its ornamentation not arranged in lines and (2) a horizontal lamina narrow medially (rounded in *Taxon N*; Gardner, 2008). *Theatoniuss* is known from Late Cretaceous deposits (Gardner and DeMar, 2013). *Theatoniuss* differs from *Taxon N* in lacking teeth on its maxillae. Thus, *Taxon N* can be excluded from Alytoidea (*Latonia*, *Alytes*), Pipimorpha, and Pelobatoidea. The only major clade left is the Neobatrachia which includes several extinct and extant hyperossified taxa.

Two neobatrachians are known in Mesozoic Africa, *Beelzebufo ampinga* Evans et al., 2008 from the Maastrichtian of Madagascar and *Cretadefdaa taouzensis* Lemierre and Blackburn, 2022 from the Cenomanian of Morocco. Fragmentary cranial remains were assigned to both taxa. *Beelzebufo*, *Cretadefdaa* and *Taxon N* shares (1) an ornamentation extending on most of the lateral surface of the maxilla and (2) the presence of a tectum supraorbitale (see Fig. IX-2I). However, *Beelzebufo* and *Cretadefdaa* can be differentiated from *Taxon N* in (1) having an ornamentation made of pits and ridges (small tubercles in *Taxon N*). Furthermore, *Beelzebufo* does not possess a distinct processus frontalis (present on *Taxon N*, see Fig. IX-2F). *Taxon N* can be furthermore differentiated from *Cretadefdaa* in lacking ornamentation on the lateral surface of the pars dentalis (Lemierre and Blackburn, 2022; Fig. IX-2B).

Another Mesozoic hyperossified neobatrachian is *Hungarobatrachus szukacsi* Szentesi and Venczel, 2010 from the Santonian of Hungary. *Taxon N* is similar to

The neobatrachians of In Becetén: The earliest coexistence of hyloid and ranoid ?

Hungarobatrachus in having (1) an ornamentation extending on most of the lateral surface of the maxilla; (2) a lamina horizontalis not projected lingually; (3) a well-developed pterygoid process of the maxilla and (4) a tectum supraorbitale. However, *Taxon N* differs from *H. szukacsi* in (1) having a well-developed lamina horizontalis (moderately developed in *H. szukacsi*; Fig. IX-2F) and (2) in having the maxillar tooth row extending posteriorly past the pterygoid process (Fig. IX-2F).

One last hyperossified neobatrachian from the Mesozoic is *Baurubatrachus pricei* Báez and Perí, 1989 from the Maastrichtian of Brazil. *Baurubatrachus* and *Taxon N* differ in the ornamentation recovered on their cranial remains (pits and ridges in *Baurubatrachus*; small tubercles in *Taxon N*). However, both taxa are similar in having (1) the medial margin of the lamina horizontalis rounded (in cross-section), (2) a pars palatina narrowing on the posterior portion of the maxilla and (3) a crista dentalis ending slightly past the pterygoid process (Fig. IX-2F).

In Africa, the next oldest hyperossified neobatrachian is the ranoid *Rocekophryne ornata* Rage et al., 2021 from the Early Eocene of Algeria. *Taxon N* can be differentiated from *Rocekophryne* in having (1) an ornamentation made of small closely spaced tubercles (pits and ridges in *Rocekophryne*) and (2) in likely having an anterodorsal process (Fig. IX-2A). However, *Taxon N* and *Rocekophryne* are similar in having (1) a rounded medial margin of the pars palatina and (2) a pars palatina narrow and shallow posteriorly near the pterygoid process. Another extinct hyperossified ranoid is *Thaumastosaurus* De Stefano, 1903, of which three taxa are known (Lemierre et al., 2021). *Taxon N* differs from *Thaumastosaurus* in (1) having an ornamentation made of small tubercles; (2) having a well-developed pterygoid process (Fig. IX-2F) and (3) in having an anterodorsal process on the maxilla.

Known extant hyperossified and ornamented neobatrachians mainly occur among hyloids, except for three genera, *Aubria*, *Cornufer* and *Pyxicephalus*. *Aubria* and *Pyxicephalus* both possess same characteristics on their maxillae as *Thaumastosaurus*, except for a more developed pterygoid process (Sheil, 1999). Therefore, *Taxon N* can be differentiated from all Pyxicephalidae (*Thaumastosaurus*, *Aubria* and *Pyxicephalus*).

The neobatrachians of In Becetén: The earliest coexistence of hyloid and ranoid ?

Cornufer is a hyperossified ranoid from Indonesia. Its maxilla does not bear any anterodorsal process, and its anterior region is low and mostly devoid of ornamentation. Furthermore, the lamina horizontalis projects lingually into a thin blade in *Cornufer*. Therefore, *Taxon N* differs from all known hyperossified ranoids.

All remaining ornamented taxa are found within the Hyloides, mainly among Ceratophrydae and Calyptocephalellidae. *Taxon N* resemble the Ceratophrydae in (likely) having an anterodorsal process on its maxilla (Muzzopappa and Báez, 2009). *Taxon N* differs from all ceratophryds in having a lamina horizontalis that is distinct on the lingual surface of the maxilla.

Calyptocephalellidae and its eponym genus, *Calyptocephalella*, are known throughout the South American fossil record since the Late Cretaceous (Agnolin, 2012; Muzzopappa, 2019; Muzzopappa et al., 2020). Incomplete specimens attributed to this clade have all been referred to *Calyptocephalella*, an attribution considered equivocal (Nicoli et al., 2016). Therefore, we will consider all materials referred to *Calyptocephalella* as Calyptocephalellidae in the following comparison. *Taxon N* resembles calyptocephalellids in having (1) an ornamentation covering the lateral surface of the maxilla, except for a thin strip of bone ventrally, and (2) in having an anterodorsal process. However, *Taxon N* differs from Calyptocephalellids in (1) lacking a distinct pars palatina on most of the length of the maxilla (in Calyptocephalellids, the pars palatina is flattened lateromedially only at the level of the orbit; Muzzopappa and Báez, 2009: fig. 3.2).

In conclusion, although we can exclude *Taxon N* from all non-neobatrachian clades, no known synapomorphies firmly attribute this taxon to Neobatrachia. However, it seems to share several characters on its maxilla with neobatrachian clades, like the presence of an anterodorsal process. To assess this affinity, we included *Taxon N* within a morphological dataset composed of extant and extinct neobatrachians.

The neobatrachians of In Becetén: The earliest coexistence of hyloid and ranoid ?

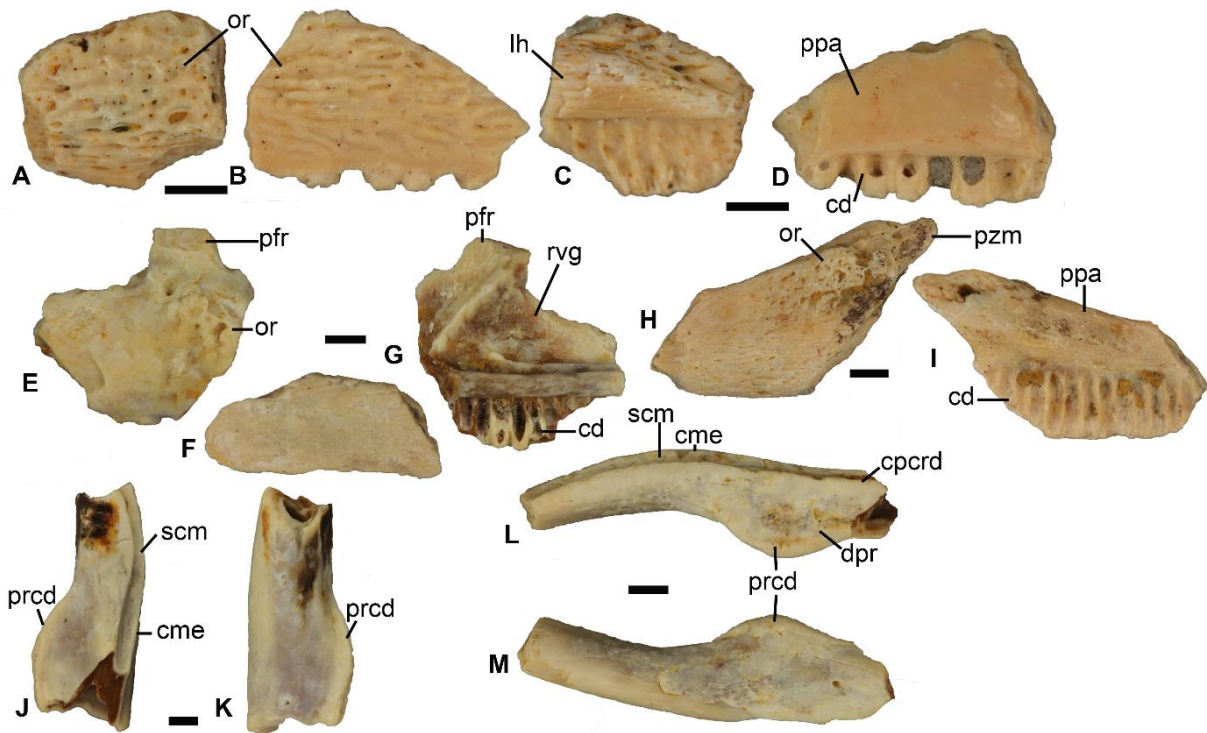


Figure IX-3. Cranial elements of indeterminate anurans. A—D, right maxilla morphotype A in A, B, labial view (MNHN.F.IBC 1989a, b) and C, D in lingual view; E—G, right maxilla morphotype B in E, F labial view (MNHN.F.IBC 1991a, b) and G, lingual view (MNHN.F.IBC 1991a); H—I, left maxilla morphotype C (MNHN.F.IBC 2063) in H, labial and I, lingual views; J—K, right angulosplenic morphotype A (MNHN.F.IBC 1988) in J, dorsal and K, ventral views; L—M, right angulosplenic morphotype B in L, dorsal and M, ventral views. **Abbreviations** : cd, crista dentalis; **cpcrd**, coronoid crest; **cme**, extern mandibular crest; **dpr**, depression; **lh**, lamina horizontalis; **obm**, orbital margin; **or**, ornamentation; **pfr**, frontal process; **ppa**, pars palatina; **prcd**, coronoid process; **prp**, palatine process; **pzm**, zygomaticomaxillaris process; **rvg**, recessus vaginiformis; **scm**, sulcus pro cartilagine Meckeli. Scale bars represent 1 mm.

The neobatrachians of In Becetén: The earliest coexistence of hyloid and ranoid ?

ANURA Duméril, 1804

INCERTAE SEDIS

Maxillae

Referred material—Eight fragments of maxillae (MNHN.F.IBC 1989a-b,1991a-e, 2063).

Three maxillar morphotypes distinct from *Taxon N* can be identified within the In Becetén material.

Description—Morphotype A (MNHN.F.IBC 1989a, b): the two fragments attributed to this morphotype bear ornamentation made of pits and ridges on their labial surface (Fig. IX-3A, B). This ornamentation covers the whole pars facialis, and most of the pars dentalis, leaving only a thin strip of smooth bone at the base of the teeth (Fig. IX-3B). The crista dentalis is shallow. One fragment (MNHN.F.IBC 1989a) bears a distinct, rounded lamina horizontalis lingually (Fig. IX-3C). On the second fragment (MNHN.F.IBC 1989b), no lamina horizontalis is present (Fig. IX-3D). Morphotype A differs from *Taxon N* mainly by the ornamentation made of pits and ridges (instead of small tubercles).

Morphotype B (MNHN.F.IBC 1991a-d): Three of the four fragments lack ornamentation on their labial surface (Fig. IX-3E, F). The only exception is the largest fragment (MNHN.F.IBC 1991c), where a faint patch of rugose ornamentation is present near the base of the frontal process (Fig. IX-3E). All fragments bear a crista dentalis, although no teeth were recovered (Fig. IX-3G). In lingual view, the rounded, prominent lamina horizontalis is distinct on all fragments (Fig. IX-3G). In lingual view, the recessus vaginiformis is shallow, but well delimited ventrally and anterodorsally by two crests (Fig. IX-3G). The anterodorsal crest (palatine process) extends dorsally onto the lingual surface of the frontal process. This morphotype can be differentiated from Morphotype A and *Taxon N* in (1) lacking ornamentation on most of its labial surface and (2) by a thin lamina horizontalis that protrudes lingually.

The neobatrachians of In Becetén: The earliest coexistence of hyloid and ranoid ?

Morphotype C (MNHN.F.IBC 1991e, 2063): The labial surface of the two fragments is covered by small pits and ornamentation that confers a rugose texture to the bone (Fig. IX-3H). This ornamentation seems to extend on the whole labial surface. The maxilla is toothed (Fig. IX-3I). The zygomaticomaxillaris process projects posterodorsally (Fig. IX-3H, I). The orbital margin strongly decreases in height posterior to the latter process (Fig. IX-3H). Lingually, the lamina horizontalis is indistinct from the pars palatina (Fig. IX-3I), and no pterygoid process is preserved. The presence of a zygomaticomaxillaris process indicates that squamosal and maxilla were articulated together. Morphotype C is therefore differentiated from Morphotype B and *Taxon N* in (1) being ornamented by pits over the whole labial surface of the maxilla. It further differs from *Taxon N* in (1) lacking a pterygoid process and (2) lacking a distinct lamina horizontalis. Morphotype C is hard to distinguish from Morphotype A, as both bear a pits and ridges ornamentation on their labial surface and assigned specimens come from different portions of the maxilla. However, the ornamentation of Morphotype C seems less developed than in Morphotype A. As the specimens of Morphotype C are far bigger than those of Morphotype A (i.e., represented a more skeletally mature individual), they likely are distinct morphotypes.

Discussion and attribution—All three morphotypes are distinct from *Taxon N* and appear to represent three other distinct taxa. It should be noted that the presence of teeth does not exclude an attribution to the four pipimorph taxa known from In Becetén (Chapters II-IV). Although most pipids lack teeth (Trueb et al., 2000), Xenopodines and extinct pipimorphs are known to have teeth (Henrici and Báez, 2001; Báez and Púgener, 2003). However, the ornamentation present in morphotypes A and C differs from that of *Pachycentrata* and the unnamed pipimorph 2 (Báez and Rage, 1998; Chapters II, IV). Therefore, Morphotypes A, B and C cannot be assigned to *Pachycentrata* and the unnamed pipimorph 2. Therefore, Morphotype B could be attributed to the unnamed pipimorph 1 or to another non-pipimorph taxon in In Becetén. Morphotypes A and C are assigned to non-pipimorph indeterminate anurans.

The neobatrachians of In Becetén: The earliest coexistence of hyloid and ranoid ?

Therefore, based on maxillar elements, between three and four non-pipimorph taxa are present in In Becetén.

Angulosplenials

Referred material—Five incomplete angulosplenials (MNHN.F.IBC 1987, 1988, 1990, 2064).

Description—The angulosplenials are all represented by posterior portions that lack their anterior and posteriormost parts. The Meckelian groove is present in the coronoid portion, excluding *Pipimorpha* (Gómez, 2016). Two morphotypes can be distinguished, morphotype A (MNHN.F.IBC 1987, 1988a, b) and morphotype B (MNHN.F.IBC 1990, 2064). However, it cannot be excluded that their differences are of ontogenetic nature.

Morphotype A: All specimens are large and thick (Fig. IX-3J). Although only the anterior region of the coronoid process is preserved, it can be inferred that an anteroposteriorly elongate coronoid crest was present (Fig. IX-3J, K). This crest did not extend as a flange (as in *Pipimorpha*). A shallow depression is present lateral to the coronoid process (Fig. IX-3J). The Meckelian groove extends on the lateral region of the angulosplénial and narrows posteriorly (Fig. IX-3J). A triangular and elongate depression is located ventral to the Meckelian groove in the coronoid region. This depression is separated from the Meckelian groove by a sharp ridge. Ventrally, a poorly developed mandibular crest delimits this triangular depression (Fig. IX-3K).

Morphotype B: This morphotype differs from morphotype A in (1) being smaller and (2) an antero-posteriorly larger coronoid process (Fig. IX-3L, M). Such as on Morphotype A, the Meckelian groove extends on the dorsal surface of the bone (Fig. IX-3M). The coronoid process forms an anteroposteriorly elongated crest.

The neobatrachians of In Becetén: The earliest coexistence of hyloid and ranoid ?

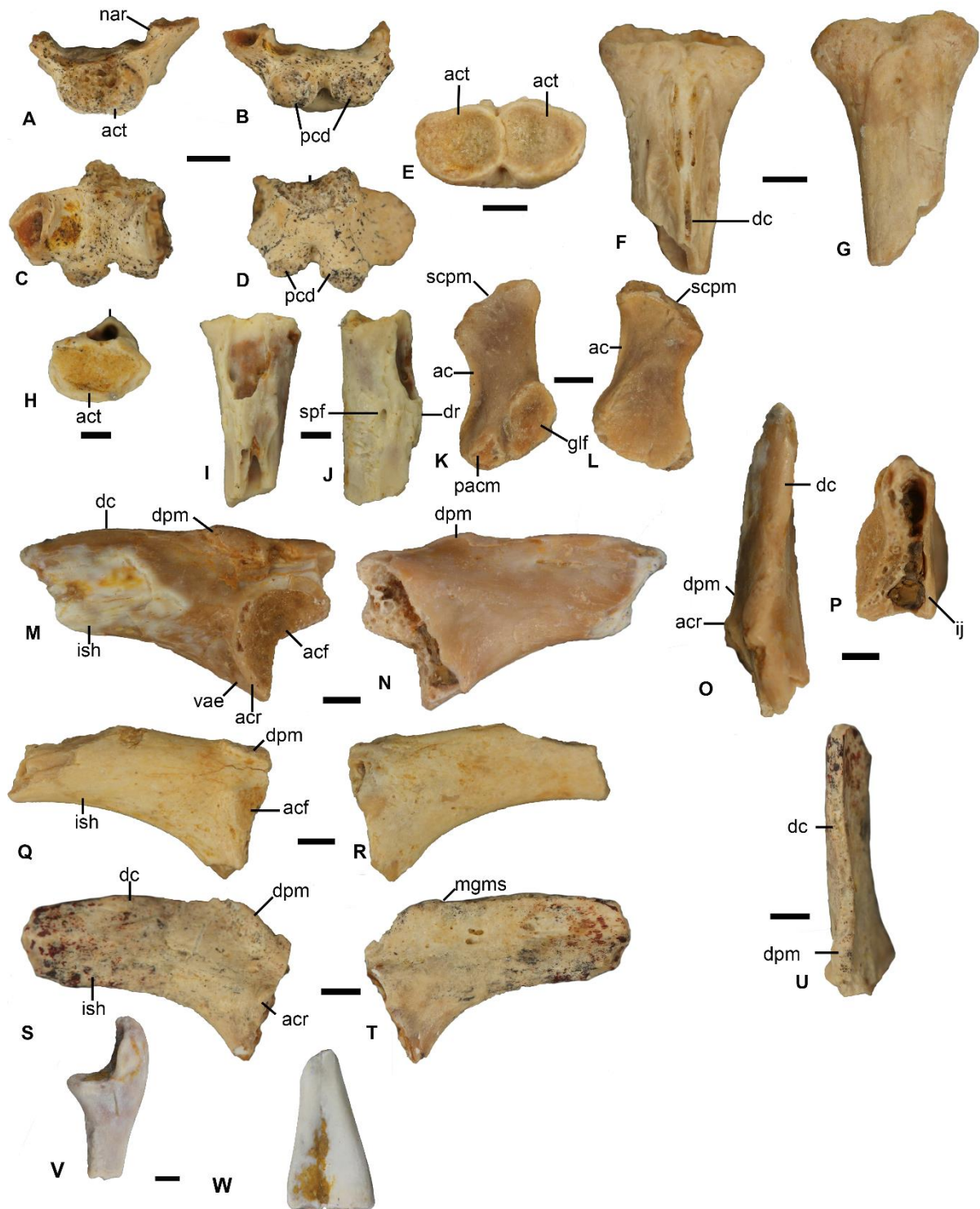


Figure IX-4. Postcranial elements of indeterminate anurans. A—D, MNHN.F.IBC 1992, incomplete sacral vertebra in A, anterior, B, posterior, C, dorsal and D, ventral views ; E—G, MNHN.F.IBC 1993, urostyle morphotype A in E, anterior, F, dorsal and G, ventral views; H—J, MNHN.F.IBC 1994, urostyle morphotype B in H, anterior, I, dorsal and J, lateral views;

The neobatrachians of In Becetén: The earliest coexistence of hyloid and ranoid ?

K—L, MNHN.F.IBC 1996, incomplete scapula in **K**, medial and **L**, lateral views; **M—P**, MNHN.F.IBC 1600, left ilium morphotype A in **M**, lateral, **N**, medial, **O**, dorsal and **P**, posterior views; **Q—R**, MNHN.F.IBC 1601, left ilium morphotype B in **Q**, lateral and **R**, medial views; **S—U**, MNHN.F.IBC 1995, left ilium morphotype C in **S**, lateral, **T**, medial and **U**, dorsal views; **V—W**, MNHN.F.IBC 1999a and b, incomplete radioulnae. **Abbreviations**: **ac**, anterior crest; **acf**, acetabular fossa; **acr**, acetabular rim; **act**, anterior cotyle; **dc**, dorsal crest; **dpm**, dorsal prominence; **dr**, dorsal ridge; **glf**, glenoid fossa; **ij**, ilioischiatric juncture; **ish**, iliac shaft; **mgms**, musculus gluteus magnus scar attachment; **nar**, neural arch remnant; **pacm**, pars acromialis; **pcd**, posterior condyle; **scpm**, suprascapular margin; **spf**, spinal foramen; **vae**, ventral acetabular expansion. Scale bars represent 1 mm.

Sacral vertebra

Referred material—One incomplete sacral vertebra (MNHN.F.IBC 1992).

Description—MNHN.F.IBC 1992 only preserves the centrum and the base of the neural arches (Fig. IX-4A-D). The vertebra bears an anterior condyle and two posterior condyles. Most of the anterior condyle is eroded, but it was likely wide (Fig. IX-4A). The posterior condyles are circular and well-separated from each other (Fig. IX-4B, C, D).

Discussion and attribution—This vertebra was attributed to Ranidae in the original study on In Becetén (de Broin et al., 1974). The presence of a bicondylar sacro-urostyler articulation and a sacral vertebra with both anterior and posterior condyles is known in Alytoidea and Ranoidea (Duellman and Trueb, 1994). Alytoidea are not known in Africa before the Neogene (Gardner and Rage, 2016). One taxon from the Late Jurassic/Early Cretaceous of Morocco, *aff. Ennabatrachus*, possesses an opisthocoelous sacral vertebra with two posterior condyles (Jones et al., 2003). However, its affinity, and the referral of non-ilium elements to this taxon, are not certain (Jones et al., 2003). In addition, MNHN.F.IBC 1992 differs from *aff. Ennabatrachus* in lacking a remnant of notochordal canal separating the posterior condyles. Regarding Ranoidea, most characters used for attribution to this clade are borne by the neural arch, here missing. In conclusion we cannot refer this element to any anuran clade.

The neobatrachians of In Becetén: The earliest coexistence of hyloid and ranoid ?

Urostyles

Referred material—Two incomplete urostyles (MNH.F.IBC 1993, 1994).

Description—The two urostyles represent two morphotypes, A (MNHN.F. IBC 1993) and B (MNHN.F. IBC 1994), both attributed to distinct taxa. As they are not fused to the sacral vertebra, they are excluded from Pipidae which usually present synsacra (fused sacral vertebra with the urostyle).

Morphotype A (MNHN.F. IBC 1993): The single specimen is an incomplete urostyle preserving most of its anterior portion (Fig. IX-4E-G). It bears two anterior cotyles for sacral articulation. The cotyles are subcircular and closely spaced, separated by a thin crest (Fig. IX-4E). Transverse processes are absent on the urostyle (Fig. IX-4F, G). Most of its neural arch is missing, but it clearly extended posteriorly into a thin dorsal crest (Fig. IX-4F). However, neither its height nor posterior extension are known. A small spinal foramen opens on each lateral surface of the urostyle.

Morphotype B (MNHN.F. IBC 1994): This urostyle also preserves only its anterior portion (Fig. IX-4H-J). MNHN.F. IBC 1994 bears one anterior cotyle for sacro-urostyler articulation (Fig. IX-4H). The cotyle is wide and slightly compressed dorsoventrally. The dorsal crest is low and forms a thin ridge (Fig. IX-4I, J).

Discussion and attribution—Morphotype A differs from morphotype B in (1) having a bicondylar sacro-urostyler articulation and (2) having a dorsal crest reduced to a ridge. These differences are not ontogenetic, so that those two morphotypes represent two distinct taxa. Morphotype A can also be differentiated from MNHN.F. IBC 1992 (the sacral vertebra) in having closely spaced articular facets (cotyles and condyles) for the sacro-urostyler articulation so that they are not compatible with each other. Therefore, and because MNHN.F. IBC 1994 is monocotylar, MNHN.F. IBC 1992 (sacral vertebra), 1993 (urostyle morphotype A) and 1994 (urostyle morphotype B) are all attributed to three distinct taxa. Bicondylar articulation on the urostyle without and absence of transverse process are known in Neobatrachia and numerous extinct Mesozoic Laurasian anurans of unknown affinities (Roček, 2013). Therefore, urostyle

The neobatrachians of In Becetén: The earliest coexistence of hyloid and ranoid ?

of Morphotype A cannot at present be attributed to any anuran clade. On Morphotype B, the presence of monocotylar articulation is uncommon among anurans. It has been recovered in several unidentified anurans from the Late Cretaceous of North America (Roček et al., 2010), in several Bombinatoridae (used as a diagnostic character; Folie et al., 2012), Discoglossinae (Rage and Hossini, 2000) and in some Pipimorphs. Within Bombinatoridae and Discoglossinae, urostyles possess transverse processes (unknown in Morphotype B) and Pipimorphs and lack any transverse processes. Therefore, Morphotype B cannot either be attributed to any anuran clade. However, it should be noted that monocotylar articulation has been associated with an increased aquatic lifestyle (Roček et al., 2010). Thus, it is possible that Morphotype B belonged to one of the two unnamed pipimorphs of In Becetén (Chapter II).

Scapula

Referred material—One incomplete scapula (MNHN.F.IBC 1996).

Description—The scapula preserves the broken base of its pars acromialis (Fig. IX-4K, L). The pars glenoid is not distinct from the scapular shaft and pars acromialis, forming a large articular facet, the glenoid fossa (Fig. IX-4K). The suprascapular region is elongate dorsoventrally. The anterior margin bears an extended crest and the level of the suprascapular margin (Fig. IX-4K, L). No assignment among anurans is possible at that time.

Ilia

Referred material—Three incomplete ilia (MNHN.F.IBC 1600, 1601, 1995).

Description—These three ilia are here tentatively interpreted as being three different morphotypes. However, all are badly preserved, and all could represent intraspecific variation. All three are excluded from Pipimorpha by (1) having a dorsal crest (Morphotype A and C) and (2) absence of an interiliac tubercle (Morphotypes A and B; present on the medial surface of pipimorphs and *Hungarobatrachus*; Gómez and Turazzini, 2016: fig. 3F).

The neobatrachians of In Becetén: The earliest coexistence of hyloid and ranoid ?

Morphotype A (MNHN.F.IBC 1600; Fig. 4M-P): the ilium bears a very low dorsal crest (Fig. IX-4M, N). The iliac shaft is strongly compressed lateromedially. The dorsal prominence is low and forms an elongate oval bulge (Fig. IX-4M, O). The dorsal prominence project laterally and is anterodorsal to the acetabular rim (Fig. IX-4M). The ventral acetabular expansion is incomplete but is likely reduced (Fig. IX-4M). The preacetabular zone is enlarged (Fig. IX-4M). A small depression beneath the ventral acetabular margin could be interpreted as a preacetabular fossa. The dorsal acetabular expansion is not preserved. No interiliac tubercle seems present (Fig. IX-4P).

Morphotype B (MNHN.F.IBC 1601): the ilium lacks a dorsal crest (at least on the preserved distal region; Fig. IX-4Q-R). The dorsal prominence is scarcely distinct from the rest of the bone, forming an ovoid bulge that projects neither medially nor laterally (Fig. IX-4Q). The acetabular region is too poorly preserved to distinguish any features.

Morphotype C (IBC. F.MNHN 1995): This right ilium is missing most of its acetabular region. The preserved iliac shaft shows a well-developed dorsal crest (Fig. IX-4S-U). Although its dorsalmost portion is not preserved, the crest is at least the height of the iliac shaft. The dorsal prominence is an anteroposteriorly elongate ovoid bulge (Fig. IX-4S). The dorsal protuberance projects lateroposteriorly (Fig. IX-4S, U). Posterior to the dorsal prominence, the notch for the attachment of the musculus gluteus magnus is present (Fig. IX-4T). The dorsal prominence is located anteriorly to the acetabular rim.

Discussion and Attribution—Morphotypes A and B are puzzling. The presence of a weakly developed dorsal prominence in Morphotype B is reminiscent of several neobatrachians, like *Telmatobius* (Gómez and Turazzini 2016) and Myobatrachidae (Tyler, 1976), and the presence of a low dorsal ridge is also known in some neobatrachians (Gómez and Turazzini, 2016). However, both ilia are far too incomplete to propose any attribution to any clade. In addition, these two morphotypes seem to differ from all known ilia from the Cretaceous of North America (Roček, 2010, 2013). Regarding morphotype C, the presence of a high dorsal crest has often been used as a characteristic of ranoids (Rage, 1984; Prasad and Rage, 2004; Rage, 2016). However, a

The neobatrachians of In Becetén: The earliest coexistence of hyloid and ranoid ?

high dorsal crest also occurs within Alytoidea, as in *Latonia* (Roček, 2013). Therefore, Morphotype C cannot either be attributed to any known clade for the moment. All three ilia represent three distinct morphotypes, and likely taxa. However, we cannot attribute them at that time to any known clade, and to any known taxa from the In Becetén fauna.

Limb bones

Referred material—25 radioulnae (MNHN.F.IBC 1999a-y), five femora (MNHN.F.IBC 2034a-e), 22 tibiofibulae (MNHN.F.IBC 2035a-v) and three metatarsals (MNHN.F.IBC 2002a-c).

Description—Radioulnae, femora, tibiofibulae and metatarsals are unfortunately too fragmentary and do not display any peculiar features (such as additional ridges) to be assigned to any anuran taxa (Fig. IX-4V, W).

The neobatrachians of In Becetén: The earliest coexistence of hyloid and ranoid ?

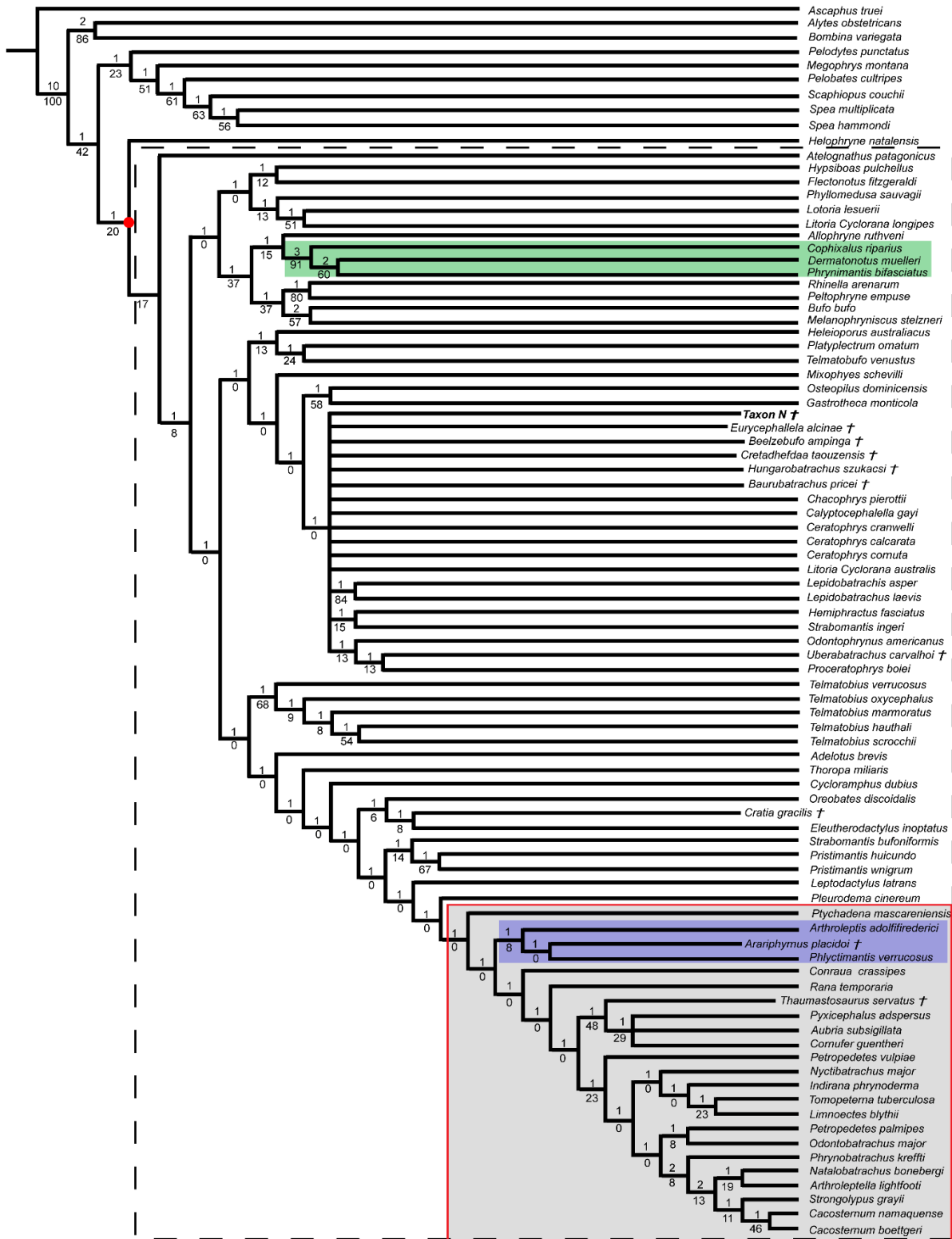


Figure IX-5. Strict consensus of the phylogenetic analysis performed under equal weight (CI = 0.163; RI = 0.520). Red circle represents Neobatrachia, dotted rectangle represents Hyloidea, light green rectangle represents Microhylidae, red outline represents "Ranoidea", light grey rectangle represents Natatanura, blue rectangle represents Afrobatrachia, numbers above and below branches represent Bremer and bootstrap values respectively.

IX.5 Phylogenetic Analyses

The analysis under equal weight analysis, with cline characters ordered, yielded 10 MPTs with score of 1362 (CI = 0.163; RI = 0.520). In the strict consensus (Figs. IX-5-6), we recovered a monophyletic Neobatrachia. However, the neobatrachian relationships are poorly resolved (Fig. IX-5). Indeed, Neobatrachia is poorly supported by four synapomorphies. *Heleophryne* is recovered as the sister-taxon to all other neobatrachians, as in molecular analyses (Hime et al., 2021). Hyloids are monophyletic (Figs. IX-5-6) but with all ranoid taxa recovered within this clade (Fig. IX-6). All Mesozoic taxa (except *Arariphrynus*) are clustered within a large unresolved polytomy (Fig. IX-5), which also includes most extant hyperossified and ornamented hyloids, like *Calyptocephalella* and the ceratophryds. This clade is poorly supported by 16 synapomorphies (See Appendix S4). *Taxon N* is also recovered as a neobatrachian within this polytomy (Fig. IX-5). Ranoidea is not recovered as monophyletic, with the natatanurans and afrobatrachians nested together (Fig. IX-6), while the microhylids are recovered within the hyloids (Fig. IX-5). This configuration is common in several analyses (Báez and Gómez, 2018; Lemierre et al., 2021) and is likely linked to pectoral girdle characters (absence of ossified omosternum in microhylids). *Thaumastosaurus* is recovered as the sister-taxon to all three hyperossified ranoids (*Pyxicephalus*, *Aubria* and *Cornufer*), a position already recovered previously (Lemierre et al., 2021; Chapter X). *Arariphrynus placidoi* is also recovered as a ranoid, within the afrobatrachians (Fig. IX-6), supported by four synapomorphies. However, it should be noted that *Arariphrynus* do not possess any synapomorphies proposed for Ranoidea or Afrobatrachia, and its position is very unstable in several analyses (Báez and Gómez, 2018). This is linked to the poor preservation of its pectoral girdle (Báez et al., 2007).

IX.6 Discussion

The neobatrachian(s) of In Becetén

Phylogenetic analyses including *Taxon N* confirm its attribution as a neobatrachian. The analyses also point to affinities to hyloids. However, a large bias exists regarding hyperossified taxa, with most hyperossified neobatrachians often clustered together (Báez and Gómez, 2018). As an example, when considering only hyperossified characters, several ranoids, like *Thaumastosaurus*, are recovered as hyloids (Báez and Gómez, 2018). Furthermore, the fragmentary remains of *Taxon N* and the few scored characters (13% of all characters) hamper establishment of its affinities. Hence, we attribute *Taxon N* to Neobatrachia only.

Thus, *Taxon N* appears to represent a neobatrachian from In Becetén. We also identify one humerus that we attribute to Neobatrachia as well. However, while *Taxon N* might have hyloid affinity, the humerus has ranoid affinities (if it is indeed a neobatrachian). Hence, we could argue that they represent two distinct neobatrachian taxa. However, a disparity between the affinity of the skull and the postcranial bones is known in several hyperossified ranoids, one of the best examples being *Thaumastosaurus* (see Laloy et al., 2013; Lemierre et al., 2021). Thus, in the absence of more elements, we consider that at least one neobatrachian is present in In Becetén, *Taxon N*. It is the third known neobatrachian in Mesozoic Africa, and the second oldest (Lemierre and Blackburn, 2022; Chapter VIII).

The oldest putative remains attributed to Ranoidea are from the Cenomanian of Sudan (Báez and Werner, 1996). However, they have never been described or illustrated, so this attribution needs to be reassessed. A neobatrachian humerus with ranoid affinities has been described from the middle Cenomanian of Morocco (Fig. VIII-6A-C), but it lacks several ranoid characters present in MNHN.F.IBC 1603. Several ilia from the Late Cretaceous (Maastrichtian) of India have been attributed to Ranoidea (~Ranoides of Frost et al., 2006) or Ranidae (Prasad and Rage, 2004) based on their

The neobatrachians of In Becetén: The earliest coexistence of hyloid and ranoid ?

overall morphology. This attribution is poorly supported, as the overall morphology of ilia are convergent within anurans (Roček, 2013) and the clade is mainly united by characters of the pectoral girdle (Frost et al., 2006; Lemierre et al., 2021). The stratigraphically oldest taxon firmly attributed to the Ranoides is *Thaumastosaurus*, from the Eocene of Western Europe (Laloy et al., 2013; Báez and Gómez, 2018; Vasilyan, 2018; Lemierre et al., 2021). Numerous African ranoid clades possess a poor fossil record, with the majority of them only identified in the Neogene (Gardner and Rage, 2016). Most of those remains are attributed to extant genera, rendering the comparison or attribution of older remains difficult.

Nevertheless, the Ranoidea are considered to have emerged in Africa during the Early Cretaceous, undergoing a rapid diversification between the Late Cretaceous and the Palaeocene (Bossuyt et al., 2006; Frazão et al., 2015; Feng et al., 2017). The presence of a ranoid in In Becetén is unsurprising, as molecular timetrees suggest that ranoids already inhabit the continent by the Cretaceous, and paleogeographic reconstructions suggest that Africa was relatively isolated at the time (Gheerbrant and Rage, 2006).

Anuran diversity in In Becetén

Based on both cranial and postcranial remains, at least 3 to 4 non-pipid anuran taxa are identified within In Becetén. Among them, at least one is referred to Neobatrachia. The presence of a neobatrachian shows that the clade was already widespread in the early Late Cretaceous in Western Africa, given the presence of *Cretadefdaa* in the Cenomanian of Morocco.

At least 7-8 anuran taxa are known in In Becetén (Chapters II-IV). This diversity is unique for Mesozoic African sites, with all others known sites yielding three taxa at the most (Gardner and Rage, 2016). In addition, In Becetén is the second richest site (for anurans) in Mesozoic Gondwana, surpassed only by the Crato Formation (Báez et al., 2021). Interestingly, at least 5 taxa from In Becetén are highly (or totally) adapted to an aquatic lifestyle. This implies that the paleoenvironment of In Becetén was

The neobatrachians of In Becetén: The earliest coexistence of hyloid and ranoid ?

composed of numerous lakes and ponds, where most aquatic anurans, in peculiar pipids, dwell (Duellman and Trueb, 1994). This is consistent with the presence of numerous actinopterygians (Gayet and Meunier, 1996).

IX.7 Conclusion

The study of the anuran fauna at In Becetén documents the presence of seven to eight distinct taxa, making it the richest site of Mesozoic and Paleogene Africa, for anurans. Among the taxa, four have been previously assigned to Pipimorpha. A new hyperossified taxon has been identified, represented mostly by fragments of maxilla. Our phylogenetic analysis suggests that this new taxon is a neobatrachian, making it the third Mesozoic occurrence of this clade in Africa. An isolated humerus also likely represents a second neobatrachian, and the oldest, and first Mesozoic occurrence of a ranoid. These neobatrachians, combined with other occurrences in Africa indicate that the clade was widespread in Western Africa in the early Late Cretaceous. Numerous isolated bones indicate that at least two other anurans were present, with one likely adapted to an aquatic lifestyle. The anuran fauna indicates that the paleoenvironment of In Beceten was likely composed of several lakes and ponds.

IX. 8 Appendix

Appendix S1. Morphological dataset used for phylogenetical analyses

The dataset used is the one from Chapter VIII, with the addition of *Taxon N*

	1	2	3	4	5	6	7	8	9	10	11	12	13	14	15	16	17	18	19	20
<i>Taxon N</i>	?	?	?	?	?	1	?	?	1&2	1&2	?	?	?	?	?	?	?	?	?	?
	21	22	23	24	25	26	27	28	29	30	31	32	33	34	35	36	37	38	39	40
<i>Taxon N</i>	?	?	?	?	?	?	?	?	?	?	?	?	?	?	?	?	?	?	?	?
	41	42	43	44	45	46	47	48	49	50	51	52	53	54	55	56	57	58	59	60

The neobatrachians of In Becetén: The earliest coexistence of hyloid and ranoid ?

<i>Taxon</i> N	?	?	1	?	?	?	?	?	?	3	2	1&2	?	?	?	?	?	?	?	?	?
	61	62	63	64	65	66	67	68	69	70	71	72	73	74	75	76	77	78	79	80	
<i>Taxon</i> N	?	?	?	?	?	?	?	?	?	?	?	?	?	?	?	?	?	?	?	?	?
	81	82	83	84	85	86	87	88	89	90	91	92	93	94	95	96	97	98	99	100	
<i>Taxon</i> N	?	?	?	?	?	?	?	?	?	?	?	?	?	?	?	?	?	?	?	?	?
	101	102	103	104	105	106	107	108	109	110	111	112	113	114	115	116	117	118	119	120	
<i>Taxon</i> N	?	?	?	?	?	?	?	?	?	?	?	?	?	?	?	?	?	?	?	?	?
	121	122	123	124	125	126	127	128	129	130	131	132	133	134	135	136	137	138	139	140	
<i>Taxon</i> N	?	?	?	?	?	?	?	?	?	?	?	?	?	?	?	?	?	?	?	?	?
	141	142	143																		
<i>Taxon</i> N	?	?	?																		

Appendix S2. Taxa list for the phylogenetical analyses

The list is the same as in Chapter VIII, with the addition of *Taxon N*.

Appendix S3. Character list

The list is the same as in Chapter VIII.

Appendix S4. List of synapomorphies for selected clades

Neobatrachia : 27: 0→1; 93: 0→1; 138: 0→1.

Neobatrachia, node excluding *Heleophryne*: 9:0→1; 119:0→2; 131:0→1; 143:0→2.

Hyperossified polytomy (including most Mesozoic taxa): 9:1→2; 36:3→4; 44:0→1;

46:1→4; 51:0→2; 52:1→2; 68:1→2; 87:0→1; 89:0→1; 92: 0→1; 120:1→2; 121:1→2; 126:1→2; 129:1→2; 136:0→2; 140:1→3.

Node *Arariprhynus* + Afrobatrachia: 67: 1→0; 102: 1→0; 112: 1→2; 131: 1→0.

Chapter X

*THE RETURN OF THE MUMMY: THAUMASTOSAURUS,
AN EOCENE PYXICEPHALID FROM WESTERN EUROPE*

The work on *Thaumastosaurus* has been published in two separated articles : Lemierre et al (2021) and Lemierre and Laurin (2021). Hence, this chapter will be divided into two unequal parts, each derived from an article. The first part has been published as Lemierre et al (2021), while the second has been published as Lemierre and Laurin (2021).

I. From Toad to Frog, a CT-based reconsideration of *Bufo servatus*, an Eocene anuran mummy from Quercy (France)

X.1 Introduction

The Quercy Phosphorites consist of an extensive series of limestones fissures within the Quercy plateau (southwestern France) that are infilled with clayey phosphates (Fig. II-1A-B; Pélissié and Sigé, 2006). Mining of these phosphates for use as fertilizer began in 1871, with the number of active quarries expanding until 1886 when the operations began to decline. Almost all quarries were closed by 1893 (Thevenin, 1903; Gèze, 1949). The Quercy Phosphorites quickly became known for their highly diverse assemblages of vertebrate fossils (e.g., Filhol, 1877) whose ages range from the Early Eocene to Early Miocene (Sigé et al., 1991; Legendre et al., 1992) but with a concentration between the Middle-Late Eocene to the Late Oligocene. This age distribution makes these fossils especially valuable for understanding the role of climate change in the “Grande Coupure” – the faunal turnover and moderate extinction event that marks the approximately 33.9 Ma Eocene-Oligocene transition (Stehlin, 1909).

The Quercy Phosphorites are best known for their highly diverse mammalian fauna (Pélissié and Sigé, 2006) and great density of amphibians (Rage, 2006), both of which are based largely on disarticulated skeletons. However, four anurans, an urodele and six snake fragments present exceptionally well-preserved tissues in 3D (Laloy et al. 2013; Tissier et al. 2016, 2017). At the time of their initial description in the late 1800s, only the external soft-tissues were known and they were referred to as “natural mummies” (see e.g. Filhol, 1877 for a brief description of the anuran skin). They were originally given or sold to Professor Henri Filhol by A. Lafont (or Lafon), a pharmacist in Villeneuve (Aveyron, France; see Fig. II-1C) during the early 1870s (see first mention in Filhol, 1873). They remained part of the

The return of the mummy: *Thaumastosaurus*, an Eocene pyxicephalid from Western Europe

private collection of H. Filhol, which housed numerous fossils from the Quercy, including the holotypes of the taxa he erected until his sudden death in 1903. Edmond J. de Rothschild then bought the entire collection to prevent its dispersal and donated it to the MNHN the same year (1903). Given their striking aspect, they were placed in the paleontological gallery of the Museum, where they remain visible to the public even now.

Reliant wholly on external morphological features, early studies assigned the anuran mummies to two different species, *Rana plicata* and *Bufo servatus* (Filhol, 1876, 1877). In the 2010s, two amphibian mummies were further analyzed using classical micro-computed tomography (on the anuran MNHN.F.QU17279; Laloy et al., 2013) and synchrotron light micro-computed tomography (on the urodele MNHN.F.QU17755; Tissier et al., 2016, 2017). Both studies evidenced internal subcomplete and articulated skeletons, soft tissues (e.g. organs) and diet contents, facilitating more complete redescriptions and assessments of their phylogenetic affinities (Laloy et al., 2013; Tissier et al., 2016). MNHN.F.QU17279, initially described by Filhol (1876) under the name *Rana plicata*, turned out to be the most complete specimen of the Eocene *Thaumastosaurus gezei* Rage and Roček, 2007, previously known only from a subcomplete skull and fragmentary remains (Rage and Roček, 2007). Later, a second mummy (MNHN unnumbered) was also assigned to *T. gezei*, based on external shape and a few visible dermal bones (Rage, 2016).

Here we focus on the third anuran specimen discovered in the 1870s and unstudied since the end of the XIXth century: MNHN.F.QU17381. This specimen was originally described as the holotype of "*Bufo servatus*" Filhol 1877. The assignment of this taxon to Bufonidae was questioned by multiple authors (e.g. Sanchiz, 1998; Rage, 2016) as its identification was based only on its external aspect. As for other exceptionally preserved specimens from Quercy, tomography revealed a subcomplete skeleton and soft tissues, enabling us to reassess the identification of MNHN.F.QU17381 and the validity of *B. servatus*. Several phylogenetic analyses are performed on this taxon as a means to discuss its general affinities among anurans. Finally, we discuss the paleobiogeographical and evolutionary implications of these phylogenetic conclusions and their impact on the anuran fossil record.

The return of the mummy: *Thaumastosaurus*, an Eocene pyxicephalid from Western Europe

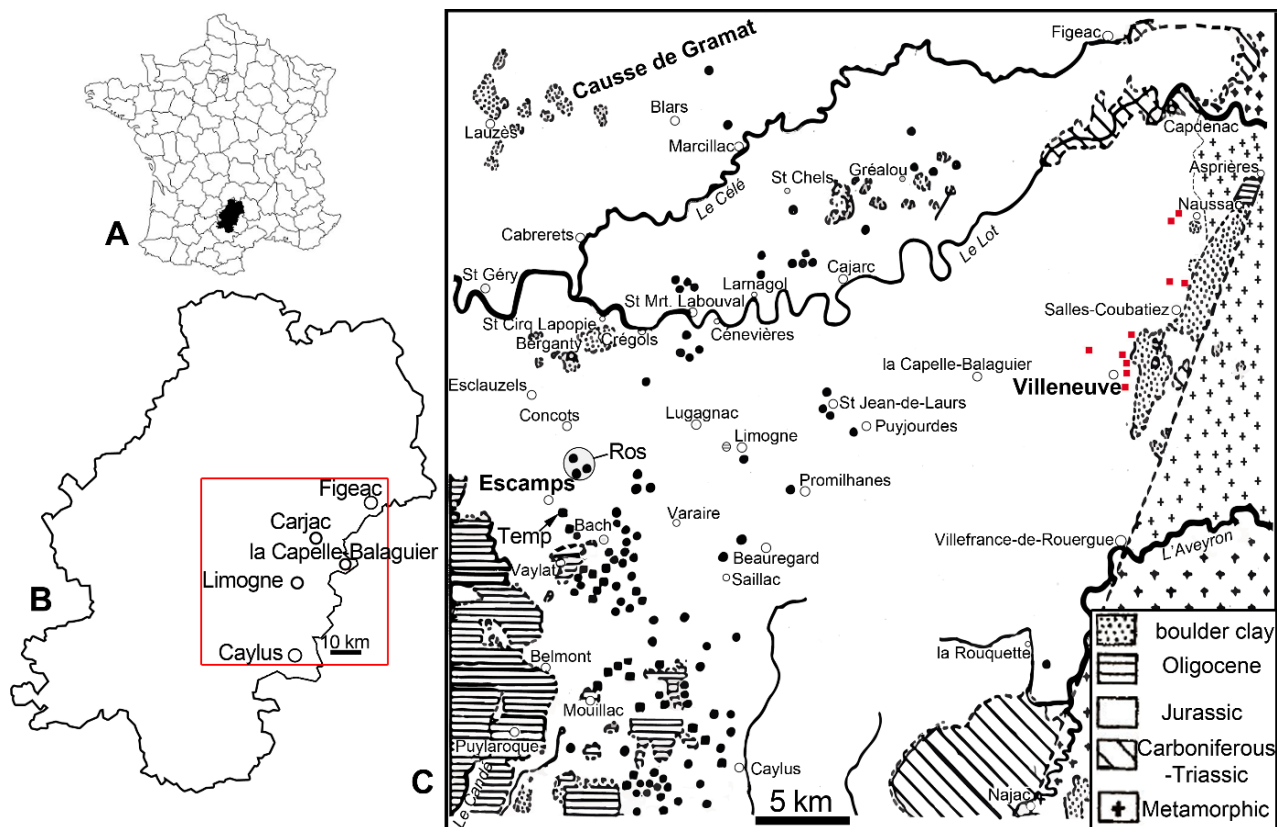


Figure X-1. Geographical maps of potential localities for the mummies. A, map of France, with the Quercy region highlighted in black; B, map of the Quercy region, with its south-eastern part highlighted in red in online version; C, close-up on the south-eastern Quercy region, modified from Gèze (1949), with the two-potential locations for sites that yielded the mummies in bold. Black dots indicate phosphorite quarries listed by Gèze (1949), red online squares indicate putative origin sites for the mummy series near Villeneuve, black arrow indicates the location of the site ‘les Tempories’, transparent circle indicates the area of the Rosières sites.

X.2 Geological Context

Locality

The specimen MNHN.F.QU17381, like the other Quercy “mummies” (Filhol, 1877), is part of the MNHN ‘old collection’ lacking information on its original location and stratigraphic assignment. However, the brief descriptions given by Filhol (Filhol, 1873, 1876, 1877) seem to indicate that all mummies come from a single quarry. We conclude that this quarry most likely belongs to one of the two localities discussed below.

The first locality is the town of Villeneuve (Fig. X-1C), where the first seller (A. Lafont) lived. The hypothesis that this locality produced the mummies is supported by the

The return of the mummy: *Thaumastosaurus*, an Eocene pyxicephalid from Western Europe

statement of Filhol (1873) that the series came from the department of Aveyron. This information was also repeated in at least two local newspapers. Both the “Journal de l’Aveyron” and the “Journal de Villefranche” published an identical small article in January 1874 based on a talk given by Filhol in Paris (1873) that placed this discovery in Aveyron. Moreover, Filhol mentioned in his talk that he had just received the fossils. It is possible that he indicated Aveyron as the origin of the mummies simply because the seller came from this place.

Near Villeneuve, approximately ten quarries are known (Fig. X-1C, red squares). Among them, one (Vielase) can be ruled out due to the nature of the phosphatic matrix, a tectonized karstic breccia (Simon-Coicon and Astruc, 1991; Legendre et al., 1992) that is clearly incompatible with the observed thin-scale phosphate replacement of the animal structures. Only one tunnel in Vielase could have housed phosphatic fillings, but it is now inaccessible, and no information exists anymore on this tunnel (T. Pélissié, pers. com). The remaining quarries are either azoic, or devoid of any phosphatic matrix still in place for comparison.

The second locality is the village of Escamps in the Lot department (Fig. X-1C). This locality was first mentioned in a local newspaper, the “Journal du Lot” on January 13th, 1874, in an article that discussed a future talk by Filhol at the ‘Société des Sciences Physiques et Naturelles de Toulouse’. Filhol indeed presented on February 6th, 1874 some exquisitely preserved fossil of anurans coming from a quarry in the Lot. The Bulletin of the above-mentioned Society gives an account of this talk, mentioning three anuran fossils (Jeanbernat, 1874). These three fossils can only correspond to the mummy series. The apparent change in the locality of origin for these fossils that occurred between Filhol’s talk in Paris (Filhol, 1873) and southern France (Toulouse) could reflect new information he received from the seller — after his 1873 talk at the Academy of Sciences (Paris). In addition to the press releases and society bulletin, there is a local memory of a discovery of a “stone” anuran in the village of Escamps, dating back to the late XIXth century (T. Pélissié and E. Cassan pers. com. October, 2020). A young miner, Emile Dutheil, discovered a stony anuran corresponding to the mummy description inside a cavity in a quarry near the town, either in the site ‘les

The return of the mummy: *Thaumastosaurus*, an Eocene pyxicephalid from Western Europe

Rosières' or 'les Tempories' (Fig. X-1C). This fossil was soon exchanged against a bottle of wine and might have ended in the hands of A. Lafont. The other mummies might have been discovered shortly thereafter. Six sites are regrouped under the name 'les Rosières' (Fig. X-1C) and are dated from Late Eocene MP17a (37.8 to 37.4 Ma) to MP19 (34.5 to 33.5 Ma; Aguilar et al., 1997; Vandenberghe et al., 2012). They have been partially studied in the previous decades (Remy et al., 1987), without any discovery of a new mummy. The other site, 'les Tempories' is dated from the MP19 (Late Eocene, 34.5–33.5 Ma). In situ layers of phosphorites are still visible today (T. Pélissié pers. com.) but most of the site was drained during its exploitation and later used as a landfill. If the series came from a layer within the quarry, this layer may have been completely cleared out more than a century ago.

Another possibility is that the series came from elsewhere in the Lot. Fossils discovered in these quarries were often appreciated by local notables and thus experienced local dispersement through exchanges or sales with surrounding towns and villages. Some of these fossils were then sold to known museum curators or even exchanged for favors (T. Pélissié pers. com.).

Until a precise account of the MNHN.F.QU17381 discovery is found that includes locality information, each of these provenance hypotheses will remain somewhat viable with its geographic (and stratigraphic) origins somewhat ambiguous. The strongest support is for the locality of Escamps, especially given the local memory of such a discovery, which does not occur in the vicinity of Villeneuve. We putatively identify the locality as the village of Escamps, Lot (France) and assign a Late Eocene age to the mummy series.

Stratigraphic Range

The genus *Thaumastosaurus* (to which two of the mummies have been attributed so far) is known from various localities in Western Europe (Vasilyan, 2018). The earliest remains of *Thaumastosaurus* are from the MP16 (Late middle Eocene ~39.5 Ma) from two Swiss localities, and the genus is present throughout the Late Eocene, with most of the localities located in the Quercy Phosphorites. The geologically most recent record of *Thaumastosaurus* is from the MP20 (~33.5 Ma, Priabonian, latest Eocene) from Escamps, in France. The

The return of the mummy: *Thaumastosaurus*, an Eocene pyxicephalid from Western Europe

complete list of the localities where *Thaumastosaurus* has been identified was compiled by Vasilyan (2018: table S1).

A recent study presented disarticulated bones from the Upper Turonian (earliest Late Cretaceous) and attributed a fragmentary maxilla to *Thaumastosaurus* (Ósi et al., 2019: fig. 6A–E) and a vertebra to an Anura indet. The tentative attribution of the vertebra to *Thaumastosaurus* is based on the presence of a ventral keel also possibly present in *T. gezei* (Laloy et al., 2013: fig. 5C; Ósi et al., 2019: fig. 6F–G). However, this ventral keel is actually the ridge of the neural spine, visible by transparency. In addition, in the vertebral column of MNHN.F.QU17381, there is no ventral keel on the vertebrae (see below). Furthermore, given the fragmentary state of this vertebra, the specimen cannot be attributed to a more exclusive clade than Batrachia (Duellman and Trueb, 1994; Tissier et al., 2016). Also, the ornamentation composed of irregular pits and ridges on the maxilla described by Ósi et al. (2019) occurs in numerous Cretaceous anuran clades (Roček and Nessov, 1993; Roček, 2008; Company and Szentesi, 2012; Báez and Gómez, 2018) as well as more recent anurans and other vertebrate taxa (e.g. squamates, crocodylians, various early stegocephalians; Buffrénil et al., 2015) and is therefore not diagnostic of *Thaumastosaurus*. Finally, the oval foramen located near the processus pterygoideus (if the fragmentary element is indeed a maxilla) as mentioned by Ósi et al. (2019) is present in other anurans (Biton et al., 2016). This makes the attribution of these Late Cretaceous fragments to the Eocene *Thaumastosaurus* unlikely and currently unsupported. Instead, these specimens may belong to a wide range of Mesozoic anuran clades. We therefore conclude that *Thaumastosaurus* has a stratigraphical range from the Late middle Eocene (~39.5 Ma) to the Terminal Late Eocene (~33.5 Ma).

X. 3 Materials and Methods

Institutional Abbreviations

IC2MP: Institut de Chimie des Milieux et Matériaux de Poitiers, Poitiers, France; **MHNT.PAL:** Muséum d'histoire Naturelle de Toulouse, Toulouse, France; **MNHN:** Muséum National d'Histoire Naturelle, Paris, France; **MNHN.F.QU:** Collection number for

The return of the mummy: *Thaumastosaurus*, an Eocene pyxicephalid from Western Europe

specimens from the 'old' Quercy Phosphorites collection, located within the paleontological collection of the MNHN; **NHMB**: Naturhistorisches Museum Basel, Basel, Switzerland; **UM. PRR**: Université de Montpellier, France, specimens from the Perrière site.

CT-scan parameters

The mummy MNHN.F.QU17381, currently displayed in the paleontology gallery of the National Natural History Museum in Paris (France), was micro-CT scanned at the PLATINA Plateforme Instrumentale d'Analyses (PLATINA platform) at the IC2MP (Poitiers, France). A microfocus beam of 160 kV of the CT-scanner was used with the following parameters: voltage, 130kV; current, 180 μ A; voxel size, 0.024 μ m; slice resolution, 1346 \times 2525 pixels. A total of 1750 virtual slices showing internal structures were reconstructed using XAct (RX solution). These slices were imported in the 3D reconstruction software Mimics 21.0 (Materialise, Leuven, Belgium). Before the importation, the slices were cropped to maximally remove the empty spaces. To decrease data size, slices were converted from 16 to 8 bits. The dataset thus includes 1256 slices with an image resolution of 1527 \times 2391 pixels and a voxel size of 2.4 μ m for the volume file (see Appendix S1). The 3D model was produced by segmentation of each bone using the 'thresholding' function (using the contrast on greyscale images). We used the same voxel resolution of 2.4 μ m, with a smoothing factor of 3 for one iteration, to homogenize the model resulting from manual segmentation. Data produced by segmentation were exported in the software 3matic 9.0 as a separate file (see Appendix S2).

Tomography revealed the internal preservation of soft tissues replicated in calcium phosphate (e.g. part of the brain and of the spinal cord, potential muscles and nerves). Unfortunately, most of the soft internal structures are either too degraded, or too similar to other structures in density and/or capacity to absorb X-rays (resulting in poor contrast) to be confidently segmented and described here. The external structures will be described in detail in a future study (N. Robin, unpublished data) and are only briefly presented here; our description focuses on the skeleton. The skull preserved inside the mummy lost its anteriormost region (snout) but is otherwise complete. Some hyobranchial bones are

The return of the mummy: *Thaumastosaurus*, an Eocene pyxicephalid from Western Europe

preserved, along with many postcranial bones, excepting the limbs and pelvic girdle (Fig. S1). An isolated ilium (UM.PRR 2002) collected in 1984 (Rage, 1984a) was recently attributed to *Thaumastosaurus* (Vasilyan, 2018) and was used here for phylogenetic analysis. This is justified given the remarkable similarity of the postcranial skeleton of the two species of *Thaumastosaurus* described in the Quercy, *T. gezei* Rage & Roček, 2007 and *T. botti* De Stefano, 1903 (Vasilyan, 2018).

The anatomical terminology used herein is based on Roček (1980) and Biton et al. (2016) for cranial features, Roček et al. (2016) for the middle ear apparatus, Sanchiz (1998) for postcranial ones, Gardner et al. (2010) for iliac characters.

Phylogenetic Analyses

Our data matrix includes 85 taxa and 143 morphological characters (62 cranial and 68 postcranial characters, 12 from the hyobranchial apparatus, and one from soft-tissues) and is derived from that of Báez and Gómez (2018; see Appendix S3 for the list of characters). We added 14 new extant natatanuran taxa (see Appendix S4) to better represent the major natatanuran clades inferred from recent molecular phylogenies (Frost et al., 2006; Pyron and Wiens, 2011; Jetz and Pyron, 2018). The new taxa were scored from both literature (Procter, 1919; Clarke, 1981; Scott, 2005; Evans et al., 2014) and 3D-models available on MorphoSource by the Blackburn Laboratory (Florida, USA) as part of the OVert program (Cross, 2017; for more information see the website: <https://www.floridamuseum.ufl.edu/overt/>).

All analyses were performed using TNT v.1.5 (Goloboff and Catalano, 2016). Half of the analyses was performed using equal weighting, whereas the other half was performed using implying weighting. Some analyses were conducted with all characters unordered and others with cline characters ordered (characters 3, 9, 10, 14, 26, 34, 51, 52, 68, 93, 112, 121, 124, 125 and 126), with or without topological constraints. All analyses consisted of heuristic searches with 1000 random addition sequences of taxa, followed by tree bisection reconnection (TBR) branch swapping, holding 10 trees per repetitions. The final trees were rooted on *Ascaphus truei* (Ascaphidae) and, when more than one tree was obtained, a strict consensus was obtained.

The return of the mummy: *Thaumastosaurus*, an Eocene pyxicephalid from Western Europe

Implied weighting was used to minimize the influence of homoplastic characters in the dataset, and achieved a better resolution of the different uncertainties recovered in the analysis under equal weighting (Goloboff, 1993, 1997), mostly for morphological characters (Goloboff et al., 2018a) and several values of k were used ($k = 1-20$) to assess sensitivity of the results due to variations of the strength of the function (Goloboff et al., 2008). Some controversies remain on the effectiveness of this method, especially when compared to Bayesian models (O'Reilly et al., 2016; Congreve and Lamsdell, 2016; Puttick et al., 2017), but some recent evidence indicates implied weighting performs well (Goloboff et al., 2018a, b). Consequently, we chose to use both equal and implied weighting parsimony methods and then compare their results. Cline characters were ordered in all but one analysis (see Appendix S5), as recent studies (Rineau et al., 2015, 2018) have shown that analyses using ordered morphocline characters outperformed analyses using unordered characters even if the ordering scheme includes some errors (Rineau et al., 2018). Constrained analyses were performed with ordered characters including both equal and implied weights ($k = 7$), using the topology of Jetz and Pyron (2018) as a constraint for extant taxa (Fig. S2). The same was done using the topology (Fig. S3) presented in Feng et al. (2017), with extinct taxa as floating taxa, in both cases. Node supports were expressed using Bremer support and standard bootstrap, with traditional searches of 1000 replicates, collapsing groups below 5% frequency. Bremer support uses tree fit score (Bremer, 1994; Goloboff and Farris, 2001). However, in implied weighting analyses, Bremer support is expressed in fractions due to the different weights that reflect the character fit (Goloboff, 1997; Jones and Butler, 2018).

The return of the mummy: *Thaumastosaurus*, an Eocene pyxicephalid from Western Europe

X.4 Systematic Paleontology

ANURA Duméril, 1805

NEOBATRACHIA Reig, 1958

RANOIDES Frost et al., 2006

NATATANURA Frost et al., 2006

PYXICEPHALOIDEA Bonaparte, 1850

PYXICEPHALIDAE Bonaparte, 1850

PYXICEPHALINAE Bonaparte, 1850

Genus *THAUMASTOSAURUS* De Stefano, 1903

Type Species—*Thaumastosaurus bottii* De Stefano, 1903

Revised Diagnosis

Hyperossified natatanuran exhibiting cranial ornamentation, composed of pits and ridges, on the frontoparietals, maxillae, nasals, squamosals and sphenethmoid; the paired nasals and frontoparietals co-ossified with each other respectively and with the sphenethmoid and prooticooccipital (frontoparietals only), rhomboid dorsal fenestra on the skull allowing a dorsal exposure of the sphenethmoid; palatines (neopalatines of Trueb, 1973) present, in medial contact with each other (by their medial margin); anterior tip of the cultriform process of the parasphenoid does not extend between palatines; processus posterolateralis and ramus paroticus of squamosal merged, articulating with the crista parotica of the otic capsules; arteria occipitalis of either side piercing the frontoparietal; medial ramus of the pterygoid well-developed, overlapping the parasphenoid alae; zygomatic ramus (lamella alaris + processus maxillaris) of the squamosal well-developed, articulating with the maxilla.

Differs from *Pyxicephalus* Tschudi, 1838 and *Aubria* Boulanger, 1917 in lacking fang-like lamellar projections on the dentaries, in having the alary process of the premaxillae oriented

The return of the mummy: *Thaumastosaurus*, an Eocene pyxicephalid from Western Europe

dorsally (posterodorsally oriented in *Pyxicephalus* and *Aubria*), the craniomandibular joint at the same level as the occiput (posterior to the occiput in *Pyxicephalus* and *Aubria*) and the clavicles oriented anteromedially to the sagittal axis (perpendicular to the sagittal axis in *Pyxicephalus* and *Aubria*).

Differs further from *Pyxicephalus* in having the alae of the parasphenoid perpendicular to its cultriform process (posterior to the cultriform process in *Pyxicephalus*), a large dorsal exposure for the sphenethmoid (in *Pyxicephalus*, the sphenethmoid is not visible in dorsal view), cotyles of the atlas fully confluent (Type III of Lynch, 1971 (instead of juxtaposed Type II in *Pyxicephalus*), bicuspid teeth on the maxillae (monocuspid teeth on the maxillae in *Pyxicephalus*) and in lacking a lateral wall of the neurocranium ossified around the optic foramen (lateral wall ossified around the optic foramen in *Pyxicephalus*).

Differs from *Aubria* in having a distinct postchoanalis processus of the vomers (no distinct process in *Aubria*).

THAUMASTOSAURUS SERVATUS Filhol, 1877 comb. nov.

Bufo servatus Filhol, 1877:493, fig. 412 (413 in error) of Filhol (1877), MNHN.F.QU17381 (original description).

Bufo serratus Filhol, 1876: 28, Filhol, 1877: fig. 412 (413 in error) (nomen nudum)

Rana plicata Filhol, 1876: 27, Filhol, 1877:figs. 401, 402, 404, 405.

Thaumastosaurus gezei Rage and Roček, 2007, figs 1, 7A.

Rana cadurcorum Martín et al., 2012: 163. Filhol, 1877: figs. 401, 402, 404, 405 (new combination).

Holotype

The holotype is MNHN.F.QU17381, a nearly complete specimen lacking the snout, appendages and pelvic region. Unrecorded locality (likely Escamps) of the Quercy Phosphorites, southwestern France. Age uncertain, but probably late Middle to Late Eocene.

The return of the mummy: *Thaumastosaurus*, an Eocene pyxicephalid from Western Europe

Referred Specimens

The specimens referred are MNHN.F.QU17748, right squamosal missing anterior tip of lamella alaris (Rage and Roček, 2007: fig. 2); MNHN.F.QU17376, holotype of *Thaumastosaurus gezei*, articulated skull missing anterior end, right side of palate, much of the right cheek region, parts of parasphenoid and both otic capsules (Rage and Roček, 2007: figs. 1, 7A); MNHN.F.QU17279, holotype of *Rana plicata*, nearly complete specimen lacking the appendages and pelvic region (Laloy et al., 2013: fig.1A–C); MNHN.F.QU17280, forelimb (Laloy et al., 2013: fig. 1D, E); MNHN unnumbered, specimen preserving the head and part of the trunk.

Revised Diagnosis

Differs from *T. wardi* by having a longer anterior extension of the squamosal alongside the dorsal margin of the maxilla, forming the whole ventral margin of the orbit; a medial margin of the lamina horizontalis of the maxilla convex rather than flat in medial view and in having the ridge separating the fossa maxillaris from the posterior part of the maxillae oriented posteriorly (instead of anteriorly).

Differs from *T. bottii* by having an elongate and slender medial process of the premaxillae, no ventral longitudinal ridge on this same process, and a groove for the vena jugularis interna shallower and wider.

The return of the mummy: *Thaumastosaurus*, an Eocene pyxicephalid from Western Europe

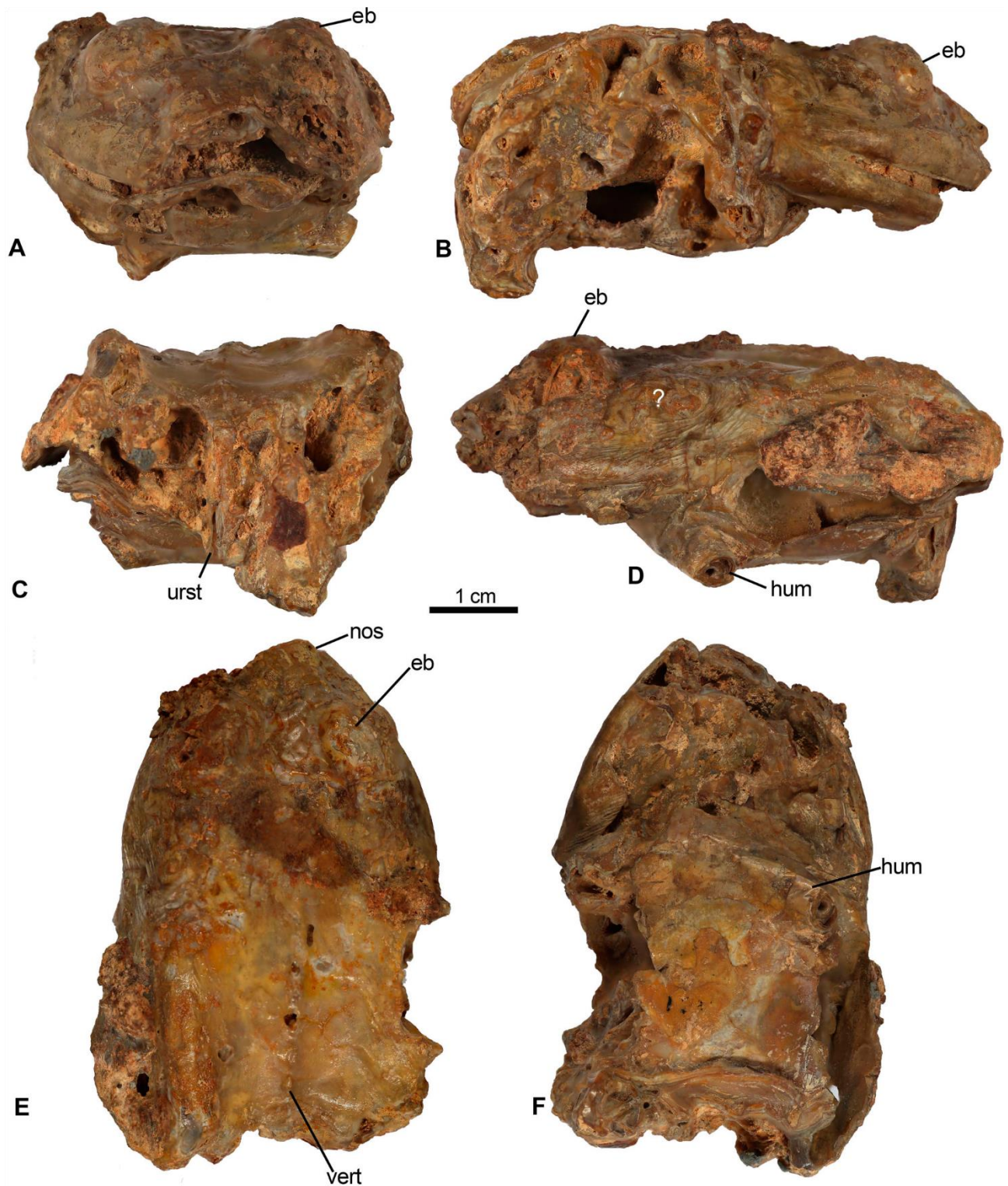


Figure X-2. External views of the specimen MNHN.F.QU17381. Holotype of “*Bufo servatus*” now attributed to *T. servatus* in **A**, anterior; **B**, right lateral; **C**, posterior; **D**, left lateral; **E**, dorsal and **F**, ventral views. ? indicate the area previously identified as a parotoid gland. **Abbreviations:** **eb**, eyeball; **nos**, nostril; **hum**, humerus; **vert**, vertebrae; **urst**, urostyle.

X.5 Description

External Preservation

As part of the Quercy old collection mummies, MNHN.F.QU17381 displays an exceptional three-dimensional preservation including most of its external soft-tissues replicated in calcium phosphate. These include the two eyeballs (Fig. X-2A) and the skin laying over 3D-preserved muscular series (Fig. X-2B–F), the striations of which are locally visible ventrally (e.g., right submaxillary muscles; Fig. X-2F). The specimen is about 6 cm from the snout to the sacrum, with its right side almost fully preserved. Hindlimbs and forelimbs are only proximally preserved. Posterior to each of the eyeball, a 1.3 cm long and 0.6 cm wide large ovoid swelling is present (Fig. X-2D, represented by a red/gray arrow and outline). This was at first identified as the outer visible deformation of a parotoid gland, typical for bufonids (Duellman and Trueb, 1994). However, other studies cast doubt on the presence of these glands in MNHN.F.QU17381 (Piveteau, 1927; Rage, 2006). The 3D model (Fig. X-3) shows that this swelling is caused by the posterior process of the squamosals, which stretches the skin in this area (Fig. X-3). This structure might have been caused by desiccation (N. Robin, unpublished data).

The outer tissues of MNHN.F.QU17381 are heterogeneously preserved. The skin is best preserved on the ventral and lateral sides of the specimen with fine sub-millimetric foldings. The latter concentrate on the mandible/maxillary complex, as well as posterior to the eye (Fig. X-2B–D). These folds, absent on extant anurans when alive, must result from post-mortem deformation of the outer tissues. Dorsally, the replicated surface tissues reveal a glassy aspect reflecting a different phosphatized texture (Fig. X-2C, E). In this region, the skin and inner tissues do not retain their *in vivo* volume but appear to be collapsed over the spine and underlying bony structure. The desiccation (or differential chemical transformation) of this dorsal part of the integument during early decay may have occasioned laterally the wrinkling of the skin resulting in observed microfolds. The left

The return of the mummy: *Thaumastosaurus*, an Eocene pyxicephalid from Western Europe

eyeball shows at the bottom a clear demarcation of the eye from the surrounding skin membrane (Fig. X-2D). Elsewhere, no distinction between the eye and the eyelid is apparent. Two other specimens of *T. servatus* display this level of exceptional 3D preservation in calcium phosphate. MNHN.F.QU17279 shows well-preserved eyelids covering the eyes fossilized in their original direction (Fig. X-4A, C). On this specimen, the skin is more stretched and homogeneously preserved over the specimen surface, revealing thinner skin (compared to MNHN.F.QU17381) microfolds and a local bulbous texture that looks original to the structure (Fig. X-4A–C). Larger skin ridges extend posteriorly from the eyes onto the dorsal surface of the trunk (Fig. X-4B). About 1 mm in width, these skin ridges correspond to the original dorsolateral folds present in many anuran taxa (Duellman and Trueb, 1994), especially in ranoids (e.g. in Pyxicephalidae, see Poynton, 1964; Channing and Baptista, 2013; Channing et al., 2016; see Dubois and Ohler, 2005 for other ranoids). On the left side of the specimen MNHN.F.QU17279, in a region between the posterior process and the postero-lateral side of the squamosal, the skin bears a slight demarcation with a faint outline (Fig. X-4C). Given the preservation of the skin on this region (Fig. X-4A–C), we do not interpret this delimitation as a reflection of the underlying bones but rather as the borders of the tympanic membrane (Duellman and Trueb, 1994).

The second best-preserved specimen, MNHN.F.QU17376, consists solely of a head whose preservation quality varies gradually from snout (best preserved) to neck (Fig. X-4D–E), with visible snout bony ornamentation (part of the nasals; Fig. X-4D). Posterolaterally, the skin looks pristine, with bulbous textural components. The aforementioned external aspects indicate that MNHN.F.QU17381 (Fig. X-2) may plausibly have undergone a longer period of decay/exposure time span prior to burial than MNHN.F.QU17279 (Fig. X-4A–C) and one comparable with, or shorter than MNHN.F.QU17376 (Fig. X-4D–E).

The return of the mummy: *Thaumastosaurus*, an Eocene pyxicephalid from Western Europe

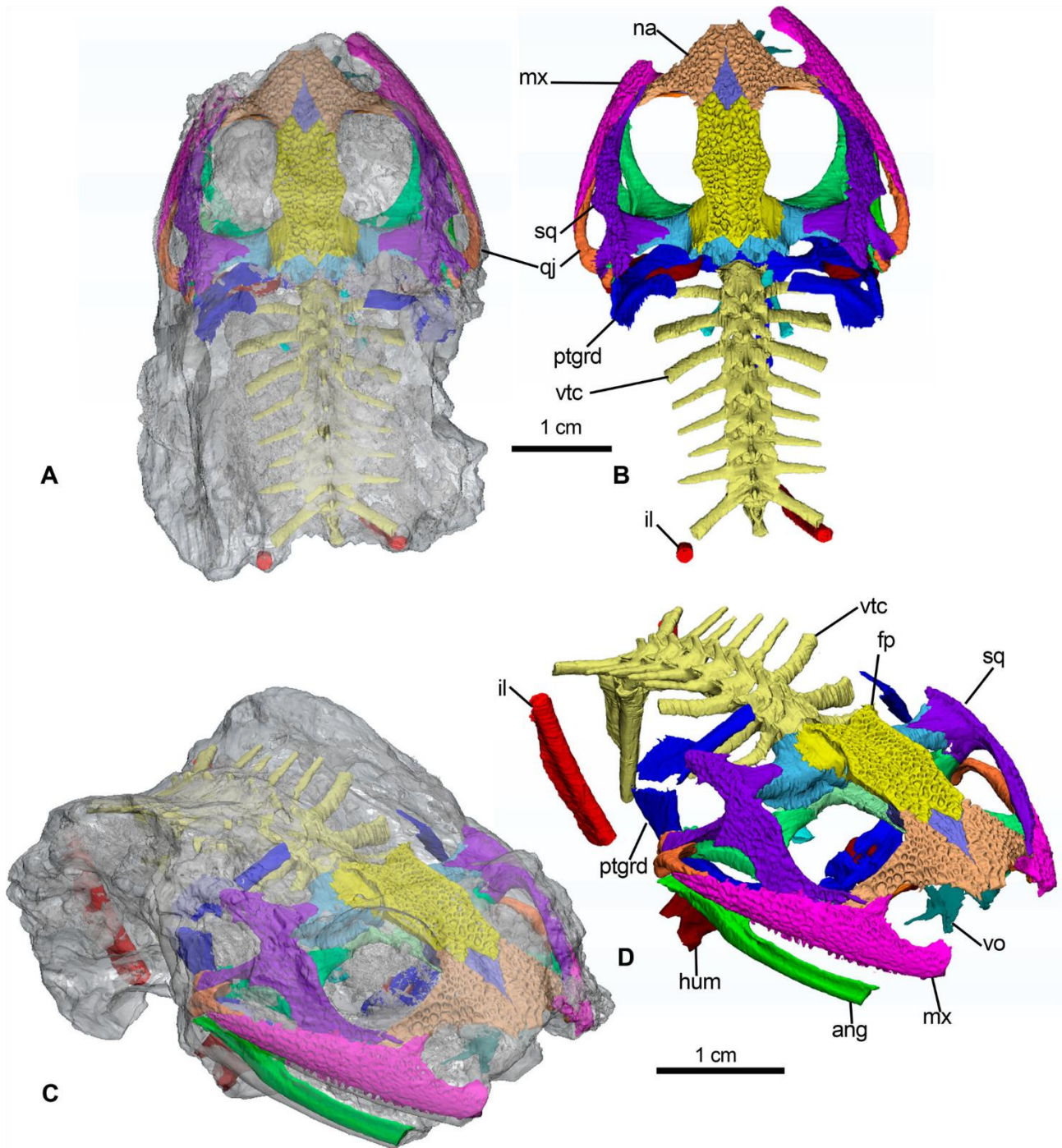


Figure X-3. 3D-model of the specimen MNHN.F.QU17381. **A**, whole specimen in dorsal view with soft tissue digitally rendered transparent to show the color-coded skeleton; **B**, dorsal view of the sole osteological component; **C**, whole specimen in right dorso-antero-lateral view with soft tissue digitally rendered transparent to show the color-coded skeleton; **D**, same view of the sole osteological component. **Abbreviations:** **ang**, angulosplenial; **fp**, frontoparietals; **hum**, humerus; **il**, ilium; **mx**, maxilla; **na**, nasal; **ptgrd**, pectoral girdle; **qj**, quadratojugal; **sq**, squamosal; **vo**, vomer; **vtc**, vertebral column.

The return of the mummy: *Thaumastosaurus*, an Eocene pyxicephalid from Western Europe

Skull

The skull is incomplete, missing the anteriormost part of the snout and the premaxillae (Figs. X-2, 3, 5). The preserved cranial bones are all articulated.

Dermal Bones—The frontoparietals, squamosals, maxillae, nasals and the dorsal part of the sphenethmoid bear an ornamentation composed of deep oval to subcircular pits and ridges with a constant thickness (Fig. X-5A). The ornamentation on the sphenethmoid is much less marked than on the other bones.

Frontoparietals—The frontoparietals are fused into a single bone, in the shape of a truncated rhomboid, longer than wide, without any clear trace of a median suture. However, anteriorly, at the posterior end of a deep notch on the midline of the nasal margin, a shallow depression on the dorsal and ventral face seems to mark the limit between the bones (Fig. X-6A). Anterolaterally, they articulate with the nasals by the external end of the nasal margin, and anteromedially, with the posteromedial margin of the dorsal exposure of the sphenethmoid. The lateral margin bears on its mid-length an external expansion (a peak), the tectum supraorbitale (Fig. X-6A–B). There is no contact between frontoparietals and squamosals (Fig. X-5A), but the lateral expansion of the tectum may indicate these two bones were joined by a ligament that would have delimited the posterior margin of the orbit, as observed in some extant anurans (Roček, 1980).

Posteriorly, the frontoparietals are fused to the prooticooccipital complex (Fig. X-5D). The processus lateralis of the frontoparietals are difficult to distinguish from the crista parotica of the prootic but seem to form an almost straight margin (Figs. X-5A, 6A). Posterolaterally, the processus paraoccipitalis of the frontoparietals is fused to the dorsal face of the prominentia ducti semicircularis posterioris of the prootic, forming a prominent ridge (Fig. X-5D). Medially, the processus paraoccipitalis delimits the foramen for the arteria occipitalis canal (Fig. X-5D). As in several extinct and recent anurans (Sanchiz, 1998), the posterior process of the frontoparietals consists of a horizontal lamina. This lamina extends the midlength of the bone posterior margin and forms a small spike-like surface that covers the dorsal exposure of the prooticooccipital (Fig. X-6A).

The return of the mummy: *Thaumastosaurus*, an Eocene pyxicephalid from Western Europe

In ventral view, the anterolateral pars contacta is a vertical lamina extending from the ventral surface of the frontoparietals (Fig. X-5B) and is fused to the dorsolateral part of the sphenethmoid (Figs. X-5B, 6A). The pars contacta increases in size posteriorly, forming a thin vertical lamina that is fused to the prootic ventrally and to the processus lateralis of the frontoparietals dorsally where it covers the prootic anterolaterally (Fig. X-5B).

Ventrally, the *incrassatio frontoparietalis* presents two structures, the *facies cerebralis anterior*, and the *facies cerebralis posterior* (Fig. X-6B). The *facies cerebralis anterior* is an unpaired lanceolate structure, extending from the posterior margin of the sphenethmoid/frontoparietals suture. The posterior limit of this structure is not clear. The *facies cerebralis posterior* is an unpaired circular impression, located postero-laterally on the left side of the bone. In another mummy (MNHN.F.QU17381), a similar condition was found for the *facies cerebralis anterior*, but the *facies cerebralis posterior* was a paired circular impression on each side (Laloy et al., 2013: fig. 4D). This condition is reminiscent of ranoids (Jarošová and Roček, 1982). In our specimen, the unpaired condition of the *facies cerebralis posterior* might be due to a non-preservation of the impression, or a lesser ossification of the right frontoparietal.

The return of the mummy: *Thaumastosaurus*, an Eocene pyxicephalid from Western Europe

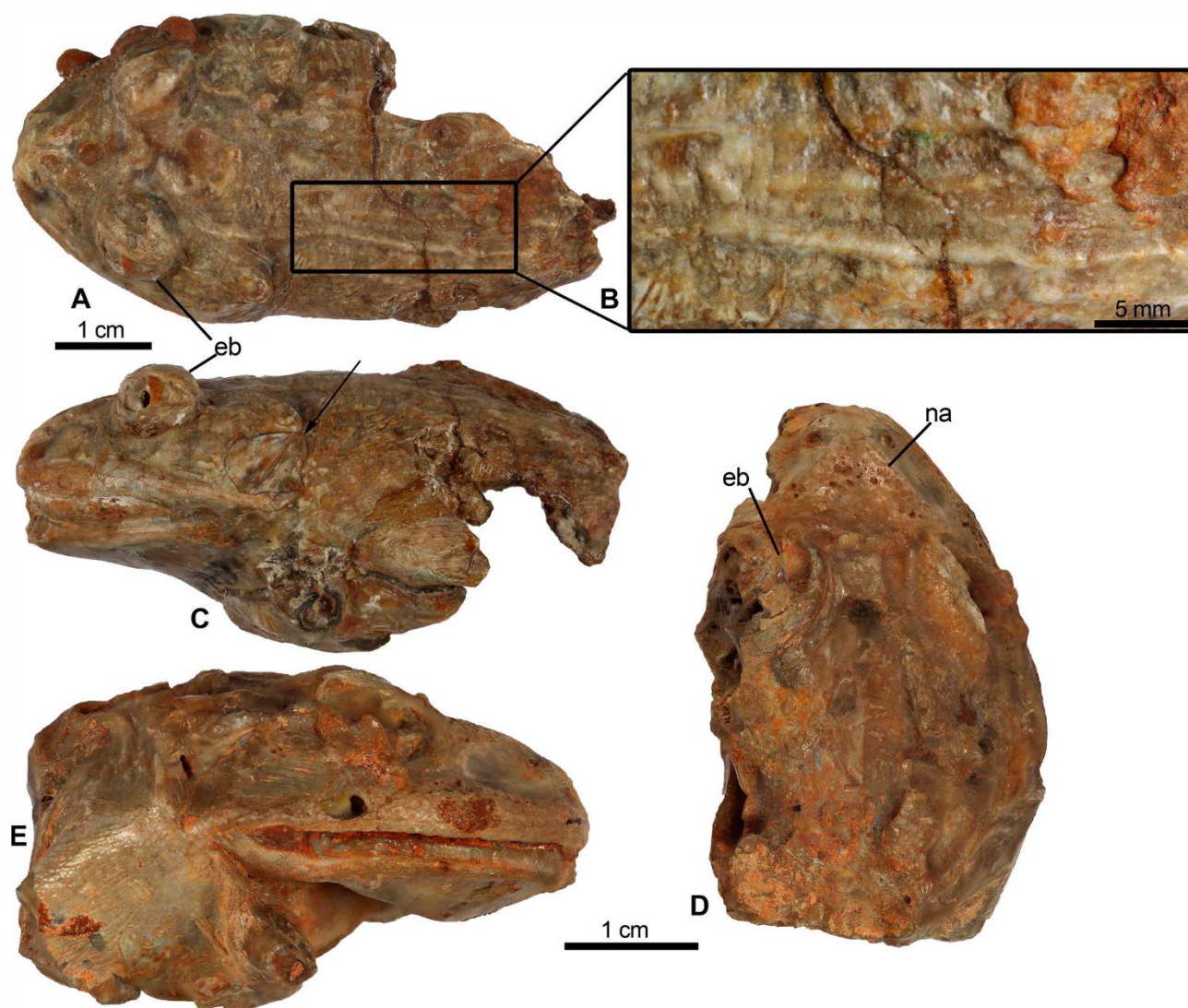


FIGURE X-4. External views of specimens MNHN.F.QU17279 and MNHN.F. unnumbered, both referred to *T. servatus*. A–C specimen QU 17279 in A dorsal view; B close-up of the rectangular region in A to show the ridges and folds of the preserved skin on the dorsal surface of the anterior trunk region; C same specimen in left lateral view; D–E specimen MNHN.F. unnumbered in D dorsal; and E right lateral views. Black arrow indicates the area of potential tympanic membrane. **Abbreviations:** eb, eyeball; na, nasals.

Squamosals—In lateral view, the lamella alaris is arch-shaped; it expands bilaterally at the base and tapers and descends ventrally towards the processus maxillaris (Fig. X-6C). It forms a thin strip of bone separating the maxilla from the orbit (Fig. X-5B). This configuration is similar to that of MNHN.F.QU1729, which also bears an elongate thin extension of the lamella alaris (Laloy et al., 2013) but is proportionally shorter than that of the holotype of *Thaumastosaurus gezei* (MNHN.F.QU17376; Rage and Roček, 2007). The

The return of the mummy: *Thaumastosaurus*, an Eocene pyxicephalid from Western Europe

anterior end of the lamella alaris forms a shallow groove with the lateral end of the nasal, identified as the groove for the nasolacrimal duct (Fig. X-5B).

The processus maxillaris is antero-posteriorly elongated (Fig. X-6C). The processus zygomatico-maxillaris of the maxilla is inserted into an incisura lateral to this processus maxillaris, fully overlapping it. This is not visible in lateral view, as it is overlapped by the lamella alaris (Fig. X-5B). The orbital margin is concave dorsally, forming the ventral wall of the orbit (Fig. 5A–B). Laterally, the lamella alaris extends posteroventrally into a spike-like extension, reaching the anterior part of the processus posterolateralis of the squamosals. Medially, the ramus paroticus is a broad dorsoventrally flat lamina, fused to the crista parotica of the otic capsule dorsomedially (Fig. X-5A). It narrows medially and ends in an almost straight margin (Fig. X-5A). The posterior process of the squamosal is short and rounded distally (Figs. X-5A–B, 6B). The processus posterolateralis is elongate and slender. In dorsal view, the surface between the ramus paroticus and the processus posterolateralis is concave (Fig. X-5A), and most likely forms the lateral wall of the tympanic cavity (Roček and Lamaud, 1995). The processus posterolateralis bears a medial flange fused to the ramus posterior of the pterygoid, making it difficult to digitally segment them (Fig. X-5B–C). The distal end of the processus posterolateralis is fused to the dorsolateral surface of the quadratojugal (Fig. X-5B).

Maxillae—The left maxilla is incomplete, lacking its anterior length starting at the level of the processus frontalis. The right maxilla, however, is almost complete, missing only its anterior tip. The posterior process of the maxillae is long, slender and has a groove posteromedially to articulate with the quadratojugal (Figs. X-5B, 6D). The processus pterygoideus, visible in medial view, is short and marked by a small posterior prominence from the lamina horizontalis. This processus delimits ventro-medially a large pit, which faces posteriorly. The lamina horizontalis is straight with a convex medial margin, moderately thickened anteriorly, where it extends onto the dorsal margin of the lamina anterior and develops into an anterodorsal anterior spine (Fig. X-6D). Posterior to the processus pterygoideus, the lamina horizontalis narrows considerably, ending in a thin,

The return of the mummy: *Thaumastosaurus*, an Eocene pyxicephalid from Western Europe

poorly marked strip extending onto the lower margin of the posterior process of the maxillae (Fig. X-6D).

In lateral view, a flattened smooth processus zygomatico-maxillaris and a well-developed processus frontalis are visible dorsally (Fig. X-6E). The dorsal margin of the pars facialis is almost straight. A weakly-pronounced notch is visible on the midline of the medial (= inner) surface of the pars facialis (Fig. X-6E). This notch was also observed in non-articulated maxillae in *Thaumastosaurus* (Roček and Lamaud, 1995; Vasilyan, 2018). The recessus vaginiformis is overlapped by a medial crista extending up to the tip of the processus frontalis. Anteriorly, the fossa maxillaris is shallow (Fig. X-6D).

The ventral margin of the lamina horizontalis delimits the base of the crista dentalis up to a triangular anterior facet of the maxillae in medial view (articulation of the premaxilla; Roček and Lamaud, 1995: fig. 6D). The teeth are present, but they are difficult to discern on either maxilla and it is not possible to determine if the tooth crowns are uni- or bicuspid, and whether or not they were pedicellate. However, Holman and Harrison (2002) described a partial maxilla attributed to *Thaumastosaurus*, where the teeth are pedicellate and bicuspid. The pedicellate condition was also retrieved in another partial maxilla (Holman and Harrison, 2003). The tooth row ends anterior to the posterior margin of the lamina horizontalis.

The anteriormost portion of the right maxilla and therefore details about the end of the lamina anterior, the rostellum and the anterior extension of the crista dentalis, are not preserved.

The return of the mummy: *Thaumastosaurus*, an Eocene pyxicephalid from Western Europe

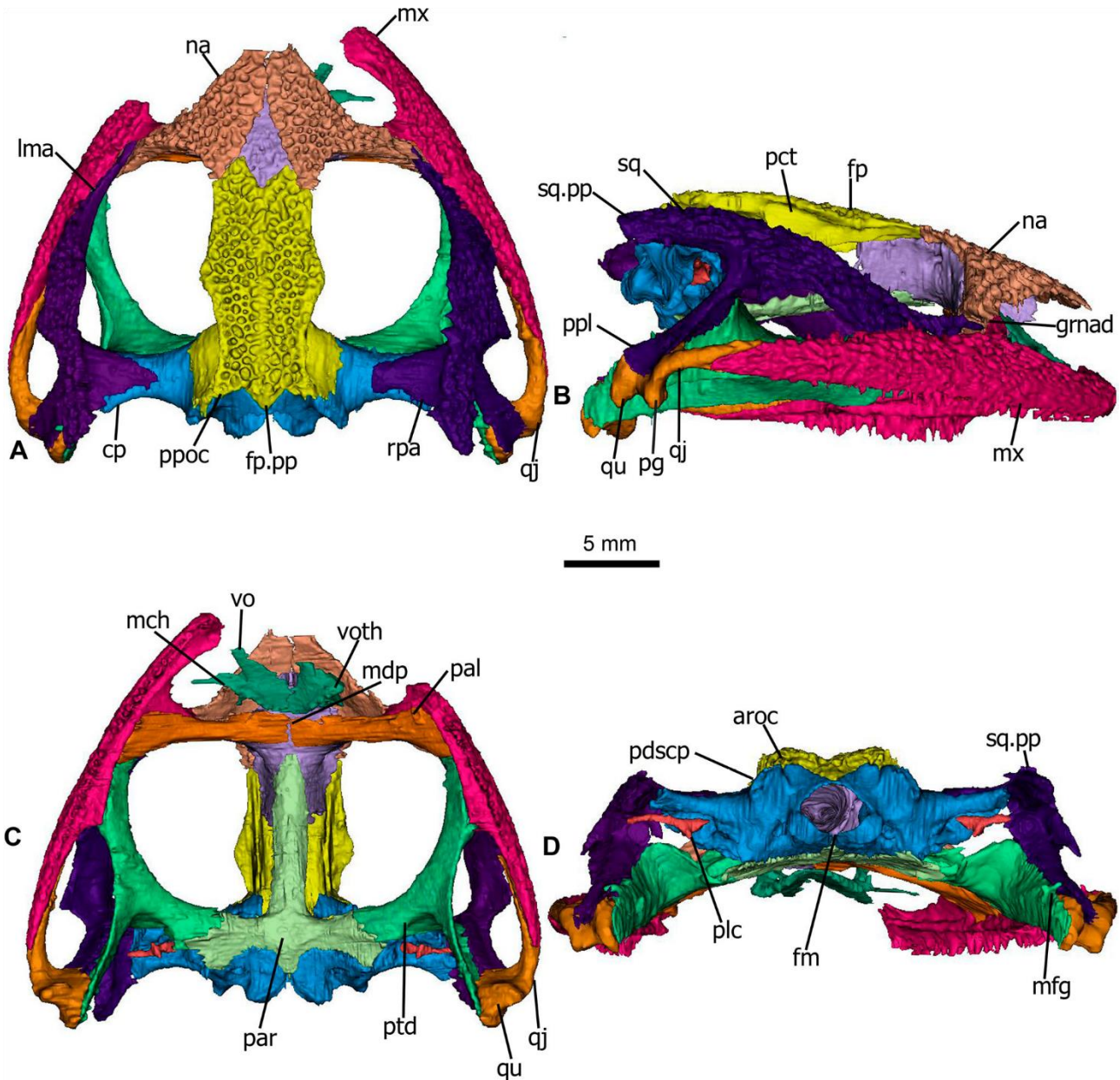


Figure X-5. The almost complete and articulated skull of the mummy MNHN.F.QU17381. Shown in **A** dorsal; **B** right lateral; **C** palatal and **D** posterior views. **Abbreviations:** aroc, canal for the arteria occipitalis; cp, crista parotica; fm, foramen magnum; fp, frontoparietals; fpp, posterior process of the frontoparietals; gnad, groove for the nasolacral duct; lma, lamella alaris; mch, choanal margin; mdp, medial process; mfg, medial flange; mx, maxilla; na, nasal; pal, palatine; par, parasphenoid; pct, pars contacta; pdscp, prominentia ducti semicircularis posterioris; pg, processus glenoidalis; plc, plectrum; ppl, processus posterolateralis; ppoc, processus prooticoccipitalis; ptd, pterygoid; qj, quadratojugal; qu, quadrate; rpa, ramus paroticus; sqpp, posterior process of the squamosal; vo, vomer; voth, vomerine teeth.

Nasals—The nasals are in close contact anteromedially and diverge from each other posteromedially, leaving the sphenethmoid exposed (Fig. 5A). This puts them in a

The return of the mummy: *Thaumastosaurus*, an Eocene pyxicephalid from Western Europe

transitory state between the condition found in the first mummy (MNHN.F.QU17279; Laloy et al., 2013), in which they are separated by an empty space, and the condition of MNHN.F.QU17376, where they are wholly fused, without midline sutures (Rage and Roček, 2007). The nasals are fused to the dorsal surface of the sphenethmoid. Both the maxillary and orbital margins are concave, with the processus paraorbitalis oriented posterolaterally at its distal end (Figs. X-5A, 6F). The processus paraorbitalis has no ornamentation distally, where it is delimited ventrally by the anterior extension of the lamella alaris of the squamosal to form a groove for the nasolacrimal duct (Figs. X-5B, 6F). The parachoanal process is a small protuberance, located at midlength of the maxillar margin (Fig. X-6F). The dermal sculpture of the nasals appeared to be more deeply pitted near the orbital margin.

Quadratojugals—The quadratojugals are elongate with an anterior slender and elongate processus jugularis. The quadratojugals articulate with the maxillae along a triangular facet, on the lateral side of the processus jugularis for nearly one half of the length of the quadratojugals (Figs. X-5B, 7A). In ventral view, the processus jugularis curves anteromedially and extends up to 80% of the lateral border of the pterygoid fossa. Posteriorly, the bone forms a thick bulge, extending medially, and with a medial groove on its posterior surface (Fig. X-5B). This bulge is interpreted as the quadrate (ossified portion of the palatoquadrate; Špinar, 1972; Duellman and Trueb, 1994; Roček, 2003). The palatoquadrate is mostly cartilaginous in anurans, but its posterior region can ossify as the quadrate. In anurans whose quadratojugals are present, the quadrates are fused to them, forming a quadratojugal+quadrate complex. The quadrate is overlapped posterodorsally by the posterolateral process of the squamosals and medially by the ramus posterior of the pterygoid. In MNHN.F.QU17279, it is also possible to see these ossified quadrates fused to the quadratojugals, with a thin suture visible between the two bones in ventral view (Laloy et al., 2013; fig. 3B).

The return of the mummy: *Thaumastosaurus*, an Eocene pyxicephalid from Western Europe

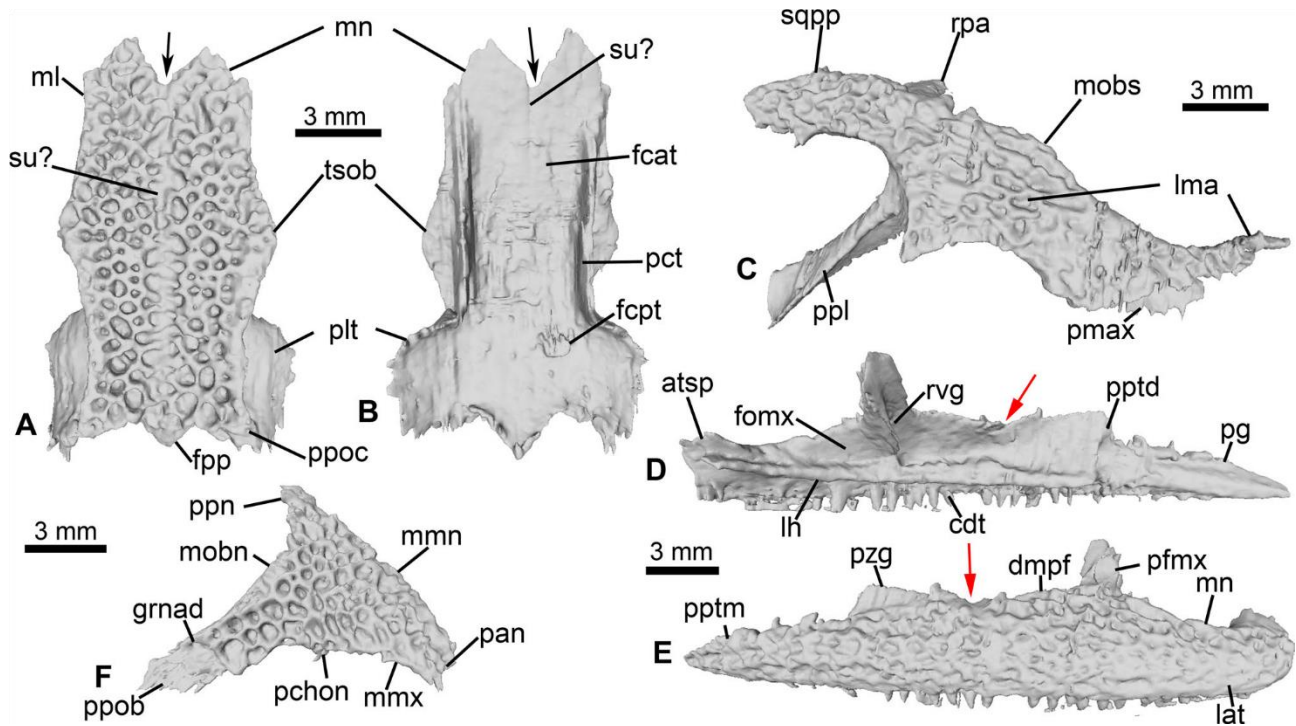


Figure X-6. Dermal bones from MNHN.F.QU17381. **A** frontoparietals in dorsal; **B** ventral views; **C** right squamosal in lateral view; **D** right maxilla in lateral; **E** medial views; **F** right nasal in lateral view. Red in arrow points to the notch on the dorsal margin of the pars facialis of the maxilla; black arrow points to the notch on the frontoparietal. **Abbreviations:** **atsp**, anterior spine; **cdt**, crista dentalis; **dmpf**, dorsal margin of the pars facialis of the maxilla; **fcat**, facies cerebralis anterior; **fcpt**, facies cerebralis posterior; **fomx**, fossa maxillaris; **fpp**, posterior process of the frontoparietals; **grnad**, groove for nasolacrimal duct; **lat**, lamina anterior; **lh**, lamina horizontalis; **lma**, lamella alaris; **ml**, lateral margin of the frontoparietals; **mn**, nasal margin; **mmx**, maxillar margin; **mmn**, medial margin of the nasals; **mobn**, orbital margin of the nasal; **mobs**, orbital margin of the squamosal; **pan**, processus anterior of the nasal; **pchon**, processus parachoanalis; **pct**, pars contacta; **pfmx**, processus frontalis; **pg**, posterior groove; **plt**, processus lateralis; **pmax**, processus maxillaris; **ppob**, processus paraorbitalis; **ppn**, posterior process of the nasals; **ppoc**, processus prooticoccipitalis; **pptm**, posterior process of the maxilla; **ppl**, processus posterolateralis; **pptd**, processus pterygoideus; **pzm**, processus zygomatico-maxillaris; **rvh**, recessus vaginiformis; **rpa**, ramus paroticus; **sqpp**, posterior process of the squamosal; **su?**, putative suture of the frontoparietals; **tsob**, tectum supraorbitale.

The return of the mummy: *Thaumastosaurus*, an Eocene pyxicephalid from Western Europe

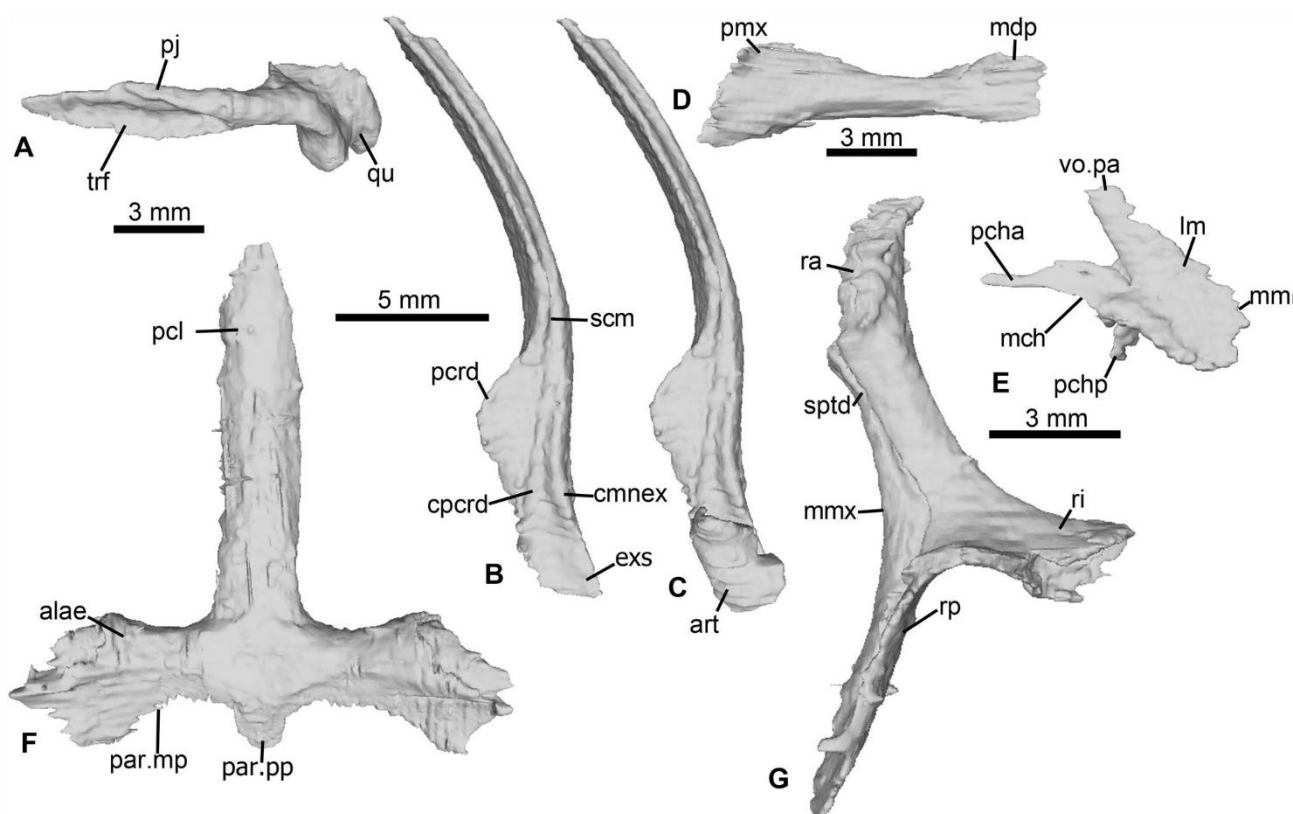


Figure X-7. Suspensorium and Palate bones from MNHN.F.QU17381. A left quadratojugal in lateral view; B right angulosplenial in dorsal view; C right angulosplenial and articular in dorsal view; D right palatine in ventral view; E right vomer in ventral view; F parasphenoid in ventral view; G left pterygoid in dorsal view. **Abbreviations:** *alae*, alae of the parasphenoid; *art*, articular; *cpcrd*, crista paracornoidea; *cmnex*, crista mandibulae externa; *exs*, extremitas spatulata; *lm*, lamina medialis; *mch*, choanal margin; *mdp*, medial process; *par.pp*, posterior process of the parasphenoid; *par.mp*, posterior margin of the parasphenoid; *pcha*, processus choanalis anterior; *pchip*, processus choanalis posterior; *pcrd*, processus coronoideus; *pclr*, cultriform process; *pj*, processus jugularis; *pmx*, processus palatinus maxillae; *qu*, quadratum; *mmx*, maxillar margin; *mm*, medial margin; *ra*, ramus anterior; *ri*, ramus interior; *rp*, ramus posterior; *scm*, sulcus pro cartilagine Meckeli; *sptd*, sulcus pterygoideus; *trf*, triangular facet; *vo.pa*, processus anterior of the vomer.

Suspensory Bones

Angulosplenials—Both angulosplenials are incompletely preserved. The left angulosplenial represents less than $\frac{1}{4}$ of the whole bone (compared to the one described in Laloy et al., 2013), and the right one represents around $\frac{2}{3}$ of a complete angulosplenial. The processus coronoideus is dorsoventrally oriented as an oval flattened plate, whereas the crista paracornoidea is poorly developed (Fig. X-7B). The crista mandibulae externa is marked laterally. The groove for Meckel’s cartilage is visible on the lateral side of the angulosplenial where it widens posterodorsally (extremitas spatulata, Fig. X-7B). In dorsal

The return of the mummy: *Thaumastosaurus*, an Eocene pyxicephalid from Western Europe

view, the articular is preserved in the posterior region of the bone. Remaining mandibular bones are not preserved in this specimen.

Articular—This bony element forms, with the quadrate, the jaw joint in anurans (Roček et al., 2016). The articular is an irregularly shaped, anteroposteriorly elongate element (Fig. X-7C). The poor ossification of this element made it difficult to delineate from the surrounding matrix in the CT data. The articular is in ventral contact with each angulosplenic but is not fused to this element. It is covered dorsally by the quadratojugal+quadrate. The quadrate and articular are not in contact, but this might be due to poor ossification/preservation of the two elements.

Palate Bones

Palatines—The palatines (neopalatines of Trueb, 1973) are elongate, dorsoventrally flattened, sub-cylindrical elements that are oriented perpendicular to the sagittal axis of the skull. In ventral view, the paired palatines articulate medially in the midline of the sphenethmoid (slightly separated by a very narrow fissure), as in MNHN.F.QU17376 (Rage and Roček, 2007). The processus palatines maxillae extends posterolaterally on the palatoquadrate groove of the maxilla (Figs. X-5C, 7D). The medial process ventrally contacts the lateral process of the sphenethmoid and nearly contacts the anterior tip of the parasphenoid posteriorly.

Vomers—Both vomers are preserved in situ and articulate with the ventral face of the sphenethmoid and with each other by their lamina medialis, forming a flat lamina that extends posteromedially (Fig. X-5C). The medial margin is convex and almost in contact with the palatine. The left vomer is damaged anterolaterally and at least half of it is missing; a few teeth are visible in ventral view (Fig. X-5C). Vomerine teeth were not visible on the right vomer during the segmentation, but their presence was observed by Laloy et al. (2013) in their segmentation of MNHN.F.QU17279. The anterior process extends anterolaterally towards, but fails to contact, the anterior spine of the lamina horizontalis of the maxilla. The processus choanalis anterior is very elongate and extends laterally without reaching the maxilla. The processus choanalis posterior is a small flattened lamina, with a crest extending

The return of the mummy: *Thaumastosaurus*, an Eocene pyxicephalid from Western Europe

dorsally (Fig. X-7E). The choanal margin (*margo choanalis* in Roček, 1994) is well-marked with an acute angle that indicates a moderately large choanal opening (Biton et al., 2016).

Parasphenoid—The parasphenoid is fused to the prooticocipital complex posterolaterally and to the sphenethmoid anteriorly. The cultriform process is long and slender, without any longitudinal ridges on its ventral surface. Posteriorly, the alae (*processus lateralis*) are short, lie perpendicular to the cultriform process, and bear a transversal and arched keel ventrally (Fig. X-7F). The posterior margin is curved (convex anteriorly) towards a short, medially borne spear-like posterior process. The parasphenoid is fused to the pterygoids by the anterolateral margin of the alae. This suture was difficult to discern during segmentation, but the alae are extensively overlapped by the ramus interior of the pterygoid anteriorly (Fig. X-5C).

Pterygoids—The pterygoids are of the standard triradiate shape for anurans (Fig. X-5A). The ramus posterior is an elongated vertical lamina (partly fused to the *processus posterolateralis* of the squamosal) in contact distally with the quadrate (Fig. X-5C). The ramus interior bears a posterodorsal flange that forms a part of the posterior wall of the orbit (Fig. X-5D). A deep sulcus extends dorsally from the ramus posterior to the ramus anterior on the maxillar margin called the *sulcus pterygoideus* (Fig. X-7G). The ramus

The return of the mummy: *Thaumastosaurus*, an Eocene pyxicephalid from Western Europe

anterior is well-developed, robust, and slightly flattened dorsoventrally.

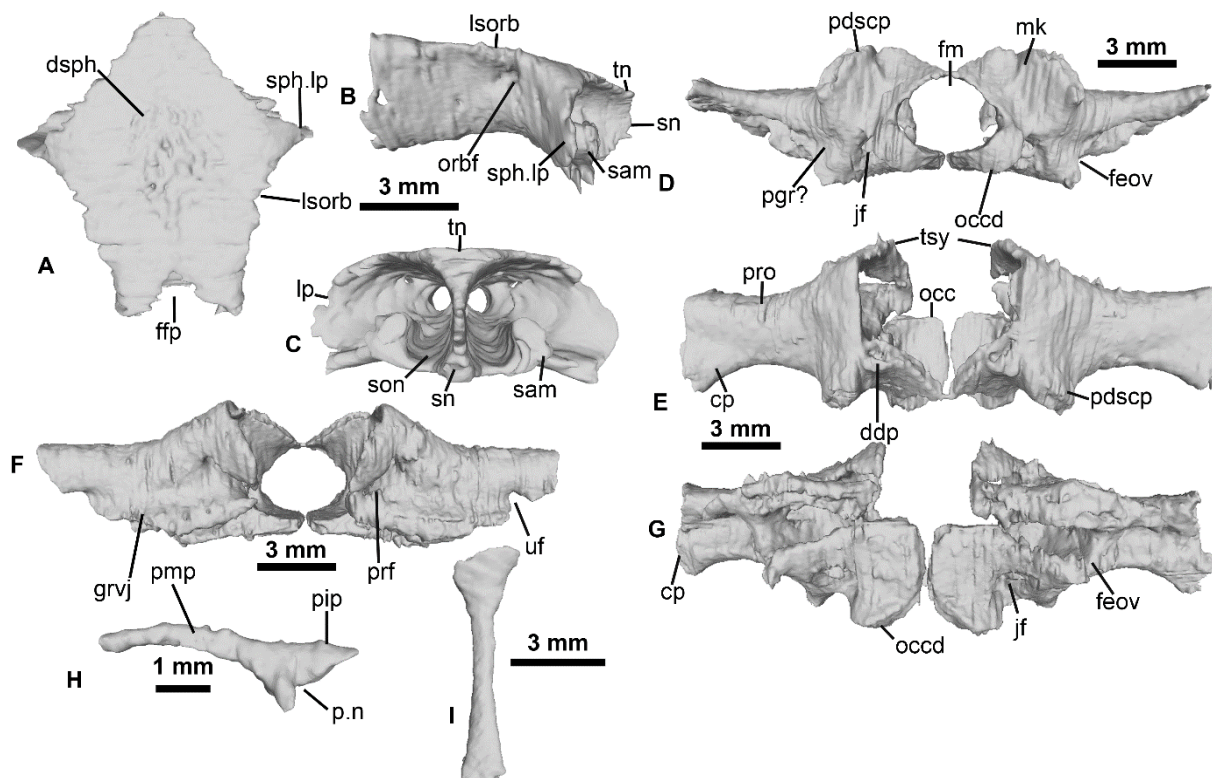


Figure X-8. Endocranial bones of MNHN.F.QU17381. A–C sphenethmoid in A dorsal; B right lateral and C anterior views; D–G prooticoccipital in D posterior; E dorsal; F anterior and G ventral views; H left stapes in posterior view; I right hyoid bone in dorsal view. **Abbreviations:** cp, crista parotica; dsph, dorsal exposure of the sphenethmoid; ddp, depression anterior to the prominentia ducti semicircularis posterioris of the prooticoccipital; ffp, fenestra frontoparietalis; feov, fenestra ovalis; jf, jugular foramen; fm, foramen magnum; grvj, groove for the vena jugularis; lsorb, lamina supraorbitalis; mk, median keel; occ, exoccipital; orbf, orbitonasal foramen; p.n, notch on the medial surface of the plectrum; pdscp, prominentia ducti semicircularis posterioris; pgr?, putative perilymphatic groove; pip, pars interna plectri; pmp, processus medialis plectri; prf, prootic foramen; pro, prootic; sam, sella amplificans; sn, septum nasi; son, solum nasi; sph.lp, lateral process of the sphenethmoid; tn, tectum nasi; tsy, tectum synotium; uf, unknown foramen?.

Endocranium

Sphenethmoid—The sphenethmoid is an unpaired bone, pentagonal in dorsal view. Most of its dorsal surface is overlapped by, and fused to, the nasals and frontoparietals. The exception is a small, rhomboid, median part that is visible dorsally (Fig. X-5A). This exposure is covered with low and poorly defined ornamentation composed of pits and ridges, nearly identical to the one covering the dermal bones (Figs. X-5A, 8A). In extant anurans, the ornamentation of the sphenethmoid (and other bones as well) thickens during growth and thus serves as an ontogenetic marker (Buffrénil et al., 2015, 2016). An even

The return of the mummy: *Thaumastosaurus*, an Eocene pyxicephalid from Western Europe

weaker ornamentation characterizes MNHN.F.QU17279 (Laloy et al., 2013), indicating that it is less mature than our specimen.

Among extant anurans, a dorsal exposure of the sphenethmoid occurs in various taxa (Duellman and Trueb, 1994; Paluh et al., 2020). However, this dorsal exposure is rarely ornamented like the neighboring dermal bones (e.g. *Aubria masako*, where the dorsal exposure is reduced to a minute rhomboidal fenestra, devoid of ornamentation). In addition, the dorsal exposure is reduced or absent in most extant or extinct hyperossified taxa (Duellman and Trueb, 1994; Sheil, 1999; Nicoli, 2019; Paluh et al., 2020), where the nasals and frontoparietals overlap the sphenethmoid. In contrast, the exposure in MNHN.F.QU17381 is rather large.

An exposed and ornamented sphenethmoid occurs in extant hylids (casque-headed tree frogs) from South America, Pelobatidae and Bombinatoridae (Trueb, 1970; Roček, 1980; Smirnov, 1997). Analysis of the ontogeny and skeletogenesis of this region in Hylidae and Bombinatoridae has shown the presence of a dermal bone called the dermal sphenethmoid (Trueb, 1966, 1970; “internasofrontal”, Smirnov, 1997). This rhomboidal neomorphic element develops by intermembranous ossification in the lower dermis (Trueb, 1966) and then cossifies with the sphenethmoid to form a single bone mass (Trueb, 1966, 1970; Smirnov, 1997). The presence of this bone is contested in Pelobatidae (Roček, 2003), as the sphenethmoid can be covered by adjacent dermal bones. Periosteal ossification of the sphenethmoid could also result in a secondary ornamentation such as for the neighboring nasals and frontoparietals. The presence of a dermal sphenethmoid is highly speculative in MNHN.F.QU17381, as it can only be differentiated in premetamorphic specimens (Trueb, 1970).

Anteriorly, the bone is divided into two chambers (cavitas nasalis) separated medially by the bony septum nasi (Fig. X-8C). The sphenethmoid is elongate posteriorly, reaching close to the mid-level of the cultriform process of the parasphenoid (Fig. X-5C). Despite the overall hyperossification of the skull, the sphenethmoid does not reach the prooticooccipital, leaving a part of the lateral walls of the braincase unossified.

The return of the mummy: *Thaumastosaurus*, an Eocene pyxicephalid from Western Europe

Posteriorly, the dorsal fenestra frontoparietalis forms a notch for the insertion of the facies cerebralis anterior (Fig. X-8A) of the frontoparietals, bearing a dorsal impression of the forebrain. Ventrally, the sphenethmoid is fused to the anterior tip of the parasphenoid and to the palatines. The lateral processes are distally short, with the posterior wall extending slightly laterally (Fig. X-8A). The dorsal surface of these processes extends slightly posterolaterally to form a poorly developed lamina supraorbitalis (Fig. X-8A). The lateral wall of each anterior chamber is pierced by an orbitonasal foramen, which conveyed the ophthalmic nerve (canalis ramus medialis nervi ophthalmici) into a large cavitas nasalis (= anterior chamber) (Fig. X-8B).

Several portions of the anterior sections of the sphenethmoid are partially ossified, which is characteristic of hyperossification. The septum nasi is ossified, without any anterior thickening, reaching the anterior part of the nasals (Fig. X-8C), and the tectum nasi is oriented anterodorsally, forming a triangular flattened area in dorsal view (Fig. X-8A). The solum nasi (ventral surface of the cavitas nasalis) bears a broad dorsal prominence, the sella amplificans (Fig. X-8C). The surface of the solum nasi and septum nasi appears smooth in the segmentation. This most likely indicates that a cartilaginous part was present (Roček and Lamaud, 1995; Duellman and Trueb, 1994). The rest of the anterior part of the sphenethmoid was most likely cartilaginous or poorly ossified, and therefore neither the postnasal wall nor anterior wall of the nasal capsule were preserved. In ventral view, the sphenethmoid is subcruciform, with the lateral expansion of the anterior chamber perpendicular to both the posterior chamber and the bony anterior extension of the septum nasi.

Prooticooccipital Complex—The prootic, occipital and exoccipital are fused into a single complex that constitutes the posterior part of the braincase and skull (Fig. X-5D). The otic capsules are poorly ossified ventrally, as indicated by their irregular ventral surface (Fig. X-8G).

The foramen magnum is large and oval (slightly compressed dorsoventrally). The two occipital condyles are crescentic, with a small dorsal ridge connecting them to the prominentia ducti semicircularis posterioris (Fig. X-8D). The latter is naturally flattened

The return of the mummy: *Thaumastosaurus*, an Eocene pyxicephalid from Western Europe

mediolaterally and extends as an elongate protuberance oriented ventrolaterally. The prominentia ducti semicircularis are flanked medially by a depression (oriented dorsoventrally) that is delimited dorsally by a small median keel (Fig. X-8D). This keel is similar to one found in MNHN.F.QU17376 (Rage and Roček, 2007: fig. 5B) and NHMB V.R31 (Vasilyan, 2018: fig. 3) but this keel was not visible in MNHN.F.QU17279 (Laloy et al., 2013). Two large jugular foramina are partially hidden in posterior view by the occipital condyles (Fig. X-8D). They open in the lateral wall of the cavum cranii and in the otic capsule. The fenestra ovalis is located on the lateral wall of the prootic (Fig. X-8D).

Dorsally, the crista parotica extends laterally into a dorsoventrally flattened processus (ramus lateralis sensu Špinar, 1978) (Fig. X-8D–E). A horizontal groove (perilymphatic groove in Fig. X-8) extends laterally from the jugular foramen on the posterior surface of the otic capsules and might have housed a perilymphatic canal. This groove is visible in both specimens MNHN.F.QU17279 and MNHN.F.QU17376 (Rage and Roček, 2007; Laloy et al., 2013). The parietal fenestra is large and completely covered dorsally by the frontoparietals.

Anteriorly, the prootic foramen is large and undivided (unlike in MNHN.F.QU17376; see Rage and Roček, 2007: fig.7). The groove for the vena jugularis is visible, extending from this foramen to the lateral margin of the anterior surface of the prooticooccipital. This groove is shallow and poorly delimited (Fig. X-8F), making it similar to the groove in MNHN.F.QU1376 (Rage and Roček, 2007: fig. 7A), and slightly different from that of MNHN.F.QU17279 (Laloy et al., 2013). On the left side of the prooticooccipital, the groove for the vena jugularis ends laterally in a small notch on the lateral side of the prootic. In MNHN.F.QU17376 and two other incomplete braincases of *Thaumastosaurus* (see Rage and Roček, 2007: fig. 7), two unidentified foramina penetrate the anterior surface of the prooticooccipital, piercing the groove for the vena jugularis. In two of the braincases (Rage and Roček, 2007: fig. X-7A, C), the most lateral of these foramina forms a notch on the lateral border of the prootic, in a similar location to the notch in MNHN.F.QU17381. These foramina are not known in MNHN.F.QU17279 (Laloy et al., 2013). Medial to the anterior surface of the prominentia ducti semicircularis posterioris, a small depression is present, as

The return of the mummy: *Thaumastosaurus*, an Eocene pyxicephalid from Western Europe

in MNHN.F.QU17279 (Fig. X-8E). This small depression might be another part of the otic canals.

The lateral wall of the cavum cranii is pierced by three foramina. As mentioned earlier, the posteriormost foramen is connected to the jugular foramen. A large, irregularly-shaped opening that leads to the otic capsules is present ventrally at approximately the midlength of the lateral wall. We interpret this single opening to have conveyed both branches of the acoustic nerve (Duellman and Trueb, 1994; Rage and Roček, 2007) whose specific bony paths are not visible due to poor preservation in this region of the otic capsule. A small rounded foramen, dorsal to this irregular opening, is interpreted as the perilymphatic foramen.

Columellae—Only the ossified portion of the columellae, the plectrum (~stapes), was identified and segmented. Both preserved plectra have the same orientation and position on each side of the braincase, implying they are in anatomical position. The posterior region of the plectrum is bifurcated, with a notch on its medial margin (Fig. X-8H). This posterior region is interpreted as the ossified pars interna plectri ('footplate' of Duellman and Trueb, 1994), with the notch on the medial surface serving as an insertion point for the cartilaginous operculum (Bolt and Lombard, 1985; Roček et al., 2016). The pars media plectri is a curved, slender rod that extends laterally between the posterior and posterolateral processes of the squamosal, where the tympanic annulus is located in anurans (Duellman and Trueb, 1994; Sheil, 1999; Roček et al., 2016). The tympanic annulus has not been identified in MNHN.F.QU17381 and MNHN.F.QU17279, although a tympanic membrane was identified in the latter specimen (Fig. X-4C), implying that a cartilaginous tympanic annulus was present (Pereyra et al., 2016). As MNHN.F.QU17381 is attributed to the same taxon (see in Taxonomy), we conclude that a tympanic annulus was present in MNHN.F.QU17381.

Hyobranchial Skeleton

Hyoid Bones—The cartilaginous hyoid plate is not visible in the scan data. However, two slender bony elements, the thyrohyal bones, corresponding to the posteromedial processes of hyoid plate, are present. The two elements are oriented anteromedially with their

The return of the mummy: *Thaumastosaurus*, an Eocene pyxicephalid from Western Europe

proximal parts almost in contact. They widen at both ends (proximal and distal; Fig. X-8I). They are placed ventrally under the first three vertebrae and the exoccipital, and dorsal to the coracoids and clavicle.

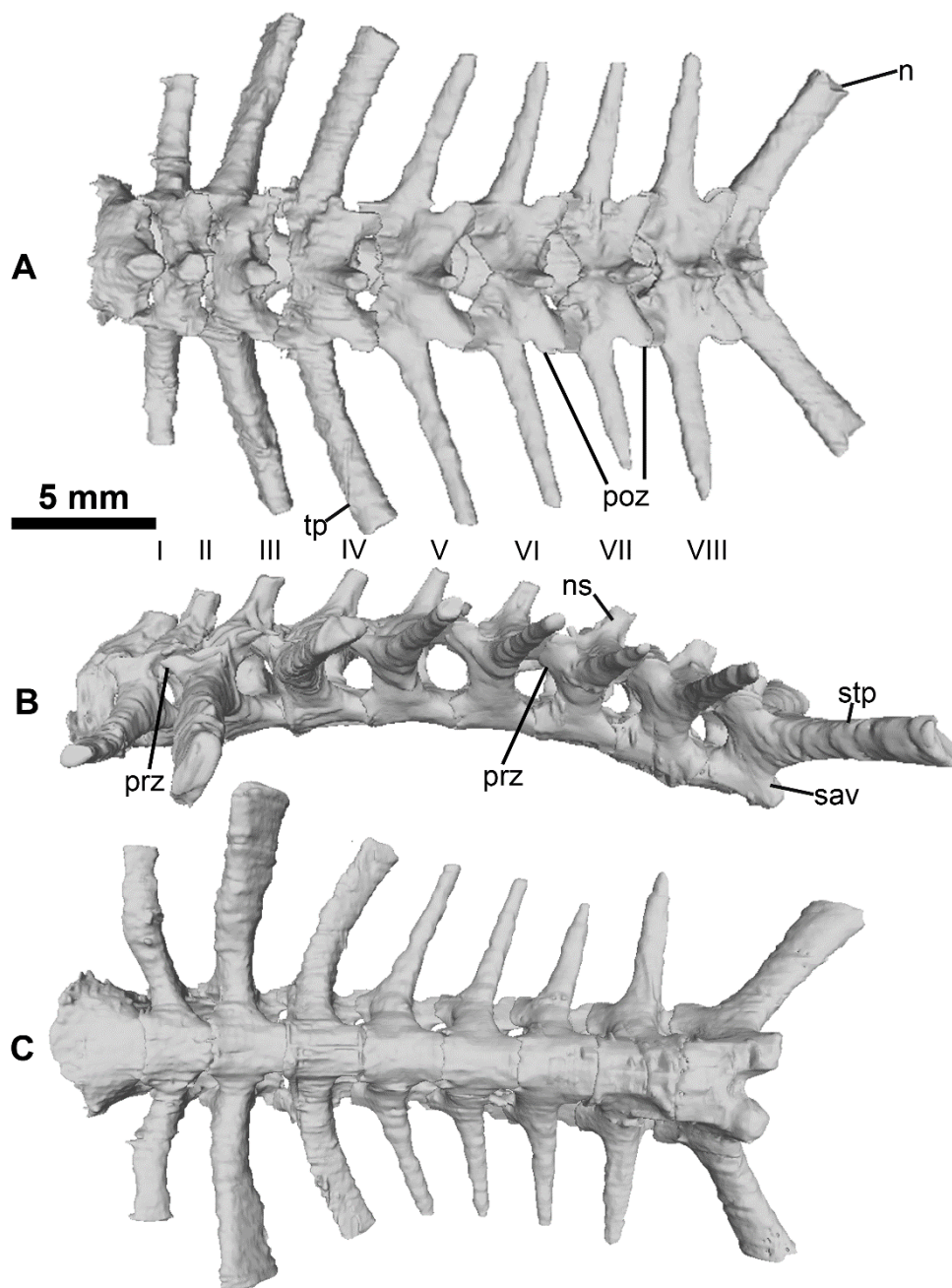


Figure X-9. Articulated diplasiocoelous vertebral column of MNHN.F.QU17381, without the urostyle in **A** dorsal; **B** left lateral and **C** ventral views. **Abbreviations:** **ns**, neural spine; **n**, notch on the sacral apophyse; **poz**, postzygapophysis; **prz**, prezygapophysis; **sav**, sacral vertebrae; **stp**, sacral transverse process; **tp**, transverse process.

The return of the mummy: *Thaumastosaurus*, an Eocene pyxicephalid from Western Europe

Vertebral Column

The vertebral column is similar to the one found and described inside the mummy by Laloy et al. (2013). It is composed of eight presacral vertebrae, one sacral vertebra and an urostyle (Fig. X-9). The seven first presacral vertebrae are procoelous (anterior cotyle and posterior condyle; Fig. X-10A, B) and the last presacral (eight vertebra) is biconcave (Fig. X-10C), indicating an amphicoelous condition. The sacral vertebra is biconvex, with an anterior cotyle and two posterior cotyles (Fig. X-10D, E). These conditions of the presacral and sacral vertebrae are characteristics of a diplasiocoelous vertebral column.

Atlas—The atlas articulates with the exoccipitals by two large and laterodorsal-ventromedially elongated cotyles (Fig. X-10A), which fuse medially to a protruding lip at the midline, forming a large articular facet with the skull (type III of Lynch, 1971). The vertebral canal is large, with thin lateral walls and thicker ventral and dorsal walls; the latter forms a large base for the short and posteriorly inclined neural spine (Fig. X-9B). The postzygapophyses are poorly developed, with a flattened articular surface inclined medioventrally. The centrum is flattened dorsoventrally and possesses a small elliptical condyle in posterior view (Fig. X-10B).

Post-atlantal Vertebrae—The centra of the post-atlantal vertebrae are longer than wider and flattened dorso-ventrally (Fig. X-9B–C). The centrum of vertebrae II–VII is concave anteriorly and convex posteriorly, indicating a procoelous condition. No vertebra bears ribs. In lateral view, the neural arch is thin, anteriorly notched, with an enlarged base (Fig. X-9B). Arches are non-imbricated. The vertebral canal remains broad until the fifth post-atlantal vertebra. The neural spines are dorsally elongated and inclined posteriorly, but do not extend beyond the posterior margin of the postzygapophysis. The posteriormost post-atlantal vertebrae (vertebra VI to VIII) possess a shorter neural spine, which are oriented less posteriorly. The zygapophyses have flat articular processes.

The first post-atlantal vertebra (Vertebra II) possesses a pair of large transverse processes, a bit shorter than the sacral transverse processes. In dorsal and ventral views, this first pair of transverse processes are slightly posteriorly arched (Fig. X-9A, C). The processes

The return of the mummy: *Thaumastosaurus*, an Eocene pyxicephalid from Western Europe

are thicker at their mid-length, with a crest appearing on the anterior face. The second post-atlantal vertebra (Vertebra III) possesses the largest transverse processes. They are oriented posterolateroventrally and are moderately widened distally. The transverse processes of vertebra IV have the same distal extension as the sacral apophyses and are oriented lateroposteriorly. The presacral vertebrae V–VII are similar in possessing transverse processes that are thinner and narrower distally than proximally. On vertebra V, they are slightly oriented posterodorsally (Fig. X-9B). On vertebrae VI and VII, they are roughly perpendicular to the long axis of the column. Presacral vertebra VIII bears thin transverse processes similar to the one of the previous presacral vertebrae. However, this vertebra is amphicoelous.

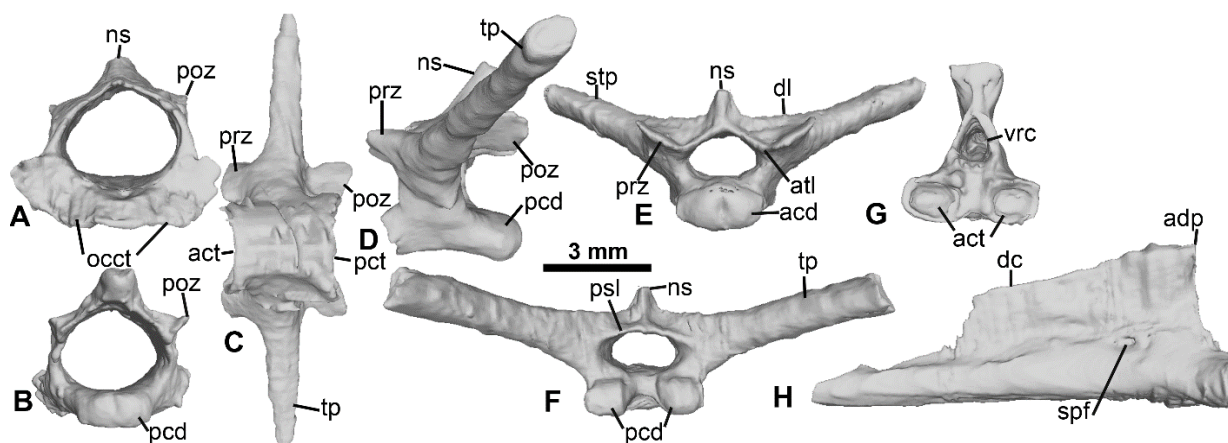


Figure X-10. Vertebral elements of the column of MNHN.F.QU17381. A–B atlas in A anterior and B posterior views; C VIII presacral vertebra in ventral view; D–F sacral vertebrae in D lateral; E anterior and F posterior views; G–H urostyle in G anterior and H lateral views. **Abbreviations:** **acd**, anterior condyle; **act**, anterior cotyle; **adp**, anterodorsal process; **atl**, anterior lamina; **dc**, dorsal crest; **dl**, diapophyseal lamina; **ns**, neural spine; **occt**, occipital cotyle; **pcd**, posterior condyle; **poz**, postzygapophysis; **prz**, prezygapophysis; **psl**, posterior lamina; **stp**, sacral transverse process; **vrc**, vertebral canal.

Sacral Vertebra—The sacral vertebra possesses two small, well-separated, posterior circular condyles that articulate with the urostyle, and one dorsoventrally flattened elliptical anterior condyle that articulates with the posterior cotyle of the last presacral vertebra (Fig. X-10D–F). On the anterodorsal border of the neural arch, a well-developed lamina extends from the base of the prezygapophyses to the base of the neural spine (Figs. X-9A, 10D). This kind of lamina is also present on the posterior border of the neural arch (Fig. X-10D–E). The sacral transverse processes are subcylindrical in cross section, slightly flattened

The return of the mummy: *Thaumastosaurus*, an Eocene pyxicephalid from Western Europe

dorsoventrally, and do not widen posterodistally. A small notch is visible dorsally at the distal margin of each transverse process (Fig. X-9A). The neural spine is reduced and anterodorsally oriented.

Urostyle—The urostyle is posteriorly incomplete. The anterior portion of the bone is articulated with the sacral vertebra with two well-separated circular anterior cotyles (fossa cotylae), which protrude laterally from the main shaft of the urostyle (Fig. X-10G). The vertebral canal is moderately high, accounting for half the height of the neural arch. The neural arch bears a well-developed thick dorsal process. This also marks the cranial end of a tall and thin dorsal crest that extends throughout the whole preserved portion of the bone and slightly decreases in size posteriorly (Fig. X-10H). A spinal foramen is present on each side of the base of the dorsal crest, posteroventrally to the thick dorsal process (Fig. X-10H). No transverse processes are present.

The return of the mummy: *Thaumastosaurus*, an Eocene pyxicephalid from Western Europe

Pectoral Girdle

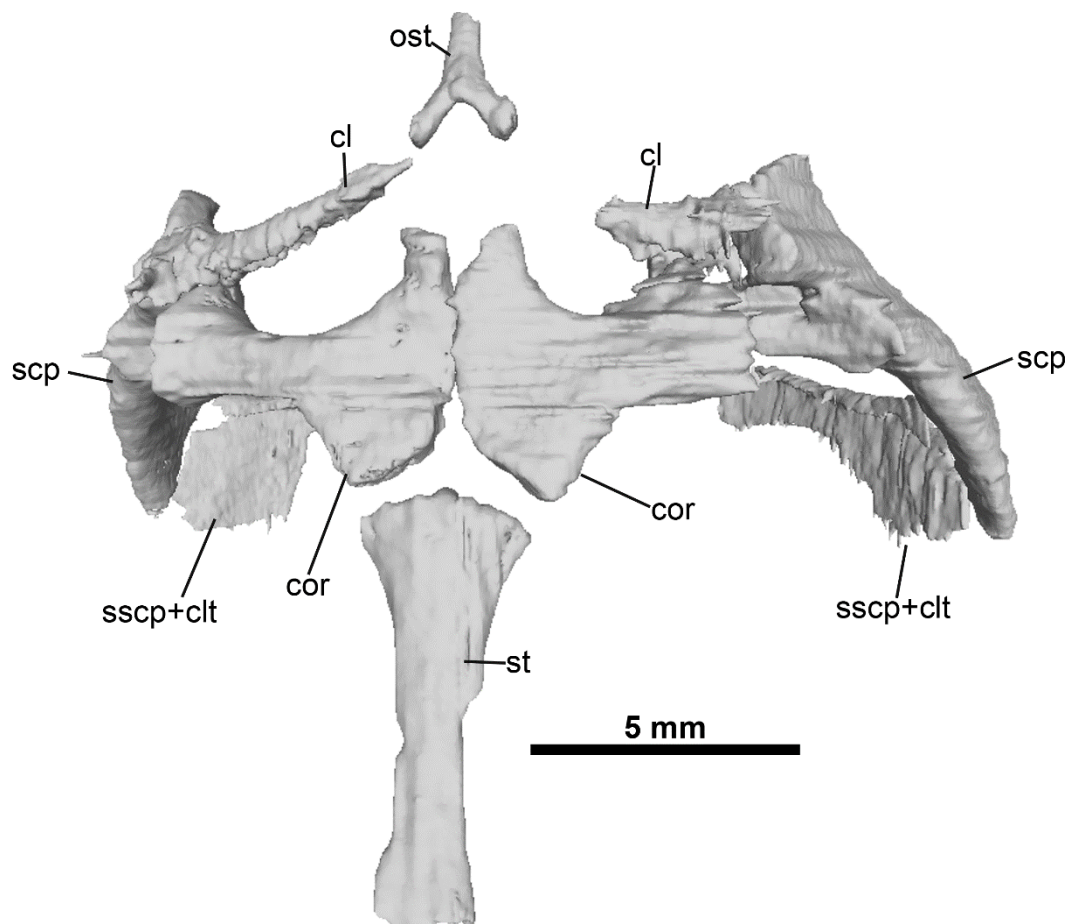


Figure X-11. Articulated bony pectoral girdle of MNHN.F.QU17381 in ventral view. Abbreviations: cl, clavicle; cor, coracoid; ost, omosternum; scp, scapula; sscp+clt, suprascapular+cleithrum; st, sternum.

All pectoral bony elements are present in anatomical position (Fig. X-11).

Cleithra-Suprascapulae Complexes—The cleithrum and the ossified portion of the suprascapula are fused together, forming a single compound element dorsomedial to the scapula. The cleithrum represents the anterior thickened portion of the compound, and the suprascapular (a mostly cartilaginous element) is ossified on its ventral and posterior margins (Fig. X-12A, B). The ramus anterior of this compound bone is long with a thickened anterior margin by the presence of a long lamina recurvata (sensu Špinar, 1972). The

The return of the mummy: *Thaumastosaurus*, an Eocene pyxicephalid from Western Europe

margines scapularis and posterior surface of the compound are rounded. There is no ramus posterior.

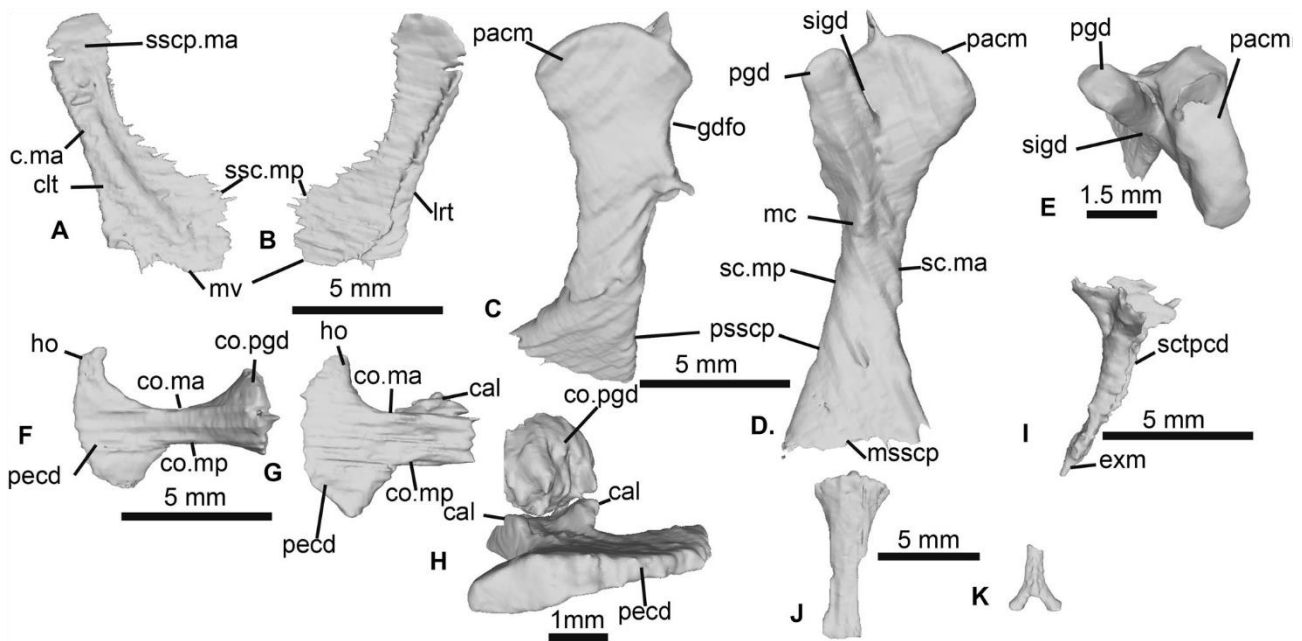


Figure X-12. Bony elements of the pectoral girdle of MNHN.F.QU17381. A–B left suprascapular + cleithrum complex in A lateral and B medial views C–E right scapula in C lateral; D medial and E ventral views (orientation follows Duellman and Trueb, 1996: 346, fig. 13-35); F right coracoid in dorsal view; G–H left coracoid in G ventral and H medial views; I right clavicle in dorsal view; J sternum in dorsal view; K omosternum in dorsal view. **Abbreviations:** cal, callus; clt, cleithrum; coma, anterior margin of the coracoid; comp, posterior margin of the coracoid; exm, extremitas medialis; gdfo, glenoid fossa; ho, hook; lrt, lamina recurvata; msscp, margo suprascapularis; mv, margo vertebralis; mc, medial crest; pacm, processus acromialis; pectd, processus epicoracoidalis, pgd, processus glenoidalis; psscp, processus suprascapularis; ra, ramus anterior; scma, anterior margin of the scapula; scmp, posterior margin of the scapula; sctpcd, sulcus cartilagine praecoracoidealis; sigd, sinus interglenoidalis; sspcma, anterior margin of the suprascapular+cleithrium.

Scapulae—The scapulae are transversally elongated, with a moderately widened distal end of the processus suprascapularis (Fig. X-12C, D). The anterior margin is concave (Fig. X-12C). There is no crest on both anterior or posterior margins of the scapulae. The processus acromialis and the processus glenoidalis are separated by a moderately wide sinus interglenoidalis (Fig. X-12E). The processus acromialis is wider than the processus glenoidalis and has a rounded lateral margin; in dorsal view, it hides the processus glenoidalis and the sinus interglenoidalis. In medial view, a well-developed medial crest is present on the processus glenoidalis and extends from the ventral border to the base of the

The return of the mummy: *Thaumastosaurus*, an Eocene pyxicephalid from Western Europe

processus anterior (Fig. X-12C). No lamina is present on the processus anterior. The glenoid fossa is moderately extended dorsoventrally (Fig. X-12C).

Coracoids—The coracoids are transversally oriented, with a thickened, cylindrical processus glenoidalis. This latter of both coracoids and scapulae are almost in contact with each other, leaving a gap for the paraglenoid cartilage. The processus epicoracoidalis is flat and anteroposteriorly enlarged (much larger than the processus glenoidalis) and bears a convex medial margin (Fig. X-12F). The processus epicoracoidalis extends anteriorly, forming a hook that extends close to the medial end of the clavicles. Both coracoids are in contact with each other medially, but do not overlap (Fig. X-11). This is characteristic of a firmsternal condition (sensu Cope, 1864; Boulenger, 1886). The left coracoid is badly damaged, with the processus glenoidalis broken off from the main shaft (Fig. X-12G–H). On the anterior and posterior margins of the main shaft, vertical laminae can be observed, forming a bony callus linking the two broken parts. This callus is also visible in ventral view, expanding the width of the shaft of the coracoid (Fig. X-12G–H). This damage can be linked to the missing part of the left clavicle. The near-absence of disarticulated bones (except the ilia) and the presence of a mineralized skin on this part of the specimen seems to exclude the diagenesis hypothesis. The absence of any hole indicating a missing part in the area of the coracoid and clavicle (the nearest holes are located anteriorly on the ventral face of the specimen) excludes the extraction hypothesis. This leaves only the hypothesis of a damage received before the burial of the animal. In extant anurans, the healing process for bone fractures is slow compared to mammals (Cameron et al., 2012; Egawa et al., 2014). Given that the broken coracoid seems partially fused back and bears a bony callus, this may represent a scar from a wound received during the life of the animal.

Clavicles—The right clavicle is completely preserved, whereas the left clavicle only preserves its lateral part (Fig. X-11). This could be linked to the injury visible on the left coracoid. The clavicles are almost as long as the coracoids and slightly arched anteriorly. In dorsal view, the lateral part is bifurcated and articulates with the processus acromialis and processus glenoidalis of the scapulae, forming a part of the articular fossa for the humeri. The sulcus cartilagine praecoracoidealis extends posteriorly on the length of the bone (Fig.

The return of the mummy: *Thaumastosaurus*, an Eocene pyxicephalid from Western Europe

X-12I). The clavicles are in contact, slightly overlapping dorsoventrally the processus glenoidalis of the coracoids. The extremitas medialis of the clavicle is not in contact with the medial part of the coracoids (Fig. X-11).

Sternum—The sternum is fully ossified as an elongate slender element. The sternum is expanded both anteriorly and posteriorly with the former being larger than the latter. (Fig. X-12J). It is strongly similar to the one found in *Pyxicephalus adpersus* (Sheil, 1999: fig. 5B).

Omosternum—The omosternum is ossified, denoting a firmisternal condition of the girdle (Cope, 1864; Boulenger, 1886; Duellman and Trueb, 1994). It is an inverted “Y”-shaped bone with a bifurcated posterior end (Fig. X-12K).

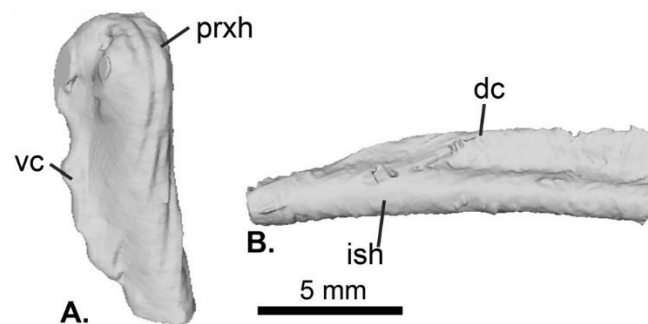


Figure X-13. Humerus and Ilium of MNHN.F.QU17381. A left humerus in lateral view; **B** right ilium in lateral view. **Abbreviations:** **dc**, dorsal crest; **ish**, iliac shaft; **prxh**, proximal head; **vc**, ventral crest.

Forelimb

Humeri—Only the proximal parts of both humeri are preserved, although badly damaged. Only the proximal articular facet of the right humerus is preserved with the glenoid fossa of the pectoral girdle. The left humerus, however, is more completely preserved, with both its proximal head and part of the diaphysis (Fig. X-13A). The left humerus displays a moderately developed crista ventralis, and lacks a proximal crista paraventralis (Fig. X-13A).

The return of the mummy: *Thaumastosaurus*, an Eocene pyxicephalid from Western Europe

Pelvic Girdle

Ilia—The two ilia are partially preserved. The left one is only a fragment of the distal part (around 1.4 mm in length), but the right one is more completely preserved, which represents about half or more of the complete iliac shaft (= ilial shaft of Gómez and Turazzini, 2016). It bears a high and well-developed dorsal crest (Fig. X-13B). Unfortunately, the rest of the ilium (distal half) is not preserved, as in the first mummy (MNHN.F.QU17279; Laloy et al., 2013).

X.6 Taxonomy

MNHN.F.QU17381 is the holotype and only known specimen of *Bufo servatus*, erected and illustrated by H. Filhol (1876; 1877: pl. 51; fig. 412) based on a first description done in 1873 (Filhol, 1873). Filhol named the specimen *Bufo servatus* (Filhol, 1876) without giving characters to diagnose the taxon or differentiate it from the other *Bufo* species. He placed it in Bufonidae based on the presence of parotoid glands (see Filhol, 1876, 1877). Martín et al. (2012) considered the name *B. servatus* as valid and did not discuss the criteria of validity. Sanchiz (1998) considered the name a nomen vanum (Mones, 1989), a taxonomic term considered in the ICZN as referring to a name based on a type inadequate for definitive diagnosis, but he did not question its validity. Our work shows that the specimen is informative, hence *B. servatus* cannot be a nomen vanum. The specimen has been figured, and according to the article 12.2.7 of the International Code of Zoological Nomenclature (ICZN), this supports the validity of a name if published before 1931. The name *B. servatus* can therefore be considered as valid. Moreover, this name has been cited several times since its original description (Piveteau, 1927; Tihen, 1962; Sanchiz, 1998; Rage, 2006) and its validity was not often discussed.

Attribution to *Bufo* was based on the presence of what Filhol identified as two parotoid glands located right behind the eyes (Filhol, 1876, 1877). However, several studies (Piveteau, 1927; Tihen, 1962; Rage, 2006, 2016) considered this observation as erroneous. We

The return of the mummy: *Thaumastosaurus*, an Eocene pyxicephalid from Western Europe

here confirm this proposition and suggest that the structures interpreted by Filhol as parotoid glands are artefactual skin ridges caused by post-mortem desiccation during the natural mummification process. In addition, on specimen MNHN.F.QU17381, we observed teeth on the maxillary, which are lost in Bufonidae (Duelleman and Trueb, 1994). Moreover, the vertebral column is diplasiocoelous, which is characteristic of Ranoidea. Finally, the presence of a firmisternal pectoral girdle as well as an ossified omosternum also reinforce the attribution to a ranoid taxon. We therefore conclude that MNHN.F.QU17381 cannot be attributed to Bufonidae or *Bufo*. Furthermore, the skeleton of specimen MNHN.F.QU17381 is almost morphologically identical to the one of MNHN.F.QU17279 and to the skull of MNHN.F.QU17376, both of which have been attributed to the genus *Thaumastosaurus* as *T. gezei* (Roček and Lamaud, 1995; Laloy et al., 2013). We therefore attribute the specimen MNHN.F.QU17381 to *Thaumastosaurus* De Stefano, 1903 by the following combination of characters: (1) dermal bones covered with ornamentation that differs from the one found in *Latonia*, *Pelobates*, *Eopelobates* and *Ceratophrys*; (2) nasals (partially) and frontoparietals co-ossified with each other and with sphenethmoid and frontoparietals co-ossified with prooticooccipital; (3) rhomboid part of sphenethmoid exposed on skull roof; (4) no bony contact between the frontoparietal and squamosal; (5) anterior tip of the parasphenoid does not extend between palatines; (6) processus posterolateralis and ramus paroticus of squamosal merged, articulating with the crista parotica of the otic capsules (Rage and Roček, 2007; Vasilyan, 2018).

At the species level, MNHN.F.QU17381 differs from *Thaumastosaurus bottii* and *T. wardi* by having the lamella alaris of the squamosal extending anteriorly along the entire ventral margin of the orbit (lamella alaris ends anteriorly at the midlength of the orbit in *T. bottii* and *T. wardi*). However, the lamella alaris of the squamosal of the neotype of *T. bottii* (Roček and Lamaud, 1995: fig. 5) is almost entirely broken off, and the length of its anterior extension cannot be assessed. Other squamosals attributed to *T. bottii* are either broken or present as an eroded anterior part of the bone (Vasilyan, 2018: fig. 4G–H), making comparison difficult. This difference on the squamosals might only result from a different

The return of the mummy: *Thaumastosaurus*, an Eocene pyxicephalid from Western Europe

preservation, as no skull of *T. bottii* is as complete as the holotype of “*T. gezei*”. This difference is not attributed to ontogeny.

The specimen MNHN.F.QU17381 furthermore differs from *T. bottii* by having a shallow, poorly delimited groove for the vena jugularis interna on the prooticooccipital complex (Fig. 8F), whereas *T. bottii* possesses a narrower and more sharply delimited groove (Roček et Lamaud, 1995; Vasilyan, 2018). Other proposed morphological differences for the two Quercy species are located on the premaxilla (Vasilyan, 2018), which is unfortunately lost in MNHN.F.QU17381, thus preventing any further comparison with *T. bottii*.

Among the mummies attributed to *Thaumastosaurus*, MNHN.F.QU17381 presents strong resemblances with MNHN.F.QU17279, the former holotype of “*Rana plicata*” (attributed to *Thaumastosaurus gezei* by Laloy et al., 2013), with the anterior extension of the squamosal separating the maxillary from the orbit by a thin strip, and a postcranial identical in both mummies. It also presents a strong resemblance to MNHN.F.QU17376, with the palatines medially in contact with each other and a groove for vena jugularis interna, which also resembles the one of MNHN.F.QU17279 (Laloy et al., 2013). However, a few differences can be seen between the skull of MNHN.F.QU17381 and those of MNHN.F.QU17279 and MNHN.F.QU17376. First, the nasals are partially fused in MNHN.F.QU17381 whereas they are separated in MNHN.F.QU17279 and fully fused in MNHN.F.QU17376. The ornamentation of the sphenethmoid in MNHN.F.QU17381 is more developed than in MNHN.F.QU17279 (Laloy et al., 2013: fig. 3A) but less than in MNHN.F.QU17376, where the limits between the sphenethmoid and the neighboring dermal bones are obscured by the ornamentation (Rage and Roček, 2007: fig. 1A). As in MNHN.F.QU17279, the prootic foramen is not divided into two portions. However, as mentioned in the description, a notch can be observed on the lateral margin of the anterior surface of this bone of MNHN.F.QU17381, which is continuous with the groove for the vena jugularis and the unknown foramina found in MNHN.F.QU17376 and other *Thaumastosaurus* sp. skulls (Rage and Roček, 2007: fig. 7A–C). The extension of the lamella alaris in MNHN.F.QU17381 is also thinner than in MNHN.F.QU17376, resembling the one found in MNHN.F.QU17279. Those differences can be linked to ontogeny (see Ontogenetic Assessment below).

The return of the mummy: *Thaumastosaurus*, an Eocene pyxicephalid from Western Europe

MNHN.F.QU17381 shares with both MNHN.F.QU17376 and MNHN.F.QU17279 (attributed to *T. gezei*) the anterior extension of the squamosal forming the whole lateral wall of the orbit and the shape of the groove for the vena jugularis interna which is shallow and wide; these are listed in the revised diagnosis. The specimen MNHN.F.QU17381 can therefore be assigned to "*Thaumastosaurus gezei*".

A consequence of this attribution is that *T. gezei* and *B. servatus* are subjective synonyms. Considering the available names and excluding those invalidated by homonymy, *Bufo servatus* Filhol, 1877 is the oldest valid name. We therefore here consider the new combination *Thaumastosaurus servatus* (Filhol, 1877).

X.7 Ontogenetic assessment

Based on Rage and Roček (2007) and Laloy et al. (2013), the following cranial characters can be used to assess the skeletal maturity of *T. servatus* specimens: relation between the nasals, palatines, and ornamentation of the sphenethmoid. In skeletally mature (sensu Griffins et al., 2021) *T. servatus*, the contralateral nasals are fused medially, as are the palatines where only a suture is still visible between the bones, and the ornamentation of the sphenethmoid is well developed, with a similar pattern present in the surrounding bones. These conditions are also present in MNHN.F.QU17376 (Rage and Roček, 2007). This specimen can therefore be considered skeletally mature. In MNHN.F.QU17279, the lack of contact between the nasals (and similarly for the palatines), and the subdued ornamentation of the sphenethmoid demonstrate skeletal immaturity (sensu Laloy et al., 2013). In MNHN.F.QU17381, the slight medial contact between the nasals, the separation of palatines by a thin fissure, and the faint ornamentation of the sphenethmoid suggest a slightly greater skeletal maturity than MNHN.F.QU17279. MNHN.F.QU17381 is therefore more skeletally mature than MNHN.F.QU17279, but less than MNHN.F.QU17376.

The return of the mummy: *Thaumastosaurus*, an Eocene pyxicephalid from Western Europe

X.8 Phylogeny

Thaumastosaurus servatus was first suggested to have affinities with Leptodactylidae, especially the South American Ceratophryidae, based on cranial characters (Roček and Lamaud, 1995; Rage and Roček, 2007). Later, Laloy et al. (2013), based on a subcomplete skeleton found within the mummy, MNHN.F.QU17279, carried out a phylogenetic analysis, using a matrix modified from Báez et al. (2009). This latter dataset (see Báez et al., 2009) was itself based on the matrix proposed by Fabrezi (2006), modified for ceratophryid phylogeny. The dataset from Báez et al. (2009) includes 42 taxa, 3 of which are extinct taxa, scored for 75 characters. Laloy et al. (2013) enlarged the sample by adding 40 taxa from Evans et al. (2008), whose matrix was also modified from the dataset of Fabrezi (2006; see Evans et al., 2008 for modifications) and included genera as OTUs. Evans et al. (2008) deleted one character (the dorsal exposure of sphenethmoid) and redefined another (character 1 in Evans et al., 2008; Laloy et al., 2013). Laloy et al. (2013) found *Thaumastosaurus* within the Natatanura, as the sister-taxon of a clade that contains *Pyxicephalus* and *Cornufer* (a ceratobatrachid).

Báez and Gómez (2018) modified the dataset from Báez et al. (2009) by adding 29 neobatrachian taxa and redefining some characters to test the impact of hyperossification characters within the dataset. The taxon sample was greatly enlarged (from 42 to 71 taxa), and 68 characters were added (for a total of 143 characters), and several characters from the old dataset were redefined. Among the taxa, *T. servatus* ("*T. gezei*" in the dataset of Báez and Gómez, 2018) was included, using the new information from MNHN.F.QU17279 described by Laloy et al. (2013). They also found *T. servatus* within hyperossified Natatanuran, but as more closely related to *Pyxicephalus adspersus* Tschudi, 1838 (African bullfrog) than to *Cornufer guentheri* Boulanger, 1884 (Solomon Island leaf frog). This topology could be explained by the limited inclusion of only five extant natatanurans taxa in their dataset. We therefore expanded the dataset of Báez and Gómez (2018) with 15 extant natatanurans taxa (See Materials and Methods). We added seven more taxa from Pyxicephalidae (*Arthroleptella*

The return of the mummy: *Thaumastosaurus*, an Eocene pyxicephalid from Western Europe

lightfooti, *Aubria subgillata*, *Cacosternum boettgeri*, *Cacosternum namaquense*, *Natalobatrachus bonebergi*, *Strongolypus grayii* and *Tomopterna tuberculosa*), represented previously only by *Pyxicephalus adpersus* (the sister-taxon to *T. servatus*, according to Báez and Gómez, 2018). Most extant anurans are placed within Neobatrachia (Feng et al., 2017), which includes two clades, Hyloidea and Ranoides. The latter clade can be divided into three subclades: Microhylidae (*Hylambates*, *Dermatonotus*, and *Asterophrys* in our dataset), Afrobatrachia (*Arthroleptis* and *Hylambates* in our dataset) and Natatanura (represented by 19 taxa in our matrix, of which 14 were not included in any of the matrices mentioned above). The phylogenetic relationship among these three clades remains contentious. Natatanura represents the vast majority of extant Ranoides (Frost et al., 2006; Pyron and Wiens, 2011), but its fossil record is scarce and mostly composed of isolated fragmentary bones (Rage, 1984b; Sanchiz, 1998; Gardner and Rage, 2016). Given the good preservation and completeness of *T. servatus* fossils and their geological age, understanding its precise position within Natatanura is essential to better understanding the evolution of the clade and assessing the timing of its diversification. For this, several phylogenetic analyses were performed.

The return of the mummy: *Thaumastosaurus*, an Eocene pyxicephalid from Western Europe

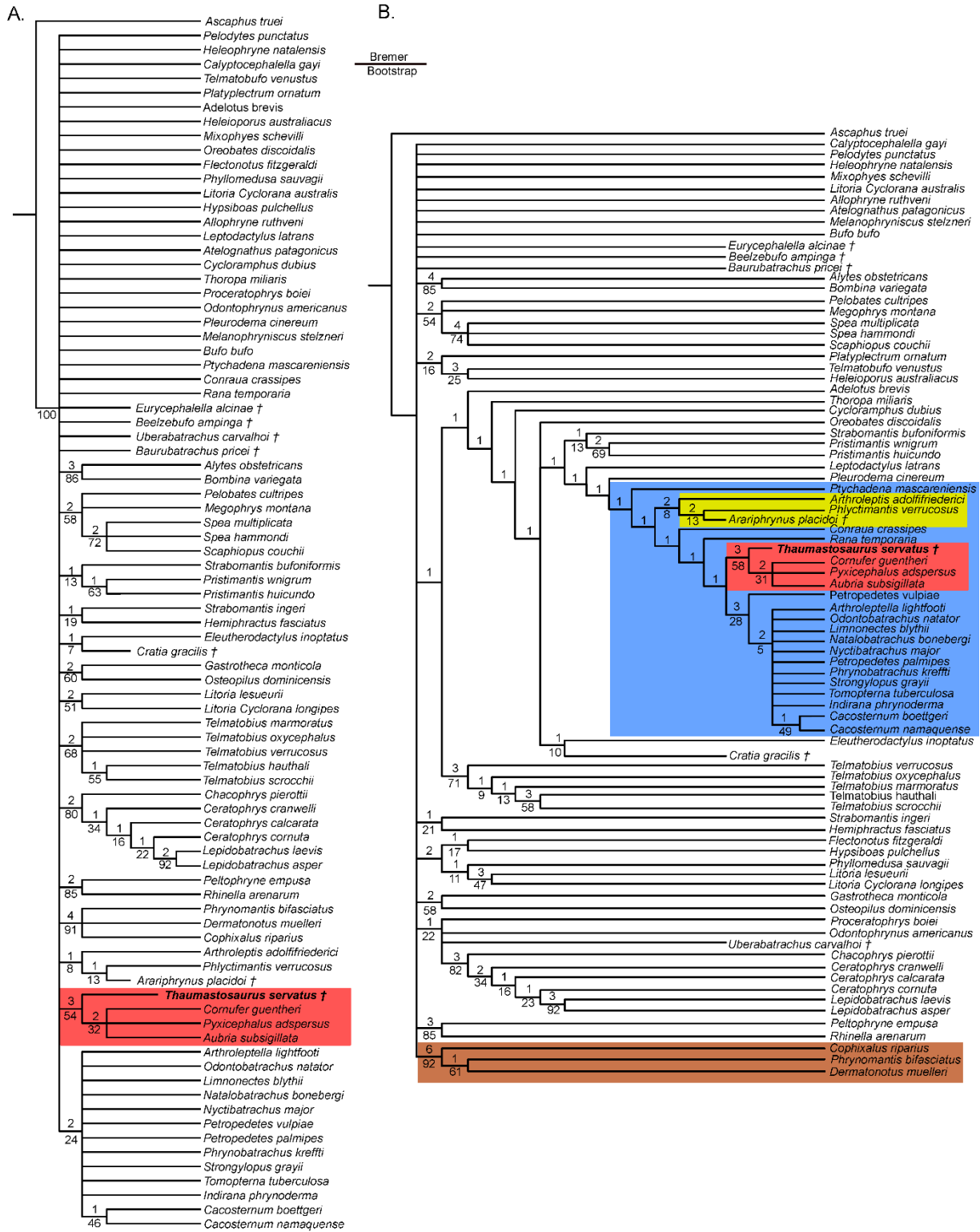


Figure X-14. **A** Strict consensus of 44 MPTs of 1354 steps from the analysis under EW, with multistate characters unordered (CI: 0.142, RI: 0.447); **B** Strict consensus of 90 MPTs of 1373 steps from the analysis under EW, with multistate characters ordered (CI: 0.137, RI: 0.422). This represents the full trees that are presented in simplified form (with fewer taxa) in Figure 14. Red represents hyperossified ranoids taxa; yellow represents the clade Afrobatrachia + *A. placidoi*; brown represents microhylids and blue represents "Ranoides"; The † symbol identifies extinct taxa.

The return of the mummy: *Thaumastosaurus*, an Eocene pyxicephalid from Western Europe

Unconstrained Analysis

Equal Weight Analysis, Unordered—We obtained 140 MPTs (most parsimonious trees) of 1355 steps (CI = 0.122; RI = 0.326) with the analysis performed under equal weight, with all multistate characters treated as unordered (Fig. X-14A). The strict consensus shows numerous polytomies, with Neobatrachia not recovered. *Thaumastosaurus servatus* is recovered as a sister-taxon to a trichotomy composed of hyperossified ranoides, *Pyxicephalus adpersus*, *Aubria subsigillata* and *Cornufer guentheri* (Fig. X-14A). The clade is supported by 26 synapomorphies. Many of them have been considered to be associated with Ranoides and Natatanura, which are not recovered in this analysis.

Equal Weight Analysis, Ordered—With cline characters ordered, we obtained 90 MPTs, of 1373 steps (CI = 0.137; RI = 0.422; Fig. X-14B). The strict consensus is more resolved than with unordered states, but it still presents numerous polytomies. A majority of the ranoids taxa (excluding the three microhylids) are clustered together (Fig. X-14A, B), forming a “Ranoides” clade. This restricted “Ranoides” is supported by nine synapomorphies but has poor bootstrap support (less than 5%) and moderate Bremer support. Among those synapomorphies, the ossification of omosternum (101: 0→1) is uniquely shared by members of this clade; it is present in almost all taxa forming the “Ranoides” clade, except in *Cacosternum*. Another one, non-overlapping coracoids (104: 0→1), is convergent with only the Microhylids (see Appendix S6 in Supplement Data 1 for the detailed list).

The presence of an ossified omosternum is particularly important in several phylogenies of Ranoides and Natatanura, as various authors have proposed it as a synapomorphy for either clade (Lynch, 1973; Laurent, 1986; Scott, 2005; Frost et al., 2006). Most natatanuran taxa display this character, although it is lost in some taxa typically ranked as genera. It is present in the Afrobatrachia but not in the Microhylidae. Another interesting synapomorphy recovered for both “Ranoides” clade and Microhylidae is the presence of non-overlapping epicoracoids (present in all extant Ranoides, as mentioned in Trueb, 1973; Lynch, 1973; Frost et al., 2006). This character represents a firmisternal condition for the pectoral girdle, classically associated with Ranoides (Lynch, 1973; Trueb, 1973; Duellman and Trueb, 1994).

The return of the mummy: *Thaumastosaurus*, an Eocene pyxicephalid from Western Europe

However, this condition is also found as a synapomorphy for Dendrobatidae (Trueb, 1973; Frost et al., 2006).

Thaumastosaurus servatus is found within “Ranoides”, recovered as a sister-taxon to a trichotomy composed of the extant hyperossified Ranoides (Fig. X-14A). Nine synapomorphies were recovered, almost all of them based on cranial elements, and six of which are hyperossification-linked characters, like the presence of a supraorbital flange on the frontoparietals (6: 0→1), a contact between squamosals and nasals (11: 0→1; lost in *Cornufer guntheri*) and the presence of a heavily ornamented external surface of the pars facialis of the maxillae (50: 0→2; see Appendix 1.6 for the detailed list). This clustering of hyperossified ranoids seems mainly moderately supported by the convergent evolution of hyperossification characters present on the skull, and is quite similar to the previous analysis, where *T. servatus* was recovered, close to extant hyperossified ranoids (Laloy et al., 2013; Báez and Gómez, 2018).

The two afrobatrachians (*Arthrolepis adolfifriederici* and *Hylambates verrucosus*) are recovered in a clade with *Arariphrynus placidoi* (Fig. X-14A), which is poorly supported by the loss of the ossified style of the sternum (102: 1→0), the reduction of the width of the glenoid fossa (112: 1→2; relative to the width of the shaft), the loss of the posterolateral process of the hyoid plate (67: 1→0) and the reduction of the posterodorsal expansion of the ischium (131: 1→0). Of those four synapomorphies, only the reduction of the glenoid fossa is scored for *A. placidoi*. The latter is recovered as the sister-taxon of *Phlyctimantis*, supported by three synapomorphies, which are the reduction of the length of the urostyle (92: 1→0), relative to the presacral vertebral length, a pars facialis of the maxillae which decrease abruptly in height in the orbital region (49: 0→1) and a change in the shape of the occipital condyles, which become stalked (40: 0→1). In addition, the *A. placidoi* postcranial is not well-known, and the synapomorphies for the “Ranoides” clade recovered (mentioned earlier) are

The return of the mummy: *Thaumastosaurus*, an Eocene pyxicephalid from Western Europe

synapomorphies, including the presence of palatines (27: 0→1; see Appendix S6 for the detailed list). Although not unique to the clade, this synapomorphy is commonly used, along other characters coded here but not recovered as synapomorphies for the clade (the loss of free ribs in adults and a bicondylar articulation between the sacral vertebra and the urostyle; Báez et al., 2009) to characterize neobatrachian taxa. Another synapomorphy proposed for this clade, the presence of a taeniae tecti medialis in the frontoparietal (Haas, 2003) was not recovered, likely for the fact that this character was not scored for a majority of the taxa in the dataset.

The return of the mummy: *Thaumastosaurus*, an Eocene pyxicephalid from Western Europe

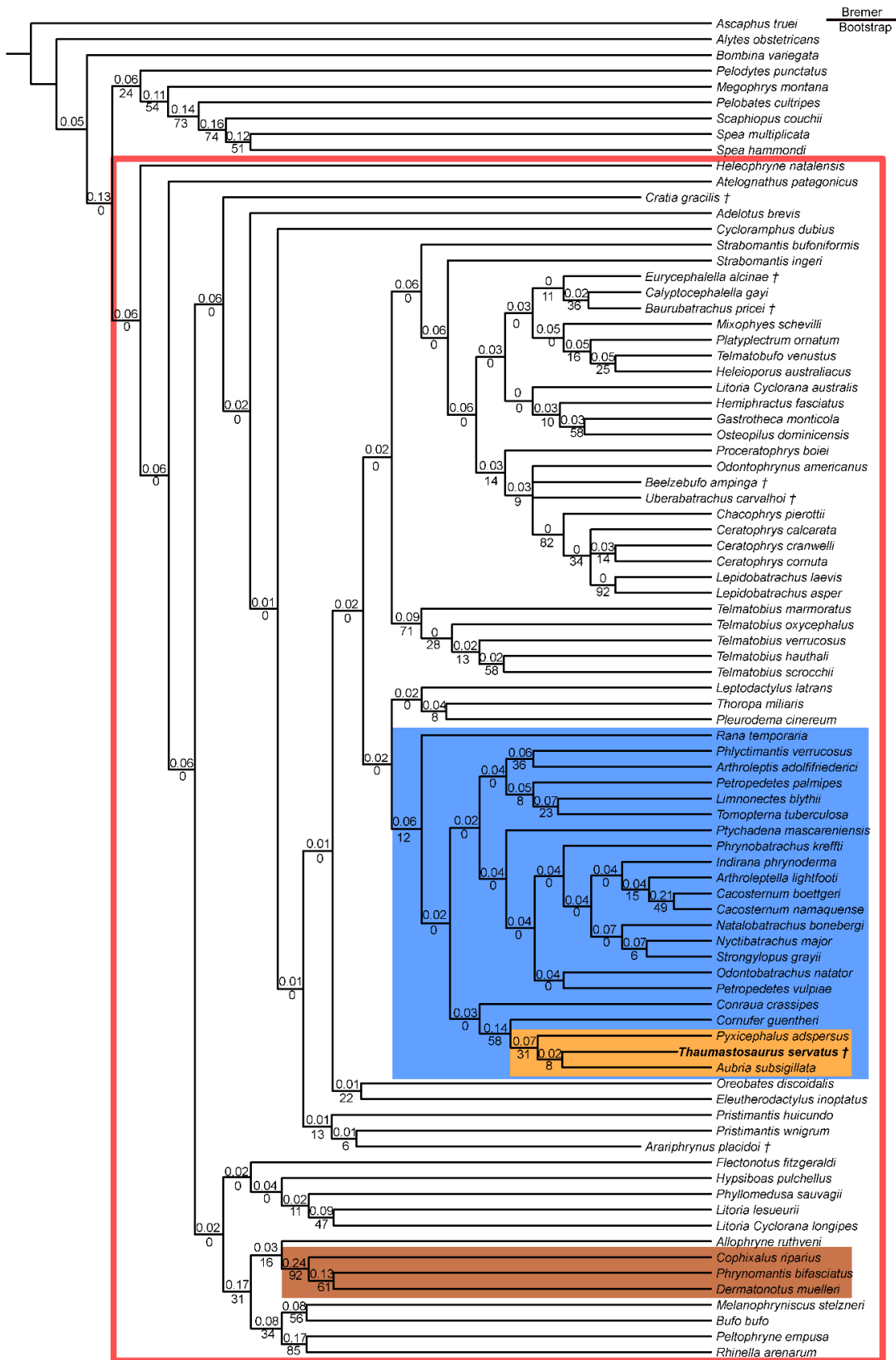


Figure X-16. Strict consensus of 2 MPTs of 66.96 steps from the analysis under IW with $k=7$, multistate characters ordered (CI: 0.168, RI: 0.548). † represent extinct taxa. This represents the full tree that is presented in simplified form (with fewer taxa) in Figure 1B. Orange represents the clade

The return of the mummy: *Thaumastosaurus*, an Eocene pyxicephalid from Western Europe

Pyxicephalinae + *T. servatus*; blue represents “Ranoides”; brown represents microhylids and the red outline represents Neobatrachia; the † symbol identifies extinct taxa.

We recovered a monophyletic “Ranoides” (excluding Microhylidae), still supported by seven synapomorphies, including six found previously. *T. servatus* is placed as a sister-taxon to the crown-clade of Pyxicephalinae (Appendix S6). This clade is moderately supported by 12 synapomorphies on cranial and postcranial characters (see Appendix S6 for the detailed list). One of them, the presence of a contact between squamosals and nasals (11: 0→1), is interesting as it is considered a marker for hyperossification (Báez and Gómez, 2018; Paluh et al., 2020) and is recovered only in Pyxicephalinae and Ceratophryidae.

When using a higher constant value ($k = 7$), we obtained two MPTs of 66.96 steps (CI = 0.168; RI = 0.548). In the strict consensus (Fig. X-16), *T. servatus* is placed within Pyxicephalinae, as a sister-taxon to *Aubria subsigillata* (brown ball frog). This clade is poorly supported by a single synapomorphy, the absence of odontoids on palatines (reversion to the plesiomorphic state). Pyxicephalinae is supported by three synapomorphies, the development of a contact between nasals and squamosals (11: 0→1), the ossification of the planum anteorbitale of the sphenethmoid (33: 0→1) and the development of a process lateral to the anterior process of the hyale (anterior process of Duellman and Trueb, 1994; such as e.g. on *Morerella cyanophthalma*, Rödel et al., 2009: fig. 5a; 64: 0→1; unknown in *T. servatus*). Only one of these was found in the previous analysis (contact between nasals and squamosals). As mentioned above, this character is retrieved as a synapomorphy for the Ceratophryidae (Báez and Gómez, 2018). *Cornufer guentheri* was placed as a sister-taxon to Pyxicephalinae (including *T. servatus*), supported by ten synapomorphies. Many of these were recovered in the equal weighting analysis, and are linked to hyperossification characters like the contact of nasals along most of their medial margin (3: 0→2), the development of tectum supraorbitale on the frontoparietals (6: 0→1) or the development of the ramus paroticus of the squamosals, overlapping prootics (14: 1→2; see Appendix S6 in Supplement Data 1 for the detailed list).

The return of the mummy: *Thaumastosaurus*, an Eocene pyxicephalid from Western Europe

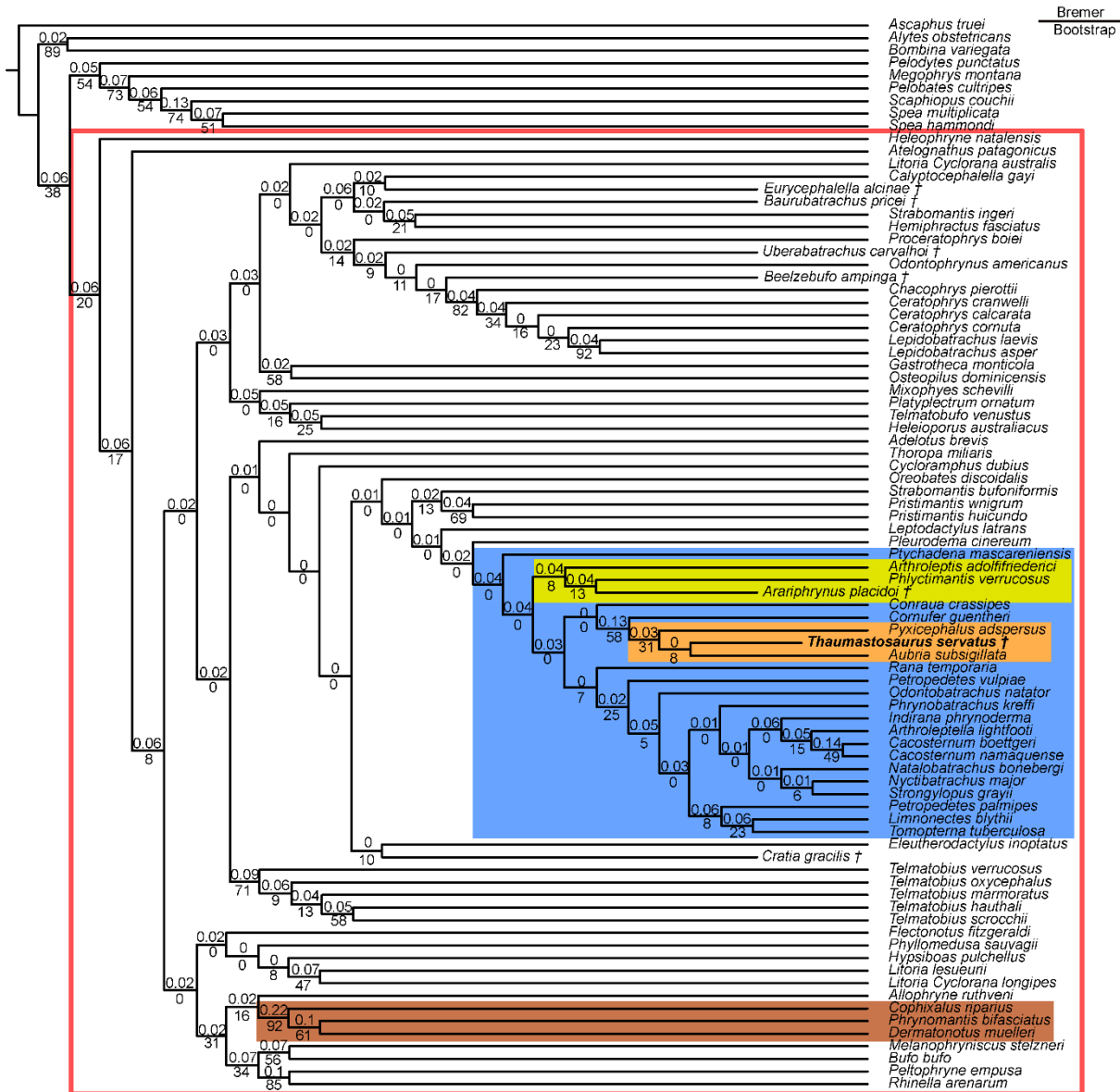


Figure X-17. Single MPT of 50.89 steps from the analysis under IW with $k = 12$, multistate characters ordered (CI: 0.171, RI:0.558). Orange represents the clade Pyxicephalinae + *T. servatus*; blue represents “Ranoides”; brown represents microhylids; yellow represents the clade Afrobatrachia + *A. placidoi* and the red outline represents Neobatrachia. The † symbol identifies extinct taxa.

When using an even higher constant value ($k=12$), we retrieved one fully resolved MPT of 50.89 steps (CI = 0.171, RI = 0.558; Fig. X-17). *T. servatus* is recovered in the same position as before, within Pyxicephalinae, with *C. guentheri* as the closest taxon to all Pyxicephalinae. *A. placidoi* is placed once again within Afrobatrachia (as when using equal weight), supported by the same synapomorphies.

The return of the mummy: *Thaumastosaurus*, an Eocene pyxicephalid from Western Europe

Constrained Analyses

Relationships within Ranoides and Natatanura have always been controversial (Clarke, 1981; Lynch, 1973; Scott, 2005; Frost et al., 2006; Pyron and Wiens, 2011), with various clades lacking morphological synapomorphies. This can be observed in our analysis as well, as we did not recover the Ranoides as a clade, but only a subset of these excluding microhylids. However, molecular datasets have yielded a better resolution of their relationships, especially with large dataset (Frost et al., 2006; Pyron and Wiens, 2011; Feng et al., 2017; Jetz and Pyron, 2018). Some uncertainties remain, with some clades still lacking clear support (see Pyron and Wiens, 2011). Conflict still exists around the position of Afrobatrachia, either as a sister-taxon to Microhylidae (Pyron and Wiens, 2011; Jetz and Pyron, 2018) or to Natatanura (Feng et al., 2017). We choose constrained analyses under two topologies, to see if changes in the relationship inside Ranoides could impact the placement of *T. servatus*.

The return of the mummy: *Thaumastosaurus*, an Eocene pyxicephalid from Western Europe

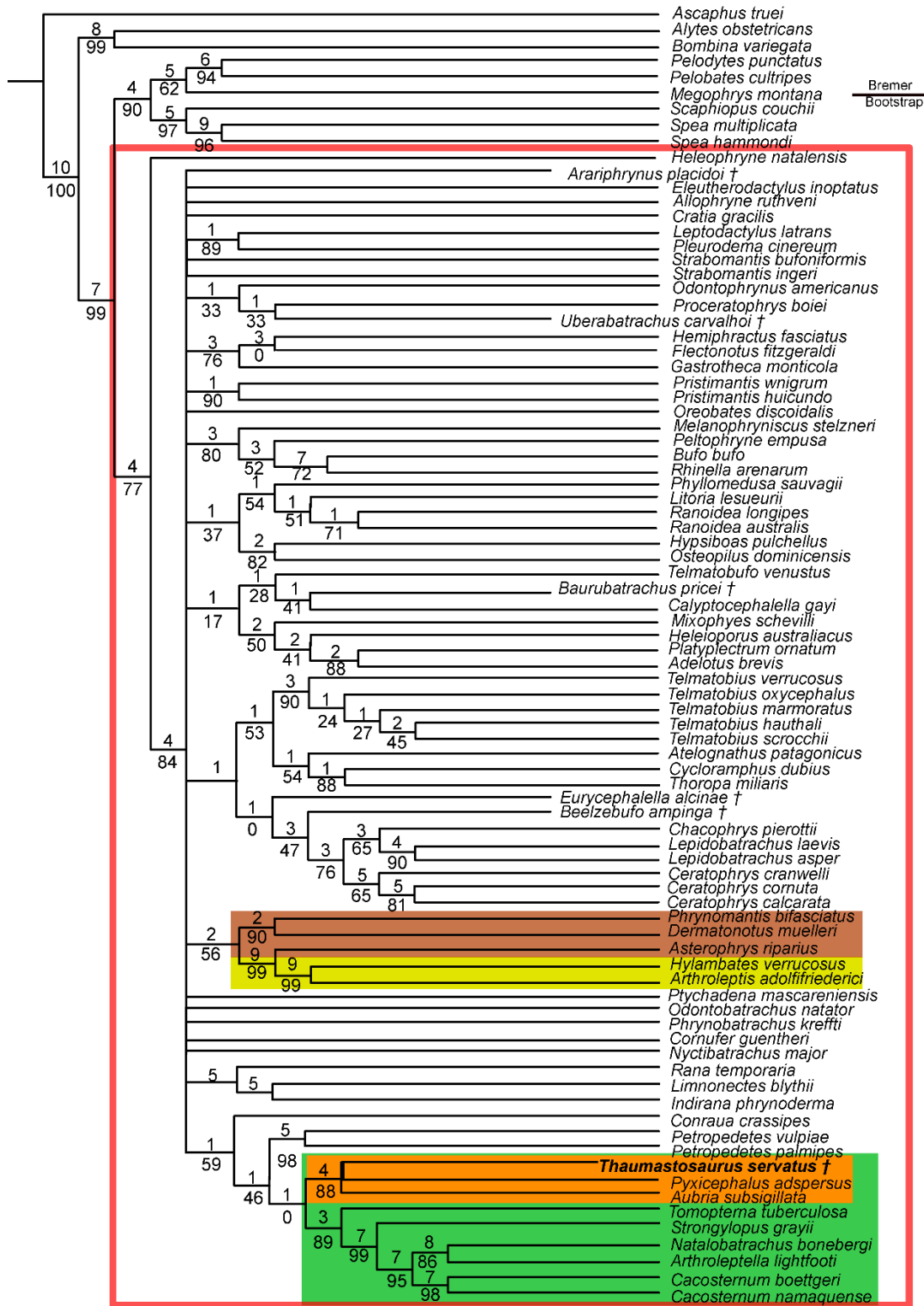


Figure X-18. Strict consensus of 22 MPTs of 1586 steps from the constrained analysis using a molecular scaffold tree from Jetz and Pyron (2018), performed under EW with multistate characters ordered (CI: 0.149, RI: 0.479). Orange represents the clade Pyxicephalinae + *T. servatus*; brown represents microhylids; yellow represents afrobatrachians and the red outline represents Neobatrachia. The † symbol identifies extinct taxa.

The return of the mummy: *Thaumastosaurus*, an Eocene pyxicephalid from Western Europe

Equal Weight Analysis, Ordered—When using a topology inferred on the phylogeny of Jetz and Pyron (2018) as a constraint, we recovered 22 MPTs with a score of 1586 steps. The strict consensus (CI = 0.149, RI = 0.479) places *T. servatus* in a trichotomy with the two pyxicephalines (Fig. X-18). The clade is strongly supported by thirteen synapomorphies, including the presence of a contact between nasals and squamosals (11: 0→1), the expansion of the zygomatic ramus of the squamosals, allowing for its articulation with the maxillae (10: 1→2), the presence of a distal expansion of the crista parotica (39: 0→1) and the enclosure of the pathway for the occipital artery into a canal (7: 0→2; see Appendix 1.6 in for the detailed list). Neither Ranoides nor Hyloidea are recovered as a clade. This is linked to the instability of one taxon, *A. placidoi*, which is recovered either as an hyloid (in 72% of the trees) or as a ranoid. When excluding this taxon, we recovered 6 MPTs with a score of 1580 (CI = 0.158, RI = 0.481). In the strict consensus, we recovered both Ranoides and Hyloidea, and *T. servatus* is placed in the same trichotomy, supported by the same synapomorphies (Fig. X-19).

The return of the mummy: *Thaumastosaurus*, an Eocene pyxicephalid from Western Europe

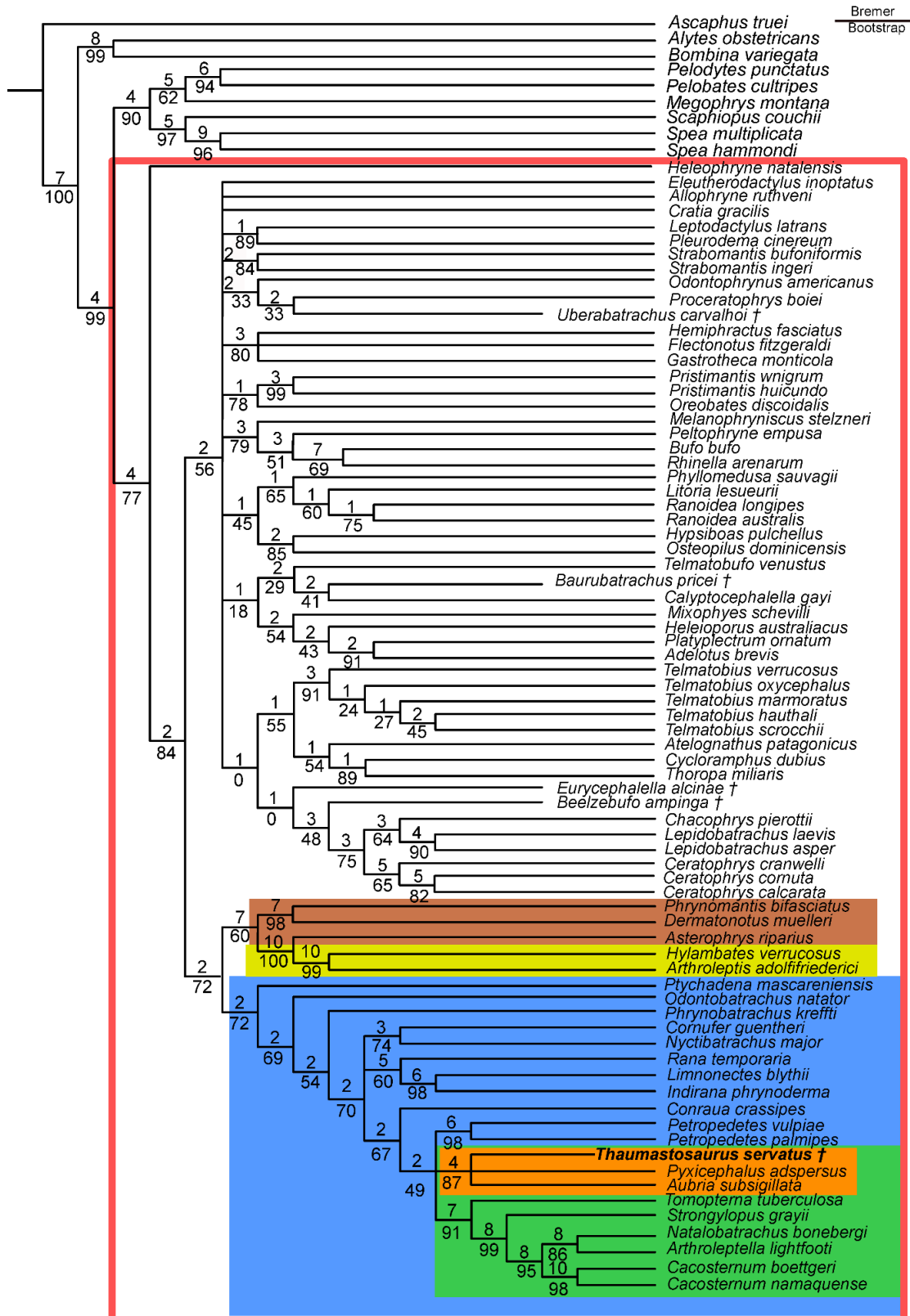


Figure X-19. Strict consensus of 6 MPTs of 1580 steps from the constrained analysis using a molecular scaffold tree from Jetz and Pyron (2018), performed under EW with multistate characters ordered excluding *Arariphrynus placidoi* (CI: 0.158, RI: 0.481). Orange represents the clade Pyxicephalinae + *T. servatus*; brown represents microhylids; yellow represents afrobatrachians; blue represents natatanurans taxa and the red outline represents Neobatrachia. The † symbol identifies extinct taxa.

The return of the mummy: *Thaumastosaurus*, an Eocene pyxicephalid from Western Europe

When using a topology inferred on the phylogeny proposed by Feng et al. (2017) as a constrain, we recovered 4 MPTs, with a score of 1574. In the strict consensus tree (CI = 0.137, RI = 0.425; Fig. X-20), *T. servatus* was recovered in the same position as with a topology inferred on the phylogeny of Jetz and Pyron (2018), in a trichotomy with the two pyxicephalinae taxa, supported by seventeen synapomorphies, thirteen of them recovered in the previous analysis, with an additional four, the partial ossification of the septum nasi of the nasal capsule (34:0→1) , the ossification of the crista parotica (38: 0→1), the translocation of the craniomandibular joint to a position well posterior to occiput (61: 0→2)

The return of the mummy: *Thaumastosaurus*, an Eocene pyxicephalid from Western Europe

and the presence of anterolateral processes on the hyoid plate (64: 0→1; not scored for *T. servatus*).

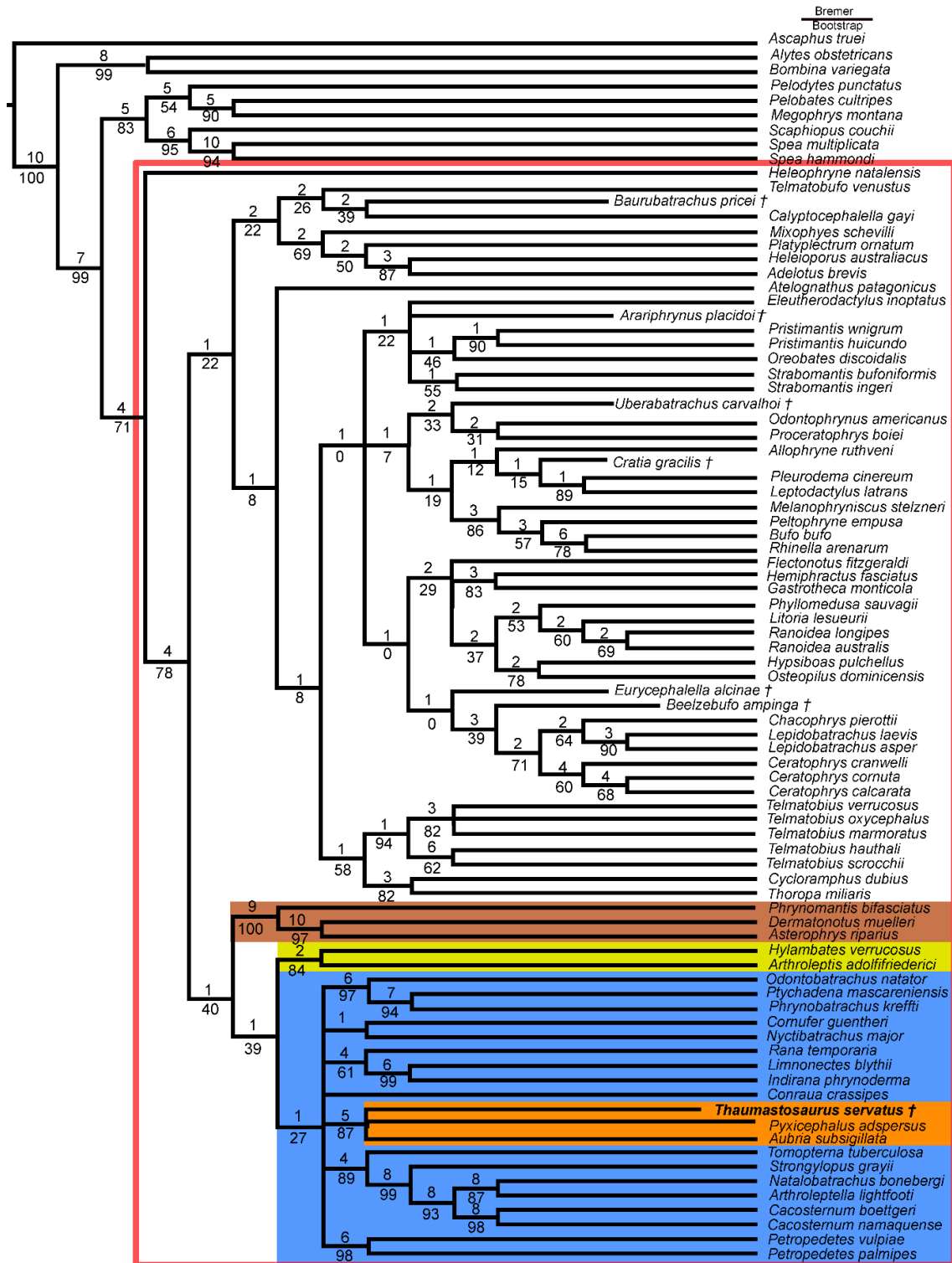


Figure X-20. Strict consensus of 4 MPTs of 1562 steps from the constrained analysis using a molecular scaffold tree from Feng & al. (2017) performed under EW with multistate characters ordered (CI: 0.151, RI: 0.486). Orange represents the clade Pyxicephalinae + *T. servatus*; brown represents microhylids; yellow represents afrobatrachians; blue represents natatanurans taxa and the red outline represents Neobatrachia. The † symbol identifies extinct taxa.

The return of the mummy: *Thaumastosaurus*, an Eocene pyxicephalid from Western Europe

Implied Weight Analyses (k = 7), Ordered—When using implied weights, and using a topology inferred on the phylogeny of Jetz and Pyron (2018) as a constraint, we obtained one tree of 72.01 steps (CI = 0.150, RI = 0.459), with *T. servatus* still found within Pyxicephalidae, as a sister-taxon to the extant Pyxicephalinae (Figs. X-21), a placement similar to the one found with a low constant value (k = 3) using implied weighting (Fig. 14). This clade is well-supported by the same 13 synapomorphies recovered in the previous analysis constrained on the same topology.

The return of the mummy: *Thaumastosaurus*, an Eocene pyxicephalid from Western Europe

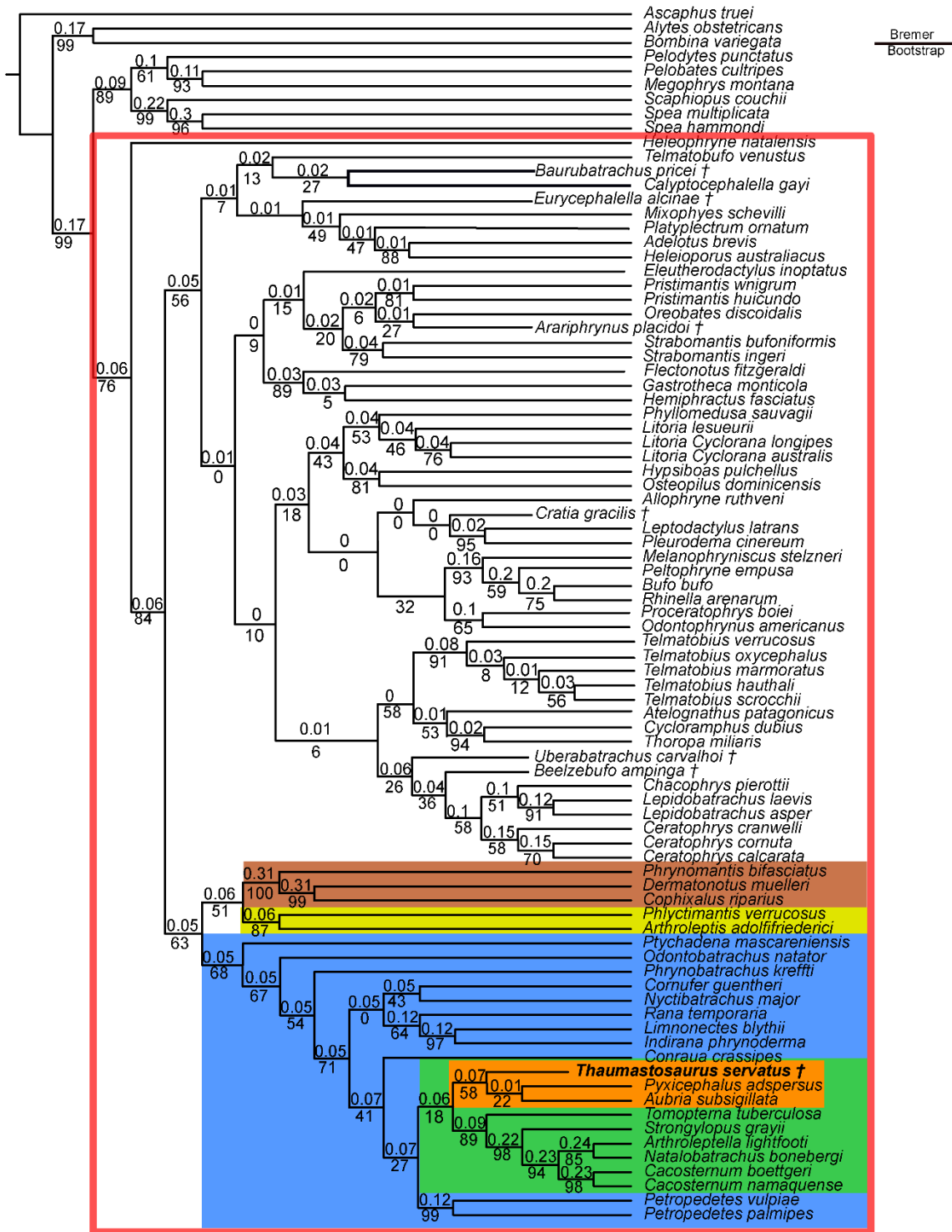


Figure X-21. Single MPT of 71.97 steps from the constrained analysis using a molecular scaffold tree from Jetz and Pyron (2018), performed under IW, with $k = 7$, with multistate characters ordered (CI: 0.151, RI: 0.485). This represents the full tree that is presented in simplified form (with fewer taxa) in Figure 15. Orange represents the clade Pyxicephalinae + *T. servatus*; green represents Pyxicephalidae; blue represents natatanurans taxa; brown represents microhylids; yellow represents afrobatrachians and the red outline represents Neobatrachia. The † symbol identifies extinct taxa.

The return of the mummy: *Thaumastosaurus*, an Eocene pyxicephalid from Western Europe

When constraining the analysis using the topology inferred from the analysis of Feng et al. (2017), we also obtained one tree of 71.79 steps (CI = 0.151, RI = 0.486) fully resolved (Fig. X-22). The position of *T. servatus* is identical as before, as the closest taxon to the Pyxicephalinae, well supported by the same thirteen synapomorphies.

The return of the mummy: *Thaumastosaurus*, an Eocene pyxicephalid from Western Europe

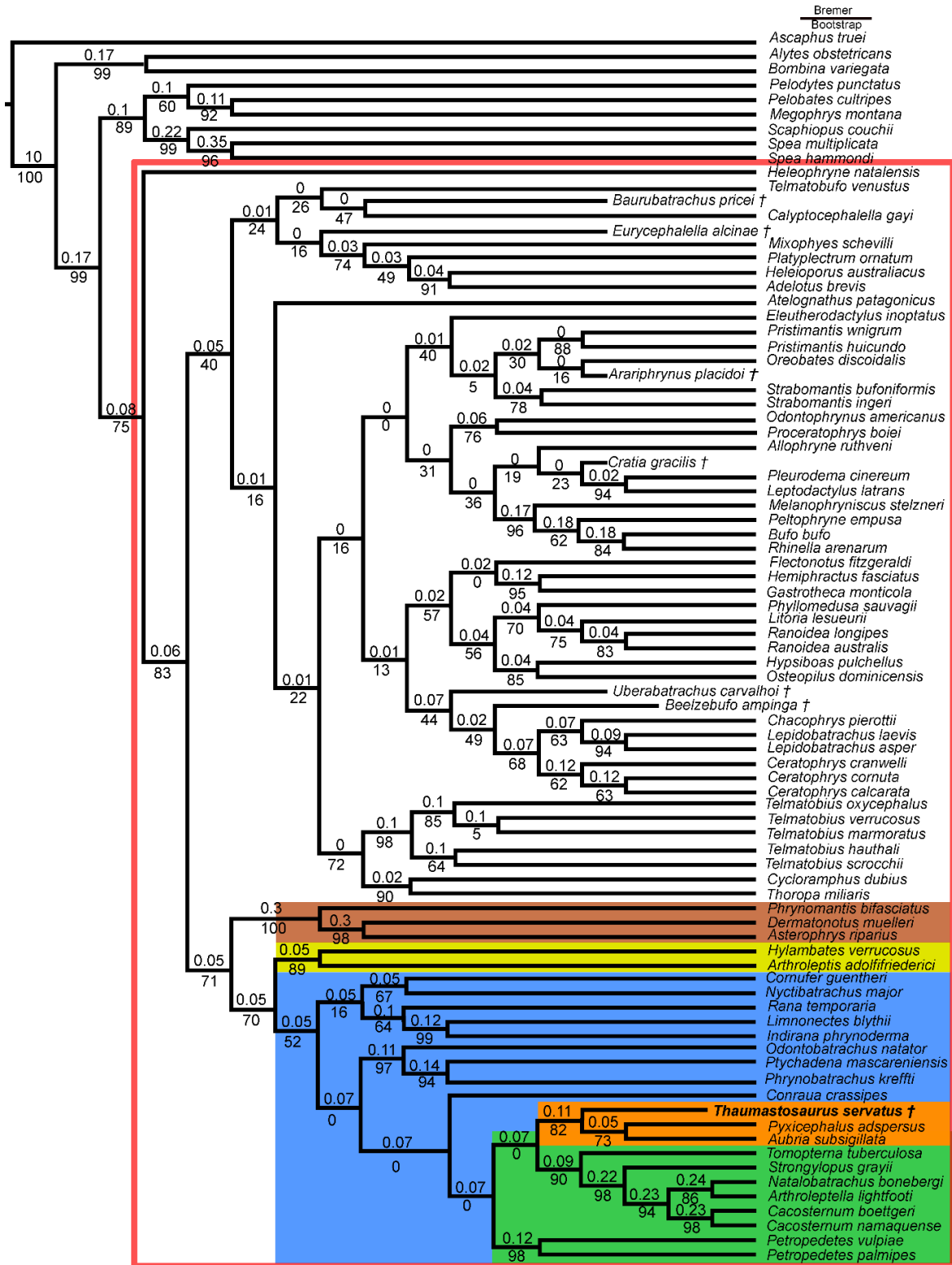


Figure X-22. Single MPT of 71.79 steps from the constrained analysis using a molecular scaffold tree from Feng & al. (2017), performed under IW with $k = 7$, with multistate characters ordered (CI: 0.151, RI: 0.486). Orange represents the clade Pyxicephalinae + *T. servatus*; green represents Pyxicephalidae; blue represents natatanurans taxa; brown represents microhylids; yellow represents afrobatrachians and the red outline represents Neobatrachia. The † symbol identifies extinct taxa.

The return of the mummy: *Thaumastosaurus*, an Eocene pyxicephalid from Western Europe

Discussion—The various analyses confirm the placement of *Thaumastosaurus* within Ranoides, more precisely within Natatanura. This position is mainly justified by several postcranial characters, such as the ossified omosternum and non-overlapping coracoids. This placement highlights the importance of postcranial characters to reduce the impact of homoplasy found in the skull characters of anurans (Duellman et Trueb, 1994; Báez and Gómez, 2018) and to correctly assess the position of extinct taxa.

In most analyses, *T. servatus* is recovered as a sister-taxon to Pyxicephalinae, or within this clade. In addition, the hyperossified *Cornufer guentheri* is also recovered close to Pyxicephalinae and *T. servatus* with both equal and implied weight, except when using a low k value (punishing heavily homoplasy; Figs. 14A, B). However, one difference can be observed between equal and implied weight analyses. With equal weights, *T. servatus* is placed as the sister-taxon to a trichotomy of the three extant taxa, whereas with implied weights, *C. guentheri* is recovered as a sister-taxon to *T. servatus* and Pyxicephalinae. This clustering of hyperossified ranoids is mostly likely driven by convergence, as the clades are based mainly on hyperossified characters (see Appendix S6). However, when using implied weight, the placement of *T. servatus* as close to Pyxicephalinae (based only on one synapomorphies on an hyperossified character) has relatively high Bremer and moderate bootstrap supports. This could be an effect of the implied weight, which tends to favor resolved trees, which may lead to false topologies. This can be observed when using low k value ($k = 3$), where *C. guentheri* is not recovered close to the other hyperossified ranoids, but also not close to its position proposed by molecular phylogenies (Fig. X-14; Jetz and Pyron, 2018). To minimize this problem, several authors proposed to use higher k value (Goloboff et al., 2018a, b). In the constrained analysis, *Thaumastosaurus* is also placed within the Pyxicephalidae, a clade composed of Pyxicephalinae and Cacosterninae. However, no osteological synapomorphy is known for this clade, because the presence of a medial lingual process on the tongue (presumed synapomorphy; Frost et al., 2006) is not known in *Thaumastosaurus*.

Conversely, as already proposed by Clarke (1981), Pyxicephalinae is supported by four morphological synapomorphies (Frost et al., 2006). One of them, the presence of an

The return of the mummy: *Thaumastosaurus*, an Eocene pyxicephalid from Western Europe

occipital canal, was also recovered as a synapomorphy for this clade in our analyses, while another one, a well-developed ramus interior (medial ramus; Clarke, 1981) of the pterygoids overlapping the parasphenoid alae, is present on *Thaumastosaurus*. The other two synapomorphies for the clade are a well-developed zygomatic ramus (= lamella alaris) of the squamosals (longer than its ramus paroticus) articulating with the maxillae, and a cranial exostosis (sensu Trueb, 1973). This latter in its typical state (a reticulate pattern of bone deposition, forming an ornamentation) is present only in Pyxicephalinae (in the Natatanura). Indeed, *C. guentheri* presents a modified pattern of exostosis, named casquing (Trueb, 1973). The articulated skulls attributed to *T. servatus* present a reticulated bone ornamentation that can be considered as skull exostosis (Figs. X-5, 6; Roček and Lamaud, 1995: fig 1–5; Rage and Roček, 2007: fig.1–6; Laloy et al., 2013: fig. 3), and possess elongated squamosals with a well-developed zygomatic ramus forming the whole ventral margin of the orbit (the maxilla does not contribute to the ventral margin of the orbit; Fig. X-5B). This character shared with both *Pyxicephalus adspersus* and *Aubria subsigillata* (both Pyxicephalinae) but not by *C. guentheri*.

Thaumastosaurus servatus shows all the synapomorphies of the Pyxicephalinae and is found in almost all analyses as the closest taxon to the pyxicephaline crown clade. It can therefore be confidently placed within Pyxicephalidae. Furthermore, we can consider *T. servatus* as a stem-Pyxicephalinae.

Several Cretaceous taxa were included in the analyses, including: *Baurubatrachus pricei*, *Eurycephalella alcinae*, *Arariphrynus placidoi*, *Beelzebufo ampinga*, *Uberabatrachus carvalhoi* and *Cratia gracilis*. Their positions throughout the analyses are similar to the ones recovered in recent analyses (Báez and Gómez, 2018). *Baurubatrachus pricei* is recovered within Atraslobatrachia, close to *Calyptocephalella gayi*. *Eurycephalella alcinae* is recovered as a sister-taxon to the extant Myobatrachidae. *Arariphrynus placidoi* is recovered within the Craugastoridae, but this position is poorly supported, as the taxon was in several analyses placed within various neobatrachian clades, even within the Ranoides, as a sister-taxa to the Afrobatrachia. This variability can be explained by the poorly known postcranial bones, especially around the pectoral girdle, where most critical characters for both Hyloidea and

The return of the mummy: *Thaumastosaurus*, an Eocene pyxicephalid from Western Europe

Ranoides are found. *Cratia gracilis* is placed in the same position as in previous analyses (Báez et al., 2009; Báez and Gómez, 2018). *U. carvalhoi* is recovered as a sister-taxon to Ceratophryidae, a position that was also recovered in some analyses of Báez and Gómez (2018) but differs from the position they retained as their preferred one (sister-taxa to *B. ampinga* clustered within Myobatrachia). *B. ampinga* is recovered in various positions, but most often as a sister-taxon to all Ceratophryidae, a position proposed by previous analyses (Evans et al., 2008; Evans et al., 2014). However, this was challenged recently (Báez and Gómez, 2018) and this uncertainty may be linked to the scarce post-cranial remains.

X. 9 Paleobiogeographic implications

Only a few sites from Africa have yielded pre-Pleistocene natatanuran fossils (Gardner and Rage, 2016). However, new material has been published in the last decade, and the fossil record of various natatanuran clades is beginning to be better documented.

The pre-Pleistocene fossil record of Ranoides is scarce, and even fewer fossil specimens older than the Miocene have been assigned to Natatanura (Sanchiz, 1998; Gardner and Rage, 2016). The few Ranoides specimens are moreover mostly fragmentary (de Broin et al., 1974; Rage, 1984a; Roček and Lamaud, 1995; Báez and Werner, 1996). The origination time estimates in molecular studies for Ranoides are around 90.7 Ma (105.6 to 76.3 Ma, according to Frazão et al., 2015), about mid-Cretaceous, which is compatible with the fossil record given that the first presumed remains attributed to this clade date from the Cenomanian (between 100.5 Ma to 93.9 Ma; Báez and Werner, 1996; Marjanović and Laurin, 2014: fig.4). However, these remains were neither described nor illustrated, making the validity of this attribution difficult to assess. Other remains are from the Santonian (86.3 Ma to 83.6 Ma) of In Beceten, Niger (de Broin et al., 1974; Rage, 1984a) and from the Paleocene (66.0 to 56.0 Ma) from Cernay, France (Estes et al., 1967; Rage, 1984a). More recent remains, clearly attributed to Ranoides, are known in multiple Eocene sites, in northern Africa (Rage et al., 2021) and in the Quercy Phosphorites (Rage, 2016), with *T. servatus* and *T. bottii* (as well as other indeterminate forms; see Rage, 2016) constituting the best-known taxa.

The return of the mummy: *Thaumastosaurus*, an Eocene pyxicephalid from Western Europe

For Natatanura, almost no fossil record is known. *Thaumastosaurus* is the oldest undisputed known taxon, as well as the oldest Ranoides with a valid taxon name (Sanchiz, 1998; Gardner and Rage, 2016; Rage, 2016). The Eocene age of this taxon is substantially more recent than the transition Cretaceous/Paleocene age for Natatanura inferred in the most recent molecular age analysis (Feng et al., 2017).

Although scarce, the fossil record of Ranoides (including Natatanura) is concentrated (in the Mesozoic at least) on the African continent (with a few exceptions in India), which suggests an African origin of the clade (Gardner and Rage, 2016). This hypothesis is strengthened by the presence of extant endemic clades on this continent (Gardner and Rage, 2016), including Pyxicephalidae. The attribution of *Thaumastosaurus*, an endemic clade of Western Europe (Vasilyan, 2018) to Pyxicephalidae extends the geographic range of Pyxicephalidae, which is otherwise limited to Sub-Saharan Africa (Van der Meijden et al., 2011) for both extant and extinct taxa (Gardner and Rage, 2016). Moreover, *Thaumastosaurus* (Middle to Late Eocene, 40.5 to 33.5 Ma) is much older than the other fossils previously attributed to that clade (around 5.1 Ma for the oldest specimen; Gardner and Rage, 2016). However, the attribution of *Thaumastosaurus* to Pyxicephalidae is well supported by our phylogenetic analysis and is compatible with the geological age proposed for the clades by molecular studies. Indeed, Pyxicephalidae diverged from its sister-clade around 60 Ma ago (Early to Middle Paleocene) according to recent molecular age (Feng et al., 2017). Within this clade, Pyxicephalinae diverged from Cacosterninae around 50 Ma ago (Hedges et al., 2015; Feng et al., 2017). The stratigraphic range for *Thaumastosaurus* is compatible with these molecular ages. Furthermore, we confirm the African affinities of *T. servatus*, proposed almost a decade ago (Laloy et al., 2013).

The presence of *Thaumastosaurus* in Europe could be linked to a faunistic exchange through an intermittent connection between Africa to Europe (Rage, 1984b; Gheerbrant and Rage, 2006). Indeed, some adapisoriculid (De Bast et al., 2012) and lousinid mammals (Sudre, 1979) may have immigrated through an intermittent connection between Africa and Eurasia in the Paleocene or Eocene. Starting in the Late Paleocene (Tanrattana et al., 2020), the temperature increased (Sluijs et al., 2006; Bohaty et al., 2009) in Western Europe, and

The return of the mummy: *Thaumastosaurus*, an Eocene pyxicephalid from Western Europe

remained warm until the end of the middle Eocene (Bohaty et al., 2009). During this period, Western Europe was characterized by a subtropical climate, with evergreen forests under warm and humid conditions (Escarguel et al., 2008; Hérán et al., 2010; Tanrattana et al., 2020).

For the herpetofauna, the timing of this wave of immigration in Europe and paleobiogeographic origins of the Early Paleogene herpetological faunas of Europe still is poorly constrained. Numerous taxa appear in Europe at the earliest Eocene (MP7; Folie et al., 2005, 2013; Rage, 2012), but could have arrived during the end of the Paleocene. Bufonidae already exhibit such a pattern with their earliest record in Europe being from the Paleocene of Cernay (Rage, 2003).

A major cooling is recorded during the Eocene-Oligocene transition (EOT). This is well established in numerous studies using different proxies (Escarguel et al., 2008; Hérán et al., 2010; Lunt et al., 2017; Tanrattana et al., 2020) and is linked to the establishment of permanent ice caps on Antarctica (Vandenberghé et al., 2012; Boscolo Galazzo et al., 2014). In Europe, the climate and environments dramatically changed. The climate became drier, with stronger seasonality and the appearance of a dry season (Escarguel et al., 2008; Tanrattana et al., 2020). The vegetation changed from forests to woodland savannah (Escarguel et al., 2008). This climate change probably triggered a moderate extinction event called the “Grande Coupure” (Stehlin, 1909), which has been particularly well-documented for mammals in Europe (Remy et al., 1987). Most of the subtropical fauna of African origin disappeared in Europe and was replaced by Eurasian taxa adapted to temperate conditions. This event is also documented in the herpetofauna (Delfino et al., 2003; Rage, 2006, 2012; Augé and Smith, 2009; Macaluso et al., 2019). Among amphibians, *Thaumastosaurus* is the best-documented victim of this turnover (Vasilyan, 2018).

The return of the mummy: *Thaumastosaurus*, an Eocene pyxicephalid from Western Europe

X.10 Conclusion

The tomography and skeletal study of the specimen MNHN.F.QU17381, firstly described as the holotype of the bufonid *Bufo servatus*, yielded numerous data. The anatomical characters led to a new taxonomic attribution to the ranoid taxon *Thaumastosaurus servatus*. MNHN.F.QU17381 is the third mummy from the Old Collections of the Quercy phosphorites attributed to this taxon, thus making it the best-known anuran in the Eocene of Western Europe.

Previous analyses placed *T. servatus* within the Natatanura, without specifying its position. Our analyses place *T. servatus* with the African hyperossified Pyxicephalinae (and likely as a stem-Pyxicephalinae and sister-taxon to the extant Pyxicephalinae), sharing a peculiar ornamentation as well as a combination of cranial features such as a contact between the squamosals and nasals, which is unique within Natatanura and Ranoides.

The position of *T. servatus* within Natatanura and Pyxicephalinae provides new insights to calibrate molecular dating analyses, as it represents the oldest fossil record for Pyxicephalidae and Pyxicephalinae, previously known only from the Pliocene (around 5 Ma) and Pleistocene respectively, extending therefore the geological range of the Pyxicephalinae of more than 33 Ma and making *T. servatus* one of the few well-known taxa firmly attributed to the Natatanura in the Paleogene. Moreover, Pyxicephalinae were previously considered to be distributed solely in Africa, whereas *T. servatus* is endemic to Western Europe. Confirmation of these affinities extends the geographical range of pyxicephalines. The main biogeographical hypothesis is that the clade originated in Africa, and then migrated into Europe through dispersal of some natatanurans during the Eocene, making *Thaumastosaurus* a member of the African herpetofauna present in Europe until the Eocene/Oligocene transition, when it was eliminated around the Grande Coupure (Delfino et al., 2003; Rage, 2006, 2012). However, given the scarce fossil record of Ranoides in Africa, especially during the Paleocene and Eocene, other hypotheses cannot be ruled out. Further findings could help to understand the evolution of Ranoides, which represents the majority of extant anurans on the African continent.

The return of the mummy: *Thaumastosaurus*, an Eocene pyxicephalid from Western Europe

X.11 Appendix

Appendix S1. CT-scan of QU17381

The appendix can be found on Morphobank at: <http://morphobank.org/permalink/?P3898>

Appendix S2. 3D model of QU17381, exported under 3-matics V19.0

The appendix can be found on Morphobank at: <http://morphobank.org/permalink/?P3898>

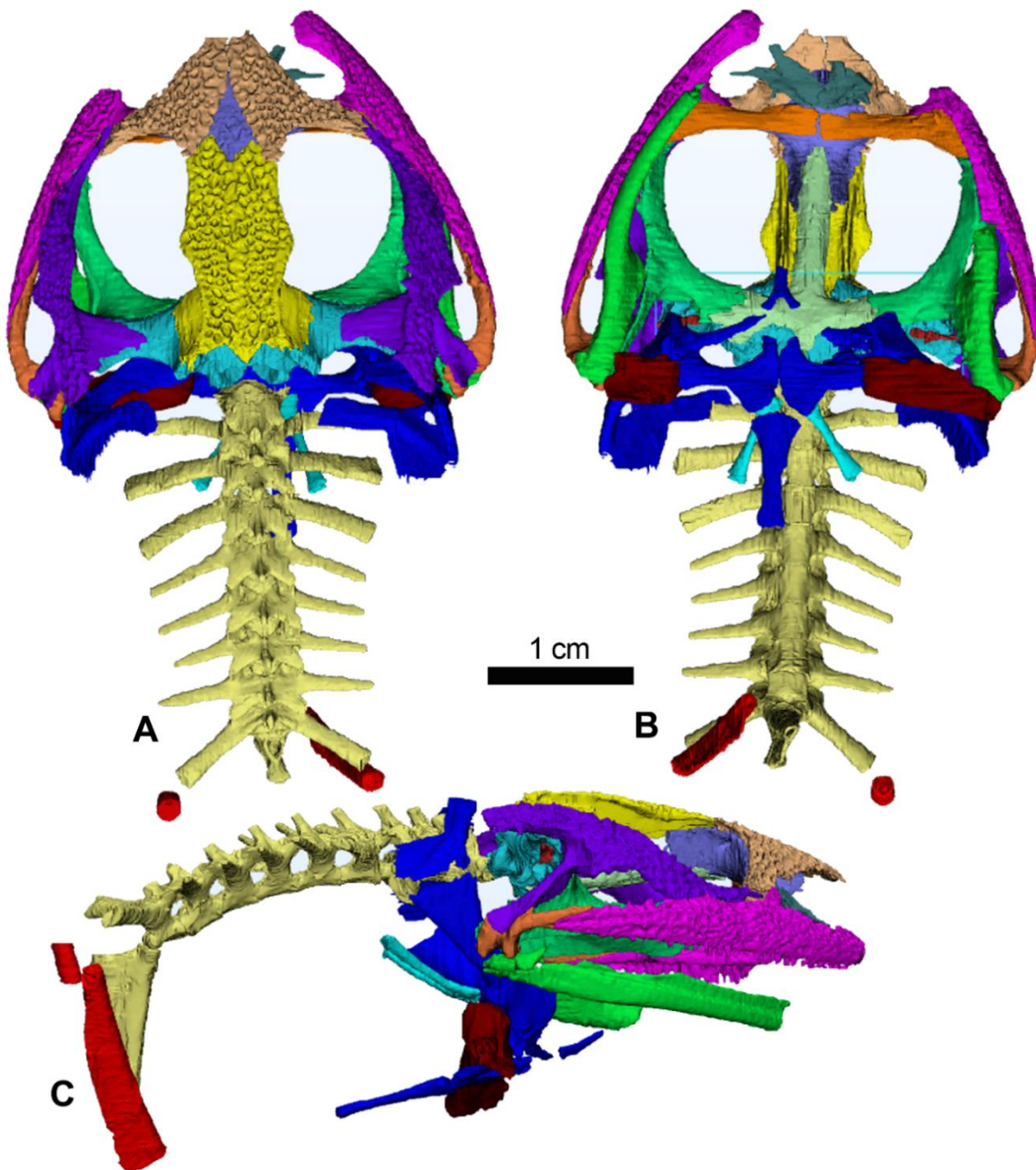


FIGURE S1. MNHN.F.QU17381, holotype of *Thaumastosaurus servatus* (*'Bufo servatus'*) in A dorsal; B ventral and C left lateral views.

The return of the mummy: *Thaumastosaurus*, an Eocene pyxicephalid from Western Europe

Appendix S3. Character list for the analyses, modified from Báez and Gómez (2018)

Symbols: *, hyperossified character (not modified from Báez and Gómez, 2018); #, modified from Báez and Gómez (2018).

Skull

1. Skull roof, orbital region, minimum width relative to maximum antorbital width: (0) less than 1/4, (1) between 1/4 and 1/3, (2) more than 1/3.
2. Skull roof, orbital region, shape: (0) posterior and anterior ends equally wide, (1) anteriorly wider than posteriorly, (2) posteriorly wider than anteriorly.
- *3. Nasals, relation to one another: (0) well separated, (1) slightly separated or in minimal contact, (2) in contact throughout most of their medial margins, or completely fused.
4. Nasal, position of anterior end relative to anterior tip of maxilla: (0) posterior, (1) same level, (2) anterior.
- *5. Frontoparietals, relation to one another: (0) separate along entire length, (1) partially sutured or in contact only partially, may be partially fused, (2) sutured along entire length, (3) azygous.
- *6. Frontoparietal, supraorbital flange: (0) absent, (1) present.
- *7. Occipital artery pathway, relation to skull roof: (0) superficial, (1) in open groove, (2) enclosed in canal.
- *8. Squamosal-frontoparietal relationship: (0) separated, (1) contact between lamella alaris of squamosal and frontoparietal, with bony bridge arching over the otic capsule to form a post temporal fenestra (*sensu* Lynch 1971: 47), (2) contact between lamella alaris and frontoparietal on the dorsal surface of the otic capsule, no post temporal fenestra present, (3) contact restricted to the otic plate of otic ramus and frontoparietal (e.g. *Bufo*).
- *9. Squamosal, otic ramus, otic plate (= ramus paroticus of Roček 2003): (0) reduced or absent, (1) small otic plate overlapping only most lateral portion of crista parotica, (2) otic plate extensively overlapping prootic.

The return of the mummy: *Thaumastosaurus*, an Eocene pyxicephalid from Western Europe

- *10. Squamosal, zygomatic ramus: (0) reduced, (1) moderately developed, free distal end, (2) well developed, articulated with maxilla.
- 11. Squamosal-nasal relationship: (0) not in contact, (1) in contact.
- 12. Pterygoid, anterior ramus, anterior extent: (0) reaching planum antorbitale, (1) not reaching planum antorbitale.
- 13. Pterygoid, anterior ramus, position relative to maxilla: (0) medial, (1) dorsal.
- #14. Pterygoid, medial ramus, configuration: (0) short, without bony contact with otic capsule, (1) moderately developed, contact with otic capsule, (2) well developed, broad contact, overlapping or sutured with parasphenoid ala.
- 15. Pterygoid, anterior ramus, ventral flange: (0) absent, (1) present.
- 16. Pterygoid, anterior ramus, dorsal flange: (0) absent, (1) present.
- 17. Parasphenoid, cultriform process, anterior extent relative to antorbital plane: (0) well posterior, (1) nearly same level, (2) anterior.
- 18. Parasphenoid, cultriform process, longitudinal ridge on ventral surface: (0) absent, (1) present.
- 19. Parasphenoid, alae, orientation in ventral aspect: (0) angled anteriorly, (1) perpendicular to cultriform process, (2) angled posteriorly.
- 20. Parasphenoid, alae, keels on ventral surface: (0) absent, (1) present.
- 21. Vomer: (0) absent, (1) present.
- 22. Vomer, teeth: (0) present, (1) absent.
- 23. Vomer, teeth, position relative to planum antorbitale: (0) clearly anterior, (1) same level.
- 24. Vomer, teeth, disposition: (0) straight rows, perpendicular to skull midline, (1) straight rows, divergent posteriorly, (2) straight rows, divergent anteriorly, (3) rows arched anteriorly, (4) rows arched posteriorly, (5) few teeth on a round bulging patch.
- 25. Vomer, anterior process, extent relative to maxillary arch: (0) reaching maxillary arch, (1) not reaching maxillary arch.
- 26. Vomer, postchoanal process: (0) not distinct, (1) distinct but short, (2) well developed, long, bordering the entire posterior margin of choana.

The return of the mummy: *Thaumastosaurus*, an Eocene pyxicephalid from Western Europe

27. Palatine, as a discrete element: (0) absent, (1) present.
28. Palatine, odontoids or ridges on ventral surface: (0) absent, (1) present.
29. Sphenethmoid, dorsal exposure between nasals and frontoparietals: (0) absent, (1) present.
30. Sphenethmoid, ventral configuration: (0) single, (1) divided.
31. Sphenethmoid, dorsal configuration: (0) single, (1) divided.
32. Sphenethmoid, orbitonasal foramen: (0) completely bound in bone, (1) incompletely bound in bone or bound in cartilage.
33. Sphenethmoid, planum antorbitale, mineralization: (0) mostly cartilaginous, (1) well ossified, at least one half of planum.
34. Nasal capsule, septum nasi, mineralization: (0) mostly cartilaginous, (1) partially ossified, (2) completely ossified.
35. Nasal capsule, septum nasi, width: (0) wide, nasal capsules medially separate, (1) narrow, nasal capsules medially close.
36. Cartilaginous roofing of cavum cranii, configuration: (0) completely open, (1) taenia tecti transversalis present only, (2) taeniae tecti transversalis and medialis present, (3) tectum parietale present, (4) almost completely chondrified, (5) taeniae tecti medialis present only.
37. Neurocranium, lateral wall at the level of the optic foramen, mineralization: (0) cartilaginous (1) partially or completely ossified.
38. Crista parotica, degree of ossification: (0) mostly cartilaginous, (1) ossified at least one half.
39. Crista parotica, distal expansion: (0) absent, (1) present.
40. Exoccipital, occipital condyles, shape: (0) not stalked, (1) stalked.
41. Tympanic annulus: (0) absent, (1) present.
42. Columella: (0) absent, (1) present.
43. Teeth on premaxilla and maxilla: (0) absent, (1) present.
44. Tooth crown, number of cuspids: (0) two, tooth bicuspid, labial cusp may be present as low blade, (1) one, tooth monocuspid.

The return of the mummy: *Thaumastosaurus*, an Eocene pyxicephalid from Western Europe

45. Premaxilla, pars palatina, palatine process, configuration: (0) distinct, projecting lingually, (1) investing alary process proximally, distinct pointed distal (posterior) tip, (2) entire process investing alary process, blunt distal tip distinct or absent.
46. Premaxilla, pars palatina, lateral end, configuration: (0) not expanded lingually nor projected posteriorly (1) expanded lingually, but less than palatine process, and slightly projected posteriorly, (2) broad but indistinct from the rest of the pars palatina, not projected posteriorly, (3) expanded lingually as much as palatine process, not projected posteriorly, (4) distinctly projected towards maxilla forming an extensive suture, slightly or not expanded lingually, a discrete lingual process may be present.
47. Premaxilla, alary process, orientation: (0) anterodorsal, (1) dorsal, (2) posterodorsal.
48. Premaxilla, contact with maxilla in labial aspect: (0) maxilla abuts premaxilla, (1) maxilla overlaps premaxilla, short anteroventral process, (2) maxilla overlaps premaxilla, long anterodorsal process, (3) maxilla overlaps premaxilla, long anteroventral process, (4) maxilla overlaps entire premaxilla.
- *49. Maxilla, pars facialis in the orbital region, shape: (0) decreases gradually in height in the orbital region, (1) decreases abruptly in height in the orbital region, (2) high along the orbital region but decreases posteriorly, (3) high throughout most of its length.
- *50. Maxilla, pars facialis external surface, aspect: (0) smooth, (1) slightly sculptured, only some ridges present, (2) heavily ornamented, usually tuberculated or pitted, sculpture lies over the external surface of the pars dentalis, (3) heavily ornamented, usually tuberculated or pitted, sculpture lies mainly in a deeper plane than that of the protruding external surface of the pars dentalis.
51. Maxilla, pars facialis, anterodorsal process: (0) absent or reduced (i.e., reaching more posteriorly than the anteroventral margin of the bone) (e.g., *Litoria australis*), (1) reaching more anteriorly than the anteroventral margin of the bone but not well differentiated from the rest of the pars facialis (e.g., *Calyptocephalella*), (2) present, long, projecting anterodorsally and well differentiated from the rest of the pars facialis (e.g., *Ceratophrys*).
52. Maxilla, pars palatina, orientation at the level of the planum anteorbitale: (0) forming a straight angle with the pars dentalis, (1) forming a wide angle with the pars dentalis, (2)

The return of the mummy: *Thaumastosaurus*, an Eocene pyxicephalid from Western Europe

forming a 180° angle with the pars dentalis and parallel to the internal surface of pars facialis.

53. Quadratojugal, pars jugalis: (0) absent, (1) present.

*54. Quadratojugal, dorsal process: (0) absent, (1) present.

*55. Quadratojugal, lateral process: (0) absent, (1) present.

56. Mentomeckelian bone: (0) absent, (1) present.

57. Mentomeckelian bone, lateral process: (0) absent, (1) present.

58. Dentary, fang-like laminar projections: (0) absent, (1) present.

59. Fang-like, symphyseal ectopic ossifications: (0) absent, (1) present.

60. Angulosplenic, coronoid process, shape: (0) poorly developed, low, (1) well developed, distinct process, (2) very well developed, long lamina.

61. Lower jaw, articulation with skull, position: (0) anterior to occiput, but lateral to otic capsule, (1) same level of occiput, (2) well posterior to occiput, (3) well anterior, anterior to otic capsule.

Hyobranchial skeleton

62. Hyoid, hyalia, general configuration: (0) complete, (1) incomplete distally, (2) incomplete proximally.

63. Hyoid, anterior process of hyale: (0) absent, (1) present.

64. Hyoid, process lateral to anterior process of hyale: (0) absent, (1) present.

65. Hyoid plate, anterolateral (alary) processes: (0) absent, (1) present.

66. Hyoid plate, anterolateral (alary) processes, shape: (0) acuminate, (1) narrow stalk and dilated distally, (2) wing-like, (3) broad stalk and dilated distally, (4) confluent with hyoid plate.

67. Hyoid plate, posterolateral process: (0) absent, (1) present.

68. Hyoid plate, posteromedial process, ossification: (0) cartilaginous stalk abuts hyoid plate, (1) ossification reaches hyoid plate, (2) ossification invades hyoid plate.

69. Hyoid plate, posteromedial process, flange on medial side: (0) absent, (1) present.

70. Hyoid, posterior projection on hyoid plate: (0) absent, (1) present.

The return of the mummy: *Thaumastosaurus*, an Eocene pyxicephalid from Western Europe

71. Hyoid plate, shape: (0) wide, width greater than, or equal to, length, (1) narrow, longer than wide.
72. Hyoid plate, calcification: (0) absent, (1) present.
73. Parahyoid bone: (0) absent, (1) present.

Vertebra Column

74. Presacral vertebrae, number (irrespective of fusions): (0) more than eight, (1) eight or less.
75. Trunk vertebrae, centrum formation: (0) perichordal, (1) epichordal.
76. Atlas, cotyle arrangement: (0) fully confluent (Type III), (1) juxtaposed (Type II), (2) widely separated (Type I).
77. Atlas, cotyle position relative to neural canal: (0) completely ventral, (1) ventrolateral.
78. Vertebrae I and II relationship: (0) completely separate, (1) neural spine I flattened, overlapping and fused to neural arch II, (2) completely fused.
79. Posterioormost presacral vertebra, centrum configuration: (0) spool-like, (1) opisthocoealous, (2) procoelous, (3) biconcave.
80. Posterior four presacrals, neural arches, imbrication: (0) present, (1) absent.
81. Anterior presacrals, neural spines: (0) absent or low, (1) high, dorsally directed, (2) high, posteriorly directed.
82. Vertebra VI, transverse processes, posterior margin orientation: (0) nearly perpendicular to longitudinal axis or slightly posterior, (1) moderately forward, (2) markedly forward.
83. Vertebra IV, transverse processes, mediolateral length relative to that of sacral diapophyses: (0) nearly equal or slightly longer, (1) much longer (25% or more).
84. Posterioormost presacral vertebra, transverse processes, mediolateral length relative to that of sacral diapophyses: (0) clearly shorter, (1) equal or subequal.
85. Vertebra III, transverse processes/associated ribs, uncinat processes: (0) present, (1) absent.

The return of the mummy: *Thaumastosaurus*, an Eocene pyxicephalid from Western Europe

86. Sacral diapophyses, distal expansion in dorsal view, evaluated as the distal length (DL) relative to the maximum distance between distal margins of diapophyses (MW) = sacral width of Trueb & Tyler (1974): (0) widely expanded ($DL \geq \frac{1}{2} MW$) (1) moderately expanded ($\frac{1}{2} MW > DL \geq \frac{1}{4} MW$), (2) slightly expanded or narrow ($DL < \frac{1}{4} MW$).
87. Sacral diapophyses, distal ends in lateral view: (0) distinctly flattened (height $< \frac{1}{2}$ anteroposterior length), (1) roughly rounded (height nearly $\frac{1}{2}$ length).
88. Sacral diapophyses, anterior margin, orientation with respect to longitudinal axis in dorsal view: (0) posterolateral, (1) nearly perpendicular, (2) anterolateral.
89. Sacral diapophyses, general orientation in posterior aspect, with respect to the horizontal plane, (0) nearly horizontal or slightly angled dorsally, (1) strongly angled dorsally, forming an angle of 15° or larger.
90. Sacral vertebra, articulation with urostyle: (0) synchondrotic, notochord persistent, (1) bicondylar, (2) monocondylar, (3) fused.
91. Urostyle, transverse processes: (0) present, (1) absent.
92. Urostyle, length relative to presacral portion of vertebral column: (0) nearly as long, or longer, (1) clearly shorter (85% or less).
93. Urostyle, dorsal crest: (0) absent or low ridge, (1) moderate or high, but extending only throughout the anterior one half of urostyle, (2) well developed, high and extending along most of the urostyle.
94. Urostyle, anterodorsal process at anterior end of dorsal crest: (0) absent or poorly developed, (1) distinct, well developed.
95. Urostyle, shape in lateral view: (0) straight, (1) arched.
96. Free ribs in adults: (0) absent, (1) present.
97. Free intervertebral discs in subadults: (0) absent, (1) present.
98. Dorsal shield formed by medial or medial and lateral elements joined to each other and to the vertebrae by ligaments: (0) absent, (1) present.
99. Dorsal shield formed by at least medial elements continuous with the neural spines: (0) absent, (1) present.

The return of the mummy: *Thaumastosaurus*, an Eocene pyxicephalid from Western Europe

Pectoral girdle

100. Pectoral girdle, omosternum: (0) absent, (1) present.
101. Pectoral girdle, omosternum, degree of ossification: (0) completely cartilaginous, (1) with ossified style.
102. Pectoral girdle, sternum, degree of ossification: (0) completely cartilaginous or irregularly calcified, (1) with an ossified style.
103. Pectoral girdle, sternum, shape: (0) short and wide, semicircular to rhomboid, (1) proximally bifurcated in long projections, (2) long and distally rounded, (3) inverted mushroom, style short and wide, (4) anchor or arrow, style long and narrow, (5) broad, longer than wide, with posterior notch, (6) narrow style, distally bifurcated, (7) wider posteriorly than anteriorly, irregular posterior margin.
104. Pectoral girdle, epicoracoids in the coracoideal region, relation to one another: (0) overlapping, (1) not overlapping.
105. Coracoid, sternal end, expansion relative to the length of bone: (0) less than $\frac{1}{2}$, (1) more than $\frac{1}{2}$.
106. Coracoid, sternal end, shape: (0) symmetrical, (1) asymmetrical.
107. Coracoid, posterodorsal process: (0) absent, (1) present.
108. Clavicle: (0) present, (1) absent.
109. Clavicle, orientation: (0) anteromedial, (1) perpendicular, (2) posterior.
110. Clavicle, medial portion, shape: (0) strongly bowed anteriorly, (1) moderately bowed anteriorly, (2) straight or nearly so, (3) bowed posteriorly.
111. Clavicle, relationship with scapula: (0) overlaps anterior margin, (1) abuts pars acromialis, (2) fused.
112. Scapula, maximum width of glenoid fossa relative to maximum width of shaft: (0) more than 1, (1) between 1 and $\frac{1}{2}$, (2) less than $\frac{1}{2}$.
113. Scapula, medial cleft: (0) absent, (1) present.
114. Scapula, anterior margin, processes or crests: (0) absent, (1) ridge or a small knob on pars acromialis, (2) moderately crest on proximal half of shaft, (3) long lamina, (4) with a short crest strongly deflected anteroventrally to form a deep basin.

The return of the mummy: *Thaumastosaurus*, an Eocene pyxicephalid from Western Europe

115. Cleithrum, overall shape in dorsal view: (0) lip of bone along the anterior margin of suprascapula, (1) lateral (scapular) margin straight, distinctly forked with anterior and posterior branches, (2) lateral margin may have a small notch at the anterior corner, distinct anterior branch, but posterolateral region of cleithrum plate-like, a small posterior branch may be present, (3) lateral margin with/out an ample notch, posterior region narrow, lacking a posterior branch, (4) extensive plate-like element investing almost entire dorsal surface of supraescapular cartilage.

Forelimb

116. Humerus, ventral condyle, diameter relative to total distal width at epicondyle level: (0) small (<0.58), (1) large (>0.58).

117. Intercalary elements: (0) absent, (1) present.

118. Preaxial carpals (element Y and distal 2), configuration: (0) separate, (1) fused.

119. Postaxial carpals (ulnare and distals 3, 4 and 5), configuration: (0) all free, (1) ulnare and 3 free, 4+5, (2) ulnare free, 3+4+5, (3) ulnare+5, 3 and 4 free.

120. Prepollex, number and shape of prepollical elements: (0) one, spherical or elongate, (1) two, distal may be elongate, (2) three or more, spherical or elongate, (3) two, distal hypermorphic, (4) two, spine-like.

121. Fingers 1 and 2 (digits II and III), relative lengths: (0) $II < III$ (1) $II = III$, (2) $II > III$.

122. Carpal torsion: (0) absent, (1) present.

Pelvic Girdle

123. Ilium, dorsal crest, development: (0) absent or low ridge, (1) moderately high (0.5 to 0.9x height of shaft), (2) high, well developed (as high as shaft or more).

124. Ilium, ventral acetabular expansion in acetabular view relative to height of acetabulum: (0) reduced (maximum length <0.4), (1) moderately developed (maximum length >0.4 and <0.8), (2) well developed (maximum length >0.8).

125. Ilium, angle between iliac shaft and ventral acetabular expansion: (0) acute, (1) straight, (2) obtuse.

The return of the mummy: *Thaumastosaurus*, an Eocene pyxicephalid from Western Europe

126. Ilium, dorsal acetabular expansion in acetabular view in relation to height of acetabulum: (0) reduced (maximum length <0.4), (1) moderately developed (maximum length >0.4 and < 0.8), (2) well developed (maximum length >0.8).
127. Ilium, ischiatic process: (0) absent, (1) present.
128. Ilium, dorsal prominence: (0) absent, (1) present.
129. Ilium, dorsal tubercle morphology: (0) low prominence, protuberance inconspicuous, (1) prominence scarcely discernible from iliac outline, elongate protuberance slightly projected laterally, (2) spike-like prominence, protuberance inconspicuous or not, (3) low prominence, rounded protuberance slightly laterally projected, (4) prominence scarcely discernible from iliac outline, elongate protuberance laterally projected.
130. Ilium, spiral groove: (0) absent, (1) present.
131. Ischium, posterodorsal expansion: (0) not developed, (1) well developed.
132. Ischium, posterior margin, shape: (0) convex, (1) straight, (2) concave.
133. Pubic region, mineralization: (0) cartilaginous, (1) mineralized.
134. Epipubis: (0) absent, (1) present.

Hindlimb

135. Femur, femoral crest: (0) absent, (1) present.
136. Femur, length relative to tibiofibula length: (0) shorter, (1) nearly equal, (2) longer.
137. Proximal tarsals (tibiale and fibulare), configuration: (0) separate, (1) proximally and distally fused, (2) completely fused.
138. Distal tarsals 3 and 2, configuration: (0) free, (1) fused.
139. Distal tarsal 1, as a discrete element: (0) absent, (1) present.
140. Prehallux, number and shape of prehallical elements: (0) one, spherical or elongate (1) two, spherical or elongate, (2) three or more, spherical or elongate, (3) two, distal hypermorphic axe-head-shaped, (4) three or more, axe-head-shaped.
141. Toe IV, terminal phalanx, general shape: (0) straight, (1) curved.
142. Toe IV, terminal phalanx, shape of distal end: (0) simple, (1) notched, (2) T-shaped, (3) Y-shaped, (4) clearly knobbed, (5) arrow-shaped.

The return of the mummy: *Thaumastosaurus*, an Eocene pyxicephalid from Western Europe

External Morphology

143. Pupil shape: (0) vertical, (1) triangular, (2) horizontal, or mainly so.

Appendix S4. Taxa list

† marks extinct taxa, taxa names in bold represent the taxa added by this study. Nomina in () represent the one used in the dataset of Báez and Gómez (2018) that were synonymized with the correct nomen (following the taxonomy proposed by Dubois et al., 2021).

Adelotus brevis

Allophryne ruthveni

Alytes obstetricans

Arariphrynus placidoi †

Arthroleptis adolfifriederici

Arthroleptella lightfooti

Ascaphus truei

Asterophrys riparius (*Cophixalus riparius*)

Atelognathus patagonicus

Aubria subsigillata

Baurubatrachus pricei †

Beelzebufo ampinga †

Bombina variegata

Bufo bufo

Cacosternum boettgeri

Cacosternum namaquense

Calyptocephalella gayi

Cornufer guentheri (*Ceratobatrachus guentheri*)

Ceratophrys calcarata

Ceratophrys cornuta

Ceratophrys cranwelli

The return of the mummy: *Thaumastosaurus*, an Eocene pyxicephalid from Western Europe

Chacophrys pierottii

Conraua crassipes

Cratia gracilis †

Cycloramphus dubius

Dermatonotus muelleri

Eleutherodactylus inoptatus

Eurycephalella alcinae †

Flectonotus fitzgeraldi

Gastrotheca monticola

Heleioporus australiacus

Heleophryne natalensis

Hemiphractus fasciatus

Hylambates verrucosus (*Phlyctimantis verrucosus*)

Hypsiboas pulchellus

Indirana phrynoderma

Lepidobatrachus asper

Lepidobatrachus laevis

Leptodactylus latrans

Limnonectes biythii

Litoria lesueurii

Megophrys montana

Melanophryniscus stelzneri

Mixophyes schevilli

Natalobatrachus bonebergi

Nyctibatrachus major

Odontobatrachus natator

Odontophrynus americanus

Oreobates discoidalis

Osteopilus dominicensis

The return of the mummy: *Thaumastosaurus*, an Eocene pyxicephalid from Western Europe

Pelobates cultripes

Pelodytes punctatus

Peltophryne empusa

Petropedetes palmipes

Petropedetes vulpiae

Phrynobatrachus kreffti

Phrynomantis bifasciatus

Phyllomedusa sauvaagii

Platyplectrum ornatum

Pleurodema cinereum

Pristimantis huicundo

Pristimantis wnigrum

Proceratophrys boiei

Ptychadena mascareniensis

Pyxicephalus adpersus

Rana temporaria

Ranoidea australis (*Litoria Cyclorana australis*)

Ranoidea longipes (*Litoria Cyclorana longipes*)

Rhinella arenarum

Scaphiopus couchii

Spea hammondi

Spea multiplicata

Strabomantis bufoniformis

Strabomantis ingeri

Strongolypus grayii

Telmatobius marmoratus

Telmatobius oxycephalus

Telmatobius verrucosus

Telmatobius hauthali

The return of the mummy: *Thaumastosaurus*, an Eocene pyxicephalid from Western Europe

Telmatobius scrocchii

Telmatobufo venustus

Thaumastosaurus servatus †

Thoropa miliaris

Tomopterna tuberculosa

Uberabatrachus carvalhoi †

Appendix S5. Nexus file containing the matrix used for all analyses

The appendix can be found on Morphobank at: <http://morphobank.org/permalink/?P3898>

Appendix S6. List of synapomorphies for selected clades

Analysis under EW, unordered

Thaumastosaurus servatus + hyperossified ranoids : 6: 0→1, 7: 0→2, 9: 1→2, 10: 1→2, 11: 0→1, 14: 1→2, 20: 0→1, 25: 1→0, 33: 0→1, 34: 0→1, 39: 0→1, 46: 1→3, 49: 0→2, 50: 0→2, 79: 2→3, 81: 0→1, 84: 0→1, 86: 1→2, 87: 0→1, 101: 0→1, 102: 0→1, 104: 0→1, 105: 0→1, 110: 1→2, 123: 0→2, 125: 1→0

Analysis under EW, ordered

“Ranoides” clade: 3: 2→0, 19: 2→1, 38: 1→0, 101: 0→1, 104: 0→1, 105: 0→1, 109: 0→2, 110: 1→2, 121: 2→1

T. servatus + hyperossified ranoids: 3: 0→2, 7: 0→2, 9: 1→2, 10: 1→2, 11: 0→1, 38: 0→1, 39: 0→1, 50: 0→2; 81: 0→1

Arthroleptis + (*Arariphrynus placidoi* + *Phlyctimantis verrucosus*): 67: 1→0, 102: 1→0, 112: 1→2, 131: 1→0

Arariphrynus placidoi + *Phlyctimantis verrucosus* : 40: 0→1, 49: 0→1, 92: 0→1

Analysis under IW (k = 3)

Neobatrachia: 27: 0→1, 78: 0→2, 86: 0→1, 87: 2→1, 0→1, 137: 0→1

‘Ranoides’ clade: 3: 2→0, 101: 0→1, 104: 0→1, 105: 0→1, 109: 0→2, 110: 1→2, 121: 2→1

The return of the mummy: *Thaumastosaurus*, an Eocene pyxicephalid from Western Europe

Thaumastosaurus servatus + Pyxicephalinae: 1:1,2→0, 3: 1→2, 6: 1→0, 7: 0→2, 9: 1→2, 10: 1→2, 11: 0→1, 14: 1→2, 25: 1→0, 39: 0→1, 50: 0→2, 81: 0→1

Analysis under IW (k = 7)

T. servatus + *A. subsigillata*: 28: 1→0

Pyxicephalinae: 11: 0→1; 33: 0→1; 64: 0→1

Cornufer guntheri + Pyxicephalinae: 3:0→2, 6: 0→1, 9: 1→2, 10: 1→2, 14: 1→2, 25: 1→0, 34: 0→1, 39: 0→1, 50: 0→2, 81: 0→1

Analysis under IW (k = 12)

T. servatus + *A. subsigillata*: 28: 1→0

Pyxicephalinae: 11: 0→1; 33: 0→1; 64: 0→1

Cornufer guntheri + Pyxicephalinae: 3:0→2, 6: 0→1, 9: 1→2, 10: 1→2, 14: 1→2, 25: 1→0, 34: 0→1, 39: 0→1, 50: 0→2, 81: 0→1

Constrained on the phylogeny of Jetz and Pyron (2018), EW

T. servatus + *P. adspersus* + *A. subsigillata*: 1: 2→0, 3: 0→2, 6: 0→1, 7:0→2, 9: 1→2, 10: 1→2, 11: 0→1, 14: 1→2, 25: 1→2, 33: 0→1, 39: 0→1, 50: 0→1, 81:0→1

Constrained on the phylogeny of Feng et al. (2017), EW

T. servatus + *P. adspersus* + *A. subsigillata*: 1: 2→0, 3: 0→2, 6: 0→1, 7:0→2, 9: 1→2, 10: 1→2, 11: 0→1, 14: 1→2, 25: 1→2, 33: 0→1, 34: 0→1, 38: 0→1, 39: 0→1, 50: 0→1, 61: 0→2, 64: 0→1, 81:0→1.

Constrained on the phylogeny of Jetz and Pyron (2018), IW (k = 7)

T. servatus + (*P. adspersus* + *A. subsigillata*): 1: 2→0, 3: 0→2, 6: 0→1, 7:0→2, 9: 1→2, 10: 1→2, 11: 0→1, 14: 1→2, 25: 1→2, 33: 0→1, 39: 0→1, 50: 0→1, 81:0→1

Constrained on the phylogeny of Feng et al. (2017), IW (k = 7)

T. servatus + (*P. adspersus* + *A. subsigillata*): 1: 2→0, 3: 0→2, 6: 0→1, 7:0→2, 9: 1→2, 10: 1→2, 11: 0→1, 14: 1→2, 25: 1→2, 33: 0→1, 39: 0→1, 50: 0→1, 81:0→1

The return of the mummy: *Thaumastosaurus*, an Eocene pyxicephalid from Western Europe

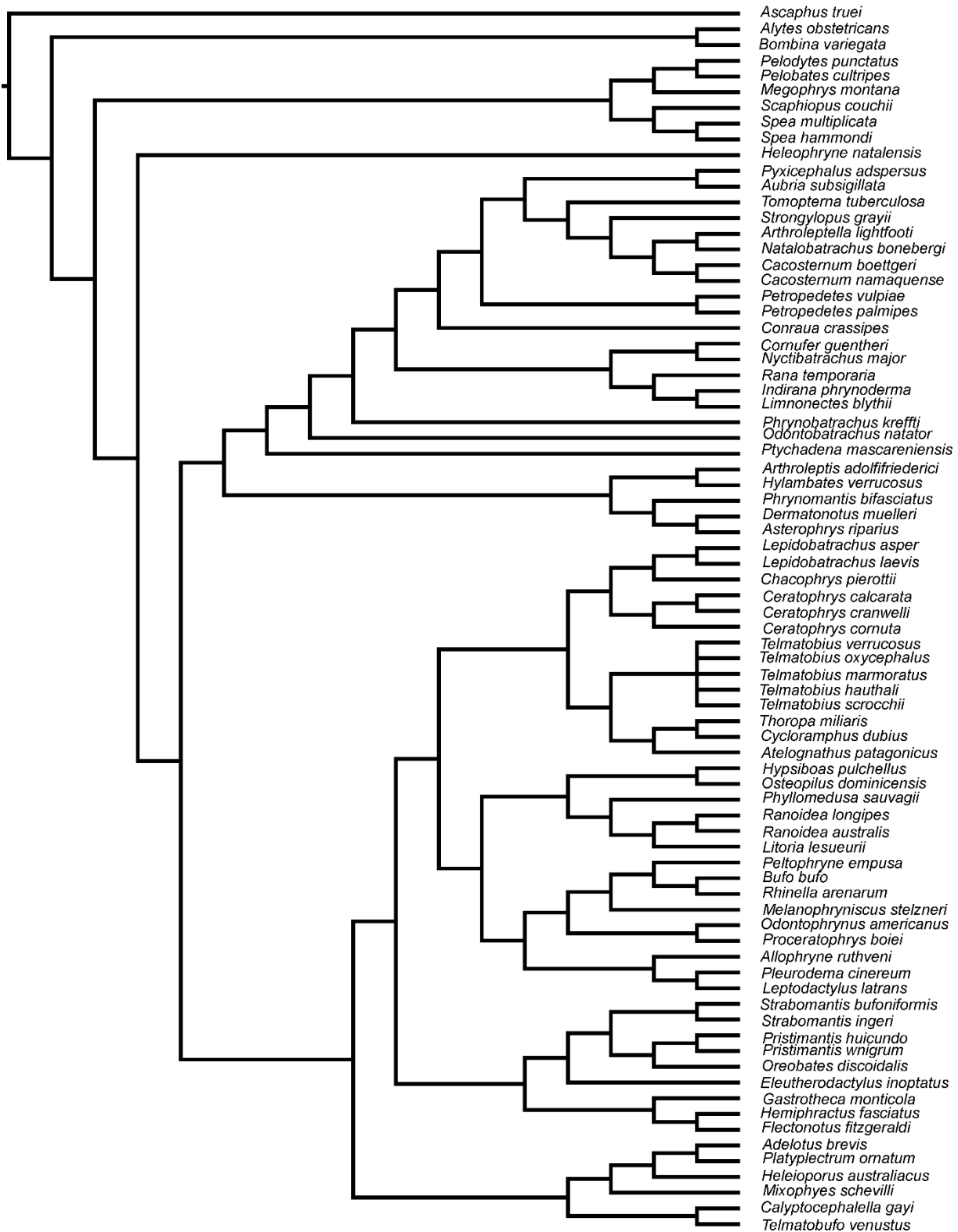


FIGURE S2. Tree used for the constrained analyses under a phylogeny inferred from Jetz and Pyron, 2018.

The return of the mummy: *Thaumastosaurus*, an Eocene pyxicephalid from Western Europe

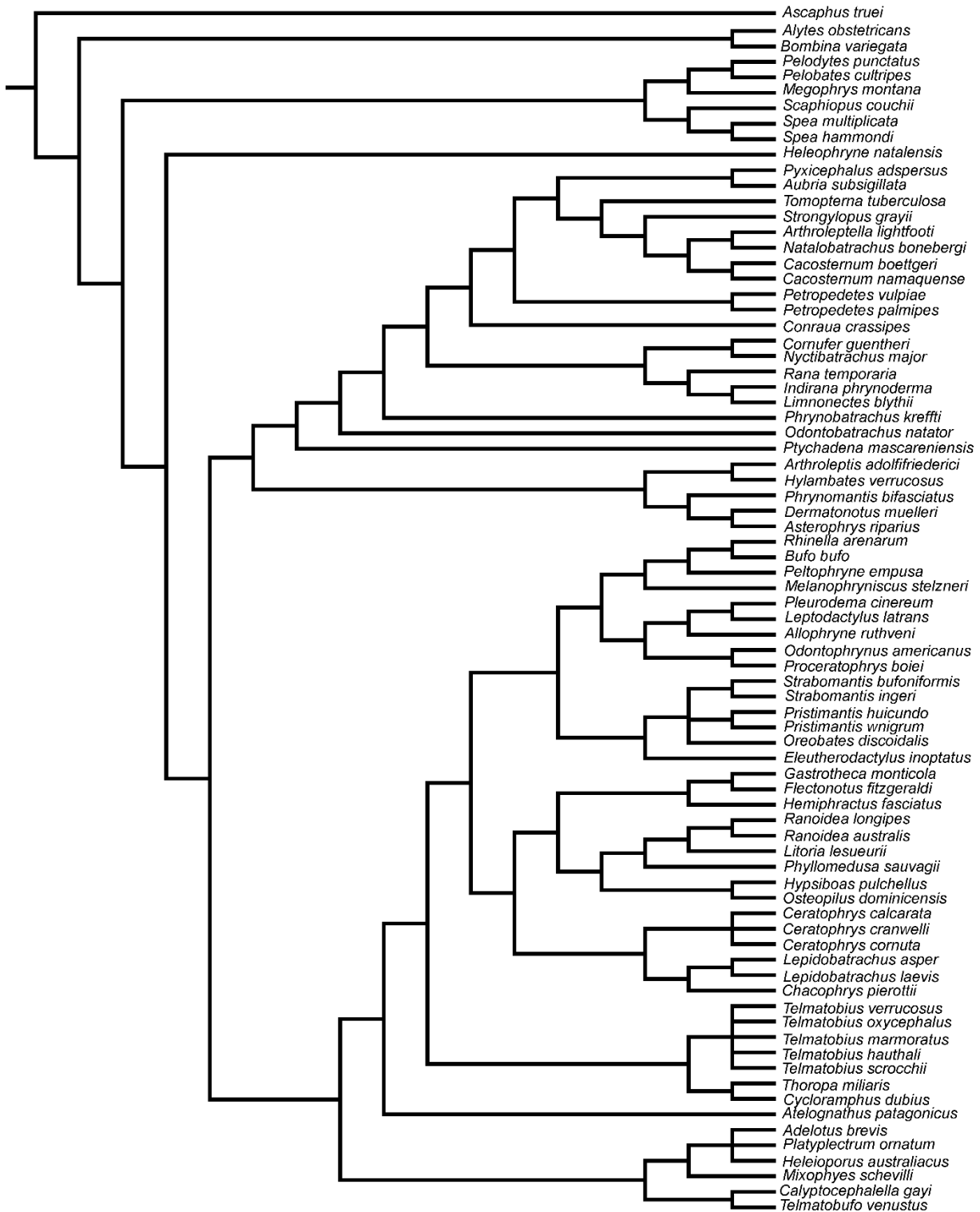


FIGURE S3. Tree used for the constrained analyses under a phylogeny inferred from Feng et al., 2017.

2. Conversion of the names Pyxicephaloidea, Pyxicephalidae and Pyxicephalinae (Anura, Ranoidea) into phylogenetic nomenclature

X.12 Introduction

Since its first edition in 2000 (Cantino & Queiroz 2020), the *PhyloCode* has evolved to propose an alternative to the rank-based nomenclature system traditionally used, by proposing a system based on phylogenetic principles. Its objective is not to replace existing names, but rather to provide another system for governing the application of said names. With the publication of the sixth edition of the *PhyloCode* (Cantino & Queiroz, 2020) and of the monograph *Phylonyms* (Queiroz & Cantino, 2020), it is now possible to publish nomenclatural acts (definitions of new or converted names that will establish priority under that code) that will have official standing under the *PhyloCode*. The first set of nomenclatural acts established under the *PhyloCode* was published in the monograph *Phylonyms* (Queiroz et al., 2020). Now, nomenclatural acts valid under the *PhyloCode* can be published in regular journals. Among amphibian taxa, much remains to be done because only *Amphibia* (Laurin et al., 2020a), *Lissamphibia* (Laurin et al., 2020b), *Caudata* (D. B. Wake, 2020) and *Gymnophiona* (M. H. Wake, 2020) have been converted so far. Building on our recent phylogenetic analysis of the “RANOIDEA” Ford and Cannatella, 2004 (~ SCOPTANURA in Dubois et al., 2021), we take the opportunity to convert three taxon names on which our recent work focuses (Lemierre et al., 2021). We follow the nomenclature proposed by Dubois et al. (2021) in their recent work regarding the names that we convert.

X.13 Typographic conventions

Throughout this paper, we use the following conventions for the writing of different kinds of nomina (scientific names):

The return of the mummy: *Thaumastosaurus*, an Eocene pyxicephalid from Western Europe

[A] Nomina managed under the current *International Code of Zoological Nomenclature* (Anonymous 1999, 2012) are presented according to the following standard formats: *italic lower-case letters* for nomina of species and genera (e.g. *Pyxicephalus*, *Pyxicephalus adspersus*); *ITALIC SMALL UPPER CASES* for nomina of families, subfamilies, tribes and related ranks (e.g., *PYXICEPHALIDAE*); **BOLD SMALL UPPER CASES** for nomina of orders, classes, phyla and taxa at other higher ranks (e.g., **AMPHIBIA**).

[B] Nomina managed under the *PhyloCode* are presented in *bold italic lower-case letters* (e.g., *Pyxicephalidae*).

Other conventions

~ : but not

∇ : clade

RegNum registration number : Registration number of the name definition on the RegNum website.

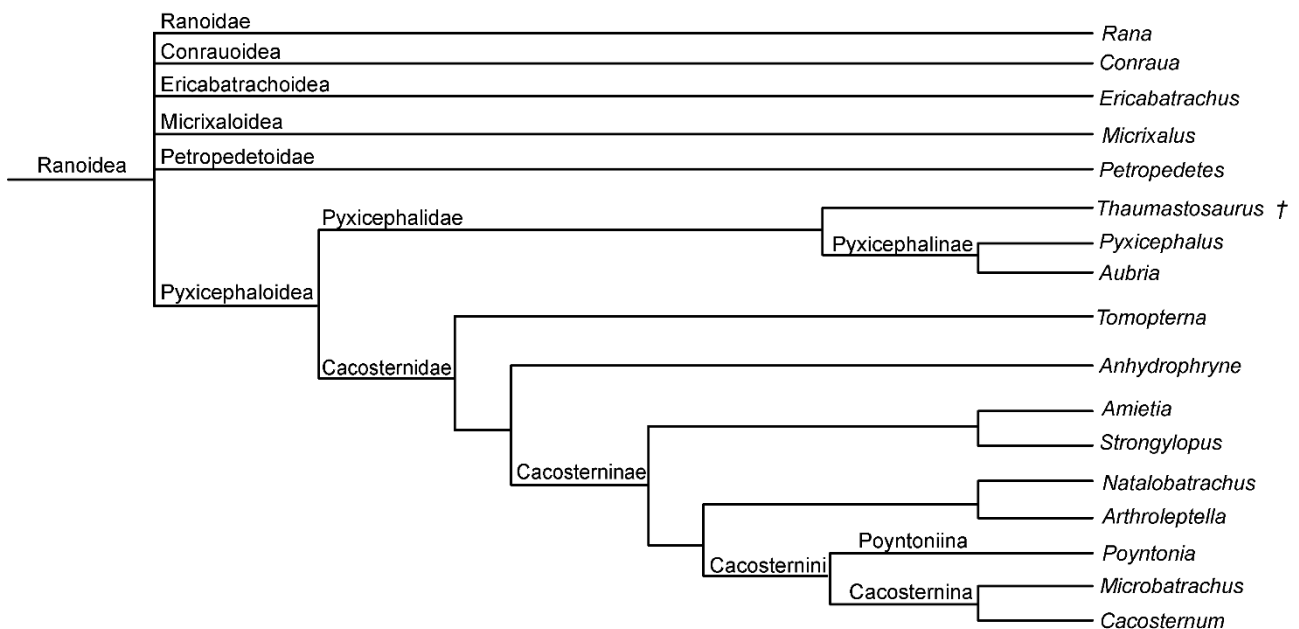


FIGURE X-23. Simplified phylogeny of the *Pyxicephaloidea* modified from the phylogeny of Dubois et al (2021). Position of *Thaumastosaurus* has been inferred from Lemierre et al (2021). Terminal taxa are at the generic level and † represents an extinct taxon.

X.14 Phylogenetic nomenclature

The return of the mummy: *Thaumastosaurus*, an Eocene pyxicephalid from Western Europe

Pyxicephaloidea Bonaparte, 1850 [Lemierre & Laurin], converted clade name
(RegNum registration number: 558)

Definition—The largest clade containing *Pyxicephalus adpersus* Tschudi, 1838, *Aubria subsigillata* Duméril, 1856, *Cacosternum boettgeri* Boulenger, 1882 and *Tomopterna natalensis* Smith, 1849, but not *Petropedetes palmipes* Boulenger, 1905 (*PETROPEDETOIDAE*), *Micrixalus fuscus* Boulenger, 1882 (*MICRIXALOIDAE*), *Ericabatrachus baleensis* Largen, 1991 (*ERICABATRACHOIDAE*), *Pelophylax ridibundus* Pallas, 1771 (*RANOIDAE*) and *Conraua goliath* Boulenger, 1906 (*CONRAUOIDAE*). Abbreviated definition: max total ∇ (*Pyxicephalus adpersus* Tschudi, 1838, *Aubria subsigillata* Duméril 1856, *Cacosternum boettgeri* Boulenger 1882 ~*Petropedetes palmipes* Boulenger, 1905, *Micrixalus fuscus*, Boulenger, 1882, *Ericabatrachus baleensis* Largen, 1991, *Pelophylax ridibundus* Pallas, 1771 and *Conraua goliath* Boulenger, 1906).

Etymology—Named after the eponymous genus *Pyxicephalus* Tschudi, 1838. Derived from the ancient Greek *pyxis* ('round' box) and *kephalē* (head). These two roots refer to the bulky head of *Pyxicephalus adpersus* Tschudi 1838.

Reference phylogeny—The primary reference phylogeny is Jetz & Pyron (2018: fig. S1; see also Dubois et al. 2021: appendix A2. tree 1) for the relationship between and within the two extant clades of *PYXICEPHALOIDAE*, *PYXICEPHALIDAE* and *CACOSTERNIDAE*, and for the position of *PYXICEPHALOIDEA* among *RANOIDEA*. Other phylogenies focused on *NATATANURA* (~*PANANURA* in Dubois et al., 2021) include Yuan et al. (2019, fig. 2) and those by Bittencourt-Silva et al. (2016, fig. 4), Cai et al. (2019, fig. 4), more focused on *PYXICEPHALOIDAE* and one more focused on *CACOSTERNIDAE* by Van der Meijden et al. (2011, fig.1–2).

Composition—*Pyxicephaloidea* encompasses two clades: [1] the *PYXICEPHALIDAE* Bonaparte, 1850, comprising *Pyxicephalus* Tschudi, 1838, *Aubria* Boulenger, 1917 and *Thaumastosaurus* De Stefano, 1903, and [2] the *CACOSTERNIDAE* Noble, 1931, comprising *Amietia* Dubois, 1987, *Anhydrophryne* Hewitt, 1919, *Arthroleptella* Hewitt, 1926, *Cacosternum* Boulenger, 1887, *Microbatrachella* Hewitt, 1926, *Natalobatrachus* Hewitt & Methuen, 1912,

The return of the mummy: *Thaumastosaurus*, an Eocene pyxicephalid from Western Europe

Nothophryne Poynton, 1963, *Poyntonina* Channing & Boycott, 1989, *Strongylopus* Tschudi, 1838 and *Tomopterna* Duméril & Bibron, 1841.

Diagnostic apomorphies—Unfortunately, no morphological synapomorphies have been identified for this clade (Frost et al., 2006), with the different taxa possessing very heterogeneous morphologies. Recent studies have been focused on molecular characters rather than morphological ones (mostly because the former yielded more robust results). However, a recent morphological analysis by Lemierre et al. (2021) recovered this clade, supported by a non-unique combination of three synapomorphies: [1] presence of an open groove for pathway of occipital artery on skull (also present in *CERATOBATRACHINAE* for example); [2] pars facialis of maxillae bearing slight ornamentation (also present in *CERATOPHRYIDAE* and *CERATOBATRACHINAE* for example); [3] digits II and III of forelimb of the same length (also present in *PTYCHADENIDAE*, for example). However, these synapomorphies are only for the smallest clade including the sampled taxa from the analyses (see Lemierre et al. 2021: Appendix S4) and were obtained on a constrained topology taken from the phylogenetic analyses of Jetz & Pyron (2018). In addition, two of these characters are further modified in *Pyxicephalidae* (see below). There is however a high molecular support for this clade (Dubois, 2005; Van der Meijden et al., 2005; Frost et al., 2006), and it is recovered in all recent molecular analyses for anurans or *RANOIDEA* (Pyron & Wiens, 2011; Van der Meijden et al., 2011; Frazão et al., 2015; Feng et al., 2017; Jetz & Pyron, 2018).

Synonyms—Synonyms are *PHRYNOPSINAE* Noble, 1931 (its type genus was synonymized with *Pyxicephalus*), as mentioned by Loveridge (1936) and Laurent (1946), *CACOSTERNINAE* Noble, 1931 (according to Dubois, 1994 and Frost et al., 2006), and *TOMOPTERNINI* Dubois, 1987 (according to Frost et al., 2006).

Comments—The name *PYXICEPHALIDAE* has been erected early to accommodate the newly described *Pyxicephalus* (Bonaparte, 1850). However, this taxon was soon considered a subgenus of *Rana*, a common situation for numerous ranoids taxa (Boulenger 1920*a–b*; Noble, 1931), and the name *Pyxicephalus* fell into disuse for more than a century. However, slowly, several subgenera were raised to generic rank (Dubois, 1981), as the large genus

The return of the mummy: *Thaumastosaurus*, an Eocene pyxicephalid from Western Europe

Rana began to be dismantled. For several taxa, including *Aubria* and *Pyxicephalus*, this work linked with the dismantling of *Rana* was still ongoing in the 1980s and 1990s, although Laurent (1953) already recognized *Aubria* as a genus. Thus, Dubois (1981, 1983) dismantled *Rana* into several subfamilies and genera, but conserved *Pyxicephalus* and *Aubria* as subgenera of *Rana*. Poynton & Broadley (1985) split *Rana* further, recognizing *Pyxicephalus* and *Aubria* as genera, but retained them within the Raninae. The two genera were considered close (see *Pyxicephalidae*) and the family *PYXICEPHALIDAE* was used to accommodate this relationship (Dubois, 1987).

In addition, several new taxa of African anurans were described (Hewitt & Methuen 1912; Hewitt 1919, 1925, 1926) and considered as distinct genera during the 20th century. To accommodate some of these taxa, Noble (1931) erected *CACOSTERNINAE* as a subfamily of *BREVICIPITIDAE* which included *Cacosternum* and *Anhydrophryne*; he considered them to be close to *ARTHROLEPTINAE*, within the much larger *RANIDAE*. A decade later, Laurent (1941), in his work on African ranids, discarded *CACOSTERNIDAE* and erected the subfamily *PHRYNOBATRACHINAE* (within the *RANIDAE*), in which he placed various African ranids, among which the cacosternins *Anhydrophryne*, *Arthroleptella*, *Cacosternum*, *Natalobatrachus*, *Microbatrachella* and *Nothophryne*. That arrangement was accepted by Dubois (1981, 1982) and Poynton & Broadley (1985). A decade later, Dubois (1992), having elevated the subfamily *PHRYNOBATRACHINAE* to family rank, proposed resurrecting the subfamily *CACOSTERNINAE* within this family.

Affinities of *PYXICEPHALIDAE* and *CACOSTERNINAE* to other *SCOPTANURA* remained unclear, at least until the application of molecular phylogenetics to anurans (Frost *et al.* 2006) and ranoids (Dubois, 2005; Scott, 2005; Van der Meijden *et al.*, 2005), in particular. These studies showed that *PYXICEPHALIDAE* and *CACOSTERNIDAE* formed a clade. The close relationship between the two families, as well as other taxa (such as *Strongylopus*), was unexpected but supported by several molecular analyses (Dubois 2005; Van der Meijden *et al.*, 2005; Frost *et al.*, 2006) that led to the recognition of a larger “Southern African Ranids” clade (*sensu* Van der Meijden *et al.*, 2005). This led Dubois (2005) to place all members of *CACOSTERNIDAE* within the subfamily *PYXICEPHALINAE*. The major analysis of Frost *et al.* (2006) showed that

The return of the mummy: *Thaumastosaurus*, an Eocene pyxicephalid from Western Europe

both clades were well supported and were sister-taxa. They recognized both *PYXICEPHALINAE* and *CACOSTERNINAE* and used the old name *PYXICEPHALIDAE* from Bonaparte (1850) as the name of the large clade encompassing both subfamilies. This topology was supported with subsequent analyses of Bossuyt et al. (2006), Pyron & Wiens (2011) and Van der Meijden et al. (2011), and more recent studies still find a close relationship between the two clades (Bittencourt-Silva et al., 2016; Feng et al., 2017; Jetz & Pyron, 2018; Cai et al., 2019). The recent work of Dubois et al (2021) also corroborated this relationship, but considered the two clades as two families, *PYXICEPHALIDAE* and *CACOSTERNIDAE*, grouped in an epifamily *PYXICEPHALOIDAE*. The relationships of *PYXICEPHALOIDAE* to other *RANOIDEA* are still unclear and unstable, forming a large hexatomy with the epifamilies *CONRAUIDAE*, *ERICABATRACHOIDAE*, *MICRIXALOIDAE*, *RANOIDEAE* and *PETROPEDETOIDAE* (Dubois et al., 2021). In addition, recent analyses (Lemierre et al., 2021) have placed the extinct *Thaumastosaurus* De Stefano, 1903 within the clade, as a member of the *PYXICEPHALIDAE*. *Thaumastosaurus* was long thought to be close to South American hyloids (Roček & Lamaud, 1995), but recent analyses incorporating new data, notably on the postcranium (Laloy et al., 2013; Báez & Gómez, 2018), placed it as a *RANOIDEA*, close to a clade that includes pyxicephalids and ceratobatrachids. Both pyxicephalids and ceratobatrachids are not sister-taxa, and this result was linked to poor *RANOIDEA* taxonomic sample and convergent hyperossified-linked characters. Recent analyses (Lemierre et al., 2021), using an expanded taxonomic sample of *RANOIDEA*, placed *Thaumastosaurus* inside the *Pyxicephaloidea* and *Pyxicephalidae*, as the sister-taxa to a clade composed of the extant *Pyxicephalinae*.

Today, *Pyxicephaloidea* are found in sub-Saharan Africa from Gambia (Western Africa; Channing & Rödel, 2019) to Southern Somalia (East range) and south to Cape Province, South Africa (Channing, 2001). *Thaumastosaurus* is known in Western Europe from the middle Eocene (around 39.5 Ma; Vasilyan, 2018) to late Eocene (around 33.5 Ma; Vasilyan, 2018), which represent the only occurrences of the clade outside of its present range.

The return of the mummy: *Thaumastosaurus*, an Eocene pyxicephalid from Western Europe

With the exception of *Thaumastosaurus*, the fossil record for *PYXICEPHALOIDAE* is limited to the Neogene, with the oldest remains attributed to the clade date to the Pleistocene, around 1 Ma (Gardner & Rage, 2016). However, molecular age estimates for the clade suggest an origin around the Cretaceous/Paleogene transition (around 60 Ma, according to Feng et al., 2017; 62, 87 Ma according to Bittencourt-Silva et al., 2016).

Pyxicephalidae Bonaparte, 1850 [Lemierre & Laurin], converted clade name.

(RegNum registration number: 571)

Definition—The largest clade containing *Pyxicephalus adpersus* Tschudi, 1838 and *Aubria subsigillata* Duméril, 1856 but not *Cacosternum boettgeri* Boulenger 1882 (*CACOSTERNIDAE*) and *Tomopterna natalensis* Smith, 1849 (*CACOSTERNIDAE*). Abbreviated definition: max total ∇ (*Pyxicephalus adpersus* Tschudi, 1838 and *Aubria subsigillata* Duméril, 1856 ~ *Cacosternum boettgeri* Boulenger 1882, *Tomopterna natalensis* Smith, 1849, and *Petropedetes palmipes* Boulenger, 1905).

Etymology—Named after the eponymous genus *Pyxicephalus* Tschudi, 1838. Derived from the ancient Greek *pyxis* ('round' box) and *kephalē* (head).

Reference phylogeny—The primary reference phylogeny is Jetz & Pyron (2018: fig. S1) for the crown-group *PYXICEPHALINAE*, and Lemierre et al. (2021: fig. S12) for the relationship between the crown-group and *Thaumastosaurus*. Other recent phylogenies for the crown group include Frost et al. (2006: fig. 50) and Pyron & Wiens (2011: fig. 2J).

Composition—The clade encompasses the extant *Pyxicephalus* Tschudi, 1838 and *Aubria* Boulenger, 1917 (forming the crown-group *PYXICEPHALINAE*) and the extinct Eocene *Thaumastosaurus* Stefano, 1903, the last of which is located on the stem of the crown-group.

Diagnostic apomorphies—According to Clarke (1981) and corroborated by Frost et al. (2006), the clade is diagnosed by the unique combination of the following apomorphies: [1] presence of enclosed canal for occipital artery (also present in *CERATOPHRYIDAE* for example); [2] well-developed zygomatic ramus of squamosal (longer than its otic ramus and articulated with maxillae; also present in *CERATOBATRACHINAE* for example); [3] well-developed medial ramus of pterygoids overlapping parasphenoid alae (also present in

The return of the mummy: *Thaumastosaurus*, an Eocene pyxicephalid from Western Europe

CERATOBATRACHINAE for example); [4] cranial exostosis (sensu Trueb, 1973; also present in *CERATOPHRYIDAE* for example). Another putative synapomorphy is the anterior extension of the squamosal forming the entire lateral margin of the orbit and in contact anteriorly with the nasal (Lemierre et al., 2021).

Synonyms—Approximate synonyms (that implicitly refer to the crown-group to the extent that only extant taxa were mentioned) are *PYXICEPHALINA* Bonaparte, 1850, *PHRYNOPSINAE* Noble, 1931, as mentioned by Loveridge (1936) and Laurent (1946), and *PYXICEPHALINI* Bonaparte, 1850 (used as a valid tribe nomen for the crown-group, see below).

Comments—As mentioned earlier, *PYXICEPHALIDAE* was proposed in the middle of the 19th century (Bonaparte, 1850), but rapidly fell into disuse, as numerous ranoids (and other anurans) were considered to be subgenera of *Rana*. Slowly, several subgenera were raised to generic rank (Dubois, 1981), as the large genus *Rana* began to be dismantled during the second half of the 20th century.

When *PYXICEPHALIDAE* was erected, it was to accommodate the genus described by Tschudi (1838) a decade earlier, and it only contained this eponymous genus. However, close affinities between *Pyxicephalus* and *Aubria* (first described as *Rana subsigillata* by Duméril in 1856) were first proposed by Procter (1919), who thought that both belonged to the same subgenus of *Rana*, in accordance to a Boulenger's unpublished manuscript on African ranids (see Clarke, 1981). These close affinities were also supported by Clarke (1981), who proposed two alternatives, either that *Pyxicephalus* and *Aubria* were congeneric as Procter (1919) had suggested, or that *Aubria* was a sister-taxon to *Pyxicephalus*. A few years later, the second phylogenetic hypothesis (*Aubria* is a sister-taxon to *Pyxicephalus*) was accepted by Dubois (1987), who resurrected *PYXICEPHALIDAE* (~*PYXICEPHALINAE* of Dubois, 1987) as a subfamily of *RANIDAE* (which encompassed various taxa previously considered subgenera of *Rana*).

However, the affinities of *PYXICEPHALIDAE* to other *RANOIDEA* remained unclear, at least until the application of molecular phylogenetics to anurans (Frost et al., 2006) and ranoids (Dubois, 2005; Scott, 2005; Van der Meijden et al., 2005), in particular. These studies showed that *PYXICEPHALIDAE* belongs to a large clade of 'southern African Ranids' (sensu Van der

The return of the mummy: *Thaumastosaurus*, an Eocene pyxicephalid from Western Europe

Meijden et al., 2005). Following these results, Dubois (2005) proposed to expand *PYXICEPHALIDAE* (~*PYXICEPHALINAE* of Dubois, 2005) to encompass cacosternins taxa. Frost et al. (2006) analysis led to the restriction of *PYXICEPHALINAE* to its eponymous genus and *Aubria*. In their recent monograph, Dubois et al. (2021) considered the latter clade as a family, and retained the name *PYXICEPHALIDAE* Bonaparte, 1850 as the valid nomen. As mentioned earlier, a recent study recovered the extinct *Thaumastosaurus* as a *PYXICEPHALIDAE* (Lemierre et al., 2021).

Pyxicephalidae are known in the fossil record since the middle Eocene, around 39.5 Ma, with the geologically oldest remains attributed to *Thaumastosaurus* (Lemierre et al., 2021). *Thaumastosaurus* extends up to the late Eocene, around 33.5 Ma. There is a large gap in the fossil record of *Pyxicephalidae* after the Eocene; the next oldest remains attributed to are from the late Pleistocene (around 12 000 years; Robbins et al., 1996) and attributed to the crown-group *Pyxicephalinae*.

Pyxicephalinae Bonaparte, 1850 [A. Lemierre, M. Laurin], converted clade name
(RegNum registration number: 572)

Definition—The smallest clade containing *Pyxicephalus adpersus* Tschudi, 1838 and *Aubria subsigillata* Duméril, 1856 but not *Thaumastosaurus* De Stefano, 1903. Abbreviated definition: min crown ∇ (*Pyxicephalus adpersus* Tschudi, 1838 and *Aubria subsigillata* Duméril, 1856 ~*Thaumastosaurus servatus* Filhol, 1877).

Etymology—Named after the eponymous genus *Pyxicephalus* Tschudi 1838. Derived from the ancient Greek *pyxis* ('round' box) and *kephalē* (head).

Reference phylogeny—The primary reference phylogeny is Jetz & Pyron (2018, fig. S1), with a majority of taxa within the clade represented. Other recent phylogenies for *PYXICEPHALINAE* include Frost et al. (2006: fig. 50) and Pyron & Wiens (2011: fig. 2J).

Composition—The clade encompasses the extant *Pyxicephalus* Tschudi, 1838 and *Aubria* Boulenger, 1917.

The return of the mummy: *Thaumastosaurus*, an Eocene pyxicephalid from Western Europe

Diagnostic apomorphies—*Pyxicephalinae* can be characterized using the following combination of skeletal synapomorphies, recovered in the analyses of Lemierre et al. (2021): [1] alary process of premaxillae oriented dorsally; [2] development of fang-like laminar projection on anterior portion of dentaries; [3] articulation for lower jaw located posterior to occiput.

Synonyms—Synonyms are the same as for *Pyxicephalidae*, as most authors used both names to refer to a clade composed only of extant taxa.

Comments—The clade is endemic to Sub-Saharan Africa, from Gambia (Western Africa; Channing and Rödel, 2019) to Southern Somalia (East range) and south to Cape Province, South Africa (Channing, 2001), with various *Pyxicephalus* taxa having the widest geographical range (Channing & Rödel, 2019).

The genus *Pyxicephalus* is represented by some of the largest extant anurans (the various taxa are dubbed the African bullfrog) and are known to be very aggressive and voracious eaters, eating anything that they can manage to capture. They are notably known for preying on small vertebrates (small anurans, squamates, rodents) and are even capable of subduing and eating small birds (Branch, 1976). This genus is also known to be consumed for its flesh by local inhabitants of southern Africa (for an example in Namibia, see Okeyo et al., 2015) and this practice has been recorded for at least 12 000 years, with the oldest remains attributed to *Pyxicephalus* being burnt, indicating that the frogs had been cooked and eaten (Robbins et al., 1996, 2009).

X.15 Concluding remarks

The *Pyxicephaloidea*, *Pyxicephalidae* and *Pyxicephalinae* are here converted in the phylogenetical nomenclatural system. We also took the opportunity to formally include the extinct *Thaumastosaurus* in two nomina. Although the phylogenetical position of *Thaumastosaurus* has strong support, its exclusion from *Pyxicephaloidea* would render *Pyxicephalidae* and *Pyxicephalinae* synonyms. As mentioned earlier, a large geographical and stratigraphic gap exist between *Thaumastosaurus* and the other *Pyxicephalidae*, and

The return of the mummy: *Thaumastosaurus*, an Eocene pyxicephalid from Western Europe

undescribed extinct taxa from Africa might fill these gaps. As an example, the recently described *Rocekophryne ornata* Rage *et al.*, 2021 from the Early Eocene of Algeria is considered a *RANOIDEA* with osteological characters similar to *Thaumastosaurus*. In addition, *R. ornata* shares several osteological synapomorphies with the *Pyxicephaloidea* (presence of an open groove for the occipital arteria pathway and ornamented pars facialis of the maxilla). This taxon could represent the oldest *Pyxicephaloidea* and would fill part of the geographical gap of the clade. Phylogenetical analyses are needed to confirm this hypothetic position.

As this work is based on our recent phylogenetical analyses of an extinct stem-*PYXICEPHALINAE*, we did not convert the *CACOSTERNIDAE*. The conversion of this family could be addressed in a more complete study of the relationships between the various genera of *CACOSTERNIDAE*.

To conclude, this work on the conversion of *PYXICEPHALOIDEA*, *PYXICEPHALIDAE* and *PYXICEPHALINAE* is only a first step toward the conversion of the numerous anuran clade nomina, as no study has yet converted **SALIENTIA** or **ANURA**, or various less inclusive clades, except for those converted here.

All definitions of names following the phylogenetical nomenclature system are stored in the RegNum website: <https://www.phyloregnum.org>.

Chapter XI

CONCLUSIONS ON THE EARLY DIVERSIFICATION OF AFRICAN NEOBATRACHIANS

Conclusions on the early diversification African neobatrachians

All previous studies point towards a Gondwanan origin of neobatrachians (Frazão et al., 2015; Feng et al., 2017). Indeed, the presence of neobatrachians in Africa (Madagascar) and in South America in Northeast Brazil around the Early/Late Cretaceous transition suggests that the first diversification of the clade was well located in Gondwana. The identification of two additional taxa *Cretadefdaa taouzensis* Lemierre and Blackburn, 2022 from the Cenomanian of Morocco (Chapter VIII) and *Taxon N* from the Coniacian-Santonian of Niger, (Chapter IX) confirm this Gondwanan origin. Moreover, the morphological similarities between *Cretadefdaa* and *Beelzebubo* suggest that these two African taxa share a common ancestor (Lemierre and Blackburn, 2022). Therefore, both lineages could have diverged during the Late Cretaceous, when the Mozambique canal opened, and Madagascar drifted away from mainland Africa (Masters et al., 2021).

The presence of a ranoid in the early Late Cretaceous of In Becetén, Niger is the oldest occurrence of the clade, and the first within the Mesozoic. Although older occurrences have been mentioned in the past (Báez and Werner, 1996) they were neither published nor illustrated. The presence of this ranoid, during the Coniacian, likely in co-existence with the neobatrachian *Taxon N*, also indicates that hyloids and ranoids had likely already diverged before the Coniacian. This confirm the molecular hypothesis with a divergence of these two clades around 125 Ma ago during the late Early Cretaceous during the fragmentation of the western Gondwana (Feng et al., 2017).

Finally, in this second section, we studied the exceptionally well-preserved mummies from the Eocene of the Quercy Phosphorites (France) and the genus *Thaumastosaurus* has been recovered as a pyxicephalid, a clade today endemic to Africa. *Thaumastosaurus* is therefore the first occurrence of pyxicephalid outside of Africa, and the stratigraphically oldest pyxicephalid. In addition, its phylogenetic position is also important for future molecular clock analyses. Previous analyses used *Thaumastosaurus* as a node constrain for Natatanura (Feng et al, 2017), a clade that has been considered to have diverged from Afrotrachia (its sister clade; Hime et al., 2021) around the Cretaceous/Paleogene transition. *Thaumastosaurus* can now more appropriately be used as node constrain for the

Conclusions on the early diversification African neobatrachians

age of origin of the pyxicephalid stem. This could help to better constrain divergence time analyses for close clades, as no other fossil older than 5 my is currently assigned to them (Gardner and Rage, 2016).

Furthermore, *Thaumastosaurus* is the first evidence of a past geographical range that stretched outside of Africa for an endemic clade from that continent. As mentioned in Chapter X, pyxicephalids are solely known in sub-Saharan Africa today, and the few fossils assigned to the clade are also within this range. However, the presence of *Thaumastosaurus* shows that the clade was likely widespread throughout northern Africa and reached Western Europe as far as England (Holman and Harrison, 2003). Interestingly, an hyperossified ornamented ranoid, *Rocekophryne ornata* Rage et al., 2021, has recently been described from Northern Africa. This taxon is morphologically similar to both *Thaumastosaurus* and extant pyxicephalids and lends support to our paleobiogeographical hypothesis. Furthermore, *R. ornata* is slightly older (Early Eocene, Rage et al., 2021) than *Thaumastosaurus*, and could also help constrain the time arrival of pyxicephalids in Europe and their establishment for at least 10 my (until the Grande Coupure, approximately). Further studies are needed to assess the phylogenetical position of *R. ornata*.

CONCLUSIONS AND PERSPECTIVES

Conclusions and Perspectives

The study of the anuran fauna of the Cretaceous of In Becetén (Chapters II-IV, IX) revealed the most diverse sites from the Mesozoic of Africa, with no more than seven taxa currently identified. The (likely) presence of one hyloid, one ranoid and at least four pipimorphs is a unique occurrence within the Cretaceous, when excluding the exceptional Crato Formation in Brazil. It shows that both neobatrachians and pipids were already diverse by the middle Late Cretaceous.

The study of the pipimorphs of In Becetén (Chapters II, III) yielded a surprisingly high number of taxa, with at least four identified taxa, including two pipids, *Pachycentrata taqueti* and *Inbecetenanura ragei*. In addition, the extreme ossification of *Pachycentrata* allows its braincase and vertebra to preserve a unique endocast of its “brain” and central nervous system (Chapter IV). The analyses of these two nervous structures allowed to infer its hearing, olfactive and optic capacities, that were similar to *Pipa*. Furthermore, it was possible to infer that *Pachycentrata* lacked a tongue, like extant pipid. Combined with the general structure of the cranial and vertebral elements, *Pachycentrata* was likely able to burrow within the muddy bottom of murky lakes or ponds. Phylogenetical analyses of pipimorphs (Chapter III) highlighted that the conflict between morphological and molecular topologies for extant pipids impacts greatly the position of numerous extinct pipids. Several pipimorphs are recovered as xenopodinomorphs when using topological constrain (using molecular topologies).

The phylogenetical analyses of pipimorphs in this dissertation all confirm that *Aygrova anoualensis* is the stratigraphically oldest pipimorph (Chapter III). It is also recovered as the sister-taxon to all pipimorphs. The resulting topologies shows that the early diversification of Pipimorpha could be placed within the lower-middle Early Cretaceous, around the Tethys margins. Several occurrences are known in the Western and Eastern margins of the Tethys. The divergence between Palaeobatrachidae (European clade) and the remaining pipimorphs (all from Gondwana) likely happened during the middle Early Cretaceous.

Pipimorphs are present across Gondwana by the end of the middle Early Cretaceous, with two closely related taxa, *Cratopipa* and *Thoraciliacus*, present during the Aptian in both Brazil

Conclusions and Perspectives

(*Cratopipa*) and Israel (*Thoraciliacus*). Pipidae emerged within the latest Early Cretaceous of Gondwana. Time estimates of the divergence between Pipidae and its sister-clade, Shelaniinae, depends on the presence (or absence) of pipid in the Early Cretaceous of Africa. If pipids are indeed present in Western Africa (Koum Basin), the divergence between Pipidae and Shelaniinae is estimated around 125 My, whereas it would be around 105 My if they are absent from the Koum Basin. The emergence of pipid was followed by a rapid evolutionary radiation in the next 10 My. This radiation could likely be linked to the opening of the Southern Atlantic Ocean, more precisely on the opening of the Central or Equatorial segment (depending on the time estimation of the pipid/shelaniin divergence). All time divergence analyses point against transatlantic dispersal events within pipid diversification, contrary to previous paleobiogeographical hypotheses. In addition, the divergence between South American and African lineages is estimated around the Early/Late Cretaceous boundaries, thus implying that long ghost lineages for the main extant pipid clades are present.

For Neobatrachia, the new newly described *Cretadhefdaa* from the Cretaceous of the Kem Kem Formation, Morocco (Chapter VIII), the oldest from Africa, shows that neobatrachians were present across Northwest Africa (Saharan Craton) in the earliest Late Cretaceous. Interestingly, this region was isolated from the rest of Africa during the lower/middle Late Cretaceous by the opening of the transaharian seaway. Thus, it could be proposed that the absence of neobatrachian from most of continental Africa until the Late Cretaceous is linked to the isolation of the Saharan Craton. However, the presence of *Beelzebubo*, a hyloid, in the Late Cretaceous of Madagascar, implies that the clade was likely already present in Africa before the separation of this continent, during the latest Early Cretaceous (Aptian). As the earliest neobatrachians were recovered from the Aptian of the Crato Formation in South America, this implies that the clade emerged before the latest Early Cretaceous, likely during the earliest/middle Early Cretaceous. In addition, the likely co-existence of a ranoid and an hyloid in In Becetén (Chapter IX) indicates that both clades were already present in the Early Cretaceous. In addition, Both the Kem Kem and In Becetén neobatrachians also fill the gap within the fossil record of Neobatrachia, who was lacking fossil occurrence from the Albian to the Campanian, leaving known only a 4 My gap, during

Conclusions and Perspectives

the Turonian. It also pushes back the oldest occurrence of the clade in Africa of more than 20 My, with *Cretadhefdaa* in the Kem Kem. Furthermore, we likely have the earliest ranoids in the current fossil record within the Kem Kem and In Becetén. If confirmed by phylogenetical analyses, it would confirm that the clade was present within the Saharan Craton almost since the Early/Late Cretaceous transition. These occurrences could be also used as a node constrain for molecular clock analyses.

Regarding *Thaumastosaurus* (Chapter X), my phylogenetical analyses confirmed its assignment to Natatanura, within Pyxicephaloidea, as a Pyxicephalidae. This confirms its African origins, as Pyxicephaloidea were only (until this dissertation) known in Sub-Saharan Africa. Thus, *Thaumastosaurus* expands the stratigraphical range of the clade from 5 My (Pliocene) to more than 35 My (middle Eocene), but also its paleobiogeographical range outside of Africa. This is indeed the first time that an endemic anuran clade from Africa is recovered (within the fossil record) outside of the continent. In addition, several ornamented ranoid have been mentioned from the Early Eocene of Northern Africa, like *Rocekophryne ornata*. Their inclusion within phylogenetical analyses could assign them to Pyxicephalidae and would confirm that the clade possessed a wider biogeographical range during the Cenozoic. The precise position of *Thaumastosaurus* will allow to use this taxon as a node constrain for Pyxicephalidae, and not just for Natatanura.

This dissertation highlights the importance of Africa during the Cretaceous for both Pipimorpha and Neobatrachia, and not only as a “stepping stone” for Neobatrachia dispersal to other continents. Although the fossil record from the Cretaceous of Africa is still very scarce (only four sites illustrated), almost all have at least a pipid and a neobatrachian taxon. This is similar to most Cretaceous South American sites, that also preserves at least a neobatrachian and a pipimorph taxon. Within Africa, the oldest occurrence of Pipidae have been recorded within the earliest Late Cretaceous. Furthermore, the Koum Basin could yield the oldest Pipidae, within the Early Cretaceous (Gardner et Rage, 2016). African sites also yielded the oldest ranoid within the Late Cretaceous. Thus, Africa played a key role within early pipid and neobatrachians diversification.

Conclusions and Perspectives

Some sites, like In Becetén, exhibit a very diverse fauna, with more taxa than any Gondwanian sites, excluding the exceptional Crato Formation in Brazil. The study of In Becetén highlights the need to fully study poorly known sites with fragmentary anurans, as more anurans could be also recovered. Although Africa is a key period for Gondwanian anurans, there is still few fossil sites known. However, several sites with anurans have been mentioned throughout the years, but never studied nor investigated (refs). It is essential to study this material to achieve a better understanding of the anuran diversity within Cretaceous Africa, in peculiar regarding neobatrachians and pipids. As an example, within the Koum Basin, more than 200 bones assigned to anurans have been identified (A. Lemierre, pers. com.). The specimens are still under study (by A. Lemierre), but at least four distinct taxa have been identified. In addition, a skull belonging to a pipimorph is known from this locality. It has recently been CT-scanned and is still under study (by A. Lemierre and D. C. Blackburn). Its inclusion within the phylogenetical dataset of this dissertation would allow to precise its position within pipimorph, and its relation to pipids. It could represent a second pipid from this Early Cretaceous site, with the putative *Pachyentrata*. Several humeri and vertebrae also bear some resemblance to neobatrachians bones from the Kem Kem and In Becetén. They could represent the earliest occurrence of the clade within the fossil record, if the affinities are confirmed by phylogenetical analyses. A second site of interest within the Early Cretaceous of Africa is the Karonga district of Malawi (Jacobs et al., 1990). Two anuran braincases (with isolated postcranial bones) have been identified there, but never described. One of them is clearly a pipimorph, while the second, bearing a frontoparietal ornamentation), resemble Cretaceous neobatrachians (A. Lemierre, pers. obs.). They could provide key information for the early diversification of these two clades and would argue that neobatrachians were present across Gondwana before its breakup. It would also be interesting to expand the scope of this study to African Paleogene sites. Several sites are known, but as in Mesozoic Africa, few have been published, but neobatrachians and pipids are mentioned in almost all sites (Gardner and Rage, 2016). Study of these sites could yield new taxa and increase our understanding of the fossil record of African clades. In addition, we could compare the Cretaceous and Paleogene fauna, to assess if the extinction crisis known at the Cretaceous/Paleogene boundary can be recorded within

Conclusions and Perspectives

anurans. We could also investigate the impact of the Early/Late Cretaceous transition on Gondwanian fauna and try to assess if the extinction crisis at the Eocene/Oligocene transition (Grande Coupure) could also be recorded within the anuran fossil record of Africa.

REFERENCES

References

- Agnolin, F.** 2012. A New Calyptocephalellidae (Anura, Neobatrachia) from the Upper Cretaceous of Patagonia, Argentina, with comments on its systematic position. *Studia Geologica Salmanticensia*, **48** (2): 129–178.
- Agnolin, F., I. de S. Carvalho, A. M. Aranciaga Rolando, F. E. Novas, J. Xavier-Neto, J. A. F. G. Andrade, and F. I. Freitas.** 2020. Early Cretaceous neobatrachian frog (Anura) from Brazil sheds light on the origin of modern anurans. *Journal of South American Earth Sciences*, **101**: 102633.
- Ahl, E.** 1926. *Xenopus stromeri* Ahl, n. sp.; pp. 141–142 in **E. Kaiser** (ed.), *Die Diamanterwüste Südwest-Afrikas, Volume 2*. Verlag von Dietrich Reimer, Germany.
- Albecker, M. A., and M. W. McCoy.** 2017. Adaptive responses to salinity stress across multiple life stages in anuran amphibians. *Frontiers in Zoology*, **14** (1): 1–16.
- Altner, H.** 1962. Untersuchungen über leistung und bau der nase des Südafrikanischen krallenfrosches *Xenopus laevis* (Daudin, 1803). *Zeitschrfft Für Vergleichende Physiologie*, **45**: 272–306.
- Anderson, M. A., and B. T. Miller.** 2011. Early iron deposition in teeth of the streamside salamander, *Ambystoma barbouri*. *Journal of Herpetology*, **45** (3): 336–338.
- Aranciaga Rolando, A. M. A., F. L. Agnolin, and J. Corsolini.** 2019. A new pipoid frog (Anura, Pipimorpha) from the Paleogene of Patagonia. Paleobiogeographical implications. *Comptes Rendus Palevol*, **18** (7): 725–734.
- Ascarrunz, E., J.-C. Rage, P. Legreneur, and M. Laurin.** 2016. *Triadobatrachus massinoti*, the earliest known lissamphibian (Vertebrata: Tetrapoda) re-examined by μ CT scan, and the evolution of trunk length in batrachians. *Contributions to Zoology*, **85** (2): 201–234.
- Aslanian, D., and M. Moulin.** 2013. Palaeogeographic consequences of conservational models in the South Atlantic Ocean. *Geological Society, London, Special Publications*, **369** (1): 75–90.
- Atkins, J. B., R. R. Reisz, and H. C. Maddin.** 2019. Braincase simplification and the origin of lissamphibians. *PLoS ONE*, **14**: e0213694.

References

- Augé, M., S. Duffaut, F. de Lapparent de Broin, J.-C. Rage, and D. Vasse. 1997. Les amphibiens et reptiles de Prémontré (Cuisien, Bassin parisien): une herpétofaune de référence pour l'Eocène inférieur. *Géologie de la France*, **1**: 23–33.
- Báez, A. M. 2013. Anurans from the Early Cretaceous Lagerstätte of Las Hoyas, Spain: New evidence on the Mesozoic diversification of crown-clade Anura. *Cretaceous Research*, **41**: 90–106.
- Báez, A. M., and S. Perí. 1989. *Baurubatrachus pricei*, nov. gen. et sp., un Anuro del Cretacico Superior de Minas Gerais. *Anais Da Academia Brasileira de Ciências*, **61** (4): 447–458.
- Báez, A. M., and C. Werner. 1996. Presencia de anuros ranoideos en el Cretácico de Sudan. *Ameghiniana*, **33** (4): 460.
- Báez, A. M., and L. Trueb. 1997. Redescription of the Paleogene *Shelania pascuali* from Patagonia and its bearing on the relationships of fossil and recent pipoid frogs. *Scientific Papers*, **4**: 1–41.
- Báez, A. M., and L. A. Púgener. 1998. A new Paleogene pipid frog from northwestern Patagonia. *Journal of Vertebrate Paleontology*, **18** (3): 511–524.
- Báez, A. M., and J.-C. Rage. 1998. Pipid frogs from the Upper Cretaceous of In Beceten, Niger. *Palaeontology*, **41** (4): 669–691.
- Báez, A. M., and L. A. Púgener. 2003. Ontogeny of a new Palaeogene pipid frog from southern South America and xenopodinomorph evolution. *Zoological Journal of the Linnean Society*, **139** (3): 439–476.
- Báez, A. M., and J.-C. Rage. 2004. *Pachycentrata*, a replacement name for *Pachybatrachus* Báez and Rage, 1998 (Amphibia, Anura). *Ameghiniana*, **41** (3): 346.
- Báez, A. M., and T. Harrison. 2005. A new pipine frog from an Eocene crater lake in North-Central Tanzania: Eocene frog from Tanzania. *Palaeontology*, **48** (4): 723–737.
- Báez, A. M., and B. Sanchíz. 2007. A review of *Neusibatrachus wilferti*, an Early Cretaceous frog from the Montsec Range, northeastern Spain. *Acta Palaeontologica Polonica*, **52** (3): 477–487.
- Báez, A. M., and R. O. Gómez. 2016. Revision of the skeletal morphology of *Eodiscoglossus santonjae*, an Early Cretaceous frog from northeastern Spain, with comments on its phylogenetic placement. *Fossil Imprint*, **72** (1-2): 67–77.

References

- Báez, A. M., and R. O. Gómez.** 2018. Dealing with homoplasy: osteology and phylogenetic relationships of the bizarre neobatrachian frog *Baurubatrachus pricei* from the Upper Cretaceous of Brazil. *Journal of Systematic Palaeontology*, **16** (4): 279–308.
- Báez, A. M., P. Muzzopappa, and L. Nicoli.** 2007. Anurans from the Candeleros Formation (?Cenomanian-Turonian) of west-central Argentina: new evidence for pipoid evolution. *Cretaceous Research*, **28**: 1005–1016.
- Báez, A. M., G. J. B. Moura, and R. O. Gómez.** 2009. Anurans from the Lower Cretaceous Crato Formation of northeastern Brazil: implications for the early divergence of neobatrachians. *Cretaceous Research*, **30** (4): 829–846.
- Báez, A. M., P. Muzzopappa, and G. J. B. de Moura.** 2021. The earliest records of pipimorph frogs from South America (Aptian, Crato Formation, Brazil): A critical evaluation. *Cretaceous Research*, **121**: 104728.
- Báez, A. M., R. O. Gómez, L. C. B. Ribeiro, A. G. Martinelli, V. P. A. Teixeira, and M. L. F. Ferraz.** 2012. The diverse Cretaceous neobatrachian fauna of South America: *Uberabatrachus carvalhoi*, a new frog from the Maastrichtian Marília Formation, Minas Gerais, Brazil. *Gondwana Research*, **22** (3-4): 1141–1150.
- Bandoni de Oliveira, F. B. de, E. C. Molina, and G. Marroig.** 2009. Paleogeography of the South Atlantic: a route for primates and rodents into the New World?; pp. 55–68 in **P. A. Garber, A. Estrada, J. C. Bicca-Marques, E. W. Heymann, and K. B. Strier** (eds.), *South American primates*. Springer New York, New York, NY.
- Barcelos, L. A., and R. O. dos Santos.** 2022. The lissamphibian fossil record of South America. *Palaeobiodiversity and Palaeoenvironments*.
- Bewick, A. J., F. J. J. Chain, J. Heled, and B. J. Evans.** 2012. The pipid root. *Systematic Biology*, **61** (6): 913–926.
- Billerman S. M., B. K. Keeney, P. G. Rodewald and T. S. Schulenberg.** 2022. Birds of the World. Cornell Laboratory of Ornithology, Ithaca, NY, USA. <https://birdsoftheworld.org/bow/home>; last access: 03/10/2022.
- Biton, R., R. Boistel, R. Rabinovich, S. Gafny, V. Brumfeld, and S. Bailon.** 2016. Osteological observations on the alytid Anura *Latonia nigrienter* with comments on functional

References

- morphology, biogeography, and evolutionary history. *Journal of Morphology*, **277** (9): 1131–1145.
- Bittencourt-Silva, G. B., Conradie, W., Siu-Ting, K., Tolley, K., Channing, A., Cunningham, M., Farooq, H., Menegon, M. and S. Loader.** 2016. The phylogenetic position and diversity of the enigmatic mongrel frog *Nothophryne* Poynton, 1963 (Amphibia, Anura). *Molecular Phylogenetics and Evolution*, **99**: 89–102.
- Blackburn, D. C., D. J. Paluh, I. Krone, E. M. Roberts, E. L. Stanley, and N. J. Stevens.** 2019. The earliest fossil of the African clawed frog (genus *Xenopus*) from Sub-Saharan Africa. *Journal of Herpetology*, **53** (2): 125–130.
- de Blainville, H. D.** 1816. Prodrome d'une nouvelle distribution systématique du règne animal. *Journal de physique, de chimie, d'histoire naturelle et des arts*, **83** (Octobre 1816): 244–267.
- Blakey, R. C.** 2008. Gondwana paleobiogeography from assembly to breakup—A 500 m.y. odyssey; pp. 1–28 in **C. R. Fielding, T. D. Frank, and J. L. Isbell** (eds.), *Resolving the Late Paleozoic Ice Age in time and space*. The Geological Society of America, Boulder, CO, USA.
- Bohaty, S. M., J. C. Zachos, F. Florindo, and M. L. Delaney.** 2009. Coupled greenhouse warming and deep-sea acidification in the Middle Eocene: Middle Eocene warming and ccd shoaling. *Paleoceanography*, **24** (2): 1–16.
- Bolt, J. R.** 1977. Dissorophoid Relationships and Ontogeny, and the Origin of the Lissamphibia. *Journal of Paleontology*, **51** (2): 235–249.
- Bolt, J. R., and R. E. Lombard.** 1985. Evolution of the amphibian tympanic ear and the origin of frogs. *Biological Journal of the Linnean Society*, **24** (1):83–99.
- Bonaparte, C.** 1850. *Conspectus Systematum. Herpetologiae et Amphibiologiae*. apud E. J. Brill Academiae typographum -- Ed. ... reformata, Leiden.
- Borsuk-Bialynicka, M., and S. E. Evans.** 2002. The scapulocoracoid of an Early Triassic stem-frog from Poland. *Acta Palaeontologica Polonica*, **47** (1): 79–96.
- Boscolo Galazzo, F., E. Thomas, M. Pagani, C. Warren, V. Luciani, and L. Giusberti.** 2014. The middle Eocene climatic optimum (MECO): A multiproxy record of paleoceanographic changes in the southeast Atlantic (ODP Site 1263, Walvis Ridge): MECO repercussions in the SE Atlantic. *Paleoceanography*, **29** (12): 1143–1161.

References

- Bossuyt, F., R. M. Brown, D. M. Hillis, D. C. Cannatella, and M. C. Milinkovitch.** 2006. phylogeny and biogeography of a cosmopolitan frog radiation: Late Cretaceous diversification resulted in continent-scale endemism in the family Ranidae. *Systematic Biology*, **55** (4): 579–594.
- Boulenger, G. A.** 1882. *Catalogue of the Batrachia Salientia s. Ecaudata in the collection of the British Museum*. Second edition. London (Taylor & Francis): 1–530.
- Boulanger G.A.** 1886. Quelques mots en réponse à la note de M. Le Dr R. Blanchard sur la classification des batraciens. *Bulletin de la société zoologique de France*, **11**: 320–321.
- Boulenger, G. A.** 1887. Descriptions of new reptiles and batrachians in the British Museum (Natural history), part III. *Annals and Magazine of natural History*, (5), **20** (115): 50–53.
- Boulenger, G. A.** 1905. Descriptions of new West-African frogs of the genera *Petropedetes* and *Bulua*. *Annals and Magazine of natural History*, (7), **15** (87): 281–283.
- Boulenger, G. A.** 1906. Descriptions of new batrachians discovered by Mr. G. L. Bates in South Cameroon. *Annals and Magazine of natural History*, (7), **17** (7): 317–323.
- Boulenger, G. A.** 1917. Sur la conformation des phalangettes chez certaines grenouilles d’Afrique. *Compte rendu hebdomadaire des Séances de l’Académie des Sciences, Paris*, **165**: 989–990.
- Boulenger, G. A.** 1918. Aperçu des principes qui doivent régir la classification des espèces du genre *Rana*. *Bulletin de la Société zoologique de France*. **43**: 111–121.
- Boulenger, G. A.** 1920a. A monograph of the South Asian, Papuan, Melanesian and Australian frogs of the genus *Rana*. *Records of the Indian Museum*, **20**: 1–226.
- Boulenger, G. A.** 1920b. A monograph of the American frogs of the genus *Rana*. *Proceeding of the American Academy of Arts and Sciences*, **55** (9): 413–480
- Branch, W. R.** 1976. Two exceptional food records for the African Bullfrog, *Pyxicephalus adspersus* (Amphibia, Anura, Ranidae). *Journal of Herpetology*, **10** (3): 266–268.
- Bremer, K.** 1994. Branch support and tree stability. *Cladistics*, **10**: 295–304.
- Brochu, C. A.** 2000. A digitally-rendered endocast for *Tyrannosaurus rex*. *Journal of Vertebrate Paleontology*, **20** (1): 1–6.

References

- de Broin, F., E. Buffetaut, J.-C. Koeniger, J. Rage, D. Russell, P. Taquet, C. Vergnaud-Grazzini, and S. Wenz.** 1974. La faune de vertébrés continentaux du gisement d'In Beceten (Sénonien du Niger). *Comptes Rendus de l'Académie des Sciences, Série 2* (279): 439–472.
- de Broin, F. de L., L. Chirio, and R. Bour.** 2020. The oldest erymnochelyine turtle skull, *Ragechelus sahelica* n. gen., n. sp., from the Iullemmeden basin, Upper Cretaceous of Africa, and the associated fauna in its geographical and geological context. *Geodiversitas*, **42** (25): 455-484.
- Brunet, M., L. L. Jacobs, J. D. Congleton, Y. Coppens, J. Dejax, L. J. Flynn, J. Hell, Y. Jehenne, G. Mouchelin, and D. R. Pilbeam.** 1988. Première découverte d'un fragment de mandibule de Mammifère dans le Crétacé inférieur d'Afrique (Cameroun, Bassin de Koum). *Compte Rendus de l'Académie des Sciences, Série 2* (307): 1675–1680.
- Buchholtz, E.** 2012. Dinosaur paleoneurology; pp. 191–208 in **M. K. Brett-Surman, T. R. Holtz and J. O. Farlow** (eds.), *The complete dinosaur*. Indiana University Press, Bloomington, Ind.
- Budgett, J. S.** 1899. Notes on the batrachians of Paraguayan Chaco, with observations upon their breeding habits and development, especially with regard to *Phyllomedusa hypochondrialis* Cope. Also a description of a new genus *Quarterly Journal of Microscopical Science. London*, **42**: 305-333.
- Buffetaut, E.** 1974a. Les crocodiliens du Sénonien Inférieur d'In Beceten (République du Niger) [PhD Thesis]. Université Paris IV, Paris, France, 146 pp.
- Buffetaut, E.** 1974b. *Trematochampsia taqueti*, un crocodylien nouveau du Sénonien inférieur du Niger. *Compte Rendus de l'Académie Des Sciences, Paris, Série D* (279): 1749–1752.
- Buffetaut, E.** 1976. Ostéologie et affinités de *Trematochampsia taqueti* (Crocodylia, Mesosuchia) du Sénonien Inférieur d'In Beceten (République du Niger). *Geobios*, **9**: 143–198.
- Buffetaut, E., G. Costa, J. L. Loeuff, M. Martin, J. C. Rage, X. Valentin, and H. Tong.** 1996. An Early Campanian vertebrate fauna from the Villeveyrac Basin (Herault, Southern France). *Neues Jahrbuch Fur Geologie Und Palaontologie Monatshefte*, **1**: 1–16.
- de Buffrénil, V., F. Clarac, A. Canoville, and M. Laurin.** 2016. Comparative data on the differentiation and growth of bone ornamentation in gnathostomes (Chordata: Vertebrata): growth of bone ornamentation in gnathostomes. *Journal of Morphology*, **277** (5): 634–670.

References

- de Buffrénil, V., F. Clarac, M. Fau, S. Martin, B. Martin, E. Pellé, and M. Laurin.** 2015. Differentiation and growth of bone ornamentation in vertebrates: a comparative histological study among the Crocodylomorpha: development of bone ornamentation in the Crocodylomorpha. *Journal of Morphology*, **276** (4): 425–445.
- Burg, J. P., B. Alabouvette, A. F. Leyreloup, T. Péliissié, J.-G. Astruc, and A. Lefavrais-Raymond.** 1998. Notice explicative, Carte géol. France (1/50 000), feuille Villefranche-de-Rouergue (882). BRGM, Orléans, 79 pp.
- Cai, Y.-Y., Shen, S.-Q., Lu, L.-X., Storey, K. B., Yu, D.-N. and J.-Y. Zhang.** 2019. The complete mitochondrial genome of *Pyxicephalus adspersus*: High gene rearrangement and phylogenetics of one of the world's largest frogs. *PeerJ*, **7**: e7532.
- Cameron, J. A., D. J. Milner, J. S. Lee, J. Cheng, N. X. Fang, and I. M. Jasiuk.** 2012. Employing the biology of successful fracture repair to heal critical size bone defects; pp. 113–132 in **E. Heber-Katz and D. L. Stocum** (eds.), *New perspectives in regeneration*. Current Topics in Microbiology and Immunology vol. 367. Springer Berlin Heidelberg, Berlin.
- Cannatella, D.** 2015. *Xenopus* in space and time: fossils, node calibrations, tip-dating, and paleobiogeography. *Cytogenetic and Genome Research*, **145** (3-4): 283–301.
- Cannatella, D. C., and L. Trueb.** 1988a. Evolution of pipoid frogs: morphology and phylogenetic relationships of *Pseudhymenochirus*. *Journal of Herpetology*, **22** (4): 439–456.
- Cannatella, D. C., and L. Trueb.** 1988b. Evolution of pipoid frogs: Intergeneric relationships of the aquatic frog family Pipidae (Anura). *Zoological Journal of the Linnean Society*, **94** (1): 1–38.
- Cannatella, D. C., D. R. Vieites, P. Zhang, M. H. Wake, and D. B. Wake.** 2009. Amphibians (Lissamphibia); pp. 353–356 in **S. B. Hedges and S. Kumar** (eds.), *The timetree of Life*. Oxford University Press.
- Cantino, P. D., and K. de Queiroz.** 2020. International Code of Phylogenetic Nomenclature (PhyloCode): Version 6, 1st ed. CRC Press, Version 6. | Boca Raton : CRC Press, 2020. | Ratified on January 20, 2019, by the Committee on Phylogenetic Nomenclature, of the International Society for Phylogenetic Nomenclature, 191 pp.
- de Carvalho, A. B.** 2006. Descrição morfológica e posição filogenética de um anuro novo (Lissamphibia, Tetrapoda) do Cretáceo Superior Continental do Brasil (Formação

References

- Adamantina, Bacia Bauru) do Município de Marília, (SP) [PhD Thesis] Universidade de São Paulo, Brazil, 167 pp.
- de Carvalho, A. B., H. Zaher, and W. R. Nava.** 2003. A new anuran (Lissamphibia: Tetrapoda) from the continental Late Cretaceous Bauru Basin, State of São Paulo. [Oral Communication], XVIII Congresso Brasileiro de Paleontologia, 188.
- Carvalho, I. S., F. Agnolin, M. A. Aranciaga Rolando, F. E. Novas, J. Xavier-Neto, F. I. Freitas, and J. A. F. G. Andrade.** 2019. A new genus of pipimorph frog (Anura) from the Early Cretaceous Crato Formation (Aptian) and the evolution of South American tongueless frogs. *Journal of South American Earth Sciences*, **92**: 222–233.
- Casamiquela, R. M.** 1960. Un pipoideo fosil de Patagonia. *Revisita del Museo de La Plata*, **4** (22): 71–123.
- Cavin, L., H. Tong, L. Boudad, C. Meister, A. Piuz, J. Tabouelle, M. Aarab, R. Amiot, E. Buffetaut, G. Dyke, S. Hua, and J. Le Loeuff.** 2010. Vertebrate assemblages from the early Late Cretaceous of southeastern Morocco: An overview. *Journal of African Earth Sciences*, **57** (5): 391–412.
- Chaboureau, A.-C., F. Guillocheau, C. Robin, S. Rohais, M. Moulin, and D. Aslanian.** 2013. Paleogeographic evolution of the central segment of the South Atlantic during Early Cretaceous times: Paleotopographic and geodynamic implications. *Tectonophysics*, **604**: 191–223.
- Channing, A.** 2001. *Amphibians of central and southern Africa*. Cornell University Press, Ithaca, NY, 496 pp.
- Channing, A. and R. C. Boycott.** 1989. A new frog genus and species from the mountains of the southwestern Cape, South Africa (Anura: Ranidae). *Copeia*, **1989** (2): 467–471.
- Channing, A., and N. Baptista.** 2013. *Amietia angolensis* and *A. fuscigula* (Anura: Pyxicephalidae) in southern Africa: A cold case reheated. *Zootaxa*, **3640** (4):501-520.
- Channing, A., and M.-O. Rödel.** 2019. *Field Guide to the Frogs & Other Amphibians of Africa*. Penguin Random House South Africa, 408 pp.
- Channing, A., J. M. Dehling, S. Lötters, and R. Ernst.** 2016. Species boundaries and taxonomy of the African river frogs (Amphibia: Pyxicephalidae: Amietia). *Zootaxa*, **4155** (1): 1-76.

References

- Clarke, B. T.** 1981. Comparative osteology and evolutionary relationships in the African Raninae (Anura Ranidae). *Monitore Zoologico Italiano. Supplemento*, **15** (1): 285–331.
- Clemen, G.** 1988. Experimental analysis of the capacity of dental laminae in *Ambystoma mexicanum* shaw. *Archives of Oral Biology*, **99**: 111–132.
- Cope, E. D.** 1865. Third contribution to the herpetology of tropical America. *Proceedings of the Academy of Natural Sciences of Philadelphia*, **17**: 185–198.
- Cope, E. D.** 1866. Fourth contribution to the herpetology of tropical America. *Proceedings of the Academy of Natural Sciences of Philadelphia*, **18**: 123–132.
- Company, J., and Z. Szentesi.** 2012. Amphibians from the Late Cretaceous Sierra Perenchiza Formation of the Chera Basin, Valencia Province, Spain. *Cretaceous Research*, **37**: 240–245.
- Congreve, C. R., and J. C. Lamsdell.** 2016. Implied weighting and its utility in palaeontological datasets: a study using modelled phylogenetic matrices. *Palaeontology*, **59** (3): 447–462.
- Cross, R.** 2017. The inside story on 20,000 vertebrates. *Science*, **357** (6353): 742–743.
- Daudin, F.** 1802. *Histoire naturelle des rainettes, des grenouilles et des crapauds*. de Bertrandet, Paris, 108 pp.
- De Robertis, E. M., and J. B. Gurdon.** 2021. *A brief history of Xenopus in Biology*. Cold Spring Harbor Protocols: pdb.top107615.
- De Stefano, G.** 1903. I Sauri del Quercy appartenenti alla collezione Rossignol. *Atti della Societa Italiana di Scienze Naturali* **4**: 382–418.
- Delfino, M., and M. R. Sánchez-Villagra.** 2018. A Late Miocene pipine frog from the Urumaco Formation, Venezuela. *Ameghiniana*, **55** (2): 210–214.
- Delfino, M., J. Rage, and L. Rook.** 2003. Tertiary mammal turnover phenomena: what happened to the herpetofauna? *DEINSEA*, **10**: 153–161.
- Dempster, W. T.** 1935. The braincase and endocranial cast of *Eryops megacephalus* (Cope). *Journal of Comparative Neurology*, **62** (1): 171–196.
- Didier, G., and M. Laurin.** 2020. Exact Distribution of Divergence Times from Fossil Ages and Tree Topologies. *Systematic Biology*, **69** (6): 1068–1087.
- Didier, G., M. Royer-Carenzi, and M. Laurin.** 2012. The reconstructed evolutionary process with the fossil record. *Journal of Theoretical Biology*, **315**: 26–37.

References

- Donato, M., P. Posadas, D. R. Miranda-Esquivel, E. O. Jaureguizar, and G. Cladera.** 2003. Historical biogeography of the Andean region: evidence from Listroderina (Coleoptera: Curculionidae: Rhytirrhinini) in the context of the South American geobiotic scenario: Historical biogeography of the Andean subregion. *Biological Journal of the Linnean Society*, **80** (2): 339–352.
- Drinkrow, D. R., and M. I. Cherry.** 1995. Anuran distribution, diversity and conservation in South Africa, Lesotho and Swaziland. *South African Journal of Zoology*, **30** (3): 82–90.
- Dubois, A.** 1981. Liste des genres et sous-genres nominaux de Ranoidea (Amphibiens Anoures) du monde, avec identification de leurs espèces-types: conséquences nomenclaturales. *Monitore zoologico italiano, (n.s.), suppl. 15*: 225–284.
- Dubois, A.** 1982. Notes sur la classification des Ranidae (Amphibiens, Anoures). *Bulletin mensuel de la Société linnéenne de Lyon*, **61** (10): 305–352.
- Dubois, A.** 1983. Classification et nomenclature supragénérique des amphibiens anoures. *Bulletin mensuel de la Société linnéenne de Lyon*, **52**: 270–276.
- Dubois, A.** 1987. Miscellanea taxinomica batrachologica (I). *Alytes*, **5**: 7–95.
- Dubois, A.** 1992. Notes sur la classification des Ranidae (Amphibiens, Anoures). *Bulletin mensuel de la Société linnéenne de Lyon*, **61**: 305–352.
- Dubois, A.** 1994. Phrynobatrachinae Laurent, 1941 (Amphibia, Anura): proposed conservation. *Bulletin of zoological Nomenclature*, **51** (3): 240–246.
- Dubois, A.** 2005. Amphibia Mundi. 1.1. An ergotaxonomy of recent amphibians. *Alytes*, **23**: 1–24.
- Dubois, A., and A. Ohler.** 2005. Taxonomic notes on the Asian frogs of the tribe Paini (Ranidae, Dicroglossinae): 1. Morphology and synonymy of *Chaparana aenea* (Smith, 1922), with proposal of a new statistical method for testing homogeneity of small samples. *Journal of Natural History*, **39** (20): 1759–1778.
- Dubois, A., A. Ohler, and R. A. Pyron.** 2021. New concepts and methods for phylogenetic taxonomy and nomenclature in zoology, exemplified by a new ranked cladonomy of recent amphibians (Lissamphibia). *Megataxa*, **5** (1): 1–738.
- Duellman, W. E., and L. Trueb.** 1994. *Biology of Amphibians*. JHU Press, 702 pp.

References

- Duméril, A. H. A., and G. Bibron.** 1841. *Erpétologie générale ou histoire naturelle complète des reptiles*. Roret, Paris, 792 pp.
- Duméril, A. H. A.** 1856. Note sur les Reptiles du Gabon. *Revue et Magasin de Zoologie pure et appliquée*, **2**: 553–562.
- Duméril, C.** 1805. *Zoologie analytique, ou méthode naturelle de classification des animaux, rendue plus facile à l'aide de tableaux synoptiques*. Allais, 386 pp.
- Dumont, M., T. Tütken, A. Kostka, M. J. Duarte, and S. Borodin.** 2014. Structural and functional characterization of enamel pigmentation in shrews. *Journal of Structural Biology*, **186** (1): 38–48.
- Dutheil, D. B.** 1999. An overview of the freshwater fish fauna from the Kem Kem beds (Late Cretaceous: Cenomanian) of southeastern Morocco; pp. 553–563 in **G. Arratia and H. P. Schultze** (eds.), *Mesozoic fishes-Systematics and fossil record*. F. Pfeil, Munich.
- Ecker, A.** 1889. *The anatomy of the frog*. Clarendon Press, Oxford, UK, 449 pp.
- Edinger, T.** 1921. Über *nothosaurus*, ein steinkern der schädelhöhle. *Senckenbergiana*, **3**: 121–129.
- Egawa, S., S. Miura, H. Yokoyama, T. Endo, and K. Tamura.** 2014. Growth and differentiation of a long bone in limb development, repair and regeneration. *Development, Growth & Differentiation*, **56** (5): 410–424.
- Eisthen, H. L.** 1992. Phylogeny of the vomeronasal system and of receptor cell types in the olfactory and vomeronasal epithelia of vertebrates. *Microscopy Research and Technique*, **23** (1): 1–21.
- Emerson, S. B.** 1976. Burrowing in frogs. *Journal of Morphology*, **149** (4): 437–458.
- Estes, R.** 1969. A new fossil discoglossid frog from Montana and Wyoming. *Breviora*, **328**: 1-7.
- Estes, R.** 1975. Fossil *Xenopus* from the Paleocene of South America and the zoogeography of pipid frogs. *Herpetologica*, **31** (3): 263–278.
- Estes, R., Ma. Hecht, and R. Hoffstetter.** 1967. Paleocene amphibians from Cernay, France. *American Museum Novitates*, **2295**: 1–25.
- Estes, R., Z. V. Špínar, and E. Nevo.** 1978. Early Cretaceous pipid tadpoles from Israel (Amphibia: Anura). *Herpetologica*, **34** (4): 374–393.
- Ettachfini, E. M., and B. Andreu.** 2004. Le Cénomanién et le Turonien de la Plate-forme Préafricaine du Maroc. *Cretaceous Research*, **25** (2): 277–302.

References

- Evans, S. E., and M. Borsuk-Bialynicka. 1998. A stem-group frog from the Early-Triassic of Poland. *Acta Palaeontologica Polonica*, **43** (4): 573–580.
- Evans, B. J., T. F. Carter, E. Greenbaum, V. Gvoždík, D. B. Kelley, P. J. McLaughlin, O. S. G. Pauwels, D. M. Portik, E. L. Stanley, R. C. Tinsley, M. L. Tobias, and D. C. Blackburn. 2015. Genetics, morphology, advertisement calls, and historical records distinguish six new polyploid species of African clawed frog (*Xenopus*, Pipidae) from West and Central Africa. *PLoS ONE*, **10** (12): e0142823.
- Evans, D. C. 2005. New evidence on brain-endocranial cavity relationships in ornithischian dinosaurs. *Acta Palaeontologica Polonica*, **50** (3): 617–622.
- Evans, S. E., A. R. Milner, and F. Musset. 1990. A discoglossid frog from the Middle Jurassic of England. *Paleontology*, **33** (2): 299–311.
- Evans, S. E., M. E. H. Jones, and D. W. Krause. 2008. A giant frog with South American affinities from the Late Cretaceous of Madagascar. *Proceedings of the National Academy of Sciences*, **105** (8): 2951–2956.
- Evans, S. E., J. R. Groenke, M. E. H. Jones, A. H. Turner, and D. W. Krause. 2014. New Material of *Beelzebufo*, a Hyperossified Frog (Amphibia: Anura) from the Late Cretaceous of Madagascar. *PLoS ONE*, **9** (1): e87236.
- Fabrezi, M. 2006. Morphological evolution of Ceratophryinae (Anura, Neobatrachia). *Journal of Zoological Systematics and Evolutionary Research*, **44** (2): 153–166.
- Fainsod, A., and S. A. Moody. 2022. *Xenopus: from basic biology to disease models in the genomic era*, 1st ed. CRC Press, Boca Raton, 360 pp.
- Fairhead, J. D. 1988. Mesozoic plate tectonic reconstructions of the central South Atlantic Ocean: The role of the West and Central African rift system. *Tectonophysics*, **155** (1-4): 181–191.
- Fairhead, J. D., and R. M. Binks. 1991. Differential opening of the Central and South Atlantic Oceans and the opening of the West African rift system. *Tectonophysics*, **187** (1-3): 191–203.
- Feng, Y.-J., D. C. Blackburn, D. Liang, D. M. Hillis, D. B. Wake, D. C. Cannatella, and P. Zhang. 2017. Phylogenomics reveals rapid, simultaneous diversification of three major clades of Gondwanan frogs at the Cretaceous–Paleogene boundary. *Proceedings of the National Academy of Sciences*, **114** (29): E5864–E5870.

References

- Filhol, H.** 1873. Sur des pièces fossiles provenant de batraciens, de lacertiens et d'ophidiens, trouvés dans les dépôts de phosphates de chaux de l'Aveyron. *Comptes Rendus de l'Académie des Sciences, Paris*, **77**: 1556–1557.
- Filhol, H.** 1876. Sur les Reptiles fossiles des phosphorites du Quercy. *Bulletin de La Société Philomathique de Paris*, **6**: 27–28.
- Filhol, H.** 1877. *Recherches sur les phosphorites du Quercy: Etude des fossiles qu'on y rencontre et spécialement des mammifères*, Librairie de l'Académie de médecine. G. Masson, Paris, 690 pp.
- Fisher, M. C., and T. W. J. Garner.** 2007. The relationship between the emergence of *Batrachochytrium dendrobatidis*, the international trade in amphibians and introduced amphibian species. *Fungal Biology Reviews*, **21** (1): 2–9.
- Fisher, M. C., T. W. J. Garner, and S. F. Walker.** 2009. Global emergence of *Batrachochytrium dendrobatidis* and amphibian chytridiomycosis in space, time, and host. *Annual Review of Microbiology*, **63** (1): 291–310.
- Fitzinger, L. J. F. J.** 1861. Eine Neue Batrachier-Gattung aus Neu-Seeland. *Verhandlungen des Zoologisch-Botanischen Vereins in Wien*, **11**: 217–220.
- Flynn, L. J., A. Brillanceau, M. Brunet, Y. Coppens, J. Dejax, G. Ekodeck, K. M. Flanagan, E. Heintz, J. Hell, L. L. Jacobs, D. R. Pilbeam', S. Sen, S. Djallo, and L. de Pal.** 1987. Vertebrate fossils from Cameroon, West Africa. *Journal of Vertebrate Paleontology*, **7** (4): 469–471.
- Folie, A., R. S. R. Rana, K. D. Rose, A. Sahini, K. Kumar, L. Singh, and T. Smith.** 2012. Early Eocene frogs from Vastan Lignite Mine, Gujarat, India. *Acta Palaeontologica Polonica*, **58** (3): 511–524.
- Ford, L. S., and D. C. Cannatella.** 1993. The major clades of frogs. *Herpetological Monographs*, **7**: 94–117.
- Fouquet, A.** 2001. Des clandestins aquatiques. *Zamensis*, **6**: 10–11.
- Fouquet, A., J. Cornuault, M. T. Rodrigues, F. P. Werneck, T. Hrbek, A. R. Acosta-Galvis, D. Massemin, P. J. R. Kok, and R. Ernst.** 2022. Diversity, biogeography, and reproductive evolution in the genus *Pipa* (Amphibia: Anura: Pipidae). *Molecular Phylogenetics and Evolution*, **170**: 107442.
- Fox, R. C.** 1976. An edentulous frog (*Theatoniuss lancensis*, new genus and species) from the Upper Cretaceous Lance Formation of Wyoming. *Canadian Journal of Earth Sciences*, **13**: 1486–1490.

References

- Franzese, J., L. Spalletti, I. G. Pérez, and D. Macdonald.** 2003. Tectonic and paleoenvironmental evolution of Mesozoic sedimentary basins along the Andean foothills of Argentina (32°–54°S). *Journal of South American Earth Sciences*, **16** (1): 81–90.
- Frazão, A., H. R. da Silva, and C. A. de M. Russo.** 2015. The Gondwana breakup and the history of the Atlantic and Indian Oceans unveils two new clades for early neobatrachian diversification. *PLoS ONE*, **10** (11): e0143926.
- Frishkopf, L. S., and M. H. Goldstein.** 1963. Responses to acoustic stimuli from single units in the eighth nerve of the bullfrog. *The Journal of the Acoustical Society of America*, **35** (8): 1219–1228.
- Frost D. R.** 2021. Amphibian species of the world: An online reference. Version 6.1 (03/10/2022). Electronic database accessible at <https://amphibiansoftheworld.amnh.org/index.php>. American Museum of Natural History, New York, USA.
- Frost, D. R., T. Grant, J. Faivovich, R. H. Bain, A. Haas, C. F. B. Haddad, R. O. De Sá, A. Channing, M. Wilkinson, S. C. Donnellan, C. J. Raxworthy, J. A. Campbell, B. L. Blotto, P. Moler, R. C. Drewes, R. A. Nussbaum, J. D. Lynch, D. M. Green, and W. C. Wheeler.** 2006. The Amphibian Tree of Life. *Bulletin of the American Museum of Natural History*, **297**: 1–291.
- Gaina, C., T. H. Torsvik, D. J. J. van Hinsbergen, S. Medvedev, S. C. Werner, and C. Labails.** 2013. The African plate: A history of oceanic crust accretion and subduction since the Jurassic. *Tectonophysics*, **604**: 4–25.
- Gao, K.-Q., and J. Chen.** 2017. A new crown-group frog (Amphibia: Anura) from the Early Cretaceous of Northeastern Inner Mongolia, China. *American Museum Novitates*, **3876**: 1–39.
- Gardner, D.** 2008. New information on frogs (Lissamphibia: Anura) from the Lance Formation (Late Maastrichtian) and Bug Creek Anthills (Late Maastrichtian and Early Paleocene), Hell Creek Formation, USA; pp. 219–249 in **J. T. Sankey and S. Baszio** (eds.), *Vertebrate Microfossil Assemblages*. Indiana University Press, Indianapolis.
- Gardner, J. D., and D. G. DeMar.** 2013. Mesozoic and Palaeocene lissamphibian assemblages of North America: a comprehensive review. *Palaeobiodiversity and Palaeoenvironments*, **93** (4): 459–515.

References

- Gardner, J. D., and J.-C. Rage.** 2016. The fossil record of lissamphibians from Africa, Madagascar, and the Arabian Plate. *Palaeobiodiversity and Palaeoenvironments*, **96** (1): 169–220.
- Gardner, J. D., A. Villa, S. Colombero, M. Venczel, and M. Delfino.** 2021. A Messinian (latest Miocene) occurrence for *Albanerpeton* Estes & Hoffstetter, 1976 (Lissamphibia: Albanerpetontidae) at Moncucco Torinese, Piedmont Basin, northwestern Italy, and a review of the European Cenozoic record for albanerpetontids. *Geodiversitas*, **43** (14): 391–404.
- Gardner, J. D., Z. Roček, T. Přikryl, J. G. Eaton, R. W. Blob, and J. T. Sankey.** 2010. Comparative morphology of the ilium of anurans and urodeles (Lissamphibia) and a re-assessment of the anuran affinities of *Nezpercius dodsoni* Blob et al., 2001. *Journal of Vertebrate Paleontology*, **30** (6): 1684–1696.
- Gaupp, E.** 1896. *Anatomie des frosches*. Pt. 3, 2nd Edition. Friedrich Vieweg Und Shon, Braunschweig, 961 pp.
- Gayet, M., and F. J. Meunier.** 1996. Nouveaux polypteriformes du gisement coniacien-sénonien d'In Becetem (Niger). *Compte Rendus de l'Académie Des Sciences, Série 2* (322): 701–707.
- Gayet, M., F. J. Meunier, and C. Werner.** 1997. Strange polypteriformes from the Upper Cretaceous of In Becetem (Niger) and Wadi Milk Formation (Sudan). *Geobios*, **30**: 249–255.
- Gèze, B.** 1949. Les Gouffres à Phosphate du Quercy. *Annales de Spéléologie*, **4** (2): 89–107.
- Gheerbrant, E., and J.-C. Rage.** 2006. Paleobiogeography of Africa: How Distinct from Gondwana and Laurasia? *Palaeogeography, Palaeoclimatology, Palaeoecology*, **241** (2): 224–246.
- Goloboff, P. A.** 1993. Estimating character weights during tree search. *Cladistics*, **9**: 83–91.
- Goloboff, P. A.** 1997. Self-weighted optimization: Tree searches and character state reconstructions under implied transformation costs. *Cladistics*, **13** (3): 225–245.
- Goloboff, P. A., and J. S. Farris.** 2001. Methods for quick consensus estimation. *Cladistics*, **17**: S26–S34.
- Goloboff, P. A., and S. A. Catalano.** 2016. TNT version 1.5, including a full implementation of phylogenetic morphometrics. *Cladistics*, **32**: 221–238.
- Goloboff, P. A., A. Torres, and J. S. Arias.** 2018a. Weighted parsimony outperforms other methods of phylogenetic inference under models appropriate for morphology. *Cladistics*, **34**: 407–437.

References

- Goloboff, P. A., J. M. Carpenter, J. S. Arias, and D. R. M. Esquivel.** 2008. Weighting against homoplasy improves phylogenetic analysis of morphological data sets. *Cladistics*, **24**: 758–773.
- Goloboff, P. A., M. Pittman, D. Pol, and X. Xu.** 2018b. Morphological data sets fit a common mechanism much more poorly than DNA sequences and call into question the mkv model. *Systematic Biology*, **68** (3): 494–504.
- Gómez, R. O.** 2016. A new pipid frog from the Upper Cretaceous of Patagonia and early evolution of crown-group Pipidae. *Cretaceous Research*, **62**: 52–64.
- Gómez, R. O., and G. F. Turazzini.** 2016. An overview of the ilium of anurans (Lissamphibia, Salientia), with a critical appraisal of the terminology and primary homology of main ilial features. *Journal of Vertebrate Paleontology*, **36** (1): e1030023.
- Gómez, R. O., and G. F. Turazzini.** 2021. The fossil record and phylogeny of South American horned frogs (Anura, Ceratophryidae). *Journal of Systematic Palaeontology*: 1–52.
- Goodrich, E. S.** 1930. *Studies on the structure and development of vertebrates*. MacMillan and co., Limited, St. Martin's street, London, 837 pp.
- Gray, E.** 1825. A synopsis of the genera of reptiles and Amphibia, with a description of some new species. *Annals of Philosophy, London* ,**10**: 193–217.
- Greigert, J.** 1966. *Description des formations Crétacées et Tertiaires du bassin Des Iullemmeden (Afrique Occidentale)*. Editions du Bureau de recherches géologiques et minières, Paris, 234 pp.
- Greigert, J., and R. Pognet.** 1967. Notice explicative sur la carte géologique de la République du Niger.
- Griffin, C. T., M. R. Stocker, C. Colleary, C. M. Stefanic, E. J. Lessner, M. Riegler, K. Formoso, K. Koeller, and S. J. Nesbitt.** 2021. Assessing ontogenetic maturity in extinct saurian reptiles. *Biological Reviews*, **96** (2): 470–525.
- Griffiths, R. A., and L. Pavajeau.** 2008. Captive breeding, reintroduction, and the conservation of amphibians. *Conservation Biology*, **22** (4):852–861.
- Günther, A. C. L. G.** 1882. Notice of a second species of *Triprion*. *Annals and Magazine of Natural History, Series 5*, **10**: 279.

References

- Gurdon, J. B., and N. Hopwood.** 2000. The introduction of *Xenopus laevis* into developmental biology: of empire, pregnancy testing and ribosomal genes. *International Journal of Developmental Biology*, **44**: 43–50.
- Haas, A.** 2003. Phylogeny of frogs as inferred from primarily larval characters (Amphibia: Anura). *Cladistics*, **19** (1): 23–89.
- Haddoumi, H., R. Allain, S. Meslouh, G. Metais, M. Monbaron, D. Pons, J.-C. Rage, R. Vullo, S. Zouhri, and E. Gheerbrant.** 2016. Guelb el Ahmar (Bathonian, Anoual Syncline, eastern Morocco): First continental flora and fauna including mammals from the Middle Jurassic of Africa. *Gondwana Research*, **29** (1): 290–319.
- Hedges, S. B., J. Marin, M. Suleski, M. Paymer, and S. Kumar.** 2015. Tree of Life rReveals clock-like speciation and diversification. *Molecular Biology and Evolution*, **32** (4): 835–845.
- Helling, H.** 1938. Das geruchsorgan der anuren, vergleichend-morphologisch betrachtet. *Zeitschrift Für Anatomie*, **108**: 587–643.
- Henrici, A. C.** 1991. *Chelomophrynus bayi* (Amphibia, Anura, Rhinophrynidae), a new genus and species from the Middle Eocene of Wyoming: ontogeny and relationships. *Annals of Carnegie Museum*, **60** (2): 97–144.
- Henrici, A. C.** 1998. A new pipoid anuran from the Late Jurassic Morrison Formation at Dinosaur National Monument, Utah. *Journal of Vertebrate Paleontology*, **18** (2): 321–332.
- Henrici, A. C., and A. M. Báez.** 2001. First occurrence of *Xenopus* (Anura: Pipidae) on the Arabian Peninsula: A new species from the Upper Oligocene of Yemen. *Journal of Paleontology*, **75** (4): 870–882.
- Hewitt, J.** 1919. *Anhydrophryne rattrayi*, a remarkable new frog from Cape Colony. *Records of the Albany Museum, Grahamstown*, **3**: 182–189.
- Hewitt, J.** 1925. On some new species of reptiles and amphibians from South Africa. *Records of the Albany Museum, Grahamstown*, **3**: 343–368.
- Hewitt, J.** 1926. Descriptions of new and little-known lizards and batrachians from South Africa. *Annals of the South African Museum*, **20**: 413–431.
- Hewitt, J. and P. A. Methuen.** 1912. Descriptions of some new Batrachia and Lacertilia from South Africa. *Transactions of the royal Society of South Africa*, **3**: 107–111.

References

- Hime, P. M., A. R. Lemmon, E. C. M. Lemmon, E. Prendini, J. M. Brown, R. C. Thomson, J. D. Kratovil, B. P. Noonan, R. A. Pyron, P. L. V. Peloso, M. L. Kortyna, J. S. Keogh, S. C. Donnellan, R. L. Mueller, C. J. Raxworthy, K. Kunte, S. R. Ron, S. Das, N. Gaitonde, D. M. Green, J. Labisko, J. Che, and D. W. Weisrock. 2021. Phylogenomics reveals ancient gene tree discordance in the amphibian Tree of Life. *Systematic Biology*, **70** (1): 49–66.
- Holman, J. A., and D. L. Harrison. 2002. A New *Thaumastosaurus* (Anura: Familia Incertae Sedis) from the Late Eocene of England, with remarks on the taxonomic and zoogeographic relationships of the genus. *Journal of Herpetology*, **36** (4): 621–626.
- Holman, J. A., and D. L. Harrison. 2003. A new helmeted frog of the genus *Thaumastosaurus* from the Eocene of England. *Acta Palaeontologica Polonica*, **48** (1): 157–160.
- Holmes J. A. 2003. *Fossil frogs and toads of North America*. Indiana University Press, Bloomington, Ind, 246 pp.
- Hopkins, G. R., and E. D. Brodie. 2015. Occurrence of amphibians in saline habitats: A review and evolutionary perspective. *Herpetological Monographs*, **29** (1): 1–27.
- Hossini, S., and J.-C. Rage. 2000. Palaeobatrachid frogs from the earliest Miocene (Agenian) of France, with description of a new species. *Geobios*, **33** (2): 223–231.
- Houssaye, A. 2009. “Pachyostosis” in aquatic amniotes: A review. *Integrative Zoology*, **4** (4): 325–340.
- Houssaye, A. 2013. Palaeoecological and morphofunctional interpretation of bone mass increase: an example in Late Cretaceous shallow marine squamates. *Biological Reviews*, **88** (1): 117–139.
- Houssaye, A., A. Herrel, R. Boistel, and J.-C. Rage. 2019. Adaptation of the vertebral inner structure to an aquatic life in snakes: Pachyophiid peculiarities in comparison to extant and extinct forms. *Comptes Rendus Palevol*, **18** (7): 783–799.
- Ibrahim, N., P. C. Sereno, D. J. Varricchio, D. M. Martill, D. B. Dutheil, D. M. Unwin, L. Baidder, H. C. E. Larsson, S. Zouhri, and A. Kaoukaya. 2020a. Geology and paleontology of the Upper Cretaceous Kem Kem Group of eastern Morocco. *ZooKeys*, **928** : 1–216.
- Ibrahim, N., S. Maganuco, C. Dal Sasso, M. Fabbri, M. Auditore, G. Bindellini, D. M. Martill, S. Zouhri, D. A. Mattarelli, D. M. Unwin, J. Wiemann, D. Bonadonna, A. Amane, J.

References

- Jakubczak, U. Joger, G. V. Lauder, and S. E. Pierce.** 2020b. Tail-propelled aquatic locomotion in a theropod dinosaur. *Nature*, **581** (7806): 67–70.
- Ihlow, F., J. Courant, J. Secondi, A. Herrel, R. Rebelo, G. J. Measey, F. Lillo, F. A. De Villiers, S. Vogt, C. De Busschere, T. Backeljau, and D. Rödder.** 2016. Impacts of climate change on the global invasion potential of the African clawed frog *Xenopus laevis*. *PLoS ONE*, **11** (6): e0154869.
- Ingle, D.** 1973a. Evolutionary perspectives on the function of the optic tectum. *Brain, Behavior and Evolution*, **8** (3): 211–237.
- Ingle, D.** 1973b. Two visual systems in the frog. *Science*, **181** (4104): 1053–1055.
- Jacobs, L. L., D. A. Winkler, and E. M. Gomani.** 1990. The Dinosaur Beds of northern Malawi, Africa. *National Geographic Research*, **6**: 196–204.
- Jacobs, L. L., J. D. Congleton, M. Brunet, J. Dejax, L. J. Flynn, J. V. Hell, and G. Mouchelin.** 1988. Mammal teeth from the Cretaceous of Africa. *Nature*, **336** (6195): 158–160.
- Jarošová, J., and Z. Roček.** 1982. The incrassatio frontoparietalis in frogs, its origin and phylogenetic significance. *Amphibia-Reptilia*, **3** : 111–124.
- Jerison, H. J.** 1973. *Evolution of the brain and intelligence*. Academic Press, New York, NY, 495 pp.
- Jerison, H. J.** 2012. Digitized fossil brains: Neocorticalization. *Biolinguistics*, **6** (3-4): 383–392.
- Jésus, V. J. P., O. Mateus, J. Milàn, and L. B. Clemmensen.** 2022. First occurrence of a frog-like batrachian (Amphibia) in the Late Triassic Fleming Fjord Group, central East Greenland. *Bulletin of the Geological Society of Denmark*, **70**: 117–130.
- Jetz, W., and R. A. Pyron.** 2018. The interplay of past diversification and evolutionary isolation with present imperilment across the amphibian tree of life. *Nature Ecology & Evolution*, **2** (5): 850–858.
- Jones, A. S., and R. J. Butler.** 2018. A new phylogenetic analysis of Phytosauria (Archosauria: Pseudosuchia) with the application of continuous and geometric morphometric character coding. *PeerJ*, **6**: e5901.
- Jones, M. E. H., S. E. Evans, and D. Sigogneau-Russell.** 2003. Early Cretaceous frogs from Morocco. *Annals of Carnegie Museum*, **72** (2): 65–99.
- Jungblut, L. D., A. G. Pozzi, and D. A. Paz.** 2013. El sistema vomeronasal y su posible funcionalidad en larvas de anuros. *Cuadernos de herpetología*, **27** (1): 47–56.

References

- Jungblut, L. D., J. O. Reiss, and A. G. Pozzi.** 2021. Olfactory subsystems in the peripheral olfactory organ of anuran amphibians. *Cell and Tissue Research*, **383** (1): 289–299.
- Kato, K., H. Nakagaki, Y. Sakakibara, J. A. Weatherell, and C. Robinson.** 1988. The dissolution rate of enamel in acid in developing rat incisors. *Archives of Oral Biology*, **33** (9): 657–660.
- Keeffe, R., and D. C. Blackburn.** 2020. Comparative morphology of the humerus in forward-burrowing frogs. *Biological Journal of the Linnean Society*, **131** (2): 291–303.
- Kobel, H. R., L. D. Pasquier, and R. C. Tinsley.** 1981. Natural hybridization and gene introgression between *Xenopus gilli* and *Xenopus laevis* (Anura: Pipidae). *Journal of Zoology*, **194** (3): 317–322.
- Kramer, K.** 1933. Untersuchungen über die Sinnesleistungen und das Orientierungsverhalten von *Xenopus laevis* Dauding. *Zoologische Jahrbucher, Abteilung Für Allgemeine Zoologie Und Physiologie*, **52** (4): 629–676.
- Laloy, F., J.-C. Rage, S. E. Evans, R. Boistel, N. Lenoir, and M. Laurin.** 2013. A re-interpretation of the Eocene anuran *Thaumastosaurus* based on microCT examination of a ‘mummified’ specimen. *PLoS ONE*, **8** (9): e74874.
- de Lapparent de Broin, F., S. Bailon, M. L. Augé, and J.-C. Rage.** 2020. Amphibians and reptiles from the Neogene of Afghanistan. *Geodiversitas*, **42** (22): 409–426.
- de Lapparent, F.** 2000. African chelonians from the Jurassic to the Present: Phases of development and preliminary catalog of the fossil record. *Palaeontologica Africana*, **36**: 43–82.
- Lasseron, M., R. Allain, E. Gheerbrant, H. Haddoumi, N.-E. Jalil, G. Métais, J.-C. Rage, R. Vullo, and S. Zouhri.** 2019. New data on the microvertebrate fauna from the Upper Jurassic or lowest Cretaceous of Ksar Metlili (Anoual Syncline, eastern Morocco). *Geological Magazine*, **157** (3): 367–392.
- Largen, M. J.** 1991. A new genus and species of petropedetine frog (Amphibia Anura Ranidae) from high altitude in the mountains of Ethiopia. *Tropical Zoology*, **4**: 139–152.
- Laurent, R. F.** 1941(‘1940’). Contribution à l’ostéologie et à la systématique des Ranides africains. Première note. *Revue de Zoologie et de Botanique africaines*, **34**: 74–96.
- Laurent, R. F.** 1946. Mises au point dans la taxonomie des Ranides. *Revue de Zoologie et de Botanique africaines*, **39**: 336–338.

References

- Laurent, R. F. (1953) Reptiles et Batraciens récemment parvenus au Musée royal du Congo belge. *Bulletin du Cercle zoologique congolais*, 21: 21–29
- Laurent, R. F.** 1986. Sous classe des lissamphibiens (Lissamphibia); pp. 594–597 in *Traité de Zoologie, Anatomie, Systématique, Biologie*, Grassé P., and M. Delsol. vol. 14. Paris.
- Laurin, M., O. Lapauze, and D. Marjanović.** 2022. What do ossification sequences tell us about the origin of extant amphibians? *Peer Community Journal*, 2: e12.
- Laurin, M., Arntzen, J. W., Báez, A. M., Bauer, A. M., Damiani, R., Evans, S. E. et al.** (2020a) Amphibia; pp.765-771 in **K. de Queiroz, P. D. Cantino and J. A. Gauthier** (eds.), *Phylonoms: an implementation of PhyloCode*, CRC Press, Boca Raton, Florida.
- Laurin, M., Arntzen, J. W., Báez, A. M., Bauer, A. M., Damiani, R., Evans, S. E. et al.** (2020b) Lissamphibia, pp. 773-778 in **K. de Queiroz, P. D. Cantino and J. A. Gauthier** (eds.), *Phylonoms: an implementation of PhyloCode*, CRC Press, Boca Raton, Florida.
- Leal, M. E. C., and P. M. Brito.** 2006. Anura do Cretáceo Inferior da Bacia do Araripe, Nordeste do Brasil; pp. 145–152 in **V. Gallo, P. M. Brito, H. M. A. Silva, and F. J. Figueiredo** (eds.), *Paleontología de Vertebrados. Grandes Temas e Contribuições Científicas*. Interciencia, Rio de Janeiro.
- Lee-Liu, D., E. E. Méndez-Olivos, R. Muñoz, and J. Larrain.** 2017. The African clawed frog *Xenopus laevis*: A model organism to study regeneration of the central nervous system. *Neuroscience Letters*, 652: 82–93.
- Lefebvre, L.** 2011. Taxonomic counts of cognition in the wild. *Biology Letters*, 7 (4): 631–633.
- Legendre, S., B. Marandat, B. Sigé, J.-Y. Crochet, M. Godinot, J.-L. Hartenberger, J. Sudre, M. Vianey-Liaud, B. Muratet, and J.-G. Astruc.** 1992. Mammalian fauna of Vielase (Phosphorites of Quercy, in the South of France): Paleontological evidence for karst formation in the Quercy area as early as the Early Eocene. *Neues Jahrbuch für Geologie und Paläontologie – Monatshefte* 1992, (7): 414–428.
- Lemierre, A., and D. C. Blackburn.** 2022. A new genus and species of frog from the Kem Kem (Morocco), the second neobatrachian from Cretaceous Africa. *PeerJ*, 10 : e13699.
- Lemierre, A., and M. Laurin.** 2021. Conversion of the names Pyxicephaloidea, Pyxicephalidae and Pyxicephalinae (Anura, Ranoidea) into phylogenetic nomenclature. *Bionomina* 25: 91–92.

References

- Lemierre, A., A. Folie, S. Bailon, N. Robin, and M. Laurin.** 2021. From toad to frog, a CT-based reconsideration of *Bufo servatus*, an Eocene anuran mummy from Quercy (France). *Journal of Vertebrate Paleontology*, **41** (3): e1989694.
- Linnaeus, C.** 1758. *Systema Naturae per Regna Tria Naturae, Secundum Classes, Ordines, Genra, Species, Cum Characteribus, Differentiis, Synonymis, Locis*, Edition decima, reformata. Laurentius, Stockholm, 828 pp.
- Longcore, J. E., A. P. Pessier, and D. K. Nichols.** 1999. *Batrachochytrium dendrobatidis* gen. et sp. nov., a chytrid pathogenic to amphibians. *Mycologia*, **91** (2): 219–227.
- Loveridge, J. P.** 1936. Scientific results of an expedition to rain forest regions in eastern Africa VII. Amphibians. *Bulletin of the Museum of comparative Zoology*, **79**: 369–430.
- Lynch, J. D.** 1971. Evolutionary Relationships, Osteology and Zoography of Leptodactyloid Frogs. *Miscellaneous Publication, Museum of Natural History, University of Kansas*, **53**: 1–238.
- Lynch, J. D.** 1973. The transition from archaic to advanced frogs; pp. 133–182 in **J. L. Vial** (ed.), *Evolutionary biology of the anurans. Contemporary research on major problems*. University of Missouri Press.
- Macaluso, L., J. E. Martin, L. Del Favero, and M. Delfino.** 2019. Revision of the crocodylians from the Oligocene of Monteviale, Italy, and the diversity of European eusuchians across the Eocene-Oligocene boundary. *Journal of Vertebrate Paleontology*, **39** (2): e1601098.
- Mackintosh, N. J., B. Wilson, and R. A. Boakes.** 1985. Differences in mechanisms of intelligence among vertebrates. *Philosophical Transactions of the Royal Society of London. B, Biological Sciences*, **308** (1135): 53–65.
- Macrini, T. E., G. W. Rougier, and T. Rowe.** 2007. Description of a cranial endocast from the fossil mammal *Vincelestes neuquenianus* (Theriiformes) and its relevance to the evolution of endocranial characters in therians. *The Anatomical Record*, **290**: 875–892.
- Maddin, H. C., M. Venczel, J. D. Gardner, and J.-C. Rage.** 2013. Micro-computed tomography study of a three-dimensionally preserved neurocranium of *Albanerpeton* (Lissamphibia, Albanerpetontidae) from the Pliocene of Hungary. *Journal of Vertebrate Paleontology*, **33** (3): 568–587.

References

- Mahony, S.** 2019. *Cordicephalus* Nevo, 1968 (Amphibia, Anura, Pipimorpha), is a junior homonym of *Cordicephalus* Wardle, 1947 (Rhabditophora, Cestoda, Diphyllbothriidae). *Journal of Vertebrate Paleontology*, **39** (2): e1593186.
- Mammal Diversity Database.** 2022. Mammal Diversity Database (Version 1.9.1)[03/10/2022]. <https://www.mammaldiversity.org/index.html>.
- Marjanović, D., and M. Laurin.** 2007. Fossils, molecules, divergence times, and the origin of lissamphibians. *Systematic Biology*, **56** (3): 369–388.
- Marjanović, D., and M. Laurin.** 2014. An updated paleontological timetree of lissamphibians, with comments on the anatomy of Jurassic crown-group salamanders (Urodela). *Historical Biology*, **26** (4): 535–550.
- Marjanović, D., and M. Laurin.** 2019. Phylogeny of Paleozoic limbed vertebrates reassessed through revision and expansion of the largest published relevant data matrix. *PeerJ*, **6**: e5565.
- Martill, D. M., G. Bechly, and R. F. Loveridge.** 2007. *The Crato fossil beds of Brazil: Window into an ancient world*. Cambridge University Press, New York, 675 pp.
- Martill, D. M., N. Ibrahim, P. M. Brito, L. Baider, S. Zhou, R. Loveridge, D. Naish, and R. Hing.** 2011. A new Plattenkalk Konservat Lagerstätte in the Upper Cretaceous of Gara Sbaa, south-eastern Morocco. *Cretaceous Research*, **32** (4): 433–446.
- Martín, C., M. A. Alonso-Zarazaga, and B. Sanchiz.** 2012. Nomenclatural notes on living and fossil amphibians. *Graellsia*, **68** (1): 159.
- Mason, M. J., J. M. Segenhout, A. Cobo-Cuan, P. M. Quiñones, and P. van Dijk.** 2015. The frog inner ear: Picture perfect? *Journal of the Association for Research in Otolaryngology*, **16** (2): 171–188.
- Masters, J. C., F. Génin, Y. Zhang, R. Pellen, T. Huck, P. P. A. Mazza, M. Rabineau, M. Doucouré, and D. Aslanian.** 2021. Biogeographic mechanisms involved in the colonization of Madagascar by African vertebrates: Rifting, rafting and runways. *Journal of Biogeography*, **48** (3): 492–510.
- Mateer, N. J., P. Wycisk, L. L. Jacobs, M. Brunet, P. Luger, M. A. Arush, F. Hendriks, T. Weissbrod, G. Gvirtzman, E. Mbede, A. Dina, R. T. J. Moody, G. Weigelt, H. A. El-Nakhal, J. Hell, and J. Stets.** 1992. Correlation of nonmarine Cretaceous strata of Africa and the Middle East. *Cretaceous Research*, **13** (3): 273–318.

References

- Matthews, T., R. Keeffe, and D. C. Blackburn.** 2019. An identification guide to fossil frog assemblages of southern Africa based on ilia of extant taxa. *Zoologischer Anzeiger*, **283**: 46–57.
- Matthews, T., E. van Dijk, D. L. Roberts, and R. M. H. Smith.** 2015. An early Pliocene (5.1 Ma) fossil frog community from Langebaanweg, south-western Cape, South Africa. *African Journal of Herpetology*, **64** (1): 39–53.
- McLoughlin, S.** 2001. The breakup history of Gondwana and its impact on pre-Cenozoic floristic provincialism. *Australian Journal of Botany*, **49** (3): 271–300.
- Measey, G. J., D. Rödder, S. L. Green, R. Kobayashi, F. Lillo, G. Lobos, R. Rebelo, and J.-M. Thirion.** 2012. Ongoing invasions of the African clawed frog, *Xenopus laevis*: A global review. *Biological Invasions*, **14** (11): 2255–2270.
- Measey, G. J., G. Vimercati, F. A. de Villiers, M. Mokhatla, S. J. Davies, C. J. Thorp, A. D. Rebelo, and S. Kumschick.** 2016. A global assessment of alien amphibian impacts in a formal framework. *Diversity and Distributions*, **22** (9): 970–981.
- Measey, J.** 2016. Overland movement in African clawed frogs (*Xenopus laevis*): a systematic review. *PeerJ*, **4**: e2474.
- Meunier, L. M. V., and H. C. E. Larsson.** 2018. *Trematochampsia taqueti* as a nomen dubium and the crocodyliform diversity of the Upper Cretaceous In Beceten Formation of Niger. *Zoological Journal of the Linnean Society*, **182** (3): 659–680.
- Meyer, H. von.** 1843. Summarische Uebersicht er fossilen Wierbelthiere des Mainzer Tertiär-Beckens, mit besonderer Rücksicht auf Weisenau. *Neues Jahrbuch für Mineralogie, Geognosie, Geologie und Petrefakten-Kunde. Stuttgart*, **1843**: 379–410.
- Miyashita, T., V. M. Arbour, L. M. Witmer, and P. J. Currie.** 2011. The internal cranial morphology of an armoured dinosaur *Euoplocephalus* corroborated by X-ray computed tomographic reconstruction: Ankylosaurid internal cranial anatomy. *Journal of Anatomy*, **219** (6): 661–675.
- Moody, R. T. J., and P. J. C. Sutcliffe.** 1991. The Cretaceous deposits of the Iullemeden Basin of Niger, central West Africa. *Cretaceous Research*, **12** (2): 137–157.

References

- Mörs, T., M. Reguero, and D. Vasilyan.** 2020. First fossil frog from Antarctica: implications for Eocene high latitude climate conditions and Gondwanan cosmopolitanism of Australobatrachia. *Scientific Reports*, **10** (1): 5051.
- Moulin, M., D. Aslanian, and P. Unternehr.** 2010. A new starting point for the South and Equatorial Atlantic Ocean. *Earth-Science Reviews*, **98** (1-2): 1–37.
- Moura, P. H. A. G., F. R. Costa, L. E. Anelli, and I. Nunes.** 2021. A new genus of fossil frog (Anura) from lower Cretaceous deposits in South America. *Anais Da Academia Brasileira de Ciências*, **93**: e20191560.
- Munsey, L. D.** 1972. Salinity tolerance of the African pipid frog, *Xenopus laevis*. *Copeia*, **1972** (3): 584–586.
- Muzzopappa, P.** 2019. *Calyptocephalella* (Anura, Australobatrachia) remains from Río Santa Cruz (Early–Middle Miocene, Santa Cruz Formation), Santa Cruz Province, Argentina. *Publicacion Electronica*, **19** (2): 48–54.
- Muzzopappa, P., and A. M. Báez.** 2009. Systematic status of the mid-Tertiary neobatrachian frog *Calyptocephalella canqueli* from Patagonia (Argentina), with comments on the evolution of the genus. *Ameghiniana*, **46** (1): 113–125.
- Muzzopappa, P., A. G. Martinelli, J. P. Garderes, and G. W. Rougier.** 2020. Exceptional avian pellet from the Paleocene of Patagonia and description of its content: a new species of calyptocephalellid (Neobatrachia) anuran. *Papers in Palaeontology* **spp2.1333**: 1-14.
- Muzzopappa, P., F. V. Iori, F. P. Muniz, and A. G. Martinelli.** 2022. A new species of *Baurubatrachus* (Anura, Neobatrachia) from the Late Cretaceous Adamantina Formation of Brazil furnishes evidence on the diversity of this bizarre genus. *Ameghiniana*, **59** (5): 297–316.
- Navas, C. A., C. R. Bevier, and A. C. Carnaval.** 2012. Integrative and objective science is the best link between amphibian decline research and conservation on the ground. *Alytes*, **29** (1-4): 119–132.
- Nevo, E.** 1968. Pipid frogs from the early cretaceous of Israel and pipid evolution. *Bulletin Museum of Comparative Zoology*, **136** (8): 255–317.
- Nicoli, L.** 2015. New fossil species of the extant genus *Lepidobatrachus* (Anura, Ceratophryidae) from the Late Miocene-Early Pliocene of central Argentina. *Journal of Vertebrate Paleontology*, **35** (5): e981636.

References

- Nicoli, L., R. L. Tomassini, and C. I. Montalvo.** 2017. The oldest record of *Ceratophrys* (Anura, Ceratophryidae) from the Late Miocene of central Argentina. *Journal of Vertebrate Paleontology*, **37** (1): e1261360.
- Noble, G. K.** 1931. *The Biology of the Amphibia*, First Edition. (A. F. Shull (ed.)). McGraw-Hill Book Company, New York ; London, 600 pp.
- Nopcsa, D. F. B.** 1908. Zur kenntnis der fossilen eidechsen. *Beitrage zur Palaontologie und Geologie Osterreich-Ungarns und des Orients*, **21**: 34–62.
- Nürnberg, D., and R. D. Müller.** 1991. The tectonic evolution of the South Atlantic from Late Jurassic to present. *Tectonophysics*, **191** (1-2): 27–53.
- Olivier, J. A.** 1951. “Gliding” in amphibians and reptiles, with a remark on an arboreal adaptation in the lizard *Anolis carolinensis carolinensis* Voigt. *The American Naturalist*, **85** (822): 171–176.
- Okeyo, D. O., Kandjenogo, L. and M., M., Kashea.** 2015. Harvesting and consumption of the giant African bullfrog, a delicacy in northern Namibia; pp. 205-219 in **K. C. Chinsebu, A. Cheikhyoussef, D. Mumbengegwi, M. Kandawa-Schilz, C. D. Kasanda, and L. Kazembe** (eds.), *Indigenous knowledge of Namibia*, UNAM Press, Windhoek, Namibia.
- O’Reilly, J. E., M. N. Puttick, L. Parry, A. R. Tanner, J. E. Tarver, J. Fleming, D. Pisani, and P. C. J. Donoghue.** 2016. Bayesian methods outperform parsimony but at the expense of precision in the estimation of phylogeny from discrete morphological data. *Biology Letters*, **12** (4): 20160081.
- Orliac, M. J., S. Ladeveze, P. D. Gingerich, R. Lebrun, and T. Smith.** 2014. Endocranial morphology of Palaeocene *Plesiadapis tricuspidens* and evolution of the early primate brain. *Proceedings of the Royal Society B: Biological Sciences*, **281**: 20132792.
- Ósi, A., M. Szabó, H. Kollmann, M. Wagneich, R. Kalmár, L. Makádi, Z. Szentesi, and H. Summesberger.** 2019. Vertebrate remains from the Turonian (Upper Cretaceous) Gosau Group of Gams, Austria. *Cretaceous Research*, **99**: 190–208.
- Otero, R. A., P. Jimenez-Huidobro, S. Soto-Acuña, and R. E. Yury-Yáñez.** 2014. Evidence of a giant helmeted frog (Australobatrachia, Calyptocephalellidae) from Eocene levels of the Magallanes Basin, southernmost Chile. *Journal of South American Earth Sciences*, **55**: 133–140.

References

- Pallas, P. S.** 1771. Reise durch verschiedene Provinzen des Russischen Reichs. *Theil 1. Saint-Petersburg (Gedruckt bey der Kayserlichen Academie der Wissenschaften)*: 1–504.
- Paluh, D. J., E. L. Stanley,** and D. C. Blackburn. 2020. Evolution of hyperossification expands skull diversity in frogs. *Proceedings of the National Academy of Sciences*, **117** (15): 8554–8562.
- Pardo, J. D., B. J. Small,** and A. K. Huttenlocker. 2017. Stem caecilian from the Triassic of Colorado sheds light on the origins of Lissamphibia. *Proceedings of the National Academy of Sciences*, **114** (27): E5389–E5395.
- Parker, H.W.** 1929. Two fossil frogs of the lower Miocene of Europe. *Annual Magazine of Natural History*, **10**: 270–281.
- Parry, R.** 1982. A revision of southern African *Pyxicephalus* Tschudi (Anura: Ranidae). *Annals of the Natal Museum*, **25**: 281–292.
- Patterson, C.** 1993. Osteichthyes: Teleostei; pp. 622–656 in M. J. Benton (ed.), *The Fossil Records 2*. Chapman and Hall Ltd, London.
- Paulina-Carabajal, A., Y.-N. Lee,** and L. L. Jacobs. 2016. Endocranial Morphology of the Primitive Nodosaurid Dinosaur *Pawpawsaurus campbelli* from the Early Cretaceous of North America. *PLoS ONE*, **11** (3) :e0150845.
- Péligri T.,** and B. Sigé (edts). 2006. 30 millions d’années de Biodiversité dynamique dans le paléokarst du Quercy. *Strata* **13**: 3–284.
- Péligri, T., M. Orliac, P. O. Antoine, V. Biot,** and G. Escarguel. 2021. Beyond Eocene and Oligocene Epochs: The Causes du Quercy Geopark and the Grande Coupure. *Geoconservation Research*, **4** (2): ***.
- Pellens R.** and P. Grandcolas (eds.). 2016. *Biodiversity Conservation and Phylogenetic Systematics*. Springer International Publishing, Cham, 386 pp.
- Pereyra, M. O., M. C. Womack, J. S. Barrionuevo, B. L. Blotto, D. Baldo, M. Targino, J. J. Ospina-Sarria, J. M. Guayasamin, L. A. Coloma, K. L. Hoke, T. Grant,** and J. Faivovich. 2016. The complex evolutionary history of the tympanic middle ear in frogs and toads (Anura). *Scientific Reports*, **6** (1): 34130.
- Piveteau, J.** 1936. Une forme ancestrale des amphibiens anoures dans le Trias inférieur de Madagascar. *Compte Rendus de l’Académie des Sciences, Série 2* (102): 1607–1608.

References

- Piveteau, J.** 1937. Paléontologie de Madagascar. XXIII. Un Amphibien du Trias inférieur. *Annales de Paléontologie*, **26**: 135–177.
- Powell, C. McA., B. D. Johnson, and J. J. Veevers.** 1980. A revised fit of East and West Gondwanaland. *Tectonophysics*, **63** (1-4): 13–29.
- Poynton, J. C.** 1963. Descriptions of southern African amphibians. *Annals of the Natal Museum*, **15**: 319–332.
- Poynton, J. C.** 1964. The amphibians of southern Africa. *Annals of the Natal Museum*, **17**: 1–334.
- Poynton, J. C. and G., Broadley.** 1985) Amphibia Zambesiaca 2. Ranidae. *Annals of the Natal Museum*, **27**: 115–181.
- Prasad, G. V. R., and J.-C. Rage.** 2004. Fossil frogs (Amphibia: Anura) from the Upper Cretaceous intertrappean beds of Naskal, Andhra Pradesh, India. *Revue de Paléobiologie, Genève*, **23** (1): 99–116.
- Procter, M. J. B.** 1919. On the skull and affinities of *Rana subsigillata* A. Dum. *Proceedings of the Zoological Society of London*, **89** (1-2): 21–27.
- Púgener, L. A.** 2002. The vertebral column and spinal nerves of anurans. [PhD Thesis] University of Kansas, Lawrence, Kansas, 480 pp.
- Púgener, L. A., A. M. Maglia, and L. Trueb.** 2003. Revisiting the contribution of larval characters to an analysis of phylogenetic relationships of basal anurans. *Zoological Journal of the Linnean Society*, **139** 1(1846): 129–155.
- Puttick, M. N., J. E. O'Reilly, A. R. Tanner, J. F. Fleming, J. Clark, L. Holloway, J. Lozano-Fernandez, L. A. Parry, J. E. Tarver, D. Pisani, and P. C. J. Donoghue.** 2017. Uncertain-tree: Discriminating among competing approaches to the phylogenetic analysis of phenotype data. *Proceedings of the Royal Society B: Biological Sciences*, **284** (): 20162290.
- Pyron, R. A.** 2011. Divergence time estimation using fossils as terminal taxa and the origins of Lissamphibia. *Systematic Biology*, **60** (4): 466–481.
- Pyron, R. A.** 2014. Biogeographic analysis reveals ancient continental vicariance and recent oceanic dispersal in amphibians. *Systematic Biology*, **63** (5): 779–797.
- Pyron, R. A., and J. J. Wiens.** 2011. A large-scale phylogeny of Amphibia including over 2800 species, and a revised classification of extant frogs, salamanders, and caecilians. *Molecular Phylogenetics and Evolution*, **61** (2): 543–583.

References

- Queiroz, K. de, Cantino, P. D. and J., A. Gauthier.** 2020 *Phylonyms: a companion to the PhyloCode*. CRC Press, Boca Raton, Florida, 1352 pp.
- Rage, J.-C.** 1984a. La “Grande Coupure” Eocène/Oligocène et les herpétofaunes (amphibiens et reptiles): Problèmes du synchronisme des événements paléobiogéographiques. *Bulletin de la société géologique de France*, **26** (6): 1251–1257.
- Rage, J.-C.** 1984b. Are the Ranidae (Anura, Amphibia) known prior to the Oligocene? *Amphibia-Reptilia*, **5** (3-4): 281–288.
- Rage, J.-C.** 2006. The lower vertebrates from the Eocene and Oligocene of the Phosphorites du Quercy (France): An overview. *Strata*, **1** (13): 161–173.
- Rage, J.-C.** 2008. Amphibia (Anura) from the Lower Miocene of the Sperrgebiet, Namibia. *Memoir of the Geological Survey of Namibia*, **20**: 75–92.
- Rage, J.-C.** 2012. Amphibians and squamates in the Eocene of Europe: what do they tell us? *Palaeobiodiversity and Palaeoenvironments*, **92** (4): 445–457.
- Rage, J.-C.** 2016. Frogs (Amphibia, Anura) from the Eocene and Oligocene of the Phosphorites du Quercy (France). An overview. *Fossil Imprint*, **72** (1-2): 53–66.
- Rage, J.-C., and Z. Roček.** 1989. Redescription of *Triadobatrachus massinoti* (Piveteau, 1936) an anuran amphibian from the Early Triassic. *Paleontographica Abteilung A*, **206**: 1–16.
- Rage, J.-C., and Z. Roček.** 2003. Evolution of anuran assemblages in the Tertiary and Quaternary of Europe, in the context of palaeoclimate and palaeogeography. *Amphibia-Reptilia*, **24** (2): 133–167.
- Rage, J.-C., and Z. Roček.** 2007. A new species of *Thaumastosaurus* (Amphibia: Anura) from the Eocene of Europe. *Journal of Vertebrate Paleontology*, **27** (2): 329–336.
- Rage, J.-C., and D. B. Dutheil.** 2008. Amphibians and squamates from the Cretaceous (Cenomanian) of Morocco - A preliminary study, with description of a new genus of pipid frog. *Paleontographica Abteilung A*, **285** (1-3): 1–22.
- Rage, J.-C., and M. Augé.** 2015. Valbro: A new site of vertebrates from the early Oligocene (MP 22) of France (Quercy). III - Amphibians and squamates. *Annales de Paléontologie*, **101** (1): 29–41.

References

- Rage, J.-C., M. Pickford, and B. Senut.** 2013. Amphibians and squamates from the middle Eocene of Namibia, with comments on pre-Miocene anurans from Africa. *Annales de Paléontologie*, **99** (3): 217–242.
- Rage, J.-C., R. Vullo, and D. Néraudeau.** 2016. The mid-Cretaceous snake *Simoliophis rochebrunei* Sauvage, 1880 (Squamata: Ophidia) from its type area (Charentes, southwestern France): Redescription, distribution, and palaeoecology. *Cretaceous Research*, **58**: 234–253.
- Rage, J.-C., G. V. R. Prasad, O. Verma, A. Khosla, and V. Parmar.** 2020. Anuran lissamphibian and squamate reptiles from the Upper Cretaceous (Maastrichtian) Deccan Intertrappean Sites in Central India, with a review of lissamphibian and squamate diversity in the Northward drifting Indian plate; pp. 99–121 in **G. V. R. Prasad and R. Patnaik** (eds.), *Biological Consequences of Plate Tectonics*. Vertebrate Paleobiology and Paleoanthropology Springer International Publishing, Cham.
- Rage, J.-C., M. Adaci, M. Bensalah, M. Mahboubi, L. Marivaux, F. Mebrouk, and R. Tabuce.** 2021. Latest Early-Middle Eocene deposits of Algeria (Glib Zegdou, HGL50) yield the richest and most diverse fauna of amphibians and squamate reptiles from the Palaeogene of Africa. *Palaeovertebrata*, **43** (2): 1–32.
- Reig, O. A.** 1956. Los anuros del Matildense. *Acta Geologica Lilloana*, **1**: 185–297.
- Reig, O. A.** 1958. Propositiones para una nueva macrosistemática de los anuros (nota preliminar). *Physis*, **21** (60): 109–118.
- Reig, O. A.** 1961. Noticia sobre un nuevo anuro fósil del Jurásico de Santa Cruz (Patagonia). *Ameghiniana*, **2**: 5–73.
- Reilly, S. M., and M. E. Jorgensen.** 2011. The evolution of jumping in frogs: Morphological evidence for the basal anuran locomotor condition and the radiation of locomotor systems in crown group anurans. *Journal of Morphology*, **272** (2): 149–168.
- Remy, J. A., J.-Y. Crochet, B. Sigé, J. Sudre, L. de Bonis, M. Vianey-Liaud, M. Godinot, J.-L. Hartenberger, B. Lange-Badré, and B. Comte.** 1987. Biochronologie des phosphorites du Quercy: Mise à jour des listes fauniques et nouveaux gisements de mammifères fossiles. *Münchener Geowissenschaftliche Abhandlungen A*, (10): 169–188.
- Rezende Oliveira, S., M. Souza Lima-Ribeiro, A. O. de Souza, C. E. dos Santos, K. Vergilio Silva, M. Zórtea, F. A. Guimarães Guilherme, F. R. de Melo, S. E. Silva Carneiro, W. Vaz**

References

- Silva, and A. Ribeiro Morais.** 2019. Are protected areas effective in preserving anurans and promoting biodiversity discoveries in the Brazilian Cerrado? *Journal for Nature Conservation*, **52**: 125734.
- Riamon, S.** 2022. Etude du premier endocrâne de l'ictonique *Sylviornis neocaledoniae* (Aves, Galliformes) et ses implications écologiques. [Oral Communication] Congress APF2022 (June 2022), Montpellier, France.
- de Ricqlès, A., and V. de Buffrénil.** 2001. Bone histology, heterochronies and the return of tetrapods to life in water: where are we?; pp. 289–310 in *Secondary adaptation of tetrapods to life in water*. Verlag Dr. Friedrich Pfeil, München.
- Rineau, V., R. Zaragüeta iBagils, and M. Laurin.** 2018. Impact of errors on cladistic inference: simulation-based comparison between parsimony and three-taxon analysis. *Contributions to Zoology*, **87** (1): 25–40.
- Rineau, V., A. Grand, R. Zaragüeta iBagils, and M. Laurin.** 2015. Experimental systematics: sensitivity of cladistic methods to polarization and character ordering schemes. *Contributions to Zoology*, **84** (2): 129–148.
- Ritland, R. M.** 1955. Studies on the post-cranial morphology of *Ascaphus truei* I Skeleton and spinal nerves. *Journal of Morphology*, **97**: 119–177.
- Robbins, L. H., Murphy, M. L., Stevens, N. J., Brook, G. A., Ivester, A. H., Haberyan, K. A., Klein, R. G., Milo, R., Stewart, K. M., Matthiesen, D. G., and A. J., Winkler.** 1996. Paleoenvironment and archaeology of Drotsky's Cave: western Kalahari Desert, Botswana. *Journal of archaeological Science*, **23**: 7–22.
- Robbins, L. H., Campbell, A. C., Murphy, M. L., Brook, G. A., Mabuse, A. A., Hitchcock, R. K., Babutsi, G., Mmolowa, M., Stewart, K.M., Steele, T. E., Klein, R. G. and C. C., Appleton.** 2009. Mogapelwa: archaeology, palaeoenvironment and oral traditions at Lake Ngami, Botswana. *South African archaeological Bulletin*, **64**: 13–32.
- Roček, Z.** 1980. Cranial anatomy of frogs of the family Pelobatidae Stanius, 1856, with outlines of their phylogeny and systematics. *Acta Universitatis Carolinae - Biologica* 1980, **3**: 1–164.
- Roček, Z.** 1994. Taxonomy and distribution of Tertiary discoglossids (Anura) of the genus *Latonia* V. Meyer, 1843. *Geobios*, **27** (6): 717–751.

References

- Roček, Z.** 2000. Mesozoic Anurans; pp. 1295–1331 in **H. Heatwole** and **R. L. Carroll** (eds.), *Palaeontology The Evolutionary History of Amphibians*, . Amphibian Biology, Surrey Beatty and Sons.
- Roček, Z.** 2003. Larval development in Oligocene palaeobatrachid frogs. *Acta Palaeontologica Polonica*, **48** (4): 595-607.
- Roček, Z.** 2008. The Late Cretaceous frog *Gobiatas* from Central Asia: its evolutionary status and possible phylogenetic relationships. *Cretaceous Research*, **29** (4): 577–591.
- Roček, Z.** 2013. Mesozoic and Tertiary Anura of Laurasia. *Palaeobiodiversity and Palaeoenvironments*, **93** (4): 397–439.
- Roček, Z.** 2019. A contribution to the herpetofauna from the late Miocene of Gritsev (Ukraine). *Comptes Rendus Palevol*, **18** (7): 817–847.
- Roček, Z.,** and **L. A. Nesson.** 1993. Cretaceous anurans from central Asia. *Palaeontographica Abteilung A*, **226** (1-3): 1–54.
- Roček, Z.,** and **P. Lamaud.** 1995. *Thaumastosaurus bottii* De Stefano, 1903, an anuran with Gondwanan affinities from the Eocene of Europe. *Journal of Vertebrate Paleontology*, **15** (3): 506–515.
- Roček, Z., J. G. Eaton, J. D. Gardner,** and **T. Přikryl.** 2010. Evolution of anuran assemblages in the Late Cretaceous of Utah, USA. *Palaeobiodiversity and Palaeoenvironments*, **90**: 341–393.
- Roček, Z., M. Wuttke, J. D. Gardner,** and **B.-A. Singh Bhullar.** 2014. The Euro-American genus *Eopelobates*, and a re-definition of the family Pelobatidae (Amphibia, Anura). *Palaeobiodiversity and Palaeoenvironments*, **94** (4): 529–567.
- Roček, Z., N. Baleeva, A. Vazeille, A. Bravin, E. van Dijk, C. Nemoz, E. M. Smirina, R. Boistel,** and **L. Claessens.** 2016. Contribution to the head anatomy of the basal frog *Barbourula busuangensis* and the evolution of the Anura. *Russian Journal of Herpetology*, **23** (3): 163–194.
- Rödel, M.-O.** 2000. *Herpetofauna of West Africa. Volume 1. Amphibians of the West African savanna.* Edition Chimaira, Frankfurt/Main, Germany, 335 pp.
- Roelants, K., D. J. Gower, M. Wilkinson, S. P. Loader, S. D. Biju, K. Guillaume, L. Moriau,** and **F. Bossuyt.** 2007. Global patterns of diversification in the history of modern amphibians. *Proceedings of the National Academy of Sciences*, **104** (3): 887–892.

References

- Rose, F. L.** 1968. Ontogenetic Changes in the tooth number of *Amphiuma tridactylum*. *Herpetologica*, **24** (2): 182–184.
- Rowe, T. B., T. E. Macrini, and Z.-X. Luo.** 2011. Fossil evidence on origin of the mammalian brain. *Science*, **332** (6032): 955–957.
- Salzburger, W., B. Van Bocxlaer, and A. S. Cohen.** 2014. Ecology and evolution of the African great lakes and their faunas. *Annual Review of Ecology, Evolution, and Systematics*, **45** (1): 519–545.
- Sanchíz, B.** 1998. *Salientia*. Pfeil, München, 275 pp.
- Sanchíz, B., and M. Młynarski.** 1979. Remarks on the fossil anurans from the Polish Neogene. *Acta Zoologica Cracoviensia*, **24** (3): 153–174.
- Santos, R. O., M. Laurin, and H. Zaher.** 2020. A review of the fossil record of caecilians (Lissamphibia: Gymnophionomorpha) with comments on its use to calibrate molecular timetrees. *Biological Journal of the Linnean Society*, **131** (4): 737–755.
- Scalia, F.** 1976. Structure of the Olfactory and Accessory Olfactory Systems; pp. 213–233 in *Frog Neurobiology*. Springer Berlin Heidelberg, Berlin, Heidelberg.
- Schaeffer, B.** 1949. Anurans from the early Tertiary of Patagonia. *Bulletin of the American Museum of Natural History*, **93** (2): 41–68.
- Schoch, R. R.** 2019. The putative lissamphibian stem-group: phylogeny and evolution of the dissorophoid temnospondyls. *Journal of Paleontology*, **93** (1): 137–156.
- Scholsser, G., and G. Roth.** 1995. Distribution of cranial and rostral spinal nerves in tadpoles of the frog *Discoglossus pictus* (Discoglossidae). *Journal of Morphology*, **226** (2): 189–212.
- Scott, E.** 2005. A phylogeny of ranid frogs (Anura: Ranoidea: Ranidae), based on a simultaneous analysis of morphological and molecular data. *Cladistics*, **21** (6): 507–574.
- Seiffert, E. R., M. F. Tejedor, J. G. Fleagle, N. M. Novo, F. M. Cornejo, M. Bond, D. de Vries, and K. E. Campbell.** 2020. A parapithecoid stem anthropoid of African origin in the Paleogene of South America. *Science*, **368** (6487): 194–197.
- Sereno, P. C., D. B. Dutheil, M. Iarochene, H. C. E. Larsson, G. H. Lyon, P. M. Magwene, C. A. Sidor, D. J. Varricchio, and J. A. Wilson.** 1996. Predatory Dinosaurs from the Sahara and Late Cretaceous Faunal Differentiation. *Science*, **272** (5264): 986–991.

References

- Shapiro, H. A., and H. Zwarenstein.** 1934. A rapid test for pregnancy on *Xenopus laevis*. *Nature*, **133**: 726.
- Sheil, C. A.** 1999. Osteology and skeletal development of *Pyxicephalus adspersus* (Anura: Ranidae: Raninae). *Journal of Morphology*, **240**: 49–75.
- Shubin, N. H., and F. A. Jenkins Jr.** 1995. An Early Jurassic jumping frog. *Nature*, **377**: 49–52.
- Sigé, B., J.-P. Aguilar, B. Marandat, and J. N.-G. Astruc.** 1991. Extension au Miocène inférieur des remplissages phosphatés du Quercy. La faune de vertébrés de Crémat (Lot, France). *Geobios*, **24** (4): 497–502.
- Sigurdson, T., D. M. Green, and P. J. Bishop.** 2012. Did *Triadobatrachus* jump? Morphology and evolution of the anuran forelimb in relation to locomotion in early salientians. *Fieldiana Life and Earth Sciences*, **5**: 77–89.
- Simon-Coinçon, R., and J.-G. Astruc.** 1991. Les pièges karstiques en Quercy: rôle et signification dans l'évolution des paysages. *Bulletin de la société géologique de France*, **162** (3): 595–605.
- Slater, B. J., K. J. Liu, M. D. Kwan, N. Quarto, and M. T. Longaker.** 2009. Cranial osteogenesis and suture morphology in *Xenopus laevis*: A unique model system for studying craniofacial development. *PLoS ONE*, **4** (1): e3914.
- Sluijs, A., S. Schouten, M. Pagani, M. Woltering, H. Brinkhuis, J. S. S. Damsté, G. R. Dickens, M. Huber, G.-J. Reichart, R. Stein, J. Matthiessen, L. J. Lourens, N. Pedentchouk, J. Backman, and K. Moran.** 2006. Subtropical Arctic Ocean temperatures during the Palaeocene/Eocene thermal maximum. *Nature*, **441** (7093): 610–613.
- Špínar, Z. V.** 1972. *Tertiary Frogs from Central Europe*. Academia, Prague; and Junk, The Hague, 463 pp.
- Špínar, Z. V.** 1976. Endolymphatic sacs and dorsal endocranial pattern: Their significance for systematics and phylogeny of frogs. *Ústředního Ústavu Geologického*, **51** (5): 285–290.
- Špínar, Z. V.** 1980. The discovery of a new species of pipid frog (Anura, Pipidae) in the Oligocene of central Libya; pp. 327–348 in **M. J. Salem and M. T. Bursrewil** (eds.), *The Geology of Libya*. Second Symposium on the Geology of Libya, held at Tripoli, September 16-21, 1978 vol. 1. Academic Press Inc. (London), London.

References

- Smith, A.** 1849. *Illustrations of the zoology of South Africa, consisting chiefly of figures and descriptions of the objects of natural history collected during an expedition into the interior of South Africa in the years 1834, 1835 and 1836... Reptilia.* London (Smith, Elder & Co.): appendix 1–28.
- Starrett, P.** 1973. Evolutionary patterns in larval morphology; pp. 251–271 in **J. L. Vial** (ed.), *Evolutionary biology of the anurans.* University of Missouri Press, Columbia, Missouri.
- Stehlin, H. G.** 1909. Remarques sur les faunules de mammifères des couches Eocène et Oligocène. *Bulletin de La Société Géologique de France*, **9** (4): 488–520.
- Stejneger, L.** 1899. Description of a new genus and species of discoglossoid toad from North America. *Proceedings of the United States National Museum*, **21**: 899–901.
- Stocker, M. R., S. J. Nesbitt, B. T. Kligman, D. J. Paluh, A. D. Marsh, D. C. Blackburn, and W. G. Parker.** 2019. The earliest equatorial record of frogs from the Late Triassic of Arizona. *Biology Letters*, **15** (2): 20180922.
- Streicher, J. W., E. C. Miller, P. C. Guerrero, C. Correa, J. C. Ortiz, A. J. Crawford, M. R. Pie, and J. J. Wiens.** 2018. Evaluating methods for phylogenomic analyses, and a new phylogeny for a major frog clade (Hyloidea) based on 2214 loci. *Molecular Phylogenetics and Evolution*, **119**: 128–143.
- Streidter, G. F., and R. G. Northcutt.** 2020. *Brains through time : A natural history of vertebrates.* Oxford University Press, New York, 523 pp.
- Suga, S., Y. Taki, and M. Ogawa.** 1992. Iron in the enameloid of perciform fish. *Journal of Dental Research*, **71** (6): 1316–1325.
- Syromyatnikova, E., Z. Roček, and S. van de Velde.** 2019. New discoveries in the frog *Latonia seyfriedi* (Anura: Alytidae) and their impact on taxonomy of the genus *Latonia*. *PalZ*, **93** (4): 669–677.
- Szentesi, Z., and M. Venczel.** 2010. An advanced anuran from the Late Cretaceous (Santonian) of Hungary. *Neues Jahrbuch Für Geologie Und Paläontologie – Abhandlungen*, **256** (3): 291–302.
- Taquet, P.** 1976. *Géologie et paléontologie du gisement de Gadoufaoua (Aptien du Niger).* Editions du Centre National de la Recherche Scientifique, Paris, 191 pp.
- Taylor, G. M., E. Nol, and D. Boire.** 1995. Brain regions and encephalization in anurans: Adaptation of stability ? *Brain, Behavior and Evolution*, **45**: 96–109.

References

- Taylor, M. P.** 2007. Phylogenetic definitions in the pre-PhyloCode era; implications for naming clades under the PhyloCode. *PaleoBios*, **27** (1): 1–6.
- Thevenin, A.** 1903. Etude géologique de la bordure Sud-Ouest du Massif Central. *Bulletin de la société géologique de France*, **14** (95): 353–555.
- Thomas, K. N., D. J. Gower, R. C. Bell, M. K. Fujita, R. K. Schott, and J. W. Streicher.** 2020. Eye size and investment in frogs and toads correlate with adult habitat, activity pattern and breeding ecology. *Proceedings of the Royal Society B: Biological Sciences*, **287** (1935): 20201393.
- Tinsley, R. C.** 1975. The morphology and distribution of *Xenopus vestitus* (Anura: Pipidae) in Central Africa. *Journal of Zoology*, **175** (4): 473–492.
- Tinsley, R. C., H. R. Kobel, and M. Fischberg.** 1979. The biology and systematics of a new species of *Xenopus* (Anura: Pipidae) from the highlands of Central Africa. *Journal of Zoology*, **188** (1): 69–102.
- Tissier, J., J.-C. Rage, and M. Laurin.** 2017. Exceptional soft tissues preservation in a mummified frog-eating Eocene salamander. *PeerJ*, **5**: e3861.
- Tissier, J., J.-C. Rage, R. Boistel, V. Fernandez, N. Pollet, G. Garcia, and M. Laurin.** 2016. Synchrotron analysis of a ‘mummified’ salamander (Vertebrata: Caudata) from the Eocene of Quercy, France: Exceptionally preserved fossil Urodele. *Zoological Journal of the Linnean Society*, **177** (1): 147–164.
- Trueb, L.** 1973. Bones, Frogs and Evolution; pp. 65–133 in J. L. Vial (ed.), *Evolutionary Biology of the Anurans*. Contemporary Research on Major Problems. University of Missouri Press, Columbia.
- Trueb, L.** 1999. The Early Cretaceous pipoid anuran, *Thoraciliacus* : Redescription, revaluation, and taxonomic status. *Herpetologica*, **55** (2): 139–157.
- Trueb, L., and J. Hanken.** 1992. Skeletal development in *Xenopus laevis* (Anura: Pipidae). *Journal of Morphology*, **214** (1): 1–41.
- Trueb, L., and A. M. Báez.** 2006. Revision of the Early Cretaceous *Cordicephalus* from Israel and an assessment of its relationships among pipoid frogs. *Journal of Vertebrate Paleontology*, **26** (1): 44–59.

References

- Trueb, L., L. A. Púgener, and A. M. Maglia.** 2000. Ontogeny of the bizarre: an osteological description of *Pipa pipa* (Anura: Pipidae), with an account of skeletal development in the species. *Journal of Morphology*, **243** (1): 75–104.
- Trueb, L., C. F. Ross, and R. Smith.** 2005. A new pipoid anuran from the Late Cretaceous of South Africa. *Journal of Vertebrate Paleontology*, **25** (3): 533–547.
- Tschudi, J. J.** 1838. Classification der Batrachier, mit Berücksichtigung der fossilen Thiere dieser Abtheilung der Reptilien. *Mémoires de la Société des Sciences naturelles de Neuchâtel*, **2**: 1–100.
- Tyler, M. J.** 1976. Comparative osteology of the pelvic girdle of Australian frogs and description of a new fossil genus. *Transactions of the Royal Society of South Australia, Incorporated*, **100**: 3–14.
- Uetz P., P. Freed, R. Aguilar and J. Hošek** (eds.). 2022. The Reptile Database [03/10/2022]. <https://www.reptile-database.org>.
- Van der Meijden, A., Vences, M., Hoegg, S. and A., Meyer.** 2005. A previously unrecognized radiation of ranid frogs in Southern Africa revealed by nuclear and mitochondrial DNA sequences. *Molecular Phylogenetics and Evolution*, **37**: 674–685.
- Van der Meijden, A., A. Crottini, J. Tarrant, A. Turner, and M. Vences.** 2011. Multi-locus phylogeny and evolution of reproductive modes in the Pyxicephalidae, an African endemic clade of frogs. *African Journal of Herpetology*, **60**: 1–12.
- Van Dijk, D. E.** 1966. Systematic and field keys to the families, genera and described species of southern African anuran tadpoles. *Annals of the Natal Museum*, **18**: 231–286.
- Van Sittert, L., and G. J. Measey.** 2016. Historical perspectives on global exports and research of African clawed frogs (*Xenopus laevis*). *Transactions of the Royal Society of South Africa*, **71** (2): 157–166.
- Vasconcellos, M. M., G. R. Colli, and D. C. Cannatella.** 2021. Paleotemperatures and recurrent habitat shifts drive diversification of treefrogs across distinct biodiversity hotspots in sub-Amazonian South America. *Journal of Biogeography*, **48** (2): 305–320.
- Vasconcelos, T. S., and V. H. M. Prado.** 2019. Climate change and opposing spatial conservation priorities for anuran protection in the Brazilian hotspots. *Journal for Nature Conservation*, **49**: 118–124.

References

- Vasilyan, D.** 2018. Eocene Western European endemic genus *Thaumastosaurus* : new insights into the question “Are the Ranidae known prior to the Oligocene?” *PeerJ*, **6**: e5511.
- Venczel, M., Z. Szentesi, and J. D. Gardner.** 2021. New material of the frog *Hungarobatrachus szukacsi* Szentesi & Venczel, 2010, from the Santonian of Hungary, supports its neobatrachian affinities and reveals a Gondwanan influence on the European Late Cretaceous anuran fauna. *Geodiversitas*, **43** (7): 187-207.
- Vidal, N., A. Azvolinsky, C. Cruaud, and S. B. Hedges.** 2008. Origin of tropical American burrowing reptiles by transatlantic rafting. *Biology Letters*, **4** (1): 115–118.
- Vogt, S., F. A. de Villiers, F. Ihlow, D. Rödder, and J. Measey.** 2017. Competition and feeding ecology in two sympatric *Xenopus* species (Anura: Pipidae). *PeerJ*, **5**: e3130.
- Vullo, R.** 2019. A new species of *Lapparentophis* from the mid-Cretaceous Kem Kem beds, Morocco, with remarks on the distribution of lapparentophiid snakes. *Comptes Rendus Palevol*, **18** (7): 765–770.
- Wagler, J.** 1827. Untitled footnote. *Isis von Oken*, **20**: 726.
- Wagler, J.** 1830. *Natürliches System der Amphibien, mit vorangehender Classification der Säugthiere und Vogel. Ein Beitrag zur vergleichenden Zoologie.* J. G. Cotta, München, Stuttgart and Tübingen.
- Wake, D. B.** 2020. Caudata, pp. 785-787 in **K. de Queiroz, P. D. Cantino and J. A. Gauthier** (eds.), *Phylonoms: an implementation of PhyloCode*. CRC Press, Boca Raton, Florida.
- Wake, M. H.** 1993. The skull as a locomotor organ; pp. 197–240 in **J. Hanken and B. K. Hall** (eds.), *The Skull. 3. Functional and evolutionary mechanisms.* The University of Chicago Press, Chicago, Illinois.
- Wake, M. H.** 2020. Gymnophiona, pp. 779-783 in **K. de Queiroz, P. D. Cantino and J. A. Gauthier** (eds.), *Phylonoms: an implementation of PhyloCode*. CRC Press, Boca Raton, Florida.
- Warkman, A. S., and P. A. Krieg.** 2007. *Xenopus* as a model system for vertebrate heart development. *Seminars in Cell & Developmental Biology*, **18** (1): 46–53.
- Weiss, L., I. Manzini, and T. Hassenklöver.** 2021. Olfaction across the water–air interface in anuran amphibians. *Cell and Tissue Research*, **383** (1): 301–325.
- Wells, K. D.** 2007. *The Ecology & Behavior of Amphibians.* The University of Chicago Press, Chicago, 1148 pp.

References

- Wever, E. G.** 1979. Middle ear muscles of the frog. *Proceedings of the National Academy of Sciences*, **76** (6): 3031–3033.
- Wever, E. G.** 1985. *The Amphibian Ear*. Princeton University Press, Princeton, New Jersey, USA, 498 pp.
- Whiting, H. P.** 1961. Pelvic girdle in amphibian locomotion; pp. 43–57 in *Vertebrate locomotion, Symposium of the Zoological Society of London 5*. Oxford University Press, London.
- Wied-Neuwied, M. A. P., Prinz zu.** 1824. Verzeichnis der Amphibien welche in zweiten Bande der Naturgeschichte Brasiliens von Prinz Max von Neuwied werden beschreiben Werden. *Isis von Oken*, **14**: 661–673.
- Wiegmann, A. F. A.** 1834. Amphibien. Meyen, F. J. F. ed., Reise um die Erde ausgeführt auf dem Königlich Preussischen Seehandlungs-Schiffe Prinzess Louise, commandiert von Captain W. Wendt, in den Jahren 1830, 1831 und 1832 von Dr. F. J. F. Meyen. Dritter Theil. Zoologischer Bericht: 433–522. Berlin, Sander'schen Buchhandlung (C. W. Eichhoff).
- Will, T. M., and H. E. Frimmel.** 2018. Where does a continent prefer to break up? Some lessons from the South Atlantic margins. *Gondwana Research*, **53**: 9–19.
- Witmer, L. M.** 1995. The extant Phylogenetic Bracket and the importance of reconstructing soft tissues in fossils; pp. 16–33 in **J. Thomason** (ed.), *Functional morphology in vertebrate paleontology*. Cambridge University Press.
- Witmer, L. M., and R. C. Ridgely.** 2008. Structure of the brain cavity and inner ear of the centrosaurine ceratopsid dinosaur *Pachyrhinosaurus* based on CT scanning and 3D visualization; pp. 117–144 in *A new horned dinosaur from an Upper Cretaceous bone bed in Alberta*. NRC Research Press, Ottawa, OH, Canada.
- Worthy, T., A. Tennyson, R. Scofield, and S. Hand.** 2013. Early Miocene fossil frogs (Anura: Leiopelmatidae) from New Zealand. *Journal of the Royal Society of New Zealand*, **43** (4): 211–230.
- Worthy, T. H.** 2001. A New species of *Platymantis* (Anura: Ranidae) from Quaternary deposits on Viti Levu, Fiji. *Palaeontology*, **44** (4): 665–680.
- Xing, L., E. L. Stanley, M. Bai, and D. C. Blackburn.** 2018. The earliest direct evidence of frogs in wet tropical forests from Cretaceous Burmese amber. *Scientific Reports*, **8**: 8770.

References

- Yuan, Z.-Y., B.-L. Zhang, C. J. Raxworthy, D. W. Weisrock, P. M. Hime, J.-Q. Jin, E. M. Lemmon, A. R. Lemmon, S. D. Holland, M. L. Kortyna, W.-W. Zhou, M.-S. Peng, J. Che, and E. Prendini. 2018. Natatanuran frogs used the Indian Plate to step-stone disperse and radiate across the Indian Ocean. *National Science Review*, 6 (1): 10–14.
- von Zittel, K. A. 1888. *Handbuch der Paläontologie. Abteilung 1. Paläozoologie Band III: Vertebrata (Pisces, Amphibia, Reptilia, Aves)*. Munich & Leipzig, Oldenbourg, 890 pp.
- Zhang, P., H. Zhou, Y.-Q. Chen, Y.-F. Liu, and L.-H. Qu. 2005. Mitogenomic perspectives on the origin and phylogeny of living amphibians. *Systematic Biology*, 54 (3): 391–400.
- Zouhri, S. 2017. *Paléontologie des vertébrés du Maroc : état des connaissances*. Société géologique de France, Paris, 614 pp.

APPENDIX – ARTICLES




From toad to frog, a CT-based reconsideration of *Bufo servatus*, an Eocene anuran mummy from Quercy (France)

Alfred Lemierre, Annelise Folie, Salvador Bailon, Ninon Robin & Michel Laurin


To cite this article: Alfred Lemierre, Annelise Folie, Salvador Bailon, Ninon Robin & Michel Laurin (2021) From toad to frog, a CT-based reconsideration of *Bufo servatus*, an Eocene anuran mummy from Quercy (France), Journal of Vertebrate Paleontology, 41:3, e1989694, DOI: 10.1080/02724634.2021.1989694

To link to this article: <https://doi.org/10.1080/02724634.2021.1989694>

 View supplementary material [↗](#)

 Published online: 23 Nov 2021.


 Submit your article to this journal [↗](#)

 Article views: 122

 View related articles [↗](#)

 View Crossmark data [↗](#)

FROM TOAD TO FROG, A CT-BASED RECONSIDERATION OF *BUFO SERVATUS*, AN EOCENE ANURAN MUMMY FROM QUERCY (FRANCE)

ALFRED LEMIERRE, ^{*1} ANNELISE FOLIE,² SALVADOR BAILON,³ NINON ROBIN,⁴ and MICHEL LAURIN¹
¹CR2P – Centre de recherche en Paléontologie–CNRS/MNHN/Sorbonnes Université, Bâtiment de Géologie, 43 rue Buffon, Paris, 75005, France, alfred.lemierre@edu.mnhn.fr, michel.laurin@mnhn.fr;
²Scientific Survey of Heritage, Royal Belgian Institute of Natural Sciences, 29 rue Vautier, 1000 Brussels, Belgium, annelise.folie@naturalscience.be;
³Département Homme & Environnement, Muséum national d’Histoire naturelle, UMR 7194 HNHP and UMR 7209 AASPE, MNHN-CNRS, 43 rue Buffon, Paris, 75005, France, salvador.bailon@mnhn.fr;
⁴School of Biological, Earth and Environmental Sciences, University College Cork, Distillery Fields, North Mall, Cork T23 N73 K, Ireland, ninonrobin23@gmail.com

ABSTRACT—In the 19th century, natural mummies of amphibians were discovered in the Quercy Phosphorites. The specific collection site was never formally reported, which hampers precise dating of these specimens. Still, the name *Bufo servatus* was erected based on the external morphology of one of the mummified specimens. A tomography of a similarly preserved specimen revealed a preserved skeleton, soft tissues and gut contents. We analyze here the holotype of *Bufo servatus* using CT-scanning in order to investigate its potentially preserved internal features. Like the previous specimen, a subcomplete articulated skeleton was identified in the *B. servatus* holotype. Surprisingly, this skeleton is almost identical to that of *Thaumastosaurus gezei*, an Eocene anuran from Western Europe to which other specimens from this mummy series were previously assigned. The few differences between the specimen skeletons highlight ontogenetic and intraspecific variations, making *T. gezei* a junior synonym of *B. servatus* and creating the new combination *Thaumastosaurus servatus*. Given its association with previously described Quercy specimens, this redescribed anuran is probably from the same time interval as *T. gezei*. Previous phylogenetic analyses assigned *T. servatus* to Ranoides, with natatanuran affinities. Using data from this newly described specimen, we tested here further its taxonomic affinities. Our analyses confirm this position, and formally identify *T. servatus* as a Natatanuran member of Pyxicephalidae (currently endemic of equatorial Africa) and more precisely, a stem-Pyxicephalinae. This result confirms the origin of *Thaumastosaurus*, a member of the African herpetofauna occupying Western Europe before the Grande Coupure at the Eocene/Oligocene transition.

SUPPLEMENTAL DATA—Supplemental materials are available for this article for free at www.tandfonline.com/UJVP.

Citation for this article: Lemierre, A., A. Folie, S. Bailon, N. Robin, and M. Laurin. 2021. From toad to frog, a CT-based reconsideration of *Bufo servatus*, an Eocene anuran mummy from Quercy (France). *Journal of Vertebrate Paleontology*. DOI: 10.1080/02724634.2021.1989694

INTRODUCTION

The Quercy Phosphorites consist of an extensive series of limestone fissures within the Quercy plateau (southwestern France) that are infilled with clayey phosphates (Fig. 1A, B; Pélissié and Sigé, 2006). Mining of these phosphates for use as fertilizer began in 1871, with the number of active quarries expanding until 1886 when the operations began to decline. Almost all quarries were closed by 1893 (Thevenin, 1903; Gèze, 1949). The Quercy Phosphorites quickly became known for their highly diverse assemblages of vertebrate fossils (e.g., Filhol, 1877) whose ages range from the early Eocene to early Miocene (Sigé et al., 1991; Legendre et al., 1992) but with a concentration between the middle–late Eocene to the late Oligocene. This age distribution makes these fossils especially valuable for understanding the role of climate change in the “Grande Coupure” – the faunal turnover and moderate extinction event that marks the ~33.9 Ma Eocene–Oligocene transition (Stehlin, 1909).

The Quercy Phosphorites are best known for their highly diverse mammalian fauna (Pélissié and Sigé, 2006) and great density of amphibians (Rage, 2006), both of which are based largely on disarticulated skeletons. However, four anurans, a urodele and six snake fragments present exceptionally well-preserved tissues in 3D (Laloy et al. 2013; Tissier et al. 2016, 2017). At the time of their initial description in the late 1800s, only the external soft tissues were known and they were referred to as “natural mummies” (see, e.g., Filhol, 1877 for a brief description of the anuran skin). They were originally given or sold to Professor Henri Filhol by A. Lafont (or Lafon), a pharmacist in Villeneuve (Aveyron, France; see Fig. 1C) during the early 1870s (see first mention in Filhol, 1873). They remained part of the private collection of H. Filhol, which housed numerous fossils from the Quercy, including the holotypes of the taxa he erected until his sudden death in 1903. Edmond J. de Rothschild then bought the entire collection to prevent its dispersal and donated it to the MNHN the same year (1903). Given their striking aspect, they were placed in the paleontological gallery of the museum, where they remain visible to the public even now.

Reliant wholly on external morphological features, early studies assigned the anuran mummies to two different species,

*Corresponding author

Color versions of one or more of the figures in the article can be found online at www.tandfonline.com/ujvp.

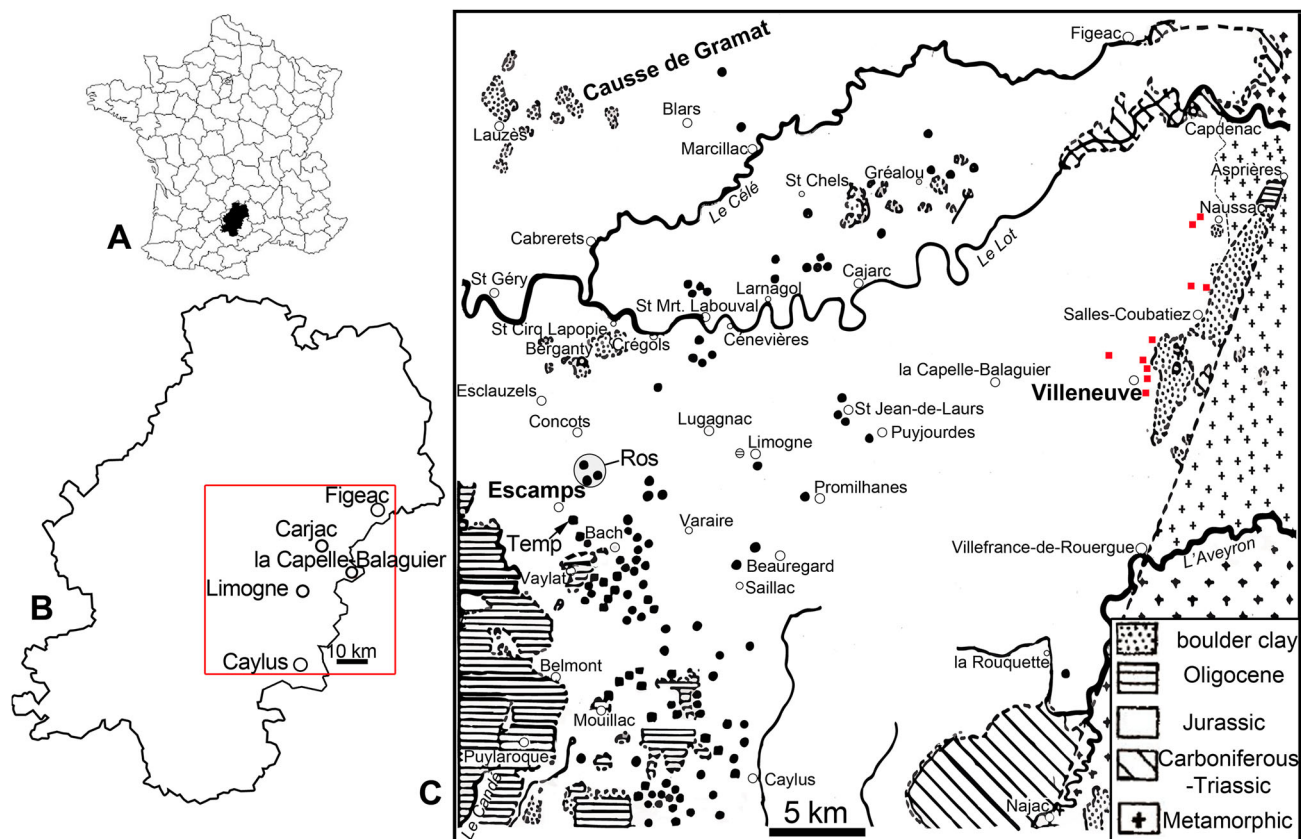


FIGURE 1. Geographic maps of potential localities for the mummies. **A**, map of France, with the Quercy region highlighted in black; **B**, map of the Quercy region, with its south-eastern part highlighted in gray square outline (red in online version); **C**, close-up of the south-eastern Quercy region, modified from Gèze (1949), with the two potential locations for sites that yielded the mummies in bold. Black dots indicate phosphorite quarries listed by Gèze (1949), gray (red online) squares indicate putative origin sites for the mummy series near Villeneuve, black arrow indicates the location of the site 'les Tempories,' transparent circle indicates the area of the Rosières sites.

Rana plicata and *Bufo servatus* (Filhol, 1876, 1877). In the 2010s, two amphibian mummies were further analysed using classical micro-computed tomography (on the anuran MNHN.F.QU17279; Laloy et al., 2013) and synchrotron light micro-computed tomography (on the urodele MNHN.F.QU17755; Tissier et al., 2016, 2017). Both studies evidenced internal subcomplete and articulated skeletons, soft tissues (e.g., organs) and diet contents, facilitating more complete redescrptions and assessments of their phylogenetic affinities (Laloy et al., 2013; Tissier et al., 2016). MNHN.F.QU17279, initially described by Filhol (1876) under the name *Rana plicata*, turned out to be the most complete specimen of the Eocene *Thaumastosaurus gezei* Rage and Roček, 2007, previously known only from a subcomplete skull and fragmentary remains (Rage and Roček, 2007). Later, a second mummy (MNHN unnumbered) was also assigned to *T. gezei*, based on external shape and a few visible dermal bones (Rage, 2016).

Here we focus on the third anuran specimen discovered in the 1870s and unstudied since the end of the 19th century: MNHN.F.QU17381. This specimen was originally described as the holotype of “*Bufo servatus*” Filhol 1877. The assignment of this taxon to Bufonidae was questioned by multiple authors (e.g., Sanchiz, 1998; Rage, 2016) as its identification was based only on its external aspect. As for other exceptionally preserved specimens from Quercy, tomography revealed a subcomplete skeleton and soft tissues, enabling us to reassess the identification of MNHN.F.QU17381 and the validity of *B. servatus*. Several phylogenetic analyses are performed on this taxon as a means

to discuss its general affinities among anurans. Finally, we discuss the paleobiogeographic and evolutionary implications of these phylogenetic conclusions and their impact on the anuran fossil record.

GEOLOGICAL CONTEXT

Locality—The specimen MNHN.F.QU17381, like the other Quercy “mummies” (Filhol, 1877), is part of the MNHN ‘old collection’ lacking information on its original location and stratigraphic assignment. However, the brief descriptions given by Filhol (Filhol, 1873, 1876, 1877) seem to indicate that all mummies come from a single quarry. We conclude that this quarry most likely belongs to one of the two localities discussed below.

The first locality is the town of Villeneuve (Fig. 1), where the first seller (A. Lafont) lived. The hypothesis that this locality produced the mummies is supported by the statement of Filhol (1873) that the series came from the department of Aveyron. This information was also repeated in at least two local newspapers. Both the “Journal de l’Aveyron” and the “Journal de Villefranche” published an identical small article in January 1874 based on a talk given by Filhol in Paris (1873) that placed this discovery in Aveyron. Moreover, Filhol mentioned in his talk that he had just received the fossils. It is possible that he indicated Aveyron as the origin of the mummies simply because the seller came from this place.

Near Villeneuve, approximately 10 quarries are known (Fig. 1C, gray squares). Among them, one (Vielase) can be ruled out due to the nature of the phosphatic matrix, a tectonized karstic breccia (Simon-Coicon and Astruc, 1991; Legendre et al., 1992) that is clearly incompatible with the observed thin-scale phosphate replacement of the animal structures. Only one tunnel in Vielase could have housed phosphatic fillings, but it is now inaccessible, and no information exists anymore on this tunnel (T. Pélissié, pers. com). The remaining quarries are either azoic, or devoid of any phosphatic matrix still in place for comparison.

The second locality is the village of Escamps in the Lot department (Fig. 1C). This locality was first mentioned in a local newspaper, the “Journal du Lot” on January 13, 1874, in an article that discussed a future talk by Filhol at the ‘Société des Sciences Physiques et Naturelles de Toulouse.’ Filhol indeed presented on February 6, 1874 some exquisitely preserved fossil of anurans coming from a quarry in the Lot. The bulletin of the above-mentioned society gives an account of this talk, mentioning three anuran fossils (Jeanbernat, 1874). These three fossils can only correspond to the mummy series. The apparent change in the locality of origin for these fossils that occurred between Filhol’s talk in Paris (Filhol, 1873) and southern France (Toulouse) could reflect new information he received from the seller—after his 1873 talk at the Academy of Sciences (Paris). In addition to the press releases and society bulletin, there is a local memory of a discovery of a “stone” anuran in the village of Escamps, dating back to the late 19th century (T. Pélissié and E. Cassan pers. comm. October, 2020). A young miner, Emile Dutheil discovered a stony anuran corresponding to the mummy description inside a cavity in a quarry near the town, either in the site ‘les Rosières’ or ‘les Tempories’ (Fig. 1C). This fossil was soon exchanged against a bottle of wine and might have ended in the hands of A. Lafont. The other mummies might have been discovered shortly thereafter. Six sites are regrouped under the name ‘les Rosières’ (Fig. 1C) and are dated in the late Eocene MP17a (37.8–37.4 Ma) to MP19 (34.5–33.5 Ma; Aguilar et al., 1997; Vandenberghe et al., 2012). They have been partially studied in the previous decades (Remy et al., 1987), without any discovery of a new mummy. The other site, ‘les Tempories’ is dated from the MP19 (late Eocene, 34.5–33.5 Ma). In situ layers of phosphorites are still visible today (T. Pélissié pers. comm.) but most of the site was drained during its exploitation and later used as a landfill. If the series came from a layer within the quarry, this layer may have been completely cleared out more than a century ago.

Another possibility is that the series came from elsewhere in the Lot. Fossils discovered in these quarries were often appreciated by local notables and thus experienced local dispersement through exchanges or sales with surrounding towns and villages. Some of these fossils were then sold to known museum curators or even exchanged for favors (T. Pélissié pers. comm.).

Until a precise account of the MNHN.F.QU17381 discovery is found that includes locality information, each of these provenance hypotheses will remain somewhat viable with its geographic (and stratigraphic) origins somewhat ambiguous. The strongest support is for the locality of Escamps, especially given the local memory of such a discovery, which does not occur in the vicinity of Villeneuve. We putatively identify the locality as the village of Escamps, Lot (France) and assign a late Eocene age to the mummy series.

Stratigraphic Range—The genus *Thaumastosaurus* (to which two of the mummies have been attributed so far) is known from various localities in Western Europe (Vasilyan, 2018). The earliest remains of *Thaumastosaurus* are from the MP16 (late middle Eocene ~39.5 Ma) from two Swiss localities, and the genus is present throughout the upper Eocene, with most of the localities located in the Quercy Phosphorites. The

geologically most recent record of *Thaumastosaurus* is from the MP20 (~33.5 Ma, Priabonian, latest Eocene) from Escamps, in France. The complete list of the localities where *Thaumastosaurus* has been identified was compiled by Vasilyan (2018:table S1).

A recent study presented disarticulated bones from the upper Turonian (early Late Cretaceous) and attributed a fragmentary maxilla to *Thaumastosaurus* (Ósi et al., 2019:fig. 6A–E) and a vertebra to an Anura indet. The tentative attribution of the vertebra to *Thaumastosaurus* is based on the presence of a ventral keel also possibly present in *T. gezei* (Laloy et al., 2013:fig. 5C; Ósi et al., 2019:fig. 6F, G). However, this ventral keel is actually the ridge of the neural spine, visible by transparency. In addition, in the vertebral column of MNHN.F.QU17381, there is no ventral keel on the vertebrae (see below). Furthermore, given the fragmentary state of this vertebra, the specimen cannot be attributed to a more exclusive clade than Batrachia (Duellman and Trueb, 1994; Tissier et al., 2016). Also, the ornamentation composed of irregular pits and ridges on the maxilla described by Ósi et al. (2019) occurs in numerous Cretaceous anuran clades (Roček and Nessov, 1993; Roček, 2008; Company and Szentesi, 2012; Báez and Gómez, 2018) as well as more recent anurans and other vertebrate taxa (e.g., squamates, crocodylians, various early stegocephalians; Buffrénil et al., 2015) and is therefore not diagnostic of *Thaumastosaurus*. Finally, the oval foramen located near the processus pterygoideus (if the fragmentary element is indeed a maxilla) as mentioned by Ósi et al. (2019) is present in other anurans (Biton et al., 2016). This makes the attribution of these Upper Cretaceous fragments to the Eocene *Thaumastosaurus* unlikely and currently unsupported. Instead, these specimens may belong to a wide range of Mesozoic anuran clades. We therefore conclude that *Thaumastosaurus* has a stratigraphic range from the late middle Eocene (~39.5 Ma) to the terminal late Eocene (~33.5 Ma).

MATERIALS AND METHODS

Institutional Abbreviations—**IC2MP**: Institut de Chimie des Milieux et Matériaux de Poitiers, Poitiers, France; **MHNT.PAL**: Muséum d’histoire Naturelle de Toulouse, Toulouse, France; **MNHN**: Muséum National d’Histoire Naturelle, Paris, France; **MNHN.F.QU**: Collection number for specimens from the ‘old’ Quercy Phosphorites collection, located within the paleontological collection of the MNHN; **NHMB**: Naturhistorisches Museum Basel, Basel, Switzerland; **UM.PRR**: Université de Montpellier, France, specimens from the Perrière site.

The mummy MNHN.F.QU17381, currently displayed in the paleontology gallery of the National Natural History Museum in Paris (France), was micro-CT scanned at the PLATINA Plateforme Instrumentale d’Analyses (PLATINA platform) at the IC2MP (Poitiers, France). A microfocus beam of 160 kV of the CT scanner was used with the following parameters: voltage, 130 kV; current, 180 μ A; voxel size, 0.024 μ m; slice resolution, 1346 \times 2525 pixels. A total of 1750 virtual slices showing internal structures were reconstructed using XAct (RX solution). These slices were imported into the 3D reconstruction software Mimics 21.0 (Materialise, Leuven, Belgium). Before the importation, the slices were cropped to maximally remove the empty spaces. To decrease data size, slices were converted from 16 to 8 bits. The dataset thus includes 1256 slices with an image resolution of 1527 \times 2391 pixels and a voxel size of 2.4 μ m for the volume file (see Appendix S1 in Supplemental Data 1). The 3D model was produced by segmentation of each bone using the ‘thresholding’ function (using the contrast on grayscale images). We used the same voxel resolution of 2.4 μ m, with a smoothing factor of 3 for one iteration, to homogenize the model resulting from manual segmentation. Data produced by

segmentation were exported in the software 3matic 9.0 as a separate file (see Appendix S2 in Supplemental Data 1).

Tomography revealed the internal preservation of soft tissues replicated in calcium phosphate (e.g., part of the brain and of the spinal cord, potential muscles and nerves). Unfortunately, most of the soft internal structures are either too degraded, or too similar to other structures in density and/or capacity to absorb X-rays (resulting in poor contrast) to be confidently segmented and described here. The external structures will be described in detail in a future study (N. Robin, unpublished data) and are only briefly presented here; our description focuses on the skeleton. The skull preserved inside the mummy lost its anteriormost region (snout) but is otherwise complete. Some hyobranchial bones are preserved, along with many postcranial bones, excepting the limbs and pelvic girdle (Fig. S1). An isolated ilium (UM.PRR 2002) collected in 1984 (Rage, 1984a) was recently attributed to *Thaumastosaurus* (Vasilyan, 2018) and was used here for phylogenetic analysis. This is justified given the remarkable similarity of the postcranial skeleton of the two species of *Thaumastosaurus* described in the Quercy, *T. gezei* Rage & Roček, 2007 and *T. bottii* De Stefano, 1903 (Vasilyan, 2018).

The anatomical terminology used herein is based on Roček (1980) and Biton et al. (2016) for cranial features, Roček et al. (2016) for the middle ear apparatus, Sanchiz (1998) for postcranial ones, Gardner et al. (2010) for iliac characters.

Phylogenetic Analyses—Our data matrix includes 85 taxa and 143 morphological characters (62 cranial and 68 postcranial characters, 12 from the hyobranchial apparatus, and one from soft tissues) and is derived from that of Báez and Gómez (2018; see Appendix S3 in Supplemental Data 1 for the list of characters). We added 14 new extant natatanuran taxa (see Appendix S4 in Supplemental Data 1) to better represent the major natatanuran clades inferred from recent molecular phylogenies (Frost et al., 2006; Pyron and Wiens, 2011; Jetz and Pyron, 2018). The new taxa were scored from both literature (Procter, 1919; Clarke, 1981; Scott, 2005; Evans et al., 2014) and 3D-models available on MorphoSource by the Blackburn Laboratory (Florida, USA) as part of the Overt program (Cross, 2017; for more information see the website: <https://www.floridamuseum.ufl.edu/overt/>).

All analyses were performed using TNT v.1.5 (Goloboff and Catalano, 2016). Half of the analyses were performed using equal weighting, whereas the other half were performed using implying weighting. Some analyses were conducted with all characters unordered and others with cline characters ordered (characters 3, 9, 10, 14, 26, 34, 51, 52, 68, 93, 112, 121, 124, 125 and 126), with or without topological constraints. All analyses consisted of heuristic searches with 1000 random addition sequences of taxa, followed by tree bisection reconnection (TBR) branch swapping, holding 10 trees per repetition. The final trees were rooted on *Ascaphus truei* (Ascaphidae) and, when more than one tree was obtained, a strict consensus was obtained.

Implied weighting was used to minimize the influence of homoplastic characters in the dataset, and achieved a better resolution of the different uncertainties recovered in the analysis under equal weighting (Goloboff, 1993, 1997), mostly for morphological characters (Goloboff et al., 2018a) and several values of k were used ($k=1-20$) to assess sensitivity of the results due to variations of the strength of the function (Goloboff et al., 2008). Some controversies remain on the effectiveness of this method, especially when compared with Bayesian models (Congreve and Lamsdell, 2016; O'Reilly et al., 2016; Puttick et al., 2017), but some recent evidence indicates implied weighting performs well (Goloboff et al., 2018a, b). Consequently, we chose to use both equal and implied weighting parsimony methods and then compare their results. Cline characters were ordered in all but one analysis (see Appendix S5 in Supplemental Data 1), as recent studies (Rineau et al., 2015, 2018) have shown

that analyses using ordered morphocline characters outperformed analyses using unordered characters even if the ordering scheme includes some errors (Rineau et al., 2018). Constrained analyses were performed with ordered characters including both equal and implied weights ($k=7$), using the topology of Jetz and Pyron (2018) as a constraint for extant taxa (Fig. S2). The same was done using the topology (Fig. S3) presented in Feng et al. (2017), with extinct taxa as floating taxa, in both cases. Node supports were expressed using Bremer support and standard bootstrap, with traditional searches of 1000 replicates, collapsing groups below 5% frequency. Bremer support uses tree fit score (Bremer, 1994; Goloboff and Farris, 2001). However, in implied weighting analyses, Bremer support is expressed in fractions due to the different weights that reflect the character fit (Goloboff, 1997; Jones and Butler, 2018).

SYSTEMATIC PALEONTOLOGY

ANURA Duméril, 1805

NEOBATRACHIA Reig, 1958

RANOIDES Frost, Grant, Faivovich, Bain, Haas, Haddad, De Sá, Channing, Wilkinson, Donnellan, Raxworthy, Campbell, Blotto, Moler, Drewes, Nussbaum, Lynch, Green, and Wheeler 2006

NATATANURA Frost, Grant, Faivovich, Bain, Haas, Haddad, De Sá, Channing, Wilkinson, Donnellan, Raxworthy, Campbell, Blotto, Moler, Drewes, Nussbaum, Lynch, Green, and Wheeler 2006

PYXICEPHALOIDEA Bonaparte, 1850

PYXICEPHALIDAE Bonaparte, 1850

PYXICEPHALINAE Bonaparte, 1850

Genus *THAUMASTOSAURUS* De Stefano, 1903

Type Species—*Thaumastosaurus bottii* De Stefano, 1903

Revised Diagnosis—Hyperossified natatanuran exhibiting cranial ornamentation, composed of pits and ridges, on the frontoparietals, maxillae, nasals, squamosals and sphenethmoid; the paired nasals and frontoparietals co-ossified with each other respectively and with the sphenethmoid and prooticoccipital (frontoparietals only), rhomboid dorsal fenestra on the skull allowing a dorsal exposure of the sphenethmoid; palatines (neopalatines of Trueb, 1973) present, in medial contact with each other (by their medial margin); anterior tip of the cultriform process of the parasphenoid does not extend between palatines; processus posterolateralis and ramus paroticus of squamosal merged, articulating with the crista parotica of the otic capsules; arteria occipitalis of either side piercing the frontoparietal; medial ramus of the pterygoid well-developed, overlapping the parasphenoid alae; zygomatic ramus (lamella alaris + processus maxillaris) of the squamosal well-developed, articulating with the maxilla.

Differs from *Pyxicephalus* Tschudi, 1838 and *Aubria* Boulenger, 1917 in lacking fang-like lamellar projections on the dentaries, in having the alary process of the premaxillae oriented dorsally (posterodorsally oriented in *Pyxicephalus* and *Aubria*), the craniomandibular joint at the same level as the occiput (posterior to the occiput in *Pyxicephalus* and *Aubria*) and the clavicles oriented anteromedially to the sagittal axis (perpendicular to the sagittal axis in *Pyxicephalus* and *Aubria*).

Differs further from *Pyxicephalus* in having the alae of the parasphenoid perpendicular to its cultriform process (posterior to the cultriform process in *Pyxicephalus*), a large dorsal exposure for the sphenethmoid (in *Pyxicephalus*, the sphenethmoid is not visible in dorsal view), cotyles of the atlas fully confluent (Type III of Lynch, 1971) (instead of juxtaposed Type II in *Pyxicephalus*), bicuspid teeth on the maxillae (monocuspid teeth on the maxillae in *Pyxicephalus*) and in lacking a lateral wall of the neurocranium ossified around the optic foramen (lateral wall ossified around the optic foramen in *Pyxicephalus*).

Differs from *Aubria* in having a distinct postchoanalis process of the vomers (no distinct process in *Aubria*).

THAUMASTOSAURUS SERVATUS (Filhol, 1877), comb. nov.

Bufo servatus Filhol, 1877:493, fig. 412 (413 in error) of Filhol (1877), MNHN.F.QU17381 (original description).

Bufo serratus Filhol, 1876:28, Filhol, 1877:fig. 412 (413 in error) (nomen nudum)

Rana plicata Filhol, 1876: 27, Filhol, 1877: figs. 401, 402, 404, 405.

Thaumastosaurus gezei Rage and Roček, 2007:figs 1, 7A.

Rana cadurcorum Martín et al., 2012:163. Filhol, 1877:figs. 401, 402, 404, 405 (new combination).

Holotype—The holotype is MNHN.F.QU17381, a nearly complete specimen lacking the snout, appendages and pelvic region. Unrecorded locality (likely Escamps) of the Quercy Phosphorites, southwestern France. Age uncertain, but probably late middle to late Eocene.

Referred Specimens—The specimens referred are MNHN.F.QU17748, right squamosal missing anterior tip of lamella alaris (Rage and Roček, 2007:fig. 2); MNHN.F.QU17376, holotype of *Thaumastosaurus gezei*, articulated skull missing anterior end, right side of palate, much of the right cheek region, parts of parasphenoid and both otic capsules (Rage and Roček, 2007:figs. 1, 7A); MNHN.F.QU17279, holotype of *Rana plicata*, nearly complete specimen lacking the appendages and pelvic region (Laloy et al., 2013:fig.1A–C); MNHN.F.QU17280, forelimb (Laloy et al., 2013:fig. 1D, E); MNHN unnumbered, specimen preserving the head and part of the trunk.

Revised Diagnosis—Differs from *T. wardi* by having a longer anterior extension of the squamosal alongside the dorsal margin of the maxilla, forming the whole ventral margin of the orbit; a medial margin of the lamina horizontalis of the maxilla convex rather than flat in medial view and in having the ridge separating the fossa maxillaris from the posterior part of the maxillae oriented posteriorly (instead of anteriorly).

Differs from *T. bottii* by having an elongate and slender medial process of the premaxillae, no ventral longitudinal ridge on this same process, and a groove for the vena jugularis interna shallower and wider.

DESCRIPTION

External Preservation

As part of the Quercy old collection mummies, MNHN.F.QU17381 displays an exceptional three-dimensional preservation including most of its external soft tissues replicated in calcium phosphate. These include the two eyeballs (Fig. 2A) and the skin laying over 3D-preserved muscular series (Fig. 2B–F), the striations of which are locally visible ventrally (e.g., right submaxillary muscles) (Fig. 2F). The specimen is about 6 cm from the snout to the sacrum, with its right side almost fully preserved. Hindlimbs and forelimbs are only proximally preserved. Posterior to each of the eyeballs, a 1.3 cm long and 0.6 cm wide large ovoid swelling is present (Fig. 2D, represented by a red/gray arrow and outline). This was at first identified as the outer visible deformation of a parotoid gland, typical for bufonids (Duellman and Trueb, 1994). However, other studies cast doubt on the presence of these glands in MNHN.F.QU17381 (Piveteau, 1927; Rage, 2006). The 3D model (Fig. 3) shows that this swelling is caused by the posterior process of the squamosals, which stretches the skin in this area (Fig. 3). This structure might have been caused by desiccation (N. Robin, unpublished data).

The outer tissues of MNHN.F.QU17381 are heterogeneously preserved. The skin is best preserved on the ventral and lateral

sides of the specimen with fine sub-millimetric folds. The latter concentrate on the mandible/maxillary complex, as well as posterior to the eye (Fig. 2B–D). These folds, absent on extant anurans when alive, must result from post-mortem deformation of the outer tissues. Dorsally, the replicated surface tissues reveal a glassy aspect reflecting a different phosphatized texture (Fig. 2C, E). In this region, the skin and inner tissues do not retain their *in vivo* volume but appear to be collapsed over the spine and underlying bony structure. The desiccation (or differential chemical transformation) of this dorsal part of the integument during early decay may have occasioned laterally the wrinkling of the skin resulting in observed microfolds. The left eyeball shows at the bottom a clear demarcation of the eye from the surrounding skin membrane (Fig. 2D). Elsewhere, no distinction between the eye and the eyelid is apparent.

Two other specimens of *T. servatus* display this level of exceptional 3D preservation in calcium phosphate. MNHN.F.QU17279 shows well-preserved eyelids covering the eyes fossilized in their original direction (Fig. 4A, C). On this specimen, the skin is more stretched and homogeneously preserved over the specimen surface, revealing thinner skin (compared with MNHN.F.QU17381) microfolds and a local bulbous texture that looks original to the structure (Fig. 4A–C). Larger skin ridges extend posteriorly from the eyes onto the dorsal surface of the trunk (Fig. 4B). About 1 mm in width, these skin ridges correspond to the original dorsolateral folds present in many anuran taxa (Duellman and Trueb, 1994), especially in ranoids (e.g., in Pyxicephalidae, see Poynton, 1964; Channing and Baptista, 2013; Channing et al., 2016; see Dubois and Ohler, 2005 for other ranoids). On the left side of the specimen MNHN.F.QU17279, in a region between the posterior process and the postero-lateral side of the squamosal, the skin bears a slight demarcation with a faint outline (Fig. 4C). Given the preservation of the skin in this region (Fig. 4A–C), we do not interpret this delimitation as a reflection of the underlying bones but rather as the borders of the tympanic membrane (Duellman and Trueb, 1994).

The second best-preserved specimen, MNHN.F.QU17376, consists solely of a head whose preservational quality varies gradually from snout (best preserved) to neck (Fig. 4D, E), with visible snout bony ornamentation (part of the nasals; Fig. 4D). Posterolaterally, the skin looks pristine, with bulbous textural components. The aforementioned external aspects indicate that MNHN.F.QU17381 (Fig. 2) may plausibly have undergone a longer period of decay/exposure time span prior to burial than MNHN.F.QU17279 (Fig. 4A–C) and one comparable with, or shorter than MNHN.F.QU17376 (Fig. 4D, E).

Skull

The skull is incomplete, missing the anteriormost part of the snout and the premaxillae (Figs. 2, 3, 5). The preserved cranial bones are all articulated.

Dermal Bones—The frontoparietals, squamosals, maxillae, nasals and the dorsal part of the sphenethmoid bear an ornamentation composed of deep oval to subcircular pits and ridges with a constant thickness (Fig. 5A). The ornamentation on the sphenethmoid is much less marked than on the other bones.

Frontoparietals—The frontoparietals are fused into a single bone, in the shape of a truncated rhomboid, longer than wide, without any clear trace of a median suture. However, anteriorly, at the posterior end of a deep notch on the midline of the nasal margin, a shallow depression on the dorsal and ventral face seems to mark the limit between the bones (Fig. 6A). Anterolaterally, they articulate with the nasals by the external end of the nasal margin, and anteromedially, with the posteromedial margin of the dorsal exposure of the sphenethmoid. The lateral margin bears on its mid-length an external expansion (a peak),

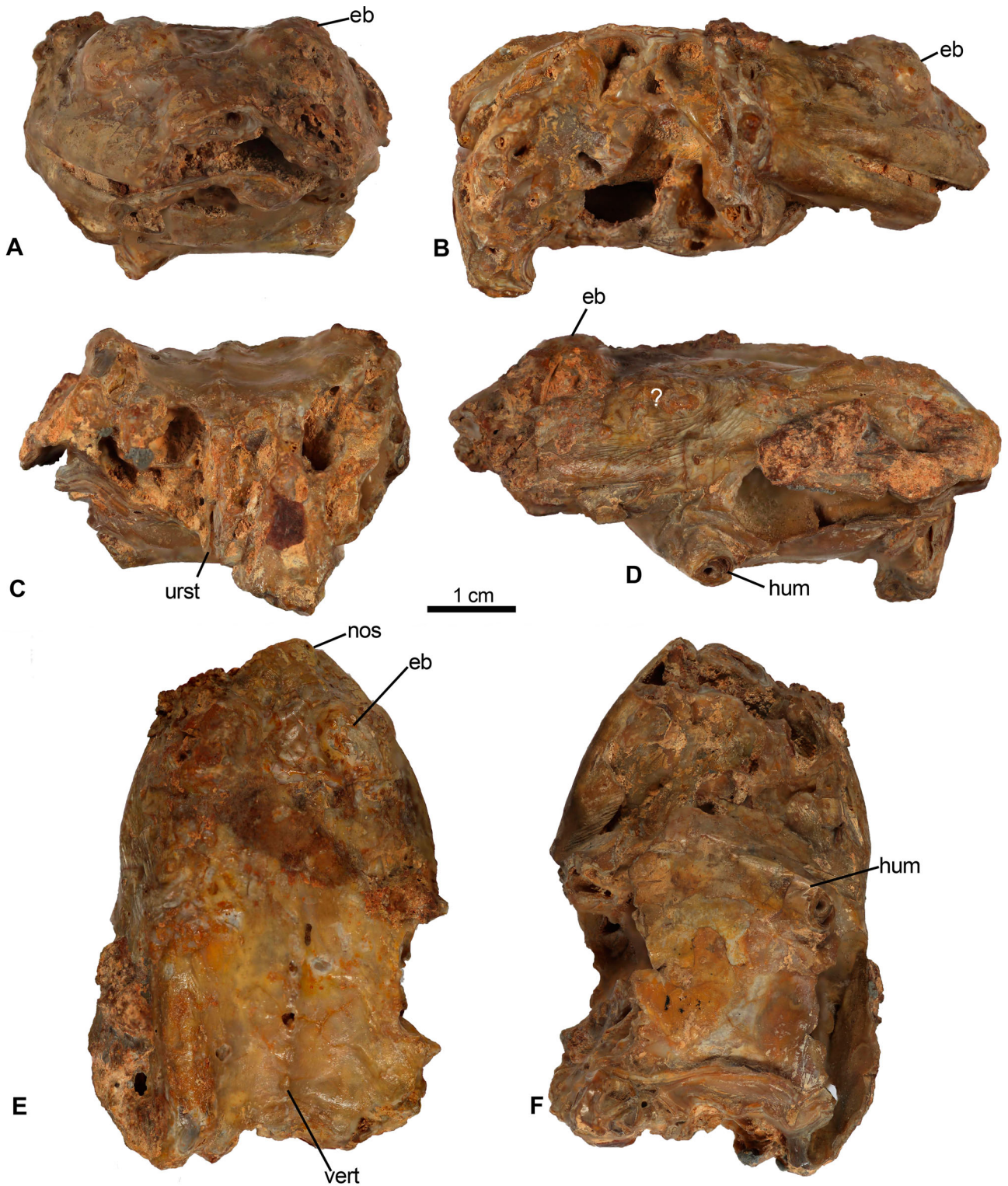


FIGURE 2. External views of the specimen MNHN.F.OU17381, holotype of *Bufo servatus* Filhol, 1877, now attributed to *T. servatus* in **A**, anterior; **B**, right lateral; **C**, posterior; **D**, left lateral; **E**, dorsal; and **F**, ventral views. ? indicates the area previously identified as a parotoid gland. **Abbreviations:** **eb**, eyeball; **hum**, humerus; **nos**, nostril; **vert**, vertebrae; **urst**, urostyle.

the tectum supraorbitale (Fig. 6A, B). There is no contact between frontoparietals and squamosals (Fig. 5A), but the lateral expansion of the tectum may indicate these two bones were joined by a ligament that would have delimited the

posterior margin of the orbit, as observed in some extant anurans (Roček, 1980).

Posteriorly, the frontoparietals are fused to the prooticoccipital complex (Fig. 5D). The processus lateralis of the

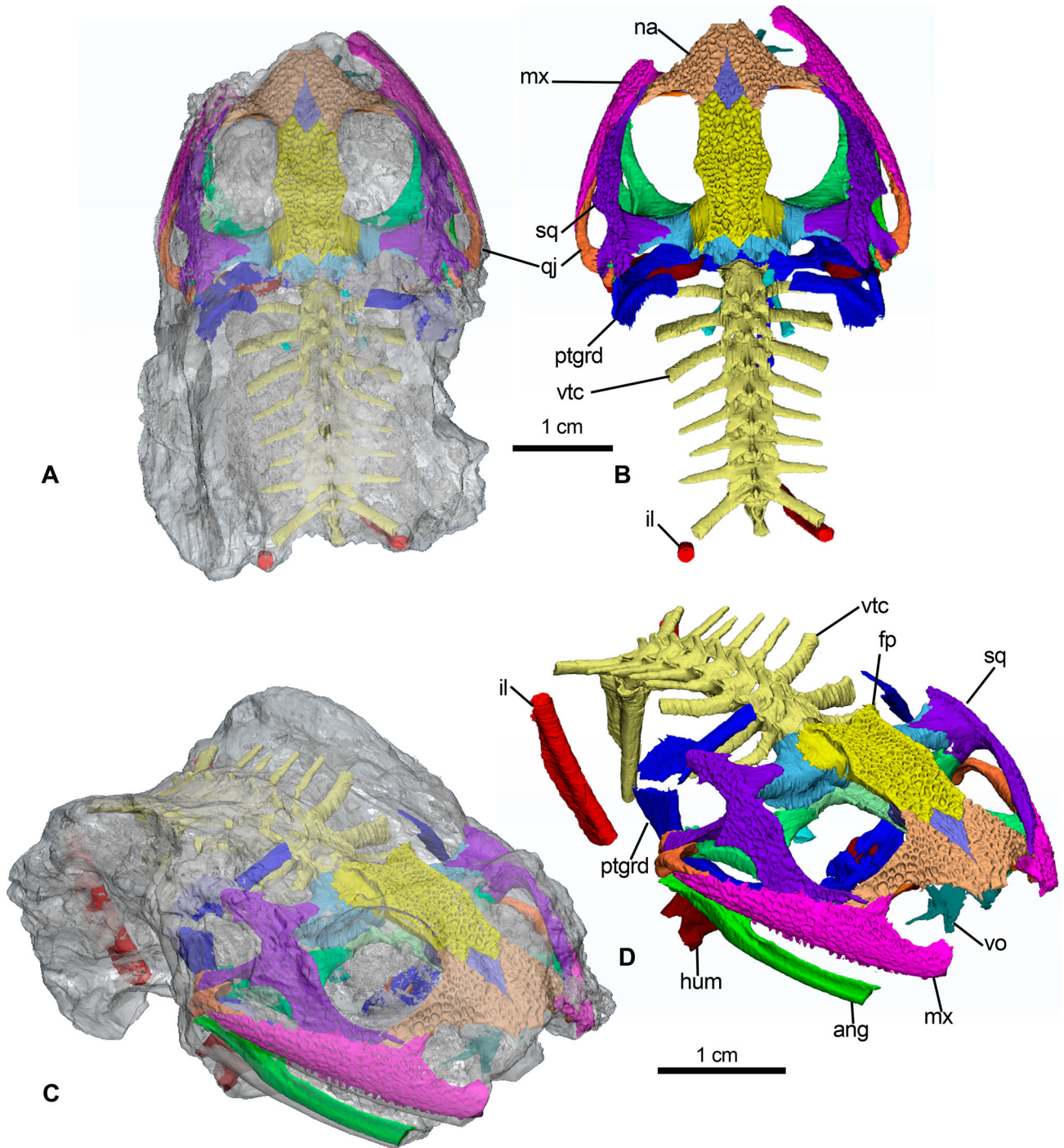


FIGURE 3. 3D-model of the specimen MNHN.F.QUI7381. **A**, whole specimen in dorsal view with soft tissue digitally rendered transparent to show the color-coded skeleton; **B**, dorsal view of the sole osteological component; **C**, whole specimen in right dorso-antero-lateral view with soft tissue digitally rendered transparent to show the color-coded skeleton; **D**, same view of the sole osteological component. **Abbreviations:** **ang**, angulosplenia; **fp**, frontoparietals; **hum**, humerus; **il**, ilium; **mx**, maxilla; **na**, nasal; **ptgrd**, pectoral girdle; **qj**, quadratojugal; **sq**, squamosal; **vo**, vomer; **vtc**, vertebral column.

frontoparietals are difficult to distinguish from the crista parotica of the prootic but seem to form an almost straight margin (Figs. 5A, 6A). Posterolaterally, the processus paraoccipitalis of the frontoparietals is fused to the dorsal face of the prominentia ducti semicircularis posterioris of the prootic, forming a prominent ridge (Fig. 5D). Medially, the processus paraoccipitalis

delimits the foramen for the arteria occipitalis canal (Fig. 5D). As in several extinct and recent anurans (Sanchiz, 1998), the posterior process of the frontoparietals consists of a horizontal lamina. This lamina extends the midlength of the bone posterior margin and forms a small spike-like surface that covers the dorsal exposure of the prooticooccipital (Fig. 6A).

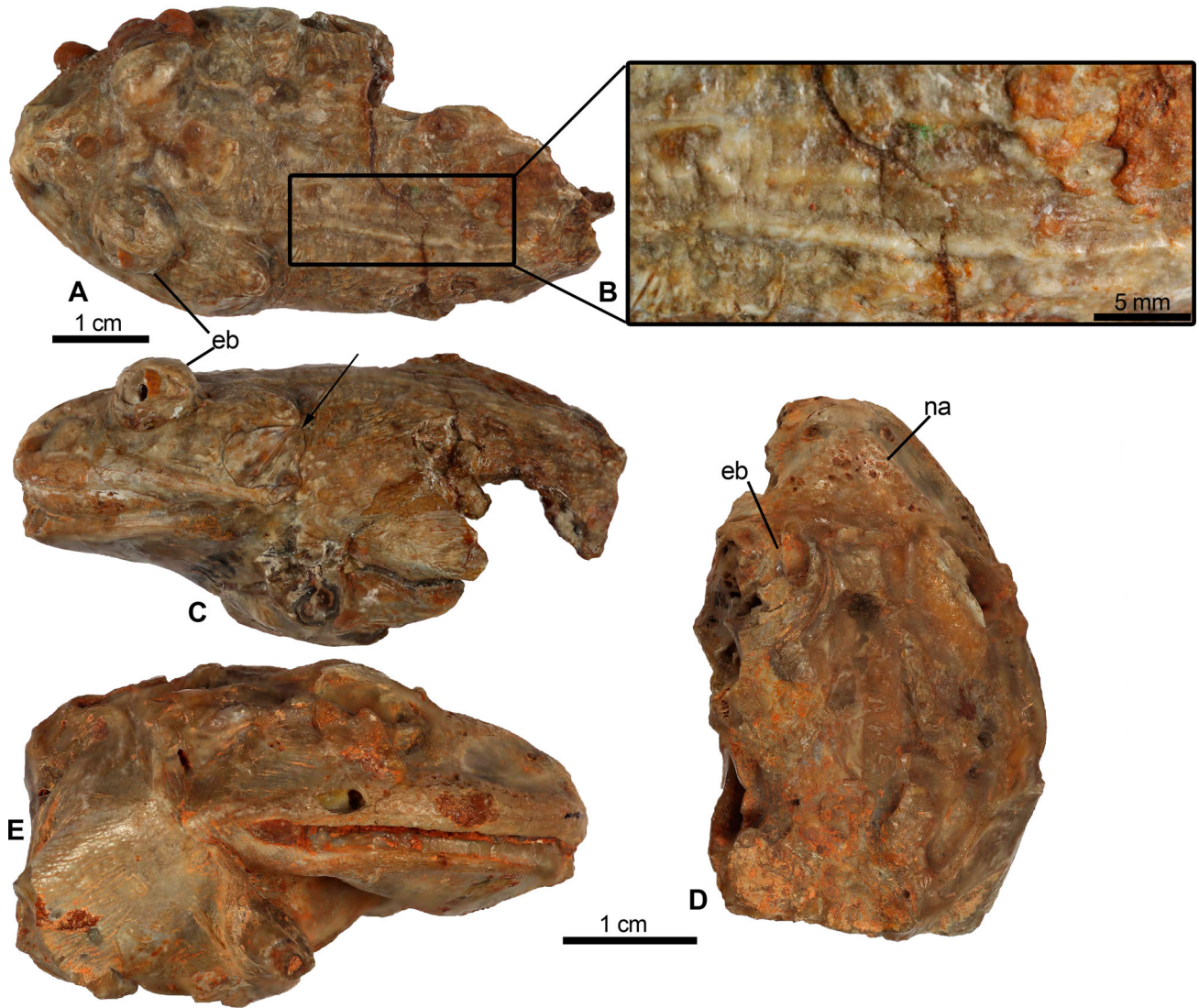


FIGURE 4. External views of specimens MNHN.F.QU17279 and MNHN.F.unnumbered, both referred to *T. servatus*. **A–C**, specimen QU 17279 in **A**, dorsal view; **B**, close-up of the rectangular region in **A** to show the ridges and folds of the preserved skin on the dorsal surface of the anterior trunk region; **C**, same specimen in left lateral view; **D–E**, specimen MNHN.F.unnumbered in **D**, dorsal and **E**, right lateral views. Black arrow indicates the area of potential tympanic membrane. **Abbreviations:** **eb**, eyeball; **na**, nasals.

In ventral view, the anterolateral pars contacta is a vertical lamina extending from the ventral surface of the frontoparietals (Fig. 5B) and is fused to the dorsolateral part of the sphenethmoid (Fig. 5B, 6A). The pars contacta increases in size posteriorly, forming a thin vertical lamina that is fused to the prootic ventrally and to the processus lateralis of the frontoparietals dorsally where it covers the prootic anterolaterally (Fig. 5B).

Ventrally, the incrassatio frontoparietalis presents two structures, the facies cerebralis anterior, and the facies cerebralis posterior (Fig. 6B). The facies cerebralis anterior is an unpaired lanceolate structure, extending from the posterior margin of the sphenethmoid/frontoparietals suture. The posterior limit of this structure is not clear. The facies cerebralis posterior is an unpaired circular impression, located postero-laterally on the left side of the bone. In another mummy (MNHN.F.QU17381), a similar condition was found for the facies cerebralis anterior, but the facies cerebralis posterior was a paired circular impression on each side (Laloy et al., 2013:fig. 4D). This condition is reminiscent of ranoids (Jarošová and Roček, 1982). In

our specimen, the unpaired condition of the facies cerebralis posterior might be due to a non-preservation of the impression, or a lesser ossification of the right frontoparietal.

Squamosals—In lateral view, the lamella alaris is arch-shaped; it expands bilaterally at the base and tapers and descends ventrally towards the processus maxillaris (Fig. 6C). It forms a thin strip of bone separating the maxilla from the orbit (Fig. 5B). This configuration is similar to that of MNHN.F.QU17279, which also bears an elongate thin extension of the lamella alaris (Laloy et al., 2013) but is proportionally shorter than that of the holotype of *Thaumastosaurus gezei* (MNHN.F.QU17376; Rage and Roček, 2007). The anterior end of the lamella alaris forms a shallow groove with the lateral end of the nasal, identified as the groove for the nasolacrimal duct (Fig. 5B).

The processus maxillaris is antero-posteriorly elongated (Fig. 6C). The processus zygomatico-maxillaris of the maxilla is inserted into an incisura lateral to this processus maxillaris, fully overlapping it. This is not visible in lateral view, as it is overlapped by the lamella alaris (Fig. 5B). The orbital margin is

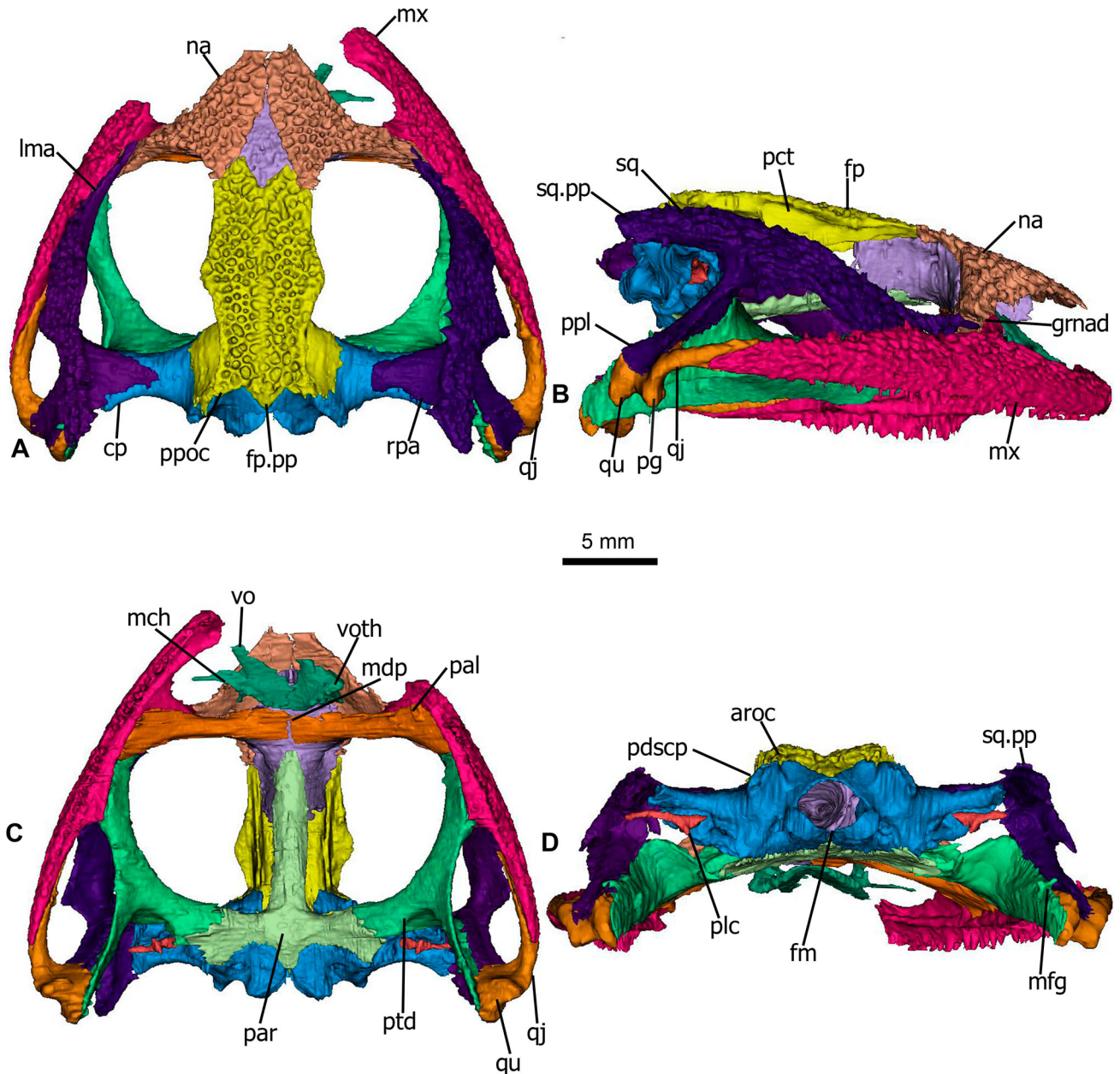


FIGURE 5. The almost complete and articulated skull of the mummy MNHN.F.QU17381. Shown in **A**, dorsal; **B**, right lateral; **C**, palatal; and **D**, posterior views. **Abbreviations:** *aroc*, canal for the arteria occipitalis; *cp*, crista parotica; *fm*, foramen magnum; *fp*, frontoparietals; *fp.p*, posterior process of the frontoparietals; *grnad*, groove for the nasolacrimal duct; *lma*, lamella alaris; *mch*, choanal margin; *mdp*, medial process; *mfg*, medial flange; *mx*, maxilla; *na*, nasal; *pal*, palatine; *par*, parasphenoid; *pct*, pars contacta; *pdscp*, prominentia ducti semicircularis posterioris; *pg*, processus glenoidalis; *plc*, plectrum; *ppl*, processus posterolateralis; *ppoc*, processus prooticoccipitalis; *ptd*, pterygoid; *qj*, quadratojugal; *qu*, quadrate; *rpa*, ramus paroticus; *sq.pp*, posterior process of the squamosal; *vo*, vomer; *voth*, vomerine teeth.

concave dorsally, forming the ventral wall of the orbit (Fig. 5A, B). Laterally, the lamella alaris extends posteroventrally into a spike-like extension, reaching the anterior part of the processus posterolateralis of the squamosals.

Medially, the ramus paroticus is a broad dorsoventrally flat lamina, fused to the crista parotica of the otic capsule dorsomedially (Fig. 5A). It narrows medially and ends in an almost straight margin (Fig. 5A). The posterior process of the squamosal is short and rounded distally (Figs. 5A, B, 6B). The processus posterolateralis is elongate and slender. In dorsal view, the surface between the ramus paroticus and the processus

posterolateralis is concave (Fig. 5A), and most likely forms the lateral wall of the tympanic cavity (Roček and Lamaud, 1995). The processus posterolateralis bears a medial flange fused to the ramus posterior of the pterygoid, making it difficult to digitally segment them (Fig. 5B, C). The distal end of the processus posterolateralis is fused to the dorsolateral surface of the quadratojugal (Fig. 5B).

Maxillae—The left maxilla is incomplete, lacking its anterior length starting at the level of the processus frontalis. The right maxilla, however, is almost complete, missing only its anterior tip. The posterior process of the maxillae is long, slender and has a

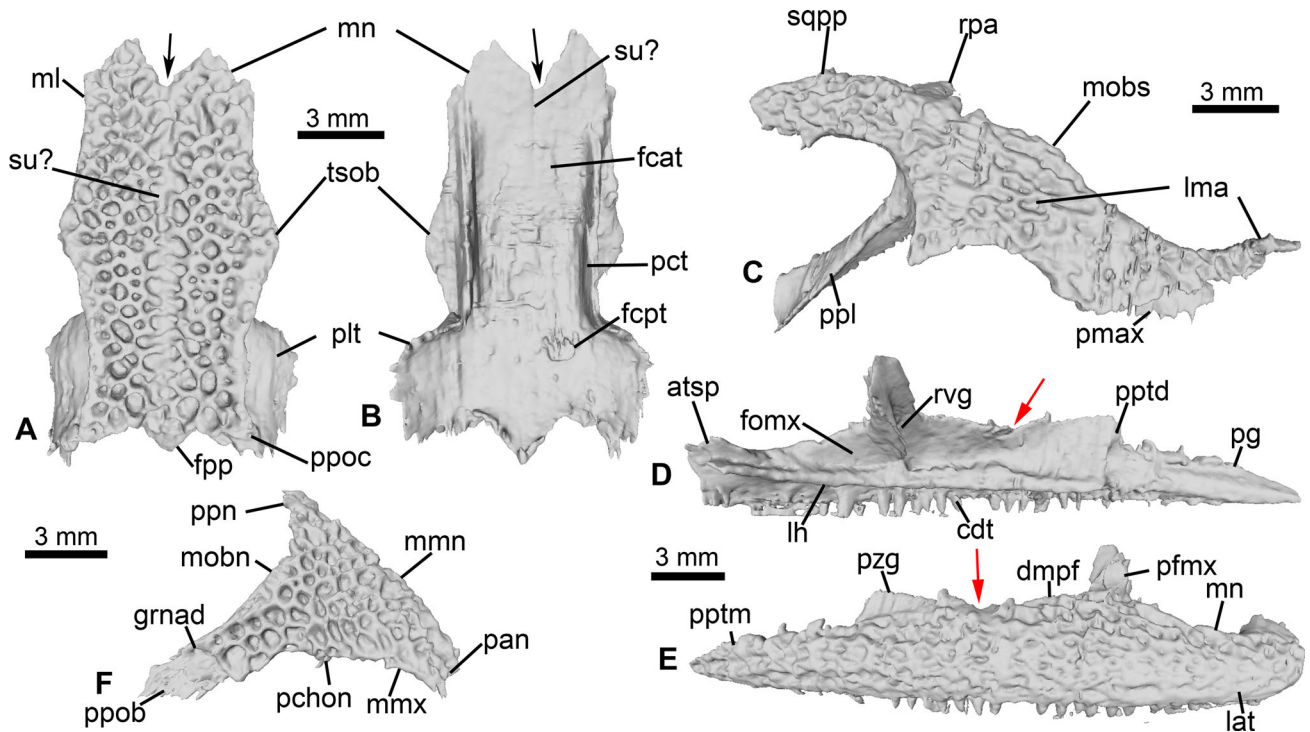


FIGURE 6. Dermal bones from MNHN.F.QU17381. **A**, frontoparietals in dorsal; **B**, ventral views; **C**, right squamosal in lateral view; **D**, right maxilla in lateral; **E**, medial views; **F**, right nasal in lateral view. Gray (red in online version) arrows point to the notch on the dorsal margin of the pars facialis of the maxilla; black arrows point to the notch on the frontoparietal. **Abbreviations:** **atsp**, anterior spine; **cdt**, crista dentalis; **dmpf**, dorsal margin of the pars facialis of the maxilla; **fcac**, facies cerebralis anterior; **fcpt**, facies cerebralis posterior; **fomx**, fossa maxillaris; **fpp**, posterior process of the frontoparietals; **grnad**, groove for nasolacrimal duct; **lat**, lamina anterior; **lh**, lamina horizontalis; **lma**, lamella alaris; **ml**, lateral margin of the frontoparietals; **mn**, nasal margin; **mmx**, maxillar margin; **mmn**, medial margin of the nasals; **mobn**, orbital margin of the nasal; **mobs**, orbital margin of the squamosal; **pan**, processus anterior of the nasal; **pchon**, processus parachoanal; **pct**, pars contacta; **pfmx**, processus frontalis; **pg**, posterior groove; **plt**, processus lateralis; **pmax**, processus maxillaris; **ppl**, processus posterolateralis; **ppob**, processus paraorbitalis; **ppn**, processus posterior of the nasals; **ppoc**, processus prooticoccipitalis; **pptd**, processus pterygoideus; **pptm**, posterior process of the maxilla; **pzm**, processus zygomatico-maxillaris; **rvg**, recessus vaginiformis; **rpa**, ramus paroticus; **sqpp**, posterior process of the squamosal; **su?**, putative suture of the frontoparietals; **tsob**, tectum supraorbitale.

groove posteromedially to articulate with the quadratojugal (Figs. 5B, 6D). The processus pterygoideus, visible in medial view, is short and marked by a small posterior prominence from the lamina horizontalis. This processus delimits ventro-medially a large pit, which faces posteriorly. The lamina horizontalis is straight with a convex medial margin, moderately thickened anteriorly, where it extends onto the dorsal margin of the lamina anterior and develops into an anterodorsal anterior spine (Fig. 6D). Posterior to the processus pterygoideus, the lamina horizontalis narrows considerably, ending in a thin, poorly marked strip extending onto the lower margin of the posterior process of the maxillae (Fig. 6D).

In lateral view, a flattened smooth processus zygomatico-maxillaris and a well-developed processus frontalis are visible dorsally (Fig. 6E). The dorsal margin of the pars facialis is almost straight. A weakly pronounced notch is visible on the midline of the medial (= inner) surface of the pars facialis (Fig. 6E). This notch was also observed in non-articulated maxillae in *Thaumastosaurus* (Roček and Lamaud, 1995; Vasilyan, 2018). The recessus vaginiformis is overlapped by a medial crista extending up to the tip of the processus frontalis. Anteriorly, the fossa maxillaris is shallow (Fig. 6D).

The ventral margin of the lamina horizontalis delimits the base of the crista dentalis up to a triangular anterior facet of the maxillae in medial view (articulation of the premaxilla; Roček and Lamaud, 1995:fig. 6D). The teeth are present, but they are difficult to discern on either maxilla and it is not possible to determine if the tooth crowns are uni- or bicuspid, and whether or

not they were pedicellate. However, Holman and Harrison (2002) described a partial maxilla attributed to *Thaumastosaurus*, where the teeth are pedicellate and bicuspid. The pedicellate condition was also retrieved in another partial maxilla (Holman and Harrison, 2003). The tooth row ends anterior to the posterior margin of the lamina horizontalis.

The anteriormost portion of the right maxilla and therefore details about the end of the lamina anterior, the rostellum and the anterior extension of the crista dentalis, are not preserved.

Nasals—The nasals are in close contact anteromedially and diverge from each other posteromedially, leaving the sphenethmoid exposed (Fig. 5A). This puts them in a transitional state between the condition found in the first mummy (MNHN.F.QU17279; Laloy et al., 2013), in which they are separated by an empty space, and the condition of MNHN.F.QU17376, where they are wholly fused, without midline sutures (Rage and Roček, 2007). The nasals are fused to the dorsal surface of the sphenethmoid. Both the maxillary and orbital margins are concave, with the processus paraorbitalis oriented posterolaterally at its distal end (Fig. 5A, 6F). The processus paraorbitalis has no ornamentation distally, where it is delimited ventrally by the anterior extension of the lamella alaris of the squamosal to form a groove for the nasolacrimal duct (Figs. 5B, 6F). The parachoanal process is a small protuberance, located at mid-length of the maxillar margin (Fig. 6F). The dermal sculpture of the nasals appeared to be more deeply pitted near the orbital margin.

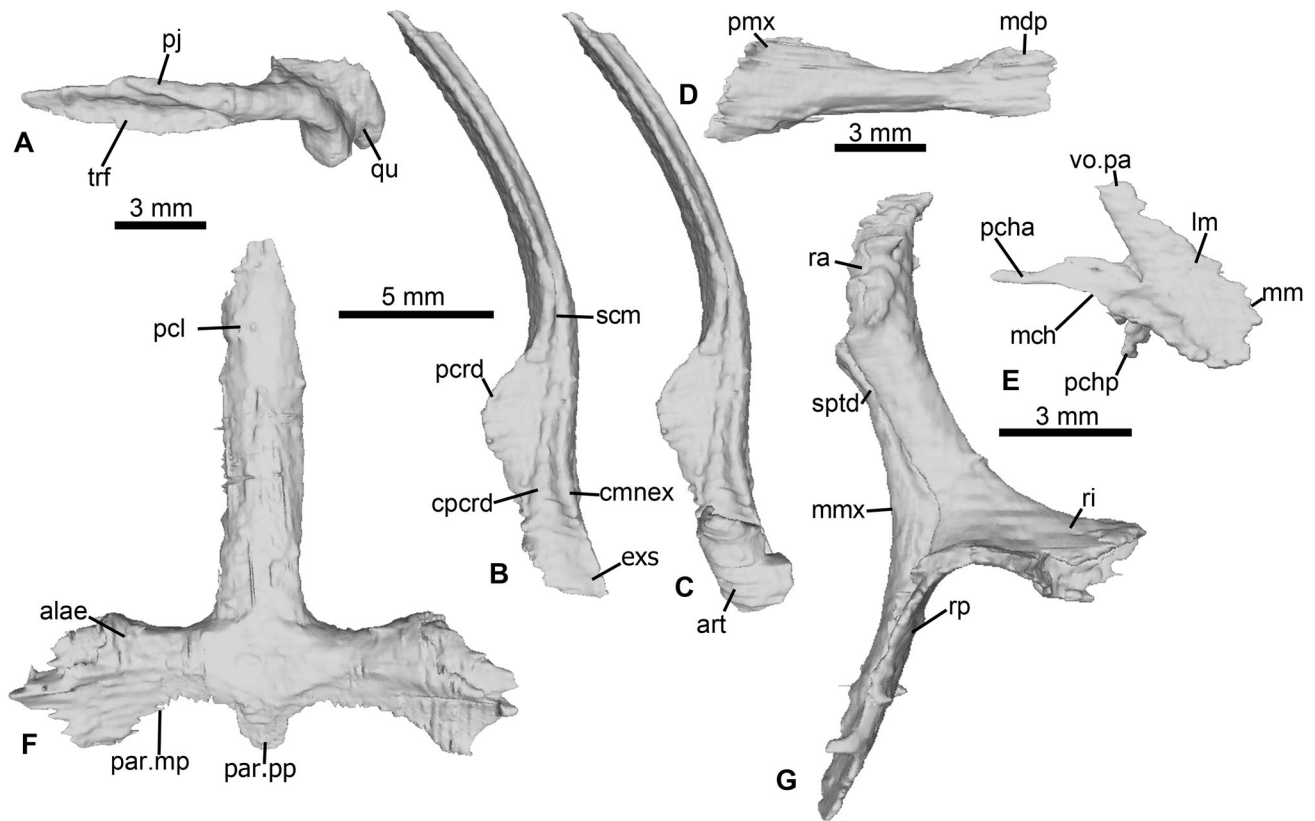


FIGURE 7. Suspensorium and palate bones from MNHN.F.QU17381. **A**, left quadratojugal in lateral view; **B**, right angulosplenic in dorsal view; **C**, right angulosplenic and articular in dorsal view; **D**, right palatine in ventral view; **E**, right vomer in ventral view; **F**, parasphenoid in ventral view; **G**, left pterygoid in dorsal view. **Abbreviations:** *alae*, alae of the parasphenoid; *art*, articular; *cmnex*, crista mandibulae externa; *cpcrd*, crista paracornoidea; *exs*, extremitas spatulate; *lm*, lamina medialis; *mch*, choanal margin; *mdp*, medial process; *par.mp*, posterior margin of the parasphenoid; *par.pp*, posterior process of the parasphenoid; *pcha*, processus choanalis anterior; *pchp*, processus choanalis posterior; *pcl*, cultriform process; *pcrd*, processus coronoideus; *pj*, processus jugularis; *pmx*, processus palatinus maxillae; *qu*, quadratum; *mm*, medial margin; *mmx*, maxillar margin; *ra*, ramus anterior; *ri*, ramus interior; *rp*, ramus posterior; *scm*, sulcus pro cartilagine Meckeli; *sptd*, sulcus pterygoideus; *trf*, triangular facet; *vo.pa*, processus anterior of the vomer.

Quadratojugals—The quadratojugals are elongate with an anterior slender and elongate processus jugularis. The quadratojugals articulate with the maxillae along a triangular facet, on the lateral side of the processus jugularis for nearly one half of the length of the quadratojugals (Figs. 5B, 7A). In ventral view, the processus jugularis curves anteromedially and extends up to 80% of the lateral border of the pterygoid fossa. Posteriorly, the bone forms a thick bulge, extending medially, and with a medial groove on its posterior surface (Fig. 5B). This bulge is interpreted as the quadrate (ossified portion of the palatoquadrate; Špinar, 1972; Duellman and Trueb, 1994; Roček, 2003). The palatoquadrate is mostly cartilaginous in anurans, but its posterior region can ossify as the quadrate. In anurans whose quadratojugals are present, the quadrates are fused to them, forming a quadratojugal + quadrate complex. The quadrate is overlapped posterodorsally by the posterolateral process of the squamosals and medially by the ramus posterior of the pterygoid. In MNHN.F.QU17279, it is also possible to see these ossified quadrates fused to the quadratojugals, with a thin suture visible between the two bones in ventral view (Laloy et al., 2013:fig. 3B).

Suspensory Bones

Angulosplenials—Both angulosplenials are incompletely preserved. The left angulosplenic represents less than 1/4 of the whole bone (compared with the one described in Laloy et al.,

2013), and the right one represents around 2/3 of a complete angulosplenic. The processus coronoideus is dorsoventrally oriented as an oval flattened plate, whereas the crista paracornoidea is poorly developed (Fig. 7B). The crista mandibulae externa is marked laterally. The groove for Meckel's cartilage is visible on the lateral side of the angulosplenic where it widens posterodorsally (extremitas spatulata, Fig. 7B). In dorsal view, the articular is preserved in the posterior region of the bone. Remaining mandibular bones are not preserved in this specimen.

Articular—This bony element forms, with the quadrate, the jaw joint in anurans (Roček et al., 2016). The articular is an irregularly shaped, anteroposteriorly elongate element (Fig. 7C). The poor ossification of this element made it difficult to delineate from the surrounding matrix in the CT data. The articular is in ventral contact with each angulosplenic but is not fused to this element. It is covered dorsally by the quadratojugal + quadrate. The quadrate and articular are not in contact, but this might be due to poor ossification/preservation of the two elements.

Palate Bones

Palatines—The palatines (neopalatines of Trueb, 1973) are elongate, dorsoventrally flattened, sub-cylindrical elements that are oriented perpendicular to the sagittal axis of the skull. In ventral view, the paired palatines articulate medially in the

midline of the sphenethmoid (slightly separated by a very narrow fissure), as in MNHN.F.QU17376 (Rage and Roček, 2007). The processus palatines maxillae extends posterolaterally on the palatoquadrate groove of the maxilla (Figs. 5C, 7D). The medial process ventrally contacts the lateral process of the sphenethmoid and nearly contacts the anterior tip of the parasphenoid posteriorly.

Vomers—Both vomers are preserved in situ and articulate with the ventral face of the sphenethmoid and with each other by their lamina medialis, forming a flat lamina that extends posteromedially (Fig. 5C). The medial margin is convex and almost in contact with the palatine. The left vomer is damaged anterolaterally and at least half of it is missing; a few teeth are visible in ventral view (Fig. 5C). Vomerine teeth were not visible on the right vomer during the segmentation, but their presence was observed by Laloy et al. (2013) in their segmentation of MNHN.F.QU17279. The anterior process extends anterolaterally towards, but fails to contact, the anterior spine of the lamina horizontalis of the maxilla. The processus choanalis anterior is very elongate and extends laterally without reaching the maxilla. The processus choanalis posterior is a small flattened lamina, with a crest extending dorsally (Fig. 7E). The choanal margin (margo choanalis in Roček, 1994) is well marked with an acute angle that indicates a moderately large choanal opening (Biton et al., 2016).

Parasphenoid—The parasphenoid is fused to the prooticoccipital complex posterolaterally and to the sphenethmoid anteriorly. The cultriform process is long and slender, without any longitudinal ridges on its ventral surface. Posteriorly, the alae (processus lateralis) are short, lie perpendicular to the cultriform process, and bear a transversal and arched keel ventrally (Fig. 7F). The posterior margin is curved (convex anteriorly) towards a short, medially borne spear-like posterior process. The parasphenoid is fused to the pterygoids by the anterolateral margin of the alae. This suture was difficult to discern during segmentation, but the alae are extensively overlapped by the ramus interior of the pterygoid anteriorly (Fig. 5C).

Pterygoids—The pterygoids are of the standard triradiate shape for anurans (Fig. 5A). The ramus posterior is an elongated vertical lamina (partly fused to the processus posterolateralis of the squamosal) in contact distally with the quadrate (Fig. 5C). The ramus interior bears a posterodorsal flange that forms a part of the posterior wall of the orbit (Fig. 5D). A deep sulcus extends dorsally from the ramus posterior to the ramus anterior on the maxillar margin called the sulcus pterygoideus (Fig. 7G). The ramus anterior is well-developed, robust, and slightly flattened dorsoventrally.

Endocranium

Sphenethmoid—The sphenethmoid is an unpaired bone, pentagonal in dorsal view. Most of its dorsal surface is overlapped by, and fused to, the nasals and frontoparietals. The exception is a small, rhomboid, median part that is visible dorsally (Fig. 5A). This exposure is covered with low and poorly defined ornamentation composed of pits and ridges, nearly identical to the one covering the dermal bones (Figs. 5A, 8A). In extant anurans, the ornamentation of the sphenethmoid (and other bones as well) thickens during growth and thus serves as an ontogenetic marker (Buffrénil et al., 2015, 2016). An even weaker ornamentation characterizes MNHN.F.QU17279 (Laloy et al., 2013), indicating that it is less mature than our specimen.

Among extant anurans, a dorsal exposure of the sphenethmoid occurs in various taxa (Duellman and Trueb, 1994; Paluh et al., 2020). However, this dorsal exposure is rarely ornamented like the neighboring dermal bones (e.g., *Aubria masako*, where the dorsal exposure is reduced to a minute rhomboidal fenestra, devoid of ornamentation). In addition, the dorsal exposure is

reduced or absent in most extant or extinct hyperossified taxa (Duellman and Trueb, 1994; Sheil, 1999; Nicoli, 2019; Paluh et al., 2020), where the nasals and frontoparietals overlap the sphenethmoid. In contrast, the exposure in MNHN.F.QU17381 is rather large.

An exposed and ornamented sphenethmoid occurs in extant hylids (casque-headed tree frogs) from South America, Pelobatidae and Bombinatoridae (Trueb, 1970; Roček, 1980; Smirnov, 1997). Analysis of the ontogeny and skeletogenesis of this region in Hylidae and Bombinatoridae has shown the presence of a dermal bone called the dermal sphenethmoid (Trueb, 1966, 1970; “internasofrontal,” Smirnov, 1997). This rhomboidal neomorphic element develops by intermembranous ossification in the lower dermis (Trueb, 1966) and then co-ossifies with the sphenethmoid to form a single bone mass (Trueb, 1966, 1970; Smirnov, 1997). The presence of this bone is contested in Pelobatidae (Roček, 2003), as the sphenethmoid can be covered by adjacent dermal bones. Periosteal ossification of the sphenethmoid could also result in a secondary ornamentation such as for the neighboring nasals and frontoparietals. The presence of a dermal sphenethmoid is highly speculative in MNHN.F.QU17381, as it can only be differentiated in premetamorphic specimens (Trueb, 1970).

Anteriorly, the bone is divided into two chambers (cavitas nasalis) separated medially by the bony septum nasi (Fig. 8C). The sphenethmoid is elongate posteriorly, reaching close to the mid-level of the cultriform process of the parasphenoid (Fig. 5C). Despite the overall hyperossification of the skull, the sphenethmoid does not reach the prooticoccipital, leaving a part of the lateral walls of the braincase unossified.

Posteriorly, the dorsal fenestra frontoparietalis forms a notch for the insertion of the facies cerebralis anterior (Fig. 8A) of the frontoparietals, bearing a dorsal impression of the forebrain. Ventrally, the sphenethmoid is fused to the anterior tip of the parasphenoid and to the palatines. The lateral processes are distally short, with the posterior wall extending slightly laterally (Fig. 8A). The dorsal surface of these processes extends slightly postero-laterally to form a poorly developed lamina supraorbitalis (Fig. 8A). The lateral wall of each anterior chamber is pierced by an orbitonasal foramen, which conveyed the ophthalmic nerve (canalis ramus medialis nervi ophthalmici) into a large cavitas nasalis (= anterior chamber) (Fig. 8B).

Several portions of the anterior sections of the sphenethmoid are partially ossified, which is characteristic of hyperossification. The septum nasi is ossified, without any anterior thickening, reaching the anterior part of the nasals (Fig. 8C), and the tectum nasi is oriented anterodorsally, forming a triangular flattened area in dorsal view (Fig. 8A). The solum nasi (ventral surface of the cavitas nasalis) bears a broad dorsal prominence, the sella amplificans (Fig. 8C). The surface of the solum nasi and septum nasi appears smooth in the segmentation. This most likely indicates that a cartilaginous part was present (Duellman and Trueb, 1994; Roček and Lamaud, 1995). The rest of the anterior part of the sphenethmoid was most likely cartilaginous or poorly ossified, and therefore neither the postnasal wall nor anterior wall of the nasal capsule were preserved. In ventral view, the sphenethmoid is subcruciform, with the lateral expansion of the anterior chamber perpendicular to both the posterior chamber and the bony anterior extension of the septum nasi.

Prooticoccipital Complex—The prootic, occipital and exoccipital are fused into a single complex that constitutes the posterior part of the braincase and skull (Fig. 5D). The otic capsules are poorly ossified ventrally, as indicated by their irregular ventral surface (Fig. 8G).

The foramen magnum is large and oval (slightly compressed dorsoventrally). The two occipital condyles are crescentic, with a small dorsal ridge connecting them to the prominencia ducti semicircularis posterioris (Fig. 8D). The latter is naturally

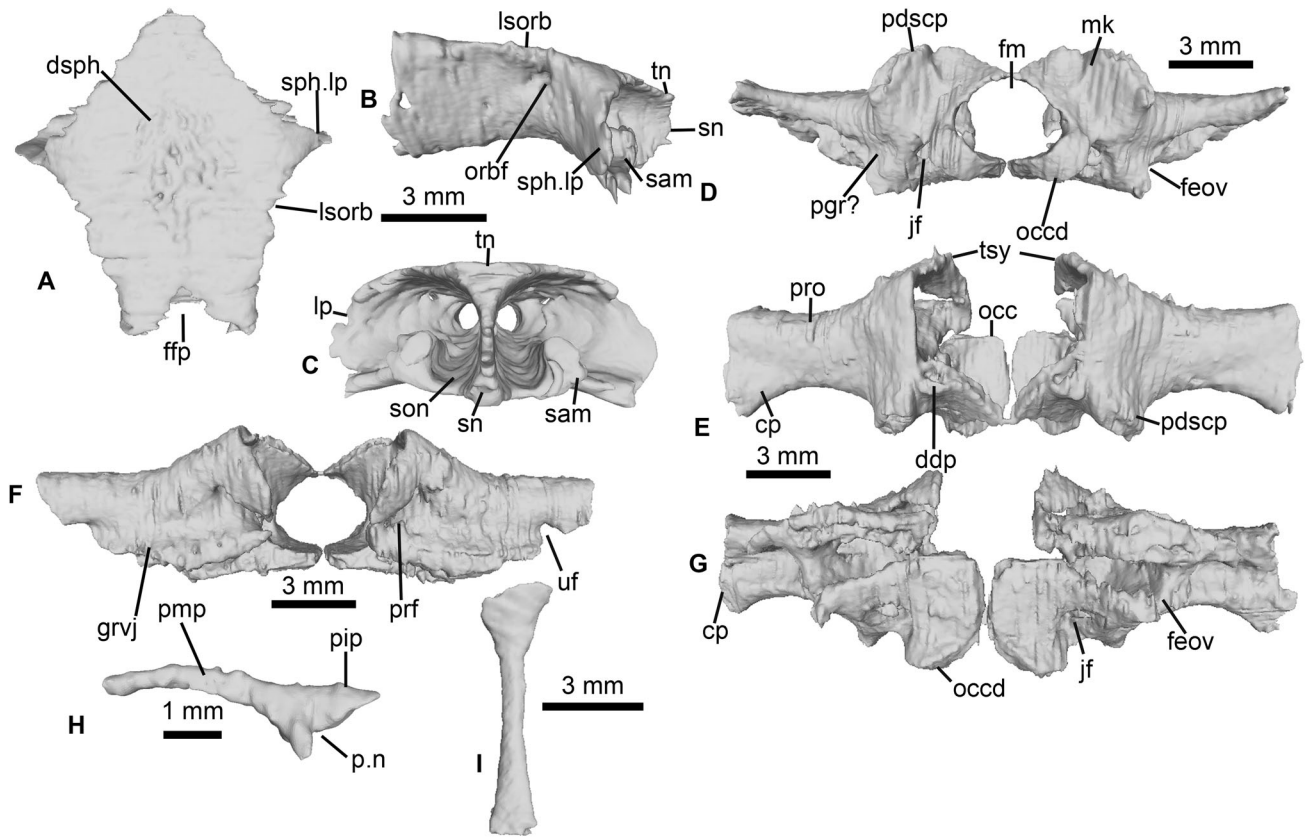


FIGURE 8. Endocranial bones of MNHN.F.QU17381. **A–C**, sphenethmoid in **A**, dorsal; **B**, right lateral and **C**, anterior views; **D–G**, prooticoccipital in **D**, posterior; **E**, dorsal; **F**, anterior; and **G**, ventral views; **H**, left stapes in posterior view; **I**, right hyoid bone in dorsal view. **Abbreviations:** **cp**, crista parotica; **ddp**, depression anterior to the prominentia ducti semicircularis posterioris of the prooticoccipital; **dsph**, dorsal exposure of the sphenethmoid; **feov**, fenestra ovalis; **ffp**, fenestra frontoparietalis; **fm**, foramen magnum; **grvj**, groove for the vena jugularis; **jf**, jugular foramen; **lsorb**, lamina supraorbitalis; **mk**, median keel; **occ**, exoccipital; **occd**, occipital condyles; **orb**, orbitonasal foramen; **pdscp**, prominentia ducti semicircularis posterioris; **pgr?**, putative perilymphatic groove; **pip**, pars interna plectri; **p.n**, notch on the medial surface of the plectrum; **pmp**, processus medialis plectri; **prf**, prootic foramen; **pro**, prootic; **sam**, sella amplificans; **sn**, septum nasi; **son**, solum nasi; **sph.lp**, lateral process of the sphenethmoid; **tn**, tectum nasi; **tsy**, tectum synotium; **uf**, unknown foramen?.

flattened mediolaterally and extends as an elongate protuberance oriented ventrolaterally. The prominentia ducti semicircularis are flanked medially by a depression (oriented dorsoventrally) that is delimited dorsally by a small median keel (Fig. 8D). This keel is similar to one found in MNHN.F.QU17376 (Rage and Roček, 2007:fig. 5B) and NHMB V.R31 (Vasilyan, 2018:fig. 3) but this keel was not visible in MNHN.F.QU17279 (Laloy et al., 2013).

Two large jugular foramina are partially hidden in posterior view by the occipital condyles (Fig. 8D). They open in the lateral wall of the cavum cranii and in the otic capsule. The fenestra ovalis is located on the lateral wall of the prootic (Fig. 8D).

Dorsally, the crista parotica extends laterally into a dorsoventrally flattened processus (ramus lateralis sensu Špinar, 1978) (Fig. 8D, E). A horizontal groove (perilymphatic groove in Fig. 8) extends laterally from the jugular foramen on the posterior surface of the otic capsules and might have housed a perilymphatic canal. This groove is visible in both specimens MNHN.F.QU17279 and MNHN.F.QU17376 (Rage and Roček, 2007; Laloy et al., 2013). The parietal fenestra is large and completely covered dorsally by the frontoparietals.

Anteriorly, the prootic foramen is large and undivided (unlike in MNHN.F.QU17376; see Rage and Roček, 2007: fig.7). The groove for the vena jugularis is visible, extending from this foramen to the lateral margin of the anterior surface of the

prooticoccipital. This groove is shallow and poorly delimited (Fig. 8F), making it similar to the groove in MNHN.F.QU17376 (Rage and Roček, 2007:fig. 7A), and slightly different from that of MNHN.F.QU17279 (Laloy et al., 2013). On the left side of the prooticoccipital, the groove for the vena jugularis ends laterally in a small notch on the lateral side of the prootic. In MNHN.F.QU17376 and two other incomplete braincases of *Thaumastosaurus* (see Rage and Roček, 2007:fig. 7), two unidentified foramina penetrate the anterior surface of the prooticoccipital, piercing the groove for the vena jugularis. In two of the braincases (Rage and Roček, 2007:fig. 7A, C), the most lateral of these foramina forms a notch on the lateral border of the prootic, in a similar location to the notch in MNHN.F.QU17381. These foramina are not known in MNHN.F.QU17279 (Laloy et al., 2013). Medial to the anterior surface of the prominentia ducti semicircularis posterioris, a small depression is present, as in MNHN.F.QU17279 (Fig. 8E). This small depression might be another part of the otic canals.

The lateral wall of the cavum cranii is pierced by three foramina. As mentioned earlier, the posteriormost foramen is connected to the jugular foramen. A large, irregularly shaped opening that leads to the otic capsules is present ventrally at approximately the midlength of the lateral wall. We interpret this single opening to have conveyed both branches of the acoustic nerve (Duellman and Trueb, 1994; Rage and Roček, 2007)

whose specific bony paths are not visible due to poor preservation in this region of the otic capsule. A small rounded foramen, dorsal to this irregular opening, is interpreted as the perilymphatic foramen.

Columellae—Only the ossified portion of the columellae, the plectrum (~stapes), was identified and segmented. Both preserved plectra have the same orientation and position on each side of the braincase, implying they are in anatomical position. The posterior region of the plectrum is bifurcated, with a notch on its medial margin (Fig. 8H). This posterior region is interpreted as the ossified pars interna plectri ('footplate' of Duellman and Trueb, 1994), with the notch on the medial surface serving as an insertion point for the cartilaginous operculum (Bolt and Lombard, 1985; Roček et al., 2016). The pars media plectri is a curved, slender rod that extends laterally between the posterior and posterolateral processes of the squamosal, where the tympanic annulus is located in anurans (Duellman and Trueb, 1994; Sheil, 1999; Roček et al., 2016). The tympanic annulus has not been identified in MNHN.F.QU17381 and MNHN.F.QU17279, although a tympanic membrane was identified in the latter specimen (Fig. 4C), implying that a cartilaginous tympanic annulus was present (Pereyra et al., 2016). As MNHN.F.QU17381 is attributed to the same taxon (see in Taxonomy), we conclude that a tympanic annulus was present in MNHN.F.QU17381.

Hyobranchial Skeleton

Hyoid Bones—The cartilaginous hyoid plate is not visible in the scan data. However, two slender bony elements, the thyrohyal bones, corresponding to the posteromedial processes of hyoid plate, are present. The two elements are oriented antero-medially with their proximal parts almost in contact. They widen at both ends (proximal and distal; Fig. 8I). They are placed ventrally under the first three vertebrae and the exoccipital, and dorsal to the coracoids and clavicle.

Vertebral Column

The vertebral column is similar to the one found and described inside the mummy by Laloy et al. (2013). It is composed of eight presacral vertebrae, one sacral vertebra and a urostyle (Fig. 9). The seven first presacral vertebrae are procoelous (anterior cotyle and posterior condyle; Fig. 10A, B) and the last presacral (eight vertebra) is biconcave (Fig. 10C), indicating an amphicoelous condition. The sacral vertebra is biconvex, with an anterior cotyle and two posterior cotyles (Fig. 10D, E). These conditions of the presacral and sacral vertebrae are characteristics of a diplasiocoelous vertebral column.

Atlas—The atlas articulates with the exoccipitals by two large and laterodorsal-ventromedially elongated cotyles (Fig. 10A), which fuse medially to a protruding lip at the midline, forming a large articular facet with the skull (type III of Lynch, 1971). The vertebral canal is large, with thin lateral walls and thicker ventral and dorsal walls; the latter forms a large base for the short and posteriorly inclined neural spine (Fig. 9B). The postzygapophyses are poorly developed, with a flattened articular surface inclined medioventrally. The centrum is flattened dorsoventrally and possesses a small elliptical condyle in posterior view (Fig. 10B).

Post-atlantal Vertebrae—The centra of the post-atlantal vertebrae are longer than wide and flattened dorso-ventrally (Fig. 9B, C). The centrum of vertebrae II–VII is concave anteriorly and convex posteriorly, indicating a procoelous condition. No vertebra bears ribs.

In lateral view, the neural arch is thin, anteriorly notched, with an enlarged base (Fig. 9B). Arches are non-imbricated. The vertebral canal remains broad until the fifth post-atlantal vertebra.

The neural spines are dorsally elongated and inclined posteriorly, but do not extend beyond the posterior margin of the postzygapophysis. The posteriormost post-atlantal vertebrae (vertebrae VI–VIII) possess a shorter neural spine, which are oriented less posteriorly. The zygapophyses have flat articular processes.

The first post-atlantal vertebra (vertebra II) possesses a pair of large transverse processes, a bit shorter than the sacral transverse processes. In dorsal and ventral views, this first pair of transverse processes are slightly posteriorly arched (Fig. 9A, C). The processes are thicker at their mid-length, with a crest appearing on the anterior face. The second post-atlantal vertebra (vertebra III) possesses the largest transverse processes. They are oriented posterolateroventrally and are moderately widened distally. The transverse processes of vertebra IV have the same distal extension as the sacral apophyses and are oriented lateroposteriorly. The presacral vertebrae V–VII are similar in possessing transverse processes that are thinner and narrower distally than proximally. On vertebra V, they are slightly oriented posterodorsally (Fig. 9B). On vertebrae VI and VII, they are roughly perpendicular to the long axis of the column. Presacral vertebra VIII bears thin transverse processes similar to the one of the previous presacral vertebrae. However, this vertebra is amphicoelous.

Sacral Vertebra—The sacral vertebra possesses two small, well-separated, posterior circular condyles that articulate with the urostyle, and one dorsoventrally flattened elliptical anterior condyle that articulates with the posterior cotyle of the last presacral vertebra (Fig. 10D–F). On the anterodorsal border of the neural arch, a well-developed lamina extends from the base of the prezygapophyses to the base of the neural spine (Figs. 9A, 10D). This kind of lamina is also present on the posterior border of the neural arch (Fig. 10D, E). The sacral transverse processes are subcylindrical in cross section, slightly flattened dorsoventrally, and do not widen posterodistally. A small notch is visible dorsally at the distal margin of each transverse process (Fig. 9A). The neural spine is reduced and anterodorsally oriented.

Urostyle—The urostyle is posteriorly incomplete. The anterior portion of the bone is articulated with the sacral vertebra with two well-separated circular anterior cotyles (fossa cotylae), which protrude laterally from the main shaft of the urostyle (Fig. 10G). The vertebral canal is moderately high, accounting for half the height of the neural arch. The neural arch bears a well-developed thick dorsal process. This also marks the cranial end of a tall and thin dorsal crest that extends throughout the whole preserved portion of the bone and slightly decreases in size posteriorly (Fig. 10H). A spinal foramen is present on each side of the base of the dorsal crest, posteroventrally to the thick dorsal process (Fig. 10H). No transverse processes are present.

Pectoral Girdle

All pectoral bony elements are present in anatomical position (Fig. 11).

Cleithra-Suprascapulae Complexes—The cleithrum and the ossified portion of the suprascapula are fused together, forming a single compound element dorsomedial to the scapula. The cleithrum represents the anterior thickened portion of the compound, and the suprascapular (a mostly cartilaginous element) is ossified on its ventral and posterior margins (Fig. 12A, B). The ramus anterior of this compound bone is long with a thickened anterior margin by the presence of a long lamina recurvata (sensu Špinar, 1972). The margins scapularis and posterior surface of the compound are rounded. There is no ramus posterior.

Scapulae—The scapulae are transversally elongated, with a moderately widened distal end of the processus suprascapularis (Fig. 12C, D). The anterior margin is concave (Fig. 12C). There is no crest on both anterior or posterior margins of the scapulae.

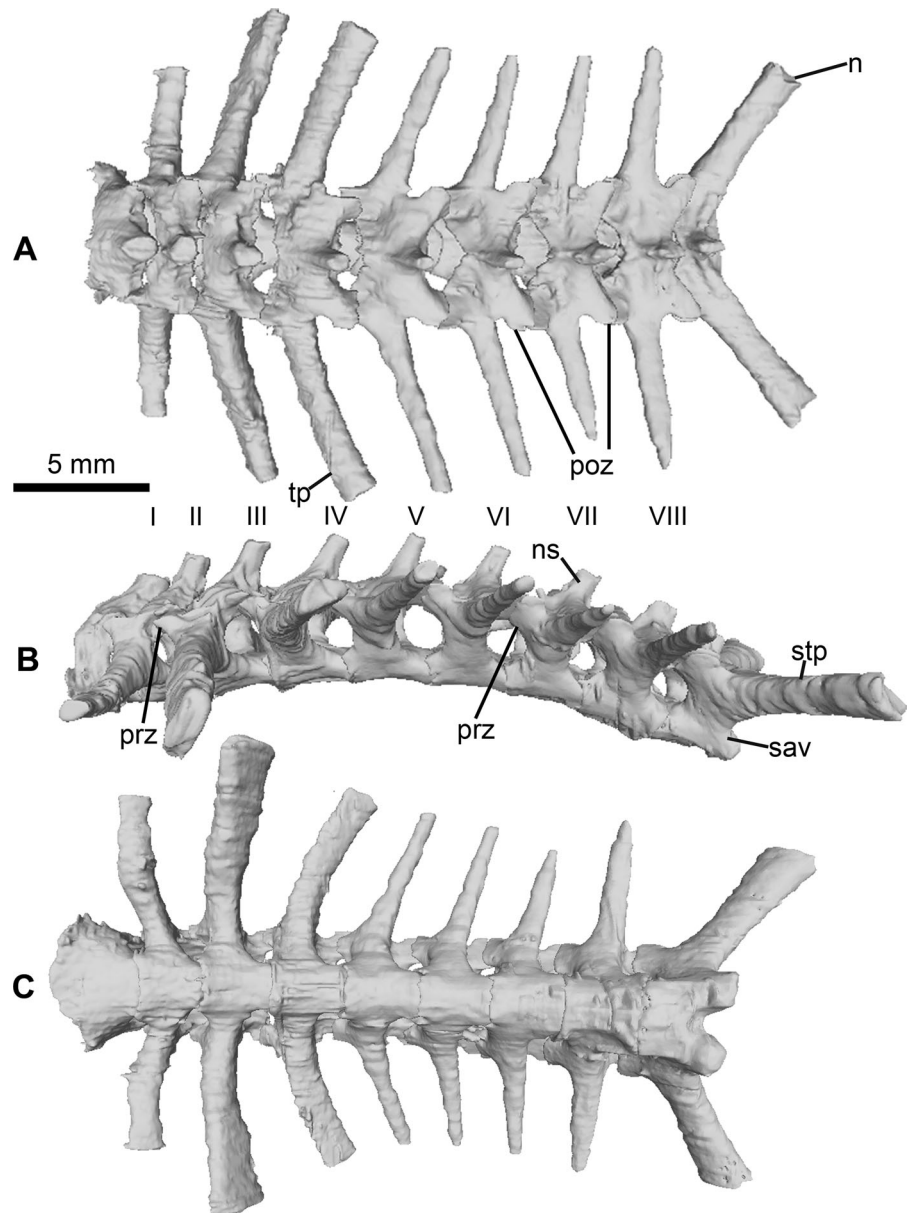


FIGURE 9. Articulated diplasiocoelous vertebral column of MNHN.F.QU17381, without the urostyle in **A**, dorsal; **B**, left lateral; and **C**, ventral views. **Abbreviations:** *ns*, neural spine; *n*, notch on the sacral apophyse; *poz*, postzygapophysis; *prz*, prezygapophysis; *sav*, sacral vertebrae; *stp*, sacral transverse process; *tp*, transverse process.

The processus acromialis and the processus glenoidalis are separated by a moderately wide sinus interglenoidalis (Fig. 12E). The processus acromialis is wider than the processus glenoidalis and has a rounded lateral margin; in dorsal view, it hides the processus glenoidalis and the sinus interglenoidalis. In medial view, a well-developed medial crest is present on the processus glenoidalis and extends from the ventral border to the base of the processus anterior (Fig. 12C). No lamina is present on the processus anterior. The glenoid fossa is moderately extended dorsoventrally (Fig. 12C).

Coracoids—The coracoids are transversally oriented, with a thickened, cylindrical processus glenoidalis. This latter of both coracoids and scapulae are almost in contact with each other, leaving a gap for the paraglenoid cartilage. The processus epicoracoidalis is flat and anteroposteriorly enlarged (much larger than the processus glenoidalis) and bears a convex medial margin (Fig. 12F). The processus epicoracoidalis extends anteriorly, forming a hook that extends close to the medial end of the clavicles. Both coracoids are in contact with each other medially, but

do not overlap (Fig. 11). This is characteristic of a firmsternal condition (sensu Cope, 1864; Boulenger, 1886). The left coracoid is badly damaged, with the processus glenoidalis broken off from the main shaft (Fig. 12G, H). On the anterior and posterior margins of the main shaft, vertical laminae can be observed, forming a bony callus linking the two broken parts. This callus is also visible in ventral view, expanding the width of the shaft of the coracoid (Fig. 12G, H). This damage can be linked to the missing part of the left clavicle. The near-absence of disarticulated bones (except the ilia) and the presence of a mineralized skin on this part of the specimen seems to exclude the diagenesis hypothesis. The absence of any hole indicating a missing part in the area of the coracoid and clavicle (the nearest holes are located anteriorly on the ventral face of the specimen) excludes the extraction hypothesis. This leaves only the hypothesis of a damage received before the burial of the animal. In extant anurans, the healing process for bone fractures is slow compared with mammals (Cameron et al., 2012; Egawa et al., 2014). Given that the broken coracoid seems partially fused back and bears a

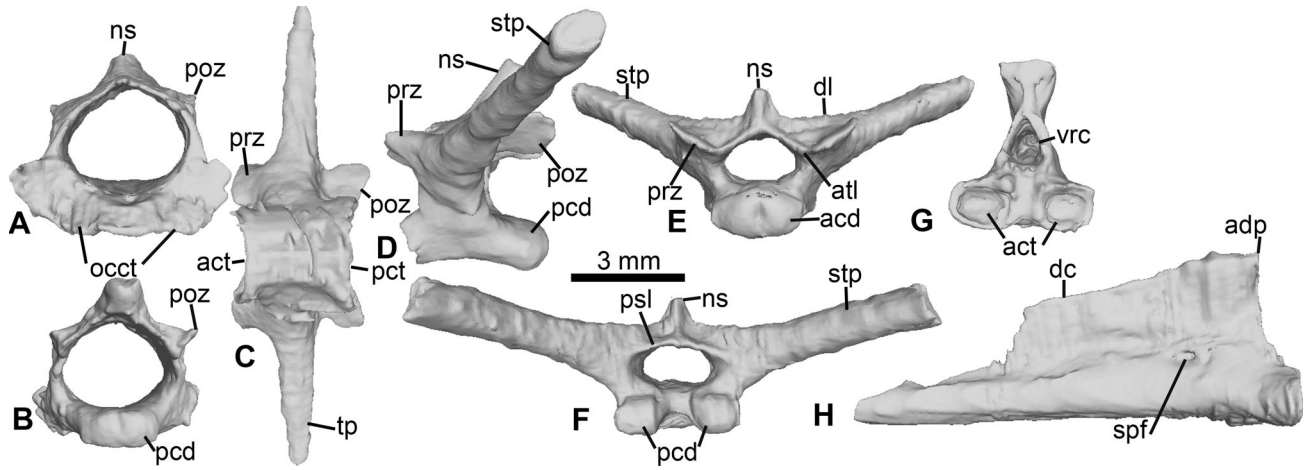


FIGURE 10. Vertebral elements of the column of MNHN.FQU17381. **A–B**, atlas in **A**, anterior and **B**, posterior views; **C**, VIII presacral vertebra in ventral view; **D–F**, sacral vertebrae in **D**, lateral; **E**, anterior and **F**, posterior views; **G–H**, urostyle in **G**, anterior and **H**, lateral views. **Abbreviations:** **acd**, anterior condyle; **act**, anterior cotyle; **adp**, anterodorsal process; **atl**, anterior lamina; **dc**, dorsal crest; **dl**, diapophyseal lamina; **ns**, neural spine; **occt**, occipital cotyle; **pcd**, posterior condyle; **poz**, postzygapophysis; **prz**, prezygapophysis; **psl**, posterior lamina; **spf**, spinal foramen; **stp**, sacral transverse process; **vrc**, vertebral canal.

bony callus, this may represent a scar from a wound received during the life of the animal.

Clavicles—The right clavicle is completely preserved, whereas the left clavicle only preserves its lateral part (Fig. 11). This could be linked to the injury visible on the left coracoid. The clavicles are almost as long as the coracoids and slightly arched anteriorly. In dorsal view, the lateral part is bifurcated and articulates with the processus acromialis and processus glenoidalis of the

scapulae, forming a part of the articular fossa for the humeri. The sulcus cartilagine praecoracoidealis extends posteriorly on the length of the bone (Fig. 12I). The clavicles are in contact, slightly overlapping dorsoventrally the processus glenoidalis of the coracoids. The extremitas medialis of the clavicle is not in contact with the medial part of the coracoids (Fig. 11).

Sternum—The sternum is fully ossified as an elongate slender element. The sternum is expanded both anteriorly and

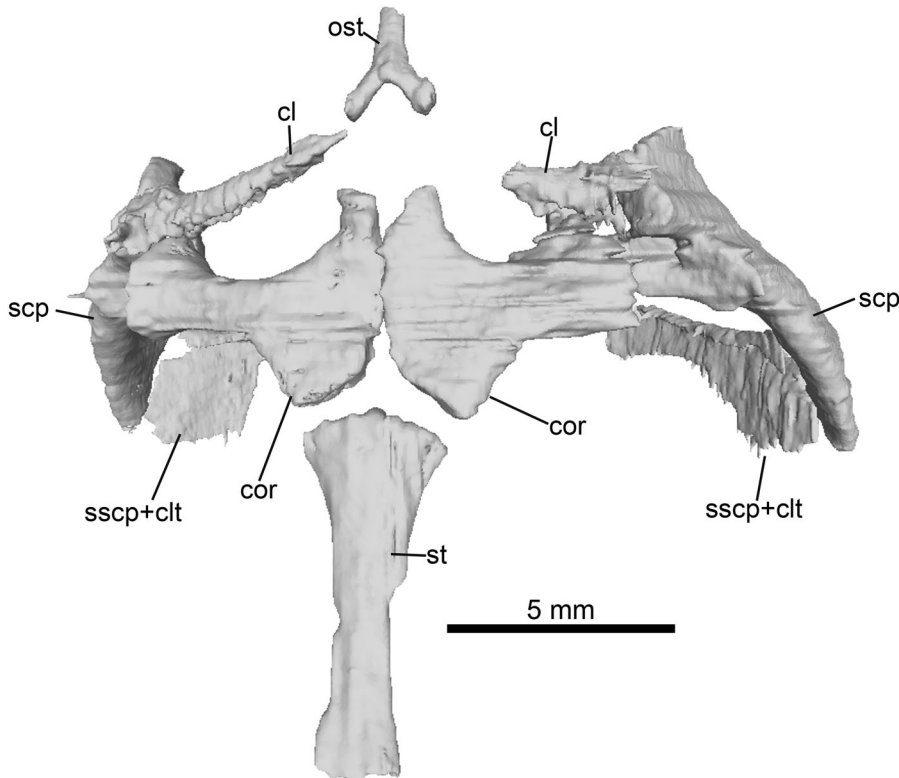


FIGURE 11. Articulated bony pectoral girdle of MNHN.FQU17381 in ventral view. **Abbreviations:** **cl**, clavicle; **cor**, coracoid; **ost**, omosternum; **scp**, scapula; **sscp + clt**, suprascapular + cleithrum; **st**, sternum.

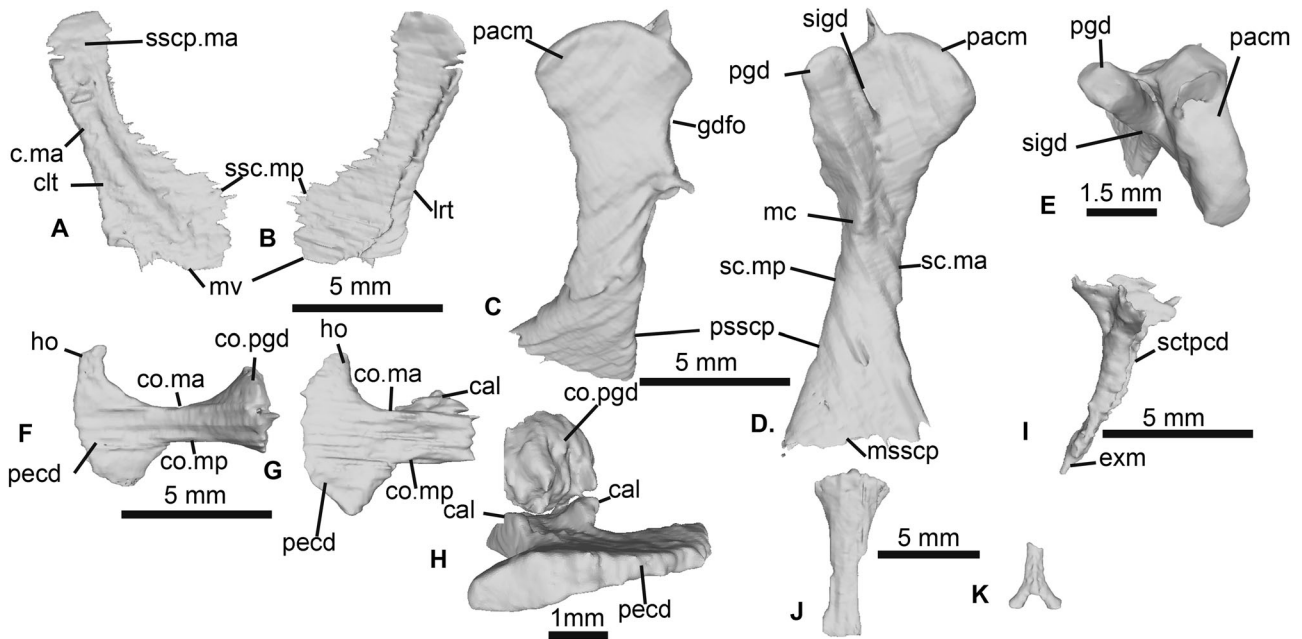


FIGURE 12. Bony elements of the pectoral girdle of MNHN.F.QU17381. **A–B**, left suprascapular + cleithrum complex in **A**, lateral and **B**, medial views; **C–E**, right scapula in **C**, lateral; **D**, medial; and **E**, ventral views (orientation follows Duellman and Trueb, 1994:346, figs. 13–35); **F**, right coracoid in dorsal view; **G–H**, left coracoid in **G**, ventral and **H**, medial views; **I**, right clavicle in dorsal view; **J**, sternum in dorsal view; **K**, omosternum in dorsal view. **Abbreviations:** **cal**, callus; **clt**, cleithrum; **c.ma**, cleithrum anterior margin; **co.ma**, anterior margin of the coracoid; **co.mp**, posterior margin of the coracoid; **co.pgd**, processus glenoidalis of the coracoid; **exm**, extremitas medialis; **ho**, hook; **lrt**, lamina recurvata; **mc**, medial crest; **msscp**, margo suprascapularis; **mv**, margo vertebralis; **pacm**, processus acromialis; **pecd**, processus epicoracoidalis; **pgd**, processus glenoidalis; **psscp**, processus suprascapularis; **ra**, ramus anterior; **sc.ma**, anterior margin of the scapula; **sc.mp**, posterior margin of the scapula; **sctpcd**, sulcus cartilagineus praecoracoidealis; **sigd**, sinus interglenoidalis; **sscp.ma**, anterior margin of the suprascapular + cleithrium; **sscp.mp**, posterior margin of the suprascapular + cleithrium.

posteriorly with the former being larger than the latter (Fig. 12J). It is strongly similar to the one found in *Pyxicephalus adspersus* (Sheil, 1999:fig. 5B).

Omosternum—The omosternum is ossified, denoting a firmisternal condition of the girdle (Cope, 1864; Boulenger, 1886; Duellman and Trueb, 1994). It is an inverted ‘Y’-shaped bone with a bifurcated posterior end (Fig. 12K).

Forelimb

Humeri—Only the proximal parts of both humeri are preserved, although badly damaged. Only the proximal articular facet of the right humerus is preserved with the glenoid fossa of the pectoral girdle. The left humerus, however, is more

completely preserved, with both its proximal head and part of the diaphysis (Fig. 13A). The left humerus displays a moderately developed crista ventralis, and lacks a proximal crista paraventralis (Fig. 13A).

Pelvic Girdle

Ilia—The two ilia are partially preserved. The left one is only a fragment of the distal part (around 1.4 mm in length), but the right one is more completely preserved, which represents about half or more of the complete iliac shaft (= iliac shaft of Gómez and Turazzini, 2016). It bears a high and well-developed dorsal crest (Fig. 13B). Unfortunately, the rest of the ilium (distal half) is not preserved, as in the first mummy (MNHN.F.QU17279; Laloy et al., 2013).

TAXONOMY

MNHN.F.QU17381 is the holotype and only known specimen of *Bufo servatus*, erected and illustrated by H. Filhol (1876, 1877: pl. 51; fig. 412) based on a first description done in 1873 (Filhol, 1873). Filhol named the specimen *Bufo servatus* (Filhol, 1876) without giving characters to diagnose the taxon or differentiate it from the other *Bufo* species. He placed it in Bufonidae based on the presence of parotoid glands (see Filhol, 1876, 1877). Martín et al. (2012) considered the name *B. servatus* as valid and did not discuss the criteria of validity. Sanchiz (1998) considered the name a nomen vanum (Mones, 1989), a taxonomic term considered in the ICZN as referring to a name based on a type inadequate for definitive diagnosis, but he did not question its validity. Our work shows that the specimen is informative, hence *B. servatus* cannot be a nomen vanum. The specimen has

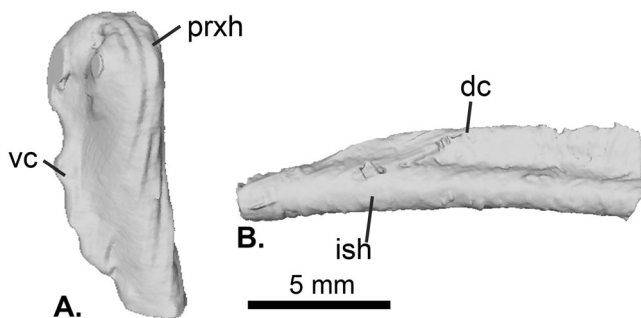


FIGURE 13. Humerus and ilium of MNHN.F.QU17381. **A**, left humerus in lateral view; **B**, right ilium in lateral view. **Abbreviations:** **dc**, dorsal crest; **ish**, iliac shaft; **prxh**, proximal head; **vc**, ventral crest.

been figured, and according to article 12.2.7 of the International Code of Zoological Nomenclature (ICZN), this supports the validity of a name if published before 1931. The name *B. servatus* can therefore be considered as valid. Moreover, this name has been cited several times since its original description (Piveteau, 1927; Tihen, 1962; Sanchiz, 1998; Rage, 2006) and its validity was not often discussed.

Attribution to *Bufo* was based on the presence of what Filhol identified as two parotoid glands located right behind the eyes (Filhol, 1876, 1877). However, several studies (Piveteau, 1927; Tihen, 1962; Rage, 2006, 2016) considered this observation as erroneous. We here confirm this proposition and suggest that the structures interpreted by Filhol as parotoid glands are artefactual skin ridges caused by post-mortem desiccation during the natural mummification process. In addition, on specimen MNHN.F.QU17381, we observed teeth on the maxillary, which are lost in Bufonidae (Duelleman and Trueb, 1994). Moreover, the vertebral column is diplasiocoelous, which is characteristic of Ranoidea. Finally, the presence of a firmisternal pectoral girdle as well as an ossified omosternum also reinforce the attribution to a ranoid taxon. We therefore conclude that MNHN.F.QU17381 cannot be attributed to Bufonidae or *Bufo*. Furthermore, the skeleton of specimen MNHN.F.QU17381 is almost morphologically identical to the one of MNHN.F.QU17279 and to the skull of MNHN.F.QU17376, both of which have been attributed to the genus *Thaumastosaurus* as *T. gezei* (Roček and Lamaud, 1995; Laloy et al., 2013). We therefore attribute the specimen MNHN.F.QU17381 to *Thaumastosaurus* De Stefano, 1903 by the following combination of characters: (1) dermal bones covered with ornamentation that differs from the one found in *Latonia*, *Pelobates*, *Eopelobates* and *Ceratophrys*; (2) nasals (partially) and frontoparietals co-ossified with each other and with sphenethmoid and frontoparietals co-ossified with prooticooccipital; (3) rhomboid part of sphenethmoid exposed on skull roof; (4) no bony contact between the frontoparietal and squamosal; (5) anterior tip of the parasphenoid does not extend between palatines; (6) processus posterolateralis and ramus paroticus of squamosal merged, articulating with the crista parotica of the otic capsules (Rage and Roček, 2007; Vasilyan, 2018).

At the species level, MNHN.F.QU17381 differs from *Thaumastosaurus bottii* and *T. wardi* by having the lamella alaris of the squamosal extending anteriorly along the entire ventral margin of the orbit (lamella alaris ends anteriorly at the midlength of the orbit in *T. bottii* and *T. wardi*). However, the lamella alaris of the squamosal of the neotype of *T. bottii* (Roček and Lamaud, 1995:fig. 5) is almost entirely broken off, and the length of its anterior extension cannot be assessed. Other squamosals attributed to *T. bottii* are either broken or present as an eroded anterior part of the bone (Vasilyan, 2018: fig. 4G–H), making comparison difficult. This difference on the squamosals might only result from a different preservation, as no skull of *T. bottii* is as complete as the holotype of “*T. gezei*”. This difference is not attributed to ontogeny.

The specimen MNHN.F.QU17381 furthermore differs from *T. bottii* by having a shallow, poorly delimited groove for the vena jugularis interna on the prooticooccipital complex (Fig. 8F), whereas *T. bottii* possesses a narrower and more sharply delimited groove (Roček and Lamaud, 1995; Vasilyan, 2018). Other proposed morphological differences for the two Quercy species are located on the premaxilla (Vasilyan, 2018), which is unfortunately lost in MNHN.F.QU17381, thus preventing any further comparison with *T. bottii*.

Among the mummies attributed to *Thaumastosaurus*, MNHN.F.QU17381 presents strong resemblances with MNHN.F.QU17279, the former holotype of “*Rana plicata*” (attributed to *Thaumastosaurus gezei* by Laloy et al., 2013), with the anterior extension of the squamosal separating the

maxillary from the orbit by a thin strip, and a postcranial identical in both mummies. It also presents a strong resemblance to MNHN.F.QU17376, with the palatines medially in contact with each other and a groove for vena jugularis interna, which also resembles the one of MNHN.F.QU17279 (Laloy et al., 2013). However, a few differences can be seen between the skull of MNHN.F.QU17381 and those of MNHN.F.QU17279 and MNHN.F.QU17376. First, the nasals are partially fused in MNHN.F.QU17381 whereas they are separated in MNHN.F.QU17279 and fully fused in MNHN.F.QU17376. The ornamentation of the sphenethmoid in MNHN.F.QU17381 is more developed than in MNHN.F.QU17279 (Laloy et al., 2013: fig. 3A) but less than in MNHN.F.QU17376, where the limits between the sphenethmoid and the neighboring dermal bones are obscured by the ornamentation (Rage and Roček, 2007:fig. 1A). As in MNHN.F.QU17279, the prootic foramen is not divided into two portions. However, as mentioned in the description, a notch can be observed on the lateral margin of the anterior surface of this bone of MNHN.F.QU17381, which is continuous with the groove for the vena jugularis and the unknown foramina found in MNHN.F.QU17376 and other *Thaumastosaurus* sp. skulls (Rage and Roček, 2007:fig.7A–C). The extension of the lamella alaris in MNHN.F.QU17381 is also thinner than in MNHN.F.QU17376, resembling the one found in MNHN.F.QU17279. Those differences can be linked to ontogeny (see Ontogenetic Assessment below).

MNHN.F.QU17381 shares with both MNHN.F.QU17376 and MNHN.F.QU17279 (attributed to *T. gezei*) the anterior extension of the squamosal forming the whole lateral wall of the orbit and the shape of the groove for the vena jugularis interna which is shallow and wide; these are listed in the revised diagnosis. The specimen MNHN.F.QU17381 can therefore be assigned to “*Thaumastosaurus gezei*.”

A consequence of this attribution is that *T. gezei* and *B. servatus* are subjective synonyms. Considering the available names and excluding those invalidated by homonymy, *Bufo servatus* Filhol, 1877 is the oldest valid name. We therefore here consider the new combination *Thaumastosaurus servatus* (Filhol, 1877).

ONTOGENETIC ASSESSMENT

Based on Rage and Roček (2007) and Laloy et al. (2013), the following cranial characters can be used to assess the skeletal maturity of *T. servatus* specimens: relation between the nasals, palatines, and ornamentation of the sphenethmoid. In skeletally mature (sensu Griffins et al., 2021) *T. servatus*, the contralateral nasals are fused medially, as are the palatines where only a suture is still visible between the bones, and the ornamentation of the sphenethmoid is well developed, with a similar pattern present in the surrounding bones. These conditions are also present in MNHN.F.QU17376 (Rage and Roček, 2007). This specimen can therefore be considered skeletally mature. In MNHN.F.QU17279, the lack of contact between the nasals (and similarly for the palatines), and the subdued ornamentation of the sphenethmoid demonstrate skeletal immaturity (sensu Laloy et al., 2013). In MNHN.F.QU17381, the slight medial contact between the nasals, the separation of palatines by a thin fissure, and the faint ornamentation of the sphenethmoid suggest a slightly greater skeletal maturity than MNHN.F.QU17279. MNHN.F.QU17381 is therefore more skeletally mature than MNHN.F.QU17279, but less than MNHN.F.QU17376.

PHYLOGENY

Thaumastosaurus servatus was first suggested to have affinities with Leptodactylidae, especially the South American

Ceratophryidae, based on cranial characters (Roček and Lamaud, 1995; Rage and Roček, 2007). Later, Laloy et al. (2013), based on a subcomplete skeleton found within the mummy, MNHN.F.QU17279, carried out a phylogenetic analysis, using a matrix modified from Báez et al. (2009). This latter dataset (see Báez et al., 2009) was itself based on the matrix proposed by Fabrezi (2006), modified for ceratophryid phylogeny. The dataset from Báez et al. (2009) includes 42 taxa, three of which are extinct taxa, scored for 75 characters. Laloy et al. (2013) enlarged the sample by adding 40 taxa from Evans et al. (2008), whose matrix was also modified from the dataset of Fabrezi (2006; see Evans et al., 2008 for modifications) and included genera as OTUs. Evans et al. (2008) deleted one character (the dorsal exposure of sphenethmoid) and redefined another (character 1 in Evans et al., 2008; Laloy et al., 2013). Laloy et al. (2013) found *Thaumastosaurus* within the Natatanura, as the sister-taxon of a clade that contains *Pyxicephalus* and *Cornufer* (a ceratobatrachid).

Báez and Gómez (2018) modified the dataset from Báez et al. (2009) by adding 29 neobatrachian taxa and redefining some characters to test the impact of hyperossification characters within the dataset. The taxon sample was greatly enlarged (from 42 to 71 taxa), and 68 characters were added (for a total of 143 characters), and several characters from the old dataset were redefined. Among the taxa, *T. servatus* (“*T. gezei*” in the dataset of Báez and Gómez, 2018) was included, using the new information from MNHN.F.QU17279 described by Laloy et al. (2013). They also found *T. servatus* within hyperossified Natatanuran, but as more closely related to *Pyxicephalus adspersus* Tschudi, 1838 (African bullfrog) than to *Cornufer guentheri* Boulenger, 1884 (Solomon island leaf frog). This topology could be explained by the limited inclusion of only five extant natatanurans taxa in their dataset. We therefore expanded the dataset of Báez and Gómez (2018) with 15 extant natatanurans taxa (see Materials and Methods). We added seven more taxa from Pyxicephalidae (*Arthroleptella lightfooti*, *Aubria subgillata*, *Cacosternum boettgeri*, *Cacosternum namaquense*, *Natalobatrachus bonebergi*, *Strongolypus grayii* and *Tomopterna tuberculosa*), represented previously only by *Pyxicephalus adspersus* (the sister-taxon to *T. servatus*, according to Báez and Gómez, 2018).

Most extant anurans are placed within Neobatrachia (Feng et al., 2017), which includes two clades, Hylroides and Ranoides. The latter clade can be divided into three subclades: Microhylidae (*Hylambates*, *Dermatonotus* and *Asterophrys* in our dataset), Afrobatrachia (*Arthroleptis* and *Hylambates* in our dataset) and Natatanura (represented by 19 taxa in our matrix, of which 14 were not included in any of the matrices mentioned above). The phylogenetic relationship among these three clades remains contentious. Natatanura represents the vast majority of extant Ranoides (Frost et al., 2006; Pyron and Wiens, 2011), but its fossil record is scarce and mostly composed of isolated fragmentary bones (Rage, 1984b; Sanchiz, 1998; Gardner and Rage, 2016). Given the good preservation and completeness of *T. servatus* fossils and their geological age, understanding its precise position within Natatanura is essential to better understanding the evolution of the clade and assessing the timing of its diversification. For this, several phylogenetic analyses were performed.

Unconstrained Analysis

Equal Weight Analysis, Unordered—We obtained 140 MPTs (most parsimonious trees) of 1355 steps (CI = 0.122; RI = 0.326) with the analysis performed under equal weight, with all multi-state characters treated as unordered (Fig. S4A). The strict consensus shows numerous polytomies, with Neobatrachia not recovered. *Thaumastosaurus servatus* is recovered as a sister-taxon to a trichotomy composed of hyperossified ranoides,

Pyxicephalus adspersus, *Aubria subsigillata* and *Cornufer guentheri* (Fig. S4A). The clade is supported by 26 synapomorphies. Many of them have been considered to be associated with Ranoides and Natatanura, which are not recovered in this analysis.

Equal Weight Analysis, Ordered—With cline characters ordered, we obtained 90 MPTs, of 1373 steps (CI = 0.137; RI = 0.422; Figs. 14A, S4B). The strict consensus is more resolved than with unordered states, but it still presents numerous polytomies. A majority of the ranoids taxa (excluding the three microhylids) are clustered together (Figs. 14A, S4B), forming a “Ranoides” clade. This restricted “Ranoides” is supported by nine synapomorphies but has poor bootstrap support (less than 5%) and moderate Bremer support. Among those synapomorphies, the ossification of omosternum (101: 0->1) is uniquely shared by members of this clade; it is present in almost all taxa forming the “Ranoides” clade, except in *Cacosternum*. Another one, non-overlapping coracoids (104: 0->1), is convergent with only the Microhylids (see Appendix S in Supplemental Data 1 for the detailed list).

The presence of an ossified omosternum is particularly important in several phylogenies of Ranoides and Natatanura, as various authors have proposed it as a synapomorphy for either clade (Lynch, 1973; Laurent, 1986; Scott, 2005; Frost et al., 2006). Most natatanuran taxa display this character, although it is lost in some taxa typically ranked as genera. It is present in the Afrobatrachia but not in the Microhylidae. Another interesting synapomorphy recovered for both “Ranoides” clade and Microhylidae is the presence of non-overlapping epicoracoids (present in all extant Ranoides, as mentioned in Lynch, 1973; Trueb, 1973; Frost et al., 2006). This character represents a firmisternal condition for the pectoral girdle, classically associated with Ranoides (Lynch, 1973; Trueb, 1973; Duellman and Trueb, 1994). However, this condition is also found as a synapomorphy for Dendrobatidae (Trueb, 1973; Frost et al., 2006).

Thaumastosaurus servatus is found within “Ranoides,” recovered as a sister-taxon to a trichotomy composed of the extant hyperossified Ranoides (Fig. 14A). Nine synapomorphies were recovered, almost all of them based on cranial elements, and six of which are hyperossification-linked characters, such as the presence of a supraorbital flange on the frontoparietals (6: 0->1), a contact between squamosals and nasals (11: 0->1; lost in *Cornufer guentheri*) and the presence of a heavily ornamented external surface of the pars facialis of the maxillae (50: 0->2; see Appendix S6 in Supplemental Data 1 for the detailed list). This clustering of hyperossified ranoids seems mainly moderately supported by the convergent evolution of hyperossification characters present on the skull, and is quite similar to the previous analysis, where *T. servatus* was recovered, close to extant hyperossified ranoids (Laloy et al., 2013; Báez and Gómez, 2018).

The two afrobatrachians (*Arthrolepis adolfifriederici* and *Hylambates verrucosus*) are recovered in a clade with *Arariphrynus placidoi* (Fig. 14A), which is poorly supported by the loss of the ossified style of the sternum (102: 1->0), the reduction of the width of the glenoid fossa (112: 1->2; relative to the width of the shaft), the loss of the posterolateral process of the hyoid plate (67: 1->0) and the reduction of the posterodorsal expansion of the ischium (131: 1->0). Of those four synapomorphies, only the reduction of the glenoid fossa is scored for *A. placidoi*. The latter is recovered as the sister-taxon of *Phlyctimantis*, supported by three synapomorphies, which are the reduction of the length of the urostyle (92: 1->0), relative to the presacral vertebral length, a pars facialis of the maxillae which decrease abruptly in height in the orbital region (49: 0->1) and a change in the shape of the occipital condyles, which become stalked (40: 0->1). In addition, the *A. placidoi* postcranial is not well-known, and the synapomorphies for the “Ranoides” clade recovered (mentioned earlier) are not known in this taxon.

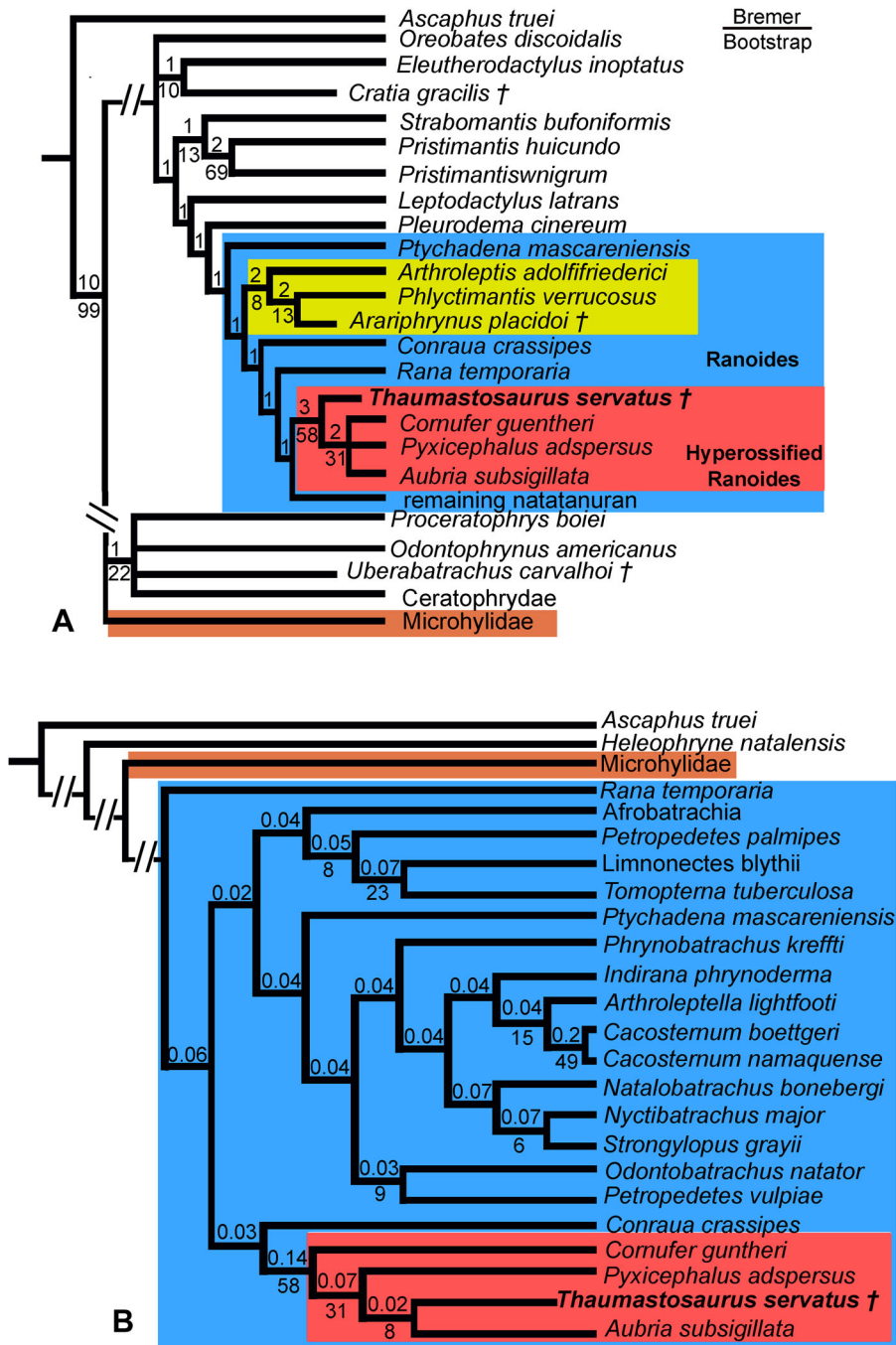


FIGURE 14. Reduced consensus trees from two analyses. **A**, simplified strict consensus of 90 MPTs of 1373 steps (CI=0.137, RI=0.422) from the analysis under equal weight (EW), multistate characters ordered; **B**, simplified strict consensus of two MPTs of 67 steps (CI=0.168, RI=0.548) from the analysis under implied weight (IW) with $k=7$, multistate characters ordered. The † symbol represents extinct taxa, the red area represents hyperossified ranoid taxa, the blue area represents the “Ranoides,” the yellow area represents the clade Afrobatrachia + *Arariphrynus placidoi*, the brown area represents the microhylids (all colors visible only online).

Implied Weighted Analyses, Ordered—When using implied weighting with a low concavity constant ($k=3$), we obtained one fully resolved tree of 91.30 steps (CI=0.164; RI=0.533; Fig. S5). Neobatrachia was recovered as monophyletic, with *Heleophryne* as a sister-taxon to all others neobatrachian. The neobatrachian clade is poorly supported by six synapomorphies, including the presence of palatines (27: 0→1; see Appendix S6 in Supplemental Data 1 for the detailed list). Although not unique to the clade, this synapomorphy is commonly used, along other characters coded here but not recovered as synapomorphies for the clade (the loss of free ribs in adults and a bicondylar articulation between the sacral vertebra and the urostyle; Báez

et al., 2009) to characterize neobatrachian taxa. Another synapomorphy proposed for this clade, the presence of a taeniae tecti medialis in the frontoparietal (Haas, 2003) was not recovered, likely due to the fact that this character was not scored for a majority of the taxa in the dataset.

We recovered a monophyletic “Ranoides” (excluding Microhylidae), still supported by seven synapomorphies, including six found previously. *T. servatus* is placed as a sister-taxon to the crown-clade of Pyxicephalinae (Fig. S5 in Supplemental Data 1). This clade is moderately supported by 12 synapomorphies on cranial and postcranial characters (see Appendix S6 in Supplemental Data 1 for the detailed list). One of them, the presence

of a contact between squamosals and nasals (11: 0→1), is interesting as it is considered a marker for hyperossification (Báez and Gómez, 2018; Paluh et al., 2020) and is recovered only in Pyxicephalinae and Ceratophryidae.

When using a higher constant value ($k=7$), we obtained two MPTs of 66.96 steps (CI = 0.168; RI = 0.548). In the strict consensus (Fig. 14B; Fig. S6), *T. servatus* is placed within Pyxicephalinae, as a sister-taxon to *Aubria subsigillata* (brown ball frog). This clade is poorly supported by a single synapomorphy, the absence of odontoids on palatines (reversion to the plesiomorphic state). Pyxicephalinae is supported by three synapomorphies, the development of a contact between nasals and squamosals (11: 0→1), the ossification of the planum anteorbitale of the sphenethmoid (33: 0→1) and the development of a process lateral to the anterior process of the hyale (anterior process of Duellman and Trueb, 1994; such as for example on *Morerella cyanophthalma*, Rödel et al., 2009:fig. 5a; 64: 0→1; unknown in *T. servatus*). Only one of these was found in the previous analysis (contact between nasals and squamosals). As mentioned above, this character is retrieved as a synapomorphy for the Ceratophryidae (Báez and Gómez, 2018). *Cornufer guentheri* was placed as a sister-taxon to Pyxicephalinae (including *T. servatus*), supported by 10 synapomorphies. Many of these were recovered in the equal weighting analysis, and are linked to hyperossification characters such as the contact of nasals along most of their medial margin (3: 0→2), the development of tectum supraorbitale on the frontoparietals (6: 0→1) or the development of the ramus paroticus of the squamosals, overlapping prootics (14: 1→2; see Appendix S6 in Supplemental Data 1 for the detailed list).

When using an even higher constant value ($k=12$), we retrieved one fully resolved MPT of 50.89 steps (CI = 0.171, RI = 0.558; Fig. S7). *T. servatus* is recovered in the same position as before, within Pyxicephalinae, with *C. guentheri* as the closest taxon to all Pyxicephalinae. *A. placidoi* is placed once again within Afrobatrachia (as when using equal weight), supported by the same synapomorphies.

Constrained Analyses

Relationships within Ranoides and Natatanura have always been controversial (Lynch, 1973; Clarke, 1981; Scott, 2005; Frost et al., 2006; Pyron and Wiens, 2011), with various clades lacking morphological synapomorphies. This can be observed in our analysis as well, as we did not recover the Ranoides as a clade, but only a subset of these excluding microhylids (see Figs. S4–S7).

However, molecular datasets have yielded a better resolution of their relationships, especially with large datasets (Frost et al., 2006; Pyron and Wiens, 2011; Feng et al., 2017; Jetz and Pyron, 2018). Some uncertainties remain, with some clades still lacking clear support (see Pyron and Wiens, 2011). Conflict still exists around the position of Afrobatrachia, either as a sister-taxon to Microhylidae (Pyron and Wiens, 2011; Jetz and Pyron, 2018) or to Natatanura (Feng et al., 2017). We choose constrained analyses under two topologies, to see if changes in the relationship inside Ranoides could impact the placement of *T. servatus*.

Equal Weight Analysis, Ordered—When using a topology inferred on the phylogeny of Jetz and Pyron (2018) as a constraint, we recovered 22 MPTs with a score of 1586 steps. The strict consensus (CI = 0.149, RI = 0.479) places *T. servatus* in a trichotomy with the two pyxicephalines (Fig. S8). The clade is strongly supported by 13 synapomorphies, including the presence of a contact between nasals and squamosals (11: 0→1), the expansion of the zygomatic ramus of the squamosals, allowing for its articulation with the maxillae (10: 1→2), the presence of a distal expansion of the crista parotica (39: 0→1) and the

enclosurement of the pathway for the occipital artery into a canal (7: 0→2; see Appendix S6 in Supplemental Data 1 for the detailed list). Neither Ranoides nor Hyloides are recovered as a clade. This is linked to the instability of one taxon, *A. placidoi*, which is recovered either as an hyloid (in 72% of the trees) or as a ranoid. When excluding this taxon, we recovered six MPTs with a score of 1580 (CI = 0.158, RI = 0.481). In the strict consensus, we recovered both Ranoides and Hyloides, and *T. servatus* is placed in the same trichotomy, supported by the same synapomorphies (Fig. S9).

When using a topology inferred on the phylogeny proposed by Feng et al. (2017) as a constraint, we recovered four MPTs, with a score of 1574. In the strict consensus tree (CI = 0.137, RI = 0.425; Fig. S10), *T. servatus* was recovered in the same position as with a topology inferred on the phylogeny of Jetz and Pyron (2018), in a trichotomy with the two pyxicephalines taxa, supported by 17 synapomorphies, 13 of them recovered in the previous analysis, with an additional four, the partial ossification of the septum nasi of the nasal capsule (34:0→1), the ossification of the crista parotica (38: 0→1), the translocation of the craniomandibular joint to a position well posterior to occiput (61: 0→2) and the presence of anterolateral processes on the hyoid plate (64: 0→1; not scored for *T. servatus*).

Implied Weight Analyses ($k=7$), Ordered—When using implied weights, and using a topology inferred on the phylogeny of Jetz and Pyron (2018) as a constraint, we obtained one tree of 72.01 steps (CI = 0.150, RI = 0.459), with *T. servatus* still found within Pyxicephalinae, as a sister-taxon to the extant Pyxicephalinae (Figs. 15, S11), a placement similar to the one found with a low constant value ($k=3$) using implied weighting (Fig. S4). This clade is well-supported by the same 13 synapomorphies recovered in the previous analysis constrained on the same topology.

When constraining the analysis using the topology inferred from the analysis of Feng et al. (2017), we also obtained one tree of 71.79 steps (CI = 0.151, RI = 0.486) fully resolved (Fig. S12). The position of *T. servatus* is identical as before, as the closest taxon to the Pyxicephalinae, well supported by the same 13 synapomorphies.

Discussion—The various analyses confirm the placement of *Thaumastosaurus* within Ranoides, more precisely within Natatanura. This position is mainly justified by several postcranial characters, such as the ossified omosternum and non-overlapping coracoids. This placement highlights the importance of postcranial characters to reduce the impact of homoplasy found in the skull characters of anurans (Duellman and Trueb, 1994; Báez and Gómez, 2018) and to correctly assess the position of extinct taxa.

In most analyses, *T. servatus* is recovered as a sister-taxon to Pyxicephalinae, or within this clade. In addition, the hyperossified *Cornufer guentheri* is also recovered close to Pyxicephalinae and *T. servatus* with both equal and implied weight, except when using a low k value (punishing heavily homoplasy; Figs. 14A, B, S4–7). However, one difference can be observed between equal and implied weight analyses. With equal weights, *T. servatus* is placed as the sister-taxon to a trichotomy of the three extant taxa, whereas with implied weights, *C. guentheri* is recovered as a sister-taxon to *T. servatus* and Pyxicephalinae. This clustering of hyperossified ranoids is mostly likely driven by convergence, as the clades are based mainly on hyperossified characters (see Appendix 6 in Supplemental Data 1). However, when using implied weight, the placement of *T. servatus* as close to Pyxicephalinae (based only on one synapomorphy on a hyperossified character) has relatively high Bremer and moderate bootstrap supports. This could be an effect of the implied weight, which tends to favor resolved trees, which may lead to false topologies. This can be observed when using low k value ($k=3$), where *C. guentheri* is not recovered close to the other hyperossified ranoids, but also not close to its position proposed by molecular

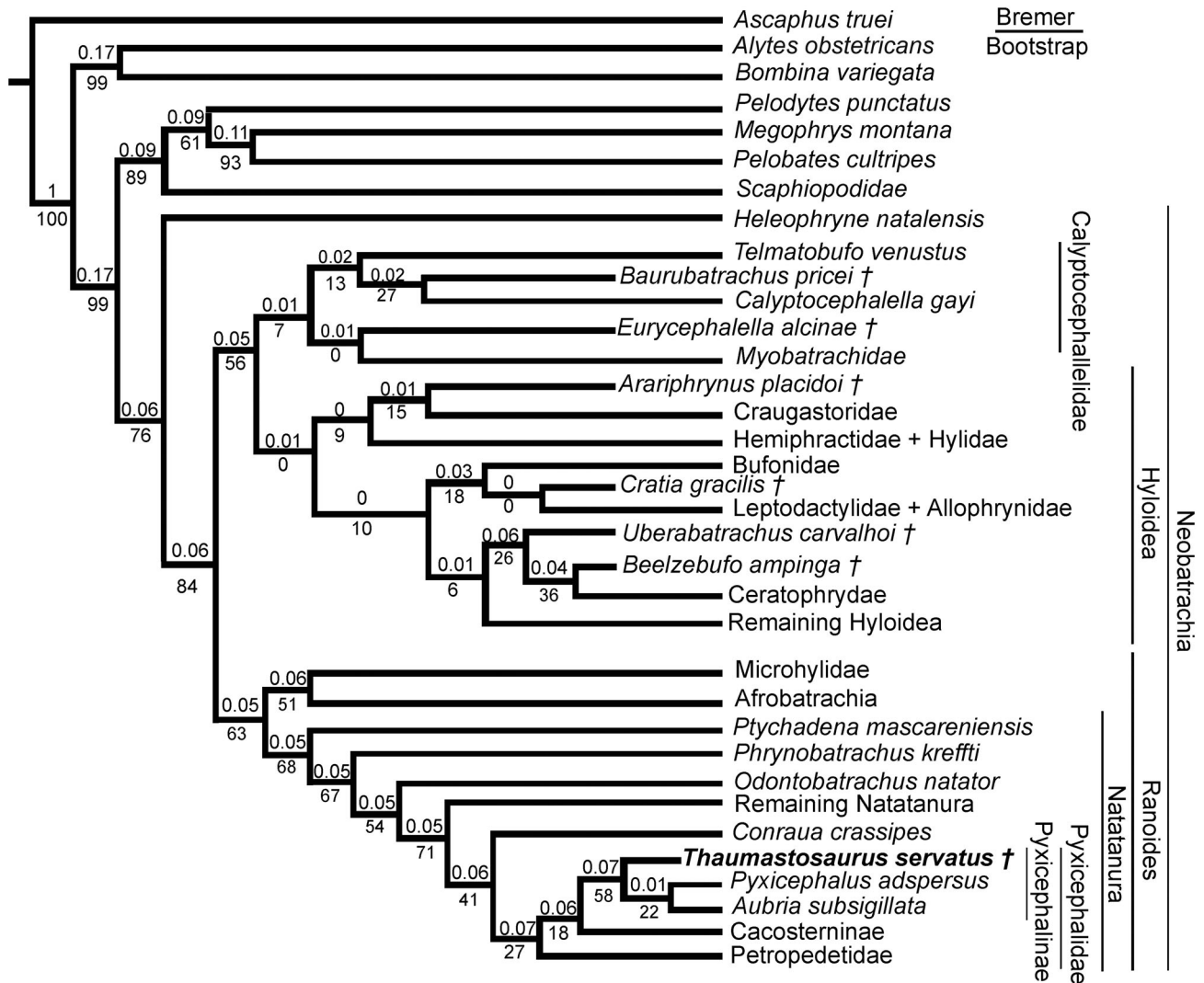


FIGURE 15. Simplified MPT from a constrained analysis. Reduced MPT of 72 steps (CI = 0.150, RI = 0.459) using a molecular scaffold tree from Jetz and Pyron (2018), performed under IW with $k = 7$, multistate characters ordered. The † symbol represents extinct taxa.

phylogenies (Fig. S4; Jetz and Pyron, 2018). To minimize this problem, several authors proposed to use a higher k value (Goloboff et al., 2018a, b). In the constrained analysis, *Thaumastosaurus* is also placed within the Pyxicephalinae, a clade composed of Pyxicephalinae and Cacosterninae. However, no osteological synapomorphy is known for this clade, because the presence of a medial lingual process on the tongue (presumed synapomorphy; Frost et al., 2006) is not known in *Thaumastosaurus*.

Conversely, as already proposed by Clarke (1981), Pyxicephalinae is supported by four morphological synapomorphies (Frost et al., 2006). One of them, the presence of an occipital canal, was also recovered as a synapomorphy for this clade in our analyses, while another one, a well-developed ramus interior (medial ramus; Clarke, 1981) of the pterygoids overlapping the parasphenoid alae, is present on *Thaumastosaurus*. The other two synapomorphies for the clade are a well-developed zygomatic ramus (= lamella alaris) of the squamosals (longer than its ramus paroticus) articulating with the maxillae, and a cranial exostosis (sensu Trueb, 1973). This latter in its typical state (a reticulate pattern of bone deposition, forming an ornamentation) is present only in Pyxicephalinae (in the Natatanura). Indeed,

C. guentheri presents a modified pattern of exostosis, named casing (Trueb, 1973). The articulated skulls attributed to *T. servatus* present a reticulated bone ornamentation that can be considered as skull exostosis (Figs. 5, 6; Roček and Lamaud, 1995:figs. 1–5; Rage and Roček, 2007:figs. 1–6; Laloy et al., 2013:fig. 3), and possess elongated squamosals with a well-developed zygomatic ramus forming the whole ventral margin of the orbit (the maxilla does not contribute to the ventral margin of the orbit; Fig. 5B). This character is shared with both *Pyxicephalus adspersus* and *Aubria subsigillata* (both Pyxicephalinae) but not by *C. guentheri*.

Thaumastosaurus servatus shows all the synapomorphies of the Pyxicephalinae and is found in almost all analyses as the closest taxon to the pyxicephaline crown clade. It can therefore be confidently placed within Pyxicephalinae. Furthermore, we can consider *T. servatus* as a stem-Pyxicephalinae.

Several Cretaceous taxa were included in the analyses, including: *Baurubatrachus pricei*, *Eurycephalella alcinae*, *Arariphrynus placidoi*, *Beelzebufo ampinga*, *Uberabatrachus carvalhoi* and *Cratia gracilis*. Their positions throughout the analyses are similar to the ones recovered in recent analyses (Báez and Gómez, 2018). *Baurubatrachus pricei* is recovered

within Australobatrachia, close to *Calyptocephalella gayi*. *Eurycephalella alcinae* is recovered as a sister-taxon to the extant Myobatrachidae. *Arariphrynus placidoi* is recovered within the Craugastoridae, but this position is poorly supported, as the taxon was in several analyses placed within various neobatrachian clades, even within the Ranoides, as a sister-taxon to the Afrobatrachia. This variability can be explained by the poorly known postcranial bones, especially around the pectoral girdle, where most critical characters for both Hyloides and Ranoides are found. *Cratia gracilis* is placed in the same position as in previous analyses (Báez et al., 2009; Báez and Gómez, 2018). *U. carvalhoi* is recovered as a sister-taxon to Ceratophryidae, a position that was also recovered in some analyses of Báez and Gómez (2018) but differs from the position they retained as their preferred one (sister-taxon to *B. ampinga* clustered within Myobatrachia). *B. ampinga* is recovered in various positions, but most often as a sister-taxon to all Ceratophryidae, a position proposed by previous analyses (Evans et al., 2008, 2014). However, this was challenged recently (Báez and Gómez, 2018) and this uncertainty may be linked to the scarce post-cranial remains.

PALEOBIOGEOGRAPHIC IMPLICATIONS

Only a few sites from Africa have yielded pre-Pleistocene natanuran fossils (Gardner and Rage, 2016). However, new material has been published in the last decade, and the fossil record of various natanuran clades is beginning to be better documented.

The pre-Pleistocene fossil record of Ranoides is scarce, and even fewer fossil specimens older than the Miocene have been assigned to Natatanura (Sanchiz, 1998; Gardner and Rage, 2016). The few Ranoides specimens are moreover mostly fragmentary (de Broin et al., 1974; Rage, 1984a; Roček and Lamaud, 1995; Báez and Werner, 1996). The origination time estimates in molecular studies for Ranoides are around 90.7 Ma (105.6–76.3 Ma, according to Frazão et al., 2015), about mid-Cretaceous, which is compatible with the fossil record given that the first presumed remains attributed to this clade date from the Cenomanian (between 100.5–93.9 Ma; Báez and Werner, 1996; Marjanović and Laurin, 2014:fig. 4). However, these remains were neither described nor illustrated, making the validity of this attribution difficult to assess. Other remains are from the Santonian (86.3–83.6 Ma) of In Beceten, Niger (de Broin et al., 1974; Rage, 1984a) and from the Paleocene (66.0–56.0 Ma) from Cernay, France (Estes et al., 1967; Rage, 1984a). More recent remains, clearly attributed to Ranoides, are known in multiple Eocene sites, in northern Africa (Rage et al., 2021) and in the Quercy Phosphorites (Rage, 2016), with *T. servatus* and *T. bottii* (as well as other indeterminate forms; see Rage, 2016) constituting the best-known taxa.

For Natatanura, almost no fossil record is known. *Thaumastosaurus* is the oldest undisputed known taxon, as well as the oldest Ranoides with a valid taxon name (Sanchiz, 1998; Gardner and Rage, 2016; Rage, 2016). The Eocene age of this taxon is substantially more recent than the transition Cretaceous/Paleocene age for Natatanura inferred in the most recent molecular age analysis (Feng et al., 2017).

Although scarce, the fossil record of Ranoides (including Natatanura) is concentrated (in the Mesozoic at least) on the African continent (with a few exceptions in India), which suggests an African origin of the clade (Gardner and Rage, 2016). This hypothesis is strengthened by the presence of extant endemic clades on this continent (Gardner and Rage, 2016), including Pyxicephalidae. The attribution of *Thaumastosaurus*, an endemic clade of Western Europe (Vasilyan, 2018) to Pyxicephalidae extends the geographic range of Pyxicephalidae, which is otherwise limited to Sub-Saharan Africa (van der Meijden et al., 2011) for both extant and extinct taxa (Gardner and Rage, 2016). Moreover,

Thaumastosaurus (middle to late Eocene, 40.5–33.5 Ma) is much older than the other fossils previously attributed to that clade (around 5.1 Ma for the oldest specimen; Gardner and Rage, 2016). However, the attribution of *Thaumastosaurus* to Pyxicephalidae is well supported by our phylogenetic analysis and is compatible with the geological age proposed for the clades by molecular studies. Indeed, Pyxicephalidae diverged from its sister-clade around 60 Ma ago (early to middle Paleocene) according to recent molecular age (Feng et al., 2017). Within this clade, Pyxicephalinae diverged from Cacosterninae around 50 Ma ago (Hedges et al., 2015; Feng et al., 2017). The stratigraphic range for *Thaumastosaurus* is compatible with these molecular ages. Furthermore, we confirm the African affinities of *T. servatus*, proposed almost a decade ago (Laloy et al., 2013).

The presence of *Thaumastosaurus* in Europe could be linked to a faunistic exchange through an intermittent connection between Africa to Europe (Rage, 1984b; Gheerbrant and Rage, 2006). Indeed, some adapisoriculid (De Bast et al., 2012) and lousinid mammals (Sudre, 1979) may have immigrated through an intermittent connection between Africa and Eurasia in the Paleocene or Eocene. Starting in the late Paleocene (Tanrattana et al., 2020), the temperature increased (Sluijs et al., 2006; Bohaty et al., 2009) in Western Europe, and remained warm until the end of the middle Eocene (Bohaty et al., 2009). During this period, Western Europe was characterized by a subtropical climate, with evergreen forests under warm and humid conditions (Escarguel et al., 2008; Héran et al., 2010; Tanrattana et al., 2020).

For the herpetofauna, the timing of this wave of immigration in Europe and paleobiogeographic origins of the early Paleogene herpetological faunas of Europe still is poorly constrained. Numerous taxa appear in Europe at the earliest Eocene (MP7; Folie et al., 2005, 2013; Rage, 2012), but could have arrived during the end of the Paleocene. Bufonidae already exhibit such a pattern with their earliest record in Europe being from the Paleocene of Cernay (Rage, 2003).

A major cooling is recorded during the Eocene–Oligocene transition (EOT). This is well established in numerous studies using different proxies (Escarguel et al., 2008; Héran et al., 2010; Lunt et al., 2017; Tanrattana et al., 2020) and is linked to the establishment of permanent ice caps on Antarctica (Vandenberghe et al., 2012; Boscolo Galazzo et al., 2014). In Europe, the climate and environments dramatically changed. The climate became drier, with stronger seasonality and the appearance of a dry season (Escarguel et al., 2008; Tanrattana et al., 2020). The vegetation changed from forests to woodland savannah (Escarguel et al., 2008). This climate change probably triggered a moderate extinction event called the “Grande Coupure” (Stehlin, 1909), which has been particularly well-documented for mammals in Europe (Remy et al., 1987). Most of the subtropical fauna of African origin disappeared in Europe and was replaced by Eurasian taxa adapted to temperate conditions. This event is also documented in the herpetofauna (Delfino et al., 2003; Rage, 2006, 2012; Augé and Smith, 2009; Macaluso et al., 2019). Among amphibians, *Thaumastosaurus* is the best-documented victim of this turnover (Vasilyan, 2018).

CONCLUSION

The tomography and skeletal study of the specimen MNHN.F.QU17381, firstly described as the holotype of the bufonid *Bufo servatus*, yielded numerous data. The anatomical characters led to a new taxonomic attribution to the ranoid taxon *Thaumastosaurus servatus*. MNHN.F.QU17381 is the third mummy from the Old Collections of the Quercy Phosphorites attributed to this taxon, thus making it the best-known anuran in the Eocene of Western Europe.

Previous analyses placed *T. servatus* within the Natatanura, without specifying its position. Our analyses place *T. servatus*

with the African hyperossified Pyxicephalinae (and likely as a stem-Pyxicephalinae and sister-taxon to the extant Pyxicephalinae), sharing a peculiar ornamentation as well as a combination of cranial features such as a contact between the squamosals and nasals, which is unique within Natatanura and Ranoides.

The position of *T. servatus* within Natatanura and Pyxicephalinae provides new insights to calibrate molecular dating analyses, as it represents the oldest fossil record for Pyxicephalidae and Pyxicephalinae, previously known only from the Pliocene (around 5 Ma) and Pleistocene respectively, extending therefore the geological range of the Pyxicephalinae of more than 33 Ma and making *T. servatus* one of the few well-known taxa firmly attributed to the Natatanura in the Paleogene. Moreover, Pyxicephalinae were previously considered to be distributed solely in Africa, whereas *T. servatus* is endemic to Western Europe. Confirmation of these affinities extends the geographic range of pyxicephalines. The main biogeographic hypothesis is that the clade originated in Africa, and then migrated into Europe through dispersal of some natatanurans during the Eocene, making *Thaumastosaurus* a member of the African herpetofauna present in Europe until the Eocene/Oligocene transition, when it was eliminated around the Grande Coupure (Delfino et al., 2003; Rage, 2006, 2012). However, given the scarce fossil record of Ranoides in Africa, especially during the Paleocene and Eocene, other hypotheses cannot be ruled out. Further findings could help to understand the evolution of Ranoides, which represents the majority of extant anurans on the African continent.

ACKNOWLEDGMENTS

We thank D. Germain (CR2P, MNHN) for providing the access to historical specimens and Y. Laurent (MHNT) for the loan and information about the specimens from MNHT. We are grateful to T. Péliissié (Global Geopark UNESCO and Parc Naturel Régional des Causses du Quercy, France) and E. Cassan (granddaughter of a miner of Escamps quarries) for sharing their knowledge on the Quercy region and sites on the search for the putative site of origin of the mummies. We thank A. Ohler (MNHN) for bringing her expertise in nomenclature in the study of the nomenclatural history of *Bufo servatus* and other taxa named on the basis of the Quercy anuran mummies. We thank D. Dosso (IBPC) and P. Prevost Marchiac (IRHIS) for fruitful discussion and exchange on the history surrounding the mummies, bringing another angle into this mystery. We warmly thank A. Mazurier (IC2MP, Poitiers University) for supporting the whole tomographic acquisition process and advising on it. We are also grateful to F. Goussard and N. Poulet (CR2P, MNHN) for their help and advice on 3D reconstructions. We are grateful to Z. Roček, J. Jia and a third anonymous reviewer for their useful comments and reviews on the manuscript. The fossil tomography was supported by the Irish grant irc4c5ffcf3b92ac2f8dda1f349764b177e (“The evolution of the integument in terrestrial vertebrates: insights from taphonomy and exceptionally preserved Eocene fossils”) awarded to N. Robin. This study was funded by a grant from the Fondation pour la Recherche sur la Biodiversité (FRB, Paris) constituted by the patronage of A., C. Lemierre; I. Baszanger; J. Tillit and P. Bernard.

ORCID

Alfred Lemierre  <http://orcid.org/0000-0003-1755-3018>

LITERATURE CITED

- Aguilar, J.-P., S. Legendre, and J. Michaux. 1997. Actes du Congrès Biochrom'97 Montpellier 14-17 Avril. Biochronologie mammalienne du Cénozoïque en Europe et domaines reliés. Mémoires et Travaux de l'Institut de Montpellier de l'Ecole Pratique des Hautes Études 21, 1-181.
- Augé, M., and R. Smith. 2009. An assemblage of early Oligocene lizards (Squamata) from the locality of Boutersem (Belgium), with comments on the Eocene–Oligocene transition. *Zoological Journal of the Linnean Society* 155:148–170.
- Báez, A. M., and R. O. Gómez. 2018. Dealing with homoplasy: osteology and phylogenetic relationships of the bizarre neobatrachian frog *Baurubatrachus pricei* from the Upper Cretaceous of Brazil. *Journal of Systematic Palaeontology* 16:279–308.
- Báez, A. M., and C. Werner. 1996. Presencia de Anuros Ranoideos en el Cretácico de Sudan. *Ameghiniana* 33:460.
- Báez, A. M., G. J. B. Moura, and R. O. Gómez. 2009. Anurans from the Lower Cretaceous Crato Formation of northeastern Brazil: implications for the early divergence of neobatrachians. *Cretaceous Research* 30:829–846.
- Biton, R., R. Boistel, R. Rabinovich, S. Gafny, V. Brumfeld, and S. Bailon. 2016. Osteological observations on the Alytid anura *Latonia nigriventer* with comments on functional morphology, biogeography, and evolutionary history. *Journal of Morphology* 277:1131–1145.
- Bohaty, S. M., J. C. Zachos, F. Florindo, and M. L. Delaney. 2009. Coupled greenhouse warming and deep-sea acidification in the Middle Eocene: Middle Eocene warming and ccd shoaling. *Paleoceanography* 24:1–16.
- Bolt, J. R., and R. E. Lombard. 1985. Evolution of the amphibian tympanic ear and the origin of frogs. *Biological Journal of the Linnean Society* 24:83–99.
- Bonaparte, C. 1850. *Conspectus Systematum. Herpetologiae et Amphibiologiae.*, Brill. Leiden, pp.
- Boscolo Galazzo, F., E. Thomas, M. Pagani, C. Warren, V. Luciani, and L. Giubertini. 2014. The middle Eocene climatic optimum (MECO): A multiproxy record of paleoceanographic changes in the southeast Atlantic (ODP Site 1263, Walvis Ridge): MECO repercussions in the SE Atlantic. *Paleoceanography* 29:1143–1161.
- Boulenger, G. A. 1884. Diagnoses of new Reptiles and Batrachians from the Solomon Islands, collected and presented to the British Museum by H. B. Guppy, Esq., M.B., H.M.S. ‘Lark’. *Proceedings of the Zoological Society of London for the year 1884*:210–213.
- Boulenger, G. A. 1886. Quelques mots en réponse à la note de M. Le Dr R. Blanchard sur la classification des Batraciens. *Bulletin de la société zoologique de France* 11:320–321.
- Boulenger, G. A. 1917. Sur la conformation des phalangettes chez certaines grenouilles d’Afrique. *Comptes rendus hebdomadaires des séances de l’Académie des sciences, Paris*, 165 : 987–990.
- Bremer, K. 1994. Branch support and Tree stability. *Cladistics* 10:295–304.
- de Broin, F., E. Buffetaut, J.-C. Koeniger, J. Rage, D. Russell, P. Taquet, C. Vergnaud-Grazzini, and S. Wenz. 1974. La faune de vertébrés continentaux du gisement d’In Beceten (Sénouien du Niger). *Comptes Rendus de l’Académie des Sciences de Paris, Série D* 279:439–472.
- de Buffrénil, V., F. Clarac, A. Canoville, and M. Laurin. 2016. Comparative Data on the Differentiation and growth of bone ornamentation in Gnathostomes (Chordata: Vertebrata): Growth of bone ornamentation in Gnathostomes. *Journal of Morphology* 277:634–670.
- de Buffrénil, V., F. Clarac, M. Fau, S. Martin, B. Martin, E. Pellé, and M. Laurin. 2015. Differentiation and growth of bone ornamentation in Vertebrates: A comparative histological study among the Crocodylomorpha: Development of bone ornamentation in the Crocodylomorpha. *Journal of Morphology* 276:425–445.
- Cameron, J. A., D. J. Milner, J. S. Lee, J. Cheng, N. X. Fang, and I. M. Jasiuk. 2012. Employing the biology of successful fracture repair to heal critical size bone defects; pp. 113–132 in E. Heber-Katz and D. L. Stocum (eds.), *New Perspectives in Regeneration. Current Topics in Microbiology and Immunology* vol. 367. Springer Berlin Heidelberg, Berlin, Heidelberg.
- Channing, A., and N. Baptista. 2013. *Amietia angolensis* and *A. fuscigula* (Anura: Pyxicephalidae) in southern Africa: A cold case reheated. *Zootaxa* 3640:501.
- Channing, A., J. M. Dehling, Lötters, and R. Ernst. 2016. Species boundaries and taxonomy of the African river frogs (Amphibia: Pyxicephalidae: *Amietia*). *Zootaxa* 4155:1.
- Clarke, B. T. 1981. Comparative osteology and evolutionary relationships in the African Raninae (Anura: Ranidae). *Monitore Zoologico Italiano. Supplemento* 15:285–331.

- Company, J., and Z. Szentesi. 2012. Amphibians from the Late Cretaceous Sierra Perenchiza Formation of the Chera Basin, Valencia Province, Spain. *Cretaceous Research* 37:240–245.
- Congreve, C. R., and J. C. Lamsdell. 2016. Implied weighting and its utility in palaeontological datasets: a study using modelled phylogenetic matrices. *Palaeontology* 59:447–462.
- Cope, E. D. 1864. On the limits and relations of the Raniformes. *Proceedings of the Academy of Natural Sciences of Philadelphia* 16:181–183.
- Cross, R. 2017. The inside story on 20,000 vertebrates. *Science* 357:742–743.
- De Bast E., Sigé B., Smith T., 2012. Diversity of the adapisoriculid mammals from the early Palaeocene of Hainin, Belgium. *Acta Palaeontologica Polonica*, 57(1):35–52
- De Stefano, G. 1903. I Sauri del Quercy appartenenti alla collezione Rossignol. *Atti della Società Italiana di Scienze Naturali* 4:382–418.
- Delfino, M., J. Rage, and L. Rook. 2003. Tertiary mammal turnover phenomena: what happened to the herpetofauna? *Deinsea* 10:153–161.
- Dubois, A., and A. Ohler. 2005. Taxonomic notes on the Asian frogs of the tribe Paini (Ranidae, Dicroglossinae): 1. Morphology and synonymy of *Chaparana aenea* (Smith, 1922), with proposal of a new statistical method for testing homogeneity of small samples. *Journal of Natural History* 39:1759–1778.
- Duellman, W. E., and L. Trueb. 1994. *Biology of Amphibians*. JHU Press, 702 pp.
- Duméril, C. 1805. *Zoologie analytique, ou Méthode naturelle de classification des animaux, rendue plus facile à l'aide de tableaux synoptiques*. Allais, Paris, XXXII + 386 pp.
- Egawa, S., S. Miura, H. Yokoyama, T. Endo, and K. Tamura. 2014. Growth and differentiation of a long bone in limb development, repair and regeneration. *Development, Growth & Differentiation* 56:410–424.
- Escarguel, G., S. Legendre, and B. Sigé. 2008. Unearthing deep-time biodiversity changes: The Palaeogene mammalian metacommunity of the Quercy and Limagne area (Massif Central, France). *Comptes Rendus Geoscience* 340:602–614.
- Estes, R., Ma. Hecht, and R. Hoffstetter. 1967. Paleocene Amphibians from Cernay, France. *American Museum Novitates* 2295:1–25.
- Evans, S. E., M. E. H. Jones, and D. W. Krause. 2008. A giant frog with South American affinities from the Late Cretaceous of Madagascar. *Proceedings of the National Academy of Sciences* 105:2951–2956.
- Evans, S. E., J. R. Groenke, M. E. H. Jones, A. H. Turner, and D. W. Krause. 2014. New material of *Beelzebufo*, a hyperossified frog (Amphibia: Anura) from the Late Cretaceous of Madagascar. *Plos One* 9:e87236.
- Fabrezi, M. 2006. Morphological evolution of Ceratophryinae (Anura, Neobatrachia). *Journal of Zoological Systematics and Evolutionary Research* 44:153–166.
- Feng, Y.-J., D. C. Blackburn, D. Liang, D. M. Hillis, D. B. Wake, D. C. Cannatella, and P. Zhang. 2017. Phylogenomics reveals rapid, simultaneous diversification of three major clades of Gondwanan frogs at the Cretaceous–Paleogene boundary. *Proceedings of the National Academy of Sciences* 114:E5864–E5870.
- Filhol, H. 1873. Sur des pièces fossiles provenant de batraciens, de lacertiens et d'ophidiens, trouvés dans les dépôts de phosphates de chaux de l'Aveyron. *Comptes Rendus de l'Académie des Sciences, Paris* 77:1556–1557.
- Filhol, H. 1876. Sur les Reptiles fossiles des phosphorites du Quercy. *Bulletin de La Société Philomathique de Paris* 6:27–28.
- Filhol, H. 1877. Recherches sur les phosphorites du Quercy: Etude des fossiles qu'on y rencontre et spécialement des mammifères, Librairie de l'Académie de médecine. Paris, 690 pp.
- Folie, A., Sigé B. and T. Smith. 2005. A new scincomorph lizard from the Palaeocene of Belgium and the origin of Scincoidea in Europe. *Naturwissenschaften* 92:542–546.
- Folie, A., Smith R. and T. Smith. 2013. New amphisbaenian lizards from the Early Paleogene of Europe and their implications for the early evolution of modern amphisbaenians. *Geologica Belgica* 16 (4): 227–235.
- Frazão, A., H. R. da Silva, and C. A. de M. Russo. 2015. The Gondwana Breakup and the History of the Atlantic and Indian Oceans Unveils Two New Clades for Early Neobatrachian Diversification. *Plos One* 10:e0143926.
- Frost, D. R., T. Grant, J. Faivovich, R. H. Bain, A. Haas, C. F. B. Haddad, R. O. De Sá, A. Channing, M. Wilkinson, S. C. Donnellan, C. J. Raxworthy, J. A. Campbell, B. L. Blotto, P. Moler, R. C. Drewes, R. A. Nussbaum, J. D. Lynch, D. M. Green, and W. C. Wheeler. 2006. *The Amphibian Tree of Life*. *Bulletin of the American Museum of Natural History* 297:1–291.
- Gardner, J. D., and J.-C. Rage. 2016. The fossil record of lissamphibians from Africa, Madagascar, and the Arabian Plate. *Palaeobiodiversity and Palaeoenvironments* 96:169–220.
- Gardner, J. D., Z. Roček, T. Prikryl, J. G. Eaton, R. W. Blob, and J. T. Sankey. 2010. Comparative morphology of the ilium of anurans and urodeles (Lissamphibia) and a re-assessment of the anuran affinities of *Nezpercius dodsoni* Blob et al., 2001. *Journal of Vertebrate Paleontology* 30:1684–1696.
- Gèze, B. 1949. Les Gouffres à Phosphate du Quercy. *Annales de Spéléologie* 4:89–107.
- Gheerbrant, E., and J.-C. Rage. 2006. Paleobiogeography of Africa: How distinct from Gondwana and Laurasia? *Palaeogeography, Palaeoclimatology, Palaeoecology* 241:224–246.
- Goloboff, P. A. 1993. Estimating character weights during tree search. *Cladistics* 9:83–91.
- Goloboff, P. A. 1997. Self-Weighted Optimization: Tree searches and character state reconstructions under implied transformation costs. *Cladistics* 13:225–245.
- Goloboff, P. A., and S. A. Catalano. 2016. TNT version 1.5, including a full implementation of phylogenetic morphometrics. *Cladistics* 32:221–238.
- Goloboff, P. A., and J. S. Farris. 2001. Methods for quick consensus estimation. *Cladistics* 17:S26–S34.
- Goloboff, P. A., A. Torres, and J. S. Arias. 2018a. Weighted parsimony outperforms other methods of phylogenetic inference under models appropriate for morphology. *Cladistics* 34:407–437.
- Goloboff, P. A., J. M. Carpenter, J. S. Arias, and D. R. M. Esquivel. 2008. Weighting against homoplasy improves phylogenetic analysis of morphological data sets. *Cladistics* 24:758–773.
- Goloboff, P. A., M. Pittman, D. Pol, and X. Xu. 2018b. Morphological data sets fit a common mechanism much more poorly than DNA sequences and call into question the Mk model. *Systematic Biology* 68:494–504.
- Gómez, R. O., and G. F. Turazzini. 2016. An overview of the ilium of anurans (Lissamphibia, Salientia), with a critical appraisal of the terminology and primary homology of main ilial features. *Journal of Vertebrate Paleontology* 36:e1030023.
- Griffins, C. T., M. R. Stocker, C. Colleary, C. M. Stefanic, E. J. Lessner, M. Riegler, K. Formoso, K. Koeller and S. J. Nesbitt. 2021. Assessing ontogenetic maturity in extinct saurian reptiles. *Biological Reviews* 96: 470–525.
- Haas, A. 2003. Phylogeny of frogs as inferred from primarily larval characters (Amphibia: Anura). *Cladistics* 19:23–89.
- Hedges, S. B., J. Marin, M. Suleski, M. Paymer, and S. Kumar. 2015. Tree of Life reveals clock-like speciation and diversification. *Molecular Biology and Evolution* 32:835–845.
- Héran, M.-A., C. Lécuyer, and S. Legendre. 2010. Cenozoic long-term terrestrial climatic evolution in Germany tracked by $\delta^{18}O$ of rodent tooth phosphate. *Palaeogeography, Palaeoclimatology, Palaeoecology* 285:331–342.
- Holman, J. A., and D. L. Harrison. 2002. A new *Thaumastosaurus* (Anura: Familia Incertae Sedis) from the Late Eocene of England, with remarks on the taxonomic and zoogeographic relationships of the genus. *Journal of Herpetology* 36:621–626.
- Holman, J. A., and D. L. Harrison. 2003. A new helmeted frog of the genus *Thaumastosaurus* from the Eocene of England. *Acta Palaeontologica Polonica* 48:157–160.
- Jarošová, J., and Z. Roček. 1982. The incrasatio frontoparietalis in frogs, its origin and phylogenetic significance. *Amphibia-Reptilia* 3:111–124.
- Jeanbernat, E. 1874. Procès-verbal de la séance du 6 février 1874. *Bulletin de la Société des Sciences Physiques et Naturelles de Toulouse* 2:502–507.
- Jetz, W., and R. A. Pyron. 2018. The interplay of past diversification and evolutionary isolation with present imperilment across the amphibian tree of life. *Nature Ecology & Evolution* 2:850–858.
- Jones, A. S., and R. J. Butler. 2018. A new phylogenetic analysis of Phytosauria (Archosauria: Pseudosuchia) with the application of continuous and geometric morphometric character coding. *PeerJ* 6:e5901.
- Laloy, F., J.-C. Rage, S. E. Evans, R. Boistel, N. Lenoir, and M. Laurin. 2013. A re-interpretation of the Eocene anuran *Thaumastosaurus*

- based on MicroCT examination of a ‘mummified’ specimen. *Plos One* 8:e74874.
- Laurent, R. F. 1986. Sous classe des Lissamphibiens (Lissamphibia) ; pp. 594–597 in Grassé P., and M. Delsol (eds), *Traité de Zoologie, Anatomie, Systematique, Biologie*. vol. 14. Paris.
- Legendre, S., B. Marandat, B. Sigé, J.-Y. Crochet, M. Godinot, J.-L. Hartenberger, J. Sudre, M. Vianey-Liaud, B. Muratet, and J.-G. Astruc. 1992. Mammalian fauna of Vielase (phosphorites of Quercy, in the South of France): paleontological evidence for karst formation in the Quercy area as early as the Early Eocene. *Neues Jahrbuch für Geologie und Paläontologie - Monatshefte* 1992:414–428.
- Lunt, D. J., T. Dunkley Jones, M. Heinemann, M. Huber, A. LeGrande, A. Winguth, C. Loptson, J. Marotzke, C. D. Roberts, J. Tindall, P. Valdes, and C. Winguth. 2017. A model-data comparison for a multi-model ensemble of early Eocene atmosphere–ocean simulations: EoMIP. *Climate of the Past* 8:1717–1736.
- Lynch, J. D. 1971. Evolutionary relationships, osteology and zoogeography of Leptodactyloid frogs. University of Kansas Museum of Natural History, Miscellaneous Publications 53: 1–238.
- Lynch, J. D. 1973. The transition from archaic to advanced frogs; pp. 133–182 in J. L. Vial (ed.), *Evolutionary Biology of the Anurans*. Contemporary research on major problems. University of Missouri Press.
- Macaluso, L., J. E. Martin, L. Del Favero, and M. Delfino. 2019. Revision of the crocodylians from the Oligocene of Monteviale, Italy, and the diversity of European eusuchians across the Eocene-Oligocene boundary. *Journal of Vertebrate Paleontology* 39:e1601098
- Marjanović, D., and M. Laurin. 2014. An updated paleontological timetree of lissamphibians, with comments on the anatomy of Jurassic crown-group salamanders (Urodela). *Historical Biology* 26:535–550.
- Martin, C., M. A. Alonso-Zarazaga, and B. Sanchiz. 2012. Nomenclatural notes on living and fossil amphibians. *Graellsia* 68:159.
- Mones A. 1989. Nomen Dubium vs Nomen Vanum. *Journal of Vertebrate Paleontology* 9: 232–234.
- Nicoli, L. 2019. The fossil record of Ceratophrys Wied-Neuwied (Anura: Ceratophryidae): a revision and update of fossil South American horned frogs. *Zootaxa* 4658:37–68.
- O’Reilly, J. E., M. N. Puttick, L. Parry, A. R. Tanner, J. E. Tarver, J. Fleming, D. Pisani, and P. C. J. Donoghue. 2016. Bayesian methods outperform parsimony but at the expense of precision in the estimation of phylogeny from discrete morphological data. *Biology Letters* 12:20160081.
- Ósi, A., M. Szabó, H. Kollmann, M. Wagreich, R. Kalmár, L. Makádi, Z. Szentesi, and H. Summesberger. 2019. Vertebrate remains from the Turonian (Upper Cretaceous) Gosau Group of Gams, Austria. *Cretaceous Research* 99:190–208.
- Paluh, D. J., E. L. Stanley, and D. C. Blackburn. 2020. Evolution of hyperossification expands skull diversity in frogs. *Proceedings of the National Academy of Sciences* 117:8554–8562.
- Pélessié T., and B. Sigé (eds). 2006. 30 millions d’années de Biodiversité dynamique dans le paléokarst du Quercy. *Strata* 13:3–284.
- Pereyra, M. O., M. C. Womack, J. S. Barrionuevo, B. L. Blotto, D. Baldo, M. Targino, J. J. Ospina-Sarria, J. M. Guayasamin, L. A. Coloma, K. L. Hoke, T. Grant, and J. Faivovich. 2016. The complex evolutionary history of the tympanic middle ear in frogs and toads (Anura). *Scientific Reports* 6:34130.
- Poynton, J. C. 1964. The Amphibians of Southern Africa. *Annals of the Natal Museum* 17:1–334.
- Piveteau, J. 1927. Etudes sur quelques Amphibiens et Reptiles fossiles. *Annales de Paléontologie* 16:59–99.
- Procter, M. J. B. 1919. On the skull and affinities of *Rana subsigillata* A. Dum. *Proceedings of the Zoological Society of London* 89:21–27.
- Puttick, M. N., J. E. O’Reilly, A. R. Tanner, J. F. Fleming, J. Clark, L. Holloway, J. Lozano-Fernandez, L. A. Parry, J. E. Tarver, D. Pisani, and P. C. J. Donoghue. 2017. Uncertain-tree: discriminating among competing approaches to the phylogenetic analysis of phenotype data. *Proceedings of the Royal Society B: Biological Sciences* 284:20162290.
- Pyron, R. A., and J. J. Wiens. 2011. A large-scale phylogeny of Amphibia including over 2800 species, and a revised classification of extant frogs, salamanders, and caecilians. *Molecular Phylogenetics and Evolution* 61:543–583.
- Rage, J.-C. 1984a. La “Grande Coupure” Eocène/Oligocène et les herpétofaunes (Amphibiens et Reptiles): Problèmes du synchronisme des événements paléobiogéographiques. *Bulletin de la société géologique de France* 26:1251–1257.
- Rage, J.-C. 1984b. Are the Ranidae (Anura, Amphibia) known prior to the Oligocene? *Amphibia-Reptilia* 5:281–288.
- Rage, J.-C. 2003. Oldest Bufonidae (Amphibia, Anura) from the Old World: a Bufonid from the Paleocene of France. *Journal of Vertebrate Paleontology* 23:462–463.
- Rage, J.-C. 2006. The Lower Vertebrates from the Eocene and Oligocene of the Phosphorites du Quercy (France): An Overview. *Strata* 1:161–173.
- Rage, J.-C. 2012. Amphibians and squamates in the Eocene of Europe: what do they tell us? *Palaeobiodiversity and Palaeoenvironments* 92:445–457.
- Rage, J.-C. 2016. Frogs (Amphibia, Anura) from the Eocene and Oligocene of the Phosphorites du Quercy (France). An overview. *Fossil Imprint* 53–66.
- Rage, J.-C., and Z. Roček. 2007. A new species of *Thaumastosaurus* (Amphibia: Anura) from the Eocene of Europe. *Journal of Vertebrate Paleontology* 27:329–336.
- Rage, J.-C., M. Adaci, M. Bensalah, M. Mahboubi, L. Marivaux, F. Mebrouk, and R. Tabuce. 2021. Latest Early-Middle Eocene deposits of Algeria (Glib Zegdou, HGL50) yield the richest and most diverse fauna of amphibians and squamate reptiles from the Palaeogene of Africa. *Paleovertebrata* 44 (1)-e1. doi: 10.18563/pv.44.1.e1.
- Reig, O. 1958. Proposiciones para una nueva macro-sistemática de los anuros (nota preliminar). *Physis* 21:109–118.
- Remy, J. A., J.-Y. Crochet, B. Sigé, J. Sudre, L. de Bonis, M. Vianey-Liaud, M. Godinot, J.-L. Hartenberger, B. Lange-Badré, and B. Comte. 1987. Biochronologie des Phosphorites du Quercy: Mise à jour des listes fauniques et nouveaux gisements de mammifères fossiles. *Münchner Geowissenschaftliche Abhandlungen A*:169–188.
- Rineau, V., A. Grand, R. Zargüeta i Bagils, and M. Laurin. 2015. Experimental systematics: sensitivity of cladistic methods to polarization and character ordering schemes. *Contributions to Zoology* 84:129–148.
- Rineau, V., R. Zargüeta i Bagils, and M. Laurin. 2018. Impact of errors on cladistic inference: simulation-based comparison between parsimony and three-taxon analysis. *Contributions to Zoology* 87:25–40.
- Roček, Z. 1980. Cranial anatomy of frogs of the family Pelobatidae Stannius, 1856, with outlines of their phylogeny and systematics. *Acta Universitatis Carolinae - Biologica* 3:1–164.
- Roček, Z. 1994. Taxonomy and distribution of Tertiary Discoglossids (anura) of The Genus *Latonia* V. Meyer, 1843. *Geobios* 27:717–751.
- Roček, Z. 2003. Larval development and evolutionary origin of the anuran skull; pp. 1877–1995 in H. Heatwole and M. Davies (eds.), *Amphibians Biology: Osteology*. vol. 5. Surrey Beatty & Sons, Chipping Norton, Australia.
- Roček, Z. 2008. The Late Cretaceous frog *Gobiates* from Central Asia: its evolutionary status and possible phylogenetic relationships. *Cretaceous Research* 29:577–591.
- Roček, Z., and P. Lamaud. 1995. *Thaumastosaurus bottii* De Stefano, 1903, an anuran with Gondwanan affinities from the Eocene of Europe. *Journal of Vertebrate Paleontology* 15:506–515.
- Roček, Z., and L. A. Nessov. 1993. Cretaceous anurans from Central Asia. *Palaeontographica Abteilung A* 226:1–54.
- Roček, Z., N. Baleeva, A. Vazeille, A. Bravin, E. van Dijk, C. Nemoz, E. M. Smirina, R. Boistel, and L. Claessens. 2016. Contribution to the head anatomy of the basal frog *Barbourula busuangensis* and the evolution of the Anura. *Russian Journal of Herpetology* 23:163–194.
- Rödel, M.-O., J. Kosuch, T. U. Grafe, R. Boistel, N. E. Asseman, N. G. Kouamé, B. Tohé, G. Gourène, J.-L. Perret, K. Henle, P. Tafforeau, N. Pollet, and M. Veith. 2009. A new tree-frog genus and species from Ivory Coast, West Africa (Amphibia: Anura: Hyperoliidae). *Zootaxa* 2044:23–45.
- Sanchiz, B. 1998. *Salientia*. Dr. Friedrich Pfeil, Munich, 275 pp.
- Scott, E. 2005. A phylogeny of ranid frogs (Anura: Ranoidea: Ranidae), based on a simultaneous analysis of morphological and molecular data. *Cladistics* 21:507–574.
- Sheil, C. A. 1999. Osteology and skeletal development of *Pyxicephalus adspersus* (Anura: Ranidae: Raninae). *Journal of Morphology* 240:49–75.
- Sigé, B., J.-P. Aguilar, B. Marandat, and J. N.-G. Astruc. 1991. Extension au Miocène inférieur des remplissages phosphatés du Quercy. *La Faune de Vertébrés de Crémant (Lot, France)*. *Geobios* 24: 497–502.

- Simon-Coincon R., and J. G. Astruc. 1991. Les pièges karstiques en Quercy : rôle et signification dans l'évolution des paysages. *Bulletin de la société géologique de France* 162:595–605.
- Sluijs, A., S. Schouten, M. Pagani, M. Woltering, H. Brinkhuis, J. S. S. Damsté, G. R. Dickens, M. Huber, G.-J. Reichart, R. Stein, J. Matthiessen, L. J. Lourens, N. Pedentchouk, J. Backman, and K. Moran. 2006. Subtropical Arctic Ocean temperatures during the Palaeocene/Eocene thermal maximum. *Nature* 441: 610–613.
- Smirnov, S. V. 1997. Additional dermal ossifications in the anuran skull: Morphological novelties or archaic elements? *Russian Journal of Herpetology* 4:17–27.
- Špinar, Z. V. 1972. Tertiary Frogs from Central Europe. *Academia, Prague and Junk, The Hague*, 463 pp.
- Špinar, Z.V. 1978. *Latonia kolebabi* Špinar, 1976 (Amphibia) and remarks on the “genus *Miopelobates*”. In Pokorny V. (ed.) *Paleontologická konference 1977*. Charles University, Prague: 289–303.
- Stehlin, H. G. 1909. Remarques sur les faunules de mammifères des couches Eocène et Oligocène. *Bulletin de la Société Géologique de France* 9:488–520.
- Sudre, J. 1979. Nouveaux mammifères éocènes du Sahara occidental. *Palaeovertebrata* 9 (3) :83-115.
- Tanrattana, M., A. Boura, F. M. B. Jacques, L. Villier, F. Fournier, A. Enguehard, S. Cardonnet, G. Volland, A. Garcia, S. Chaouch, and D. De Franceschi. 2020. Climatic evolution in Western Europe during the Cenozoic: insights from historical collections using leaf physiognomy. *Geodiversitas* 42:151.
- Thevenin, A. 1903. Etude géologique de la bordure Sud-Ouest du Massif Central. *Bulletin de la société géologique de France* 14:353–555.
- Tihen, J. 1962. A review of New World fossil Bufonids. *The American Midland Naturalist* 68:1–50.
- Tissier, J., J.-C. Rage, and M. Laurin. 2017. Exceptional soft tissues preservation in a mummified frog-eating Eocene salamander. *PeerJ* 5:e3861.
- Tissier, J., J.-C. Rage, R. Boistel, V. Fernandez, N. Pollet, G. Garcia, and M. Laurin. 2016. Synchrotron analysis of a ‘mummified’ salamander (Vertebrata: Caudata) from the Eocene of Quercy, France: Exceptionally Preserved Fossil Urodele. *Zoological Journal of the Linnean Society* 177:147–164.
- Trueb, L. 1966. Morphology and development of the skull in the frog *Hyla septentrionalis*. *Copeia* 1966:562-573.
- Trueb, L. 1970. Evolutionary relationships of casque-headed tree frog with co-ossified skulls (family Hylidae). University of Kansas Publications, Museum of Natural History 18:547–716.
- Trueb, L. 1973. Bones, frogs and evolution; pp. 65–133 in J. L. Vial (ed.), *Evolutionary biology of the anurans: Contemporary research on major problems*. University of Missouri Press, Columbia.
- Tschudi, J. J. 1838. Classification der Batrachier, MitBerücksichtigung der FossilienThiere Dieser Abtheilungder Reptilien. *Der Buchdruckerei von Petitpierre. Mémoires de la Société des Sciences Naturelles de Neuchâtel* 2: 1–100.
- Vandenbergh, N., F.J. Hilgen, R. P. Speijer, J. G. Ogg, F. M. Gradstein, O. Hammer, C. J. Hollis, and J. J. Hooker. 2012. The Paleogene Period; pp. 855-921 in F. Gradstein, J. Ogg, M. Schmitz, and G. Ogg (eds), *The Geologic Time Scale*. Elsevier.
- Van der Meijden, A., A. Crottini, J. Tarrant, A. Turner, and M. Vences. 2011. Multi-locus phylogeny and evolution of reproductive modes in the Pyxicephalidae, an African endemic clade of frogs. *African Journal of Herpetology* 60:1–12.
- Vasilyan, D. 2018. Eocene Western European endemic genus *Thaumastosaurus*: new insights into the question “Are the Ranidae known prior to the Oligocene?” *PeerJ* 6:e5511.

Submitted December 27, 2020; revisions received September 20, 2021; accepted September 28, 2021.

Handling Editor: Gabriel Bever.



Conversion of the names Pyxicephaloidea, Pyxicephalidae and Pyxicephalinae (Anura, Ranoidea) into phylogenetic nomenclature

Alfred LEMIERRE* & Michel LAURIN*

*CR2P- Centre de recherche en Paléontologie-Paris, CNRS/MNHN/Sorbonnes Université, Bâtiment de Géologie, 43 rue Buffon, Paris, 75005, France.

✉ alfred.lemierre@edu.mnhn.fr; <https://orcid.org/0000-0003-1755-3018>

✉ michel.laurin@mnhn.fr; <https://orcid.org/0000-0003-2974-9835>

Abstract

The recent publications of the sixth edition of the *PhyloCode* and of the monograph *Phylonyms* now allow the publication of nomenclatural acts that will establish priority under that code. This includes defining existing and newly proposed taxon names in conformity with the *PhyloCode*. Among amphibian taxa, very few names have been converted so far, and we take the opportunity of our recent phylogenetic analysis of neobatrachians focusing on an extinct genus of *PYXICEPHALIDAE*, *Thaumastosaurus*, from the Eocene of Western Europe, to convert the names *Pyxicephaloidea*, *Pyxicephalidae* and *Pyxicephalinae* into phylogenetic nomenclature, following the *PhyloCode* rules.

Keywords

Phylogenetic nomenclature, *PhyloCode*, amphibians, *PYXICEPHALIDAE*.

Typographic conventions

Throughout this paper, we use the following conventions for the writing of different kinds of nomina (scientific names):

[A] Nomina managed under the current *International Code of Zoological Nomenclature* (Anonymous 1999, 2012) are presented according to the following standard formats: *italic lower-case letters* for nomina of species and genera (e.g. *Pyxicephalus*, *Pyxicephalus adpersus*); *ITALIC SMALL UPPER CASES* for nomina of families, subfamilies, tribes and related ranks (e.g., *PYXICEPHALIDAE*); **ITALIC SMALL UPPER CASES** for nomina of orders, classes, phyla and taxa at other higher ranks (e.g., **AMPHIBIA**).

[B] Nomina managed under the *PhyloCode* are presented in **bold italic lower-case letters** (e.g., ***Pyxicephalidae***).

Other conventions (phylogenetic definitions only)

~ : but not.

∇ : clade.

RegNum registration number: registration number of the name definition on the RegNum website <<https://www.phyloregnum.org>>.

1. Introduction

Since its first edition in 2000 (Cantino & Queiroz 2020), the *PhyloCode* has evolved to propose an alternative to the rank-based nomenclature system traditionally used, by proposing a system based on phylogenetic principles. Its objective is not to replace existing names, but rather to provide another system for governing the application of said names. With the publication of the sixth edition of the *PhyloCode* (Cantino & Queiroz 2020) and of the monograph *Phylonyms* (Queiroz & Cantino 2020), it is now possible to publish nomenclatural acts (definitions of new or converted names) that will have official standing under the *PhyloCode*. The first set of nomenclatural acts established under the *PhyloCode* was published in the monograph *Phylonyms* (Queiroz *et al.* 2020). Now, nomenclatural acts valid under the *PhyloCode* can be published in regular journals. Among amphibian taxa, much remains to be done because only *Amphibia* (Laurin *et al.* 2020a), *Lissamphibia* (Laurin *et al.* 2020b), *Caudata* (D. B. Wake 2020) and *Gymnophiona* (M. H. Wake 2020) have been converted in *Phylonyms*. Building on our recent phylogenetic analysis of the ‘RANOIDEA’ Ford & Cannatella, 2004 (~ *SCOPTANURA* in Dubois *et al.*, 2021), we take the opportunity to convert three taxon names on which our recent work focuses (Lemierre *et al.* 2021). We follow the phylogeny (Fig. 1) and the nomenclature proposed by Dubois *et al.* (2021) in their recent work regarding the names that we convert.

2. Phylogenetic nomenclature

2.1. *Pyxicephaloidae* Bonaparte, 1850 [Lemierre & Laurin], converted clade name (RegNum registration number: 558)

2.1.1. Definition

The largest clade containing *Pyxicephalus adspersus* Tschudi, 1838, *Aubria subsigillata* Duméril, 1856, *Cacosternum boettgeri* Boulenger, 1882 and *Tomopterna natalensis* Smith, 1849, but not *Petropedetes palmipes* Boulenger, 1905 (*PETROPEDETOIDAE*), *Micrixalus fuscus* Boulenger, 1882 (*MICRIXALOIDAE*), *Ericabatrachus baleensis* Largen, 1991 (*ERICABATRACHOIDAE*), *Pelophylax ridibundus* Pallas, 1771 (*RANOIDEAE*) and *Conraua goliath* Boulenger, 1906 (*CONRAUOIDAE*). Abbreviated definition: max total ∇ (*Pyxicephalus adspersus* Tschudi, 1838, *Aubria subsigillata* Duméril 1856, *Cacosternum boettgeri* Boulenger 1882 ~ *Petropedetes palmipes* Boulenger, 1905, *Micrixalus fuscus*, Boulenger, 1882, *Ericabatrachus baleensis* Largen, 1991, *Pelophylax ridibundus* Pallas, 1771 and *Conraua goliath* Boulenger, 1906).

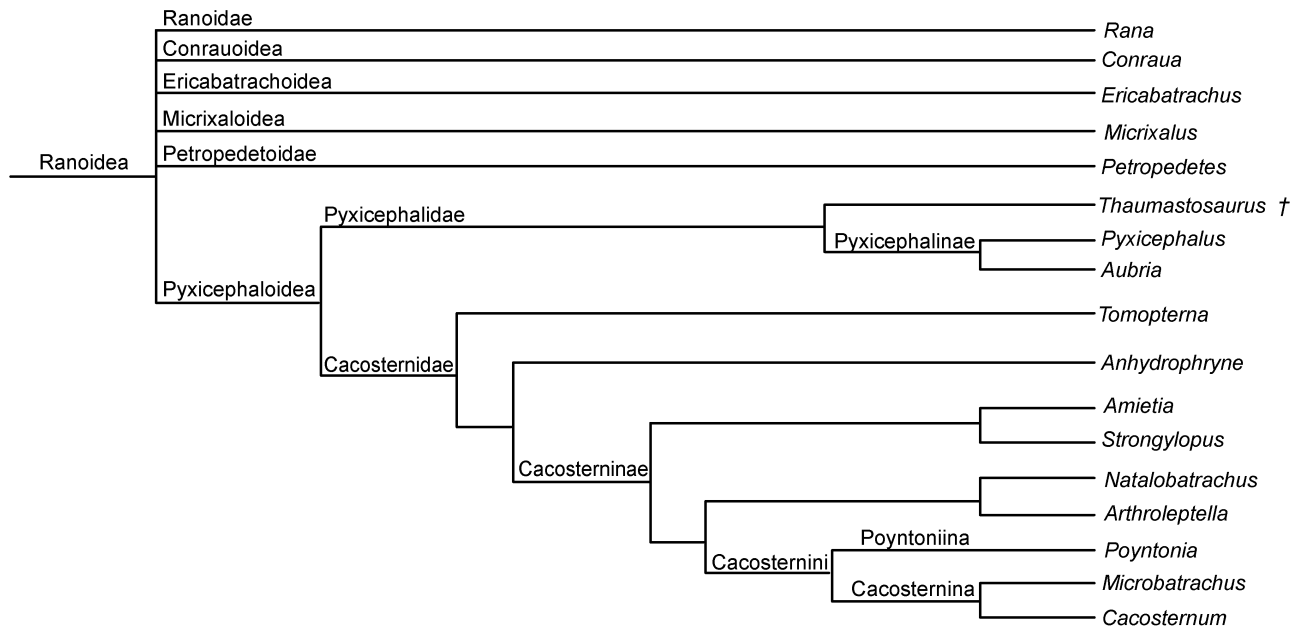


FIGURE 1. Simplified phylogeny of the *Pyxicephaloidea* modified from the phylogeny of Dubois *et al.* (2021: fig.6). Position of *Thaumastosaurus* has been inferred from Lemierre *et al.* (2021). Terminal taxa are at the generic level and † represents an extinct taxon.

2.1.2. Etymology

Named after the eponymous genus *Pyxicephalus* Tschudi, 1838. Derived from the ancient Greek *pyxis* (cylindrical box) and *kephalē* (head). These two roots refer to the bulky head of *Pyxicephalus adspersus* Tschudi 1838.

2.1.3. Reference phylogeny

The primary reference phylogeny is Jetz & Pyron (2018: fig. S1; see also Dubois *et al.* 2021: appendix A2, tree 1) for the relationship between and within the two extant clades of *PYXICEPHALOIDEA*, *PYXICEPHALIDAE* and *CACOSTERNIDAE*, and for the position of *PYXICEPHALOIDEA* among *RANOIDEA*. Other phylogenies focused on *NATATANURA* (~ *PANANURA* in Dubois *et al.* 2021) include Yuan *et al.* (2019, fig. 2) and those by Bittencourt-Silva *et al.* (2016, fig. 4), Cai *et al.* (2019, fig. 4), more focused on *PYXICEPHALOIDEA* and one more focused on *CACOSTERNIDAE* by Van der Meijden *et al.* (2011, fig.1–2).

2.1.4. Composition

Pyxicephaloidea encompasses two main clades: [1] the *PYXICEPHALIDAE* Bonaparte, 1850, comprising *Pyxicephalus* Tschudi, 1838, *Aubria* Boulenger, 1917 and *Thaumastosaurus* De Stefano, 1903, and [2] the *CACOSTERNIDAE* Noble, 1931, comprising *Amietia* Dubois, 1987, *Anhydrophryne* Hewitt, 1919, *Arthroleptella* Hewitt, 1926, *Cacosternum* Boulenger, 1887, *Microbatrachella* Hewitt, 1926, *Natalobatrachus* Hewitt & Methuen, 1912, *Nothophryne* Poynton, 1963, *Poyntonia* Channing & Boycott, 1989, *Strongylopus* Tschudi, 1838 and *Tomopterna* Duméril & Bibron, 1841.

2.1.5. Diagnostic apomorphies

Unfortunately, no morphological synapomorphies have been identified for this clade (Frost *et al.* 2006), with the different taxa possessing very heterogeneous morphologies. Recent studies have focused on molecular characters rather than morphological ones (mostly because the former yielded more robust results). However, a recent morphological analysis by Lemierre *et al.* (2021) recovered this clade, supported by a non-unique combination of three synapomorphies: [1] presence of an open groove for pathway of occipital artery on skull (also present in *CERATOBATRACHINAE*, for example); [2] pars facialis of maxillae bearing slight ornamentation (also present in *CERATOPHRYIDAE* and *CERATOBATRACHINAE*, among others); [3] digits II and III of forelimb of the same length (also present in *PTYCHADENIDAE*, for instance). However, these synapomorphies are only for the smallest clade including the sampled taxa from the analyses (see Lemierre *et al.* 2021: Appendix S4 in Supplemental Data 1) and were obtained on a constrained topology taken from the phylogenetic analyses of Jetz & Pyron (2018). In addition, two of these characters are further modified in *Pyxicephalidae* (see below). There is however a high molecular support for this clade (Dubois 2005; Van der Meijden *et al.* 2005; Frost *et al.* 2006), and it is recovered in all recent molecular analyses for anurans or *RANOIDEA* (Pyron & Wiens 2011; Van der Meijden *et al.* 2011; Frazão *et al.* 2015; Feng *et al.* 2017; Jetz & Pyron 2018).

2.1.6. Synonyms

Synonyms are *PHRYNOPSINAE* Noble, 1931 (its type genus was synonymized with *Pyxicephalus*), as mentioned by Loveridge (1936) and Laurent (1946), *CACOSTERNINAE* Noble, 1931 (according to Dubois 1994 and Frost *et al.* 2006), and *TOMOPTERNINI* Dubois, 1987 (according to Frost *et al.* 2006).

2.1.7. Comments

The name *PYXICEPHALIDAE* has been erected early to accommodate the newly described *Pyxicephalus* (Bonaparte 1850). However, this taxon was soon considered a subgenus of *Rana*, a common situation for numerous ranoids taxa (Boulenger 1920*a–b*; Noble 1931), and the name *Pyxicephalus* fell into disuse for more than a century. However, slowly, several subgenera were raised to generic rank (Dubois 1981), as the large genus *Rana* began to be dismantled. For several taxa, including *Aubria* and *Pyxicephalus*, this work linked with the dismantling of *Rana* was still ongoing in the 1980s and 1990s, although Laurent (1953) already recognized *Aubria* as a genus. Thus, Dubois (1981, 1983) dismantled *Rana* into several subfamilies and genera, but conserved *Pyxicephalus* and *Aubria* as subgenera of *Rana*. Poynton & Broadley (1985) split *Rana* further, recognizing *Pyxicephalus* and *Aubria* as genera, but retained them within the *RANINAE*. The two genera were considered close (see *Pyxicephalidae*) and the family *PYXICEPHALIDAE* was used to accommodate this relationship (Dubois 1987).

In addition, several new taxa of African anurans were described (Hewitt & Methuen 1912; Hewitt 1919, 1925, 1926) and considered as distinct genera during the 20th century. To accommodate some of these taxa, Noble (1931) erected *CACOSTERNINAE* as a subfamily of *BREVICIPITIDAE* which included *Cacosternum* and *Anhydrophryne*; he considered them to be close to *ARTHROLEPTINAE*, within the much larger *RANIDAE*. A decade later, Laurent (1941), in his work on African ranids, discarded *CACOSTERNIDAE* and erected the subfamily *PHRYNOBATRACHINAE* (within the *RANIDAE*), in which

he placed various African ranids, among which the cacosternins *Anhydrophryne*, *Arthroleptella*, *Cacosternum*, *Natalobatrachus*, *Microbatrachella* and *Nothophryne*. That arrangement was accepted by Dubois (1981, 1982) and Poynton & Broadley (1985). A decade later, Dubois (1992), having elevated the subfamily *PHRYNOBATRACHINAE* to family rank, proposed resurrecting the subfamily *CACOSTERNINAE* within this family.

Affinities of *PYXICEPHALIDAE* and *CACOSTERNINAE* to other **SCOPTANURA** remained unclear, at least until the application of molecular phylogenetics to anurans (Frost *et al.* 2006) and ranoids (Dubois 2005; Scott 2005; Van der Meijden *et al.* 2005), in particular. These studies showed that *PYXICEPHALIDAE* and *CACOSTERNINAE* formed a clade. The close relationship between the two families, as well as other taxa (such as *Strongylopus*), was unexpected but supported by several molecular analyses (Dubois 2005; Van der Meijden *et al.* 2005; Frost *et al.* 2006) that led to the recognition of a larger ‘Southern African Ranids’ clade (*sensu* Van der Meijden *et al.* 2005). This led Dubois (2005) to place all members of *CACOSTERNINAE* within the subfamily *PYXICEPHALINAE*. The major analysis of Frost *et al.* (2006) showed that both clades were well supported and were sister-taxa. They recognized both *PYXICEPHALINAE* and *CACOSTERNINAE* and used the old name *PYXICEPHALIDAE* from Bonaparte (1850) as the name of the large clade encompassing both subfamilies. This topology was supported with subsequent analyses of Bossuyt *et al.* (2006), Pyron & Wiens (2011) and Van der Meijden *et al.* (2011), and more recent studies still find a close relationship between the two clades (Bittencourt-Silva *et al.*, 2016; Feng *et al.* 2017; Jetz & Pyron 2018; Cai *et al.* 2019). The recent work of Dubois *et al.* (2021) also corroborated this relationship, but considered the two clades as two families, *PYXICEPHALIDAE* and *CACOSTERNINAE*, grouped in an epifamily *PYXICEPHALOIDEA*. The relationships of *PYXICEPHALOIDEA* to other *RANOIDEA* are still unclear and unstable, forming a large hexatomy with the epifamilies *CONRAUIDAE*, *ERICABATRACHOIDAE*, *MICRIXALOIDAE*, *RANOIDEA* and *PETROPEDETOIDAE* (Dubois *et al.* 2021). In addition, recent analyses (Lemierre *et al.* 2021) have placed the extinct *Thaumastosaurus* De Stefano, 1903 within the clade, as a member of the *PYXICEPHALIDAE*. *Thaumastosaurus* was long thought to be close to South American hylids (Roček & Lamaud 1995), but recent analyses incorporating new data, notably on the postcranium (Laloy *et al.* 2013; Báez & Gómez 2018), placed it as a *RANOIDEA*, close to a clade that includes pyxicephalids and ceratobatrachids. Pyxicephalids and ceratobatrachids are not sister-taxa, and this result was linked to poor *RANOIDEA* taxonomic sample and convergent hyperossified-linked characters. Recent analyses (Lemierre *et al.* 2021), using an expanded taxonomic sample of *RANOIDEA*, placed *Thaumastosaurus* inside the *Pyxicephaloidea* and *Pyxicephalidae*, as the sister-taxa to a clade composed of the extant *Pyxicephalinae*.

Today, *Pyxicephaloidea* are found in sub-Saharan Africa from Gambia (Western Africa; Channing & Rödel 2019) to Southern Somalia (East range) and south to Cape Province, South Africa (Channing 2001). *Thaumastosaurus* is known in Western Europe from the middle Eocene (around 39.5 Ma; Vasilyan 2018) to late Eocene (around 33.5 Ma; Vasilyan 2018), which represent the only occurrences of the clade outside of its present range.

With the exception of *Thaumastosaurus*, the fossil record for *PYXICEPHALOIDEA* is limited to the Neogene, with the oldest remains attributed to the clade date to the Pleistocene, around 1 Ma (Gardner & Rage 2016). However, molecular age estimates for the clade suggest an origin around the Cretaceous/Paleogene transition (around 60 Ma, according to Feng *et al.* 2017; about 63 Ma according to Bittencourt-Silva *et al.* 2016).

2.2. *Pyxicephalidae* Bonaparte 1850 [Lemierre & Laurin], converted clade name.
(RegNum registration number: 571)

2.2.1. *Definition*

The largest clade containing *Pyxicephalus adpersus* Tschudi, 1838 and *Aubria subsigillata* Duméril, 1856 but not *Cacosternum boettgeri* Boulenger 1882 (*CACOSTERNIDAE*) and *Tomopterna natalensis* Smith, 1849 (*CACOSTERNIDAE*). Abbreviated definition: max total ∇ (*Pyxicephalus adpersus* Tschudi, 1838 and *Aubria subsigillata* Duméril, 1856 ~ *Cacosternum boettgeri* Boulenger 1882, *Tomopterna natalensis* Smith, 1849, and *Petropedetes palmipes* Boulenger, 1905).

2.2.2. *Etymology*

Named after the eponymous genus *Pyxicephalus* Tschudi, 1838. Derived from the ancient Greek *pyxis* (cylindrical box) and *kephalē* (head).

2.2.3. *Reference phylogeny*

The primary reference phylogeny is Jetz & Pyron (2018: fig. S1) for the crown-group *PYXICEPHALINAE*, and Lemierre *et al.* (2021: fig. S12) for the relationship between the crown-group and *Thaumastosaurus*. Other recent phylogenies for the crown group include Frost *et al.* (2006: fig. 50) and Pyron & Wiens (2011: fig. 2J).

2.2.4. *Composition*

The clade encompasses the extant *Pyxicephalus* Tschudi, 1838 and *Aubria* Boulenger, 1917 (forming the crown-group *PYXICEPHALINAE*) and the extinct Eocene *Thaumastosaurus* Stefano, 1903, the last of which is located on the stem of the crown-group.

2.2.5. *Diagnostic apomorphies*

According to Clarke (1981) and corroborated by Frost *et al.* (2006), the clade is diagnosed by the unique combination of the following apomorphies: [1] presence of enclosed canal for occipital artery (also present in *CERATOPHRYIDAE*, for example); [2] well-developed zygomatic ramus of squamosal (longer than its otic ramus and articulated with maxillae; also present in *CERATOBATRACHINAE*, among others); [3] well-developed medial ramus of pterygoids overlapping parasphenoid alae (also present in *CERATOBATRACHINAE*, for example); [4] cranial exostosis (*sensu* Trueb 1973; also present in *CERATOPHRYIDAE*, for instance). Another putative synapomorphy is the anterior extension of the squamosal forming the entire lateral margin of the orbit and in contact anteriorly with the nasal (Lemierre *et al.* 2021).

2.2.6. Synonyms

Approximate synonyms (that implicitly refer to the crown-group to the extent that only extant taxa were mentioned) are *PYXICEPHALINA* Bonaparte, 1850, *PHRYNOPSINAE* Noble, 1931, as mentioned by Loveridge (1936) and Laurent (1946), and *PYXICEPHALINI* Bonaparte, 1850 (used as a valid tribe nomen for the crown-group, see below).

2.2.7. Comments

As mentioned earlier, *PYXICEPHALIDAE* was proposed in the middle of the 19th century (Bonaparte 1850), but rapidly fell into disuse, as numerous ranoids (and other anurans) were considered to be subgenera of *Rana*. Slowly, several subgenera were raised to generic rank (Dubois 1981), as the large genus *Rana* began to be dismantled during the second half of the 20th century.

When *PYXICEPHALIDAE* was erected, it was to accommodate the genus described by Tschudi (1838) a decade earlier, and it only contained this eponymous genus. However, close affinities between *Pyxicephalus* and *Aubria* (first described as *Rana subsigillata* by Duméril in 1856) were first proposed by Procter (1919), who thought that both belonged to the same subgenus of *Rana*, in accordance to a Boulenger's unpublished manuscript on African ranids (see Clarke 1981). These close affinities were also supported by Clarke (1981), who proposed two alternatives, either that *Pyxicephalus* and *Aubria* were congeneric as Procter (1919) had suggested, or that *Aubria* was a sister-taxon to *Pyxicephalus*. A few years later, the second phylogenetic hypothesis (*Aubria* is a sister-taxon to *Pyxicephalus*) was accepted by Dubois (1987), who resurrected *PYXICEPHALIDAE* (~ *PYXICEPHALINAE* of Dubois 1987) as a subfamily of *RANIDAE* (which encompassed various taxa previously considered subgenera of *Rana*).

However, the affinities of *PYXICEPHALIDAE* to other *RANOIDEA* remained unclear, at least until the application of molecular phylogenetics to anurans (Frost *et al.* 2006) and ranoids (Dubois 2005; Scott 2005; Van der Meijden *et al.* 2005), in particular. These studies showed that *PYXICEPHALIDAE* belongs to a large clade of 'Southern African Ranids' (sensu Van der Meijden *et al.* 2005). Following these results, Dubois (2005) proposed to expand *PYXICEPHALIDAE* (~ *PYXICEPHALINAE* of Dubois 2005) to encompass cacosternins taxa. Frost *et al.* (2006) analysis led to the restriction of *PYXICEPHALINAE* to its eponymous genus and *Aubria*. In their recent monograph, Dubois *et al.* (2021) considered the latter clade as a family, and retained the name *PYXICEPHALIDAE* Bonaparte, 1850 as the valid nomen. As mentioned earlier, a recent study recovered the extinct *Thaumastosaurus* as a *PYXICEPHALIDAE* (Lemierre *et al.* 2021).

Pyxicephalidae are known in the fossil record since the middle Eocene, around 39.5 Ma, with the geologically oldest remains attributed to *Thaumastosaurus* (Lemierre *et al.* 2021). *Thaumastosaurus* extends up to the late Eocene, around 33.5 Ma. There is a large gap in the fossil record of *Pyxicephalidae* after the Eocene; the next oldest remains attributed to are from the late Pleistocene (around 12 000 years; Robbins *et al.* 1996) and attributed to the crown-group *Pyxicephalinae*.

2.3. *Pyxicephalinae* Bonaparte, 1850 [A. Lemierre, M. Laurin], converted clade name (RegNum registration number: 572)

2.3.1. *Definition*

The smallest clade containing *Pyxicephalus adspersus* Tschudi, 1838 and *Aubria subsigillata* Duméril, 1856 but not *Thaumastosaurus* De Stefano, 1903. Abbreviated definition: min crown ∇ (*Pyxicephalus adspersus* Tschudi, 1838 and *Aubria subsigillata* Duméril, 1856 ~ *Thaumastosaurus servatus* Filhol, 1877).

2.3.2. *Etymology*

Named after the eponymous genus *Pyxicephalus* Tschudi 1838. Derived from the ancient Greek *pyxis* (cylindrical box) and *kephalē* (head).

2.3.3. *Reference phylogeny*

The primary reference phylogeny is Jetz & Pyron (2018, fig. S1), with a majority of taxa within the clade represented. Other recent phylogenies for *PYXICEPHALINAE* include Frost *et al.* (2006: fig. 50) and Pyron & Wiens (2011: fig. 2J).

2.3.4. *Composition*

The clade encompasses the extant *Pyxicephalus* Tschudi, 1838 and *Aubria* Boulenger, 1917.

2.3.5. *Diagnostic apomorphies*

Pyxicephalinae can be characterized using the following combination of skeletal synapomorphies, recovered in the analyses of Lemierre *et al.* (2021): [1] alary process of premaxillae oriented dorsally; [2] development of fang-like laminar projection on anterior portion of dentaries; [3] articulation for lower jaw located posterior to occiput.

2.3.6. *Synonyms*

Synonyms are the same as for ***Pyxicephalidae***, as most authors used both names to refer to a clade composed only of extant taxa.

2.3.7. *Comments*

The clade is endemic to Sub-Saharan Africa, from Gambia (Western Africa; Channing and Rödel 2019) to Southern Somalia (East range) and south to Cape Province, South Africa (Channing 2001), with various *Pyxicephalus* taxa having the widest geographical range (Channing & Rödel 2019).

The genus *Pyxicephalus* is represented by some of the largest extant anurans (the various taxa are dubbed the African bullfrog) and are known to be very aggressive and voracious eaters, eating anything that they can manage to capture. They are notably known for preying on small vertebrates (small anurans, squamates, rodents) and are even capable of subduing and eating small birds (Branch 1976). This genus is also known to be consumed for its flesh by local inhabitants of southern Africa (for an example in Namibia, see Okeyo *et al.* 2015) and this practice has been recorded for at least 12 000 years, with the oldest remains attributed to *Pyxicephalus* being burnt, indicating that the frogs had been cooked and eaten (Robbins *et al.* 1996, 2009).

3. Concluding remarks

The *Pyxicephaloidea*, *Pyxicephalidae* and *Pyxicephalinae* are here converted into the phylogenetic nomenclatural system. We also took the opportunity to formally include the extinct *Thaumastosaurus* in the definition of two nomina. Although the phylogenetic position of *Thaumastosaurus* has strong support, its exclusion from *Pyxicephaloidea* would render *Pyxicephalidae* and *Pyxicephalinae* redundant but not synonymous. As mentioned earlier, a large geographical and stratigraphic gap exist between *Thaumastosaurus* and the other *Pyxicephalidae*, and undescribed extinct taxa from Africa might fill these gaps. As an example, the recently described *Rocekophryne ornata* Rage *et al.*, 2021 from the lower Eocene of Algeria is considered a *RANOIDEA* with osteological characters similar to *Thaumastosaurus*. In addition, *R. ornata* shares several osteological synapomorphies with the *Pyxicephaloidea* (presence of an open groove for the occipital arterial pathway and ornamented pars facialis of the maxilla). This taxon could represent the oldest *Pyxicephaloidea* and would fill part of the geographical gap of the clade. Phylogenetic analyses are needed to confirm this hypothetical position.

As this work is based on our recent phylogenetic analyses of an extinct stem-*PYXICEPHALINAE*, we did not convert the *CACOSTERNIDAE*. The conversion of this name could be addressed in a more thorough study of the relationships between the various genera of *CACOSTERNIDAE*.

To conclude, this work on the conversion of *PYXICEPHALOIDEA*, *PYXICEPHALIDAE* and *PYXICEPHALINAE* is only a first step toward the conversion of the numerous anuran clade nomina, as no study has yet converted *SALIENTIA* or *ANURA*, or various less inclusive clades, except for those converted here.

All definitions of names following the phylogenetic nomenclature system are stored in the RegNum website: <https://www.phyloregnum.org>.

4. References

- Báez, A. M. & Gómez, R. O. (2018) Dealing with homoplasy: osteology and phylogenetic relationships of the bizarre neobatrachian frog *Baurubatrachus pricei* from the Upper Cretaceous of Brazil. *Journal of systematic Palaeontology*, **16**: 279–308. <<https://doi.org/10.1080/14772019.2017.1287130>>.
- Bittencourt-Silva, G. B., Conradie, W., Siu-Ting, K., Tolley, K., Channing, A., Cunningham, M., Farooq, H., Menegon, M. & Loader, S. (2016) The phylogenetic position and diversity of the enigmatic mongrel frog *Nothophryne* Poynton, 1963 (Amphibia, Anura). *Molecular Phylogenetics and Evolution*, **99**: 89–102. <<https://doi.org/10.1016/j.ympev.2016.03.021>>.
- Bonaparte, C. (1850) *Conspectus Systematum. Herpetologiae et Amphibiologiae*. Leiden (Brill): 1 pl.
- Bossuyt, F., Brown, R. M., Hillis, D. M., Cannatella, D. C. & Milinkovitch, M. C. (2006) Phylogeny and biogeography of a cosmopolitan frog radiation: Late Cretaceous diversification resulted in continent-scale endemism in the family Ranidae. *Systematic Biology*, **55**: 579–594. <<https://doi.org/10.1080/10635150600812551>>.
- Boulenger, G. A. (1882) *Catalogue of the Batrachia Salientia s. Ecaudata in the collection of the British Museum*. Second

- edition. London (Taylor & Francis): 1–530.
- Boulenger, G. A. (1887) Descriptions of new reptiles and batrachians in the British Museum (Natural history), part III. *Annals and Magazine of natural History*, (5), **20** (115): 50–53. <<https://doi.org/10.1080/00222938709460009>>.
- Boulenger, G. A. (1905). Descriptions of new West-African frogs of the genera *Petropedetes* and *Bulua*. *Annals and Magazine of natural History*, (7), **15** (87): 281–283. <<https://doi.org/10.1080/03745480509443042>>.
- Boulenger, G. A. (1906) Descriptions of new batrachians discovered by Mr. G. L. Bates in South Cameroon. *Annals and Magazine of natural History*, (7), **17** (7): 317–323. <<https://doi.org/10.1080/00222930608562529>>.
- Boulenger, G. A. (1917) Sur la conformation des phalangettes chez certaines grenouilles d’Afrique. *Compte rendu hebdomadaire des Séances de l’Académie des Sciences*, Paris, **165**: 989–990. <<https://doi.org/10.5962/bhl.part.1217>>.
- Boulenger, G. A. (1918) Aperçu des principes qui doivent régir la classification des espèces du genre *Rana*. *Bulletin de la Société zoologique de France*. **43**: 111–121. <<https://doi.org/10.5962/bhl.part.29706>>.
- Boulenger, G. A. (1920a) A monograph of the South Asian, Papuan, Melanesian and Australian frogs of the genus *Rana*. *Records of the Indian Museum*, **20**: 1–226. <<https://doi.org/10.5962/bhl.title.12471>>.
- Boulenger, G. A. (1920b) A monograph of the American frogs of the genus *Rana*. *Proceeding of the American Academy of Arts and Sciences*, **55** (9): 413–480. <<https://doi.org/10.2307/20025810>>.
- Branch, W. R. (1976) Two exceptional food records for the African Bullfrog, *Pyxicephalus adspersus* (Amphibia, Anura, Ranidae). *Journal of Herpetology*, **10** (3): 266–268. <<https://doi.org/10.2307/1562997>>.
- Cai, Y.-Y., Shen, S.-Q., Lu, L.-X., Storey, K. B., Yu, D.-N. & Zhang, J.-Y. (2019) The complete mitochondrial genome of *Pyxicephalus adspersus*: high gene rearrangement and phylogenetics of one of the world’s largest frogs. *PeerJ*, **7** [e7532]. <<https://doi.org/10.7717/peerj.7532>>.
- Cantino, P. D. & Queiroz, K. de (2020) *International Code of Phylogenetic Nomenclature (PhyloCode): a phylogenetic code of biological nomenclature*. Boca Raton, Florida (CRC Press): 1–189. <<https://doi.org/10.1201/9780429446320-1>>.
- Channing, A. (2001) *Amphibians of central and southern Africa*. Ithaca, NY (Cornell University Press): 1–496. <<https://doi.org/10.7591/9781501733697>>.
- Channing, A. & Boycott, R. C. (1989) A new frog genus and species from the mountains of the southwestern Cape, South Africa (Anura: Ranidae). *Copeia*, **1989** (2): 467–471. <<https://doi.org/10.2307/1445445>>.
- Channing, A. & Rödel M.-O. (2019) *Field guide to the frogs & other amphibians of Africa*. Cape Town, South Africa (Struik Nature): 1–395.
- Clarke, B. T. (1981) Comparative osteology and evolutionary relationships in the African Raninae (Anura Ranidae). *Monitore zoologico italiano*, (n.s.), suppl. **15**: 285–331. <<https://doi.org/10.1080/03749444.1981.10736638>>.
- De Stefano, G. (1903) I sauri del Quercy appartenenti alla collezione Rossignol. *Atti della Società italiana di Scienze naturali*, **4**: 382–418.
- Dubois, A. (1981) Liste des genres et sous-genres nominaux de Ranoidea (Amphibiens Anoures) du monde, avec identification de leurs espèces-types: conséquences nomenclaturales. *Monitore zoologico italiano*, (n.s.), suppl. **15**: 225–284. <<https://doi.org/10.1080/03749444.1981.10736637>>.
- Dubois, A. (1982) Notes sur la classification des Ranidae (Amphibiens, Anoures). *Bulletin mensuel de la Société linnéenne de Lyon*, **61** (10): 305–352. <<https://doi.org/10.3406/linly.1992.11011>>.
- Dubois, A. (1983) Classification et nomenclature supragénérique des Amphibiens Anoures. *Bulletin mensuel de la Société linnéenne de Lyon*, **52**: 270–276. <<https://doi.org/10.3406/linly.1983.10607>>.
- Dubois, A. (1987) Miscellanea taxinomica batrachologica (I). *Alytes*, **5**: 7–95.
- Dubois, A. (1992) Notes sur la classification des Ranidae (Amphibiens, Anoures). *Bulletin mensuel de la Société linnéenne de Lyon*, **61**: 305–352. <<https://doi.org/10.3406/linly.1992.11011>>.
- Dubois, A. (1994) Phrynobatrachinae Laurent, 1941 (Amphibia, Anura): proposed conservation. *Bulletin of zoological Nomenclature*, **51** (3): 240–246. <<https://doi.org/10.5962/bhl.part.7204>>.
- Dubois, A. (2005) Amphibia Mundi. 1.1. An ergotaxonomy of recent amphibians. *Alytes*, **23**: 1–24.
- Dubois, A., Ohler, A. & Pyron, R. A. (2021) New concepts and methods for phylogenetic taxonomy and nomenclature in zoology, exemplified by a new ranked cladonomy of recent Amphibians (Lissamphibia). *Megataxa*, **5** (1): 1–738. <<https://doi.org/10.11646/megataxa.5.1.1>>.
- Duméril, A. H. A. (1856) Note sur les Reptiles du Gabon. *Revue et Magasin de Zoologie pure et appliquée*, **2**: 553–562.
- Duméril, A. H. A. & Bibron, G. (1841) *Erpétologie générale ou Histoire naturelle complète des Reptiles*. Volume **8**. Paris (Roret): 1–792.
- Feng, Y.-J., Blackburn, D. C., Liang, D., Hillis, D. M., Wake, D. B., Cannatella D. C. & Zhang, P. (2017) Phylogenomics reveals rapid, simultaneous diversification of three major clades of Gondwanan frogs at the Cretaceous–Paleogene boundary. *Proceedings of the national Academy of Sciences*, **114**: E5864–E5870. <<https://doi.org/10.1073/pnas.1704632114>>.
- Filhol, H. 1877. *Recherches sur les phosphorites du Quercy: étude des fossiles qu’on y rencontre et spécialement des Mammifères*. Paris (Librairie de l’Académie de médecine): 1–690.
- Frazão, A., Silva, H. R. da & Russo, C. A. de M. (2015) The Gondwana breakup and the history of the Atlantic and Indian Oceans unveils two new clades for early neobatrachian diversification. *PLoS One*, **10** [e0143926]. <<https://doi.org/10.1371/journal.pone.0143926>>.

- org/10.1371/journal.pone.0143926>.
- Frost, D. R., Grant, T., Faivovich, J., Bain, R. H., Haas, A., Haddad, C. F. B., de Sá, R. O., Channing, A., Wilkinson, M., Donnellan, S. C., Raxworthy, C. J., Campbell, J. A., Blotto, B. L., Moler, P., Drewes, R. C., Nussbaum, R. A., Lynch, J. D., Green, D. M. & Wheeler, W. C. (2006) The Amphibian Tree of Life. *Bulletin of the American Museum of Natural History*, **297**: 1–291. <[https://doi.org/10.1206/0003-0090\(2006\)297\[0001:TATOL\]2.0.CO;2](https://doi.org/10.1206/0003-0090(2006)297[0001:TATOL]2.0.CO;2)>.
- Gardner, J. D. & Rage, J.-C. (2016) The fossil record of lissamphibians from Africa, Madagascar, and the Arabian Plate. *Palaeobiodiversity and Palaeoenvironments*, **96**: 169–220. <<https://doi.org/10.1007/s12549-015-0221-0>>.
- Hewitt, J. (1919) *Anhydrophryne rattrayi*, a remarkable new frog from Cape Colony. *Records of the Albany Museum, Grahamstown*, **3**: 182–189.
- Hewitt, J. (1925) On some new species of reptiles and amphibians from South Africa. *Records of the Albany Museum, Grahamstown*, **3**: 343–368.
- Hewitt, J. (1926) Descriptions of new and little-known lizards and batrachians from South Africa. *Annals of the South African Museum*, **20**: 413–431.
- Hewitt, J. & Methuen, P. A. (1912) Descriptions of some new Batrachia and Lacertilia from South Africa. *Transactions of the Royal Society of South Africa*, **3**: 107–111. <<https://doi.org/10.1080/00359191309519682>>.
- Jetz, W. & Pyron, R. A. (2018) The interplay of past diversification and evolutionary isolation with present imperilment across the amphibian tree of life. *Nature, Ecology & Evolution*, **2**: 850–858. <<https://doi.org/10.1038/s41559-018-0515-5>>.
- Laloy, F., Rage, J. C., Evans, S. E., Boistel, R., Lenoir, N. & Laurin, M. (2013) A re-interpretation of the Eocene anuran *Thaumastosaurus* based on microCT examination of a ‘mummified’ specimen. *PLoS One*, **8** [e74874]. <<https://doi.org/10.1371/annotation/f7988d67-24b9-493c-9aef-c5c715948a1e>>.
- Largen, M. J. (1991) A new genus and species of petropedetine frog (Amphibia Anura Ranidae) from high altitude in the mountains of Ethiopia. *Tropical Zoology*, **4**: 139–152. <<https://doi.org/10.1080/03946975.1991.10539483>>.
- Laurent, R. F. (1941) Contribution à l’ostéologie et à la systématique des Ranides africains. Première note. *Revue de Zoologie et de Botanique africaines*, **34**, ‘1940’: 74–96.
- Laurent, R. F. (1946) Mises au point dans la taxonomie des Ranides. *Revue de Zoologie et de Botanique africaines*, **39**: 336–338.
- Laurent, R. F. (1953) Reptiles et Batraciens récemment parvenus au Musée royal du Congo belge. *Bulletin du Cercle zoologique congolais*, **21**: 21–29.
- Laurin, M., Arntzen, J. W., Báez, A. M., Bauer, A. M., Damiani, R., Evans, S. E. et al. (2020a) Amphibia. In: K. de Queiroz, P. D. Cantino & J. A. Gauthier (ed.), *Phylonoms: an implementation of PhyloCode*, Boca Raton, Florida (CRC Press): 765–771.
- Laurin, M., Arntzen, J. W., Báez, A. M., Bauer, A. M., Damiani, R., Evans, S. E. et al. (2020b) Lissamphibia. In: K. de Queiroz, P. D. Cantino & J. A. Gauthier (ed.), *Phylonoms: an implementation of PhyloCode*, Boca Raton, Florida (CRC Press): 773–778.
- Lemierre, A., Folie, A., Bailon, S., Robin N. & Laurin, M. (2021) From toad to frog, a CT-based reconsideration of *Bufo servatus*, an Eocene anuran mummy from Quercy (France). *Journal of Vertebrate Paleontology*, **41** (3) [e1989694].
- Loveridge, J. P. (1936) Scientific results of an expedition to rain forest regions in eastern Africa VII. Amphibians. *Bulletin of the Museum of Comparative Zoology*, **79**: 369–430.
- Noble, G. K. (1931) *The biology of the Amphibia*. New York & London (McGraw-Hill Book Company): 1–600. <<https://doi.org/10.5962/bhl.title.82448>>.
- Okeyo, D. O., Kandjenogo, L. & Kashea, M. M. (2015) Harvesting and consumption of the giant African bullfrog, a delicacy in northern Namibia. In: K. C. Chinsembu, A. Cheikhyoussef, D. Mumbengegwi, M. Kandawa-Schilz, C. D. Kasanda, & L. Kazembe (ed.), *Indigenous knowledge of Namibia*, Windhoek, Namibia (UNAM Press): 205–219. <<https://doi.org/10.2307/j.ctvvc619h.15>>.
- Parry, R. (1982) A revision of southern African *Pyxicephalus* Tschudi (Anura: Ranidae). *Annals of the Natal Museum*, **25**: 281–292.
- Pallas, P. S. (1771) *Reise durch verschiedene Provinzen des Russischen Reichs*. Theil **1**. Saint-Petersburg (Gedruckt bey der Kayserlichen Academie der Wissenschaften): 1–504.
- Poynton, J. C. (1963) Descriptions of southern African amphibians. *Annals of the Natal Museum*, **15**: 319–332.
- Poynton, J. C. & Broadley, G. (1985) Amphibia Zambesiaca 2. Ranidae. *Annals of the Natal Museum*, **27**: 115–181.
- Procter, M. J. B. (1919) On the skull and affinities of *Rana subsigillata* A. Dum. *Proceedings of the Zoological Society of London*, **89**: 21–27. <<https://doi.org/10.1111/j.1096-3642.1919.tb02109.x>>.
- Pyron, R. A. & Wiens, J. J. (2011) A large-scale phylogeny of Amphibia including over 2800 species, and a revised classification of extant frogs, salamanders, and caecilians. *Molecular Phylogenetics and Evolution*, **61**: 543–583. <<https://doi.org/10.1016/j.ympev.2011.06.012>>.
- Queiroz, K. de, Cantino, P. D. & Gauthier, J. A. (2020) *Phylonoms: a companion to the PhyloCode*. Boca Raton, Florida (CRC Press): 1–1352. <<https://doi.org/10.1201/9780429446276>>.
- Rage, J.-C., Adaci, M., Bensalah, M., Mahboubi, M., Marivaux, L., Mebrouk, F. & Tabuce, R. (2021) Latest early-middle Eocene deposits of Algeria (Glib Zegdou, HGL50) yield the richest and most diverse fauna of amphibians and squamate

- reptiles from the Palaeogene of Africa. *Paleovertebrata*, **44** (1) [e1]. <<https://doi.org/10.18563/pv.44.1.e1>>.
- Robbins, L. H., Murphy, M. L., Stevens, N. J., Brook, G. A., Ivester, A. H., Haberyan, K. A., Klein, R. G., Milo, R., Stewart, K. M., Matthesen, D. G., & Winkler, A. J. (1996) Paleoenvironment and archaeology of Drotzky's Cave: western Kalahari Desert, Botswana. *Journal of archaeological Science*, **23**: 7–22. <<https://doi.org/10.1006/jasc.1996.0002>>.
- Robbins, L. H., Campbell, A. C., Murphy, M. L., Brook, G. A., Mabuse, A. A., Hitchcock, R. K., Babutsi, G., Mmolowa, M., Stewart, K.M., Steele, T. E., Klein, R. G. & Appleton, C. C. (2009). Mogapelwa: archaeology, palaeoenvironment and oral traditions at Lake Ngami, Botswana. *South African archaeological Bulletin*, **64**: 13–32.
- Roček, Z. & Lamaud P. (1995) *Thaumastosaurus bottii* De Stefano, 1903, an anuran with Gondwanan affinities from the Eocene of Europe. *Journal of Vertebrate Paleontology*, **15**: 506–515. <<https://doi.org/10.1080/02724634.1995.10011244>>.
- Rödel, M.-O. (2000) *Herpetofauna of West Africa*. Volume 1. *Amphibians of the West African savanna*. Frankfurt/Main (Edition Chimaira): 1–335.
- Scott, E. (2005) A phylogeny of ranid frogs (Anura: Ranoidea: Ranidae), based on a simultaneous analysis of morphological and molecular data. *Cladistics*, **21**: 507–574. <<https://doi.org/10.1111/j.1096-0031.2005.00079.x>>.
- Smith, A. (1849) *Illustrations of the zoology of South Africa, consisting chiefly of figures and descriptions of the objects of natural history collected during an expedition into the interior of South Africa in the years 1834, 1835 and 1836... Reptilia*. London (Smith, Elder & Co.): appendix 1–28. <<https://doi.org/10.5962/bhl.title.120442>>.
- Trueb, L. (1973) Bones, frogs and evolution. In: J. L. Vial (ed.), *Evolutionary biology of the Anurans, Contemporary research on major problems*, Columbia (University of Missouri Press): 65–133.
- Tschudi, J. J. (1838) Classification der Batrachier, mit Berücksichtigung der fossilen Thiere dieser Abtheilung der Reptilien. *Mémoires de la Société des Sciences naturelles de Neuchâtel*, **2**: 1–100. <<https://doi.org/10.5962/bhl.title.4883>>.
- Van der Meijden, A., Crottini, A., Tarrant, J., Turner, A. & Vences, M. (2011) Multi-locus phylogeny and evolution of reproductive modes in the Pyxicephalidae, an African endemic clade of frogs. *African Journal of Herpetology*, **60**: 1–12. <<https://doi.org/10.1080/21564574.2010.523904>>.
- Van der Meijden, A., Vences, M., Hoegg, S. & Meyer, A. (2005) A previously unrecognized radiation of ranid frogs in Southern Africa revealed by nuclear and mitochondrial DNA sequences. *Molecular Phylogenetics and Evolution*, **37**: 674–685. <<https://doi.org/10.1016/j.ympev.2005.05.001>>.
- Van Dijk, D. E. (1966) Systematic and field keys to the families, genera and described species of southern African anuran tadpoles. *Annals of the Natal Museum*, **18**: 231–286.
- Vasilyan, D. (2018) Eocene Western European endemic genus *Thaumastosaurus*: new insights into the question “Are the Ranidae known prior to the Oligocene?” *PeerJ*, **6** [e5511]. <<https://doi.org/10.7717/peerj.5511>>.
- Wake, D. B. (2020) Caudata. In: K. de Queiroz, P. D. Cantino & J. A. Gauthier (ed.), *Phylonoms: an implementation of PhyloCode*. Boca Raton, Florida (CRC Press): 785–787.
- Wake, M. H. (2020) Gymnophiona. In: K. de Queiroz, P. D. Cantino & J. A. Gauthier (ed.), *Phylonoms: an implementation of PhyloCode*. Boca Raton, Florida (CRC Press): 779–783.
- Yuan, Z.-Y., Zhang, B.-L., Raxworthy, C. J., Weisrock, D. W., Hime, P. M., Jin, J.-Q., Lemmon, E. M., Lemmon, A. R., Holland, S. D., Kortyna, M. L., Zhou, W.-W., Peng, M.-S., Che, J., & Prendini, E. (2019) Natatanuran frogs used the Indian Plate to step-stone disperse and radiate across the Indian Ocean. *National Science Review*, **6**: 10–14. <<https://doi.org/10.1093/nsr/nwy092>>.

Submitted: 24 February 2021. Accepted: 20 November 2021. Published: 17 December 2021.
Corresponding Editor: Alain Dubois.

A new genus and species of frog from the Kem Kem (Morocco), the second neobatrachian from Cretaceous Africa

Alfred Lemierre¹ and David C. Blackburn²

¹Département Origine et Evolution, UMR 7207, Centre de recherche en Paléontologie, CNR/Sorbonne Université/MNHN, Muséum national d'Histoire naturelle, Paris, France

²Department of Natural History, Florida Museum of Natural History, University of Florida, Gainesville, FL, United States of America

ABSTRACT

Neobatrachia, a clade representing the majority of extant anuran diversity, is thought to have emerged and diversified during the Cretaceous. Most of the early diversification of neobatrachians occurred in southern Gondwana, especially the regions that are today South America and Africa. Whereas five extinct neobatrachians have been described from the Cretaceous of South America in the last decade, only one is known from Africa. This difference in the known extinct diversity is linked to the lack of well-preserved specimens, understudy of fragmentary remains, and lack of known Cretaceous sites in Africa. Study of fragmentary anuran remains from Africa could allow for the identification of previously unknown neobatrachians, allowing for a better understanding of their early diversification. We reanalysed several previously described anuran specimens from the well-known Kem Kem beds, including using CT-scanning. Through our osteological study, we determined that several cranial bones and vertebrae represent a new hyperossified taxon for which we provide a formal description. Comparison to other hyperossified anurans revealed similarities and affinity of this new taxon with the neobatrachians *Beelzebufo* (extinct) and *Ceratophrys* (extant). Phylogenetic analyses supported this affinity, placing the new taxon within Neobatrachia in an unresolved clade of Ceratophryidae. This taxon is the oldest neobatrachian from Africa, and reveals that neobatrachians were already widespread throughout southern Gondwana during the earliest Late Cretaceous.

Submitted 4 March 2022

Accepted 17 June 2022

Published 15 July 2022

Corresponding author

Alfred Lemierre,
alfred.lemierre@edu.mnhn.fr

Academic editor

Diogo Provete

Additional Information and
Declarations can be found on
page 28

DOI 10.7717/peerj.13699

© Copyright
2022 Lemierre and Blackburn

Distributed under
Creative Commons CC-BY 4.0

OPEN ACCESS

Subjects Biodiversity, Evolutionary Studies, Paleontology, Taxonomy, Zoology

Keywords Anura, Cretaceous, Africa, Phylogeny, Neobatrachia, Taxonomy, Tomography

INTRODUCTION

The Cretaceous is a key period in anuran evolution and diversification including the emergence of major extant clades such as Neobatrachia and Pipidae (*Frazão, Da Silva & Russo, 2015; Feng et al., 2017*). The breakup of the Western Gondwana palaeocontinent during the Late Jurassic and Early Cretaceous (*McLoughlin, 2001; Blakey, 2008*)—leading to the creation of the Central and Southern Atlantic Oceans—may have contributed to the early diversification of the Neobatrachia, just as it likely did for the Pipidae (*Frazão, Da Silva & Russo, 2015; Feng et al., 2017*). Several neobatrachian taxa have been described in the last decade from the Cretaceous beds of South America (*Báez, Moura & Gómez, 2009; Báez et*

al., 2012; Báez & Gómez, 2018; Agnolin et al., 2020), contributing to a better understanding of early diversification of the Neobatrachia. Unfortunately, the fossil record of Neobatrachia is scarce for the Cretaceous of Africa and includes only a single described taxon: *Beelzebulo ampinga* (Evans, Jones & Krause, 2008) from the Cretaceous of Madagascar (Evans et al., 2014). However, the lack of both study and sampling is not limited to either African Cretaceous outgroups or extinct Neobatrachia. In general, there are few well-preserved and identifiable anuran fossils in Africa, with numerous sites yielding only few and fragmentary remains (e.g., De Broin et al., 1974; Báez & Werner, 1996; Rage, 2008; Gardner & Rage, 2016) that are not easily incorporated into phylogenetic analyses. This contrasts with South American neobatrachians, several of which are known from well-preserved and mostly articulated specimens preserving much or all of the skeleton (Báez et al., 2012). In Africa, only a handful of sites contain enough fragmentary fossils referred to the same taxon to allow for comparisons to other frogs and inclusion in phylogenetic analyses (Evans, Jones & Krause, 2008; Evans et al., 2014). These few sites are critical to filling the gap in the fossil record of Neobatrachia and central to understanding their early diversification in Africa.

The Kem Kem beds of Morocco (Cretaceous, 100–95 Ma; Ibrahim et al., 2020) are known for their rich terrestrial vertebrate fauna with numerous dinosaurs, fishes, sharks, turtles, and crocodiles (Zouhri, 2017). This fauna has been studied extensively in recent decades (Ibrahim et al., 2020) but there is only a single study of its amphibians. Rage & Dutheil (2008) provided evidence for three different anurans, including one pipid that they described as *Oumtkoutia anae* based on a neurocranium, as well as two indeterminate non-pipid anurans based on postcranial remains (Rage & Dutheil, 2008). They attributed several cranial fragments to an undescribed species (mainly based on relative size of the cranial and postcranial elements) with an ornamented and hyperossified skull, one of the earliest known from the Cretaceous of Africa. A decade ago, Agnolin (2012) described a neobatrachian taxon (Calyptocephalellidae) from the Late Cretaceous of Argentina and reviewed several Gondwanan anurans with hyperossified skulls. In that study, Agnolin (2012: 156) included Kem Kem fossils which he referred to Calyptocephalellidae based on cranial and postcranial characters. Because several subsequent studies (Báez & Gómez, 2018; Muzzopappa et al., 2020) highlighted anatomical and analytical errors in Agnolin (2012), attribution of the Kem Kem fossils to the Calyptocephalellidae is questionable. Because Agnolin (2012) considered all of the “indeterminate” anuran remains from the Kem Kem Formation to be a single taxon in his study, several characters supporting the affiliation of these fossils with the Neobatrachia are based on postcranial elements that are not clearly referable to the hyperossified cranial elements. Further, because Agnolin (2012) did not include the Kem Kem fossils in his phylogenetic analysis, their relationships were never formally tested. Reevaluation of the anatomy and phylogenetic affinities of this hyperossified Kem Kem frog may be important for deciphering the early diversification of neobatrachians during the Lower Late Cretaceous of Gondwana and filling a notable gap in the fossil record of African anurans.

Here, we use microcomputed tomographic scans (MicroCT scans) to provide new information about the anatomy of the hyperossified Kem Kem frog. These new data allow for a more complete anatomical study of this taxon, comparisons to other Cretaceous

anurans, and a phylogenetic analysis to estimate its relationships. We describe this material as a new genus and discuss its importance for understanding neobatrachian diversification in Gondwana during the Cretaceous.

Geological context

The specimens were collected in 1995 during an expedition organized by the University of Chicago and the Service géologique du Maroc at four different localities near Taouz and Oum Tkout (OT1c, TD1, TZ8a1 and TZ8a2 from [Dutheil, 1999](#)) from the Kem Kem beds ([Ettachfni & Andreu, 2004](#); [Cavin et al., 2010](#)). The term “Kem Kem beds” ([Sereno et al., 1996](#)) refers to a large escarpment extending across southeastern Morocco, near the Morocco-Algerian border ([Ibrahim et al., 2020](#): figs. 1A and 1C), with numerous exposures along its length. More recently, these beds have been referred to as the Kem Kem group ([Ibrahim et al., 2020](#)), containing two formations: the Gara Sbaa and the Douira Formations. The anuran specimens discussed here were recovered from layers that can be correlated to the Douira Formation of the Kem Kem group (upper part of the Kem Kem; [Ibrahim et al., 2020](#)). The Douira Formation (as well as the Gara Sbaa Formation) has been correlated to the Bahariya Formation in Egypt ([Sereno et al., 1996](#); [Cavin et al., 2010](#)), which is dated to the Early Cenomanian ([Cavin et al., 2010](#)). The Kem Kem group is topped by marine sediments correlated to the Cenomanian-Turonian transition ([Cavin et al., 2010](#)). Other analyses have confirmed the Cenomanian age ([Ibrahim et al., 2020](#)) and considered the Kem Kem group a single continuous deposit sequence from 100 to 95 Ma. The boundary between the Gara Sbaa and the Douira Formations is dated to 96 Ma and linked to the Mid-Cenomanian Event ([Ibrahim et al., 2020](#)). The Douira Formation—and the anuran specimens discussed here—are thus dated to the middle Cenomanian, approximately 96 to 95 Ma ([Ibrahim et al., 2020](#)).

The Douira Formation contains strata that show a marine influence that increases over time. The deposits in the lower part of the formation, composed of sandstones and mudstones, are consistent with a river delta, whereas the deposits in the upper part, composed of interbedded mudstone with claystone, are characteristic of coastal and sabkha environments (see [Ibrahim et al., 2020](#) for a complete description). There is no indication of whether the materials came from either lower or upper part of the Douira Formation.

MATERIAL AND METHODS

The anuran fossils are curated in the vertebrate palaeontology research collection of the University of Chicago. We generated MicroCT scans at the University of Florida’s Nanoscale Research Facility using a Phoenix v|tome|x M (GE Measurement & Control Solutions, Boston, MA, USA). Voltage and current were customized for each specimen to balance resolution and intensity contrast; scanning parameters are included in the metadata associated with the scans on MorphoSource. The X-ray images were converted into tomogram slices using GE’s reconstruction software [datos|x](#) (see [Table S1](#) in [Data S1](#)). Each stack of slices produced was imported in the 3D reconstruction software Mimics 21.0 (Materialise, Leuven, Belgium); before importation, slices were cropped to remove empty spaces. To further decrease the data size, the slices were converted from 16 bits to 8 bits.

The resulting slices have an image resolution of $1,580 \times 2,144$ pixels and a voxel size of $5.7 \mu\text{m}$ for the volume size. 3D models were produced by segmenting each element using the ‘thresholding’ function (using the contrast on greyscale images). A 3D model of the endocast was produced by segmenting each element using the “add” function. We used the same voxel resolution of $5.7 \mu\text{m}$, with a smoothing factor of 3 for one iteration, to homogenize the model resulting from the segmentation. Data produced by segmentation were exported in the software 3matic 9.0 as separate files (see [Table S1](#) in [Data S1](#)).

The electronic version of this article in Portable Document Format (PDF) will represent a published work according to the International Commission on Zoological Nomenclature (ICZN), and hence the new names contained in the electronic version are effectively published under that Code from the electronic edition alone. This published work and the nomenclatural acts it contains have been registered in ZooBank, the online registration system for the ICZN. The ZooBank LSIDs (Life Science Identifiers) can be resolved and the associated information viewed through any standard web browser by appending the LSID to the prefix <http://zoobank.org/>. The LSID for this publication is: urn:lsid:zoobank.org:pub:DCACD333-53AA-4A6D-A0F0-9F9C180F0DDC. The online version of this work is archived and available from the following digital repositories: PeerJ, PubMed Central SCIE, and CLOCKSS.

Phylogenetic analyses

Our data matrix includes 88 taxa and 150 morphological characters (62 cranial and 75 postcranial characters, 12 from the hyobranchial apparatus, and one from soft-tissues) and is derived from that of [Lemierre et al. \(2021\)](#); see [Appendices S1](#), [S2](#), [S3](#)). We added two extinct hyperossified neobatrachian taxa (the new taxon described below from the Kem Kem, and *Hungarobatrachus szukacsi*) to test their affinities. *Hungarobatrachus szukacsi* ([Szentesi & Venczel, 2010](#)) has recently been included in a reduced phylogenetic analysis ([Venczel, Szentesi & Gardner, 2021](#)) and is considered a neobatrachian. It is the oldest neobatrachian outside of Gondwana and essential to understand the diversification of the clade during the Cretaceous. These new taxa were scored from observation on 3D mesh files created for this study based on segmenting newly generated MicroCT scans (see above) and from literature ([Szentesi & Venczel, 2010](#); [Venczel, Szentesi & Gardner, 2021](#)).

All analyses were performed using TNT v.1.5 ([Goloboff & Catalano, 2016](#)). All analyses were conducted with cline (also called multi-state) characters ordered (characters 3, 9, 10, 14, 26, 34, 51, 52, 68, 93, 112, 121, 124, 125 and 126). Cline characters were ordered as several studies ([Rineau et al., 2015](#); [Rineau, Bagils & Laurin, 2018](#)) showed that analyses using ordered morphocline characters outperformed analyses using unordered characters, even when the ordering scheme is wrong ([Rineau, Bagils & Laurin, 2018](#)). Analyses consisted of heuristic searches with 1,000 random addition sequences of taxa, followed by tree bisection reconnection (TBR) branch swapping, withholding 10 trees per repetition. The final trees were rooted using *Ascaphus Stejneger 1899* (Ascaphidae, Anura) and a strict consensus was created. Node supports were evaluated using Bremer support and standard nonparametric bootstrapping, with searches of 1,000 replicates and collapsing groups below 5% frequency.

Because the phylogeny resulting from the above analysis is strongly at odds with relationships inferred from those inferred with molecular genetic data, we performed an additional analysis using a constraint tree reflecting a consensus of recent molecular phylogenetic analyses. This included constraining the backbone of the tree to reflect early divergences in anuran evolution, as well as large-scale patterns of relationships within the two major clades of Neobatrachia (Hyoidea, Ranoidea). Within Hyoidea, we constrained four clades: Calyptocephalellidae, Neoaustrarana ([Feng et al., 2017](#); [Streicher et al., 2018](#)), the genus *Telmatobius* Wiegmann, 1834 as monophyletic, and a clade representing all other hyloids. Within Ranoidea, we constrained three clades: Afrobatrachia, Microhylidae, and Natatanura. We did not constrain the placement of any extinct taxa and we also left relationships within constraint clades (e.g., Pelobatoidea, Myobatrachoidea, Natatanura) as polytomies so that relationships within them could be inferred by our morphological data. This constraint tree (available in the Supplemental Materials) was generated by hand and represents a broad-scale consensus of phylogenetic relationships presented in recent phylogenomic analyses for most frog families ([Feng et al., 2017](#): fig. 1; [Hime et al., 2021](#): fig. 1) and those specific to hyloids ([Streicher et al., 2018](#): fig. 6) and ranoids ([Yuan et al., 2018](#): fig. 2).

The anatomical terminology used herein is based on [Roček \(1981\)](#), [Sanchiz \(1998\)](#), and [Biton et al. \(2016\)](#) for cranial features, [Sanchiz \(1998\)](#) for postcranial ones, [Gómez & Turazzini \(2021\)](#) for humerus anatomy, and [Gómez & Turazzini \(2016\)](#) for ilium anatomy. Anatomical terminology for cranial nerves follows [Gaupp \(1896\)](#).

RESULTS

Systematic Paleontology

Anura Duméril, 1804
Neobatrachia Reig, 1958
Cretadhefdaa gen. nov.

Type (and only known) species

Cretadhefdaa taouzensis sp. nov.
CRETADHEFDAA TAOUZENSIS sp. nov.

Holotype

UCRC-PV94, posterior portion of the skull preserving co-ossified and incomplete frontoparietals, parasphenoid, and the prooticooccipital (the co-ossified prootics and exoccipitals sensu [Roček, 1981](#)).

Type locality

TD1, near the city of Taouz in southeastern Morocco (see [Dutheil, 1999](#) for more information on Kem Kem localities).

Stratigraphic range

Middle Cenomanian (96–95 Ma).

Referred materials

One incomplete squamosal from TD1 (UCRC-PV95); one incomplete maxilla from Tz8a1 (UCRC-PV96); three incomplete presacral vertebrae, two from TD1 (UCRC-PV97–98) and one from Tz8a1 (UCRC-PV101); one incomplete sacral vertebra from OT1c (UCRC-PV103).

Etymology

The genus nomen *Cretadhefdaa* is a combination of the word Cretaceous and a transliteration of the Arabic word *dhefdaa* (also sometimes written as *dheftha* or *thedfaa*), meaning “frog”. The specific epithet *taouzensis* recognizes the type locality, Taouz.

Diagnosis

A neobatrachian anuran with a hyperossified skull differing from all other anurans by the following unique combination of characters: (1) frontoparietals coossified, lacking a midline suture, and covered in ornamentation of pits and ridges; (2) frontoparietals bearing a smooth occipital flange; (3) no *incrassatio frontoparietalis* on the ventral surface of the frontoparietals; (4) presence of a deep, groove-like central recess on the posterodorsal surface of the braincase to each side of the foramen magnum, and housing the foramen for the *arteria occipitalis*.

Cretadhefdaa can be differentiated from *Beelzebufo* in (1) having a smooth occipital flange on the posterior margin of the frontoparietals; (2) having a ventral extension of maxillary ornamentation on the *pars dentalis* and (3) lacking an ornamented table sitting atop neural spine of anterior presacral vertebrae. *Cretadhefdaa* can be differentiated from *Baurubatrachus* in (1) having a fully ossified dorsal margin of the foramen magnum; (2) lacking a distinct palatine shelf of the maxilla; (3) having a smooth occipital flange on the posterior margin of the frontoparietals; and (4) having a slender and shorter neural spine on presacral vertebrae. *Cretadhefdaa* can be differentiated from *Calyptocephalella satan Agnolin, 2012* in (1) lacking a distinct shelf on the maxilla; (2) having a smooth occipital flange on the posterior margin of the frontoparietals; (3) lacking median suture between frontoparietals; and (4) having weakly expanded sacral transverse processes. *Cretadhefdaa* can be differentiated from *Hungarobatrachus* in (1) lacking an *incrassatio frontoparietalis* on the ventral surface of the frontoparietals; (2) having the *arteria occipitalis* foramen within a deep recess; and (3) lacking a distinct palatine shelf of the maxilla. Diagnosis for the species is same as for the genus.

Description of the holotype (UCRC-PV94)

Osteological description

UCRC-PV94 is the preserved posterior region of the skull of *Cretadhefdaa*. All bones are co-ossified and the sutures between prooticoccipitals and the frontoparietals are difficult to discern (Figs. 1A–1G).

The posterior portion of the frontoparietals is preserved. The two frontoparietals are coossified to one another, and no suture is visible on the frontoparietal table (Fig. 1A). The frontoparietal table is large and covered in an ornamentation of pits and ridges. The posterior margin of the frontoparietals is flanked by a large occipital flange that

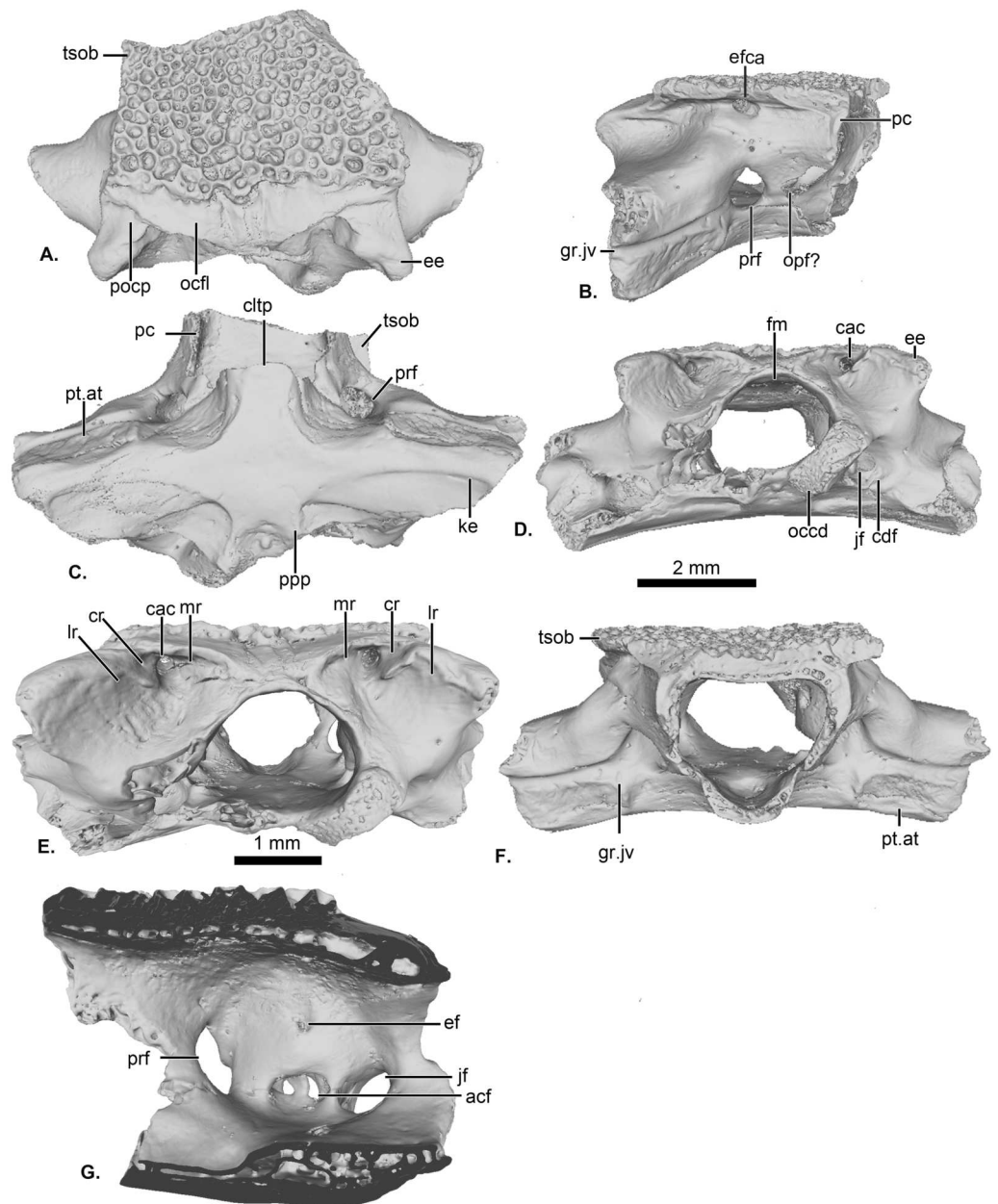


Figure 1 UCRC-PV64, holotype of *Cretadhefdaa*. Incomplete braincase in (A) dorsal; (B) right lateral; (C) ventral; (D) posterior; (E) posterodorsal view with a close up on the recesses system; (F) anterior and (G) medial views. Abbreviations: acf?, fused acoustic foramina; cac, canal for arteria occipitalis; cdf, condyloid fossa; cltp, cultriform process; cr?, central recess; ee, epiotic eminence; ef, endolymphatic foramen; efca, exit foramen for arteria orbitonasalis; fm, foramen magnum; gr.jv, groove for the jugular vein; jf, foramen jugulare; ke, median keel; lr, lateral recess; mr, medial recess; occd, occipital condyle; opt?, optic foramen; pc, pars contacta; pocp, paraoccipital process; ppp, posterior process of the parasphenoid; prf, prootic foramen; pt.at, pterygoid attachment area; tsob, tectum supraorbitale.

Full-size DOI: 10.7717/peerj.13699/fig-1

lacks ornamentation (Fig. 1A). The paraoccipital processes are reduced and fused to the underlying epiotic eminence (prominentia circularis ducti posterior of Roček & Lamaud, 1995), and the posterior process of the frontoparietals is not distinct (Fig. 1A). There is no pineal foramen visible. In lateral view, the preserved portion of the pars contacta is a straight vertical lamina (Fig. 1B). In ventral view, the frontoparietal table extends lateral to the pars contacta into a tectum supraorbitale, but its full extent is unknown because it is broken (Figs. 1A and 1B). There is no visible frontoparietal incassation on the ventral surface of the frontoparietals (*i.e.*, there is no imprint of the dorsal surface of the endocranium). The absence of frontoparietal incassation could be linked to the coossification of the tecta and thickening of this region of the frontoparietals (Z. Roček, pers. com.). In posterior view, the boundary between the frontoparietals and prooticoccipitals bears a series of deep recesses (Figs. 1D and 1E). The recesses are located between the tall epiotic eminence and the posterior margin of the frontoparietal table and appear to form a single large, deep groove on each side of the braincase. However, three different recesses can be distinguished within each groove (medial, central, and lateral recesses in Fig. 1E) that are each separated by well-defined ridges. Both the lateral and medial recesses are shallow, whereas the central recess is deep and houses a large, circular foramen for the arteria occipitalis. The foramen for the arteria orbitonasalis is visible on each lateral surface of the frontoparietal, ventral to the lateral extension of the table (Fig. 1B).

The posterior region of the parasphenoid is preserved. The cultriform process is broken, preserving only its base. The alae are large and cover the ventral surface of the otic capsules. In ventral view, the alae bear a median keel on its surface, extending from its lateral margin to and slightly curving towards the posterior process of the bone (Fig. 1C). The posterior process is divided into two well-separated small extensions, oriented posterolaterally. These expansions are fused to the base of the occipital condyles (Fig. 1C).

The prootic and exoccipital are coossified into a single prooticooccipital complex without a visible suture. Each prooticooccipital is co-ossified to the other along their medial margins, as well as to the frontoparietals (dorsally) and parasphenoid (ventrally). In dorsal view, the epiotic eminence is large, forming a broad lamina (Figs. 1A and 1D). The dorsal surface of the prootic is smooth. The crista parotica is not fully persevered, but likely had an ossified lateral expansion. There is no trace of an articulation facet for the squamosal on the preserved portion of the prooticooccipital (Fig. 1A). In anterolateral view, a large prootic foramen is present on the anterior surface of the prooticooccipital (Figs. 1B and 1G), and is fully enclosed in bone. In lateral view, anterior to the prootic foramen, a notch is visible on the anteriormost bony margin of the braincase (Fig. 1B) and might represent the posterior portion of the optic foramen. In anterior view, a well-delimited, narrow groove, likely for the jugular vein, extends from a large depression at the border of the prootic foramen to the lateral margin of the prootic (Fig. 1F). Beneath this groove, a large depression is present from the lateral margin of the prootic to the midpoint of its anterior surface. This is likely an articular facet for the medial ramus of the pterygoid. In posterior view, the left occipital condyle is missing (Fig. 1D), but the right occipital condyle is slightly ventrolateral to the large foramen magnum (Fig. 1D). The occipital condyle obscures the foramen jugulare that remains partially visible laterally (Fig. 1D). In

medial view, several foramina are visible in the wall of the braincase. The posteriormost opening is the foramen jugulare (Fig. 1G). Separated from the latter foramen by a thin bony pillar, a large opening is present on the lateral braincase wall (Fig. 1G). This opening likely represents the fused acoustics foramina, a fusion that is common in many anurans (Z. Roček, pers. comm.). A similar preservation is also present in the exceptionally preserved *Thaumastosaurus servatus* Filhol, 1877 (Lemierre et al., 2021).

Inner ear

The preservation of the endocast of the otic capsule allowed us to segment the otic chamber and semi-circular canals (vestibular apparatus) of *Cretadhefdaa*. The anterior, posterior, and lateral canals are all preserved and clearly identifiable (Figs. 2A and 2B). In anterior view, the base of the anterior canal bears a bulge, containing the anterior ampulla (Fig. 2A). In dorsal view, at the base of both anterior and lateral canals, the bulges contain the anterior and lateral ampullae (Fig. 2C). At the base of the posterior sinus (connecting the lateral and posterior canals), a similar bulge contains the posterior ampulla (Figs. 2B and 2D). In anterior and posterior views, the common crus (superior sinus), connecting the anterior and posterior canals, is well preserved (Figs. 2A–2C). The base of the superior sinus is thick, and is part of the utricle. The utricle forms the ventral portion of the vestibular apparatus. The vestibular apparatus occupies approximately half of total height of the endocast. The auditory region is large and bulbous (Fig. 2), and the posterior region (perilymphatic cistern + sacculus + lagena) occupies most of the endocast.

Within this posterior region, the perilymphatic cistern occupies the posteromedial region (Fig. 2B), while the sacculus occupies the anteriormost portion of this region (Fig. 2A). Lateral to the posterior region, a small region is delimited from the rest of the ventral volume by a slight constriction (Figs. 2A and 2B). This region can be identified as the transverse section through the perilymphatic space close to the fenestra ovalis. Near the perilymphatic cistern, a short and large canal, representing the perilymphatic ducts, opens posteriorly (Figs. 2B and 2D) into the braincase and the condyloid fossa (fused perilymphatic foramina). Another large duct is visible in the medial region of the otic chamber, entering the braincase through the fused acoustic foramina. However, this canal comprises two smaller ducts that are fused medially (Fig. 2) and housed the pathway of the cranial nerve VIII (Gaupp, 1896), representing the auditory nerve (Duellman & Trueb, 1994). A second medial, smaller duct is visible in the medial region of the vestibular apparatus, leading to the dorsalmost foramen of the lateral wall of the braincase (Fig. 1G). This duct is identified as the endolymphatic duct, leading to the endolymphatic sac that was present in the braincase (Frishkopf & Goldstein, 1963; Duellman & Trueb, 1994).

Referred cranial material

UCRC-PV95

The specimen is a fragment of a right squamosal preserving part of the lamella alaris (otic plate of Evans et al., 2014) and the base of the processus posterolateralis (Fig. 3). The dorsal and lateral surfaces of the bone are covered with an ornamentation made of deep longitudinal pits and ridges in the orbital and lateral region, and deep, nearly circular pits and ridges in the posterior and otic region (Fig. 3A). This ornamentation is slightly

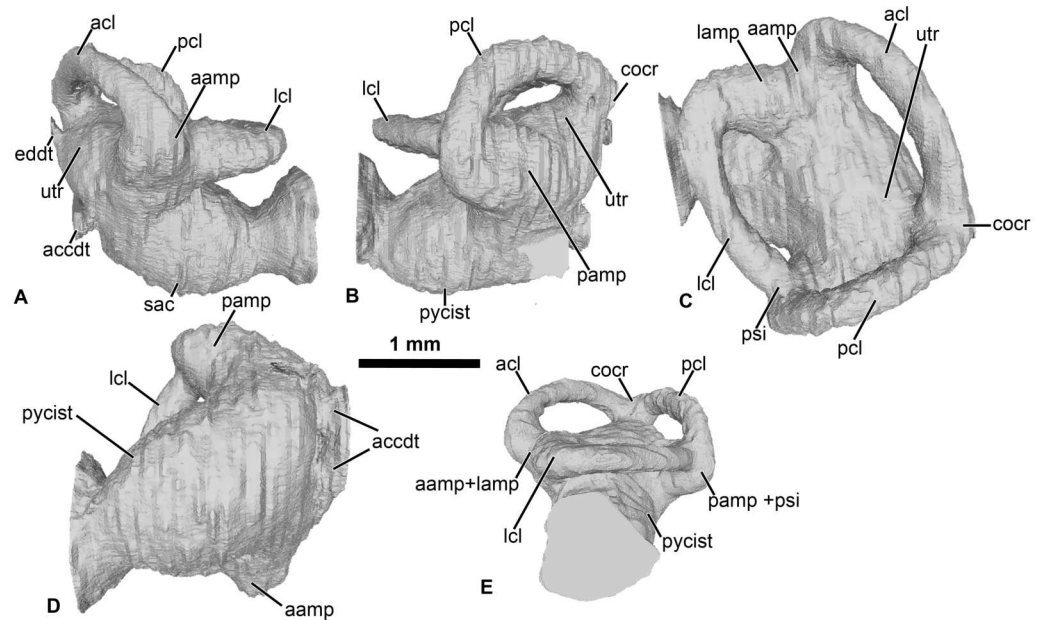


Figure 2 Internal morphology of the otic capsule of *Cretadhefdaa*. Endocast of the left otic capsule in (A) anterior; (B) posterior; (C) dorsal; (D) ventral and (E) lateral views. Abbreviations: aamp, anterior ampulla; accdt, transverse section through perilymphatic space containing stat-acoustic nerve; acl, anterior semicircular canal; cocr, common crus; eddt, endolymphatic duct; lamp, lateral ampulla; lcl, lateral semicircular canal; otr, otic chamber; pamp, posterior ampulla; pcl, posterior semicircular canal; psi, posterior sinus; pycist, perilymphatic cistern; sac, sacculus; utr, utricle.

Full-size [DOI: 10.7717/peerj.13699/fig-2](https://doi.org/10.7717/peerj.13699/fig-2)

different from that observed in UCRC-PV94, though it is not uncommon for anuran cranial bones to display variation in ornamentation within an individual (*de Buffrénil et al., 2015; de Buffrénil et al., 2016*). Thus, we interpret UCRC-PV95 as belonging to the same taxon as UCRC-PV94. The size of the squamosal is consistent with the size of the braincase (UCRC-PV94), but there is no indication that the two bones belong to the same individual. The lamella alaris is well developed (~3 mm length preserved, anterior to posterior) with an anterior extension ventrolaterally oriented (*Fig. 3B*). Posteriorly, the lamella alaris bears a vertical lamina, likely the base of the processus posterolateralis (*Fig. 3C*). Near this lamina, on the ventral surface of the lamella alaris, a small broken ridge is present. It might be the base of the ramus paroticus.

UCRC-PV96

This represents a partial anterior portion of a right maxilla. The maxilla is toothed and its lateral surface is covered in a pits and ridges ornamentation. The ornamentation covers almost all of the lateral surface, save for a thin strip of bone ventrally and its dorsalmost portion. Dorsally, the base of the large processus frontoparietalis is preserved (*Figs. 3E and 3F*). In medial view, the pars dentalis is straight, with a small sulcus dentalis (*Figs. 3F and 3G*; also visible in ventral view). The lamina horizontalis is faint, almost non-distinct from the medial surface of the maxilla (*Fig. 3F*). It forms a small ridge, with a shallow dorsal groove for the palatoquadrate (*Fig. 3G*). A deep maxillary recess is present medially (*Fig.*

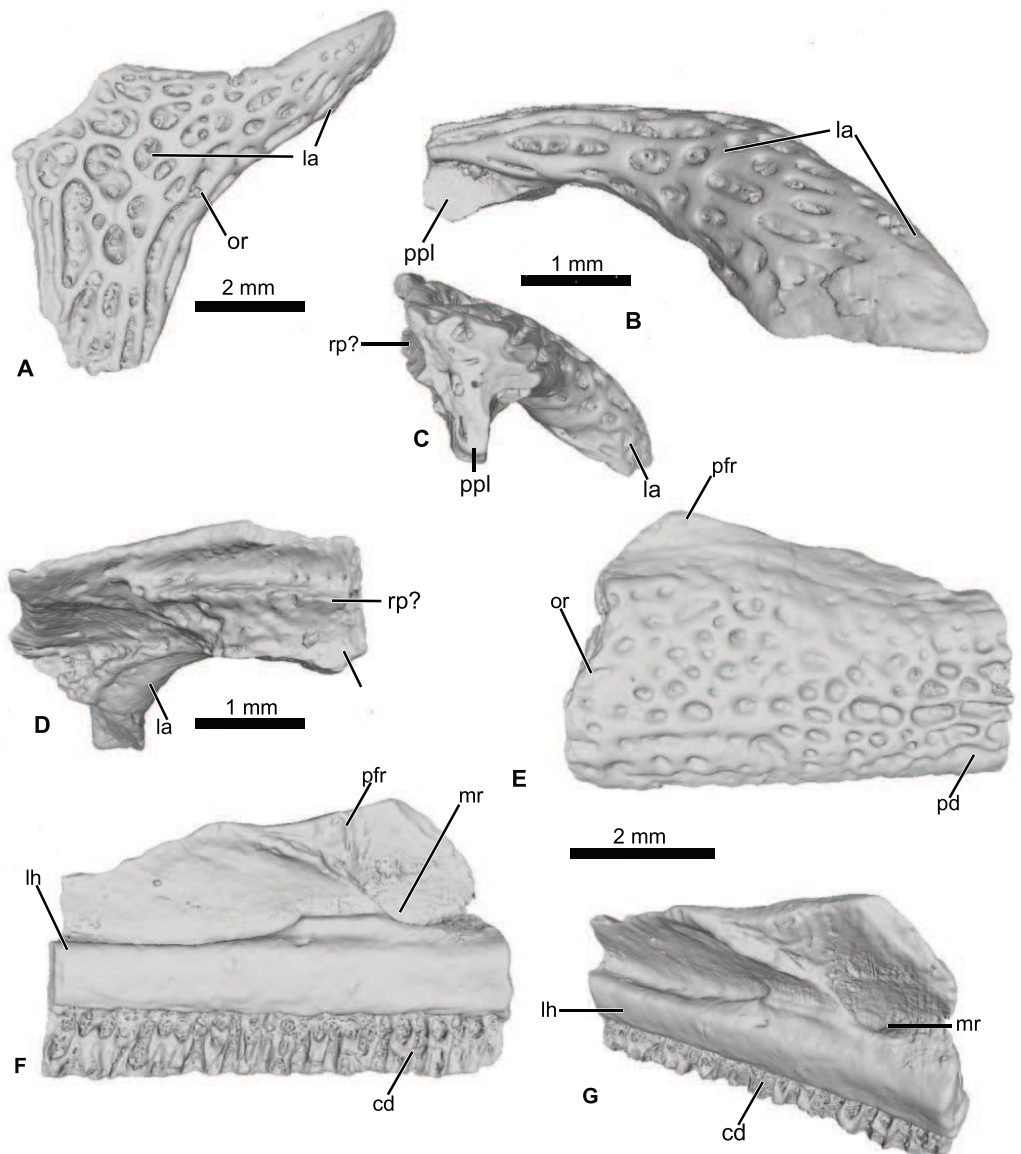


Figure 3 Cranial elements of *Cretadhefdaa*. (A–D) UCRC-PV95, incomplete squamosal in (A), dorsal; (B) lateral; (C) posterior and (D) ventral views; (E–G) UCRC-PV94, incomplete maxilla in (E) lateral, (F) medial and (G) dorsomedial views. Abbreviations: cd, crista dentalis; la, lamella alaris; lh, lamina horizontalis; mr, maxillary recess; or, ornamentation; pfr, processus frontalis; ppl, processus posterolateralis; rp?, ramus paroticus?.

Full-size  DOI: [10.7717/peerj.13699/fig-3](https://doi.org/10.7717/peerj.13699/fig-3)

3F). A groove for maxillary nerves extends dorsally from the maxillary recess to the dorsal part of the maxilla. Because only the bases of several teeth are preserved, nothing can be said of the tooth morphology of *Cretadhefdaa*.

Referred Vertebrae

The four vertebrae attributed to *Cretadhefdaa* all have an anterior cotyle and a posterior condyle, indicating a procoelous condition of the vertebral column. Although the length

of the centrum varies among these specimens (UCRC-PV97, UCRC-PV101 and UCRC-PV103 are shorter than UCRC-PV98), their similar size and the shape of articular facets and zygapophyses suggests that they all represent the same taxon. In addition, the two best preserved vertebrae, UCRC-PV101 and UCRC-PV98, have a similarly shaped low and short neural spine that is oriented posteriorly. In other anurans, there is documented variation in the length of the centra of presacral vertebrae throughout the vertebral column (Trueb, 1973; Duellman & Trueb, 1994; Púgner, 2002; Evans et al., 2014; Lemierre et al., 2021: fig. 9). We attribute the above cranial elements and these vertebrae to *Cretadhefdaa* because they all represent non-pipid individuals of similar body size (following Rage & Dutheil, 2008).

UCRC-PV97

This specimen is a centrum of a procoelous vertebra, with the neural walls not preserved (Figs. 4A–4C). The centrum is longer than wide (Figs. 4A and 4B). The posterior condyle is large and wide.

UCRC-PV98

This presacral vertebra is better preserved than UCRC-PV97, with most of the transverse process, one postzygapophysis, and the distal end of the neural spine missing (Figs. 4D–4I). The width of the posterior condyle is the same as that of the vertebral canal. The neural walls are thick, with the base of the transverse processes protruding laterally. In dorsal view, the remnants of the transverse processes are subcylindrical and oriented posteriorly. Each prezygapophysis bears a large flat and ovoid-shaped articular facet that is oriented dorsomedially (Fig. 4F). The medial margin of this articular facet is a sharp, straight lamina constituting the medial end of the dorsal wall of the vertebral canal. The neural spine is low and was likely short, though it is broken distally. The postzygapophysis is long, with an ovoid and flattened articular surface that is oriented ventrally (Fig. 4F). A small posterior lamina connects the neural spine and the medial margin of the postzygapophysis. The centrum is more elongate than UCRC-PV97 (Fig. 4G). In ventral view, the centrum is compressed lateromedially at midlength, giving the ventral surface an hourglass shape (Fig. 4G). In lateral view, a shallow fossa is visible at the midpoint of the vertebra and might be a remnant of a spinal foramen (Figs. 4H and 4I). The elongate centrum indicates that this vertebra is from the mid-column of *Cretadhefdaa*, possibly representing presacral vertebra IV.

UCRC-PV101

This element is an incomplete presacral vertebra preserving the centrum and neural arch (Figs. 4J–4N). The centrum is short, almost as wide as long. The vertebra is procoelous, with an anterior cotyle and a posterior condyle (Figs. 4J and 4K). The condyle is poorly preserved but seems elongated lateromedially. The prezygapophyses bear a flat articular facet that is oriented dorsomedially (Fig. 4L). In dorsal view, the anterior margin of the neural arch is concave, and a sharp ridge is visible on the dorsal surface of the neural arch, marking the beginning of the neural spine. The neural spine is very short (shorter than the one recovered in UCRC-PV98) and oriented posteriorly. Each postzygapophysis

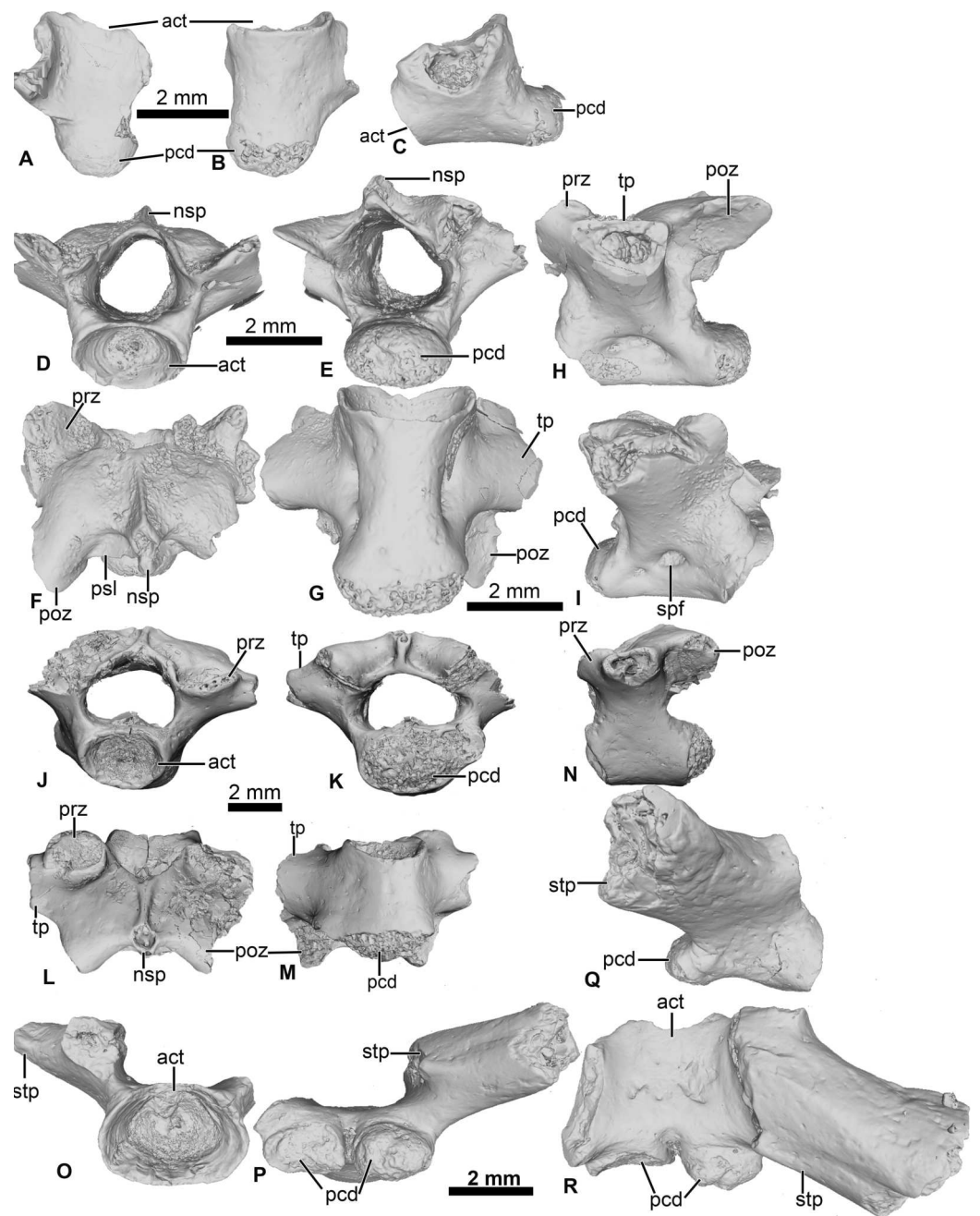


Figure 4 Vertebral element of *Cretadhefdaa*. (A–C) UCRC-PV97, presacral centrum in (A) dorsal; (B) ventral and (C) right lateral views; (D–I) UCRC-PV98 incomplete possible presacral vertebra IV in (D) anterior; (E) posterior; (F) dorsal; (G) ventral; (H) left lateral and I right lateral views; (J–N) UCRC-PV101, incomplete possible presacral VIII in (J) anterior; (K) posterior; (L) dorsal; (M) ventral and N left lateral views; (O–R) UCRC-PV103, incomplete sacral vertebra in (O) anterior; (P) posterior; (Q) right lateral and (R) ventral views. Abbreviations: act, anterior cotyle; nsp, neural spine; pcd, posterior condyle; poz, postzygapophysis; prz, prezygapophysis; psl, posterior lamina; spf, spinal foramen; stp, sacral transverse process; tp, transverse process.

Full-size DOI: 10.7717/peerj.13699/fig-4

bears a flat articular surface that is oriented ventrolaterally. The transverse processes are broken at their bases. The base of these processes is cylindrical in shape and elongate anteroposteriorly, oriented perpendicular to the anteroposterior axis of the centrum (Figs. 4L and 4N). The anteroposteriorly short centrum and the low and posteriorly oriented neural spine indicate that UCRC-PV101 is one of the posterior presacral vertebrae (VI to VIII). The posterior condyle of UCRC-PV101 is similar in size to the anterior cotyle of the identified sacral vertebra (UCRC-PV103) and the inferred position of the prezygapophyses of UCRC-PV103 seems to match the position of the postzygapophyses of UCRC-PV101. UCRC-PV101 might represent the last presacral vertebra (VIII).

UCRC-PV103

This incomplete sacral vertebra bears an anterior cotyle and two posterior condyles (Figs. 4O–4R). The centrum of UCRC-PV103 is shorter than the other three vertebrae, but the anterior cotyle is similar to those of UCRC-PV97–98 and 101. The two posterior condyles are well separated and are wider than tall, and thus elliptical. The preserved transverse process is posterolaterally oriented and the preserved portion does not expand distally. In lateral view, the sacral transverse process is extended anteroposteriorly, and is not cylindrical or rod-like. The dorsal expansion of the transverse process is visible in dorsal view (Fig. 4R).

Osteological comparison to hyperossified anurans

Hyperossified (sensu *Trueb, 1973*) ornamented cranial bones occur in both extinct and extant anurans, from pipoids (*Báez & Rage, 1998; Trueb, Pügener & Maglia, 2000*) to diverse lineages of neobatrachians, and is a condition that has evolved more than 20 times independently across extant frogs (*Paluh, Stanley & Blackburn, 2020*). Hyperossified cranial elements are known in numerous Cretaceous anurans from both Laurasian and Gondwanan sites (*Jacobs, Winkler & Gomani, 1990; Rage & Roček, 2003; Roček, 2013; Gardner & Rage, 2016*). In the Gondwanan fossil record, Cretaceous hyperossified anurans are known that belong to both the Pipimorpha and Neobatrachia (*Gardner & Rage, 2016; Báez & Gómez, 2018*).

Comparison to non-neobatrachian taxa

Ornamented and co-ossified cranial bones are relatively uncommon in the first four diverging lineages of extant frogs: Leiopelmatoidea, Alytoidea, Pipoidea, and Pelobatoidea. Neither of the two extant leiopelmatoids, *Ascaphus* and *Leiopelma* Fitzinger 1861, exhibit any characteristics unique to hyperossified anuran skulls. Among the extant alytoids, ornamented dermal bones are found only in the genus *Latonia* Meyer 1843 which is known from the Paleogene and Neogene of Laurasia and Africa (*Roček, 1994; Roček, 2013; Biton et al., 2016*). However, *Cretadhefdaa* differs from *Latonia* in having a foramen for the occipital artery (lacking in *Latonia*) and frontoparietals that fuse with the prooticooccipitals (see *Roček, 1994*: fig. 7). The extinct Gobiidae from the Cretaceous of Asia (*Roček, 2008; Roček, 2013*) also exhibits ornamented dermal bones. However, *Cretadhefdaa* can be differentiated from all Gobiidae in having fused frontoparietals without a visible suture (frontoparietals not fused or in contact with each other in Gobiidae), complete fusion of the prootic and

exoccipital (suture visible between the two bones in Gobiidae; [Roček, 2008](#)), and presacral vertebrae that are procoelous (amphicoelous in Gobiidae).

Cretadhefdaa can be differentiated from all pipoid anurans in having alae of the parasphenoid that cover the ventral surface of the otic capsules ([Fig. 1C](#)). Some members of the Pelobatoidea also have ornamented skull bones, but as an integral part of the bone and not as a secondary exostosis ([Rage & Roček, 2007](#); [Roček, 2013](#); [Roček et al., 2014](#)). *Cretadhefdaa* can be differentiated from *Eopelobates* Parker, 1929 in (1) having ornamentation as a secondary exostosis (ornamentation is an integral part of the bones in *Eopelobates*); and (2) lacking anteroposterior expansion of the distal part of the sacral apophyses ([Roček et al., 2014](#)).

In addition, several fragmentary remains of ornamented maxillae and procoelous vertebrae were recovered in the Cretaceous outcrops of Texas and might represent one the early diverging frog lineages, but the phylogenetic affinities of these fossils remain unclear ([Roček, 2013](#)).

Two hyperossified taxa of uncertain affinities are known from the Late Cretaceous of North America: *Scotiophryne* Estes, 1969 and *Theatoniuss* Fox, 1976. *Cretadhefdaa* can be differentiated from *Scotiophryne* in (1) having ornamentation made of pits and ridges (fine beadlike tubercles in *Scotiophryne*; [Gardner, 2008](#)); (2) having fused frontoparietals without a median suture (frontoparietals not fused in *Scotiophryne*); (3) having a well-delimited lamina horizontalis on the maxilla; and (4) having a well-developed ramus paroticus of the squamosal that articulates with the frontoparietal. *Cretadhefdaa* can be differentiated from *Theatoniuss* in (1) having teeth on the maxillae (maxillae are edentate in *Theatoniuss*; [Gardner, 2008](#)); and (2) having fused frontoparietals without a median suture (frontoparietal fused with a median suture in *Theatoniuss*; [Gardner, 2008](#)).

Based on the above comparisons, we exclude *Cretadhefdaa* from the Leiopelmatoidea, Alytoidea, Pipoidea, and Pelobatoidea. The vast majority of extant frog species belong to the Neobatrachia. *Cretadhefdaa* shares with Neobatrachia the presence of well-separated occipital condyles and a bicondylar articulation between the sacrum and urostyle. However, others synapomorphies used to diagnose Neobatrachia (in combination with the two mentioned above), such as the presence of palatines (also called neopalatines in neobatrachians; [Báez, Moura & Gómez, 2009](#)) cannot be assessed based on the preserved elements of *Cretadhefdaa*.

Comparison to Cretaceous hyperossified taxa

The best known non-pipimorph ornamented taxon described from the Mesozoic fossil record of Africa is *Beelzebufo ampinga*, from the Maastrichtian of Madagascar ([Evans, Jones & Krause, 2008](#); [Evans et al., 2014](#)). *Beelzebufo* is known from numerous cranial and some postcranial elements. The ornamentation of *Cretadhefdaa*, comprised of pits and ridges, is similar to that of *Beelzebufo*. Both taxa also have a series of three recesses on the posterodorsal surface of the skull, with the foramen for the arteria occipitalis located within the central recess, which is the deepest recess in both taxa ([Fig. 5](#)). *Cretadhefdaa* also differs from *Beelzebufo* in having a smooth occipital flange on the posterior region of the frontoparietals. The poor preservation of the tectum supraorbitale of the frontoparietals

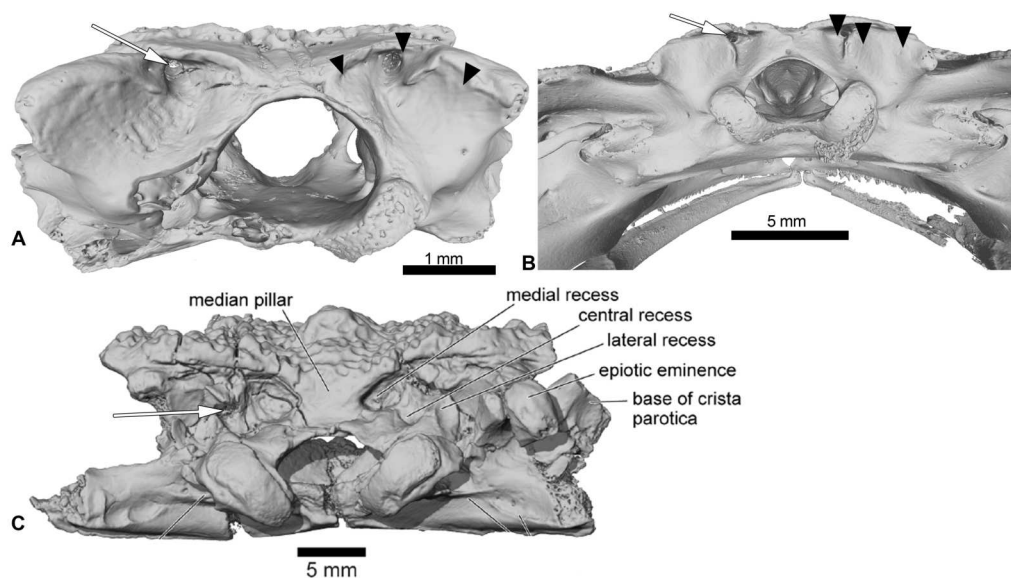


Figure 5 Comparison between the braincases of *Cretadhefdaa*, *Beelzebufo* and *Ceratophryidae*. (A) *Cretadhefdaa* in posterior view (UCRC-PV64); (B) *Beelzebufo* braincase in posterior view (taken from (Evans et al., 2014): fig. 22C) and (C) braincase of *Ceratophrys aurita* in posterior view (CAS:Herp:84998; MorphoSource ARK: ark:/87602/m4/M16099). Black arrows point to the recesses discussed in the text and white arrows point to the foramen for the arteria occipitalis.

Full-size DOI: 10.7717/peerj.13699/fig-5

of *Cretadhefdaa* (UCRC-PV94) means that we cannot evaluate whether it is similar to the expansion in *Beelzebufo*, in which the tectum supraorbitale is elongate laterally along on its entire length, covering the lateral region of the braincase (Evans et al., 2014). The parasphenoid of *Cretadhefdaa* is similar to that of *Beelzebufo* in having narrow alae (alary process of Evans et al., 2014) with a median keel. *Cretadhefdaa* is similar to *Beelzebufo* in lacking a distinct palatine shelf on the medial surface of the maxilla, but differs in having ornamentation of the pars facialis on the lateral surface of the maxilla that extends ventrally to the pars dentalis (the ornamentation ends before the pars dentalis in *Beelzebufo*).

The presacral vertebrae of *Cretadhefdaa* differ from most of those referred to *Beelzebufo* by lacking a well-developed neural spine, and lacking an expanded and ornamented “table” sitting atop the spine (Evans et al., 2014: figs. 34–36). In addition, even the shortest neural spine of the posteriormost presacral of *Beelzebufo* is taller than that of any vertebrae that we refer to *Cretadhefdaa* (Figs. 4F and 1L). The sacral vertebra of *Cretadhefdaa* is similar to that of *Beelzebufo* in having two elliptical posterior condyles for the sacro-urostylar articulation and a centrum that is wider than longer (Fig. 4P). However, the sacral transverse processes of *Beelzebufo* are slightly more expanded distally than that preserved for *Cretadhefdaa* (Fig. 4R).

Another neobatrachian from Gondwana with an ornamented skull is *Baurubatrachus pricei* Báez & Perí, 1989 from the Crato Formation of Brazil (Upper Early Cretaceous). The poor preservation of the frontoparietals of the holotype (and only known specimen), which is still embedded in matrix, prevents comparisons of the braincase of *Cretadhefdaa* to

Baurubatrachus. However, its frontoparietals seem to be similar in having ornamentation comprised of pits and ridges that extend posteriorly to the margin of the foramen magnum. *Cretadhefdaa* also differs from *B. pricei* in having a fully ossified dorsal margin of the foramen magnum, and a foramen for the arteria orbitonasalis dorsal to the prootic foramen. The maxilla of *Cretadhefdaa* is similar to *B. pricei* in having ornamentation on the lateral surface of the pars facialis that extends ventrally to the pars dentalis, but differs in lacking a distinct palatine shelf. *Cretadhefdaa* differs from *B. pricei* in having an occipital flange and a system of recesses on the posterodorsal region of the braincase. *Cretadhefdaa* also differs from *B. pricei* in having more slender and shorter neural spines on presacral vertebrae and slightly expanded sacral transverse processes.

In his 2012 review, Agnolin described several specimens as *Calyptocephalella satan*, the oldest calyptocephalellid described (Agnolin, 2012). Although these specimens need to be reassessed (Báez & Gómez, 2018) and likely represent more than one taxon (Muzzopappa et al., 2020), their attribution to Neobatrachia is certain. *Cretadhefdaa* resembles *C. satan* in having dermal skull bones covered with an ornamentation of pits and ridges, but differs in lacking a distinct palatine shelf (all calyptocephalellids exhibit a distinct palatine shelf; Muzzopappa & Báez, 2009; Agnolin, 2012), in having fused frontoparietals without a median suture, and in having an occipital flange on the frontoparietals (Fig. 1A). The postcranial elements of *Cretadhefdaa* resemble *C. satan* in having procoelous vertebrae with anteroposteriorly elongate centra for the anterior presacral vertebrae, and shorter centra for posterior presacral and sacral vertebrae (Agnolin, 2012). The sacral vertebra bears a bicondylar articulation in both taxa, but *Cretadhefdaa* differs in having sacral transverse processes that are weakly expanded distally, whereas *C. satan* exhibits greatly expanded sacral transverse processes (Agnolin, 2012: figs. 10A and 10B).

One last ornamented Cretaceous neobatrachian taxon is *Hungarobatrachus szukacsi* from the Late Cretaceous of Hungary. Its vertebral elements are not known, but several skull fragments were recently described (Venczel, Szentesi & Gardner, 2021). Both taxa have fused frontoparietals without a trace of suture along their medial margin. However, *Cretadhefdaa* differs from *H. szukacsi* in having a system of recesses on each side of the posterior surface of its frontoparietals (divided by the foramen magnum) with the foramen for the occipital artery opening in a deep recess and an occipital flange on the frontoparietals. In *H. szukacsi*, the posterior surface of the frontoparietals is smooth with a slight depression and the foramen for the occipital artery opens on each side of the foramen magnum (Venczel, Szentesi & Gardner, 2021: fig. 3). The frontoparietals of *H. szukacsi* also bear an *incrassatio frontoparietalis* on the ventral surface whereas *Cretadhefdaa* does not. The maxilla of *Cretadhefdaa* differs from that of *H. szukacsi* in lacking a distinct palatine shelf (Venczel, Szentesi & Gardner, 2021: fig. 5).

Comparison to hyperossified extinct ranoids

Two other hyperossified taxa are relevant for comparisons to *Cretadhefdaa*: *Rocekophryne ornata* (Rage et al., 2021) from the Early Eocene of Algeria (Rage et al., 2021) and *Thaumastosaurus servatus* from the Middle to Late Eocene of southwestern France (Lemierre

et al., 2021). These are the oldest occurrences of ornamented ranoids in the fossil record (Lemierre *et al.*, 2021; Rage *et al.*, 2021).

Rocekophryne ornata is known from fragmentary cranial and postcranial remains. *Cretadhefdaa* resembles *Rocekophryne* in having fused frontoparietals without a median suture and bearing an ornamentation of pits and ridges, an occipital flange, and in lacking an *incrassatio frontoparietalis* on the ventral surface of the frontoparietals. In addition, *Cretadhefdaa* and *Rocekophryne* both bear ornamentation on the lateral surface of the pars facialis of the maxilla that extends ventrally to the pars dentalis (Fig. 3F). However, *Cretadhefdaa* differs in lacking a lateral flange on the posterior surface of the frontoparietal, lacking a distinct palatine shelf, and in having very short paraoccipital processes (well-developed in *Rocekophryne*; Rage *et al.*, 2021: figs. 3A–3F) and a series of recesses on the posterodorsal surface of the braincase. In addition, the sacral vertebra of *Rocekophryne* bears an anterior condyle (instead of an anterior cotyle in *Cretadhefdaa*) that indicates that the vertebral column is diplasiocoelous (Rage *et al.*, 2021: figs. 4A and 4B) and possesses transverse processes that are circular in lateral view (not circular in *Cretadhefdaa*).

Thaumastosaurus servatus is known from fragmentary remains and three partially complete and articulated skeletons (Rage & Roček, 2007; Lemierre *et al.*, 2021). As with *R. ornata*, *Cretadhefdaa* and *T. servatus* have fused and ornamented frontoparietals without a medial suture. The anterior surface of the prooticoccipitals of both taxa exhibit a well-delimited but shallow and narrow groove for the jugular vein (Rage & Roček, 2007: fig. 7; Lemierre *et al.*, 2021: fig. 8F). However, *Cretadhefdaa* differs from *T. servatus* in having an occipital flange and reduced paraoccipital processes, lateromedially compressed occipital condyles (instead of crescent shaped), and a series of recesses in the posterodorsal surface of the braincase (Fig. 1). *Cretadhefdaa* also differs from *T. servatus* in lacking a single, tapered posterior process of the parasphenoid and an *incrassatio frontoparietalis* on the ventral surface of the frontoparietals (Fig. 1C). In addition, the vertebral column of *T. servatus* is diplasiocoelous instead of procoelous as in *Cretadhefdaa*.

Comparisons to extant hyperossified hyloids

Cretadhefdaa shares numerous characters with ornamented extant Neobatrachia. Most of these similarities are associated with hyperossification, but two characters deserve further attention. The first is the presence of contact between the squamosal and frontoparietals, which occurs frequently (but not uniquely) in Hyloidea (*e.g.*, Calyptocephalellidae, Ceratophryidae, or the hylid *Tripriion* Cope, 1866). The second is the series of recesses on the posterodorsal surface of the braincase in *Cretadhefdaa*. This is known only in *Beelzebufo* and in *Ceratophrys* Wied-Neuwied, 1824 (Evans *et al.*, 2014; Figs. 5B and 5C). However, both *Cretadhefdaa* and *Beelzebufo* differ from *Ceratophrys* in having the foramen for the occipital artery located in the central recess, whereas it is found in the medial recess in extant taxa (Fig. 5). The braincase of *Ceratophrys* is similar to *Cretadhefdaa* in having fused frontoparietals, no distinct posterior process, and barely distinct paraoccipital processes. *Cretadhefdaa* differs from *Ceratophrys* in having an occipital flange, a well-delimited groove for the jugular vein, and in lacking the expanded “table” atop the neural spine of presacral vertebrae. The extant *Tripriion* differs from *Cretadhefdaa* in having a frontoparietal

extending posteriorly up to the end of the epiotic eminence, covering it dorsally. *Tripriion petasatus* Cope, 1865 also lacks the system of recesses on the posterodorsal surface of the braincase. *Tripriion spatulatus* Günther, 1882 bears recesses on its posterodorsal region of the braincase, but differs from *Cretadhefdaa* in having the foramen for the arteria occipitalis not located within a recess.

Neobatrachia? Reig, 1958

Ranoidea? Rafinesque, 1814

Forelimb (UCRC-PV104)

This specimen is an incomplete humerus missing its proximal end and part of the diaphysis (Fig. 6). The diaphysis is straight, and a thin ventral ridge on the proximal end of the bone extends distally to the midlength of the diaphysis (Figs. 6A and 6C). The fossa cubitalis is very reduced, being shallow and not well-delimited, and visible in ventral view only as a thin crescent around the humeral ball (Fig. 6A). The humeral ball is large and in-line with the main axis of the diaphysis. The epicondyles are not symmetrical, with the ulnar epicondyle well-developed and the radial epicondyle reduced and barely visible in ventral view (Fig. 6A). In dorsal view, the olecranon scar is short, with a tapered and pointed end (Fig. 6B).

Comparisons

The combination of a large humeral ball and asymmetrically developed epicondyles is diagnostic for most *Neobatrachia* (Prasad & Rage, 2004; Rage, Pickford & Senut, 2013), although this combination of characters has not been evaluated in phylogenetic analyses. The presence of a straight diaphysis, a humeral ball in line with the axis of the diaphysis, and a shallow, poorly delimited fossa cubitalis are found in most ranoids (Rage, Pickford & Senut, 2013; De Lapparent de Broin et al., 2020). It differs from the humerus of *Thaumastosaurus servatus*, one of the earliest known ranoids, in having a crescent-shaped fossa cubitalis (triangular in *T. servatus*) and a less developed ulnar epicondyle. Among the Cretaceous neobatrachian taxa, only *Eurycephalella alcinae* (Báez, Moura & Gómez, 2009) and *Arariphrynus placidoi* (Leal & Brito, 2006) have preserved humeri with their ventral surface exposed. The humerus of *A. placidoi* differs from UCRC-PV104 in having two well-developed epicondyles (instead of a reduced radial epicondyle) and a deep fossa cubitalis (instead of a shallow fossa in UCRC-PV104).

These comparisons suggest that UCRC-PV104 should be referred to the *Neobatrachia*. UCRC-PV104 shares several characters with extant and extinct *Ranoidea*, as well as with the oldest (putative) member of the *Ranoidea* (*Thaumastosaurus servatus*). However, because no phylogenetic analyses have yet shown synapomorphies for *Ranoides* related to the humerus, we refer this fossil to the *Neobatrachia* and recognize the assignment to *Ranoidea* as tentative.

Incertae Sedis

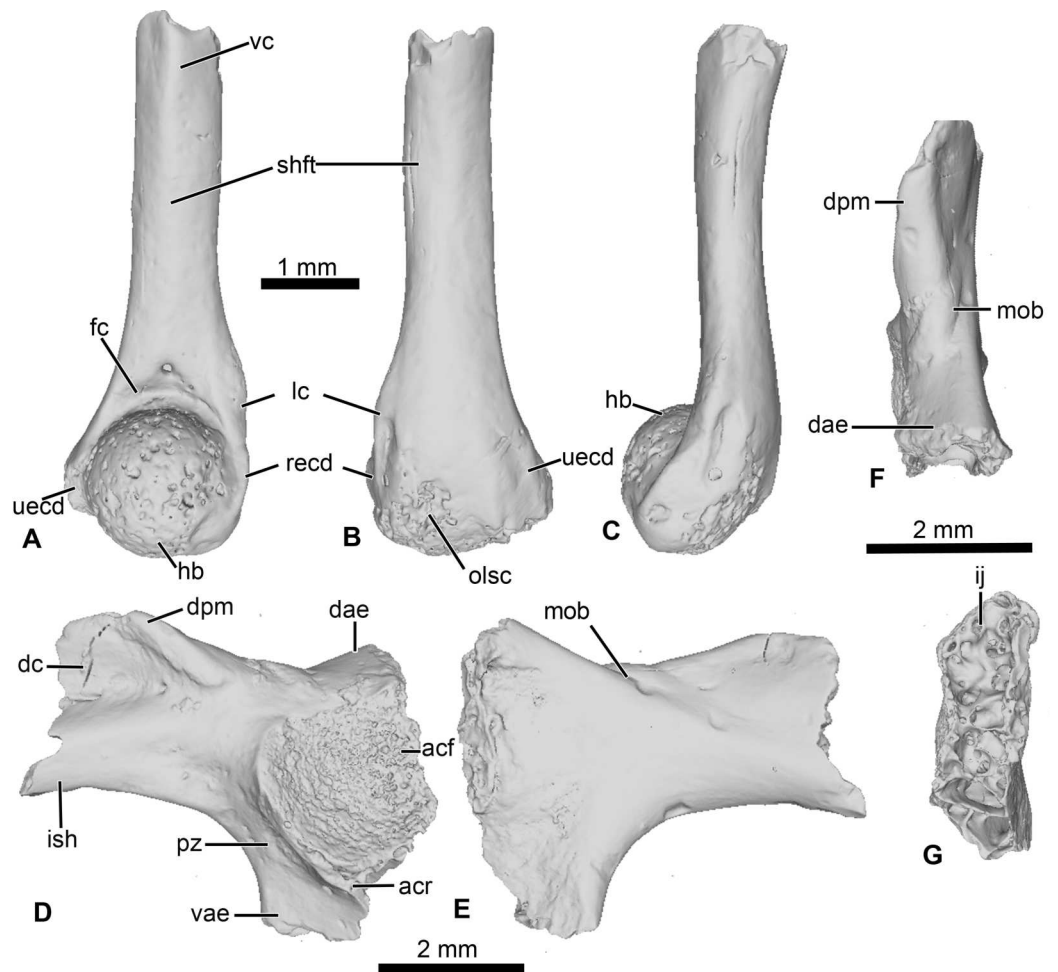


Figure 6 Neobatrachia? and indeterminate ilium from Kem Kem beds. (A–C) UCRC-PV104, incomplete humerus in (A) ventral; (B) dorsal and (C) lateral views; (D–G) UCRC-PV105, left ilium in (D) lateral; (E) medial; (F) posterior and (G) dorsal views. Abbreviations: acf, acetabular fossa; acr, acetabular rim; dae, dorsal acetabular expansion; dc, dorsal crest; dpm, dorsal prominence; fc, fossa cubitalis; hb, humeral ball; ij, ilioischial juncture; ish, iliac shaft; lc, lateral crest; mob, medial oblique ridge; olsc, olecranon scar; pz, preacetabular zone; reed, radial (lateral) epicondyle; shft, shaft; uecd, ulnare (medial) epicondyle; vae, ventral acetabular expansion; vc, ventral crest.

Full-size DOI: [10.7717/peerj.13699/fig-6](https://doi.org/10.7717/peerj.13699/fig-6)

Pelvic girdle (UCRC-PV105)

This element is an incomplete left ilium, preserving most of its acetabular region. UCRC-PV105 bears a high and well-developed dorsal crest, although its extension on the iliac shaft is unknown (Figs. 7I–7J). The dorsal crest appears to be lacking its dorsalmost portion, indicating that it was more extensive (Figs. 7I and 7K). The dorsal prominence is low and elongate anteroposteriorly, and the dorsal protuberance is strongly oriented laterally (Fig. 7K). The acetabular rim is well developed on its ventral region. Although not complete, both the dorsal and ventral acetabular expansions are developed. The dorsal acetabular expansion is inclined posteromedially (Fig. 7I). The ventral acetabular expansion is poorly preserved. However, the preserved portion shows it was well-developed (Fig. 4I). The

preacetabular angle is obtuse and the preacetabular zone is narrow (Fig. 7I). In medial view, a shallow but well delimited medial ridge is present, starting from the base or the dorsal acetabular expansion to the anteriormost preserved portion (Fig. 7J). In posterior view, the ilioischadic juncture is moderately wide and an interiliac tubercle is absent (Fig. 7L).

Comparisons

Ilia are one of the most common anuran elements recovered in the fossil record (Roček, 2000; Rage & Roček, 2003; Roček, 2013; Roček et al., 2013; Gardner & Rage, 2016) and several authors have proposed characters to identify the ilia of the different clades (Gardner et al., 2010; Gómez & Turazzini, 2016; Matthews, Keeffe & Blackburn, 2019). However, these are largely based on extant anurans and can be difficult to apply to Mesozoic anurans (Roček et al., 2010; Roček, 2013). The presence of a well-developed dorsal crest is found in several clades (Alytoidea, Pipoidea, and Neobatrachia, especially Ranoidea), but likely reflects similarity in locomotion rather than close phylogenetic relationships (Roček, 2013). The absence of an interiliac tubercle is diagnostic for many neobatrachians, with notable exceptions such as *H. szukacsi* and the aquatic hyloid *Pseudis* Wagler 1830 (Gómez & Turazzini, 2016; Venczel, Szentesi & Gardner, 2021). However, the utility of this character has not been tested thoroughly in a taxon-rich phylogenetic analysis (Gómez & Turazzini, 2016). Agnolin (2012) argued that the presence of a broad preacetabular zone and large acetabular fossa was diagnostic for the Calyptocephalellidae but this was not evaluated in a phylogenetic analysis and may represent an example of convergent evolution. There are no characters that allow for a precise attribution of this ilium (UCRC-PV105) to the other anurans from the Kem Kem or other specific anuran lineages.

Phylogenetic analyses

Recent phylogenetic analyses (Báez & Gómez, 2018; Lemierre et al., 2021) are based on a similar dataset. This dataset was first elaborated by Báez, Moura & Gómez (2009), based on the dataset of Fabrezi (2006) that was developed for a phylogenetic analysis of ceratophryids. The dataset from Báez, Moura & Gómez (2009) includes 42 taxa—three of which are extinct taxa—and 75 characters. In a separate analysis, Báez & Gómez (2018) modified the dataset from Fabrezi (2006) further by adding 29 neobatrachian taxa and redefining some characters to test the impact of characters related to hyperossification. They expanded the taxon sampling to 71 taxa and added 68 characters (for a total of 143 characters), as well as redefined several characters. Finally, Lemierre et al. (2021) further enlarged the dataset from Báez & Gómez (2018), by adding 15 extant natatanuran ranoid taxa (for a total of 20 natatanuran taxa). The vast majority of extant anurans belong to the Neobatrachia (Feng et al., 2017), which includes two large clades, Hyloidea and the Ranoidea. To date, phylogenetic analyses based solely on morphological characters (e.g., Scott, 2005) do not recover many of the clades found in recent molecular phylogenetic analyses (e.g., Roelants et al., 2007; Feng et al., 2017; Jetz & Pyron, 2018; Hime et al., 2021). To evaluate the phylogenetic placement of *Cretadhefdaa*, we analyzed our character matrix using different sets of assumptions as well as one analysis using a constraint tree reflecting recent results from molecular phylogenetic analyses.

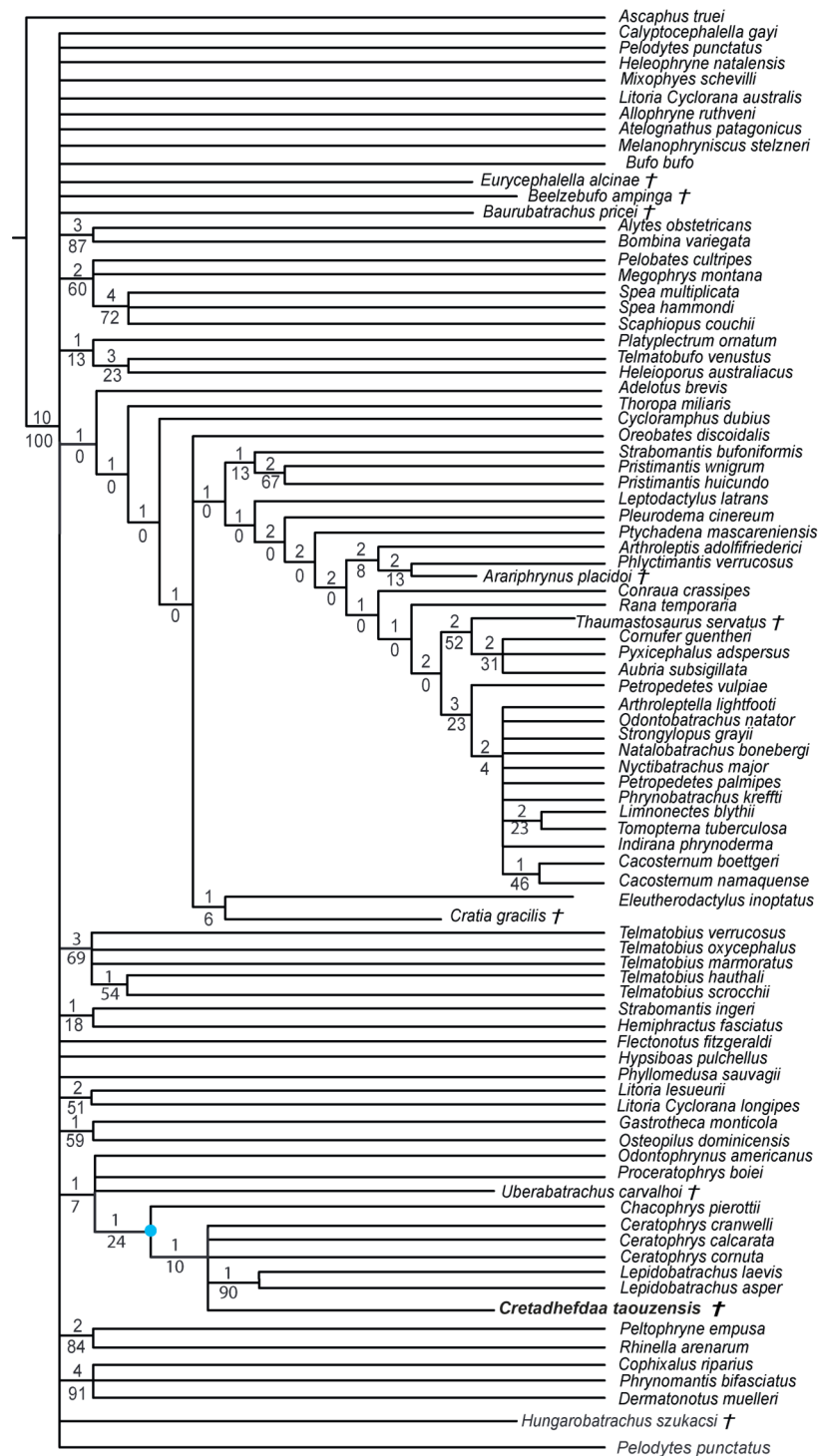


Figure 7 Strict consensus of 60 MPTs of 1362 steps (CI = 0.139; RI = 0.418) from the analysis under EW. † represents extinct taxon, light blue circle represents Ceratophryidae node; numbers above branches designate Bremer support; those below are bootstrap frequencies.

Full-size DOI: 10.7717/peerj.13699/fig-7

RESULTS

We obtained 60 MPTs (most parsimonious trees) of 1362 steps (CI = 0.139; RI = 0.418) with the analysis performed under equal weight with cline characters ordered. The strict consensus (Fig. 7) shows large polytomies, and the monophyly of the Neobatrachia is not recovered. This seems related to the uncertainties regarding the position of *Arariphrynus placidoi*, and the lack of characters scored for *Cretadhefdaa* and *Hungarobatrachus szukacsi* (13 and 11% of characters scored, respectively). *Cretadhefdaa* is recovered within a clade containing *Uberabatrachus carvalhoi* Baéz et al. 2012 and the Ceratophryidae. This clade is supported by three synapomorphies, all of which are character states found in other groups of frogs: (1) a position of articulation of lower jaw and skull at the level of occiput (character 61: 0 >1); (2) cotyle of the atlas widely separated (76: 1 >2) and (3) angle between iliac shaft and ventral acetabular expansion obtuse (125: 1 >2). *Cretadhefdaa* is placed within this clade in a polytomy with the Ceratophryidae. This clade is supported by five synapomorphies mainly related to hyperossified cranial characters (see Appendix S4).

When excluding *Arariphrynus*, we obtained 10 trees of 1,355 steps. The strict consensus (CI = 0.174; RI = 0.556; Fig. 8) shows a trichotomy with Pelobatoidae, *Heleophryne* Sclater 1898, and the remaining Neobatrachia. The 'Neobatrachia' (the clade exclusive of *Heleophryne*) is supported by a five synapomorphies: (1) otic ramus of the squamosal short, overlapping only the most lateral portion of the crista parotica (9: 0 >1); (2) absence of process or crest on the anterior margin of the scapula (114: 3 >0); (3) configuration of the postaxial carpals as ulnare free, 3+4+5 (119: 0 >2); (4) well developed posterodorsal expansion of the ischium (131: 0 >1) and (5) horizontal pupil shape (143: 0 >2). Among the Neobatrachia, we recovered a large hyperossified clade, supported by six synapomorphies (see Appendix S4). *Hungarobatrachus* is within a poorly supported trichotomy with *Eurycephalella* and *Calyptocephalella* Strand 1928, for which there are three synapomorphies: (1) contact between lamella alaris of the squamosal and frontoparietals on the dorsal surface of the otic capsule (8: 0 >2); (2) anterior ramus of the pterygoid not reaching planum antorbitale (12: 0 >1) and (3) postaxial carpal with ulnare and 3 free (119: 2 >1). *Cretadhefdaa* is recovered within a large polytomy with extant Ceratophryidae, poorly supported by four synapomorphies (see Appendix S4).

In analyses using a topological constraint (and excluding *Arariphrynus placidoi*), we obtained 190 trees, with a score of 1,395 steps. The strict consensus (CI = 0.126, RI = 0.247; Fig. 9) shows a monophyletic Neobatrachia, Ranoidea, and Hyloidea, but all of the monophyly of each was enforced in the constraint tree. Within Hyloidea, most taxa are placed within a large unresolved clade (Fig. 9). *Cretadhefdaa* is recovered in a large polytomy within Hyloidea as are *Baurubatrachus*, *Beelzebufo*, *Cratia* (Baéz, Moura & Gómez, 2009), *Eurycephalella*, *Hungarobatrachus*, and *Uberabatrachus*. The only extinct taxon to be recovered elsewhere in the phylogeny is *Thaumastosaurus*, which is recovered in a clade of Ranoidea with *Aubria* Boulenger 1917, *Cornufer* Tschudi 1838, and *Pyxicephalus* Tschudi 1838.



Figure 8 Strict consensus of 10 MPTs of 1355 steps (CI = 0.174; RI = 0.556) from the analysis under EW excluding *Arariphrynus placidoi*. † represents extinct taxon, red circle represents Neobatrachia node (excluding *Heleophryne*); numbers above branches designate Bremer support; those below are bootstrap frequencies and light blue circle represents Ceratophryidae node.

Full-size DOI: 10.7717/peerj.13699/fig-8

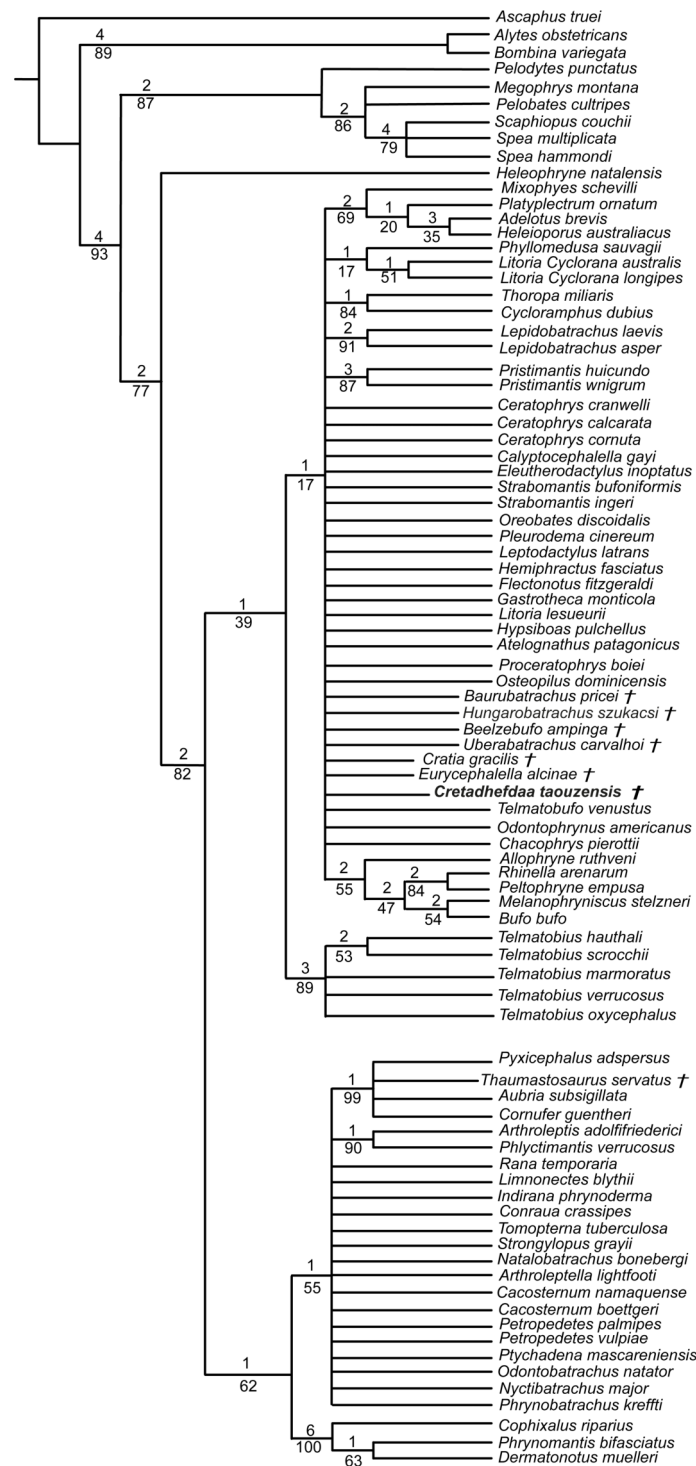


Figure 9 Strict consensus of 190 MPTs of 1395 steps (CI = 0.126; RI = 0.247) from the analysis under EW, excluding *Arariphrynus placidoi* and using a constraint topology based on molecular phylogenetic analyses. † represents extinct taxon and numbers above branches designate Bremer support; those below are bootstrap frequencies.

Full-size DOI: 10.7717/peerj.13699/fig-9

DISCUSSION

Phylogenetic analyses

The poor resolution of the topology obtained when performing phylogenetic analysis under equal weights is not surprising. *Hungarobatrachus szukacsi* has only 16 scored characters within the dataset, none of which are clear neobatrachian synapomorphies, and the skeleton of *Arariphrynus* is very incomplete leading to few scored characters, especially those for the pectoral girdle and vertebrae (51 scored characters in total; see [Báez, Moura & Gómez, 2009](#)). In addition, most of the scored cranial characters for *Hungarobatrachus* and *Cretadhefdaa* are linked to hyperossification, a recurrent feature in anuran evolution (see above) that likely obscures the phylogenetic relationships of *Cretadhefdaa*.

The phylogenetic positions of *Cretadhefdaa* and *Hungarobatrachus* are similar to several hyperossified extinct Cretaceous taxa by being close to either the Ceratophryidae or Calyptocephalellidae. Recent analyses ([Báez & Gómez, 2018](#)) have highlighted that convergence due to hyperossification likely plays a role in the position recovered for other hyperossified extinct neobatrachian taxa. This could influence the position of *Cretadhefdaa* as well. Nevertheless, the combination of characters of *Cretadhefdaa* confirms its assignment to Neobatrachia. In addition, one character mentioned in the description of the braincase, the presence of a series of recesses in posterodorsal region of the braincase, deserves attention. In addition to *Cretadhefdaa*, a similar (but not clearly homologous) morphology has only been identified in *Beelzebufo* and in the Ceratophryidae (except in *Chacophrys* Reig and Limeses 1963). To our knowledge, this character has not been used in phylogenetic analyses (e.g., [Gómez & Turazzini, 2021](#)). However, the two extant taxa possessing these recesses are closely related (*Ceratophrys* and *Lepidobatrachus* Budgett, 1899), and the extinct *Beelzebufo* has been proposed as a stem member of the Ceratophryidae ([Báez & Gómez, 2018](#); [Lemierre et al., 2021](#)). Interestingly, *Cretadhefdaa* is recovered in a more crownward position within Ceratophryidae than *Beelzebufo*, even in other analyses ([Báez & Gómez, 2018](#); [Lemierre et al., 2021](#)). It is necessary to test the phylogenetic significance of this character to confirm this hypothesis, which is beyond the scope of this paper. When using a topological constraint based on recent phylogenomic analyses, most extinct taxa—including *Cretadhefdaa*—included in the analysis were recovered as part of Hyloidea, though as part of a large polytomy. In conclusion, our phylogenetic analyses point to *Cretadhefdaa* being within the Neobatrachia, even if most of the synapomorphies diagnostic of this clade are not scored, and several analyses support a hyloid affinity.

Paleobiogeographical implications

Neobatrachians are known in the fossil record during the Late Cretaceous from three main locations: Madagascar (Maastrichtian; [Evans et al., 2014](#)), Europe (Campanian; [Venczel, Szentesi & Gardner, 2021](#)), and South America (Maastrichtian; [Báez & Gómez, 2018](#)). The South American fossil record is of particular importance with numerous taxa known from articulated specimens ([Báez, Moura & Gómez, 2009](#); [Báez & Gómez, 2018](#); [Agnolin et al., 2020](#); [Moura et al., 2021](#)). In contrast, only fragmentary remains of two taxa have been recovered from Madagascar and Europe ([Evans, Jones & Krause, 2008](#); [Evans et al., 2014](#); [Venczel, Szentesi & Gardner, 2021](#)). There are other reports of neobatrachians from the

Cretaceous ([Báez & Werner, 1996](#); [Prasad & Rage, 2004](#); [Rage, 1984](#); [Rage et al., 2020](#)) but the attribution of these to the Neobatrachia remains uncertain because diagnostic elements are often not preserved and these other fossils have not been included in phylogenetic analyses. Because *Cretadhefdaa* is from the Mid-Cenomanian, it is the oldest neobatrachian of Africa.

The oldest occurrence of the Neobatrachia is from the Brazilian Crato Formation ([Leal & Brito, 2006](#); [Báez, Moura & Gómez, 2009](#); [Agnolin et al., 2020](#); [Moura et al., 2021](#)), which preserves extinct anurans from the Aptian (Early Cretaceous). However, *Cretadhefdaa* is still the oldest occurrence of Neobatrachia outside of South America. The Neobatrachia began to diversify during the earliest Cretaceous, including an early split into two major lineages, Hyloidea and Ranoidea, each of which was largely restricted to a portion of western Gondwana, respectively, South America and Africa ([Frazão, Da Silva & Russo, 2015](#); [Feng et al., 2017](#)). Time-calibrated molecular phylogenetic analyses (e.g., [Feng et al., 2017](#)) suggest that by 96–95 Ma (i.e., the period from which *Cretadhefdaa* was recovered), the Neobatrachia was already separated into a number of lineages that are restricted today to specific biogeographic regions. These include the Myobatrachidae of Australia, the hyloids of South America, the Microhylidae (widespread today across the tropics), the Afrobatrachia of sub-Saharan Africa, the natatanuran ranoids, and the lineage leading to the Sooglossidae and Nasikabatrachidae that are today restricted, respectively, to the Seychelles Islands and the Western Ghats of India. There remains ample opportunity for both additional sampling and study of neobatrachian fossils from Gondwanan landmasses that could add new insights into the early evolution and biogeography of these major extant frog lineages that diversified in the Early Cretaceous.

The current absence of Ranoidea from the Cretaceous fossil record is puzzling. Except for undescribed and unillustrated material that was attributed to Ranoidea two decades ago ([Báez & Werner, 1996](#)), there are surprisingly few ranoid fossils especially in comparison to the hyloid fossils discovered in South America, Europe, and Africa. Their absence could be due to several factors. The first and most obvious is the lack of anuran specimens from the fossil record of Africa, due both to a lack of targeted collecting and little academic research on existing material. One example that highlights this problem is the Pyxicephalidae, a clade of ranoids endemic to Africa ([Channing & Rödel, 2019](#)) and for which time-calibrated molecular phylogenetic analyses suggest a divergence from other natatanurans around 60 Ma (Early Palaeocene). Yet, the oldest occurrence of this family is *Thaumastosaurus* from the Middle-Late Eocene of Europe, whereas the earliest African fossil is from only 5 Ma ([Matthews et al., 2015](#); [Lemierre et al., 2021](#)). The large gap in the fossil record of this family is found in many other families of Ranoidea, and many clades with an African origin completely lack a fossil record. Another bias could be that the vast majority of Ranoidea are not hyperossified anurans, including many small-sized species, and thus less likely to be preserved as intact and diagnosable fossils. In addition, numerous synapomorphies of Ranoidea are for postcranial elements, such as the vertebrae and the pectoral girdle, that are less likely to be identified and/or preserved ([Scott, 2005](#); [Frost et al., 2006](#)). A final bias is simply that there has been sustained interest from South American paleontologists in

the fossil record of anurans from countries such as Bolivia, Brazil, and Argentina, whereas there have been exceedingly few African paleontologists dedicated to studying anurans.

CONCLUSION

Our study confirms the report of *Rage & Dutheil (2008)* that at least three anuran taxa are present in the Kem Kem beds of Morocco. The newly described *Cretadhefdaa taouzensis* can be attributed to the Neobatrachia, making it both the oldest occurrence of the clade outside of South America and only the second occurrence in the Cretaceous of Africa. Several postcranial bones also point to an affinity with the Neobatrachia but cannot be associated definitively with either *Cretadhefdaa* or another taxon. The presence of a neobatrachian in the Kem Kem in the Cenomanian demonstrates that neobatrachians were already widespread on Gondwana during the earliest Late Cretaceous.

Institutional abbreviations

MNHN Muséum National d'Histoire Naturelle, Paris (France)

UCRC-PV University of Chicago research collection, Chicago (USA)

ACKNOWLEDGEMENTS

We thank Paul Sereno (University of Chicago) for access to and loan of the specimens, and Edward Stanley (University of Florida) for CT-scanning them. Processing of tomographic data was undertaken at the 3D imaging facilities Lab of the UMR 7207 CR2P (MNHN CNRS UPMC, Paris). We thank María Vallejo-Pareja for comments on a draft of this manuscript and both Zbyněk Roček and David Cannatella for constructive criticism.

ADDITIONAL INFORMATION AND DECLARATIONS

Funding

Funding for CT-scanning of both fossils and comparative material was supported by the US National Science Foundation (DBI-1701714 to David C. Blackburn). Funding for study of materials was supported by a grant from the Fondation pour la Recherche sur la Biodiversité (FRB, France) to Alfred Lemierre. The funders had no role in study design, data collection and analysis, decision to publish, or preparation of the manuscript.

Grant Disclosures

The following grant information was disclosed by the authors:

US National Science Foundation: DBI-1701714.

Fondation pour la Recherche sur la Biodiversité.

Competing Interests

The authors declare there are no competing interests.

Author Contributions

- Alfred Lemierre conceived and designed the experiments, performed the experiments, analyzed the data, prepared figures and/or tables, authored or reviewed drafts of the article, and approved the final draft.
- David C. Blackburn conceived and designed the experiments, authored or reviewed drafts of the article, and approved the final draft.

Data Availability

The following information was supplied regarding data availability:

The phylogenetic dataset is available in the [Supplemental File](#).

The CT-scan and 3D models are available on MorphoSource: Project 000426961.

<https://www.morphosource.org/projects/000426961?locale=en>

- UCRC-PV94, Incomplete posterior braincase, *Cretadhefdaa taouzensis*, CT Scan, <https://doi.org/10.17602/M2/M168041>; 3D Model, <https://doi.org/10.17602/M2/M427199>.
- UCRC-PV94_Inner ear, Endocast of Inner Ear, *Cretadhefdaa taouzensis*, CT Scan, <https://doi.org/10.17602/M2/M168041>; 3D Model, <https://doi.org/10.17602/M2/M427199>.
- UCRC-PV95, Incomplete squamosal, *Cretadhefdaa taouzensis*, CT Scan, <https://doi.org/10.17602/M2/M351726>; 3D Model, <https://doi.org/10.17602/M2/M427218>.
- UCRC-PV96, Incomplete maxilla, *Cretadhefdaa taouzensis*, CT Scan, <https://doi.org/10.17602/M2/M389771>; 3D Model, <https://doi.org/10.17602/M2/M427196>.
- UCRC-PV97, presacral vertebra, *Cretadhefdaa taouzensis*, CT Scan, <https://doi.org/10.17602/M2/M351731>; 3D Model, <https://doi.org/10.17602/M2/M427215>.
- UCRC-PV98, presacral vertebra, *Cretadhefdaa taouzensis*, CT Scan, <https://doi.org/10.17602/M2/M351736>; 3D Model, <https://doi.org/10.17602/M2/M427212>.
- UCRC-PV101, presacral vertebra, *Cretadhefdaa taouzensis*, CT Scan, <https://doi.org/10.17602/M2/M351753>; 3D Model, <https://doi.org/10.17602/M2/M427227>.
- UCRC-PV103, Sacral vertebra, *Cretadhefdaa taouzensis*, CT Scan, <https://doi.org/10.17602/M2/M351822>; 3D Model, <https://doi.org/10.17602/M2/M427202>.
- UCRC-PV104, Humerus, *Neobatrachia* ?, CT Scan, <https://doi.org/10.17602/M2/M351812>; 3D Model, <https://doi.org/10.17602/M2/M427209>.
- UCRC-PV105, Ilium, *Anura* Indet., CT Scan, <https://doi.org/10.17602/M2/M351817>; 3D Model, <https://doi.org/10.17602/M2/M427206>.

New Species Registration

The following information was supplied regarding the registration of a newly described species:

Publication LSID: urn:lsid:zoobank.org:pub:DCACD333-53AA-4A6D-A0F0-9F9C180F0DDC

Genus name: *Cretadhefdaa*: urn:lsid:zoobank.org:act:F144A555-3232-4FA0-8405-217E3DA55331

Species name: *Cretadhefdaa taouzensis*: urn:lsid:zoobank.org:act:A16F9829-615A-4405-AEBF-E62785E1BB7D

Supplemental Information

Supplemental information for this article can be found online at <http://dx.doi.org/10.7717/peerj.13699#supplemental-information>.

REFERENCES

- Agnolin F. 2012.** A New Calyptocephalellidae (Anura, Neobatrachia) from the Upper Cretaceous of Patagonia, Argentina, with comments on its systematic position. *Studia Geologica Salmanticensia* **48**:129–178.
- Agnolin F, Carvalho IDS, Aranciaga Rolando AM, Novas FE, Xavier-Neto J, Andrade JAFG, Freitas FI. 2020.** Early Cretaceous neobatrachian frog (Anura) from Brazil sheds light on the origin of modern anurans. *Journal of South American Earth Sciences* **101**:102633 DOI [10.1016/j.jsames.2020.102633](https://doi.org/10.1016/j.jsames.2020.102633).
- Báez AM, Gómez RO. 2018.** Dealing with homoplasy: osteology and phylogenetic relationships of the bizarre neobatrachian frog *Baurubatrachus pricei* from the Upper Cretaceous of Brazil. *Journal of Systematic Palaeontology* **16**:279–308 DOI [10.1080/14772019.2017.1287130](https://doi.org/10.1080/14772019.2017.1287130).
- Báez AM, Gómez RO, Ribeiro LCB, Martinelli AG, Teixeira VPA, Ferraz MLF. 2012.** The diverse Cretaceous neobatrachian fauna of South America: *Uberabatrachus carvalhoi*, a new frog from the Maastrichtian Marília Formation, Minas Gerais, Brazil. *Gondwana Research* **22**:1141–1150 DOI [10.1016/j.gr.2012.02.021](https://doi.org/10.1016/j.gr.2012.02.021).
- Báez AM, Moura GJB, Gómez RO. 2009.** Anurans from the Lower Cretaceous Crato Formation of northeastern Brazil: implications for the early divergence of neobatrachians. *Cretaceous Research* **30**:829–846 DOI [10.1016/j.cretres.2009.01.002](https://doi.org/10.1016/j.cretres.2009.01.002).
- Báez AM, Perí S. 1989.** *Baurubatrachus pricei*, nov. gen. et sp. un Anuro del Cretacico Superior de Minas Gerais. *Anais da Academia Brasileira de Ciências* **61**:447–458.
- Báez AM, Rage J-C. 1998.** Pipid frogs from the Upper Cretaceous of In Beceten, Niger. *Palaeontology* **41**:669–691.
- Báez AM, Werner C. 1996.** Presencia de anuros ranoideos en el Cretácico de Sudan [Abstract 460]. *Ameghiniana* **33**.
- Biton R, Boistel R, Rabinovich R, Gafny S, Brumfeld V, Bailon S. 2016.** Osteological observations on the Alytid Anura *Latonia nigriventer* with comments on functional morphology, biogeography, and evolutionary history. *Journal of Morphology* **277**:1131–1145 DOI [10.1002/jmor.20562](https://doi.org/10.1002/jmor.20562).
- Blakey RC. 2008.** Gondwana paleobiogeography from assembly to breakup—a 500 m.y. odyssey. In: Fielding CR, Frank TD, Isbell JL, eds. *Resolving the Late Paleozoic Ice Age in time and space. The geological society of america special paper*, Boulder: Geological Society of America, 1–28.
- Cavin L, Tong H, Boudad L, Meister C, Piuz A, Tabouelle J, Aarab M, Amiot R, Buffetaut E, Dyke G, Hua S, Le Loeuff J. 2010.** Vertebrate assemblages from the early Late Cretaceous of southeastern Morocco: an overview. *Journal of African Earth Sciences* **57**:391–412 DOI [10.1016/j.jafrearsci.2009.12.007](https://doi.org/10.1016/j.jafrearsci.2009.12.007).

- Channing A, Rödel M-O. 2019.** *Field guide to the frogs & other Amphibians of Africa*. Cape Town: Penguin Random House South Africa.
- De Broin F, Buffetaut E, Koeniger J-C, Rage J, Russell D, Taquet P, Vergnaud-Grazzini C, Wenz S. 1974.** La faune de vertébrés continentaux du gisement d'In Beceten (Sénonien du Niger). *Comptes Rendus de l'Académie des Sciences, Paris* **279**:439–472.
- de Buffrénil V, Clarac F, Canoville A, Laurin M. 2016.** Comparative data on the differentiation and growth of bone ornamentation in gnathostomes (Chordata: Vertebrata): growth of bone ornamentation in gnathostomes. *Journal of Morphology* **277**:634–670 DOI [10.1002/jmor.20525](https://doi.org/10.1002/jmor.20525).
- de Buffrénil V, Clarac F, Fau M, Martin S, Martin B, Pellé E, Laurin M. 2015.** Differentiation and growth of bone ornamentation in vertebrates: a comparative histological study among the Crocodylomorpha: development of bone ornamentation in the Crocodylomorpha. *Journal of Morphology* **276**:425–445 DOI [10.1002/jmor.20351](https://doi.org/10.1002/jmor.20351).
- De Lapparent de Broin F, Bailon S, Augé ML, Rage J-C. 2020.** Amphibians and reptiles from the Neogene of Afghanistan. *Geodiversitas* **42**:409–426.
- Duellman WE, Trueb L. 1994.** *Biology of amphibians*. Baltimore: John Hopkins University Press.
- Dutheil DB. 1999.** An overview of the freshwater fish fauna from the Kem Kem beds (Late Cretaceous: Cenomanian) of southern Morocco. In: Arratia G, Schultze HP, eds. *Mesozoic fishes-systematics and fossil record*. Munich: F. Pfeil, 553–563.
- Ettachfani EM, Andreu B. 2004.** Le Cénomanien et le turonien de la plate-forme préafricaine du Maroc. *Cretaceous Research* **25**:277–302 DOI [10.1016/j.cretres.2004.01.001](https://doi.org/10.1016/j.cretres.2004.01.001).
- Evans SE, Groenke JR, Jones MEH, Turner AH, Krause DW. 2014.** New material of *Beelzebufo*, a hyperossified frog (Amphibia: Anura) from the Late Cretaceous of Madagascar. *PLOS ONE* **9**:e87236 DOI [10.1371/journal.pone.0087236](https://doi.org/10.1371/journal.pone.0087236).
- Evans SE, Jones MEH, Krause DW. 2008.** A giant frog with South American affinities from the Late Cretaceous of Madagascar. *Proceedings of the National Academy of Sciences of the United States of America* **105**:2951–2956 DOI [10.1073/pnas.0707599105](https://doi.org/10.1073/pnas.0707599105).
- Fabrezi M. 2006.** Morphological evolution of Ceratophryinae (Anura, Neobatrachia). *Journal of Zoological Systematics and Evolutionary Research* **44**:153–166 DOI [10.1111/j.1439-0469.2005.00349.x](https://doi.org/10.1111/j.1439-0469.2005.00349.x).
- Feng Y-J, Blackburn DC, Liang D, Hillis DM, Wake DB, Cannatella DC, Zhang P. 2017.** Phylogenomics reveals rapid, simultaneous diversification of three major clades of Gondwanan frogs at the Cretaceous–Paleogene boundary. *Proceedings of the National Academy of Sciences of the United States of America* **114**:E5864–E5870 DOI [10.1073/pnas.1704632114](https://doi.org/10.1073/pnas.1704632114).
- Filhol H. 1877.** *Recherches sur les phosphorites du Quercy: étude des fossiles qu'on y rencontre et spécialement des mammifères*. Paris: G. Masson.
- Frazão A, Da Silva HR, Russo CADM. 2015.** The Gondwana breakup and the history of the Atlantic and Indian Oceans unveils two new clades for early neobatrachian diversification. *PLOS ONE* **10**:e0143926 DOI [10.1371/journal.pone.0143926](https://doi.org/10.1371/journal.pone.0143926).

- Frishkopf LS, Goldstein MH. 1963.** Responses to acoustic stimuli from single units in the eighth nerve of the bullfrog. *Journal of the Acoustical Society of America* 35:1219–1228 DOI [10.1121/1.1918676](https://doi.org/10.1121/1.1918676).
- Frost DR, Grant T, Faivovich J, Bain RH, Haas A, Haddad CFB, De Sá RO, Channing A, Wilkinson M, Donnellan SC, Raxworthy CJ, Campbell JA, Blotto BL, Moler P, Drewes RC, Nussbaum RA, Lynch JD, Green DM, Wheeler WC. 2006.** The Amphibian tree of life. *Bulletin of the American Museum of Natural History* 297:1–291 DOI [10.1206/0003-0090\(2006\)297%5b0001:TATOL](https://doi.org/10.1206/0003-0090(2006)297%5b0001:TATOL).
- Gardner D. 2008.** New information on frogs (Lissamphibia: Anura) from the Lance Formation (Late Maastrichtian) and Bug Creek Anthills (Late Maastrichtian and Early Paleocene). Hell Creek Formation, USA. In: Sankey JT, Baszio S, eds. *Vertebrate microfossil assemblages*. Indianapolis: Indiana University Press, 219–249.
- Gardner JD, Rage J-C. 2016.** The fossil record of lissamphibians from Africa, Madagascar, and the Arabian Plate. *Palaeobiodiversity and Palaeoenvironments* 96:169–220 DOI [10.1007/s12549-015-0221-0](https://doi.org/10.1007/s12549-015-0221-0).
- Gardner JD, Roček Z, Přikryl T, Eaton JG, Blob RW, Sankey JT. 2010.** Comparative morphology of the ilium of anurans and urodeles (Lissamphibia) and a reassessment of the anuran affinities of *Nezpercius dodsoni* Blob others, 2001. *Journal of Vertebrate Paleontology* 30:1684–1696 DOI [10.1080/02724634.2010.521605](https://doi.org/10.1080/02724634.2010.521605).
- Gaupp E. 1896.** *Anatomie des Frosches. Pt. 3.* Braunschweig: Friedrich Vieweg Und Shon.
- Goloboff PA, Catalano SA. 2016.** TNT version 1.5, including a full implementation of phylogenetic morphometrics. *Cladistics* 32:221–238 DOI [10.1111/cla.12160](https://doi.org/10.1111/cla.12160).
- Gómez RO, Turazzini GF. 2016.** An overview of the ilium of anurans (Lissamphibia, Salientia), with a critical appraisal of the terminology and primary homology of main ilial features. *Journal of Vertebrate Paleontology* 36:e1030023 DOI [10.1080/02724634.2015.1030023](https://doi.org/10.1080/02724634.2015.1030023).
- Gómez RO, Turazzini GF. 2021.** The fossil record and phylogeny of South American horned frogs (Anura, Ceratophryidae). *Journal of Systematic Palaeontology* 19:91–130 DOI [10.1080/14772019.2021.1892845](https://doi.org/10.1080/14772019.2021.1892845).
- Hime PM, Lemmon AR, Lemmon ECM, Prendini E, Brown JM, Thomson RC, Kratovil JD, Noonan BP, Pyron RA, Peloso PLV, Kortyna ML, Keogh JS, Donnellan SC, Mueller RL, Raxworthy CJ, Kunte K, Ron SR, Das S, Gaitonde N, Green DM, Labisko J, Che J, Weisrock DW. 2021.** Phylogenomics reveals ancient gene tree discordance in the amphibian tree of life. *Systematic Biology* 70:49–66 DOI [10.1093/sysbio/syaa034](https://doi.org/10.1093/sysbio/syaa034).
- Ibrahim N, Sereno PC, Varricchio DJ, Martill DM, Dutheil DB, Unwin DM, Baidder L, Larsson HCE, Zouhri S, Kaoukaya A. 2020.** Geology and paleontology of the Upper Cretaceous Kem Kem Group of eastern Morocco. *ZooKeys* 928:1–216 DOI [10.3897/zookeys.928.47517](https://doi.org/10.3897/zookeys.928.47517).
- Jacobs LL, Winkler DA, Gomani EM. 1990.** The dinosaur beds of northern Malawi, Africa. *National Geographic Research* 6:196–204.

- Jetz W, Pyron RA. 2018.** The interplay of past diversification and evolutionary isolation with present imperilment across the amphibian tree of life. *Nature Ecology & Evolution* 2:850–858 DOI [10.1038/s41559-018-0515-5](https://doi.org/10.1038/s41559-018-0515-5).
- Leal MEC, Brito PM. 2006.** Anura do Cretáceo Inferior da Bacia do Araripe, Nordeste do Brasil. In: Gallo V, Brito PM, Silva HMA, Figueiredo FJ, eds. *Paleontologia de Vertebrados. Grandes Temas e Contribuições Científicas*. Rio de Janeiro: Interciencia, 145–152.
- Lemierre A, Folie A, Bailon S, Robin N, Laurin M. 2021.** From toad to frog, a CT-based reconsideration of *Bufo servatus*, an Eocene anuran mummy from Quercy (France). *Journal of Vertebrate Paleontology* 41:e1989694 DOI [10.1080/02724634.2021.1989694](https://doi.org/10.1080/02724634.2021.1989694).
- Matthews T, Keffe R, Blackburn DC. 2019.** An identification guide to fossil frog assemblages of southern Africa based on ilia of extant taxa. *Zoologischer Anzeiger* 283:46–57 DOI [10.1016/j.jcz.2019.08.005](https://doi.org/10.1016/j.jcz.2019.08.005).
- Matthews T, Van Dijk E, Roberts DL, Smith RMH. 2015.** An early Pliocene (5.1 Ma) fossil frog community from Langebaanweg, south-western Cape, South Africa. *African Journal of Herpetology* 64:39–53 DOI [10.1080/21564574.2014.985261](https://doi.org/10.1080/21564574.2014.985261).
- McLoughlin S. 2001.** The breakup history of Gondwana and its impact on pre-Cenozoic floristic provincialism. *Australian Journal of Botany* 49:271–300 DOI [10.1071/BT00023](https://doi.org/10.1071/BT00023).
- Moura PHAG, Costa FR, Anelli LE, Nunes I. 2021.** A new genus of fossil frog (Anura) from lower Cretaceous deposits in South America. *Anais da Academia Brasileira de Ciências* 93:e20191560 DOI [10.1590/0001-3765202120201560](https://doi.org/10.1590/0001-3765202120201560).
- Muzzopappa P, Báez AM. 2009.** Systematic status of the mid-Tertiary neobatrachian frog *Calyptocephalella canqueli* from Patagonia (Argentina), with comments on the evolution of the genus. *Ameghiniana* 46:113–125.
- Muzzopappa P, Martinelli AG, Garderes JP, Rougier GW. 2020.** Exceptional avian pellet from the Paleocene of Patagonia and description of its content: a new species of calyptocephalellid (Neobatrachia) anuran. *Papers in Palaeontology* 7(2):1–14 DOI [10.1002/spp2.1333](https://doi.org/10.1002/spp2.1333).
- Paluh DJ, Stanley EL, Blackburn DC. 2020.** Evolution of hyperossification expands skull diversity in frogs. *Proceedings of the National Academy of Sciences of the United States of America* 117:8554–8562 DOI [10.1073/pnas.2000872117](https://doi.org/10.1073/pnas.2000872117).
- Prasad GVR, Rage J-C. 2004.** Fossil frogs (Amphibia: Anura) from the Upper Cretaceous intertrappean beds of Naskal, Andhra Pradesh, India. *Revue de Paléobiologie, Genève* 23:99–116.
- Púgener LA. 2002.** The Vertebral Column and Spinal Nerves of Anurans. Unpublished Ph.D. thesis, University of Kansas, USA 480.
- Rage J-C. 1984.** Are the Ranidae (Anura, Amphibia) known prior to the Oligocene? *Amphibia-Reptilia* 5:281–288 DOI [10.1163/156853884X-005-03-09](https://doi.org/10.1163/156853884X-005-03-09).
- Rage J-C. 2008.** Amphibia (Anura) from the Lower Miocene of the Sperrgebiet, Namibia. *Memoir of the Geological Survey of Namibia* 20:75–92.

- Rage J-C, Adaci M, Bensalah M, Mahboubi M, Marivaux L, Mebrouk F, Tabuce R. 2021.** Latest Early-Middle Eocene deposits of Algeria (Glib Zegdou, HGL50) yield the richest and most diverse fauna of amphibians and squamate reptiles from the Palaeogene of Africa. *Paleovertebrata* **43**:1–32.
- Rage J-C, Dutheil DB. 2008.** Amphibians and squamates from the Cretaceous (Cenomanian) of Morocco—A preliminary study, with description of a new genus of pipid frog. *Palaeontographica Abteilung A* **285**:1–22 DOI [10.1127/pala/285/2008/1](https://doi.org/10.1127/pala/285/2008/1).
- Rage J-C, Pickford M, Senut B. 2013.** Amphibians and squamates from the middle Eocene of Namibia, with comments on pre-Miocene anurans from Africa. *Annales de Paléontologie* **99**:217–242 DOI [10.1016/j.annpal.2013.04.001](https://doi.org/10.1016/j.annpal.2013.04.001).
- Rage J-C, Prasad GVR, Verma O, Khosla A, Parmar V. 2020.** Anuran lissamphibian and squamate reptiles from the Upper Cretaceous (Maastrichtian) Deccan Intertrappean Sites in Central India, with a review of lissamphibian and squamate diversity in the northward drifting Indian Plate. In: Prasad GVR Patnaik R eds., ed. *Biological Consequences of Plate Tectonics. Vertebrate Paleobiology and Paleoanthropology*. Cham: Springer International Publishing, 99–121 DOI [10.1007/978-3-030-49753-8_6](https://doi.org/10.1007/978-3-030-49753-8_6).
- Rage J-C, Roček Z. 2003.** Evolution of anuran assemblages in the Tertiary and Quaternary of Europe, in the context of palaeoclimate and palaeogeography. *Amphibia-Reptilia* **24**:133–167 DOI [10.1163/156853803322390408](https://doi.org/10.1163/156853803322390408).
- Rage J, Roček Z. 2007.** A new species of *Thaumastosaurus* (Amphibia: Anura) from the Eocene of Europe. *Journal of Vertebrate Paleontology* **27**:329–336 DOI [10.1671/0272-4634\(2007\)27%5b329:ANSOTA](https://doi.org/10.1671/0272-4634(2007)27%5b329:ANSOTA).
- Rineau V, Bagils RZi, Laurin M. 2018.** Impact of errors on cladistic inference: simulation-based comparison between parsimony and three-taxon analysis. *Contributions to Zoology* **87**:25–40 DOI [10.1163/18759866-08701003](https://doi.org/10.1163/18759866-08701003).
- Rineau V, Grand A, Zaragüeta R, Laurin M. 2015.** Experimental systematics: sensitivity of cladistic methods to polarization and character ordering schemes. *Contributions to Zoology* **84**:129–148 DOI [10.1163/18759866-08402003](https://doi.org/10.1163/18759866-08402003).
- Roček Z. 1981.** Cranial anatomy of frogs of the family Pelobatidae Stanius, 1856, with outlines of their phylogeny and systematics. *Acta Universitatis Carolinae—Biologica* **1980**:1–164.
- Roček Z. 1994.** Taxonomy and distribution of Tertiary discoglossids (Anura) of the genus *Latonia* V. Meyer, 1843. *Geobios* **27**:717–751 DOI [10.1016/S0016-6995\(94\)80058-8](https://doi.org/10.1016/S0016-6995(94)80058-8).
- Roček Z. 2000.** Mesozoic Anurans. In: Heatwole H, Carroll RL, eds. *Amphibian biology. 4. Palaeontology. The evolutionary history of amphibians*. Surrey Beatty and Sons Pty. Limited, 1295–1331.
- Roček Z. 2008.** The Late Cretaceous frog *Gobiates* from Central Asia: its evolutionary status and possible phylogenetic relationships. *Cretaceous Research* **29**:577–591 DOI [10.1016/j.cretres.2008.01.005](https://doi.org/10.1016/j.cretres.2008.01.005).
- Roček Z. 2013.** Mesozoic and tertiary anura of Laurasia. *Palaeobiodiversity and Palaeoenvironments* **93**:397–439 DOI [10.1007/s12549-013-0131-y](https://doi.org/10.1007/s12549-013-0131-y).

- Roček Z, Eaton JG, Gardner JD, Přikryl T. 2010.** Evolution of anuran assemblages in the Late Cretaceous of Utah, USA. *Palaeobiodiversity and Palaeoenvironments* **90**:341–393 DOI [10.1007/s12549-010-0040-2](https://doi.org/10.1007/s12549-010-0040-2).
- Roček Z, Gardner JD, Eaton JG, Přikryl T. 2013.** Anuran ilia from the Upper Cretaceous of Utah—diversity and stratigraphic patterns. In: Titus AL, Loewen MA, eds. *At the top of the grand staircase*. Bloomington: Indiana University Press, 273–294.
- Roček Z, Lamaud P. 1995.** *Thaumastosaurus bottii* De Stefano, 1903, an anuran with Gondwanan affinities from the Eocene of Europe. *Journal of Vertebrate Paleontology* **15**:506–515 DOI [10.1080/02724634.1995.10011244](https://doi.org/10.1080/02724634.1995.10011244).
- Roček Z, Wuttke M, Gardner JD, Singh Bhullar B-A. 2014.** The Euro-American genus *Eopelobates*, and a re-definition of the family Pelobatidae (Amphibia, Anura). *Palaeobiodiversity and Palaeoenvironments* **94**:529–567 DOI [10.1007/s12549-014-0169-5](https://doi.org/10.1007/s12549-014-0169-5).
- Roelants K, Gower DJ, Wilkinson M, Loader SP, Biju SD, Guillaume K, Moriau L, Bossuyt F. 2007.** Global patterns of diversification in the history of modern amphibians. *Proceedings of the National Academy of Sciences of the United States of America* **104**:887–892 DOI [10.1073/pnas.0608378104](https://doi.org/10.1073/pnas.0608378104).
- Sanchiz B. 1998.** *Salientia*. Munich: F. Pfeil.
- Scott E. 2005.** A phylogeny of ranid frogs (Anura: Ranoidea: Ranidae), based on a simultaneous analysis of morphological and molecular data. *Cladistics* **21**:507–574 DOI [10.1111/j.1096-0031.2005.00079.x](https://doi.org/10.1111/j.1096-0031.2005.00079.x).
- Sereno PC, Dutheil DB, Iarochene M, Larsson HCE, Lyon GH, Magwene PM, Sidor CA, Varricchio DJ, Wilson JA. 1996.** Predatory dinosaurs from the sahara and late cretaceous faunal differentiation. *Science* **272**:986–991 DOI [10.1126/science.272.5264.986](https://doi.org/10.1126/science.272.5264.986).
- Streicher JW, Miller EC, Guerrero PC, Correa C, Ortiz JC, Crawford AJ, Pie MR, Wiens JJ. 2018.** Evaluating methods for phylogenomic analyses, and a new phylogeny for a major frog clade (Hyloidea) based on 2214 loci. *Molecular Phylogenetics and Evolution* **119**:128–143 DOI [10.1016/j.ympev.2017.10.013](https://doi.org/10.1016/j.ympev.2017.10.013).
- Szentesi Z, Venczel M. 2010.** An advanced anuran from the Late Cretaceous (Santonian) of Hungary. *Neues Jahrbuch für Geologie und Paläontologie - Abhandlungen* **256**:291–302 DOI [10.1127/0077-7749/2010/0054](https://doi.org/10.1127/0077-7749/2010/0054).
- Trueb L. 1973.** Bones, frogs and evolution. In: Vial JL, ed. *Evolutionary biology of the anurans. Contemporary research on major problems*. Columbia: University of Missouri Press, 65–133.
- Trueb L, Pügener LA, Maglia AM. 2000.** Ontogeny of the bizarre: an osteological description of *Pipa pipa* (Anura: Pipidae), with an account of skeletal development in the species. *Journal of Morphology* **243**:75–104 DOI [10.1002/\(SICI\)1097-4687\(200001\)243:1<75::AID-JMOR4>3.0.CO;2-L](https://doi.org/10.1002/(SICI)1097-4687(200001)243:1<75::AID-JMOR4>3.0.CO;2-L).
- Venczel M, Szentesi Z, Gardner JD. 2021.** New material of the frog *Hungarobatrachus szukacsi* (Szentesi & Venczel, 2010), from the Santonian of Hungary, supports its neobatrachian affinities and reveals a Gondwanan influence on the European Late Cretaceous anuran fauna. *Geodiversitas* **43**(7):187–207 DOI [10.5252/geodiversitas2021v43a7](https://doi.org/10.5252/geodiversitas2021v43a7).

Yuan ZY, Zhang BL, Raxworthy CJ, Weisrock DW, Hime PM, Jin JQ, Lemmon EM, Lemmon AR, Holland SD, Kortyna ML, Zhou WW. 2018. Natatanuran frogs used the Indian Plate to step-stone disperse and radiate across the Indian Ocean. *National Science Review* **6**:10–14 DOI [10.1093/nsr/nwy092](https://doi.org/10.1093/nsr/nwy092).

Zouhri S (ed.) 2017. *Paléontologie des vertébrés du Maroc: état des connaissances*. Paris: Société Géologique de France.